Sustainable Cross-linked Polymers

A DISSERTATION

SUBMITTED TO THE FACULTY OF THE GRADUATE SCHOOL

OF THE UNIVERSITY OF MINNESOTA

BY

Guilhem Xavier Roger De Hoe

IN PARTIAL FULFILLMENT OF THE REQUIREMENT

FOR THE DEGREE OF

DOCTOR OF PHILOSOPHY

Marc A. Hillmyer, Advisor

September 2019

Acknowledgments

This thesis marks an incredible achievement for me, but it would not exist were it not for some incredible mentorship along the way. Were you to ask me ten years ago if a Ph.D. in Chemistry was in my future, I would have answered that I barely know what a doctoral program is, and that even if I did know, chemistry is certainly not my strong suit. In fact, exactly ten years ago (September 2009) was the start of my senior year in high school, and I was still recovering from the aftershocks of my A.P. Chemistry course in my junior year. It is here where my acknowledgements begin, because that experience created a ripple effect that has made me into the person I am today.

In the latter half of my junior year, Mr. Nafrada—endearingly referred to as Narf—and I had a personal meeting to address my performance in his (notoriously difficult) A. P. Chemistry course, which was becoming a steady downward spiral. I am hopefully not misquoting, but I believe his exact words were "rise up, De Hoe!" From then until the end of the year, improving my almost-failing grade was a grueling adventure that ultimately rewarded me with a B; thankfully Narf teaches some organic chemistry near the end, and I happened to be decent at that. His recognition of my accomplishment is immortalized in a yearbook gathering dust at my parents' house in California; on one of the blank pages, Narf wrote nothing more than "you rose up." I credit Narf for nucleating my interest in chemistry, and without him I may not have chosen it as my undergraduate major. More importantly, the values I learned from Narf carried me through my academic career: work hard, have integrity, and aim to be your best rather than better than those around you. Thank you, Narf, for keeping it real and being a hardass—I will continue to appreciate the struggle more than the result.

My undergraduate advisor, Prof. Philip Costanzo, is next in line for acknowledgment. He raised me from a research embryo to research tadpole, and then pushed me into the big boy pond of graduate school. I value the tenacious support and encouragement he gives his students, although I often ask myself how and why he tolerated me for so long. Perhaps it was because he could periodically call me "knucklehead" or perhaps it was because I had potential; whatever the reason, I am grateful that he persisted because I became well prepared for a top tier doctoral program in spite of the fact that I had never been exposed to one at my undergraduate institution. Interestingly enough, both Phil and Narf—who, just to be clear, do not know each other—were in the habit of endearingly referring to me and others as "fools"; I always appreciated the informality but also feel like it kept me humble, and humility is one of the most important virtues. From Phil I also learned the importance of optimism and momentum; the latter refers to his ability to charge ahead in work and in life, or as he would say: "keeping it cranking and moving forward so we can bust it out." (That's the abridged impression.) Lastly, I thank Phil for his continued support, advice, and inspiration.

At the start of this doctoral program, I was fortunate enough to join the research group of Prof. Marc Hillmyer, who has been an incredible mentor. During the past five years, I have metamorphosed from research tadpole to independent researcher, and it is thanks to Marc that I have been able to perform high quality research that I can call my own. Marc was always available to provide feedback or advice when needed, and in general he trusted me to be responsible for my research progress. He also gave me plenty of leeway to initiate my own projects and collaborations as well as participate in non-research activities (conference organizing, outreach, and a student group) that greatly benefitted my

overall professional development. I have appreciated and been inspired by Marc's enthusiasm for science, impeccable communication, and exceptional efficiency. Thank you, Marc, for being an exemplary advisor, professor, and individual.

I am grateful for the wonderful cohort of graduate students and postdocs in the Hillmyer group—although the personnel have changed significantly over five years, the environment has remained supportive and enjoyable. Dr. Jake Brutman deserves special mention because he was my mentor during the early stages of my metamorphosis and he remains an invaluable resource and friend. I would also like to highlight (in no particular order) a few past and current members of the group who have helped me directly either inside or outside of the lab: Prof. Christophe Sinturel, Prof. Madalyn Radlauer, Prof. Philip Dirlam, Dr. Luke Kassekert, Dr. Sebla Onbulak, Dr. Thomas Vidil, Dr. Deborah (Debbie) Schneiderman, Dr. Luis (Leo) Oquendo, Dr. Gereon Wuu-Yee, Dr. Lindsay Johnson, Dr. James Gallagher, Dr. Stacey Saba, Dr. Annabelle Watts, David Goldfeld, Nicholas Hampu, and Derek Batiste. David also deserves extra thanks for helping me proofread the introductory chapter of this thesis, for being my YouTube co-star, and for lending me his car, some mousetraps, and anything else I've forgotten.

I have also been fortunate to work with many talented scientists at the University of Minnesota and elsewhere, all of whom have positively influenced me in some way: Prof. Geoffrey Coates, Prof. William Dichtel, Prof. Kristopher McNeill, Prof. Thomas Hoye, Prof. Christopher Alabi, Dr. Michael Sander, Dr. Michael Zumstein, Dr. Grant Fahnhorst, Dr. Emily Hoff, Dr. David Fortman, Dr. Maria Sanford, Dr. Gordon Getzinger, Dr. Kyungtae Kim, Rachel Snyder, and Claire Lidston. Further thanks are in order for Dr.

Letitia Yao, David Giles, and Prof. Chris Macosko, each of whom have helped me when I was struggling with NMR spectroscopy or rheology.

I am especially grateful to a few key people who have given me continual encouragement during the past several years. First and foremost is my primary source of scientific and emotional support for the past few years, Dr. Angelika Neitzel. Next are Dr. Aakriti Kharel and Dr. Courtney Elwell, who have been my two graduate school sidekicks (or maybe I am their sidekick) since the beginning and have made the Ph.D. journey an enjoyable one both on- and off-campus. I must also thank Michael Loeper, who has little idea what I really do in lab but is always willing to listen to me rant or help me celebrate whenever necessary. Finally, I must thank my family and a few old friends who have always been actively supportive even though we are physically separated: Ella Pravetz, Alex London, Tristan Kleine, and Molly Burns.

Pour mes parents: Marie-Hélène et Alain

Abstract

Plastics, which are composed of long molecules called polymers, are useful materials whose versatility, low cost, and durability has caused their annual production to surpass that of most other man-made materials. The manufacturing of plastics is almost exclusively dependent on petrochemicals derived from nonrenewable fossil fuels and virtually all major plastics today are so durable that they persist long past their functional lifetime, resulting in a staggering exponential increase in plastic waste generation. Unfortunately, only a small fraction of this waste is collected for value recovery (e.g., recycling and incineration) while the majority ends up stagnating in landfills or polluting the environment. Certain important subsets of plastics, such as those with cross-linked molecular architectures, cannot be recycled at all. Therefore, the sourcing and end-of-life landscape for plastics is unsustainable in the long term. One avenue of research which aims to provide workable solutions to these problems is the development of new, competitive materials which can be sourced from annually renewable feedstocks (i.e., biomass) and/or have more sustainable end-of-life fates (e.g., improved capacity for recycling or degradation). In this thesis, four projects are presented investigating various aspects of sustainable cross-linked plastics. Chapter 1 provides a summary of plastic use and sustainable plastic development, with emphasis on cross-linked polymers. Chapter 2 investigates a component of biodegradability for a commercial mulch film which cross-links under UV light. Chapters 3 and 4 describe the development of sustainable cross-linked elastomers, and Chapter 5 comprises a study of potentially recyclable polymers with dynamic urethane cross-links.

Table of Contents

List of Tables

List of Figures

Chapter 1. Challenges Regarding the Sustainable Use of Cross-linked Plastics*

* Small sections and a few figures in this chapter have been reprinted (adapted) with permission from Fortman, D. J.; Brutman, J. P.; De Hoe, G. X.; Snyder, R. L.; Dichtel, W. R.; Hillmyer, M. A. Approaches to Sustainable and Continually Recyclable Cross-Linked Polymers. *ACS Sus. Chem. Eng.* **2018**, *6*, 11145–11159.

1.1. Plastics as Tools for Humankind

Since before the development of ancient civilizations, humankind has been adept at making tools from natural resources in order to perform complicated tasks that enhance the quality of life and prolong the average lifespan. Throughout the societal evolution of our species, we have mastered the use of raw materials like stone, minerals, ceramics, metals, and even those obtained from living organisms. This last category of materials includes plant matter (e.g., wood, fibers, natural rubber), animal parts (e.g., feathers, shells, horns, hides) and secretions (e.g., silk, shellac), as well as coal and related substances (e.g., bitumen, oil shale, crude oil, and natural gas).[1,2] These substances are effectively derived from dead organisms—primarily plants—after a long process involving biological/bacterial degradation followed by immense heat and pressure in the Earth's crust.[3] Their origin from prehistoric living matter coupled with their eventual application for the industrial production of common chemicals is the reason that coal, oil shale, bitumen, crude oil, and natural gas have been termed *fossil fuels*. Another relevant term that is important to define is *petroleum*, which literally means *rock oil* and refers to gaseous, liquid, semisolid, and solid hydrocarbons that are found in fossil fuels.[4]

Fossil fuels have been in humankind's toolbox for millennia. Bitumen, also known as asphalt, was used in construction as a waterproofing agent and mortar by early cultures such as the Sumerians and the Babylonians.[4] Interestingly, the archaic uses of fossil fuels can also be related to different stages of life and death: Ancient Egyptians embalmed corpses using cloth permeated with bitumen, eventually also using it to fill the inside of the bodies (preservation after death); the Byzantines used so-called *Greek fire*, an incendiary mixture probably containing a petroleum distillate, during naval warfare (a source of

death); and Middle Eastern physicians touted curative uses for bitumen obtained from mummies (extension of life).[4,5] While these uses of fossil fuels were small-scale, there were also relatively early reports (ca. 1270 A.D.) by traveling merchant Marco Polo describing a commercial petroleum industry in northern Persia; the presence of this early industry can presumably be attributed to the use of volatile petroleum substances (i.e., distilled fractions) as illuminants.[4] It would be several hundred years before the first instance of modern commercial petroleum distillation, but the prime motive would remain the same: fuel.

At approximately the same time as the erection of the first modern oil wells (ca. 1840 to 1860), several inventors were embarking on a quest that would yield the earliest plastics. Independently from one another, they began to investigate the chemical modification of natural substances. Two American brothers, Charles and Nelson Goodyear, discovered that heating sulfur with natural rubber could furnish useful materials with vastly different properties: a highly elastic solid if only a few percent of sulfur was used, whereas much greater quantities of sulfur resulted in a very hard solid.[2,6] In both cases, these materials had the peculiar characteristics of retaining their elasticity or stiffness over a wide range of temperatures as well as resistance to solvents (i.e., no dissolution). The molecular reasons for these characteristics were not understood until much later, but it is worth taking an aside to explain these reasons and provide a working definition for the word *plastic*.

Plastics are composed of long molecules known as macromolecules or polymers, which are chains of repeating chemical units made from small molecules called monomers **(Figure 1.1A**). These polymers generally become malleable with an increase in temperature (or the presence of solvent), and thus the term *thermoplastic* is typically used.

However, there also exists polymers that cannot be re-molded once they are shaped due to the chemical junctions—also known as chemical cross-links—between separate polymer strands (**Figure 1.1B**); these cross-linked materials are classically referred to as *thermosets*, and the working definition of the word *plastic* has evolved to include both thermosets and thermoplastics. Although they did not necessarily know the full scientific significance of their discoveries, Charles and Nelson Goodyear had transformed a thermoplastic—natural rubber, or poly(isoprene)—into the first thermosets. The sulfur had reacted with the natural rubber and generated chemical junctions between different poly(isoprene) chains, and inclusion of more sulfur created a more densely cross-linked and thus much harder rubber (**Figure 1.1C**). The cross-linked nature of both the elastic and hard materials was the underlying reason for their remarkable thermal and chemical resistance; heating did not significantly affect their dimensional stability or material properties because the chains could not move past one another, and immersion in solvent only swelled the network of chains rather than dissolved it.

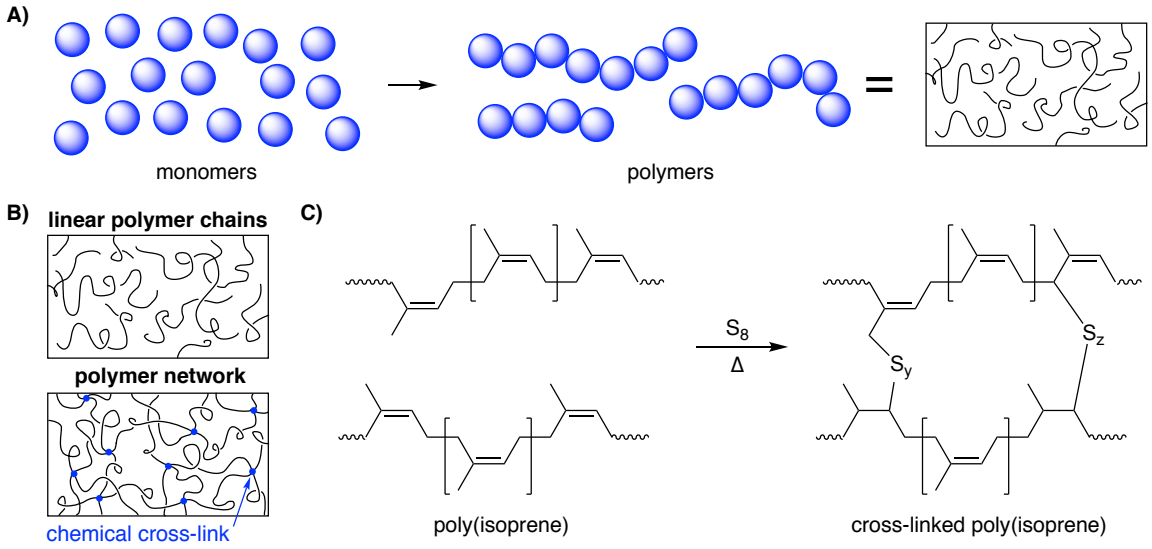

Figure 1.1. A) Schematic representation of polymerization. B) Comparison of linear and chemically cross-linked polymer architectures. C) Reaction of sulfur with poly(isoprene), which yields a cross-linked material.

Not long after the discoveries regarding natural rubber took place, the development of other semi-synthetic plastics continued with chemical modifications of a different natural polymer: cellulose. The controlled nitration of cellulose had just been established in Europe, and an English inventor named Alexander Parkes found that solutions of nitrocellulose—then commonly used in photography—could be evaporated to yield a thermoplastic material that he named Parkesine. Parkes is credited with the first attempt of the commercial production of a thermoplastic; unfortunately, his venture failed and the ultimate victor of nitrocellulose-derived plastics was John Wesley Hyatt, an American inventor. Hyatt realized that camphor, a compound obtained from plants, was an effective plasticizer for nitrocellulose and was essential for reproducible and profitable material production; the manufacture and sale of this plastic, which he termed Celluloid, was a commercial success. Besides cross-linked rubber, celluloid, and a few natural materials (e.g., shellac), no other plastics were available until 1900, when a new material derived

from casein (a milk protein) and formaldehyde was unveiled. This material, known as Galalith or Erinoid, is a cross-linked thermoset and the predecessor of the first fully synthetic plastic.

In the 20th century, the fossil fuel and materials industries merged to create a new industry which is now inextricable from human life. The beginning of this transition is the invention of Bakelite by Leo Baekeland (US patent filed in 1907).[7] His creation—a thermoset derived from phenol and formaldehyde—drew upon earlier work on aldehyde-derived resins, but Baekeland was the first to control and modify the phenol-formaldehyde reaction such that commercialization was possible.[8] Importantly, the modern petroleum industry had been growing steadily since the mid-19th century, and its refined products (aromatics and olefins) now enabled the production of many *petrochemicals* that were not readily accessible from natural materials. Because formaldehyde and phenol are petrochemicals, Bakelite is considered the first fully synthetic plastic, although it bears strong structural similarities to a natural polymer called lignin (**Figure 1.2**). The invention and successful commercialization of Bakelite demonstrated the immense potential for petrochemicals to be used as feedstocks for something other than fuels: plastics. However, it took 20 to 30 more years before the initial industrial production of some of today's major synthetic plastics: poly(styrene), poly(ethylene), poly(methyl methacrylate), and poly(vinyl chloride).[2] World War II began shortly thereafter and with it came huge demand for the aforementioned plastics as well as the development of new plastics like nylon and synthetic rubber.[2,9] Less than a decade after the war ended in 1945, the fossil fuel-based plastics industry was in full swing. Improvements in material quality and cost of production

occurred quickly and the mass production of plastics rapidly became a lucrative and tangible reality.

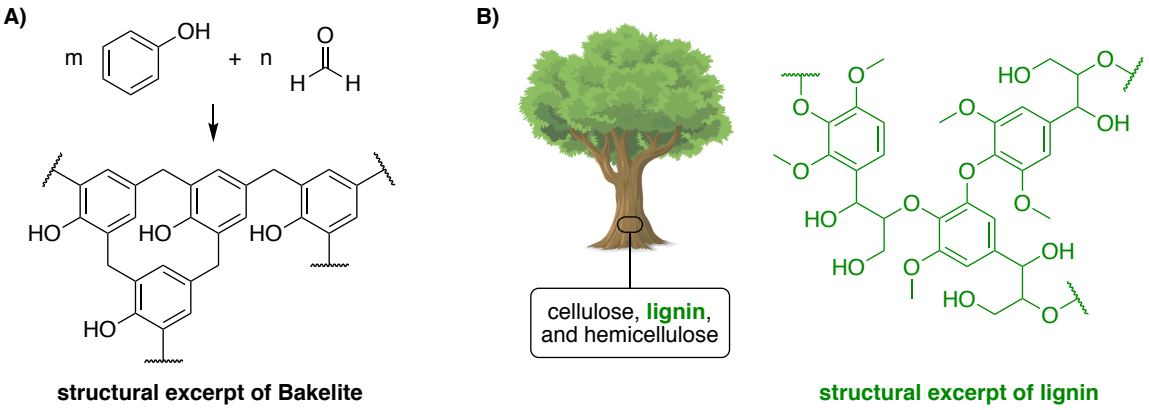

Figure 1.2. A) Production of Bakelite from phenol and formaldehyde. B) Molecular structure of lignin, a structural component of plants.

Since these early developments of petrochemical-derived plastics, humankind has become inexorably dependent on our plastic tools. We require polymers to perform many crucial tasks like keeping our food fresh (i.e., packaging) and our hearts beating (i.e., pacemakers). Not only are we leveraging plastics for crucial functions, but we also employ plastics as solutions to trivial problems such as altering the aesthetics of clothes (e.g., bejeweling jeans) or celebrations (e.g., confetti). It is virtually impossible to imagine a developed or developing society without polymers; their low cost, durability, and versatility have created a culture permeated with plastic. Nothing emphasizes the reality of our global obsession more than the data describing polymer production. The trend is exponential and spans across practically every market. The total amount of primary plastics produced (i.e., virgin material, including polymer fibers) between 1950 and 2015 has been estimated at 7800 million metric tons (**Figure 1.3**); half of this amount was generated in

the last 13 years alone.[10] Extrapolating this trend beyond this time period suggests that by 2050, humankind will have produced over 26,000 Mt of primary plastics.[10]

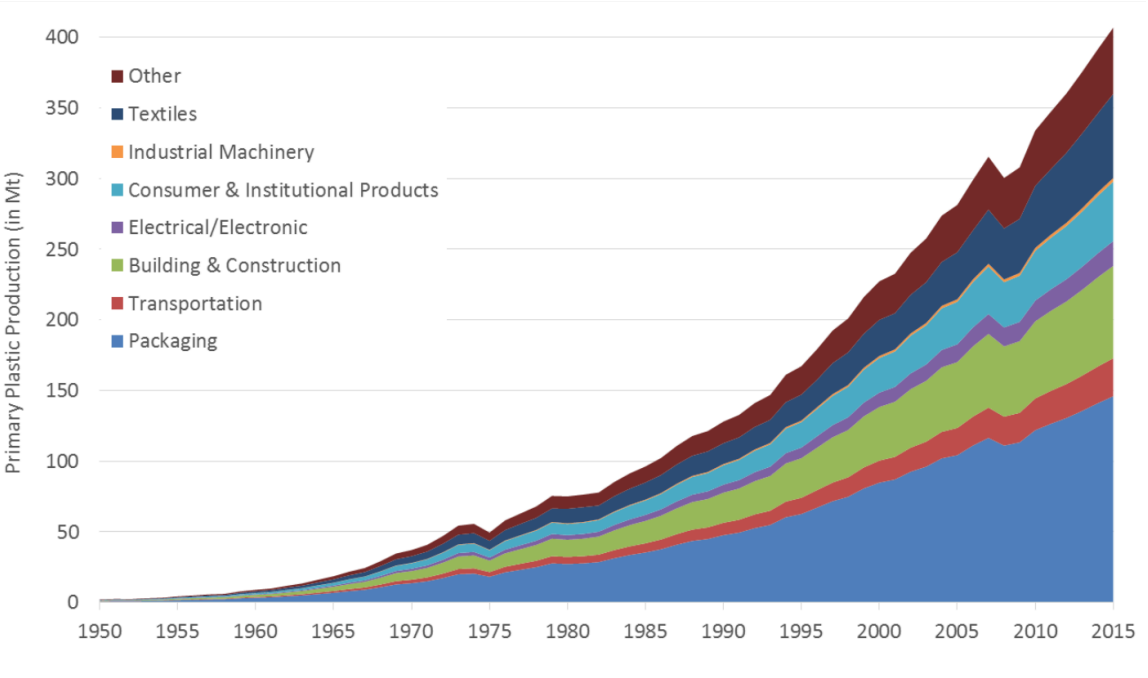

Figure 1.3. The time trends in primary plastic production (i.e., not including recycled plastic) for various industries; reprinted with permission from AAAS.[10]

1.2. The Case for Sustainable Plastic Development

The extensive and successful use of plastics for both simple and sophisticated tasks begs the question: if plastics are so useful, what is there to worry about? There are certainly many positive outcomes—people live longer and arguably more comfortably—but these come at a severe cost to the environment and the economy. Given the widespread utility of plastics, it is certain that human societies will never stray completely from their use. However, the current paradigm is short-sighted: the benefits exist while the plastic lasts, but when it is no longer performing its function, the plastic is discarded and a new one is purchased—repeat *ad infinitum*. If humans had access to an endless amount of fossil fuels, a never-ending supply of energy, and a black hole within which we could dispose of our

waste, the current paradigm would be inconsequential. Unfortunately, humankind has not been blessed with such fortunate circumstances, and we are instead expending finite resources (i.e., fossil fuels), using an increasing amount of energy, and polluting the environment. Furthermore, we are losing the inherent value in the majority of scrap plastic by not successfully collecting it for energy retrieval or recycling.

Almost all plastic materials in use today are entirely or in large part derived from fossil fuels. Although the majority of fossil fuels are used for transport, electricity, and heating, between 4 and 8% of global oil production goes into the sourcing and manufacturing of plastics.[11,12] This figure will reach 20% by 2050 if the current trends in plastics production continue (annual growth of 3.5–3.8%).[12] These oil consumption statistics do not consider the use of natural gas feedstocks, which further contribute to the codependence of the plastics and fossil fuel industries. Humans are becoming ever more efficient in the extraction of fossil fuels from the Earth, but these reserves are finite. Only 0.1% of ancient living matter escaped chemical and biological degradation to become fossil fuels, and it is only thanks to the enormously long timeframe between their existence and ours that fossil fuels have accumulated in significant quantities.[3] Our current society therefore consumes this resource—as a carbon source as well as an energy source—much faster than it can be adequately replenished, and this approach is unsustainable in the long term. Understanding what is meant by *sustainable* warrants a precise working definition, in this case adapted from the United Nations World Commission on Environment and Development: *sustainability* is "meeting the needs of the present without compromising the ability to meet those of the future".[13] It appears straightforward that the depletion of a finite resource on a faster timescale than its production should be considered unsustainable,

but there are some caveats. For example, the adoption of plastics as suitable alternatives to heavier materials (e.g., metals) in vehicles has increased fuel efficiency, which offsets (but does not neutralize) concerns regarding the sustainability of fossil fuel-based plastics production.[14,15]

The most important consequence of this growth in production is the immense and ever-increasing amount of plastic waste being generated. The average functional lifetime of plastics ranges from less than one year in packaging applications to decades in more demanding applications like building and construction. In either case, the existence of the plastic itself far exceeds the functional lifetime and discarded plastic waste accumulates in landfills or in the environment unless it is recycled or destroyed by other means (e.g., incineration). The amount of plastic waste that is generated on a global scale is staggering: recent estimates reported that 6300 million metric tons (Mt) of plastic have been discarded to date—just over three quarters of the amount that has ever been produced (8300 Mt).[10] These enormous quantities are difficult to comprehend; for context, 6300 Mt of plastic waste (assuming a conservative average density estimate of 1 g/cm^3) would cover the entire state of Minnesota with an even layer of plastic 28 meters thick. The exponential increase in production unsurprisingly results in a similar trend for waste generation, and extrapolation coupled with the assumption that human use patterns remain consistent suggests that over 25,000 Mt of plastic waste will have been generated by 2050 (**Figure 1.4**).[10] Fortunately, the collection of plastics for value recovery, which was virtually nonexistent before 1980, has started to gain some momentum in recent years. Regardless, the sheer quantity of plastic waste and the accelerating trajectory of plastics production

represent daunting challenges that must be addressed to ensure a sustainable future for humans and other living organisms.

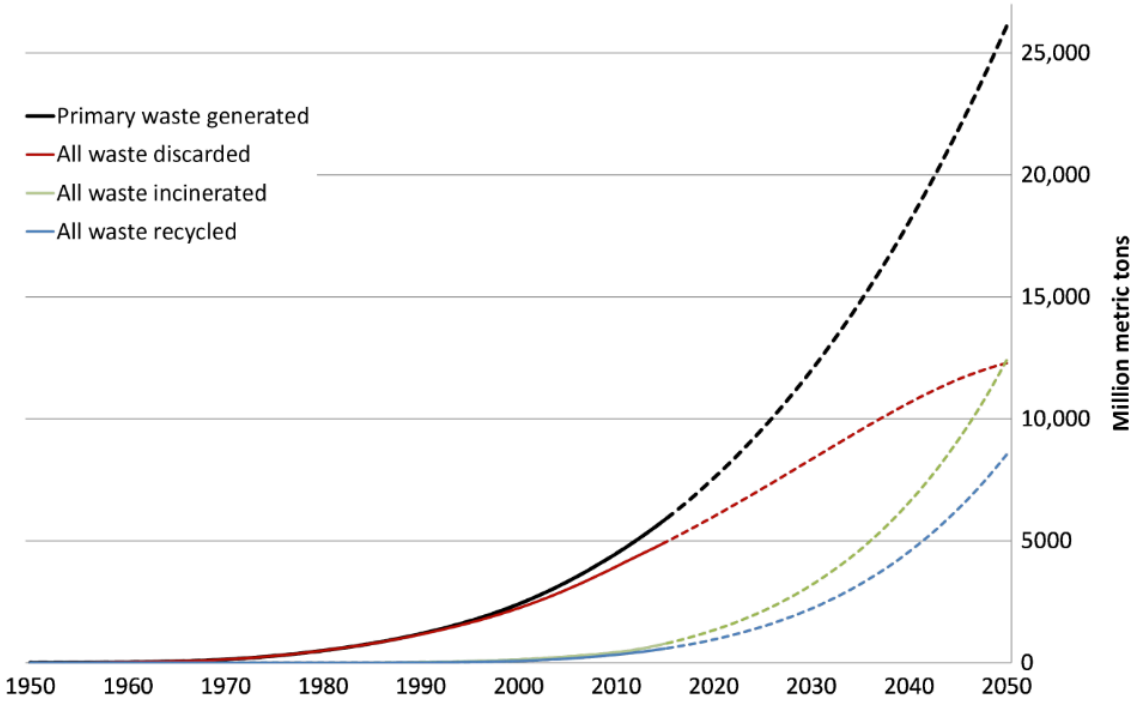

Figure 1.4. Extrapolated time trends for plastic waste generation and management; reprinted with permission from AAAS.[10]

Landfilling is the practice of compacting and burying solid waste, which is the simplest and cheapest method for waste management.[16] The buried waste is not exposed to much moisture, oxygen, or light, but there are microorganisms present that can degrade cellulose and other natural materials.[17] However, virtually all plastic entering this environment is too durable to undergo biotic or abiotic degradation processes and consequently persists for hundreds to thousands of years.[18] Although short-term environmental consequences are limited for a well-managed landfill, there can be long-term consequences including soil and groundwater contamination.[11,15] When plastic waste is mismanaged, either intentionally or unintentionally, it ends up leaking into terrestrial or

marine systems; once introduced, the plastic waste will remain there for similar timescales as it would in landfills.[19,20] The environmental consequences begin immediately—the plastic itself does not degrade quickly, but the ecosystems contaminated with plastic do.

The three major ecological threats from plastic pollution are entanglement, ingestion, and exposure to organic pollutants (i.e., small molecules). Entanglement is particularly common in marine environments and can cause animals to drown or die by injury or starvation.[21] Ingestion can be accidental or intentional, either of which may result in acute and/or chronic symptoms which could potentially pass from one animal to another (i.e., up the food chain).[18] Organic pollutants can leach from plastic waste (e.g., additives or residual monomers), but those already present in the environment may also concentrate themselves on the surface of the plastic (i.e., partitioning) and present more significant of a hazard than when dilute.[22] The extent of each of these hazards depends on the size, shape, and chemical nature of the plastic, all of which can change over time due to environmental *weathering* (i.e., exposure to solar radiation, heat/cold, moisture, oxygen, mechanical forces, and atmospheric contaminants).[23] Over time, weathering generates progressively smaller particles, increasing the likelihood of ingestion as well as the potential to leach and/or concentrate compounds (i.e., by increasing the surface area-to-volume ratio).[24,25]

When considered alongside our increasing population and plastic waste generation, these end-of-life options—environmental pollution or filling finite landfills—strongly suggest that our current paradigm of plastic use and disposal is unsustainable. The plastic subject to these fates will persist as worthless and potentially harmful garbage for many years to come. There are two main efforts to collect and recover value from plastic: energy recovery and recycling. Almost all energy recovery is done by incineration, which is

amenable to mixed waste streams and is therefore more easily implemented on a large scale.[11,26] However, incineration produces harmful gases that must be managed to avoid atmospheric pollution and the remaining charred material is classified as hazardous waste.[27] Recycling avoids both these hazards and is more energy efficient than incineration, which does not generate enough energy to outweigh the amount needed to extract raw materials and produce more virgin plastic.[28] However, recycling requires efficient sorting of commingled waste to ensure reprocessing inputs are relatively pure because contamination will diminish the material properties and value of the product. Repeated reprocessing cycles can also increase the risk of contaminant buildup and degradation of the plastic.[26,29] For these reasons, recycling is currently performed by blending scrap and virgin plastic and thus cannot fully displace virgin plastic production. Overall, the technical challenges and energy costs regarding the large-scale development, operation, and expansion of recycling and incineration facilities do not currently contend with the ease of virgin plastic production and disposal through other means (i.e., domestic landfilling or international export).

The case study that best exemplifies the current global paradigm for plastic production and end-of-life is its largest market: packaging. Almost 80 million metric tons of plastic packaging are produced each year, virtually all of which comes from petroleum-derived virgin plastic.[12] After the functional lifetime of packaging expires, only 28% enters recycling or energy recovery/incineration pipelines while the remaining 72% is destined to pollute the environment or arrive at a landfill (**Figure 1.5**).[12] A small fraction of plastic that enters the recycling stream is used for further production of similar-value products, and the rest is either made into lower-value products or lost during the recycling process.

The current landscape for production and disposal is a direct consequence of a shift toward single-use plastic packaging. Importantly, this shift has resulted in an annual net loss of 95% of the material value for packaging, which represents 80–120 billion US dollars lost to the global economy.[12] Furthermore, there are additional economic penalties to be considered regarding the management of plastic waste: litter removal from coastlines costs taxpayers hundreds of millions of dollars per year and landfill disposal can cost hundreds of dollars per metric ton.[27,30] Lastly, the generation of millions of tons of plastic waste will not only continue to disrupt animal habitats, but also infringe upon the amount of livable, clean space for the increasing human population.

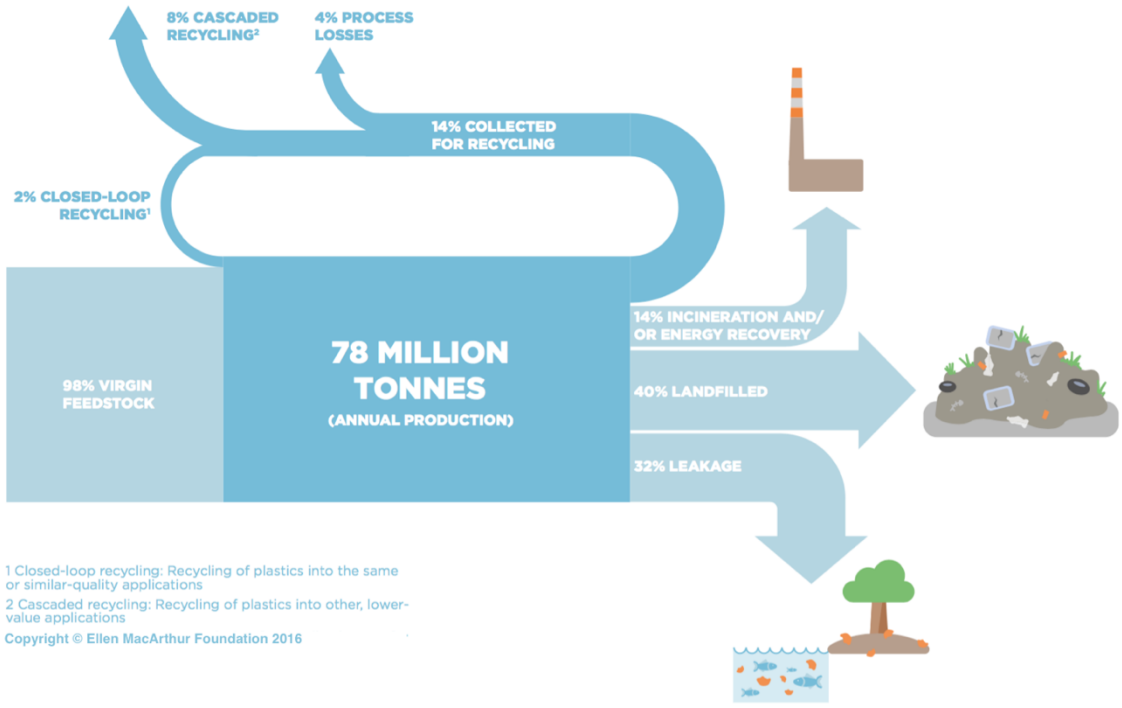

Figure 1.5. A schematic of the global material flow analysis for plastic packaging; used with permission from the Ellen MacArthur Foundation.[12]

Managing large volumes of domestic plastic waste is such a difficult task that developed countries will often export some fraction to other nations for landfilling or

recycling, but the global landscape surrounding this industry are changing now more than ever. An analysis published in 2014 revealed that on average, U.S. municipal solid waste streams contain around 11% plastics by mass.[31] However, these figures were reported several years before the Chinese government began to limit their importation of scrap plastic.[32] In 2016 alone, the U.S. exported almost 700,000 tons of plastic waste to China.[33] Just two years later, China banned almost all plastic waste imports, which created a financial opportunity—or shifted the burden, depending on your outlook—for other countries to acquire unwanted plastic waste; for example, Malaysia became a major destination for U.S. plastic waste in 2018.[34] However, China's ban has also set a precedent. Malaysia and other southeast Asian countries have quickly realized that the overwhelming influx of waste motivates illegal recycling plants to crop up, which diminish the profits of legitimate recyclers while damaging the environment by illegally burning, burying, or dumping plastic; as a result, these countries are also restricting or banning plastic waste imports.[35,36] These global shifts in waste management have undoubtedly begun to affect U.S. recycling and landfilling practices, and we will likely see an increase in plastic in the next thorough analysis of municipal solid waste.

To maximize the overall economic benefits of plastic use while minimizing the negative social and environmental impacts, it is clear we must implement significant, widespread changes to shift toward a more sustainable model. This momentum must come from both the public and private sectors working together to incentivize a more circular lifecycle for plastic, manufacture conventional polymers more sustainably, and develop new sophisticated plastics that are robust during application but offer better end-of-life options. It is the responsibility of industrial, academic, and governmental researchers to

provide the fundamental technological advances required to catalyze this transition toward a more sustainable future. In particular, this dissertation will focus on contributions toward the design of new cross-linked plastics that can compete with their conventional analogs while offering various benefits in the arena of sustainability.

1.3. Sustainable Material Design

Designing more sustainable alternatives to conventional plastics is a key step toward addressing the concerns of economic and environmental stewardship. Unsurprisingly, this thesis is not the first scientific publication that has reported the need for a change in the plastics paradigm, and there has (fortunately) been much interest in recent decades in developing new plastics and in sustainably producing traditional plastics. It is important to provide definitions for three key parameters that can be used to evaluate a material through the lens of sustainable design: 1) renewability, 2) recyclability, and 3) degradability.

Renewability refers to the sourcing of our plastics. As in, how does the material's functional lifetime compare to the timescale required to generate the feedstock from which the material is sourced? For example, a plastic grocery bag made from poly(ethylene) is typically used for days, months, or years, which is much shorter than the millions of years required for organic matter to transform into the feedstock for polyethylene (natural gas, either pure or as a byproduct of petroleum refining). On this basis, the grocery bag is deemed non-renewable. This argument is commonly extended to many other traditional plastic products because a majority of them are also derived from fossil fuels and their functional lifetime is likely less than a million years.

Assessing *recyclability* requires an evaluation of how value can be recovered from the plastic product after its functional lifetime. Recycling has traditionally been subdivided

by the scientific community into four categories: primary (mechanical), secondary (mechanical), tertiary (chemical), and quaternary (energy recovery).[11] Both primary and secondary recycling involve the processing of scrap plastic, but the products of the former are similar in characteristics and value to the original plastic, whereas the products of the latter have different characteristics and are lesser in value than the original plastic. For these reasons, they are commonly referred to as closed-loop recycling and downgrading/downcycling, respectively. Tertiary recycling is commonly referred to as chemical or feedstock recycling because its products are basic chemicals or fuels. Lastly, quaternary recycling is defined as the retrieval of energy (heat, steam, electricity) from scrap plastic by directly using it as a fuel; this is commonly referred to as energy recovery and sometimes valorization.

Degradability also focuses on the ultimate fate of plastic materials but is less straightforward to define given the frequency, variability, and context-dependence regarding its use (and mis-use) in the scientific literature. To provide an accurate definition, we must delineate between *chemical* and *physical* changes in the material; only the former is typically considered when it comes to the term *degradation*, whereas *deterioration* can be used for the latter.[17] Exposure of plastics to heat, light, microorganisms, oxygen, chemicals, and/or mechanical forces can trigger these chemical changes, which in turn either diminish the size of polymer chains (i.e., chain scission) or affect their chemical composition.[17] Although either result has historically been enough to justify the use of the word *degradation*,[37,17] recent literature has emphasized that the suggested use of these words (*degradable*, *degradation*, *degradability*) is specific to chemical changes that progressively decrease the molar mass of polymer chains.[38] It is worth noting, however,

that a change in the chemical composition of the polymer—for example, from sunlight exposure—can render it more susceptible to chain scission processes.[23] Finally, whether or not a material is degradable depends heavily on its environment, which makes comparison across different conditions difficult. As such, degradability must be evaluated with the following question: under which conditions can this plastic be degraded, and how quickly?

Given the wide variety of degradation pathways available to polymers, it is prudent to elaborate on and define those most salient to the work presented in this dissertation: abiotic and enzymatic hydrolysis. In general, *hydrolysis* is defined as the rupture of covalent bonds in a chemical by reaction with water.[39] Typically, this requires the presence of electrophilic chemical functionalities that are susceptible to nucleophilic attack by a water molecule; a relevant example is the hydrolysis of an ester bond, which produces an alcohol and carboxylic acid (**Figure 1.6A**). The term *abiotic hydrolysis* can be used if biological facilitation is absent;[38] however, this process is relatively slow at ambient conditions (i.e., neutral pH and low temperatures). Hydrolysis can be accelerated by changes in pH, temperature, and/or the presence of certain microorganisms.[23,40] In natural and engineered environments (i.e., composts), the microorganisms—typically bacteria, algae, and/or fungi—will adhere to and colonize the surface of the plastic, then secrete extracellular hydrolytic enzymes which degrade the polymer through a process termed *enzymatic hydrolysis*.[40,17] Unfortunately, a majority of the most common petroleum-derived polymers have hydrocarbon backbones (**Figure 1.6B**) which are not typically amenable to hydrolysis without prior modification (e.g., photooxidation).[40]

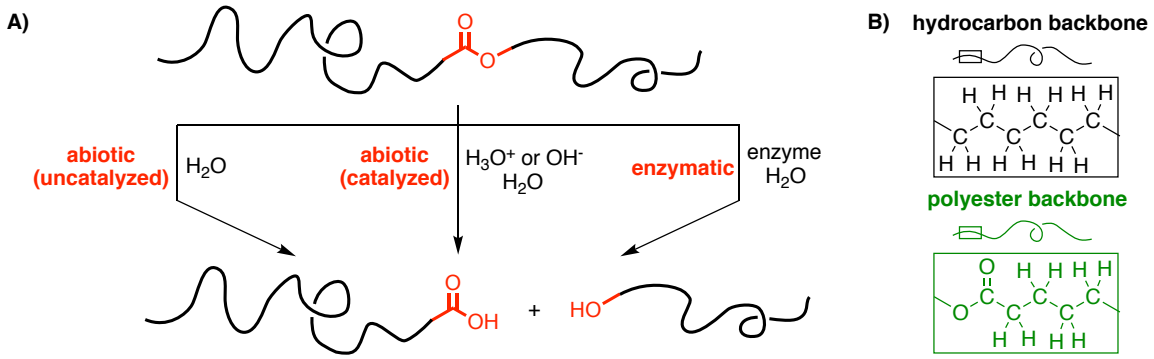

Figure 1.6. A) The hydrolysis of an ester bond in a polymer backbone under various conditions. B) Comparison of a hydrocarbon polymer backbone and a polyester backbone.

If microorganisms are facilitating the degradation of polymers, the term *biodegradation* can be applied.[38] Just as with its more general analogue, claims of biodegradability are sometimes misleading, presumptive, or exaggerative. One key example is the promotion of *oxo-degradable* plastics as biodegradable; these are simply conventional plastics with additives that accelerate abiotic oxidation of the polymer, yielding small fragments that do not readily biodegrade and continue to pose a threat to the environment. This and other examples demonstrate why the judicious use of *biodegradability* and related terms (*biodegradable*, *biodegradation*) is necessary. As in the case of its general analogue, this demands specification of the environmental conditions under which biodegradability is being evaluated. Furthermore, microorganisms must be present during testing—for example, enzymatic hydrolysis *in vitro* is not considered a direct demonstration of biodegradation.

Lastly, it is important to elaborate on the possibilities regarding the ultimate fate of biodegraded plastic. In the worst-case scenario, the degradation products are themselves toxic or persistent and thereby harmful to the environment. A better scenario would be that the fragments are water-soluble and can be taken up by the surrounding microorganisms,

which then convert the carbon in the degradation products to biomass and small molecules such as CO_2 under aerobic conditions and/or CH_4 under anaerobic conditions (**Figure 1.7**).[17,38] This process, which is typically concomitant with biodegradation, is known as *(bio)mineralization*. The ideal fate for a biodegradable plastic is that all carbon from the original material is mineralized by microorganisms, which is sometimes referred to as *ultimate biodegradation*.[38] The rate-limiting step in ultimate biodegradation is typically enzymatic degradation; subsequent mineralization (if possible) is often relatively rapid.[41]

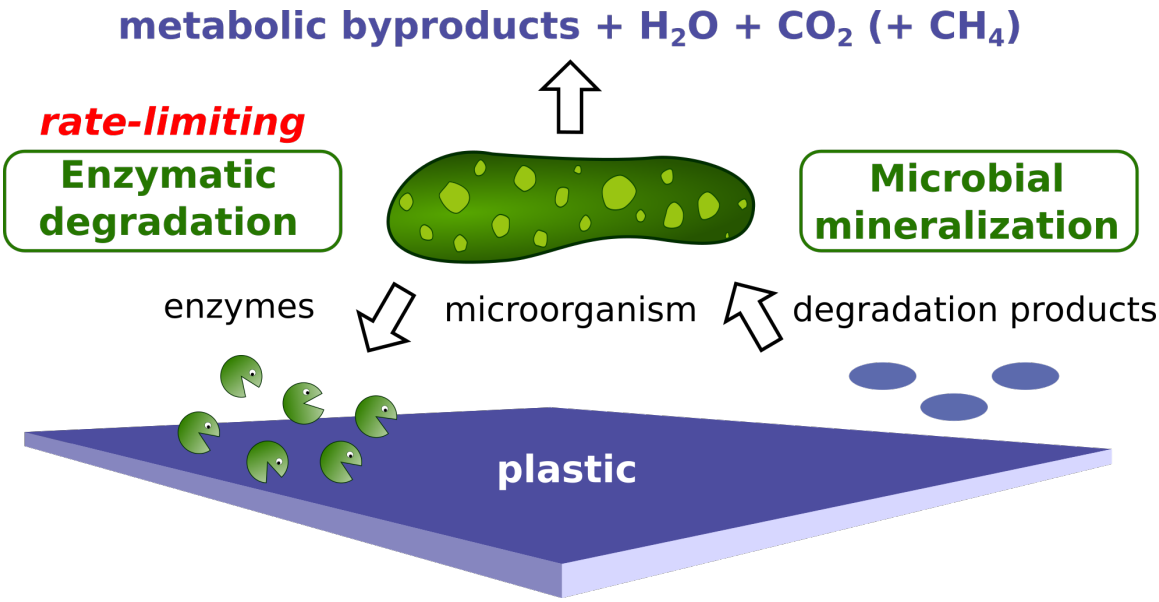

Figure 1.7. A schematic of the ultimate biodegradation process for a plastic: extracellular enzymes convert the plastic into smaller, soluble products that can be taken up by the microorganism and converted into small molecules and biomass; methane is typically produced only when the environment is anaerobic.

All three aspects of sustainable material design are featured in this dissertation, but emphasis is placed on end-of-life options for cross-linked plastics. **Chapter 2** focuses entirely on enzymatic hydrolysis. **Chapter 3** includes emphasis on renewability, tertiary recycling, and abiotic hydrolysis. **Chapter 4** features enzymatic hydrolysis and has slight emphasis on renewability. **Chapter 5** is focused entirely on primary recycling. The projects

presented in **Appendices A, B,** and **C** are motivated to varying degrees by the themes of renewability, recyclability, and (ultimate) biodegradability.

1.4. Improving the sustainability of cross-linked polymers

Cross-linked polymers comprise ca. 15-20% of plastics produced and are crucial in applications such as elastomers, insulation, adhesives, automotive parts, coatings, and foams.[42] As with almost all types of plastics used today, synthetic cross-linked polymers are sourced from petroleum and do not readily degrade in landfills or the environment. In addition, the mechanical reprocessing most commonly employed in primary plastics recycling is only compatible with thermoplastic materials; primary recycling of cross-linked polymers is impractical because their structures preclude flow, even at elevated temperatures. Their insolubility also prevents solution reprocessing. Although some of these materials are down-cycled into lower value products, most thermosets are incinerated, sent to landfills, or escape collection and pollute the environment. Still, the high strength, thermal stability, and solvent resistance of thermosets renders them essential for certain applications, and there is therefore a responsibility to develop technological advances that address the challenges in sustainable use of cross-linked polymers.

Improving the renewability of cross-linked polymers (and even thermoplastics) can be done using two approaches: drop-in replacements and new material design. The first approach relies on the production of the same (or functionally equivalent) precursors for commodity plastics from biomass rather than petroleum or natural gas; these bio-based chemicals can be used directly because no modifications to existing manufacturing facilities or processes are required.[18] The major targets for drop-in replacements are the monomers used on the largest scale in the plastics industry: ethylene, propylene, styrene,

isoprene, ethylene glycol, and terephthalic acid.[43] Fortunately, there have been significant advances for several of these chemicals and researchers are continuing to tackle the fundamental challenges regarding the scalability and efficiency of the biomass-to-product processes.[18,43] However, this small list of monomers better represents the thermoplastics market than that of common thermosets. Some thermoplastics are converted into thermosets (e.g., vulcanization of isoprene), but many mass-produced cross-linked polymers—phenolics, aminos, polyesters, silicones, polyurethanes, polyimides, epoxy, and more—are not produced from common thermoplastics or their monomers. As such, the drop-in replacement strategy should be used for conventional cross-linked polymers if possible, otherwise the development of new bio-based materials is necessary.

Renewable material design requires the sourcing of biomass-derived feedstocks such as natural oils, proteins, saccharides, and polyphenols.[44] The most appealing of these feedstocks are either byproducts from established industries—for example, phenol-containing cashew nut shell liquid (agricultural industry) or glycerol (biodiesel and soap-making industries)—or those already present in high abundance such as plant oils, cellulose, starch, lignin, and plant proteins.[45,46,47] Extensive reviews of thermosets derived from renewable resources are already available and generally focus on four main thermoset types: phenolics, epoxies, polyurethanes, and polyesters.[46,47] The first two of these categories typically involve more rigid materials, whereas the latter two describe a range of properties from soft foams to flexible elastomers to rigid resins. The work presented in **Chapter 4** describes the production of cross-linked elastomers derived from 4-methylcaprolactone, a monomer that could potentially be sourced from either lignin or plant oils (**Figure 1.8**).

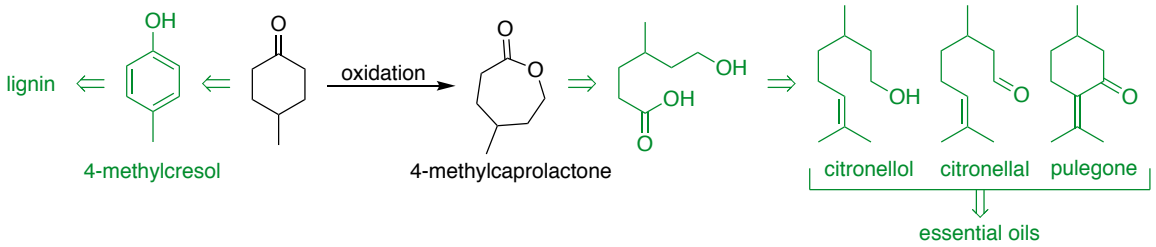

Figure 1.8. Two feasible synthetic routes for the production of 4-methylcaprolactone monomer from renewable resources.

In addition to renewable feedstocks obtained from physical and chemical transformations of biomass, one can genetically engineer microorganisms to produce chemicals from their food (e.g., glucose). With sufficient knowledge of the vast array of metabolic pathways available to bacteria, algae, and fungi, synthetic routes can be designed to target precursors to either established or novel monomers and polymers.[48] An important consideration when using engineered microorganisms is that the synthetic route can leverage both biological and chemical transformations; the biosynthetic production of a precursor that can be effectively converted into the desired chemical using simple organic reactions is often more desirable than a less efficient, fully-biosynthetic route.[48] These concepts are related to the work presented in **Chapter 3**, which involves the preparation of cross-linked elastomers from β-methyl-δ-valerolactone; this monomer can be produced from glucose using a total biosynthetic pathway or a more efficient integrated approach involving chemical modification of a biosynthesized precursor, mevalonate (**Figure 1.9**).[49]

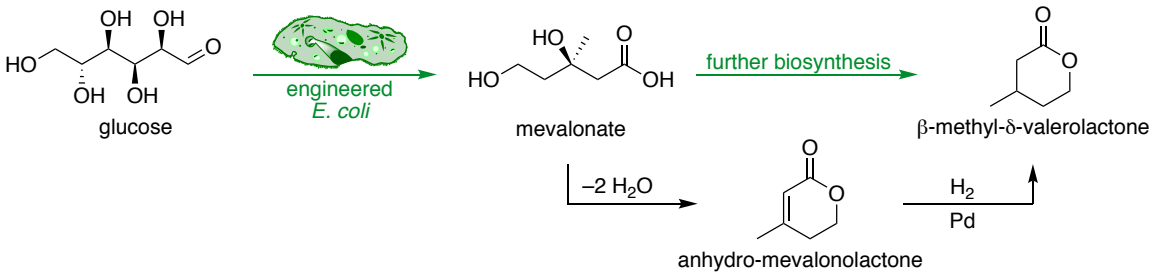

Figure 1.9. The total biosynthetic and integrated approaches reported for the production of β-methyl-δ-valerolactone from glucose using a strain of engineered bacteria.

Due to the environmental persistence of virtually all major plastics, another key milestone in sustainable plastic development is to design new alternatives that remain robust during application yet undergo triggered degradation after disposal. Abiotic hydrolysis, biodegradation, and oxo-biodegradation (i.e., oxidation followed by biodegradation) are focused on as the main chemical pathways to promote more sustainable end-of-life options for plastics (cross-linked or otherwise).[50,51] Of these three, biodegradation has spurred the most research effort because it is relatively straightforward to implement without compromising durability and is amenable to both natural and managed systems (i.e., composts and landfills).

Polymer biodegradability is dictated by a host of interrelated factors other than degradation conditions: chemical structure, molar mass, dispersity, degree of branching, presence of hydrogen bonding, crystallinity, melting point, storage modulus, hydrophobicity, molar mass, and even the surface area of the product it composes.[40] The degradability of thermosets is therefore expected to be different from thermoplastics because the cross-linked architecture affects many of these parameters. Biodegradability requires the presence of enzymatically-cleavable chemical bonds along the polymer backbone, which typically excludes carbon-carbon bonds except in a few rare cases [e.g.,

water-soluble poly(vinyl alcohol)].[52] Polyamides, polyurethanes, and polycarbonates have been shown to be biodegradable to small extents, but the functionalities that are most susceptible to enzymatic degradation—the rate-limiting step of biodegradation—are glycosidic linkages and ester linkages (**Figure 1.10**).[40] The incorporation of these moieties into cross-linked plastics is the best approach to enable the possibility for triggered degradation after their use; this concept is demonstrated using polyester materials in **Chapters 2, 3,** and **4**. Furthermore, **Chapter 2** entails a systematic investigation of the correlation between the degree of cross-linking and the enzymatic hydrolyzability.

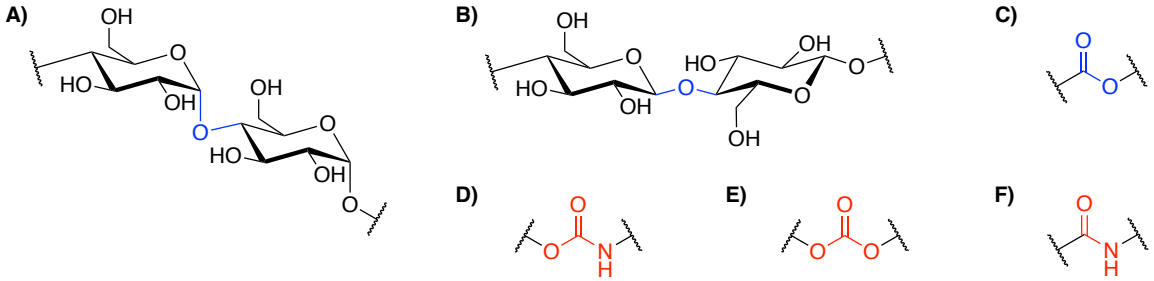

Figure 1.10. Hydrolyzable chemical bonds that can impart biodegradability to polymers. A) α-glycosidic bond, B) β-glycosidic bond, C) ester bond, D) urethane bond, E) carbonate bond, and F) amide bond. The bonds shown in blue (A-C) are generally more readily hydrolyzable than those shown in red (D-F).

A separate way to address the end-of-life issues of cross-linked polymers is to circumvent their inherently limited options for recycling. One strategy is to optimize the recovery of fuels or other chemicals from scrap material (i.e., tertiary recycling). The most straightforward technique for tertiary recycling is pyrolysis, wherein large molecules are converted into smaller ones at high temperatures (typically >600 °C), such as in petroleum cracking. Both thermoplastic and cross-linked polymers are capable of complete breakdown via pyrolysis,[53,54,55] which yields complex mixtures of potentially valuable chemicals. In industry, the mixtures obtained from petroleum cracking are separated; a

similar process could be envisioned for recovering high-value chemical feedstocks from complex mixtures of waste plastics. While industrial-scale pyrolysis has been demonstrated as a reliable method to produce fuel mixtures,[56,57] the production of useful polymer feedstocks via pyrolysis is not commonly practiced due to the complex, energy-intensive separations it would require. Plastics that selectively depolymerize to recover pure, reusable monomer feedstocks would prevent the need for complex purifications and could require less energy (**Figure 1.11**).

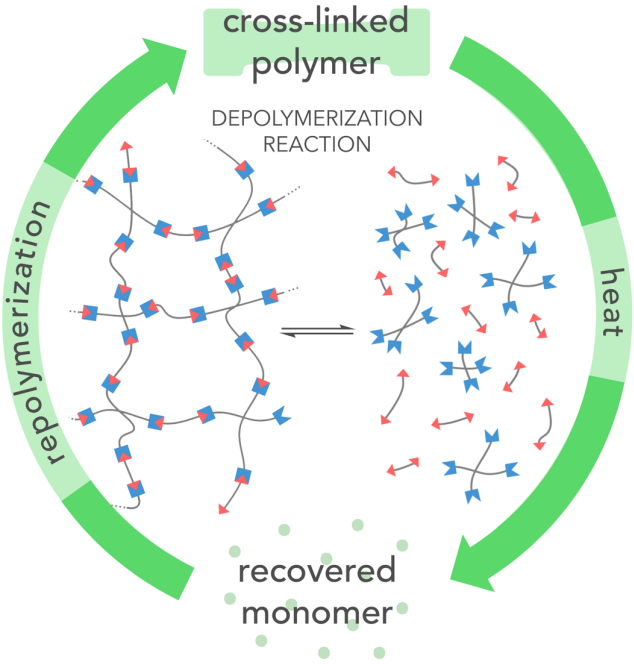

Figure 1.11. Depolymerization strategies, such as pyrolysis, solvolysis, hydrolysis, or the design of polymers that depolymerize or dissociate under mild conditions, enable reprocessing through conversion of polymers to monomers that can be repolymerized to products of similar performance. Used with permission.[58]

Selective depolymerization at lower temperatures than those required for pyrolysis (<200 °C) has been demonstrated for several polymers.[59,60,61,62] The most common examples are lactone-based polyesters, but poly(phthalaldehyde),[63] poly(tetramethylene oxide),[64] poly(methyl methacrylate),[65] certain polycarbonates,[66] and poly(trimethylene

urethane)[67] also depolymerize to regenerate their monomers. Depolymerization is induced by heating above the ceiling temperature (T_c), at which the rate of polymerization and depolymerization are equal under the prevailing conditions. Typical recovery processes yield high-purity monomers, reducing the need for further purification. This strategy is applicable to any polymer with an appropriate T_c, and a prime example is presented in **Chapter 3**: high-performance cross-linked elastomers based on poly(β-methyl-δ-valerolactone) were depolymerized to recover over 90% of the original monomer (**Figure 1.12**).

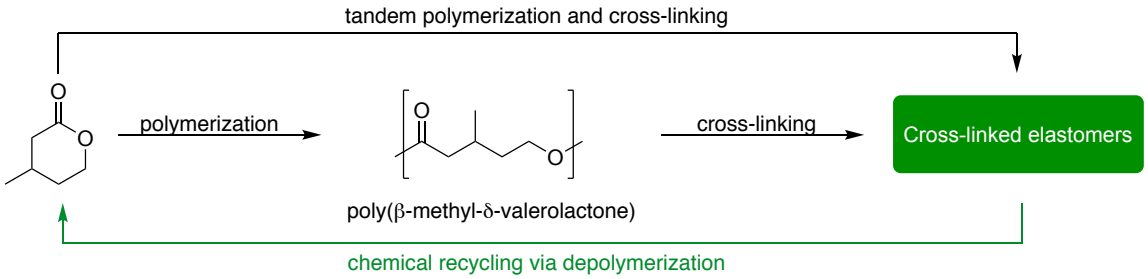

Figure 1.12. Two approaches for the production of chemically recyclable cross-linked elastomers based on poly(β-methyl-δ-valerolactone).

Almost all polymers can be pyrolyzed, but the recovered compounds cannot necessarily be used to manufacture similar-value products (i.e., reprocessed). For instance, polyesters[68,69,70,71] and polyurethanes[72,73] are difficult to pyrolyze into useful small-molecules, but the ester and urethane functional groups of these polymers are still susceptible to reactions with nucleophiles such as water or methanol, allowing them to be depolymerized to compounds suitable for repolymerization. This strategy is amenable to any material in which a hydrolyzable functional group is part of the polymer backbone. The most successful application of solvent-assisted depolymerization is the hydrolysis or alcoholysis of poly(ethylene terephthalate), a common commodity thermoplastic.[68,70,74]

Although polyurethane foams are traditionally considered non-recyclable, they also can be subjected to alcoholysis to obtain various urethane-alcohols that can be used to produce materials of similar value.[72] The development of efficient catalysts[75] and optimization of engineering processes could make this strategy practical for the recycling of cross-linked polyesters, polyurethanes, polyamides, and polyacetals.

Another effective approach towards continually reprocessable cross-linked polymers is to control the reversible transformation between a cross-linked and uncross-linked state, allowing the polymers to flow without complete depolymerization. Thermoreversible Diels-Alder (DA) reactions between furans and maleimides (FurMal) are the most prominently explored for these applications (**Figure 1.13**). Several reprocessable FurMal polymer networks have been reported since the original patent in 1969,[76] and a recent comprehensive review indicates that interest in FurMal linkages has by not waned over time.[77,78,79,80] This interest is due to their ease of access; attractive equilibrium thermodynamics; and remarkable tunability via sterics, regiochemistry, and diene/dienophile selection.[81] Because their formation and dissociation is rapid in temperature ranges compatible with many polymer backbones, FurMal linkages have been successfully incorporated into networks based on polyolefins, polyesters, polyethers, polyurethanes, polyamides, polyoxazolines, polyketones, and polysiloxanes.[80] There are also several notable examples of FurMal moieties in degradable and/or renewable cross-linked materials[82,83,84,85,86,87] as well as industrially relevant thermosets.[78,88,89]

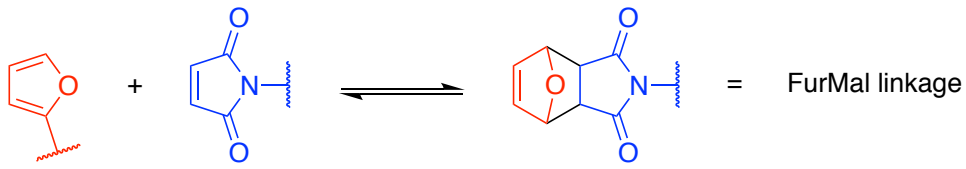

Figure 1.13. The Diels-Alder and retro-Diels-Alder equilibrium for a furan-maleimide (FurMal) linkage.

The transition from cross-linked and uncross-linked state is accompanied by a significant, rapid drop in the viscosity of the material due to the dissociative nature of the reversible reaction, which decreases the number of chemical cross-links and causes a loss of network integrity at elevated temperature. In the last decade, a separate approach for direct recyclability of cross-linked plastics has been developed, whereby dynamic bonds that undergo associative exchange reactions are incorporated into polymer networks (**Figure 1.14**).[90] The materials retain their cross-link density during recycling because the breaking of one chemical junction is simultaneous with the formation of another; consequently, the decrease in viscosity at elevated temperature is more gradual than that of dynamic materials with dissociative chemistries. Since the seminal publication on transesterification-based vitrimers,[90] the field has expanded to include many more chemistries including disulfide exchange, olefin metathesis, alkoxyamines, imine exchange, vinylogous urethane exchange, urea/urethane exchange, siloxane exchange, and boronic ester exchange.[91,92,93,94,58] In certain cases, these materials demonstrate vitrimer-like behavior (e.g., they remain insoluble at high temperature and exhibit gradual viscosity changes) even though the embedded dynamic chemistry proceeds via dissociative intermediates, presumably due to high association constants in the intermediate. The work in **Chapter 5** demonstrates that the reprocessability of polyester materials with urethane cross-links is due to Sn-catalyzed dissociation of the urethane bonds rather than

transesterification, which classifies it—and the polyether-based material used for comparison—as vitrimer-like materials (**Figure 1.15**).

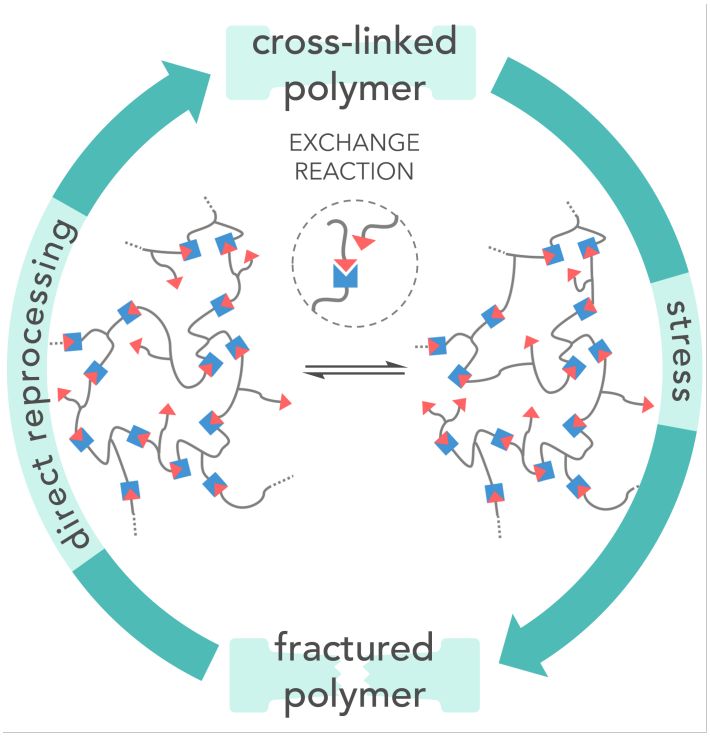

Figure 1.14. Illustration of vitrimer recycling: a fractured cross-linked polymer can be directly reprocessed into a similar value material due to dynamic covalent exchange reactions within the network. Used with permission.[58]

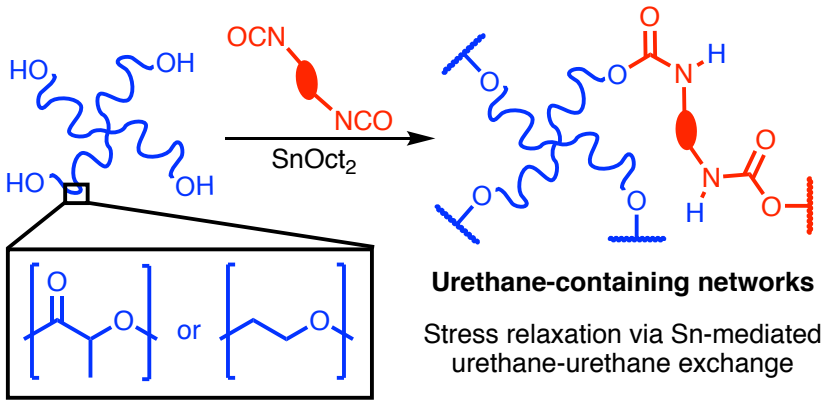

Figure 1.15. Cross-linking of polyether or polyester tetraols with diisocyanates, which yields materials that with dynamic urethane linkages. Used with permission.[95]

1.5. References.

[1] Gao, J. Coal, Oil Shale, Natural Bitumen, Heavy Oil, and Peat. In *Coal, Oil Shale, Natural Bitumen, Heavy Oil, and Peat*; Gao, J., Ed.; Eolss Publishers Co. Ltd.: Oxford, UK, 2009; Vol. 1, pp 1–39.

[2] Brydson, J. A. *Plastics Materials*, 6th ed.; Butterworth Heinemann: Oxford, 1995.

[3] Sato, M. Thermochemistry of the formation of fossil fuels. In *Fluid-Mineral Interactions: A Tribute to H.P. Eugster*; Spencer, R. J., Chou, I. M., Eds.; Geological Society of America, 1990; Special Publication 2, pp 271−283.

[4] Speight, J. G. *The Chemistry and Technology of Petroleum*; Marcel Dekker: New York, 1980.

[5] Prioreschi, P. *A History of Medicine: Primitive and ancient medicine*, 2nd ed.; Horatius Press: Omaha, NE, 1996.

[6] Kauffman, G. B.; Seymour, R. B. Elastomers: I. Natural Rubber. *J. Chem. Educ.* **1990**, *67*, 422–425.

[7] Baekeland, L. H. Method of making insoluble products of phenol and formaldehyde. U.S. Patent 942699A, December 7. 1909.

[8] Kaufmann, C. B. *Grand Duke, Wizard, and Bohemian*; Meta4Press LLC: 2012.

[9] Freinkel, S. *Plastic: A Toxic Love Story*; Houghton Mifflin Harcourt Publishing Company: New York, 2011.

[10] Geyer, R.; Jambeck, J. R.; Law, K. L. Production, use, and fate of all plastics ever made. *Sci. Adv.* **2017**, *3*, e1700782.

[11] Hopewell, J.; Dvorak, R.; Kosior, E. Plastics Recycling: Challenges and Opportunities. *Philos. Trans. R. Soc., B* **2009**, *364*, 2115−2126.

[12] World Economic Forum, Ellen MacArthur Foundation and McKinsey and Company, The New Plastics Economy Rethinking the Future of Plastics; 2016; [report] http://www.ellenmacarthurfoundation.org/publications.

[13] Our Common Future, Report of the World Commission on Environment and Development, World Commission on Environment and Development, 1987. Published as Annex to General Assembly document A/42/427, Development and International Co-operation: Environment August 2, 1987.

[14] Andrady, A. L.; Neal, M. A. Applications and societal benefits of plastics. *Phil. Trans. R. Soc., B* **2009**, *364*, 1977–1984.

[15] Thompson, R. C.; Moore, C. J.; vom Saal, F. S.; Swan, S. H. Plastics, the environment and human health: current consensus and future trends. *Phil. Trans. R. Soc., B* **2009**, *364*, 2153–2166.

[16] Santa Barbara County Resource Recovery & Waste Management Division, What happens to trash? http://lessismore.org/materials/177-what-happens-to-trash/ (accessed on 3 September 2019).

[17] Andrady, A. J. Assessment of Environmental Biodegradation of Synthetic Polymers. *Macromol. Sci., Polym. Rev.* **1994**, *34*, 25−76.

[18] Schneiderman, D. K.; Hillmyer, M. A. 50th Anniversary Perspective: There Is a Great Future in Sustainable Polymers. *Macromolecules* **2017**, *50*, 3733–3749.

[19] Barnes, D. K. A.; Galgani, F.; Thompson, R. C.; Barlaz, M. Accumulation and fragmentation of plastic debris in global environments. *Philos. Trans. R. Soc., B* **2009**, *364*, 1985−1998.

[20] Jambeck, J. R.; Geyer, R.; Wilcox, C.; Siegler, T. R.; Perryman, M.; Andrady, A.; Narayan, R.; Law, K. L. Plastic waste inputs from land into the ocean. *Science*, **2015**, *347*, 768–771.

[21] Gregory, M. R. Environmental implications of plastic debris in marine settings—entanglement, ingestion, smothering, hangers-on, hitch-hiking and alien invasions. *Phil. Trans. R. Soc., B* **2009**, *364*, 2013–2025.

[22] Teuten, E. L.; Saquing, J. M.; Knappe, D. R. U.; Barlaz, M. A.; Jonsson, S.; Björn, A.; Rowland, S. J.; Thompson, R. C.; Galloway, T. S.; Yamashita, R.; Ochi, D.; Watanuki, Y.; Moore, C.; Viet, P. H.; Tana, T. S.; Prudente, M.; Boonyatumanond, R.; Zakaria, M. P.; Akkhavong, K.; Ogata, Y.; Hirai, H.; Iwasa, S.; Mizukawa, K.; Hagino, Y.; Imamura, A.; Saha, M.; Takada, H. Transport and release of chemicals from plastics to the environment and to wildlife. *Philos. Trans. R. Soc., B* **2009**, *364*, 2027−2045.

[23] Searle, N. D. Environmental Effects on Polymeric Materials. In *Plastics and the Environment*; Andrady, A., Ed.; John Wiley & Sons, Inc.: Hoboken, NJ, 2003; pp 311–358.

[24] Galloway, T. S.; Cole, M.; Lewis, C. Interactions of microplastic debris throughout the marine ecosystem. *Nat. Ecol. Evol.* **2017**, *1*, 0116.

[25] Romera-Castillo, C.; Pinto, M.; Langer, T. M.; Álvarez-Salgado, X. A.; Herndl, G. J. Dissolved organic carbon leaching from plastics stimulates microbial activity in the ocean. *Nat. Comm.* **2018**, *9*, 1430.

[26] Rahimi, A.; García, J. Chemical recycling of waste plastics for new materials production. *Nat. Rev. Chem.* **2017**, *1*, 0046.

[27] United Nations Environmental Programme (UNEP) Valuing Plastic: The business Case for Measuring Managing and Disclosing Plastic Use in the Consumer Goods Industry, 2014.

[28] Morris, J. Recycling versus incineration: an energy conservation analysis. *J. Hazard. Mater.* **1996**, *47*, 277–293.

[29] Geyer, R.; Kuczenski, B; Zink, T.; Henderson, A. Common Misconceptions about Recycling. *J. Ind. Ecol.* **2015**, *20*, 1010–1017.

[30] Rochman, C. M.; Browne, M. A.; Halpern, B. S.; Hentschel, B, T.; Hoh, E.; Karapanagioti, H. K.; Rios-Mendoza, L. M.; Takada, H.; Teh, S.; Thompson, R. C. Classify plastic waste as hazardous. *Nature* **2013**, *494*, 169−171.

[31] Themelis, N. J., Mussche, C. 2014 Energy and Economic Value of Municipal Solid Waste (MSW) and Non-Recycled Plastics (NRP) Currently Landfilled in the Fifty States. Columbia University Earth Engineering Center; http://www.seas.columbia.edu/earth/wtert/sofos/2014_Energy_value_of_MSW.pdf (accessed on 9 September 2019).

[32] McNaughton, S.; Nowakowski, K. How China's plastic waste ban forced a global recycling reckoning. *National Geographic*, June 2019.

[33] Brooks, A. L.; Wang, S.; Jambeck, J. R. The Chinese import ban and its impact on global plastic waste trade. *Sci. Adv.* **2018**, *4*, eaat0131.

[34] Parker, L. China's ban on trash imports shifts waste crisis to Southeast Asia. Laura Parker. *National Geographic*, November 16, 2018.

[35] Lee, Y. N. Malaysia, following in China's footsteps, bans imports of plastic waste. *CNBC News*, January 25, 2019.

[36] Taylor, M. Dumping plastic waste in Asia found destroying crops and health. *Reuters*, April 22, 2019.

[37] Horie, K.; Barón, M.; Fox, R. B.; He, J.; Kahovec, J.; Kitayama, T.; Kubisa, P.; Maréchal, E.; Mormann, W.; Stepto, R. F. T.; Tabak, D.; Vohlídal, T.; Wilks, E. S.;

Work, W. J. Definitions of terms relating to reactions of polymers and to functional polymeric materials (IUPAC Recommendations 2003). *Pure Appl. Chem.* **2004**, *76*, 889–906.

[38] Vert, M.; Doi, Y.; Hellwich, K.-H.; Hess, M.; Hodge, P.; Kubisa, P.; Rinaudo, M.; Schué, F. Terminology for biorelated polymers and applications (IUPAC Recommendations 2012). *Pure Appl. Chem.* **2012**, *84*, 377–410.

[39] Muller, P. Glossary of terms used in physical organic chemistry (IUPAC Recommendations 1994). *Pure Appl. Chem.* **1994**, *66*, 1077–1184.

[40] Tokiwa, Y.; Calabia, B. P.; Ugwu, C. U.; Aiba, S. Biodegradability of Plastics. *Int. J. Mol. Sci.* **2009**, *10*, 3722–3742.

[41] Shah, A. A.; Hasan, F.; Hameed, A.; Ahmed, S. Biological degradation of plastics: A comprehensive review. *Biotechnol. Adv.* **2008**, *26*, 246–265.

[42] American Chemistry Council, U.S. Resin Production and Sales, March 2017. https://plastics.americanchemistry.com/Sales-Data-by-Resin.pdf

[43] Hillmyer, M. A. The promise of plastics from plants. *Science* **2017**, *358*, 868–870.

[44] Gandini, A.; Lacerda, T. M.; Carvalho, A. J. F.; Trovatti, E. Progress of Polymers from Renewable Resources: Furans, Vegetable Oils, and Polysaccharides. *Chem. Rev.* **2016**, *116*, 1637−1669.

[45] Sun, Z.; Fridrich, B.; de Santi, A.; Elangovan, S.; Barta, K. Bright Side of Lignin Depolymerization: Toward New Platform Chemicals. *Chem. Rev.* **2018**, *118*, 614−678.

[46] Raqueza, J.-M.; Deléglise, M; Lacrampe, M.-F.; Krawczak, P. Thermosetting (bio)materials derived from renewable resources: A critical review. *Prog. Polym. Sci.* **2010**, *35*, 487–509.

[47] Dotan, A. Biobased Thermosets. In *Handbook of Thermoset Plastics*, 3rd Ed.; Dodiuk, H. and Goodman, S. H., Eds.; Elsevier Inc.: Oxford, UK, 2013; pp 572–622.

[48] Lee, S.Y., Kim, H.U., Chae, T.U., Cho, J.S., Kim, J.W., Shin, J.H., Kim, D.I., Ko, Y.-S., Jang, W.D., Jang, Y.-S. A comprehensive metabolic map for production of bio-based chemicals. *Nat. Catal.* **2019**, *2*, 18–33.

[49] Xiong, M.; Schneiderman, D. K.; Bates, F. S.; Hillmyer, M. A.; Zhang, K. Scalable production of mechanically tunable block polymers from sugar. *Proc. Natl. Acad. Sci. U. S. A.* **2014**, *111*, 8357−8362.

[50] Ammala, A.; Bateman, S.; Dean, K.; Petinakis, E.; Sangwan, P.; Wong, S.; Yuan, Q.; Yu, L.; Patrick, C.; Leong, K. H. An overview of degradable and biodegradable polyolefins. *Prog. Polym. Sci.* **2011**, *36*, 1015–1049.

[51] McCarthy, S. Biodegradable Polymers. In *Plastics and the Environment*; Andrady, A., Ed.; John Wiley & Sons, Inc.: Hoboken, NJ, 2003; pp 359–377.

[52] Eubeler, J. P.; Bernhard, M.; Knepper, T. P. Environmental biodegradation of synthetic polymers II. Biodegradation of different polymer groups. *Trends Anal. Chem.* **2010**, *29*, 84–100.

[53] Buekens, A. Introduction to Feedstock Recycling of Plastics. In *Feedstock Recycling and Pyrolysis of Waste Plastics*, John Wiley & Sons, Ltd: 2006; pp 1–41.

[54] Butler, E.; Devlin, G.; McDonnell, K. Waste Polyolefins to Liquid Fuels via Pyrolysis: Review of Commercial State-of-the-Art and Recent Laboratory Research. *Waste and Biomass Valoriz.* **2011,** *2*, 227–255.

[55] Kaitz, J. A.; Lee, O. P.; Moore, J. S. Depolymerizable polymers: preparation, applications, and future outlook. *MRS Comm.* **2015,** *5*, 191–204.

[56] American Chemistry Council, Economic Impact of Plastics-to-Oil Facilities in the U.S. October, 2014.

[57] Sharuddin, S. D. A.; Abnisa, F.; Daud, W. M. A. W.; Aroua, M. K. A Review on Pyrolysis of Plastic Wastes. *Energy Convers. Manag*. **2016**, *115*, 308–326.

[58] Fortman, D. J.; Brutman, J. P.; De Hoe, G. X.; Snyder, R. L.; Dichtel, W. R.; Hillmyer, M. A. Approaches to Sustainable and Continually Recyclable Cross-Linked Polymers. *ACS Sus. Chem. Eng.* **2018**, *6*, 11145–11159.

[59] Schneiderman, D. K.; Vanderlaan, M. E.; Mannion, A. M.; Panthani, T. R.; Batiste, D. C.; Wang, J. Z.; Bates, F. S.; Macosko, C. W.; Hillmyer, M. A. Chemically Recyclable Biobased Polyurethanes. *ACS Macro Lett.* **2016**, 515–518.

[60] Hong, M.; Chen, E. Y. X. Completely recyclable biopolymers with linear and cyclic topologies via ring-opening polymerization of γ-butyrolactone. *Nat. Chem.* **2016,** *8*, 42–49.

[61] MacDonald, J. P.; Shaver, M. P. An aromatic/aliphatic polyester prepared via ring-opening polymerisation and its remarkably selective and cyclable depolymerisation to monomer. *Polym. Chem.* **2016,** *7*, 553–559.

[62] Hong, M., Chen, E. Y. X. Chemically Recyclable Polymers: A Circular Economy Approach to Sustainability. *Green Chem.* **2017**, 19, 3692–3706.

[63] Ito, H.; Willson, C. G. Chemical amplification in the design of dry developing resist materials. *Polym. Eng. Sci.* **1983,** *23*, 1012–1018.

[64] Enthaler, S.; Trautner, A. Iron-Catalyzed Ring-Closing Depolymerization of Poly(tetrahydrofuran). *ChemSusChem* **2013,** *6*, 1334–1336.

[65] Kaminsky, W.; Franck, J. Monomer recovery by pyrolysis of poly(methyl methacrylate) (PMMA). *J. Anal. Appl. Pyrolysis* **1991**, *19*, 311−318.

[66] Olsén, P.; Undin, J.; Odelius, K.; Keul, H.; Albertsson, A-C. Switching from Controlled Ring-Opening Polymerization (cROP) to Controlled Ring-Closing Depolymerization (cRCDP) by Adjusting the Reaction Parameters that Determine the Ceiling Temperature. *Biomacromolecules* **2016**, *17*, 3995–4002.

[67] Neffgen, S.; Keul, H.; Höcker, H. Ring-opening polymerization of cyclic urethanes and ring-closing depolymerization of the respective polyurethanes. *Macromol. Rapid Commun.* **1996**, *17*, 373–382.

[68] Paszun, D.; Spychaj, T. Chemical Recycling of Poly(ethylene terephthalate). *Ind. Eng. Chem. Res.* **1997,** *36*, 1373–1383.

[69] Bassampour, Z. S.; Budy, S. M.; Son, D. Y. Degradable epoxy resins based on bisphenol A diglycidyl ether and silyl ether amine curing agents. *J. Appl. Polym. Sci.* **2017,** *134*, 44620.

[70] Fukushima, K.; Lecuyer, J. M.; Wei, D. S.; Horn, H. W.; Jones, G. O.; Al-Megren, H. A.; Alabdulrahman, A. M.; Alsewailem, F. D.; McNeil, M. A.; Rice, J. E.; Hedrick, J. L. Advanced chemical recycling of poly(ethylene terephthalate) through organocatalytic aminolysis. *Polym. Chem.* **2013,** *4*, 1610–1616.

[71] Shi, Q.; Yu, K.; Dunn, M. L.; Wang, T.; Qi, H. J. Solvent Assisted Pressure-Free Surface Welding and Reprocessing of Malleable Epoxy Polymers. *Macromolecules* **2016**, *49*, 5527–5537.

[72] Zia, K. M.; Bhatti, H. N.; Ahmad Bhatti, I. Methods for polyurethane and polyurethane composites, recycling and recovery: A review. *React. Funct. Polym.* **2007,** *67*, 675–692.

[73] Yang, W.; Dong, Q.; Liu, S.; Xie, H.; Liu, L.; Li, J. Recycling and Disposal Methods for Polyurethane Foam Wastes. *Procedia Environ. Sci.* **2012,** *16*, 167–175.

[74] Fukushima, K.; Coulembier, O.; Lecuyer, J. M.; Almegren, H. A.; Alabdulrahman, A. M.; Alsewailem, F. D.; McNeil, M. A.; Dubois, P.; Waymouth, R. M.; Horn, H. W.; Rice, J. E.; Hedrick, J. L. Organocatalytic Depolymerization of Poly(ethylene terephthalate). *J. Polym. Sci. Part A – Polym. Chem.* **2011**, *49*, 1273–1281.

[75] Zhang, X.; Fevre, M; Jones, G. O.; Waymouth, R. M. Catalysis as an Enabling Science for Sustainable Polymers. *Chem. Rev.* **2018**, *118*, 839–885.

[76] Craven, J. M. Cross-linked thermally reversible polymers produced from condensation polymers with pendant furan groups cross-linked with maleimides. US Patent 3,435,003, March 25, 1969.

[77] Chujo, Y.; Sada, K.; Saegusa, T. Reversible gelation of polyoxazoline by means of Diels-Alder reaction. *Macromolecules* **1990**, *23*, 2636–2641.

[78] Canary, S. A.; Stevens, M. P. Thermally reversible crosslinking of polystyrene via the furan-maleimide Diels-Alder reaction. *J. Polym. Sci. A Polym. Chem.* **1992**, *30*, 1755–1760.

[79] Chen, X.; Dam, M. A.; Ono, K.; Mal, A.; Shen, H.; Nutt, S.; Sheran, K.; Wudl, F. A. Thermally Re-mendable Cross-linked Polymeric Material. *Science* **2002**, *295*, 1698–1702.

[80] Gandini, A. The furan/maleimide Diels-Alder reaction: A versatile click-unlick tool in macromolecular synthesis. *Prog. Polym. Sci.* **2013**, *38*, 1–29.

[81] Boutelle, R. C.; Northrop, B. H. Substituent Effects on the Reversibility of Furan-Maleimide Cycloadditions. *J. Org. Chem.* **2011**, *76*, 7994–8002.

[82] Ikeda, T.; Oikawa, D.; Shimasaki, T.; Teramoto, N.; Shibata, M. Organogelation behavior, thermal and mechanical properties of polymer network formed by the Diels-Alder reaction of furan- and maleimide-terminated four-arm star-shaped ε-caprolactone oligomers. *Polymer* **2013**, *54*, 3206–3216.

[83] Iji, M.; Inoue, K.; Yamashiro, M. Recyclable shape-memory and mechanical strength of poly(lactic acid) compounds cross-linked by thermo-reversible Diels-Alder reaction. *Polym. J.* **2008**, *40*, 657–662.

[84] Nimmo, C. M.; Owen, S. C.; Shoichet, M. S. Diels-Alder click cross-linked hyaluronic acid hydrogels for tissue engineering. *Biomacromolecules* **2011**, *12*, 824–830.

[85] Zhang, D.; Dumont, J-M. Reprocessable 5-hydroxymethylfurfural derivative-based thermoset elastomers synthesized through the thiol-Michael and Diels-Alder reactions. *J. Mater. Sci*. **2018**, *53*, 11116–11129.

[86] Amato, D. N.; Strange, G. A.; Swanson, J. P.; Chavez, A. D.; Roy, S. E.; Varney, K. L.; Machado, C. A.; Amato, D. V.; Costanzo, P. J. Synthesis and evaluation of thermally-responsive coatings based upon Diels-Alder chemistry and renewable materials. *Polym. Chem.* **2013**, *5*, 69–76.

[87] Teramoto, N.; Arai, Y.; Shibata, M. Thermo-reversible Diels-Alder polymerization of difurfurylidene trehalose and bismaleimides. *Carbohydr. Polym.* **2006**, *64*, 78–84.

[88] Bai, N.; Saito, K.; Simon, G. P. Synthesis of a diamine cross-linker containing Diels-Alder adducts to produce a self-healing thermosetting epoxy polymer form a widely used epoxy monomer. *Polym. Chem.* **2013**, *4*, 724–730.

[89] Bai, J.; Li, Z.; Shi, Z.; Yin, J. An eco-friendly scheme for the cross-linked polybutadiene elastomer via thiol-ene and Diels-Alder click chemistry. *Macromolecules* **2015**, *48*, 3539–3546.

[90] Montarnal, D.; Capelot, M.; Tournilhac, F.; Leibler, L. Silica-Like Malleable Materials from Permanent Organic Networks. *Science* **2011,** *334*, 965–968.

[91] Zhang, Z. P.; Rong, M. Z.; Zhang, M. Q. Polymer engineering based on reversible covalent chemistry: A promising innovative pathway towards new materials and new functionalities. *Prog. Polym. Sci.* **2018**, *80*, 39–93.

[92] Denissen, W.; Winne, J.; Du Prez, F. Vitrimers: Permanent Organic Networks with Glass-like Fluidity. *Chem. Sci*. **2016**. *7*, 30–38.

[93] Imbernon, L.; Norvez, S. From Landfilling to Vitrimer Chemistry in the Rubber Life Cycle. *Eur. Polym. J.* **2016,** *82*, 347–376.

[94] Zou, W. K.; Dong, J. T.; Luo, Y. W.; Zhao, Q.; Xie, T. Dynamic Covalent Polymer Networks: from Old Chemistry to Modern Day Innovations. *Adv. Mater*. **2017**, *29*, 1606100.

[95] Brutman, J. P.; Fortman, D. J.; De Hoe, G. X.; Dichtel, W. R.; Hillmyer, M. A. A Mechanistic Study of Stress Relaxation in Urethane-Containing Polymer Networks. *J. Phys. Chem. B* **2019**, *123*, 1432–1441.

Chapter 2. Photochemical transformation of poly(butylene adipate-co-terephthalate) and its effects on enzymatic hydrolyzability*

* Reprinted (adapted) with permission from De Hoe, G. X.; Zumstein, M. T.; Getzinger, G. J.; Rüegsegger, I.; Kohler, H.-P. E.; Maurer-Jones, M. A.; Sander, M.; Hillmyer, M. A.; McNeill, K. Photochemical transformation of poly(butylene adipate-co-terephthalate) and its effects on enzymatic hydrolyzability. *Environ. Sci. Technol.* **2019**, *123*, 1432–1441. Copyright © 2019 American Chemical Society.

2.1. Abstract

Biodegradable polyesters are increasingly used to replace conventional, non-degradable polymers in agricultural applications such as plastic film for mulching. For many of these applications, poly(butylene adipate-co-terephthalate) (PBAT) is a promising biodegradable material. However, PBAT is also susceptible to photochemical transformations. To better understand how photochemistry affects the biodegradability of PBAT, we irradiated blown, non-stabilized, transparent PBAT films and studied their enzymatic hydrolysis, which is considered the rate-limiting step in polyester biodegradation. In parallel, we characterized the irradiated PBAT films by dynamic mechanical thermal analysis. The rate of enzymatic PBAT hydrolysis decreased when the density of light-induced cross-links within PBAT exceeded a certain threshold. Mass-spectrometric analysis of the enzymatic hydrolysis products of irradiated PBAT films provided evidence for radical-based cross-linking of two terephthalate units that resulted in the formation of benzophenone-like molecules. In a proof-of-principle experiment, we demonstrated that the addition of photostabilizers to PBAT films mitigated the negative effect of UV irradiation on the enzymatic hydrolyzability of PBAT. This work advances the understanding of light-induced changes on the enzyme-mediated hydrolysis of aliphatic-aromatic polyesters and will therefore have important implications for the development of biodegradable plastics.

2.2. Introduction

Modern agriculture heavily relies on the use of synthetic polymers in various applications. For example, approximately two million metric tons of plastic mulch films are used annually around the world.[1] As most of these plastic materials are not

biodegradable, these agricultural applications of plastics—also referred to as plasticulture—facilitate entry of non-degradable polymer materials into environmental systems and thus contribute to the accumulation of plastics in the environment.[2] Substituting non-degradable plastics with biodegradable alternatives is a promising strategy to mitigate the growing problem of plastic accumulation.[3,4,5,6] Polyesters are an important class of plastics because they can exhibit high performance while offering the potential for biodegradability. Ester bond hydrolysis, which can be catalyzed by extracellular microbial esterases,[7] is considered the rate-limiting step in the overall biodegradation of polyester materials in receiving environments; subsequent microbial uptake and utilization of oligomers and monomers formed during hydrolysis are comparatively fast.[8,9]

Among biodegradable polyesters, the aliphatic-aromatic co-polyester poly(butylene adipate-co-terephthalate) (PBAT) is a commercially important material used extensively for plastic mulch film.[5] Several studies have shown that the ester bonds in PBAT can be hydrolyzed by extracellular carboxylesterases from microorganisms that are commonly found in terrestrial systems.[10,11,12] Cutinases, one particular class of extracellular carboxylesterases which hydrolyze cutin on plant surfaces, were particularly effective in hydrolyzing PBAT as well as other polyesters containing aromatic units.[13,14,15,16,17] We also demonstrated that carbon from all monomeric units in PBAT (i.e., butanediol, adipate, and terephthalate) was microbially utilized and converted to carbon dioxide and microbial biomass during incubation of PBAT films in an agricultural soil.[9]

During application, mulch films encounter various weathering processes that alter the physicochemical properties of the product. Photochemical weathering of mulch films

is particularly important due to the high rate of photo-exposure in the field; for this reason, industrial polymer films often contain additives that mitigate photochemical weathering (i.e., photostabilizers). While non-irradiated PBAT has been shown to be enzymatically hydrolyzable and to undergo biodegradation in soils, the effect of photochemical transformations resulting from sunlight exposure on the enzymatic hydrolysis of PBAT films remains unclear. Light irradiation of PBAT films, including photostabilized films, causes simultaneous cross-linking and cleavage of PBAT chains; these chemical reactions therefore result in the formation of both an insoluble polyester network and low molar mass PBAT chain fragments within the network.[18,19,20,21] Furthermore, light-induced cross-linking decreased the extent to which PBAT films were microbially utilized (i.e., biodegraded) during a 45-day incubation in manure compost.[20]

The goal of this study was to systematically assess the effect of UV-light irradiation on the enzymatic hydrolyzability of PBAT. To this end, we first irradiated PBAT films under controlled laboratory conditions for variable times. To directly assess photochemical changes in native PBAT, we chose films without commonly applied photostabilizers. After photo-exposure, we monitored the enzymatic hydrolysis of the irradiated PBAT films by a cutinase from *Fusarium solani* (FsC), using both a pH-stat titration approach and and approach based on the quantification of released hydrolysis products by total organic carbon (TOC) analysis. In parallel, we characterized the irradiated PBAT films using dynamic mechanical thermal analysis (DMTA), gel fraction measurements, differential scanning calorimetry (DSC), and wide-angle X-ray scattering (WAXS). We then related the irradiation-induced changes of PBAT films to their enzymatic hydrolyzability. In a next step, we analyzed the products from the enzymatic hydrolysis of PBAT by high-

performance liquid chromatography coupled to high-resolution mass spectrometry (HPLC-HRMS) and found mechanistic support for the light-induced cross-linking of PBAT chains. Finally, we repeated selected experiments with PBAT films containing a photostabilizer to assess the extent to which photostabilization mitigates irradiation-induced changes in PBAT hydrolyzability.

2.3. Materials and Methods

2.3.1. Polymer and Chemicals.

Potassium chloride (KCl, product number: P4504), terephthalic acid (185361), pyridine (Pyr, 270407), deuterated chloroform ($CDCl_3$, 151823**),** and hydrochloric acid (HCl, 30721) were obtained from Sigma-Aldrich. Chloroform (C/4966/17) and acetonitrile (A/0627/17) were obtained from Fisher Chemical. 4-nitroanisole (PNA, 10354-3), 2-(2-benzotriazolyl)-4-methylphenol (533203), and 4-benzoylbenzoic acid (1240-7) were obtained from Aldrich. 1,4-dimethoxybenzene (D0629) was obtained from TCI. Blown films of poly(butylene adipate-co-terephthalate) (PBAT) with a thickness of 25 μm were provided by BASF SE; these films did not contain any photostabilizers.

2.3.2. Enzyme.

Fusarium solani cutinase (FsC, molecular weight: 20.8 kDa, isoelectric point: 8.4, both calculated from the RCSB Protein Data Base (PDB) entry 1AGY[22] with the pI/MW compute tool from expasy[23]) was obtained from ChiralVision as a solution (concentration of FsC of 4.2 mM, as determined from solution absorbance at 280 nm and the molar extinction coefficient of FsC of 13610 $M^{-1}\cdot cm^{-1}$).[24] We prepared a stock solution of FsC

(4.1 $mg_{FsC}\cdot(mL)^{-1}$) in a pH 7 buffered solution (3 mM phosphate) and stored aliquots at – 20 °C until used.

2.3.3. Solutions.

All solutions were prepared in Milli-Q water (resistivity = 18.2 MΩ cm; Barnstead Nanopure Diamond).

2.3.4. Solvent Casting of PBAT Films.

We dissolved PBAT in chloroform to obtain a 0.5 % (w/w) solution. For photostabilized films, we added 2-(2-benzotriazolyl)-4-methylphenol (BMP) to the solution to a final concentration of 0.0001 % (w/w, BMP/chloroform) and horizontally orbit-shook the solution (40 min). To obtain solvent-cast PBAT films, we added 27 mL of the solution to a glass petri dish (diameter 9.1 cm) and evaporated the chloroform by horizontally orbit-shaking the petri dish at 100 rpm in the fume hood for 14 h. To release the film from the petri dish, we dipped the dish into liquid nitrogen and then carefully peeled the film from the dish and stored the film in the dark until the hydrolysis experiments.

2.3.5. Irradiation of PBAT Films by UV-light and Sunlight.

PBAT films were cut into rectangular pieces (dimensions: 7 cm × 14 cm) and fixed to cardboard. The cardboard pieces were mounted on the outside of a carousel sample holder (diameter: 13 cm) of a Rayonet merry-go-round photoreactor. The films were subsequently irradiated with UV light from eight 300 nm bulbs (Rayonet, USA, lamp spectrum is shown in Results and Discussion) while the sample holder was continuously rotating. We confirmed that the lightbulbs in the photoreactor did not heat the samples

enough to expect any thermally induced physicochemical changes in the films (the temperature was ≤ 36 °C). After the irradiation, the films were stored in 15 mL plastic tubes in the dark until subsequent analyses. In addition to the irradiation experiments performed in the Rayonet photoreactor, we performed complementary irradiation experiments with natural sunlight. For these studies, blown films of PBAT were cut into pieces of 8 x 8 cm. We then stapled these films onto a EUR-palette that was placed at a shade-free location on the roof of our institute's building (the Institute of Biogeochemistry and Pollutant Dynamics) in Zurich, Switzerland. At indicated times, we sampled films and stored them in the dark until we determined their gel fraction.

2.3.6. Actinometry.

To control the intensity of the Rayonet photoreactor, we performed PNA/Pyr-based actinometry.[25] For a typical actinometry procedure, a borosilicate glass test tube (VWR, PYREX, 99445-15) was charged with 10 µL of a PNA solution (10 mM in acetonitrile), 50 µL of a pyridine solution (100 mM in acetonitrile), and 9.94 mL of Milli-Q water. The test tube was then transferred into the carousel sample holder of the photo reactor. The remaining positions of the sample holder were filled with test tubes containing water only. The irradiation was performed with eight bulbs (maximal light intensity at 300 nm) while the carousel was rotating. At specific times during the irradiation, a 150 µL aliquot of the PNA/Pyr solution was transferred into an amber vial, which was subsequently stored in the dark at 4 °C.

To determine the concentration of PNA in the irradiated solutions, we used an Agilent 1100 Series HPLC equipped with a ZORBAX Eclipse XDB C18 column (4.6 x 150 mm, Agilent 993967-902), a C18 guard column (4.6 x 12.5 mm, Agilent 820950-926),

and a G1314A UV detector (absorbance measured at 316 nm). The aqueous fraction of the mobile phase consisted of acetate buffer (30 mM acetate/acetic acid, pH 6.0) containing 5% (v/v) acetonitrile, while the organic fraction was pure acetonitrile. Throughout the time of the experiment (4.5 min), the organic fraction of the mobile phase was constantly held at 70%, the flow rate at 1 mL/min. Absorbance peaks were integrated with the Agilent OpenLAB CDS ChemStation Edition C.01.05 software. PNA concentrations were calculated based on calibration solutions ranging between 1 and 20 µM.

2.3.7. Quantification of PBAT Hydrolysis by pH-Stat Titration.

The hydrolyzability of untreated and irradiated PBAT films by FsC was determined by pH-stat titration using an assay adapted from Marten et al.[26] In brief, circular pieces (diameter: 2.3 cm) were punched out of the PBAT films and placed into a thermo-jacketed beaker (40 °C) containing 10 mL of a 10 mM KCl solution. The pH of the solution was maintained at a constant pH of 7.0 by automated pH-stat titration with a Titrando 907 (Metrohm) that delivered a KOH solution (15 mM, diluted from a precise Titrisol solution; Merck: 1.09918.0001). Following the addition of the circular PBAT pieces into the solution, the system was allowed to equilibrate for 24 hours prior to the addition of FsC from the stock solution (200 µL; final concentration: 82 $\mu g_{FsC} \cdot mL^{-1}$). Given that hydrolysis of ester bonds at pH 7 releases an equimolar amount of H^+ into solution, the number of ester bonds in PBAT that were hydrolyzed by FsC was determined from the number of hydroxide ions added to maintain a constant pH. Dividing the number of hydrolyzed ester bonds by the total number of ester bonds present in the added amount of PBAT yields the percentage of ester bonds cleaved during enzymatic hydrolysis (i.e., OH^- added / ester

bonds in PBAT (%)). At the end of the experiment, the solution was collected and stored at –20 °C.

2.3.8. Quantification of PBAT Hydrolysis by TOC Measurements.

Complementary to the pH-stat titration experiments, we used an approach based on quantifying the total organic carbon (TOC) of a solution to study the hydrolysis of PBAT films. For these experiments, we punched circular film pieces (diameter 2.3 cm) out of the blown PBAT films and incubated these pieces at 40 °C in 20 mL glass vials containing 15 mL of buffer (90 mM potassium phosphate, 10 mM potassium chloride, pH 7.0, filtered at 0.22 μm). Incubations were performed in the dark under orbital shaking at 140 rpm. Approximately 50 h after the addition of the PBAT films, we added a stock solution of *Fusarium solani* cutinase (300 μL; final concentration: 82 μg_{FsC}/mL). At indicated times during the experiment, we took 250 μL of the incubation solution into a 1.5 mL plastic tube and stored these aliquots at 4 °C. After all samples had been collected, we centrifuged the samples (2000 x g, 3 min) to make sure that PBAT particles that potentially detached from the film were collected at the bottom of the tube. Subsequently, we transferred 80 μL from the top of the solution into a test tube for TOC measurements, added Milli-Q water to a total volume of 8 mL, and measured these solutions with a TOC analyzer (TOC-L, Shimadzu). The obtained signal was converted to a TOC concentration employing a standard calibration curve (0 to 20 mg C/L) prepared from a TOC standard (Sigma-Aldrich, 76067). For all experiments monitored by solution TOC analysis, we performed background measurements of the incubation medium and enzyme in order to effectively subtract out their contribution to the measured carbon content.

2.3.9. Liquid Extraction and ^{1}H NMR Analysis of Hydrolysis Products.

We complemented our HPLC-HRMS-based analysis of the hydrolysis products with ^{1}H nuclear magnetic resonance (NMR) spectroscopy. Therefore, we thawed the solutions that were stored after the pH-stat titration experiments and added a few drops of HCl solution (1 M) to 0.75 mL of the solution containing the hydrolysis products (resulting pH < 1.5). For the extraction of the hydrolysis products, we added 0.75 mL of deuterated chloroform ($CDCl_3$) to the acidified samples and vortexed the resulting mix for 15 s. The organic phase was then transferred into a sample tube for the NMR measurement. Chloroform addition, vortexing, and transferring of the organic phase were repeated twice. For absolute quantification of the hydrolysis products, we added a solution of 1,4-dimethoxybenzene as an internal standard to our analytes. ^{1}H NMR spectra were acquired on a Bruker, Avance III 400 MHz NMR spectrometer equipped with a 5 mm BBFO Z-Gradient high-resolution probe (relaxation time was set to 15 s). All ^{1}H NMR spectra were baseline and phase corrected. The chemical shifts were referenced to the proton of $CHCl_3$ that is present in $CDCl_3$.

2.3.10. Identification of PBAT Hydrolysis Products by HPLC-HRMS.

To identify the predominant enzymatic hydrolysis products from PBAT films, we analyzed the solutions from the pH-stat titration experiments by high-performance liquid chromatography coupled to high-resolution mass spectrometry (HPLC-HRMS). Centrifuged aliquots (20 µL) were separated by gradient elution and reversed phase chromatography (Hypersil Gold aQ, 150 x 4.6 mm, 5 µm particles, flow rate = 1 mL·min^{-1}, thermostatted to 50 °C). The mobile phase consisted of water (aqueous) and methanol (organic), both containing 0.1% (v/v) formic acid. The initial solvent mixing ratio was 85%

aqueous to 15% organic and was held constant for one minute after sample injection. The ratio was subsequently decreased linearly to 5% aqueous and 95% organic over 35 minutes, after which it was held constant for 5 minutes. Finally, to prepare for the next sample injection, the solvent ratio was re-adjusted to the initial conditions for seven minutes. The eluent from the HPLC column was split post-column prior to introduction into the heated electrospray ionization (ESI) source of an Orbitrap Exactive high resolution mass spectrometer (Thermo Scientific) and into the UV/Vis detector, respectively. Positive and negative polarity, high-resolution (R = 25k FWHM at m/z 200, automatic gain control target = 10^6, injection time = 100 ms, m/z range: 100-2000) mass spectra (HRMS) were acquired in full-scan and all-ion higher-energy collisional dissociation (HCD, collision energy = 30 eV) modes throughout the chromatographic separation. UV/Vis spectra were acquired concurrently with a diode array detector.

2.3.11. Dynamic Mechanical Thermal Analysis.

Dynamic mechanical thermal analysis (DMTA) was performed using a TA Instruments RSA-G2 analyzer (tensile mode). A sinusoidal, oscillatory strain (constant frequency) is applied to a sample and the resultant axial force is monitored as a function of temperature. This force is converted to a complex modulus (i.e., a measure of the sample's rigidity) by dividing by the cross-sectional area and the applied strain. Ultimately, the complex modulus is deconvoluted into the storage modulus E' (in-phase with the oscillatory strain, elastic solid-like behavior) and the loss modulus E'' (out-of-phase with the oscillatory strain, viscous liquid-like behavior). DMTA therefore gives insight into the viscoelastic behavior of polymeric materials as a function of temperature; furthermore, the elasticity (i.e., storage modulus) of a cross-linked polymer (above T_g and T_m) is directly

related to its cross-link density ν_e, and therefore this technique can be used to quantify the extent of cross-linking in the polymer. The cross-link density can be expressed in terms of the average molar mass between cross-links M_x as shown by equation 1, where ρ denotes the density of PBAT (1.25 g·cm^{-3}), R is the ideal gas constant, and T is the temperature in Kelvin:[27]

$$E' = 3RT\nu_e = \frac{3\rho RT}{M_x} \quad (1)$$

The calculated M_x from this equation can reflect the cross-link density corresponding to covalent cross-links, physical cross-links (e.g., chain entanglements), or both. Each DMTA measurement was performed using rectangular PBAT specimens [0.025 mm (T) x *ca.* 4 mm (W) x *ca.* 25 mm (L) with a gauge length of *ca.* 6 mm] which were cut out using a razor blade. Due to the thinness of the samples, a specialized method (described below) was developed to obtain data in the range of –80 °C to 200 °C without breaking the films.

A typical procedure for each DMTA measurement was as follows. The transducer was zeroed and tared at room temperature with the oven closed after the stream of nitrogen gas (from the liquid nitrogen chamber) equilibrated. A PBAT sample was then loaded in the tensile fixtures using a torque wrench (40 cN·m) to ensure that the sample maintained continuous contact with the fixtures during the temperature sweep. Liquid nitrogen was used to cool the sample to –80 °C, and the axial force was continuously adjusted to 20.0 g (sensitivity 1.0 g) to ensure no buckling of the film. The proportional force mode was set to force tracking to maintain an axial force that was at least 100% greater than the dynamic oscillatory force. The compensate for modulus feature was not used and the adjustment time out for the axial force was set to 4.0 s. The minimum axial force was set to 2.0 g and

the minimum and maximum oscillatory force were set to 1.0 g and 20.0 g, respectively. The strain adjust was set to 30% with minimum and maximum strain values of 0.05% and 5.0%, respectively. The sample was then heated to 200 °C at a rate of 5 °C·min^{-1} at an angular frequency of 6.28 rad·s^{-1} (1 Hz). Data acquisition was performed in correlation mode with 0.5 delay cycles and 0.5 s of delay time.

2.3.12. Gel Fraction Measurements.

Extractions of sol fractions were performed using $CHCl_3$ as the swelling solvent. These experiments reveal the mass fraction that is actually incorporated into an insoluble polymer network. Although measuring the gel fraction is convenient and common,[18,28,29] it is a relatively crude way to evaluate the extent of cross-linking present in the sample (as shown below). The gel fraction determinations for UV-irradiated samples were performed slightly differently than those for sunlight-irradiated samples. For swell tests on UV-irradiated PBAT, a small amount of sample (*ca.* 35-40 mg) was placed in a 20 mL vial, which was subsequently filled with solvent. The solvent was decanted after 48 h, and the swollen sample was then dried under reduced pressure—first at 200 mTorr for 48 h, then at 20 mTorr for 48 h—to ensure no solvent remained when the final mass was measured. The gel fraction was calculated by taking the ratio of the final mass of the polymer sample to the initial mass. The sol fraction was also dried at 20 mTorr for 48 h to confirm closed mass balances. For swell tests on sunlight-irradiated PBAT, we first stuffed disposable glass Pasteur pipets with glass wool and determined its mass (m_1). We then added the PBAT film (ca. 12 mg) onto the glass wool and determined its mass (m_2). Subsequently, we loaded the pipet with chloroform, incubated it at room temperature for 1 h, and pushed the chloroform out of the pipet. Then, the pipet was washed three times with chloroform,

dried at 70 °C (1 h), and mass its mass (m_3) was determined. We calculated the gel fraction as $(m_3-m_1)/(m_2-m_1)$.

2.3.13. Differential Scanning Calorimetry.

DSC was performed on the untreated and irradiated PBAT films using a TA Instruments Discovery Series differential scanning calorimeter. Samples subjected to calorimetry (ca. 4 mg) were placed in T-Zero hermetic pans and cooled to –80 °C before the first and second heating ramp to 250 °C; all temperature sweeps were performed at 10 °C min^{-1}. We used the *Trios* software to determine the glass transition temperatures (midpoints of each transition) and the melting temperatures (maximum of the endotherm). These temperatures were measured using the first heat so as to account for the thermal history from the PBAT film processing conditions.

2.3.14. Wide-angle X-ray Scattering.

Room-temperature wide-angle x-ray scattering (WAXS) data were collected on the Dupont-Northwestern-Dow Collaborative Access Team (DND-CAT) insertion device beamline at Sector 5 of the Advanced Photon Source at Argonne National Laboratory, using 17 keV X-rays (λ = 0.7293 Å) and a sample-to-detector distance of 201.31 mm. PBAT films (original thickness 0.025 mm), both untreated and irradiated, were folded to generate squares of PBAT with thicknesses of 0.1 mm, which were sandwiched between two layers of Kapton tape and mounted to Teflon washers. Each sample was exposed to the beam for 5 s; isotropic scattering patterns were azimuthally averaged to give one-dimensional plots of scattered intensity I as a function of the scattering wavevector q. Scattered intensity was calibrated using a glassy carbon standard and q was calibrated using

a silicon diffraction grating. The raw scattering data for 2 sheets of Kapton tape was subtracted from the raw sample data, which was then corrected for the actual sample thickness (i.e., 0.1 mm).

2.3.15. Size-exclusion Chromatography.

SEC was performed at 35 °C using an HP/Agilent 1100 series size-exclusion chromatograph equipped with a HP 1047A refractive index detector. The mobile phase was chloroform (1 mL min^{-1} flow rate); prior to reaching the detector, the sample passed through a PLgel 5 μm guard column before passing through three successive PLgel Mixed C columns. We used a 10-point calibration curve generated using EasiCal polystyrene standards purchased from Agilent to determine M_n and $Đ$ for untreated PBAT and the sol fractions of UV-irradiated PBAT.

2.4. Results and Discussion

2.4.1. Properties of Untreated PBAT Films.

To investigate the molar mass distribution and thermal properties of the untreated PBAT film, we respectively employed size-exclusion chromatography and differential scanning calorimetry (**Figure 2.1** and **Figure 2.2**). The size-exclusion chromatography was performed using a chloroform mobile phase, and the molar mass distribution was evaluated with respect to polystyrene standards; the number average molar mass was determined to be 37 kg/mol with a dispersity of 2.2. The differential scanning calorimetry profile for the first heating cycle revealed a glass transition temperature at –30 °C as well as a broad melting transition containing two maxima at 59 °C and 121 °C. These maxima respectively represent the melting of adipate-rich crystallites and terephthalate-rich crystallites.[30] We

note that the latter of these crystallite types is the one that is predominantly observed by wide-angle x-ray scattering (discussed later in the Results and Discussion). Overall, the thermal properties and scattering signals are consistent with prior literature reports.[30,31,32]

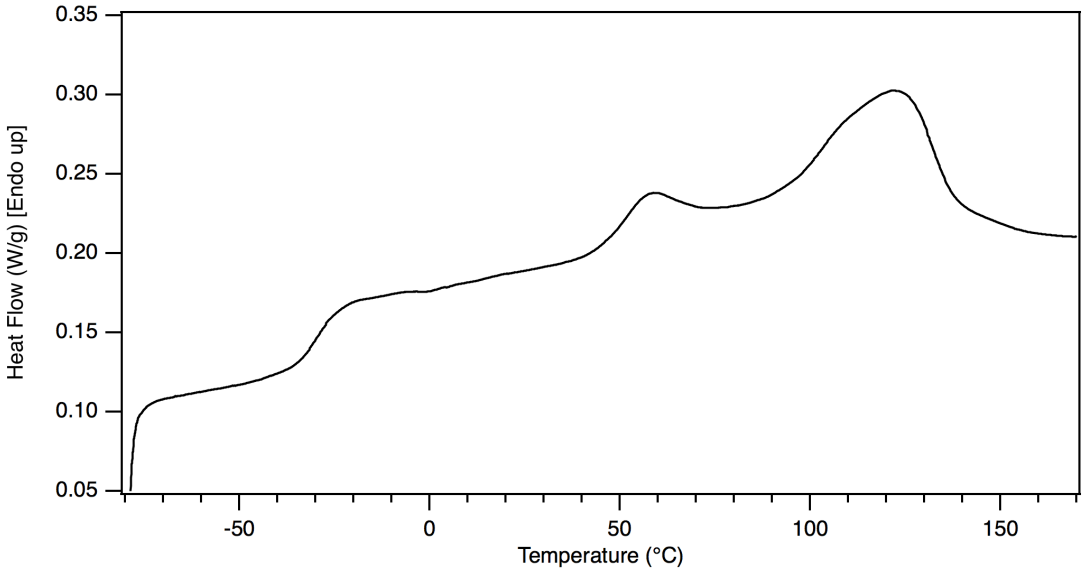

Figure 2.1. Differential scanning calorimetry trace of untreated poly(butylene adipate-co-terephthalate), which shows a glass transition at –30 °C and a broad melting transition between 40 °C and 150 °C.

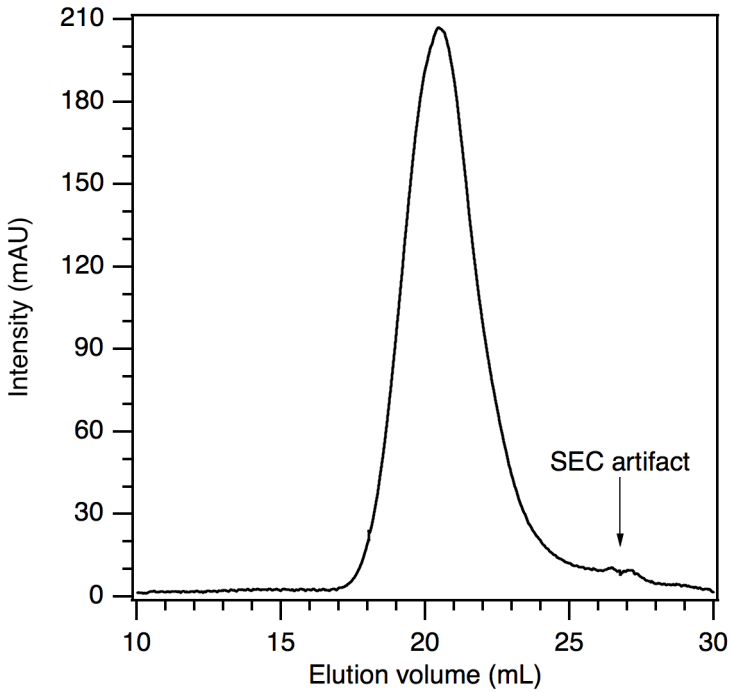

Figure 2.2. Size-exclusion chromatography trace (chloroform mobile phase) of untreated poly(butylene adipate-co-terephthalate).

To determine the chemical composition of the PBAT film, we dissolved a small piece in $CDCl_3$ and analyzed the solution by ^1H NMR spectroscopy (**Figure 2.3**). We used the integrals of the peaks corresponding to the aryl protons (8.1 ppm) and the –OC**H**$_2$– protons of the butanediol unit (4.4 and 4.1 ppm) to determine the ratio of terephthalate units to adipate units; The molar ratio of terephthalate (T) to adipate (A) of the PBAT was 0.936 $mol_T \cdot (mol_A)^{-1}$.

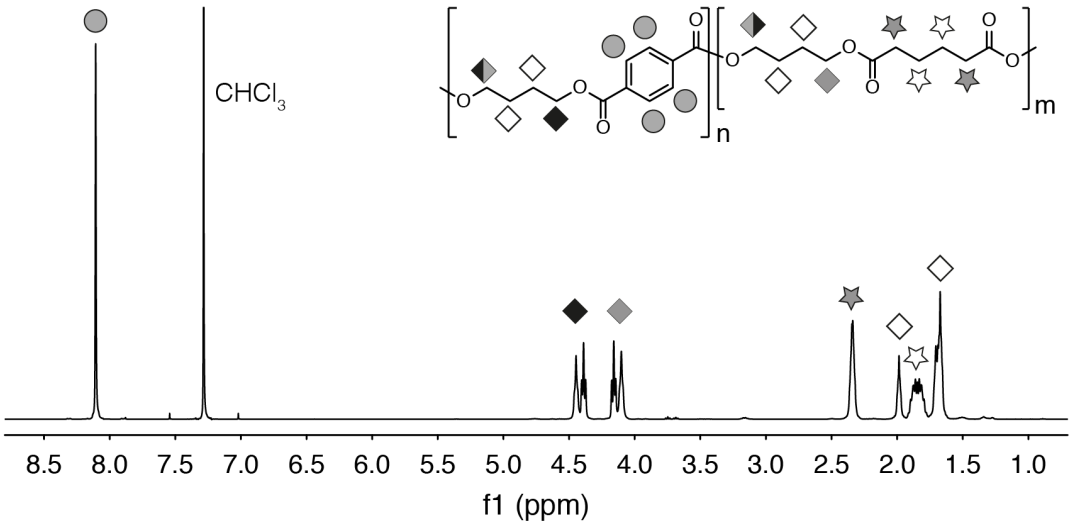

Figure 2.3. ^{1}H NMR spectrum ($CDCl_3$, 400 MHz) of a poly(butylene adipate-co-terephthalate) (PBAT) film. The symbols next to the peaks in the spectrum and next to the protons in the structural formula depict the peak assignment.

2.4.2. Irradiation of PBAT Films.

To study the effect of light-induced photochemical changes in PBAT films on their enzymatic hydrolyzability, we irradiated both sides of blown, non-photostabilized, transparent PBAT films with UV light (lamp spectrum shown in **Figure 2.4**) for varying times between 6 and 24 hours per side. We performed actinometry experiments with 4-nitroanisole (PNA) in pyridine-containing solutions to verify constant light intensity in the photoreactor (**Figure 2.5**).[25] We found that the first-order rate constants for the photochemical degradation of PNA were very similar between experiment 1 (0.0102 min^{-1}, before film irradiation) and experiment 2 (0.0103 min^{-1}, after film irradiation). These results confirmed that the light in the photoreactor had a constant intensity over the course of the film irradiations.

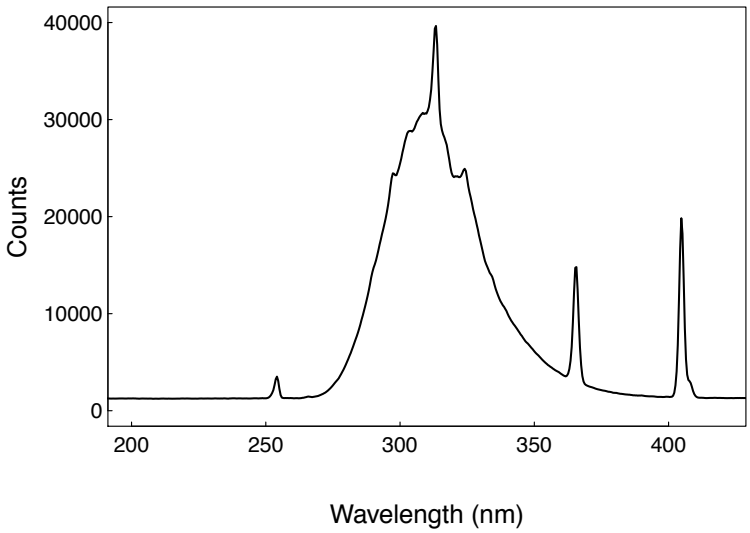

Figure 2.4. Spectrum emitted by the UV bulbs used in this study as measured with a Jaz Spectrometer (Ocean Optics).

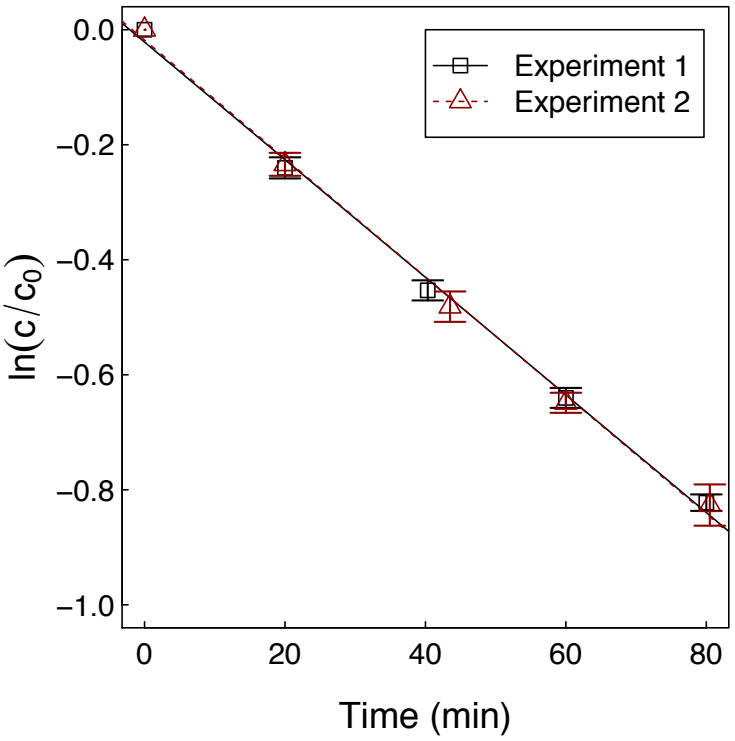

Figure 2.5. Logarithmic plot of the photochemical degradation of 4-nitroanisole (PNA) in a solution containing pyridine. Experiments 1 (black squares) and 2 (red triangles) were performed before and after the irradiations of the polyester films, respectively. Error bars represent standard deviations of triplicate measurements.

2.4.3. Titration experiments of PBAT films.

We assessed the hydrolyzability of untreated and irradiated PBAT films by pH-stat titration. Titration experiments were conducted in duplicate and showed high reproducibility (**Figure 2.6** and **Figure 2.7**).

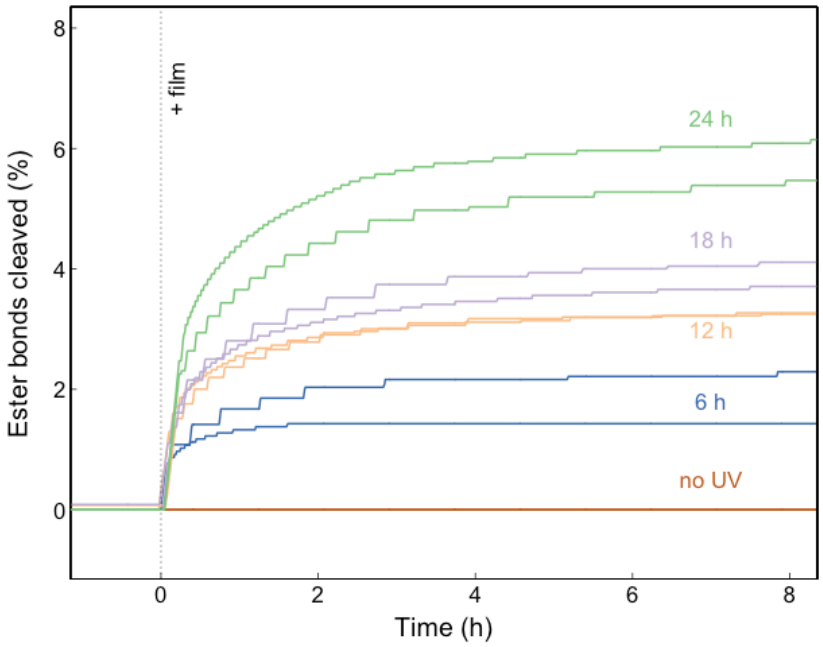

Figure 2.6. Cumulative number of released protons, relative to the number of ester bonds in the poly(butylene adipate-co-terephthalate) (PBAT) films, quantified by automated pH-stat titration. Each side of the PBAT film was irradiated with UV light for the time indicated next to the curve. PBAT films were added to the system at the time indicated by the vertical dashed line. Duplicate experiments are shown in the same color.

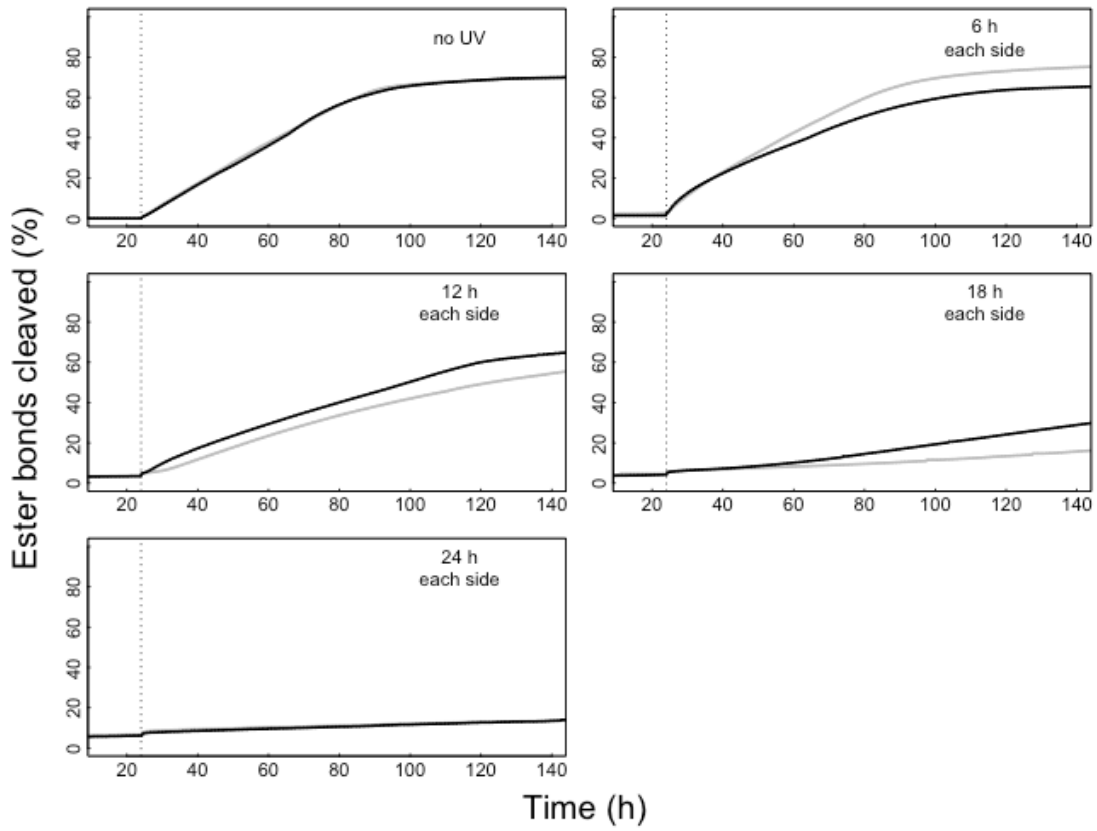

Figure 2.7. Hydrolysis of irradiated poly(butylene adipate-co-terephthalate) (PBAT) films by *Fusarium solani* cutinase (FsC). The plots show the cumulative number of released protons, relative to the number of ester bonds in the PBAT film, quantified by automated pH-stat titration. PBAT films were irradiated with UV light for the time indicated in each panel. FsC was added to the system at the time indicated by the vertical dashed lines. Duplicate experiments are depicted in black and grey.

Figure 2.9a and **Figure 2.9b** show the titration results for one of the two replicates for the different irradiation times. The addition of untreated PBAT films to an enzyme-free solution at pH 7 did not result in the decrease of the pH of the solution (**Figure 2.6** and **Figure 2.9a**). Conversely, when adding irradiated films to an enzyme-free solution, protons were released from the films, as evidenced from the KOH that was titrated to maintain a constant pH. We attributed the release of protons from irradiated PBAT films to carboxylic acid moieties produced by Norrish-type photochemical reaction mechanisms (**Figure 2.8**)

that have previously been reported for polyesters containing aromatic moieties.[20,33,34] For all irradiated films, titration rates were highest immediately after the film addition and subsequently slowed down and reached a plateau. The cumulative amounts of added KOH, and thus the amount of acidity generated by UV-irradiation, increased linearly with increasing irradiation time (**Figure 2.9c**). For films irradiated for the longest time studied here (24 h per side), the plateau of released protons corresponded to approximately 6 % of the ester bonds in the added PBAT.

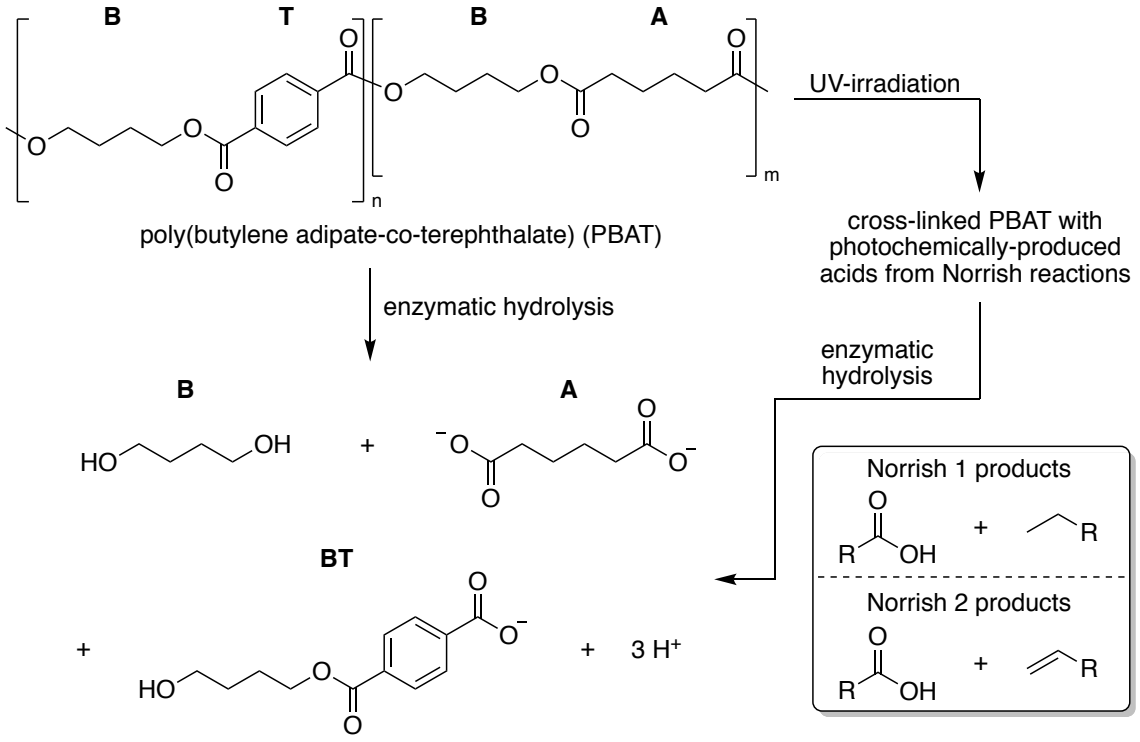

Figure 2.8. Photochemical and enzymatic cleavage of chemical bonds in poly(butylene adipate-co-terephthalate) (PBAT).

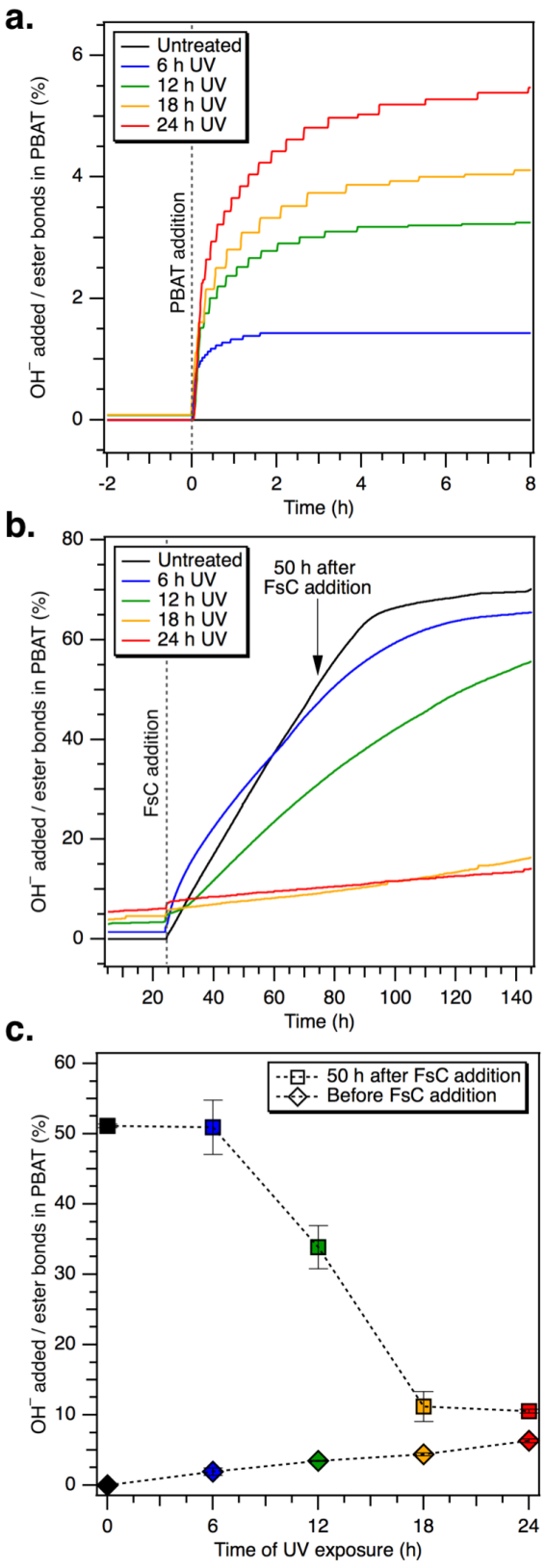
a.
Untreated
6 h UV
12 h UV
18 h UV
24 h UV
PBAT addition
OH⁻ added / ester bonds in PBAT (%)
Time (h)
b.
Untreated
6 h UV
12 h UV
18 h UV
24 h UV
50 h after
FsC addition
FsC addition
OH⁻ added / ester bonds in PBAT (%)
Time (h)
c.
50 h after FsC addition
Before FsC addition
OH⁻ added / ester bonds in PBAT (%)
Time of UV exposure (h)

Figure 2.9. Results of pH-stat titration experiments at pH 7 and 40 °C on untreated and UV-irradiated films of poly(butylene adipate-co-terephthalate) (PBAT). Both sides of the films were irradiated with UV light for the time indicated in the legend (panels a. and b.) and on the x-axis (panel c.). In all panels the y-axis represents the cumulative amount of OH^- added relative to the number of ester bonds in the PBAT film; this includes titration of carboxylic acids produced by photochemical transformations and by enzymatic hydrolysis. **a.** Initial portion of the pH-stat titration experiments with only PBAT film present in the solution. **b**. The rest of the pH-stat titration experiments, with PBAT and *Fusarium solani* cutinase (FsC) present in the solution. **c.** The amount of OH^- added before and 50 h after the addition of FsC (indicated by the arrow at 74 h in panel b). Error bars represent ranges of independent duplicates from their means.

When the release of protons from photochemically produced acids reached a plateau (i.e., approximately 24 h after addition of PBAT films), we added *Fusarium solani* cutinase (FsC) to the solution. This enzyme addition resulted in the immediate rapid hydrolysis of ester bonds and the subsequent release of protons into the solution (**Figure 2.9b** and **Figure 2.7**). For untreated PBAT films, the cumulative number of cleaved ester bonds increased linearly for approximately 70 h before reaching a plateau at values corresponding to approximately 70% of the ester bonds in the added PBAT films. Consistent with this high extent of ester bond cleavage, the film had disappeared, which provided a visual indication of the transformation of untreated PBAT into soluble hydrolysis products. Although enzymatic hydrolysis of the untreated PBAT films was extensive, approximately 30% of the ester bonds were not cleaved. This incomplete hydrolysis was not due to FsC inactivation: re-addition of new FsC solution to the titration solution did not result in a significant increase in the cumulative number of hydrolyzed ester bonds (**Figure 2.10**). Taken together, these findings suggest that FsC did not cleave some specific ester bonds in the soluble hydrolysis products during the experiment.

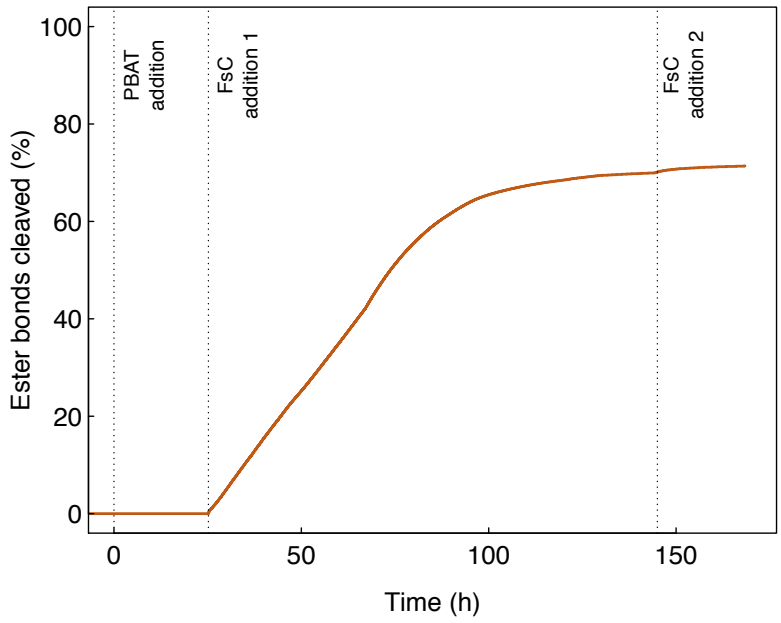

Figure 2.10. Hydrolysis of an untreated poly(butylene adipate-co-terephthalate) (PBAT) film by *Fusarium solani* cutinase (FsC). The plot shows the cumulative number of released protons, relative to the number of ester bonds in the PBAT film, quantified by automated pH-stat titration. PBAT film was added at t = 0 h. FsC was added to the system at the times indicated by the additional vertical dashed lines at t = 24 h and t = 145 h.

To identify incompletely hydrolyzed products, we analyzed the solution that remained after the pH-stat titration experiments by HPLC-HRMS and ^{1}H NMR spectroscopy. The signals observed by HPLC-HRMS were assigned to adipate (A), terephthalate (T), and 4-hydroxylbutyl terephthalate (butanediol-terephthalate dyad; BT); butanediol (B) was not detected (**Figure 2.11**). The strong signal detected for BT, which contains an ester bond that was not hydrolyzed by FsC, supports the incomplete ester hydrolysis measured by automated pH-stat titration. To assess the presence of BT more quantitatively, we performed ^{1}H NMR analysis on hydrolysis products isolated by liquid-liquid extraction (**Figure 2.12**). The peaks indicative of the hydrolysis products were the aryl protons from terephthalate units and protons adjacent to a hydroxyl moiety; the

integrals from these peaks (1:0.5:0.5) could be explained by the presence of pure BT or an equimolar mix of the terephthalate-butanediol-terephthalate triad (TBT) and butanediol (B). Given the likely difference between the partitioning of TBT and B in chloroform, the finding that the peak ratio was the same for three consecutive extractions strongly suggests that BT was the predominant terephthalate-containing hydrolysis product isolated by extraction. We quantified the concentration of terephthalate units by adding 1,4-dimethoxybenzene as an internal standard. To relate the quantified number of terephthalate protons to the number of terephthalate protons that was added to the hydrolysis experiment in the form of PBAT, we extrapolated the amounts that we quantified in the three consecutive extractions with an exponential decay fit. Extrapolating for 10 extractions resulted in a recovery of 86 ± 8 %. These ^{1}H NMR results corroborate the HPLC-HRMS analysis and confirm that BT is the predominant terephthalate-containing product of the hydrolysis of PBAT by FsC. Thereby, these experiments match the extents of cleaved ester bonds we detected by pH-stat titration (**Figure 2.9**).

Both ^{1}H NMR and HPLC-HRMS analyses consistently showed the formation of three predominant hydrolysis products: butanediol (B), adipate (A), and 4-hydroxylbutyl terephthalate (butanediol-terephthalate dyad; BT) (**Figure 2.8**). The identification of BT as the major terephthalate-containing hydrolysis product explained the incomplete hydrolysis of ester bonds in PBAT observed by pH-stat titration. Furthermore, BT accumulation implies that the rate of FsC-mediated ester hydrolysis of a B-T-B sequence is rapid for the first aryl ester bond and then is strongly decreased for the second aryl ester bond.

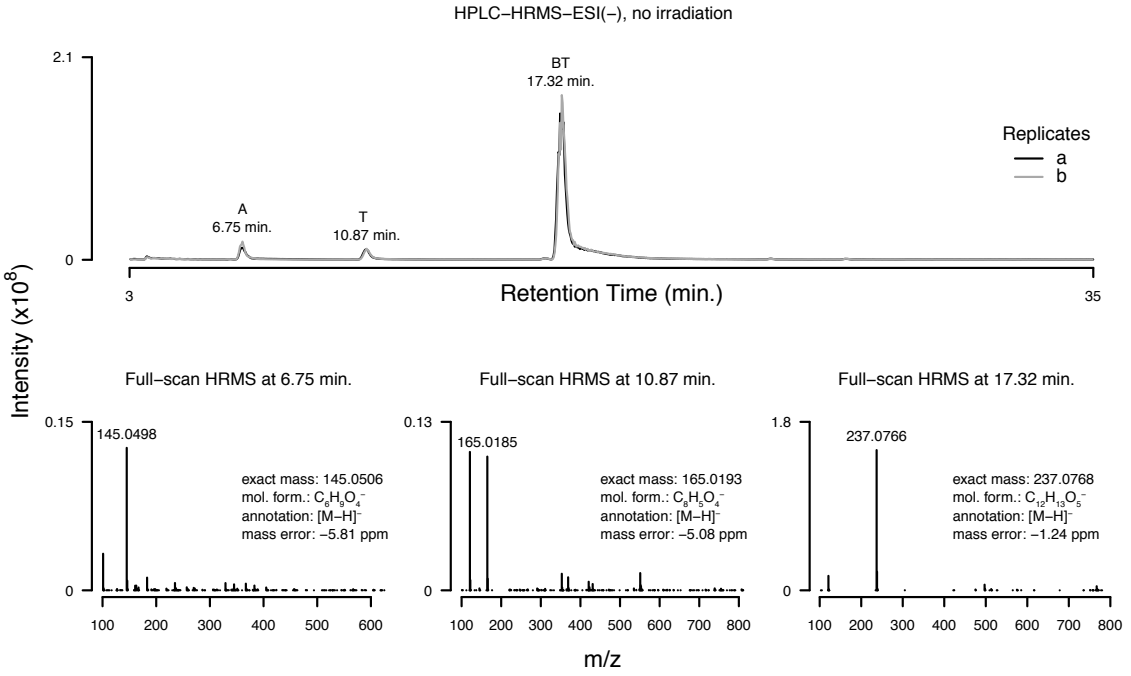

Figure 2.11. Product identification of the enzymatic hydrolysis of poly(butylene adipate-co-terephthalate) (PBAT). **Top.** Base peak chromatograms generated by high-pressure liquid chromatography coupled to high-resolution mass spectrometry (HPLC-HRMS) in negative mode electrospray ionization (ESI). Curves of independent duplicates (grey and black) overlap. **Bottom.** Full-scan HRMS spectra acquired at the indicated retention times; additional information on the molecule assigned to the predominant masses are provided in each panel.

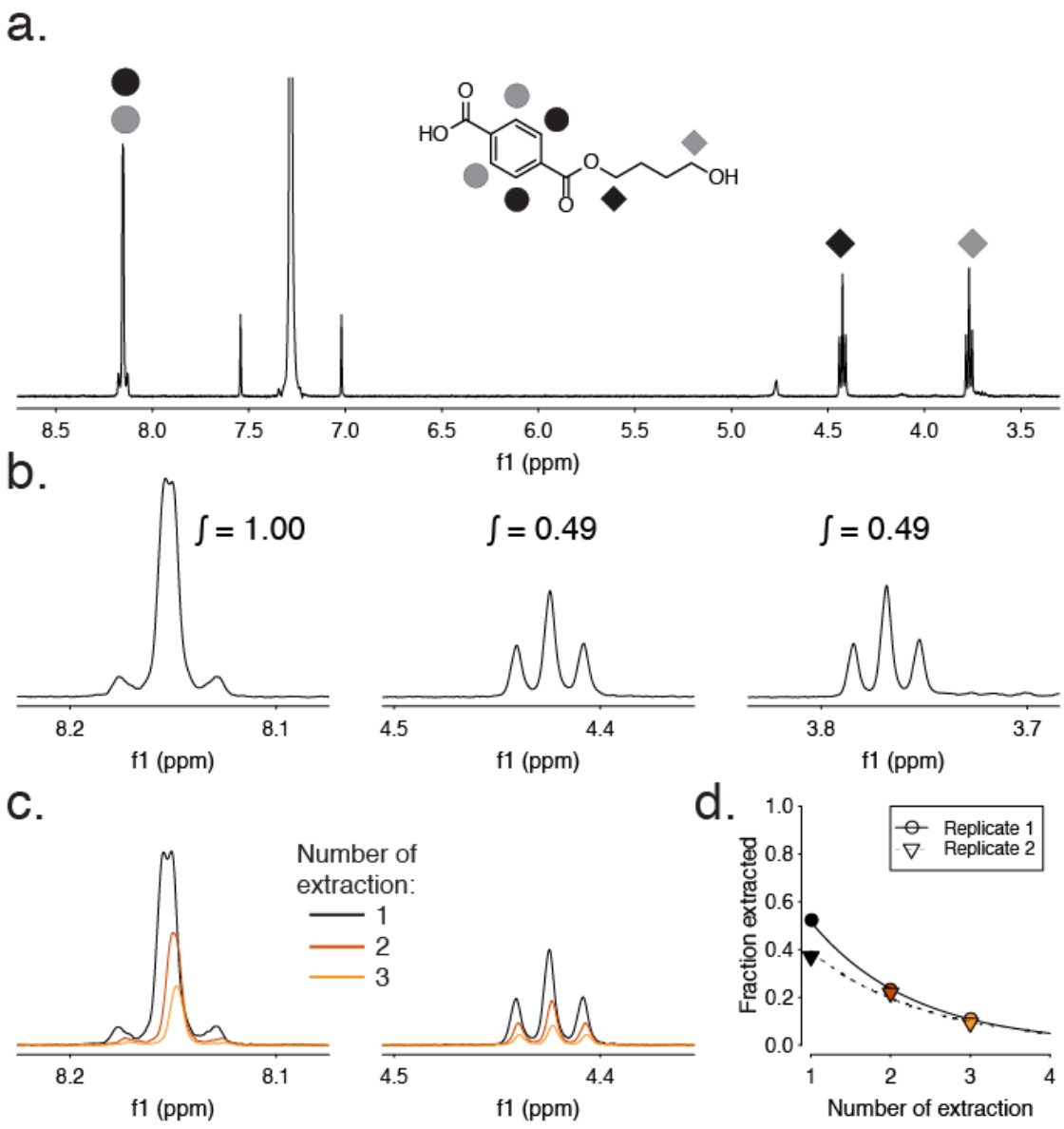

Figure 2.12. ^{1}H NMR analysis of the products from the enzymatic hydrolysis of untreated poly(butylene adipate-co-terephthalate) (PBAT) after liquid-liquid extraction. **a.** ^{1}H NMR spectrum of hydrolysis products and structural formula of the butanediol-terephthalate dyad (BT). The symbols depict the assignment of the characteristic protons to the peaks in the spectrum. **b.** Enhanced regions containing the spectral peaks assigned to the characteristic protons of BT and their integration values. **c.** Enhanced regions of two spectral peaks assigned to the characteristic protons of BT. Spectra obtained after consecutive extractions are shown in different colors. **d.** Fraction of extracted PBAT-derived terephthalate for three consecutive extractions of duplicate hydrolysis experiments. The lines depict exponential fits for the points.

The PBAT films that were irradiated with UV light for 6 h per side were hydrolyzed by FsC on similar timescales as the untreated films (**Figure 2.7** and **Figure 2.9b**). However, the enzymatic hydrolysis curves of the 6 h UV-irradiated and the untreated PBAT films had slightly different shapes. While the hydrolysis rate of untreated films was constant for the first 70 h after FsC addition, the hydrolysis rate for the 6 h UV-irradiated films was initially higher, but subsequently decreased to rates smaller than for the untreated films. We speculate that the high initial rate is a result of the photochemical cleavage of some PBAT chains, which produced smaller and thus more hydrolyzable fragments.[35] We ascribe the subsequent regime with slower hydrolysis to photochemical cross-linking of PBAT chains that decreases their flexibility and hence their enzymatic hydrolyzability. This explanation is consistent with previous studies, in which chain flexibility was used to explain polyester hydrolysis rates.[12,36,37,38] Films that were UV-irradiated for 12 h and longer per side were hydrolyzed considerably slower than the untreated films. Less than 5% of ester bonds were enzymatically hydrolyzed in films that were exposed to UV light for 24 h per side during incubation with FsC for 50 h.

As a complementary approach to pH-stat titration, we assessed the enzymatic hydrolysis of these PBAT films in batch incubation reactors containing pH-buffered solutions; aliquots were removed at various times and their total organic carbon (TOC) content was measured to monitor the release of hydrolysis products over time (**Figure 2.13**). Although this is a convenient approach, we note that it is more error-prone and less time-resolved than the pH-stat titration approach. Nonetheless, these independent experiments confirmed the results obtained with the pH-stat titration setup: PBAT films that were UV-irradiated for 12 h or more showed significantly decreased enzymatic

hydrolysis rates. We also used the TOC-based approach to show that the rate of PBAT hydrolysis by FsC did not increase when we doubled the solution concentration of FsC (**Figure 2.14**). Thereby, we demonstrated that for all enzymatic hydrolyses presented herein (i.e., pH-stat titrations and incubations coupled to solution TOC analysis) the PBAT surfaces were saturated with FsC.

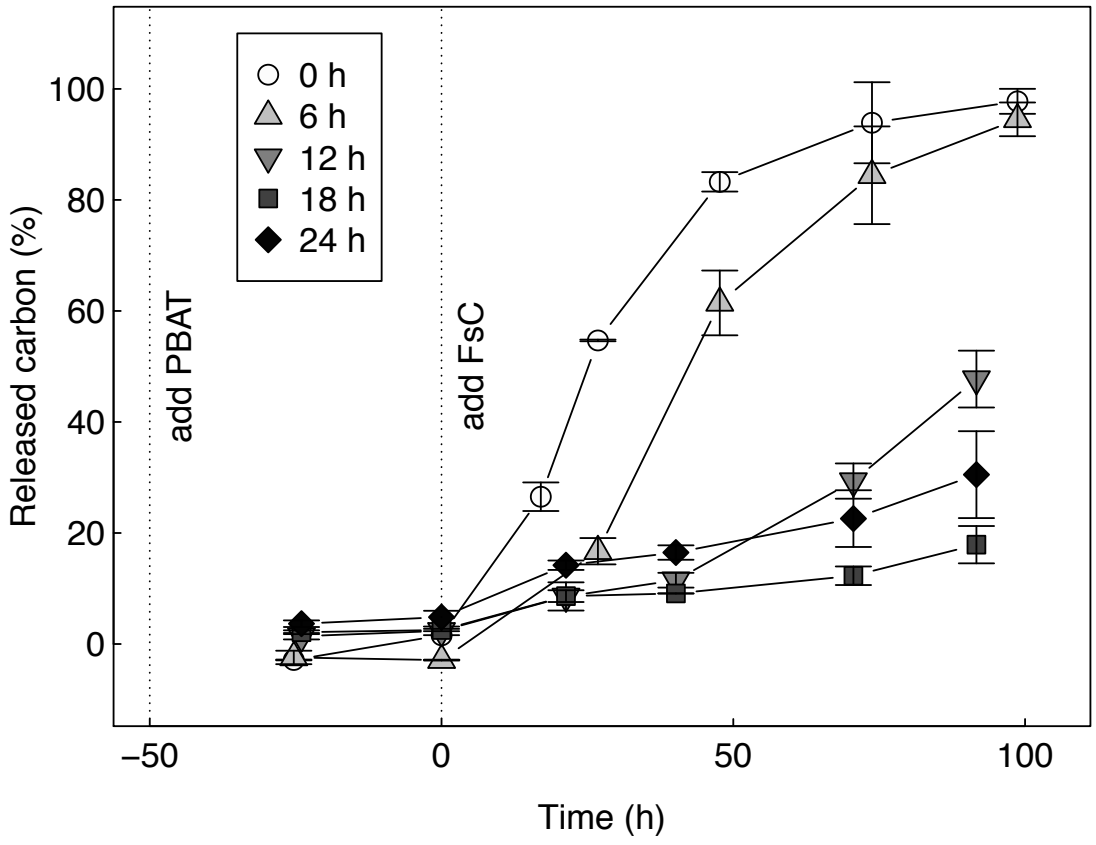

Figure 2.13. Hydrolysis of irradiated poly(butylene adipate-co-terephthalate) (PBAT) films by *Fusarium solani* cutinase (FsC). The plot shows the cumulative amount of organic carbon that was released into the solution, relative to the amount of organic carbon in the PBAT film initially added to the experiment. We quantified released carbon by total organic carbon (TOC) measurements of the hydrolysis solution. PBAT films were irradiated on both sides with UV light for the time indicated in the legend. PBAT films and FsC were added to the system at the times indicated by the vertical dashed lines at –50 and 0 h, respectively. Error bars represent the ranges of independent duplicates from their means.

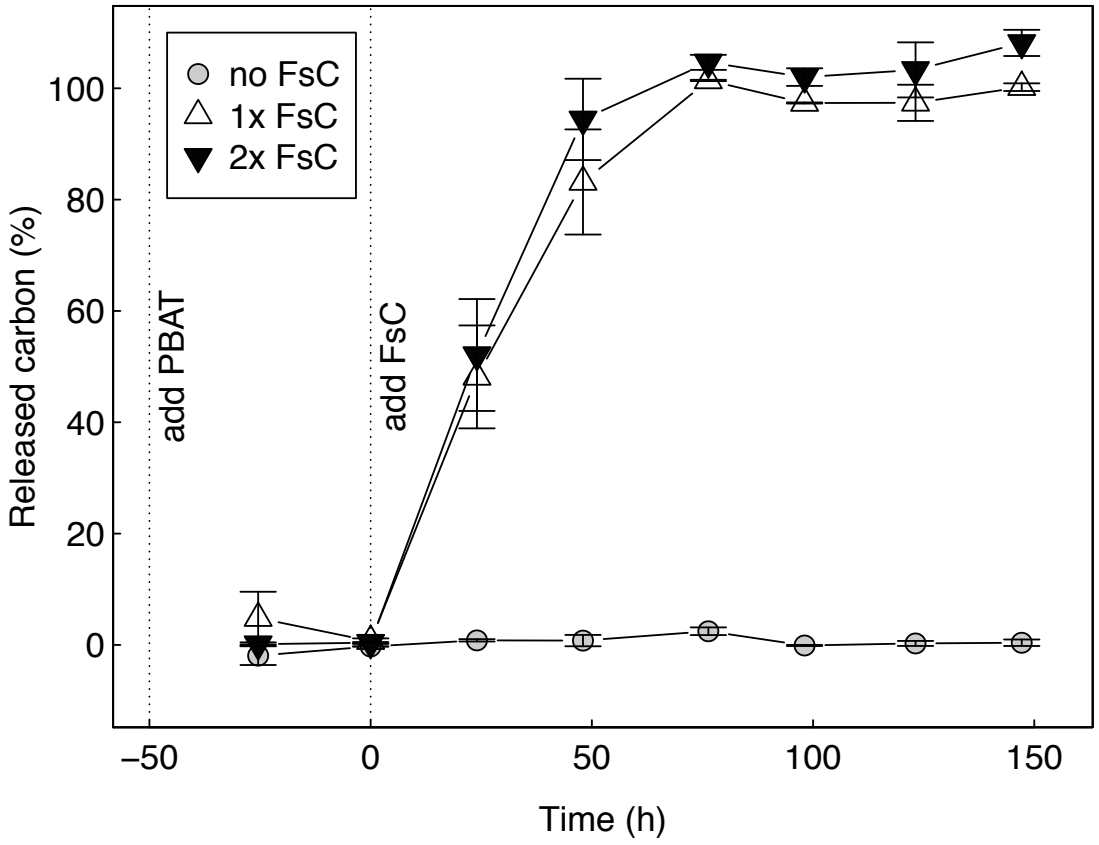

Figure 2.14. Hydrolysis of poly(butylene adipate-co-terephthalate) (PBAT) films by *Fusarium solani* cutinase (FsC). The plot shows the cumulative amount of carbon that was released into the solution, relative to amount of carbon in the PBAT film, quantified by total organic carbon (TOC) measurements of the hydrolysis solution. PBAT films and FsC were added to the system at the times indicated by the vertical dashed lines at -50 and 0 h, respectively. Error bars represent the ranges of independent duplicates from their means. Circles, triangles, and inverted triangles represent experiments with different concentrations of FsC (i.e., zero, standard concentration used in all experiments of the manuscript, and doubled concentration, respectively).

2.4.4. Characterization of physicochemical properties of untreated and UV-irradiated PBAT films.

First, we investigated the crystallinity of untreated and irradiated films, as crystallinity is an important parameter for polyester biodegradation (higher degrees of crystallinity decrease the enzymatic hydrolyzability).[39,40] To probe the crystallinity of these

PBAT films, we employed two complementary methods: differential scanning calorimetry (DSC) and wide-angle x-ray scattering (WAXS). The enthalpy of melting (ΔH_m) values obtained by DSC are directly related to the % crystallinity of a polymer.[41] For the UV-irradiated films, a quantitative analysis of the melting transition by DSC indicated that there was no substantial change in the % crystallinity as compared to untreated PBAT (**Figure 2.15** and **Table 2.1**). We furthermore note that the DSC measurements revealed that the melting temperature T_m for the crystalline domains, which has previously been shown to negatively correlate with enzymatic hydrolyzability,[12,37,38,39] decreased with increasing UV exposure time (**Table 2.1**). Although the data shown is for the first heat, the same trend was observed after erasing the thermal history (i.e., on the second heat). Due to the low % crystallinity of commercial PBAT films (e.g., EcoFlex, 11%), there are few crystallites present and the network that is formed from UV-irradiation is thus essentially a network of randomly oriented chains. In such networks, it has been empirically observed that a small degree of cross-linking can drastically reduce the melting temperature (both onset and maximum), which has been explained by a change in the entropy of fusion.[41] This melting point depression trend continues—though not as drastically—as cross-link density is increased.

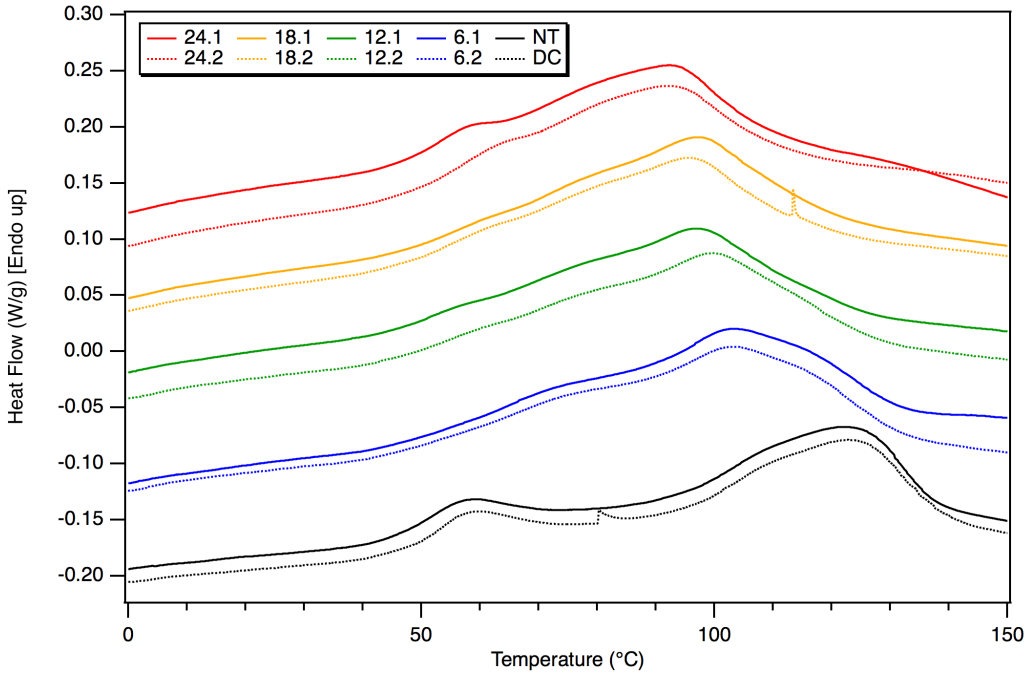

Figure 2.15. An overlay of differential scanning calorimetry (DSC) traces of untreated PBAT (denoted NT), a dark control (DC), and PBAT irradiated on both sides with UV light for the time indicated in the legend (i.e., 6-24 h). Duplicate measurements for the irradiated films are shown as solid and dotted lines in the same color (denoted X.1 or X.2, where X is the irradiation time in hours). Traces are vertically scaled for clarity.

Table 2.1. Thermal properties of PBAT samples measured by DSC.

Sample ID[a]	ΔH_m (J/g)[b]	T_m (°C)[c]
NT	29	121
DC	27	123
6.1	28	103
6.2	31	103
12.1	28	97
12.2	29	99
18.1	27	97
18.2	26	99
24.1	27	92
24.2	25	91

[a] Nomenclature: untreated PBAT is denoted NT, a dark control is denoted DC, and duplicate samples of UV-irradiated are denoted X.1 or X.2, where X is the irradiation time in hours. [b] Enthalpy of melting was determined by integrating the signal produced by the melting transition. [c] The melting temperature was defined as the global maximum of the melting transition.

We sought to corroborate the DSC results using WAXS. The data obtained by WAXS for the untreated and irradiated PBAT samples is in good agreement with the expected crystal structure for PBAT: the crystalline domains are dominated by poly(butylene terephthalate) (PBT) crystals rather than poly(butylene adipate) crystals. The reported values for the triclinic unit cell (α form) of PBT are a = 4.83 Å, b = 5.94 Å, c = 11.59 Å, α = 99.7°, β = 115.2°, and γ = 110.8°.[42] Using very slightly modified values (a = 4.89 Å, b = 5.94 Å, c = 11.78 Å, α = 100.3°, β = 115.0°, and γ = 111.1°), the experimental data can be indexed according to the expected reflections from this unit cell. There is good agreement between these reflections and the observed peaks (**Figure 2.16**). Importantly, there was no change in the crystal structure with UV irradiation and very little change in the peak intensities, which suggested that the % crystallinity remains constant with prolonged UV exposure (**Figure 2.17**). Based on the DSC and WAXS results, we therefore cannot ascribe the observed decrease in enzymatic hydrolyzability with increasing UV-irradiation to changes in PBAT crystallinity.

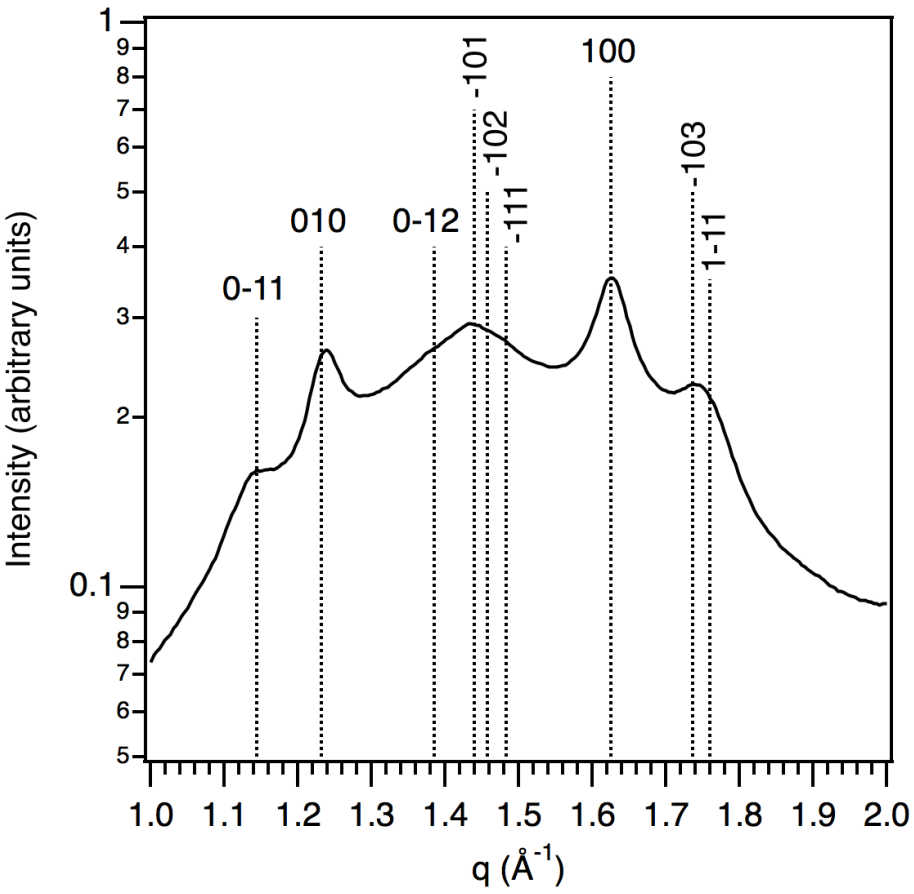

Figure 2.16. Wide-angle x-ray scattering (WAXS) data of untreated poly(butylene adipate-co-terephthalate) (PBAT) with Miller indices shown for the expected reflections of the triclinic poly(butylene terephthalate) (PBT) unit cell (α form). The parameters used to index the peaks were: a = 4.89 Å, b = 5.94 Å, c = 11.78 Å, α = 100.3°, β = 115.0°, and γ = 111.1°. Although poorly developed along the c axis, the peaks corresponding to the a and b axis are very distinct (100 and 010, respectively). The underlying broad bump is due to scattering from amorphous material.

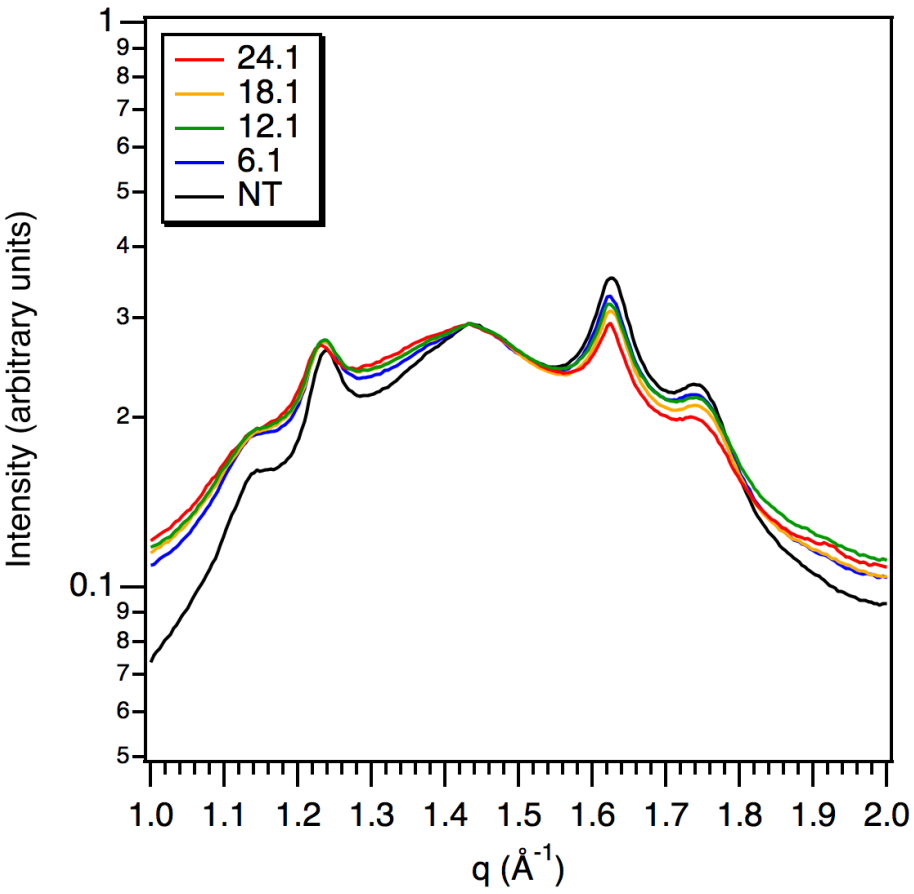

Figure 2.17. Wide-angle x-ray scattering (WAXS) data of untreated poly(butylene adipate-co-terephthalate) (PBAT) (denoted NT) and PBAT irradiated on each side for the time indicated in the legend (6-24 h). The irradiated PBAT curves were vertically shifted to align with the NT data at q = 1.432 Å^{-1}.

Second, we used the commonly employed technique of gel fraction measurements to assess the formation of cross-links in polymers. To this end, we determined the chloroform-soluble and chloroform-insoluble mass fractions of the untreated and the UV-irradiated PBAT films (**Figure 2.18a** and **Figure 2.19**). These measurements showed that the soluble fraction of PBAT films strongly decreased from 1.0 (i.e., fully soluble) for the untreated PBAT to less than 0.4 for films that were irradiated for 6 h per side. Additional irradiation further decreased the chloroform-soluble fraction—though less drastically—until it reached approximately 0.2 for samples that were irradiated for 24 h per side. Taken

qualitatively, the swelling experiments confirmed that UV-irradiation induced cross-linking between chains in PBAT films. Furthermore, the monotonic decrease in the soluble fraction with increasing irradiation time suggested that more cross-links were formed with increasing UV exposure. As photochemical reactions are limited by the penetration depth of the light, we sought to demonstrate whether our procedure (i.e., irradiation on both sides) generated cross-links throughout the film. We therefore irradiated samples on one side for 24 h and compared their chloroform-insoluble (gel) fractions (ca. 0.41) to those of the 24 h samples shown in **Figure 2.18a** (ca. 0.84); the finding that one-sided irradiation resulted in gel fractions that were approximately half the value measured for samples irradiated on both sides is consistent with our supposition that our procedure was successfully generating cross-links throughout the films. As these cross-linking events were expected to be accompanied by chain scission events, we analyzed the soluble fractions by size-exclusion chromatography (SEC); indeed, the SEC results demonstrated that increased irradiation time yielded smaller PBAT fragments in the soluble fractions (**Figure 2.20**).

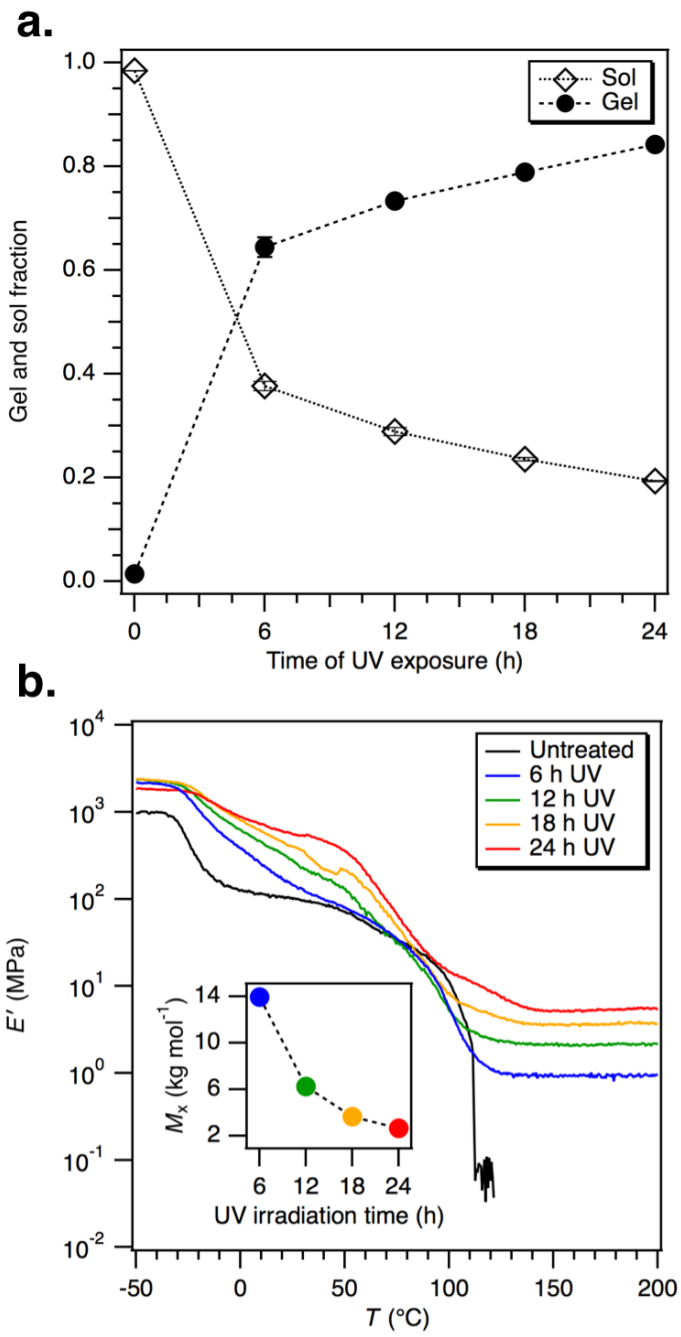

Figure 2.18. Characterization data for untreated and UV-irradiated poly(butylene adipate-co-terephthalate) (PBAT) films. **a.** Chloroform-insoluble (gel) and chloroform-soluble (sol) fraction of PBAT as a function of UV-irradiation time; error bars represent ranges of independent duplicates from their means. **b.** Representative dynamic mechanical thermal analysis curves showing storage modulus (E') as a function of temperature for untreated and irradiated films; the inset shows representative molar masses between cross-links (M_x) for the irradiated PBAT samples, which were calculated from the plateau storage modulus at 150 °C using equation 1.

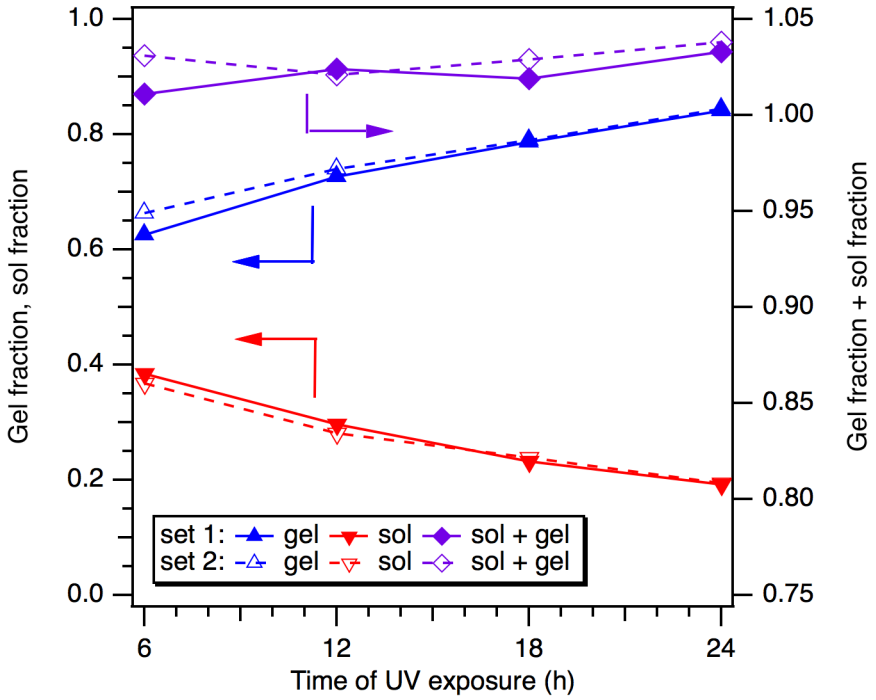

Figure 2.19. Chloroform-insoluble (i.e., gel), chloroform-soluble (i.e., sol) and total (i.e., sol+gel) mass fractions of PBAT films that were irradiated on both sides for the time indicated on the x-axis. Duplicate experiments are depicted as open and closed symbols in the same color.

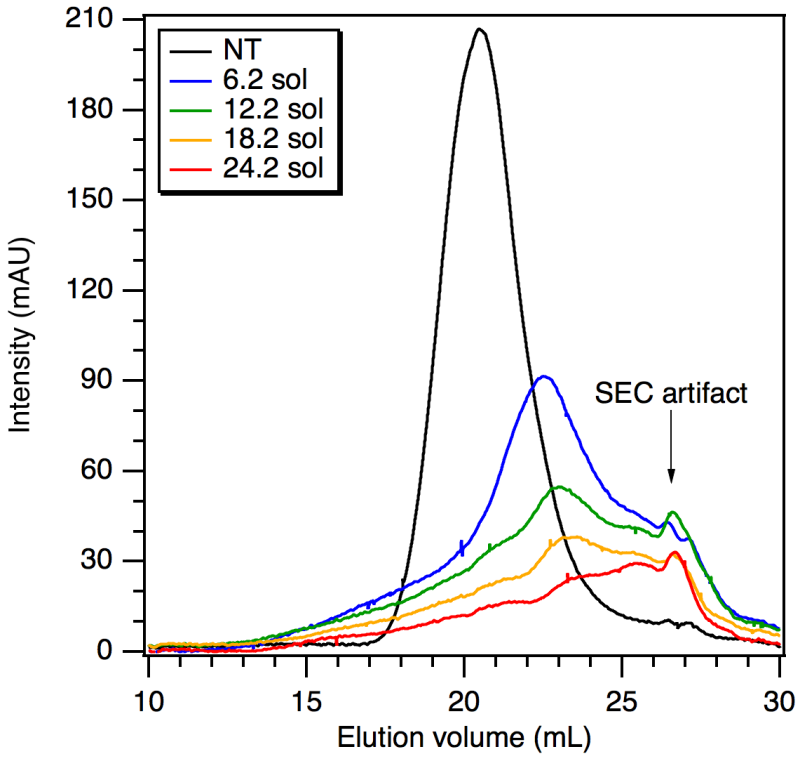

Figure 2.20. An overlay of size-exclusion chromatography (SEC) traces of untreated PBAT (denoted NT) and sol fractions from the PBAT samples irradiated with UV light for 6, 12, 18, and 24 h per side. There is an artifact at ca. 26.5 mL that contributes to the signal; it is seen in all traces obtained on this size-exclusion chromatograph.

Third, we sought to obtain a quantitative measure of the number of cross-links formed by UV-irradiation. To this end, we characterized untreated and UV-irradiated PBAT films using dynamic mechanical thermal analysis (DMTA). As we heated the untreated PBAT film through its melting transition (*ca.* 110 °C), the storage modulus E' dropped precipitously (**Figure 2.18b** and **Figure 2.21**). In contrast, heating the irradiated PBAT films through their melting transitions resulted in a more gradual drop in E', which was afterwards steady throughout the rest of each experiment (**Figure 2.18b**, **Figure 2.21**, and **Figure 2.22**). The relatively constant storage modulus above the melting transition for the UV-irradiated films confirmed that they were indeed cross-linked, which corroborated the qualitative conclusion drawn from the swelling experiments. The storage modulus in

this regime can be related to the cross-link density in the PBAT films and thus the average molar mass between cross-links M_x, as shown by equation 1. As expected, increasing the irradiation time resulted in increasing storage moduli as the samples become more extensively cross-linked (**Figure 2.18b**, **Figure 2.21**, and **Figure 2.22**); the calculated M_x (using the value of E' at 150 °C) decreased with increasing irradiation time (**Figure 2.18b** and **Figure 2.23)**. The M_x for the sample irradiated for 6 h per side was 14 kg·mol^{-1}, and it decreased to 6.2, 3.7, and 2.7 kg·mol^{-1} for samples irradiated for 12, 18, and 24 h per side, respectively. Using an average monomer molar mass of 105 g·mol^{-1}, these M_x values respectively correspond to an average number of monomers between cross-links of approximately 130, 60, 35, and 26.

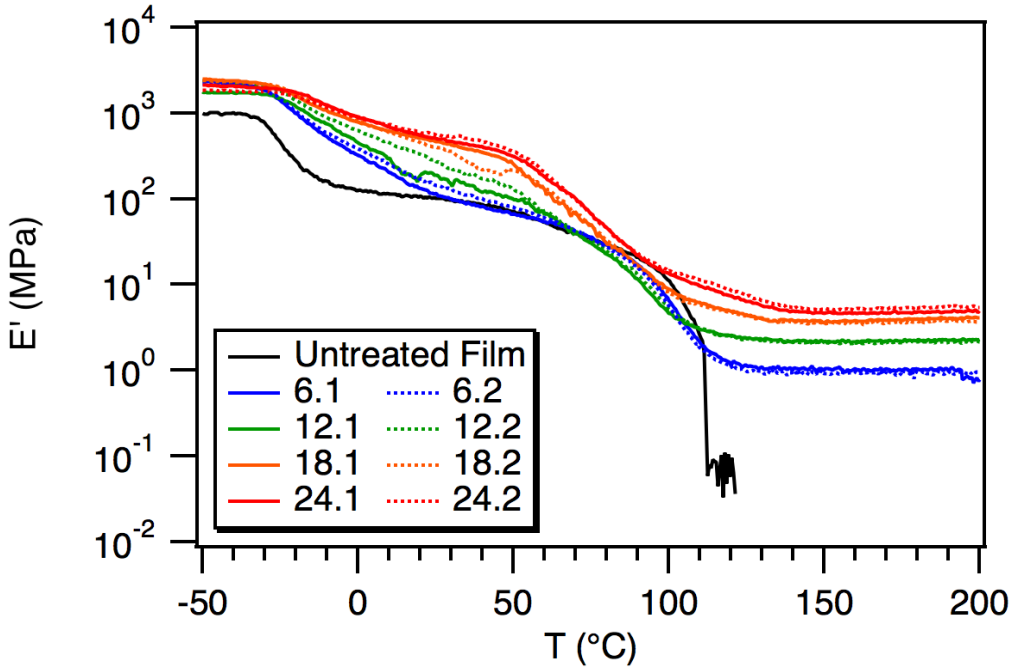

Figure 2.21. Dynamic thermal mechanical analysis (DMTA) of irradiated and untreated poly(butylene adipate-co-terephthalate) (PBAT) films. DMTA was performed on parts of the same film samples used for enzymatic hydrolysis experiments; films were irradiated with UV light for the time indicated in the legend (i.e., 6-24 h per side). Duplicate measurements for the irradiated films are shown as solid and dotted lines in the same color.

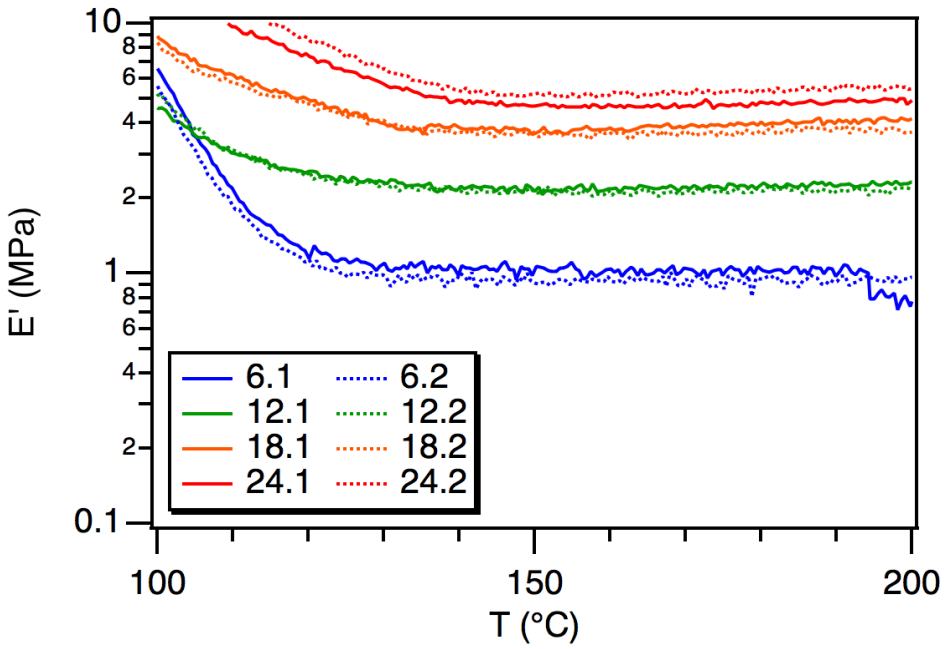

Figure 2.22. Enhanced view of the dynamic thermal mechanical analysis (DMTA) of irradiated poly(butylene adipate-co-terephthalate) (PBAT) films above their melting transition. Both sides of the films were irradiated for the time indicated in the legend (i.e., 6-24 h). Duplicate measurements for the irradiated films are shown as solid and dotted lines in the same color.

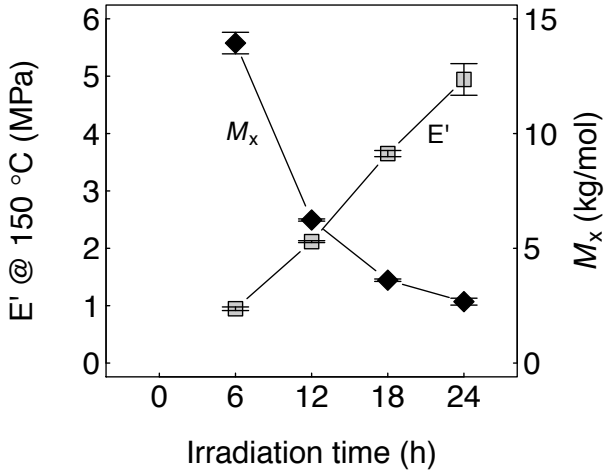

Figure 2.23. Graphical depiction of the storage modulus (E') at 150 °C measured by dynamic mechanical thermal analysis (DMTA) and the corresponding average molar mass between cross-links (M_x) for irradiated poly(butylene adipate-co-terephthalate) (PBAT) films. Error bars represent the ranges of independent duplicate measurements from their means.

2.4.5. Relating enzymatic hydrolyzability to changes in the physicochemical properties of PBAT films upon UV-irradiation.

In **Figure 2.24a** and **Figure 2.24b**, we related the changes in the enzymatic hydrolyzability to changes in the physicochemical properties of the PBAT films determined by swelling experiments and DTMA, respectively.

The decreases in enzymatic hydrolyzability were not well correlated with changes in the sol fraction (**Figure 2.24a**): although the extent of PBAT hydrolysis by FsC over 50 h was comparable for the untreated and the PBAT film UV-irradiated for 6 h per side, the 6 h of UV irradiation causes the soluble mass fraction to decrease from 1.0 to 0.4 (**Figure 2.18a** and **Figure 2.24a**). This comparison demonstrated that the density of interchain cross-links formed within 6 h of UV-irradiation per side was sufficient to render the majority of the PBAT insoluble while not significantly impacting the enzymatic hydrolyzability; we propose that at this low cross-link density, the overall chain flexibility of PBAT remains largely unaffected on the length scales required to access the active site of the enzymes. Irradiation for more prolonged periods of time (> 6 h per side) resulted in small decreases in the sol fraction yet quite substantial decreases in the extent of ester hydrolysis, which strongly suggests the change in sol fraction (i.e., gel content) is not a good indicator of the expected change in enzymatic hydrolyzability.

As compared to gel content, the decrease in enzymatic hydrolyzability of UV-irradiated PBAT correlated more closely with the average molar mass between cross-links determined by DMTA (**Figure 2.24b**). This linear relationship shows that substantial increases in the cross-link density (i.e., decreases in M_x) significantly reduce the enzymatic hydrolyzability of PBAT chains, likely due to the reduced probability that these chains will

be able to readily enter the active site of FsC. Our findings agree well with the previously suggested concept that the enzymatic hydrolysis of polyesters is highly dependent on the flexibility of the polyester chains.[12,36,37,38]

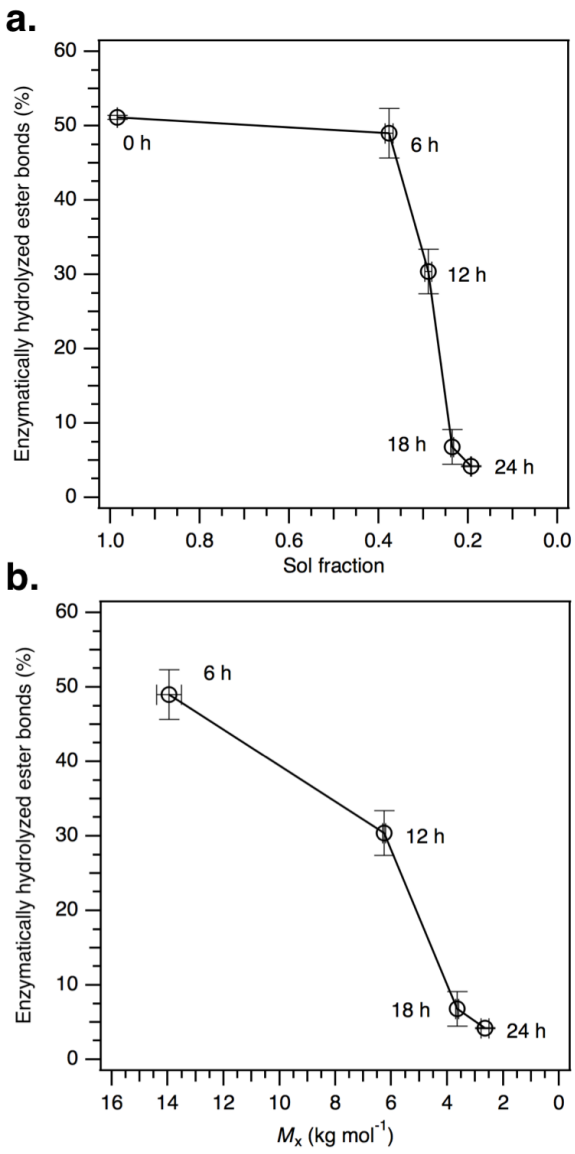

Figure 2.24. a. Correlation between the chloroform-soluble fractions of untreated and irradiated PBAT with the percentage of enzymatically hydrolyzed ester bonds 50 h after *Fusarium solani* cutinase (FsC) addition. **b.** Correlation between the average molar masses between cross-links (M_x) for irradiated PBAT with the percentage of enzymatically hydrolyzed ester bonds 50 h after FsC addition. In both panels, error bars represent ranges of independent duplicates from their means and the UV-irradiation time is specified next to each data point. The y-axes are distinct from those in **Figure 2.9** because here the

contribution of the photochemically-produced acids (i.e., titration before FsC addition) is intentionally not considered.

The data in **Figure 2.24b** show that hydrolyzability of PBAT by FsC becomes impaired at cross-link densities corresponding to M_x values in the range of 14 to 6 kg·mol^{-1}. In the photoreactors used in this study, M_x values of approximately 6 kg·mol^{-1} were reached when films had been irradiated for 12 h per side. To frame our experimental results in a more environmentally-relevant context, we performed natural sunlight exposure experiments of PBAT films in Zurich, Switzerland (47° latitude). We collected film samples at various time points, determined their chloroform-insoluble mass fractions (i.e., gel fractions), and compared the initial rate of gel formation to that of films subjected to UV-irradiation in the photoreactor (**Figure 2.25**). We note that these films were only irradiated on one side and that these measurements were performed differently than the gel fraction measurements shown above (i.e., in **Figure 2.18a**, **Figure 2.19**, and **Figure 2.24a**). As the purpose of these experiments was to ensure that cross-linking is triggered by natural sunlight and to provide a comparison between natural and artificial light exposures, we considered gel fraction measurements, which can be done much more rapidly than dynamic mechanical thermal analyses, to be sufficient.

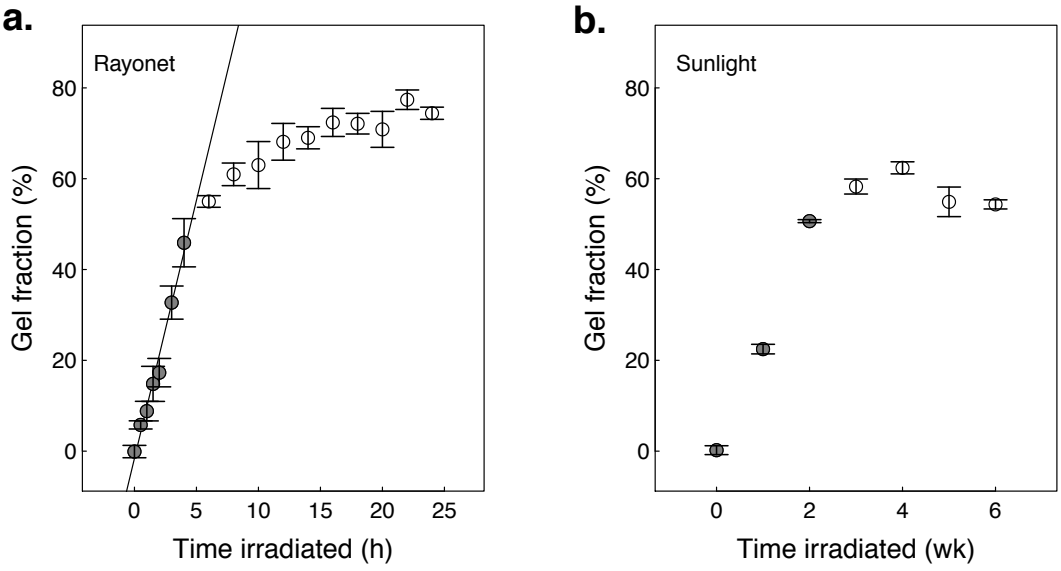

Figure 2.25. Chloroform-insoluble mass (i.e., gel) fractions of PBAT films that were irradiated on one side for the time indicated on the x-axes either in the Rayonet photoreactor (panel a) or by sunlight (panel b). Error bars represent standard deviations of triplicates. Filled circles represent the data points comprising the linear phase of gel formation; these data were thus used for the quantitative comparison.

During the initial 4 h of irradiation in the photoreactor, the gel fraction of PBAT films increased linearly with a slope of 11.4%/h. We compared this rate to the rate of gel formation during the first two weeks of the sunlight irradiation experiment (linear phase). To frame these measurements in terms of the number of sunny days that would cause degrees of cross-linking similar to those caused by UV-irradiation in the photoreactor, we used irradiance data that was collected on the roof of the building where the sunlight-irradiation experiments were performed (**Figure 2.26**). More specifically, the number of sunny days per week was calculated by dividing the integral of the illuminance curves for the entire week by the integral of the illuminance curve measurement on June 7 (i.e., an almost perfectly sunny day, **Figure 2.27**). These estimations suggested that a 12 h irradiation in the photoreactor corresponds to ~26 sunny days in central Europe in early June.

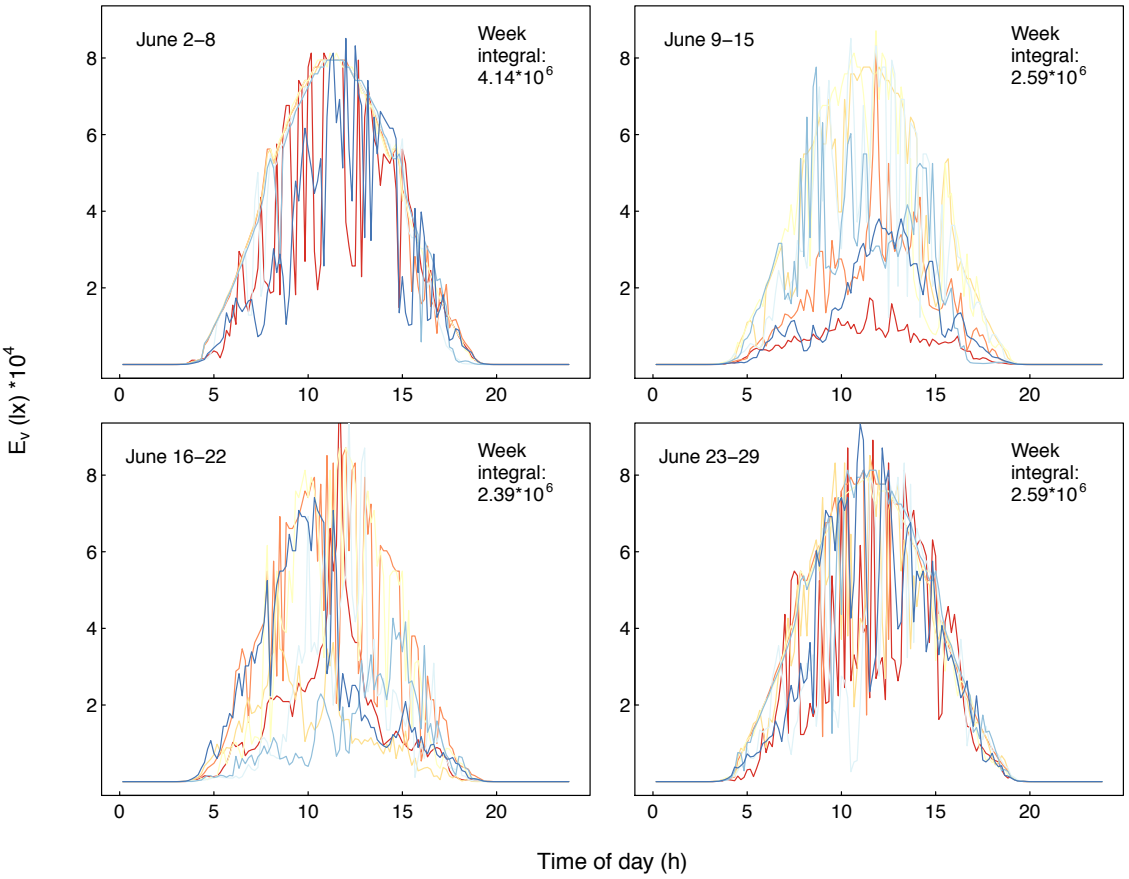

Figure 2.26. Illuminance data collected on the roof of our institute's building (the Institute of Biogeochemistry and Pollutant Dynamics) in Zurich Switzerland on June 2015. The curve for each day of a week is shown in a different color. The integrals of the curves (over the entire week) are provided in the top right corner of each panel. The dates are provided on the top left corner of each panel. Data was collected by researchers from the Institute of Atmospheric and Climate Science (IAC) at ETH Zurich.

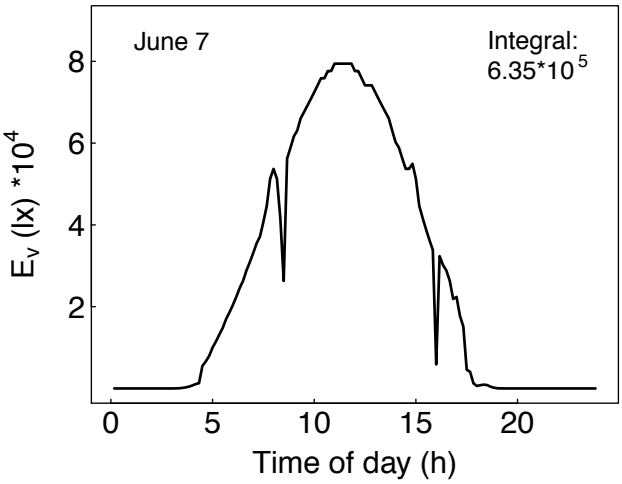

Figure 2.27. Illuminance data collected on the roof of our institute's building (the Institute of Biogeochemistry and Pollutant Dynamics) in Zurich Switzerland on June 7, 2015. The integral of the curve is provided in the top right corner. Data was collected by researchers from the Institute of Atmospheric and Climate Science (IAC) at ETH Zurich.

In summary, our experiments show that the decrease in enzymatic hydrolyzability of UV-irradiated PBAT correlates better to the increase in the cross-link density than to the decrease in the soluble PBAT mass fractions. Although swelling experiments provide insight as to the mass fraction that is present in a cross-linked state, they do not necessarily provide a correlation to how densely cross-linked—and thus how flexible—the polymer chains are in the network. For future studies assessing potential effects of photoirradiation of polymers on their enzymatic hydrolyzability, we therefore recommend quantifying the cross-link density by DMTA. Future research on PBAT-containing films may also assess whether light-induced changes in film surface properties or the formation of leachable photo-transformation products impact enzymatic hydrolysis.

2.4.6. HPLC-HRMS Analysis of Cross-linked Hydrolysis Products.

Given the importance of cross-linking density on enzymatic hydrolyzability, we aimed to identify the chemical nature of the formed cross-links. To this end, we compared

the enzymatic hydrolysis products of untreated PBAT films to those of films irradiated for 6 h per side. We found a chromatographic peak (retention time of 26.6 min) that was significantly larger among the hydrolysis products from UV-irradiated films than among those from untreated PBAT films (**Figure 2.28a**). Negative-ionization, full-scan HRMS at this elution time provided evidence for an $[M-H]^-$ ion of $C_{20}H_{18}O_8$ (*m/z*: exact 385.0929, found 385.0932) (**Figure 2.28b**).

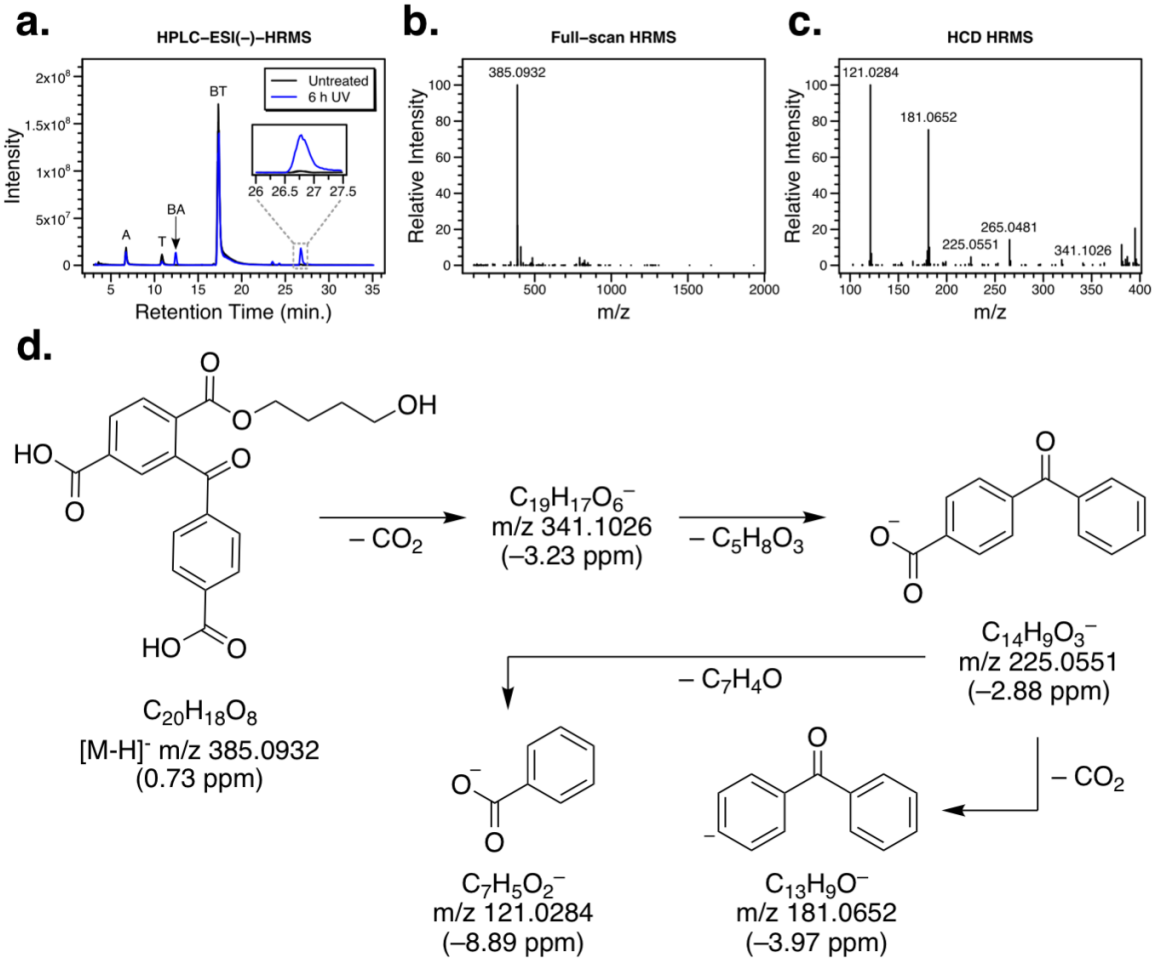

Figure 2.28. Analysis of the enzymatic hydrolysis products of poly(butylene adipate-co-terephthalate) (PBAT) by high-performance liquid chromatography coupled to high-resolution mass spectrometry (HPLC-HRMS). **a.** Base peak chromatograms for untreated and irradiated PBAT with peaks assigned to the hydrolysis products adipate (A), terephthalate (T), butanediol-adipate dyad (BA), and butanediol-terephthalate dyad (BT).

b. and **c.** Full-scan HRMS (panel b) and higher-energy collisional dissociation (HCD) $HRMS^2$ (panel c) of the peak eluting at 26.6 min. **d.** Proposed structures and fragmentation mechanisms for the observed ions in panels b and c.

Figure 2.28c and **Figure 2.28d** depict the associated higher-energy collisional dissociation (HCD) $HRMS^2$ and proposed structure annotations for the observed product. HCD $HRMS^2$ showed neutral losses of CO_2 suggestive of terminal carboxylate moieties. Furthermore, neutral loss of $C_5H_8O_3$ to give $C_{19}H_{17}O_6^-$ (*m/z:* exact 341.1031, found 341.1026) was consistent with cleavage of a butanediol benzoate ester. Finally, an intense fragment ion was observed with the sum formula $C_{13}H_9O^-$ (*m/z:* exact 181.0659, found 181.0652), which strongly supported the presence of a benzophenone substructure. To further support this assignment, we analyzed authentic 4-benzyolybenzoic acid by ESI(-)-HRMS, which gave the deprotonated pseudo-molecular ion (*m/z*: exact 225.0557, found 225.0556) and decarboxylated when treated with HCD to form the same benzophenone anion (*m/z*: exact 181.0659, found 181.0654, data not shown).

Taken together, these data provided strong evidence for the photochemical production of substituted benzophenone cross-links in PBAT films during their irradiation. This structure is also consistent with the findings of Kijchavengkul et al., who used Fourier-transform infrared (FTIR) spectroscopy to show that a signal corresponding to 1,2,4-trisubstituted benzene becomes increasingly prominent with increasing irradiation time of PBAT.[18] Based on our results, we propose that the cross-links between chains in PBAT are formed by the radical-based mechanism depicted in **Figure 2.29**. A similar mechanism has been proposed for the formation of benzophenone cross-links in terephthalate-containing polymers.[43]

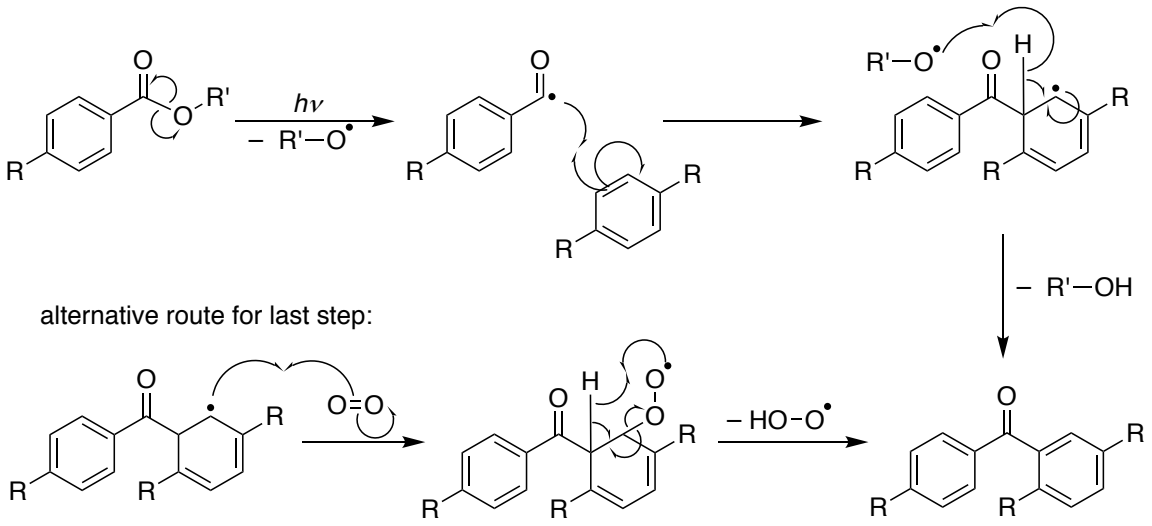

Figure 2.29. Proposed molecular mechanism for the photochemical formation of cross-links between chains in poly(butylene adipate-co-terephthalate) (PBAT).

2.4.7. Photostabilization of PBAT Films.

We have demonstrated that extensive photochemical cross-linking of non-photostabilized PBAT films impairs their enzymatic hydrolyzability. We therefore assessed the extent to which photostabilizers added to the PBAT films prevent the decrease in enzymatic hydrolyzability. In a proof-of-principle experiment, we solvent-casted PBAT films both with and without 2% (w/w) of the photostabilizer 2-(2-benzotriazolyl)-4-methylphenol (BMP) and studied whether its presence decreased the effect of UV irradiation on the enzymatic hydrolysis of PBAT (**Figure 2.30**). BMP was chosen because it is a commonly used photostabilizer for polymeric materials.[44,45] We found that FsC-mediated hydrolysis after UV irradiation (24 h per side) was indeed faster for photostabilized films than for those without BMP. Photochemical production of carboxylic acids was reduced—but not completely inhibited—by the addition of the photostabilizer to the films. Furthermore, enzymatic hydrolysis rates of untreated films were not significantly different between photostabilized and non-photostabilized films. These findings

demonstrate that the addition of photostabilizers to PBAT films can mitigate photochemical transformations while maintaining the hydrolyzability of PBAT by extracellular enzymes that may be present in natural soil environments.

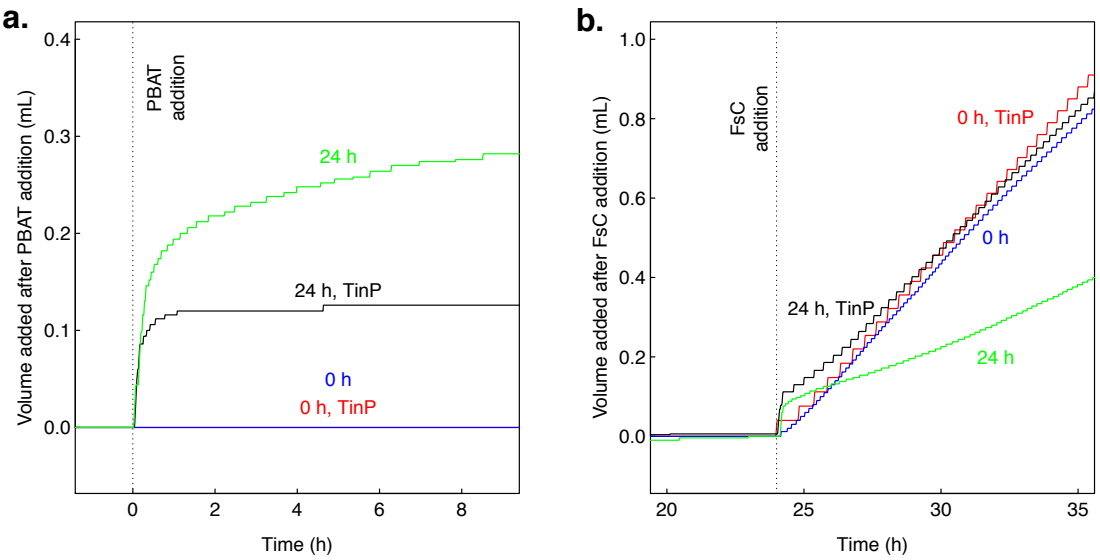

Figure 2.30. Hydrolysis of solvent-cast poly(butylene adipate-co-terephthalate) (PBAT) films—both irradiated and non-irradiated—by *Fusarium solani* cutinase (FsC). Both panels show the cumulative volume of potassium hydroxide solution that was added to keep pH 7 constant. **a.** Volume added after the addition of the solvent-casted PBAT films to the solution (addition is represented by the vertical dashed line at t=0 h). **b.** Volume added after the addition of FsC to the solution (addition is represented by the vertical dashed line at t=24 h). For the experiments represented by black and green curves, each side of the PBAT films was irradiated with UV light for 24 h. Red and blue curves represent dark controls. Films used for experiments represented by red and black curves contained 2% (w/w) of the photostabilizer 2-(2-benzotriazolyl)-4-methylphenol. Duplicate experiments exhibited similar rates, but were not included for the sake of clarity.

2.4.8. Implications.

We have demonstrated that UV-irradiation of a non-photostabilized, transparent film of PBAT, an aliphatic-aromatic co-polyester, results in cross-links between polyester chains that can severely decrease the ability of the film to be enzymatically hydrolyzed, which is a key step in polyester biodegradation. Our results highlight the relevance of considering photochemical reactions when studying the environmental fate of

biodegradable polyesters and the importance of employing photostabilizing additives to biodegradable polyesters.[46,47] Such additives not only aid in maintaining the desired material properties (e.g., preventing embrittlement) during the application of the material but also in ensuring that it remains biodegradable after its functional lifetime.

On a molecular level, we demonstrated that the enzymatic hydrolyzability of irradiated films negatively correlated with the density of cross-links formed between polyester chains. We attribute this trend to the decreased flexibility of polyester chains in a densely cross-linked network and thus the lower probability of polyester chains at the sample surface from readily accessing the active site of adsorbed esterases. Our findings extend the previously suggested hypothesis that enzymatic hydrolysis of polyesters is determined by the degree of flexibility of chains in the polyester: whereas previous work showed that crystalline regions in the polyesters have impaired chain flexibility and thus enzymatic hydrolyzability, we herein show that extensive cross-linking of polyester chains is a second characteristic that restrains chain flexibility and hence impairs enzymatic hydrolyzability.

Lastly, we showed that UV-irradiation results in the formation of benzophenone-containing structures in PBAT, suggesting that cross-links between PBAT chains are formed by a radical mechanism coupling two terephthalate units. We note that benzophenone moieties are well-known photosensitizers and that such cross-links may accelerate photochemical changes during long term UV exposure of these materials.[48,49] This mechanistic insight will help in assessing the performance of existing photostabilizers and guide the development of environmentally friendly photostabilizers for aliphatic-

aromatic polyesters. In future work, the environmental fate of photostabilizers and the formation of coupling products under field conditions need to be assessed.

2.5. References.

[1] Liu, E. K.; He, W. Q.; Yan, C. R. 'White revolution' to 'white pollution'— agricultural plastic film mulch in China. *Environ. Res. Lett.* **2014**, *9*, 1–4.

[2] Sander, M. Biodegradation of Polymeric Mulch Films in Agricultural Soils: Concepts, Knowledge Gaps, and Future Research Directions. *Environ. Sci. Technol.* **2019**, *53*, 2304–2315.

[3] Rillig, M. C. Microplastic in Terrestrial Ecosystems and the Soil? *Environ. Sci. Technol.* **2012**, *46*, 6453–6454.

[4] Gross, R. A. Biodegradable Polymers for the Environment. *Science* **2002**, *297* (5582), 803–807.

[5] Künkel, A.; Becker, J.; Börger, L.; Hamprecht, J.; Koltzenburg, S.; Loos, R.; Schick, M. B.; Schlegel, K.; Sinkel, C.; Skupin, G.; et al. Polymers, Biodegradable. In *Ullmann's Encyclopedia of Industrial Chemistry*; Wiley-VCH Verlag GmbH & Co. KGaA: Weinheim, 2016.

[6] Sintim, H. Y.; Flury, M. Is Biodegradable Plastic Mulch the Solution to Agriculture's Plastic Problem? *Environ Sci Technol* **2017**, *51*, 1068–1069.

[7] Tokiwa, Y.; Suzuki, T. Hydrolysis of polyesters by lipases. *Nature* **1977**, *270*, 76–78.

[8] Mueller, R.-J. Biological degradation of synthetic polyesters—Enzymes as potential catalysts for polyester recycling. *Process Biochem.* **2006**, *41*, 2124–2128

[9] Zumstein, M. T.; Schintlmeister, A.; Nelson, T. F.; Baumgartner, R.; Woebken, D.; Wagner, M.; Kohler, H.-P. E.; McNeill, K.; Sander, M. Biodegradation of synthetic polymers in soils: Tracking carbon into CO_2 and microbial biomass. *Science Advances* **2018**, *4*, eaas9024.

[10] Zumstein, M. T.; Kohler, H.-P. E.; McNeill, K.; Sander, M. Enzymatic Hydrolysis of Polyester Thin Films: Real-Time Analysis of Film Mass Changes and Dissipation Dynamics. *Environ. Sci. Technol.* **2016**, *50*, 197–206.

[11] Perz, V.; Bleymaier, K.; Sinkel, C.; Kueper, U.; Bonnekessel, M.; Ribitsch, D.; Guebitz, G. M. Substrate specificities of cutinases on aliphatic-aromatic polyesters and on their model substrates. *New Biotechnol.* **2016**, *33*, 295–304.

[12] Marten, E.; Müller, R.-J.; Deckwer, W.-D. Studies on the enzymatic hydrolysis of polyesters. II. Aliphatic–aromatic copolyesters. *Polym. Degrad. Stab.* **2005**, *88*, 371–381.

[13] Yoshida, S.; Hiraga, K.; Takehana, T.; Taniguchi, I.; Yamaji, H.; Maeda, Y.; Toyohara, K.; Miyamoto, K.; Kimura, Y.; Oda, K. A bacterium that degrades and assimilates poly(ethylene terephthalate). *Science* **2016**, *351*, 1196–1199

[14] Han, X.; Liu, W.; Huang, J.-W.; Ma, J.; Zheng, Y.; Ko, T.-P.; Xu, L.; Cheng, Y.-S.; Chen, C.-C.; Guo, R.-T. Structural insight into catalytic mechanism of PET hydrolase. *Nat. Commun.* **2017**, *8*, 1–6.

[15] Ronkvist, Å. M.; Xie, W.; Lu, W.; Gross, R. A. Cutinase-Catalyzed Hydrolysis of Poly(ethylene terephthalate). *Macromolecules* **2009**, *42*, 5128–5138.

[16] Herrero Acero, E.; Ribitsch, D.; Steinkellner, G.; Gruber, K.; Greimel, K.; Eiteljoerg, I.; Trotscha, E.; Wei, R.; Zimmermann, W.; Zinn, M.; et al. Enzymatic Surface Hydrolysis of PET: Effect of Structural Diversity on Kinetic Properties of Cutinases from Thermobifida. *Macromolecules* **2011**, *44*, 4632–4640.

[17] Araujo, R.; Silva, C.; O'Neill, A.; Micaelo, N.; Guebitz, G.; Soares, C. M.; Casal, M.; Cavaco-Paulo, A. Tailoring cutinase activity towards polyethylene terephthalate and polyamide 6,6 fibers. *J. Biotechnol.* **2007**, *128*, 849–857.

[18] Kijchavengkul, T.; Auras, R.; Rubino, M. Measuring gel content of aromatic polyesters using FTIR spectrophotometry and DSC. *Polym. Test.* **2008**, *27*, 55–60.

[19] Kijchavengkul, T.; Auras, R.; Rubino, M.; Ngouajio, M.; Fernandez, R. T. Assessment of aliphatic–aromatic copolyester biodegradable mulch films. Part I: Field study. *Chemosphere* **2008**, *71*, 942–953.

[20] Kijchavengkul, T.; Auras, R.; Rubino, M.; Ngouajio, M.; Fernandez, R. T. Assessment of aliphatic–aromatic copolyester biodegradable mulch films. Part II: Laboratory simulated conditions. *Chemosphere* **2008**, *71*, 1607–1616.

[21] Kijchavengkul, T.; Auras, R.; Rubino, M.; Alvarado, E.; Montero, J. R. C.; Rosales, J. M. Atmospheric and soil degradation of aliphatic-aromatic polyester films. *Polym. Degrad. Stab.* **2010**, *95*, 99–107.

[22] Longhi, S.; Czjzek, M.; Lamzin, V.; Nicolas, A.; Cambillau, C. Atomic resolution (1.0 A) crystal structure of Fusarium solani cutinase: stereochemical analysis. *J. Mol. Biol.* **1997**, *268*, 779–799.

[23] Gasteiger, E.; Hoogland, C.; Gattiker, A.; Duvaud, S.; Wilkins, M.; Appel, R.; Bairoch, A. *Protein identification and analysis tools on the ExPASy server*; Humana Press: Totowa, NJ, 2005; pp 571–607.

[24] Baker, P. J.; Poultney, C.; Liu, Z.; Gross, R.; Montclare, J. K. Identification and comparison of cutinases for synthetic polyester degradation. *Appl. Microbiol. Biotechnol.* **2011**, *93*, 229–240.

[25] Laszakovits, J. R.; Berg, S. M.; Anderson, B. G.; O'Brien, J. E.; Wammer, K. H.; Sharpless, C. M. p-Nitroanisole/Pyridine and p-Nitroacetophenone/Pyridine Actinometers Revisited: Quantum Yield in Comparison to Ferrioxalate. *Environ. Sci. Technol. Lett.* **2017**, *4*, 11–14.

[26] Marten, E.; Müller, R.-J.; Deckwer, W.-D. Studies on the enzymatic hydrolysis of polyesters I. Low molecular mass model esters and aliphatic polyesters. *Polym. Degrad. Stab.* **2003**, *80*, 485–501.

[27] Hiemenz, P. C.; Lodge, T. P. *Polymer Chemistry,* Second Edition; CRC Press, 2007.

[28] ASTM D 2765–16 Standard Test Methods for Determination of Gel Content and Swell Ratio of Cross-linked Ethylene Plastics, ASTM International, West Conshohocken, PA, 2016.

[29] ISO 10147:2011, Pipes and fittings made of crosslinked polyethylene (PE-X)—estimation of the degree of cross-linking by determination of the gel content, International Organization for Standardization: Geneva, Switzerland, 2011.

[30] Herrera, R.; Franco, L.; Rodríguez-Galán, A.; Puiggalí, J. Characterization and degradation behavior of poly(butylene adipate- co-terephthalate)s. *J. Polym. Sci. A Polym. Chem.* **2002**, *40*, 4141–4157.

[31] Sangroniz, A.; Sangroniz, L.; Aranburu, N.; Fernández, M.; Santamaria, A.; Iriarte, M.; Etxeberria, A. Blends of biodegradable poly(butylene adipate-co-terephthalate) with poly(hydroxi amino ether) for packaging applications: Miscibility, rheology and transport properties. *Eur. Polym. J.* **2018**, *105*, 348–358.

[32] Kuwabara, K.; Gan, Z.; Nakamura, T.; Abe, H.; Doi, Y. Crystalline/Amorphous Phase Structure and Molecular Mobility of Biodegradable Poly(butylene adipate-co-butylene terephthalate) and Related Polyesters. *Biomacromolecules* **2002**, *3*, 390–396.

[33] Rivaton, A.; Gardette, J.-L. Photo-oxidation of aromatic polymers. *Angew. Makromol. Chem.* **1998**, *261-262*, 173–188.

[34] Gewert, B.; Plassmann, M.; Sandblom, O.; MacLeod, M. Identification of Chain Scission Products Released to Water by Plastic Exposed to Ultraviolet Light. *Environ. Sci. Technol. Lett.* **2018**, *5*, 272–276.

[35] Tokiwa, Y.; Suzuki, T. Hydrolysis of Polyesters by Rhizopus delemar Lipase. *Agric. Biol. Chem.* **1978**, *42*, 1071–1072.

[36] Tokiwa, Y.; Suzuki, T. Hydrolysis of copolyesters containing aromatic and aliphatic ester blocks by lipase. *J. Appl. Polym. Sci.* **1981**, *26*, 441–448.

[37] Zumstein, M. T.; Rechsteiner, D.; Roduner, N.; Perz, V.; Ribitsch, D.; Guebitz, G. M.; Kohler, H.-P. E.; McNeill, K.; Sander, M. Enzymatic Hydrolysis of Polyester Thin Films at the Nanoscale: Effects of Polyester Structure and Enzyme Active-Site Accessibility. *Environ. Sci. Technol.* **2017**, *51*, 7476–7485.

[38] Zumstein, M. T.; Kohler, H.-P. E.; McNeill, K.; Sander, M. High-Throughput Analysis of Enzymatic Hydrolysis of Biodegradable Polyesters by Monitoring Cohydrolysis of a Polyester-Embedded Fluorogenic Probe. *Environ. Sci. Technol.* **2017**, *51*, 4358–4367.

[39] Tokiwa, Y.; Calabia, B. P.; Ugwu, C. U.; Aiba, S. Biodegradability of plastics. *Int. J. Mol. Sci.* **2009**, *10*, 3722–3742.

[40] Kijchavengkul, T.; Auras, R.; Rubino, M.; Selke, S.; Ngouajio, M.; Fernandez, R. T. Biodegradation and hydrolysis rate of aliphatic aromatic polyester. *Polym. Degrad. Stab.* **2010**, *95*, 2641–2647.

[41] Mandelkern, L. *Crystallization of Polymers*, Second Edition. Cambridge University Press: New York, 2004; Vol. 1.

[42] Yokouchi, M.; Sakakibara, Y.; Chatani, Y.; Tadokoro, H.; Tanaka, T.; Yoda, K. Structures of Two Crystalline Forms of Poly(butylene terephthalate) and Reversible Transition between Them by Mechanical Deformation. *Macromolecules* **1976**, *9*, 266–273.

[43] Tabankia, M. H.; Gardette, J.-L. Photo-oxidation of Block Copoly(Ether-Ester) Thermoplastic Elastomers: Part 2—Origins of the Photo-Yellowing. *Polym. Degrad. Stab.* **1987**, *19*, 113-123.

[44] Guillory, J. P.; Cook, C. F. Mechanism of stabilization of polypropylene by ultraviolet absorbers. *J. Polym. Sci., Part A-1: Polym. Chem.* **1971**, *9*, 1529–1536.

[45] Carlsson, D. J.; Wiles, D. M. The Photooxidative Degradation of Polypropylene. Part I. Photooxidation and Photoinitiation Processes. *J. Macromol. Sci., Polym. Rev.* **1976**, *14*, 65–106.

[46] Kijchavengkul, T.; Auras, R.; Rubino, M.; Selke, S.; Ngouajio, M.; Fernandez, R. T. Formulation selection of aliphatic aromatic biodegradable polyester film exposed to UV/solar radiation. *Polym. Degrad. Stab.* **2011**, *96*, 1919–1926.

[47] Souza, P. M. S.; Morales, A. R.; Sanchez, E. M. S.; Mei, L. H. I. Study of PBAT Photostabilization with Ultraviolet Absorber in Combination with Hindered Amine Light Stabilizer and Vitamin E, Aiming Mulching Film Application. *J. Polym. Environ.* **2018**, *15*, 125.

[48] Blossey, E. C.; Neckers, D. C. Concerning the use of polymer based photosensitizers. *Tetrahedron Lett.* **1974**, *15*, 323–326.

[49] Chinmayanandam, B. R.; Melville, H. W. Photosensitization of polymerization reactions. *Trans. Faraday Soc.* **1954**, *50*, 73–10.

Chapter 3. Renewable, Degradable, and Chemically Recyclable Cross-linked Elastomers*

* Reprinted (adapted) with permission from Brutman, J. P.; De Hoe, G. X.; Schneiderman, D. K.; Le, T.N.; Hillmyer, M. A. Renewable, Degradable, and Recyclable Cross-Linked Elastomers. *Ind. Eng. Chem. Res.* **2016**, *55*, 11097–11106.

3.1. Abstract

Most commercial elastomers, typified by vulcanized natural rubber, are cross-linked polymers and as such cannot easily be reprocessed or recycled. While some are derived from renewable resources, the majority are produced from petroleum feedstocks and do not easily degrade. In this study, renewable elastomers based on β-methyl-δ-valerolactone were produced using two different methodologies: 1) tandem copolymerization/cross-linking with a bis(6-membered cyclic carbonate) and 2) cross-linking of a linear poly(β-methyl-δ-valerolactone) homopolymer with a free-radical generator. The mechanical properties of these materials were investigated; tensile strengths of up to 12 MPa and elongations up to 2000% were observed. Inclusion of a filler (fumed silica) was used to enhance the performance of the elastomers without significant loss of elasticity with some composites exhibiting tensile strengths nearly double the neat elastomer. Aqueous degradation studies indicated that the materials were capable of degradation in acidic and basic conditions at 60 °C. Moreover, these cross-linked elastomers can also be chemically recycled, yielding monomer in high purity and yield (>91% and 93%, respectively).

3.2. Introduction

Cross-linked polymers (CPs) encompass almost a third of the synthetic polymer industry and are vital in a wide variety of products including tires, contact lenses, elastomers, adhesives, and foams.[1] While cross-linking confers a number of advantages, including high thermal stability and solvent resistance, this structure also prevents these materials from being reprocessed. Postconsumer CPs are consequentially disposed of in landfills or by incineration, leading to significant loss of value.[1] Additionally, the vast

majority of synthetic polymers—including CPs—are petroleum-derived and non-degradable. Their production and disposal is therefore unsustainable in the long term. In recent years, considerable effort has been devoted to the development of CPs that are recyclable, some of which are also renewable.[2,3,4,5,6,7,8]

Among the palate of renewable polymers, aliphatic polyesters are particularly attractive because they are easily synthesized and in many cases are also biodegradable and biocompatible.[9,10,11] In numerous previous examples, aliphatic polyesters have been used to prepare thermoplastic elastomers (TPEs) that mimic styrenic block polymers in both design and performance.[12,13,14,15,16,17,18,19,20,21,22] Conveniently, the thermal and mechanical properties of these TPEs can be easily tuned by altering the size and composition of the discrete polymer blocks. Unfortunately, TPEs typically have poor solvent resistance, low thermal stability, and often exhibit significant stress softening (known as the Mullins effect).[23] Finally, polyester TPEs often require rigorous reaction conditions to ensure proper morphology; variations in dispersity and the presence of adventitious initiators can result in a dramatic reduction of toughness.

These issues are often resolved by the use of CPs, as they exhibit both high thermal stability and solvent resistance. A number of methods have been developed for cross-linking polyesters to improve their thermal, physical, and mechanical properties. These methodologies frequently employ hydroxy-multifunctional polyesters, or polyesterols, such as poly(lactide) (PLA) and poly(ε-caprolactone) (PCL). Polyesterols can be cross-linked using condensation reactions or further functionalized and subsequently cross-linked.[6,24,25,26,27,28,29,30] As the polyesterols are synthesized by either step growth condensation or ring-opening transesterification polymerization (ROTEP), their reactive

groups are generally terminal. In theory, the coupling efficiency should not be influenced by molar mass; in practice, low molar mass ($M_n \leq 5$ kg mol^{-1} to end group) is often necessary to precisely target a balanced stoichiometry for the cross-linking reaction such that it reaches high conversion. As a result, the range of accessible molar masses between cross-links (M_x) is rather constrained. Improvements in the mechanical properties of CPs have been attributed to large M_x values. Most notably, ultimate elongation increases with M_x. Furthermore, higher M_x allows entanglements to form, which behave as transient physical cross-links; a lower molar mass between entanglements (M_e) in the constituent polymer will increase the number of physical cross-links, also improving the mechanical properties.[31]

Other strategies have been developed for polyesters to overcome these deficiencies. One method, tandem copolymerization/cross-linking, allows for direct conversion of monomers to CPs. Although this approach eliminates processing steps, it comes with its own challenges. For example, due to problems with solubility, high concentrations of bis(ε-caprolactone) cross-linkers (8 to 28 mol%) are often required, rendering it difficult to tune the mechanical properties of the CPs in a controlled manner.[32,33] Bis(6-membered cyclic carbonates) have been utilized at much lower loadings (1 mol%) when copolymerized directly with ε-caprolactone (CL), but this system likely suffered from reactivity differences as well.[34,35] The inclusion of trimethylene carbonate (50 mol%) allowed for lower concentrations of cross-linker (0.05 mol%) and resulted in an amorphous material; however, the mechanical properties of the resulting material are poor.

A second method that has been used to access tunable polyester elastomers is ROTEP of alkene-functionalized lactone comonomers with saturated aliphatic lactones (e.g., CL)

to produce statistical copolymers.[36,37,38] These copolymers can be cross-linked in subsequent steps using free radical or thiol-ene click reactions. While the properties of these CPs can be easily tuned, the alkene comonomers are often prohibitively expensive and/or challenging to synthesize on a large scale.[37] Alkene functionalized macrolactones are more economical, however, their polymerization may also require the use of enzymatic polymerization catalysts, which can be limiting.[38] Interestingly, free radical generators are capable of cross-linking fully saturated polyesters.[34,39,40,41,42] Typically, this involves the thermal cross-linking of the polyester with an organic peroxide. Though this allows for facile tuning of the mechanical properties, these studies have been confined to high glass transition temperature (T_g) and/or semi-crystalline materials, which are not ideal for elastomers. In fact, there is a dearth of literature on tough cross-linked amorphous, low T_g polyesters; preceding examples have indicated poor tensile properties due to limits on M_x dictated by the methodologies used.[26,27,43,44] Those with competitive properties generally have a T_g that is above –40 °C, limiting the scope of their potential applications.[27,33,35]

We have demonstrated that β-methyl-δ-valerolactone (MVL) can be produced renewably on a large scale and can be polymerized in the bulk to afford poly(β-methyl-δ-valerolactone) (PMVL).[17] The properties of amorphous PMVL (T_g = −52 °C and M_e = 4.3 kg mol^{-1}) make it an attractive polymer for use in a wide range of applications. For example, we have explored the use of PMVL in tough plastics, thermoplastic elastomers, soft polyurethane foams, and thermoplastic polyurethanes.[17,20,45] Furthermore, PMVL has been shown to depolymerize in the presence of catalyst, allowing for controlled recovery of pure monomer.[45]

Herein, we report the production cross-linked elastomers prepared from PMVL. We use two different synthetic strategies: tandem copolymerization/cross-linking reaction of MVL with a bis(6-membered cyclic carbonate) and cross-linking of linear PMVL with a free-radical generator. We investigate the impact of synthetic conditions and fumed silica incorporation on the mechanical properties of PMVL elastomers. Furthermore, we study the degradation of these materials in aqueous media. Finally, we show that these materials can be recycled to recover MVL in high purity and yield.

3.3. Experimental

3.3.1. Materials.

All reagents were purchased from Sigma-Aldrich (Milwaukee, WI) and were used as received unless otherwise stated. 1,5,7-triazabicyclodec-5-ene (TBD) was purified by vacuum sublimation (70 °C, 30 mTorr). Dichloromethane (DCM), tetrahydrofuran (THF), and methanol were purchased from Fisher Scientific (Hampton, NH); DCM and THF were purified via a GC-SPS-4-CM glass contour 800-L solvent purification system obtained from Pure Process Technologies (Nashua, NH). 3-Methyl-1,5-pentanediol was obtained from TCI (Portland, OR) and used without further purification. MVL was produced by one of two methods as described in previous studies and purified by fractional distillation (3X) over calcium hydride (72 °C, 1 Torr).[45,46] 5,5'-(oxybis(methylene))bis(5-ethyl-1,3-dioxan-2-one) (B6CC), a bis(6-membered cyclic carbonate), was also produced as described in a previous study and recrystallized from THF (3X).[7] Aerosil® R 812 was kindly provided by Evonik Industries (Parsippany, NJ). Rubber bands were purchased from the University

of Minnesota chemistry stockroom; they were manufactured in Thailand for Universal® (Deerfield, IL). All glassware was heated to 105 °C overnight prior to use.

3.3.2. Modified synthesis of MVL from 3-methyl-1,5-pentanediol[46]

3-Methyl-1,5-pentanediol (1 L, 974 g, 8.24 mol) and copper chromite (50 g, 0.16 mol, 2 mol%) were charged into a 2-L 3-neck round bottom flask fitted with a Dean-Stark apparatus, a thermometer, and a glass stopper. The apparatus was then attached to a bubbler filled with silicon oil. A heating mantle was used to heat the round bottom flask to 240 °C under vigorous stirring. The temperature of the reaction rapidly rose to 170 °C, followed by collection of water (*ca.* 5 mL) and an unknown organic liquid (*ca.* 5 mL). Following removal of these impurities, the reaction temperature rose rapidly to *ca.* 210-220 °C followed by evolution of H_2 gas. The reaction was allowed to continue for 20 h and then cooled. At this time the ^{1}H NMR spectrum of the solution indicated *ca.* 95% conversion of the diol. The crude product, a mixture of MVL monomer and PMVL polymer, was then purified by fractional distillation under reduced pressure.

First, a forerun was removed (1 Torr, 55-72 °C, 50 g) followed by a second fraction (1 Torr, 72-75 °C, 850 g). The higher boiling fraction was a clear, colorless liquid containing a minor amount of 4-methyl-3,4,5,6-tetrahydro-2H-pyran-2-ol. The concentration of this impurity in MVL was estimated to be ~0.2 mol% using the ^{1}H NMR signal corresponding to the methine proton at δ 5.3 ppm. To remove the lactol, the crude MVL was stirred with phosphorous pentoxide (5 g) at 120 °C for 12 h; this resulted in the dehydration of the lactol impurity and polymerization of the MVL (~60% conversion of MVL was observed) presumably with water or lactol as the initiating species. The solution of polymer in monomer was then distilled under the conditions previously described until

ca. 10% of the liquid remained in the pot. Analysis of the resulting MVL via ^{1}H NMR spectroscopy indicated that it no longer contained any lactol impurity, within the detection limit of the instrument used. To obtain high purity monomer, the MVL was then distilled two more times under reduced pressure from calcium hydride, each time discarding the first 5% of distillation liquid, to yield a clear a colorless liquid (65-75% yield).

To evaluate the monomer purity, test polymerizations were conducted in the bulk at room temperature using 0.1 mol% TBD as a catalyst in the absence of exogenous initiator. The molar mass of the resultant polymer is expected to depend on the concentration of adventitious initiators which can be roughly estimated via size-exclusion chromatography. For this work we classified the MVL as low purity if polymerization results in PMVL with M_n < 100 kg/mol, moderate purity if M_n >100 kg/mol, and high purity if M_n > 200 kg/mol. The copper chromite residue after the first distillation has been used in up to four successive reactions without significant/noticeable decreased in activity. ^{1}H NMR (500 MHz, $CDCl_3$; 25 °C): δ (ppm) = 4.40 [m, -O-*C*H$_2$-CH$_2$-, 1H], 4.25 [m, -O-*C*H$_2$-CH$_2$-, 1H], 2.66 [m, -CO-*C*H$_2$-CH(CH$_3$)-, 1H], 2.20 [m, -CO-*C*H$_2$-CH(CH$_3$)-, 1H], 2.03-2.13 [m, CO-CH$_2$-*C*H(CH$_3$)-CH$_2$- and -CO-*C*H$_2$-CH(CH$_3$)-, 2H], 1.9 [m, -CH(CH$_3$)-*C*H$_2$-CH$_2$-O, 1H], 1.55 [m, -CH(CH$_3$)-*C*H$_2$-CH$_2$-, 1H], 1.05 [d, -CH$_2$-CH(*C*H$_3$)-CH$_2$-, 3H].

3.3.3. Synthesis of a cyclic carbonate cross-linked PMVL (CC)

Under a nitrogen atmosphere, MVL (7.00 g, 61.4 mmol, high purity) was charged into a 20-mL scintillation vial along with varying amounts of B6CC (46 to 371 mg, 0.15 to 1.23 mmol, 0.25 to 2 mol% to MVL) and 1,4-benzenedimethanol (BDM, 0 to 19 mg, 0 to 0.14 mmol). The mixture was stirred until completely homogenous, then a solution of TBD in DCM (100 mg/mL, 85 μL solution, TBD = 0.1 mol% relative to MVL) was injected

using a gastight syringe. The polymerization solution was allowed to stir for *ca.*10 s and then poured into a Pyrex® petri dish (inner diameter = 90 mm). The contents of petri dish were allowed to cure overnight at room temperature under nitrogen (*ca.* 20 h) to ensure maximum conversion. The resulting elastomer was then removed from the dish and a 1 M solution of acetic anhydride and triethylamine in DCM (0.35 to 1.40 mL, *ca.* 5 eq relative to hydroxyl moieties or TBD if no BDM was used) was dripped over the top of the film via a syringe. The elastomer was allowed to sit in air for another 20 h and then placed in an oven under reduced pressure at 80–90 °C for 48 h to remove DCM, acetic anhydride, triethylamine, and residual MVL monomer. This process afforded a clear, colorless, and odorless cross-linked PMVL film (88 to 91% mass yield). Samples prepared using this method are named as CC-*X*-*Y*, where *X* and *Y* represent the mol% B6CC and the theoretical molar mass (kg mol^{-1}) if no cross-linking were to occur, respectively. For example, a sample with 1.00 mol% B6CC and a theoretical molar mass of 100 kg/mol based on the amount of BDM added (assuming 100% monomer conversion and no cross-linker added) would be denoted CC-1.00-100.

3.3.4. Synthesis of MVL homopolymer

Under a nitrogen atmosphere, MVL (100.00 g, 875 mmol, moderate purity) was charged into a 1-L round bottom flask with a Teflon® coated magnetic stir bar. A solution of TBD in DCM (1.22 mL, 100 mg TBD/mL DCM, 0.1 mol% TBD to MVL) was added to the monomer, then the flask was sealed with a rubber septum and the mixture was stirred for 16 hours. Following this, a 1 M benzoic acid solution in DCM was added (9 mL, 10 eq. benzoic acid to TBD) and the polymer solution was diluted with additional DCM to *ca.* 500 mL. Once the polymer was fully dissolved, the solution was precipitated into methanol

(5 L), then dried over a stream of nitrogen for 2 days, dried under vacuum at room temperature for 3 days, and finally dried in an oven under reduced pressure at 60–70 °C for 2 days. The resulting PMVL was a highly viscous, clear and, colorless (85-88% yield). ^{1}H NMR (500 MHz, $CDCl_3$; 25 °C): δ (ppm) = 4.13 [m, -O-*C*H_2-CH_2-, 2H], 2.34 [m, -CO-*C*H_2-CH(CH_3)-, 1H], 2.20 [m, -CO-*C*H_2-CH(CH_3)-, 1H], 2.10 [m, -CH_2-*C*H(CH_3)-CH_2-, 1H] 1.72 [m, -CH(CH_3)-*C*H_2-CH_2-, 1H], 1.55 [m, m, -CH(CH_3)-*C*H_2-CH_2-, 1H], 1.00 [d, -CH_2-CH(*C*H_3)-CH_2-, 3H]. RI-SEC ($CHCl_3$): M_n = 162 kg mol^{-1}, $Đ$ = 1.29. DSC: T_g = –52 °C. TGA: T_d (5% mass loss, Air) = 240 °C.

3.3.5. Production of peroxide cross-linked PMVL (PC) and PC-fumed silica composities (PC-FS)

PMVL homopolymer (2.00 g) and benzoyl peroxide (BPO, 20 to 100 mg, 1 to 5 wt%) were loaded into a twin-screw extruder (DSM Xplore 5 mL micro compounder; Geleen, Netherlands) at 70 °C (10 h half-life for BPO) and allowed to mix for 10 min before extruding a grayish yellow material (*ca.* 80% recovery). Composites were also prepared with 10, 20, or 30 wt% fumed silica (FS) fed into the extruder (2 wt% BPO relative to PMVL was used for all composites), yielding a colorless and translucent material. The homogenous polymer mixture was placed in a 5 cm (W) × 5 cm (L) × 0.05 cm (T) aluminum mold that was placed between two 12 cm x 12 cm aluminum plates with a thin Teflon® sheet (0.05 mm thick) over each plate. This was then placed in a press mold (Wabash MPI; Wabash, IN) at 150 °C and 3 tons of pressure for 10 min and rapidly cooled to room temperature over 5 min, affording a translucent, grayish yellow elastomer. In the presence of FS, the materials appeared colorless and translucent. Samples are named as PC-*Z*-FS*Q* where *Z* represents the wt% BPO relative to PMVL and *Q* represents wt% FS

fed into the extruder. For instance, a sample with 1 wt% BPO and 0 wt% FS would be denoted PC-1.0-FS0.

3.3.6. Depolymerization of CC-0.50-100 or PC-2.0-FS0

CC-0.50-100 or PC-2.0-FS0 (*ca.* 1.00 g cut into small pieces), stannous octoate (1 drop, *ca.* 20 mg), and pentaerythritol ethoxylate (1 drop, *ca.* 20 mg, M_n = 797 g/mol) were placed in a 10-mL round bottom flask equipped with a simple vacuum distillation apparatus. The mixture was heated to 150 °C overnight at 1 Torr, yielding a clear and colorless liquid (91% recovery for CC-0.50-100 and 93% for PC-2.0-FS0 after a mass correction for cross-linker was performed). The ^{1}H NMR spectrum of the distillate was identical to that of pure MVL.

3.3.7. Characterization Methods[6]

^{1}H NMR spectroscopy was performed on a 500 MHz Bruker Avance III HD with SampleXpress spectrometer (Billerica, MA). Solutions were prepared in 99.8% $CDCl_3$ (Cambridge Isotope Laboratories). All spectra were acquired at 20 °C with 64 scans and a 2 s delay. Chemical shifts are reported in ppm with respect to $CHCl_3$ (7.26 ppm).

Uniaxial tensile testing and hysteresis measurements were conducted using dogbone-shaped tensile bars (*ca.* 0.5 mm (T) × 3 mm (W) × 25 mm (L) and a gauge length of 14 mm for PC samples or 0.5 mm (T) × 5 mm × 38 mm (L) and a gauge length of 22 mm for CC samples). The samples were aged for 48 hours at 25 °C in a desiccator prior to testing. Tensile measurements were performed on a Shimadzu Autograph AGS-X Series tensile tester (Columbia, MD) at 25 °C with a uniaxial extension rate of 50 mm min^{-1}. Young's modulus (E) values were calculated using the Trapezium software by taking the slope of

the stress-strain curve from 0 to 10% strain. Reported values are the average and standard deviations of five replicates from the same sample. Twenty cycles were performed during hysteresis measurements to 67% strain at 50 mm min^{-1} and the energy loss was calculated by subtracting the area under the curve of the contraction from the area under the curve of the extension in each cycle. The residual strain was taken as the point at which the return cycle reached its minimum stress. All graphical representation of hysteresis data was smoothed using a 100-point adjacent-averaging smoothing function in Origin® data analysis software in order to remove noise.

Dynamic mechanical thermal analysis (DMTA) was performed on a TA Instruments RSA-G2 analyzer (New Castle, DE) using dog bone shape films (*ca.* 0.5 mm (T) × 3 mm (W) × 25 mm (L) and a gauge length of 14 mm). DMTA experiments were conducted in tension film mode, where the axial force was first adjusted to 0.2 N of tension (sensitivity of 0.01 N) to ensure no buckling of the sample. The proportional force mode was set to force tracking to ensure that the axial force was at least 100% greater than the dynamic oscillatory force. The strain adjust was then set to 30% with a minimum strain of 0.05%, a maximum strain of 5%, and a maximum force of 0.2 N in order to prevent the sample from going out of the specified strain range. A temperature ramp was then performed from –70 °C to 200 °C at a rate of 5 °C min^{-1}, with an oscillating strain of 0.05% and an angular frequency of 6.28 rad s^{-1}. The T_g was calculated from the maximum value of the loss modulus. The effective molar mass between cross-links ($M_{x,eff}$), which consists of contributions from cross-links and entanglements, was calculated using the storage modulus (E') at 25 °C and equation 1.

$$E'(T) = 3G'(T) = 3RT\nu_e = \frac{3\rho RT}{M_{x,eff}} \quad (1)$$

Where *E*' and *G*' are the storage and shear modulus respectively, *R* is the universal gas constant, *T* refers to the absolute temperature in the rubbery region (*ca.* 298 K), ν_e is the cross-link density, and ρ is the density of PMVL[17] (*ca.* 1.1 g cm^{-3}).

Differential scanning calorimetry (DSC) was conducted on a TA Instruments Discovery DSC (New Castle, DE). The instrument was calibrated using an indium standard. All samples were prepared using T-Zero hermetic pans (*ca.* 5 mg) under a N_2 purge of 50 mL min^{-1}. The samples were initially cooled to –80 °C and then heated to 100 °C at 10 °C min^{-1}. The samples were then cooled back to –80 °C at 10 °C min^{-1} and heated again to 100 °C at the same rate. Values for T_g were acquired at the mid-point of each transition in the second heating curve using the Trios® software. Thermogravimetric analysis (TGA) was performed on a TA Instruments Q500 (New Castle, DE) under air at a heating rate of 10 °C/min to 550 °C. A typical sample size was between 8-15 mg.

Solvent extraction experiments were performed by placing a small amount of cross-linked polymer (*ca.* 20 to 100 mg) into a 20-mL vial filled with DCM. The vial was then closed and stirred for 48 h before removing the solvent by gravity filtration. The recovered sample was dried under reduced pressure for 48 h at 20 mTorr, after which the sample was weighed and the gel percent was determined.

The hydrolytic degradation of the elastomers was investigated in accelerated conditions using 1 M aqueous solutions of NaOH or HCl at 60 °C as well as in biologically relevant conditions by using an aqueous phosphate-buffered saline (PBS, pH = 7.4) solution at 37 °C. Nine replicates of each cross-linked polymer sample were prepared (50

mg each). The replicates were immersed in triplicate in the aforementioned aqueous solutions in separate 20-mL scintillation vials and heated to their respective temperatures. The insoluble mass was recorded after removing each sample from the solution and patting it dry with a Kimwipe™, after which the sample was re-immersed in the same solution. Solutions were checked weekly with litmus paper to ensure their pH remained stable; none of the solutions showed pH variance by this method. The data presented in the plots of insoluble mass % (percentage of original mass) over time includes the averages and standard deviations of the triplicate samples in their respective medium.

Refractive index size exclusion chromatography (RI-SEC) was performed on an HP/Agilent 1100 series SEC at 35 °C using three successive PLgel Mixed C Columns and a PLgel 5 μm guard column with an HP 1047A RI detector (Santa Clara, CA). $CHCl_3$ was used as the mobile phase with an elution rate of 1 mL min^{-1}. The M_n and $Đ$ were determined based on a 10-point calibration curve using EasiCal™ polystyrene standards purchased from Agilent.

3.4. Results and Discussion

We first investigated PMVL elastomers synthesized using a tandem methodology (**Figure 3.1**). A bis(6-membered cyclic carbonate) was chosen as a cross-linker due to its high solubility in neat MVL, and also because it was anticipated that MVL and B6CC would have similar reactivity. The equilibrium monomer concentration of MVL is 90% at room temperature, thus we removed residual monomer post-polymerization prior to testing the material properties.[17]

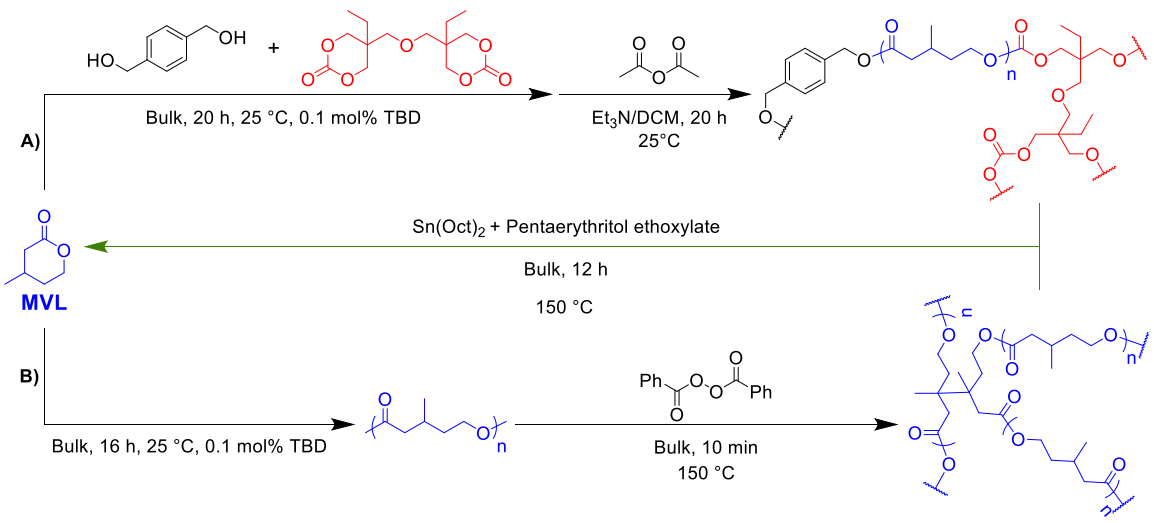

Figure 3.1. Synthesis of Cross-linked PMVLs.

As PMVL is able to depolymerize in the presence of catalyst, we scanned a variety of methodologies to deactivate TBD so that any residual monomer could be removed under reduced pressure and the material could operate at elevated temperatures without uncontrollable depolymerization. Guanidine-based organocatalysts are most commonly deactivated using a large excess of benzoic acid, yet we observed that the excess benzoic acid sublimed under vacuum and that the films depolymerized in these conditions. We posit that there remained an acid adduct of TBD that was capable of depolymerizing PMVL, as similar acid adducts of organocatalysts are capable of transesterification.[47] Additionally, deactivation of TBD through exposure to air generally took up to two weeks at ambient conditions, suggesting that diffusion of oxygen and carbon dioxide into the polymer is slow.

Therefore, we developed a method to convert the hydroxyl end-groups of PMVL to acetate groups; we suspected that acetylation chemistries would also deactivate the residual TBD. To accomplish this, we applied a solution of acetic anhydride and triethylamine in

DCM (5 equivalents with respect to hydroxyl moieties or TBD if no added initiator was added) to the surface of the film. After allowing the solution to diffuse through the film for 20 h, we subjected the material to reduced pressure to remove residual monomer. We found that this could be accomplished with mild heating (80 to 90 °C) without significant depolymerization. We observed that this end-capping strategy also increased the decomposition temperature of the polymers by 10–15 °C when compared with CC samples in which we deactivated TBD with two weeks of air exposure. The significant increase in the decomposition temperature can be attributed to the lack of hydroxyl groups, which are required for depolymerization of PMVL to occur via an "unzipping" mechanism. The amount of cross-linker did not appear to affect the mass recovery after excess monomer removal, nor was there a significant difference in their decomposition temperatures. On the other hand, the yield of an elastomer produced with no initiator was significantly lower (76%), likely owing to a slower polymerization rate; if the polymerization had been allowed to proceed, it is possible that a higher conversion could have been obtained. This indicates that some initiator is necessary to attain high monomer conversion in a reasonable period of time.

Once the monomer removal protocol was established, two sets of CC samples were investigated. At a fixed ratio of MVL to added BDM initiator (specifically, 876:1), we first varied the concentration of B6CC from 0.25 to 2.0 mol% relative to MVL. All of the materials with B6CC concentrations greater than or equal to 0.25 mol% gelled within 10 min. To ensure conversion of MVL monomer reached equilibrium, the films were allowed to cure overnight (*ca.* 20 h). After monomer removal, extraction experiments revealed high gel percentages that increased slightly with cross-linker content (**Table 3.1**). Next, we fixed

the ratio of MVL to B6CC (specifically at 100:1) and varied the amount of added initiator. No clear trend in gel percentage was observed when the concentration of initiator was varied. Furthermore, the T_g of all the materials was between –47 and –49 °C compared to –52 °C for PMVL homopolymer, implying that the molecular structure and amount of cross-linker did not significantly contribute to the thermal properties of the material.

Table 3.1. Tandem Cross-linking of PMVL with B6CC.

CC-*X*-*Y*[a]	Yield (%)[b]	Gel %[c]	*E'* (MPa)[c]	$M_{x,eff}$ (kg mol^{-1})[c,d]	$M_{x,theo}$ (kg mol^{-})[c,e]	T_g,DMTA (°C)[c,f]	T_g,DSC (°C)[c,h]	T_d (°C)[c,i]
CC-0.25-100	88	89	1.2	6.8	40	–49	–48	274
CC-0.50-100	91	95	1.8	4.5	21	–48	–48	262
CC-0.75-100	89	98	1.9	4.3	13	–48	–47	266
CC-1.0-100	89	99	2.1	3.9	10	–48	–48	269
CC-2.0-100	89	100	2.7	3.0	5.1	–47	–46	269
CC-1.0-NI[g]	76	98	2.8	2.9	10	–47	–47	268
CC-1.0-50	88	97	1.8	4.5	10	–48	–47	262
CC-1.0-75	89	96	1.6	5.1	10	–48	–47	263
CC-1.0-150	89	99	2.2	3.7	10	–48	–47	266
CC-1.0-200	89	100	1.7	4.8	10	–48	–47	262

[a] *X* is the mol% B6CC to MVL and *Y* is the theoretical M_n (kg mol^{-1}) assuming no cross-linker was added and 100% monomer conversion. [b] Recovery of mass after heating in a vacuum oven for 48 h at 80 °C. [c] Determined at 25 °C after removing residual monomer. [d] Determined using *E'* from DMTA in equation 1. [e] Calculated by dividing the mass of the polymer recovered by the moles of B6CC and assuming no contribution from entanglements. [f] Calculated from the maximum of the loss modulus. [g] NI stands for no initiator; M_n in the presence of no B6CC with high purity monomer is >200 kg mol^{-1} relative to polystyrene standards in RI-SEC with $CHCl_3$ as the mobile phase. [h] Taken on the second heating ramp at a rate of 10 °C min^{-1}. [i] Taken under air, defined as the temperature at which 5% mass loss is observed.

With the materials in hand, we sought to determine their tensile properties and compare them to those of a conventional elastomer, specifically vulcanized natural rubber (generic rubber band, Universal®, Deerfield, IL). Remarkably, CC-0.25-100 and CC-0.50-100 both exhibited significantly higher tensile strength and elongation than rubber bands

as well as a substantial strain hardening effect (**Figure 3.2**). Interestingly, CC-0.75-100 and CC-1.00-100 both showed uniaxial extension properties very similar to that of a rubber band, although their tensile strength drops significantly compared to the samples with lower cross-linker content. A second batch of analogous materials exhibited nearly identical properties, indicating this behavior is reproducible. As expected, increasing the amount of cross-linker resulted in a reduction of the strain at break while slightly increasing Young's modulus (**Figure 3.3** and **Table 3.2**). However, there was no clear correlation between cross-linker content and ultimate tensile strength (**Figure 3.3** and **Table 3.2**). Cross-linked rubbers often show a maximum in tensile strengths at intermediate cross-link densities which would initially explain this trend.[48] However, the increase in tensile strength for CC-2.0-100 does not correlate, suggesting other undeterminable factors may be involved.

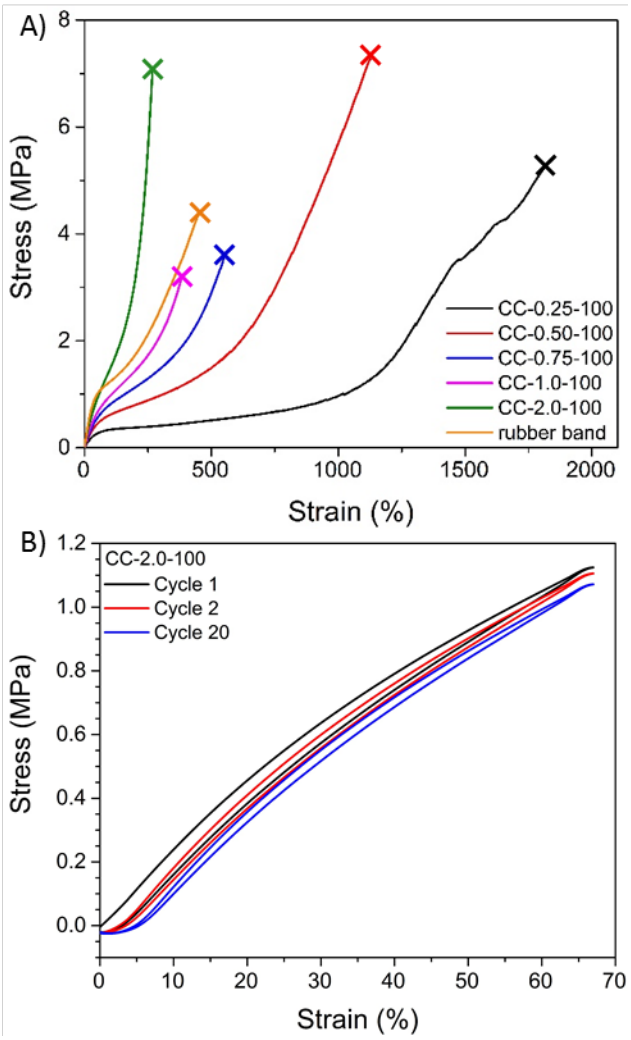

Figure 3.2. A) Representative tensile data for CC elastomers cross-linked with varying amounts of B6CC and keeping BDM constant. **B)** Representative hysteresis data for a cross-linked elastomer (CC-1.0-100).

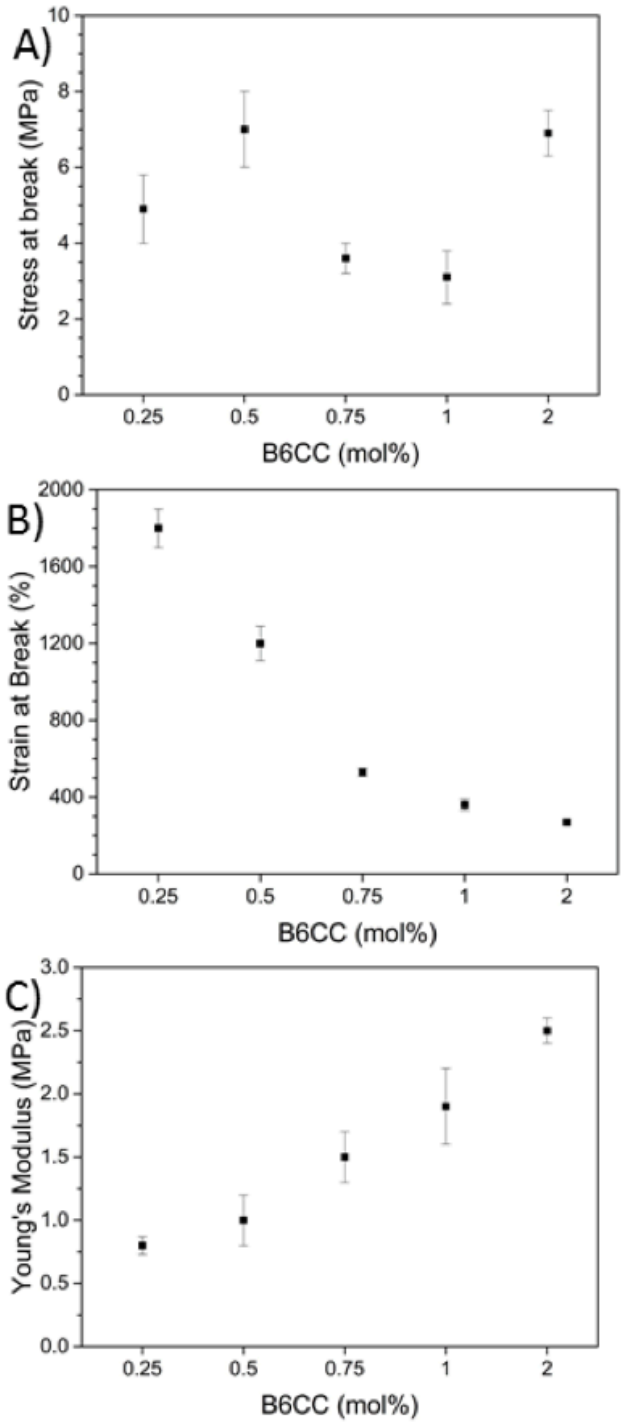

Figure 3.3. Tensile properties of PC while varying mol% of B6CC. The amount of initiator was kept at a constant amount such that $M_{n,theo}$ of PMVL would be 100 kg/mol if 100% conversion were achieved and no cross-linking occurred. **A)** Stress at break, **B)** strain at break, and **C)** Young's modulus.

Table 3.2. Tensile properties of CC materials.

CC-*X*-*Y*[a]	Stress at break (MPa)	Strain at break (%)	Young's modulus (MPa)[b]
CC-0.25-100	4.9 ± 0.9	1800 ± 100	0.80 ± 0.07
CC-0.50-100	7 ± 1	1200 ± 90	1.0 ± 0.2
CC-0.75-100	3.6 ± 0.4	530 ± 20	1.5 ± 0.2
CC-1.0-100	3.1 ± 0.7	360 ± 30	1.9 ± 0.3
CC-2.0-100	6.9 ± 0.6	270 ± 9	2.5 ± 0.1
CC-1.0-NI[c]	4 ± 1	350 ± 40	1.9 ± 0.1
CC-1.00-50	1.8 ± 0.1	300 ± 20	1.5 ± 0.3
CC-1.0-75	1.5 ± 0.2	220 ± 40	1.4 ± 0.1
CC-1.0-150	4 ± 1	390 ± 50	1.8 ± 0.2
CC-1.0-200	5 ± 1	390 ± 40	2.1 ± 0.3

[a] *X* is the mol% B6CC added and *Y* is the theoretical M_n (kg mol^{-1}) assuming no cross-linker was added. [b] Calculated from the slope of the stress-strain data from 0-10% strain. [c] NI stands for no initiator; M_n in the presence of no B6CC with high purity monomer is >200 kg mol^{-1}.

Hysteresis experiments revealed that the energy loss and residual strain per cycle decreased monotonically with B6CC content, with the sample containing 2.0 mol% B6CC exhibiting the least amount of hysteresis loss over 20 cycles (**Figure 3.2**, **Figure 3.4**, and **Table 3.3**). The results obtained via DMTA indicated a similar trend in the stiffness of the elastomers; samples with more cross-linker exhibited a higher plateau modulus (**Figure 3.5**). Samples with the least amount of cross-linker displayed a slightly negative sloping plateau modulus at temperatures above the T_g. This effect is likely due to dangling chain ends as this phenomenon has been seen previously in materials with high levels of this network defect.[49] The effective molar mass between cross-links ($M_{x,eff}$) of the materials was much lower than expected (**Table 3.1**); as the M_e of linear PMVL is 4.3 kg/mol, this result is likely due to inherent entanglements contributing to $M_{x,eff}$.[50] Therefore, it is also possible that the relaxation of transient entanglements within the network are also

contributing to the negatively sloping modulus exhibited by samples with low cross-linker content.

Table 3.3. Hysteresis energy loss and residual strain in CC and PC elastomers.

	Energy Loss (%)[a]			Residual Strain (%)[b]		
Sample Name	**Cycle 1**	**Cycle 2**	**Cycle 20**	**Cycle 1**	**Cycle 2**	**Cycle 20**
CC-0.25-100	51	46	53	6.8	8.7	17
CC-0.50-100	31	25	25	2.4	3.7	8.3
CC-0.75-100	19	14	12	4.9	6.4	9.2
CC-1.00-100	15	10	9.3	2.6	3.3	5.3
CC-2.00-100	7.9	4.9	4.0	0.9	1.9	2.2
CC-1.00-NI	19	14	12	1.9	6.1	10
CC-1.00-50	9.3	6.4	5.9	0.8	1.9	3.1
CC-1.00-75	9.9	6.6	5.7	0.1	0.5	2.4
CC-1.00-150	12	7.7	5.8	2.1	3.6	6.9
CC-1.00-200	13	8.0	5.8	1.4	2.8	6.8
PC-1.0-FS0	41	34	36	7.2	10	16
PC-2.0-FS0	22	16	15	4.1	5.4	8.5
PC-3.0-FS0	14	10	8.5	2.3	3.5	4.5
PC-4.0-FS0	11	6.7	5.8	2.1	2.9	3.5
PC-5.0-FS0	6.5	3.6	3.4	0.6	0.7	1.1
PC-2.0-FS10	21	16	15	3.3	4.1	6.3
PC-2.0-FS20	28	21	20	3.4	4.3	7.5
PC-2.0-FS30	43	32	20	5.0	6.9	11
Rubber Band	21	9.5	7.4	0.1	0.20	1.1

[a] Calculated by dividing the area under the contraction by the area under the extension.
[b] Determined as the point at which the contraction reaches a plateau stress.

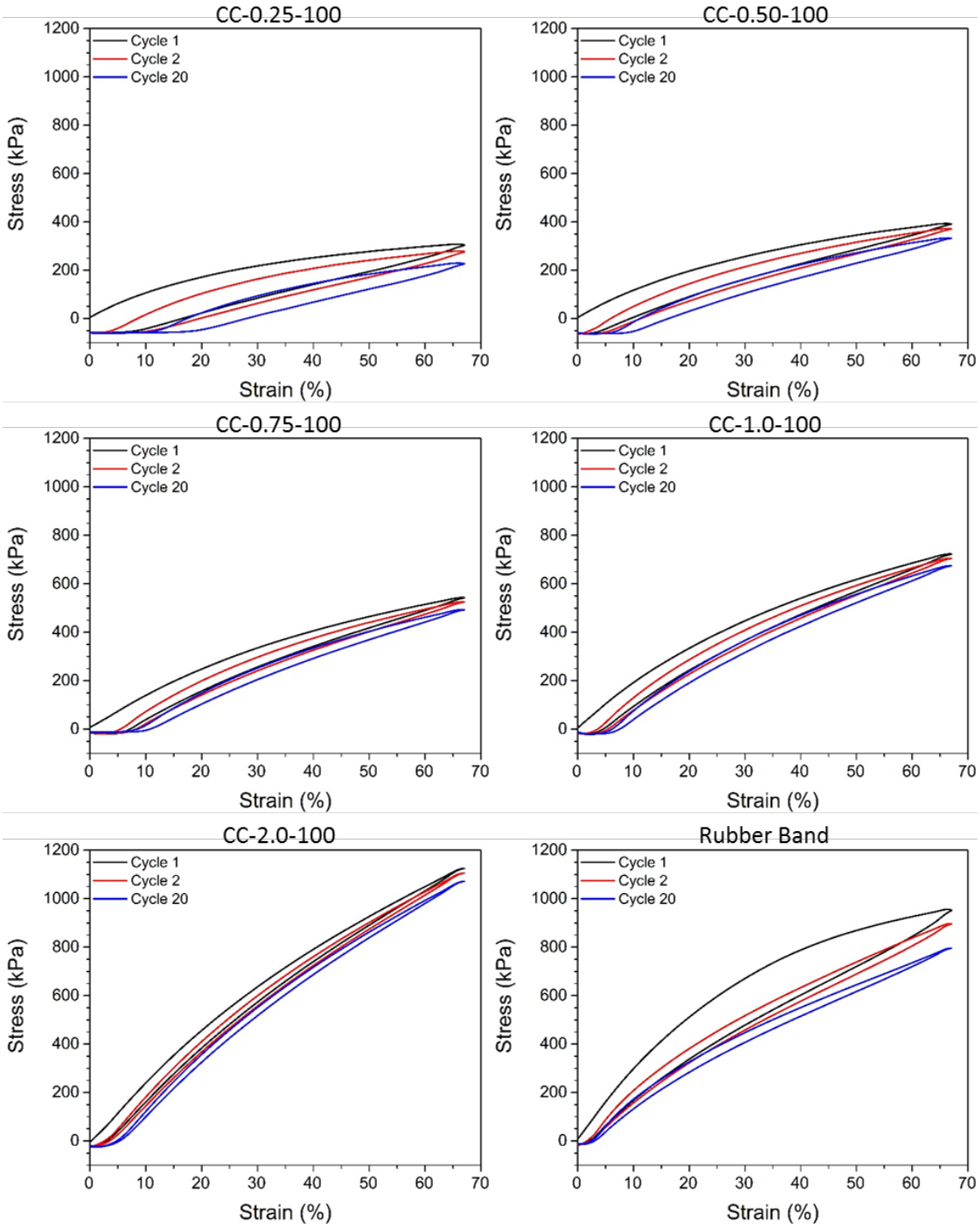

Figure 3.4. Cycles 1, 2, and 20 of the hysteresis of CC while varying B6CC. The amount of initiator was kept at a constant amount such that $M_{n,theo}$ of PMVL would be 100 kg/mol if 100% conversion were achieved in the absence of cross-linker. The hysteresis of a rubber band is also shown. Samples were stretched at a rate of 50 mm min^{-1}.

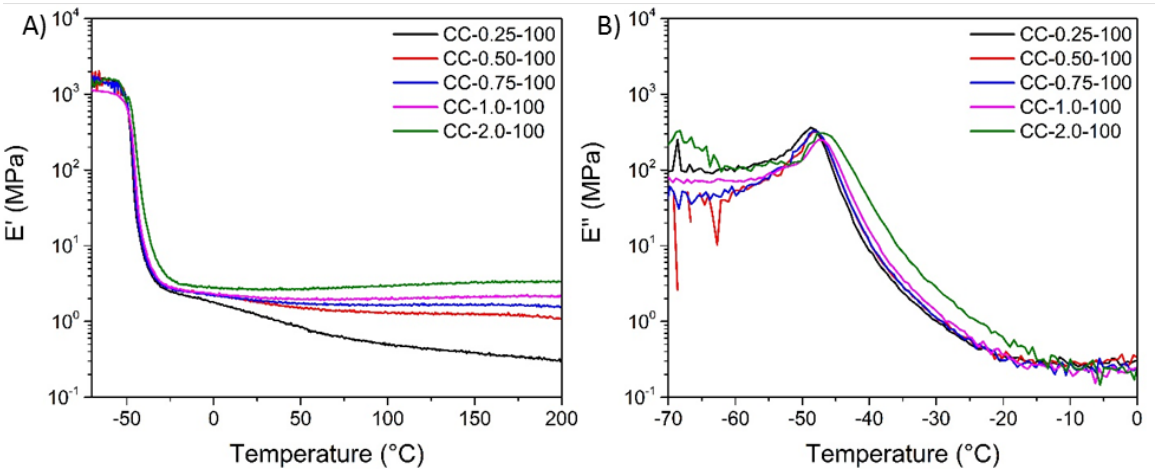

Figure 3.5. DMTA of CC while varying the mol% of B6CC. The amount of initiator was kept at a constant amount such that $M_{n,theo}$ of PMVL would be 100 kg/mol if 100% conversion were achieved and no cross-linking occurred. **A)** Storage modulus (*E'*) and **B)** loss modulus (*E''*). Samples were measured from –70 to 200 °C at a strain rate of 0.05% and a frequency of 1 Hz.

We next tested the set of materials prepared at fixed B6CC content with varying amounts of initiator. Uniaxial extension tests revealed that increasing the amount of initiator caused the material to lose significant toughness (**Table 3.2**, **Figure 3.6,** and **Figure 3.7**), though no significant change in hysteresis loss was observed (**Figure 3.8** and **Table 3.3**). We hypothesize that the loss of toughness is due to an increase in network defects from a higher amount of active initiation sites; network defects can cause a significant reduction in mechanical properties because the applied stress will be localized rather than equally divided among the strands in the network.[30] Furthermore, the absence of initiator did not produce a more desirable material, thus, the addition of some initiator is preferred to obtain higher mass recovery after monomer removal high conversion of monomer.

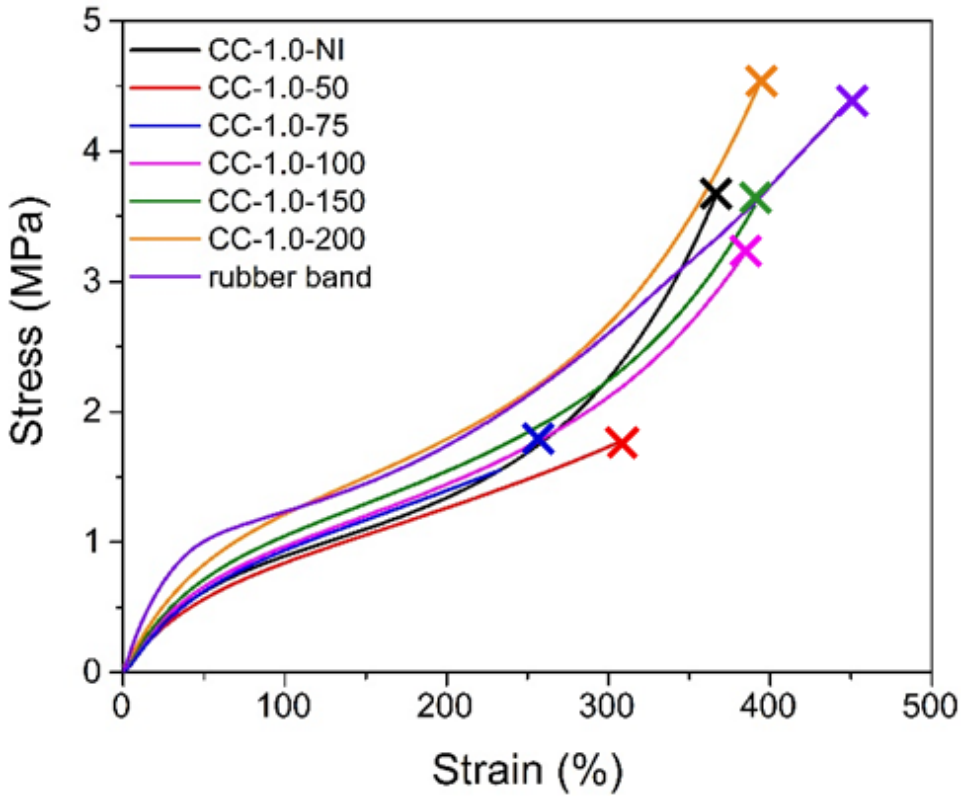

Figure 3.6. Representative tensile data showing the influence of varying amounts of BDM, while keeping B6CC constant, on tensile properties.

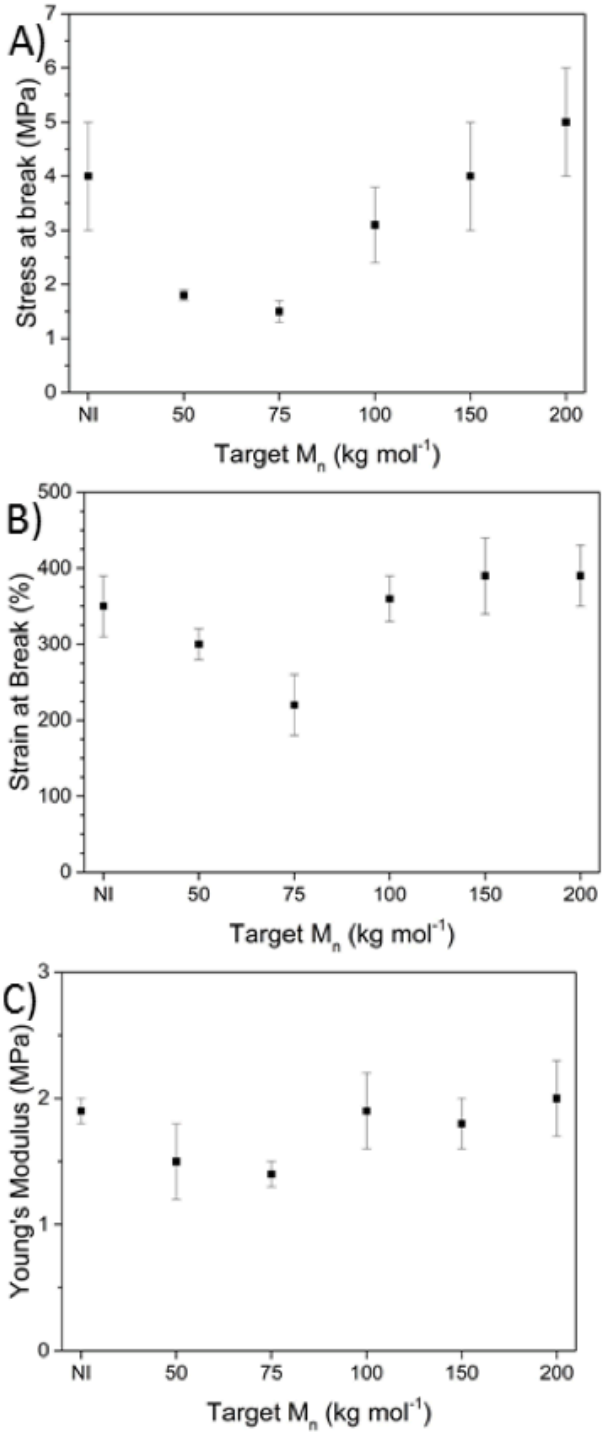

Figure 3.7. Tensile properties of CC while varying target M_n while keeping mol% of B6CC fixed. Target M_n is determined by calculating the theoretical M_n of the polymer assuming no cross-linker were added and 100% conversion of monomer. **A)** Stress at break, **B)** strain at break, and **C)** Young's modulus.

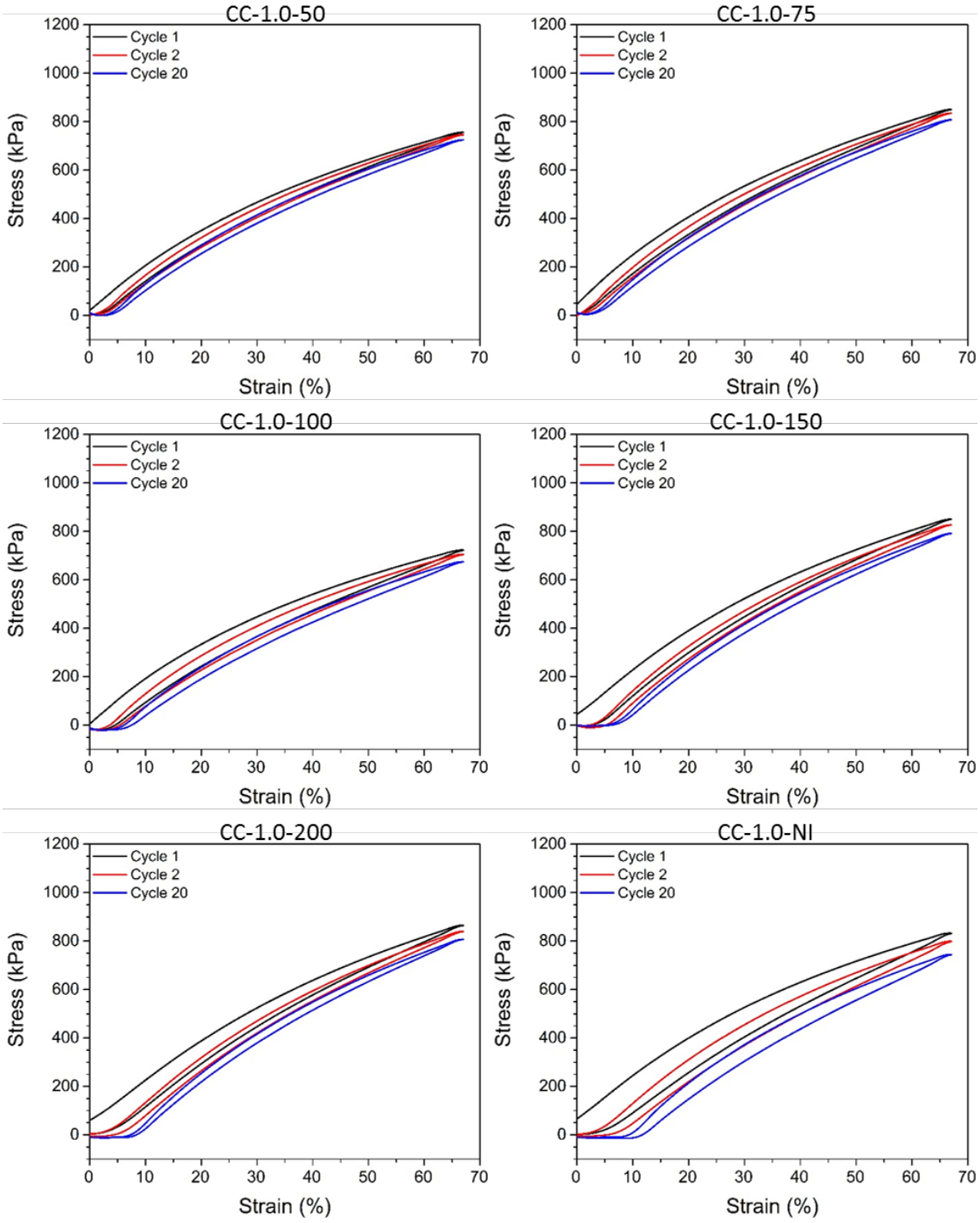

Figure 3.8. Cycles 1, 2, and 20 of the hysteresis of CC while varying amount of BDM and keeping a constant 1 mol% B6CC. Samples were stretched at a rate of 50 mm min^{-1}.

Neglecting the impact of reactivity ratio differences, if the ratio of MVL to BDM is fixed, M_x should increase with a decreasing amount of B6CC in the initial feed because less tetrafunctional junctions will be formed. On the other hand, M_x should not vary significantly if the ratio of MVL to BDM is varied as BDM is difunctional and will not introduce cross-link junctions. Indeed, the plateau modulus and $M_{x,eff}$ increase as the amount of B6CC is decreased, whereas no clear trend is seen when varying the amount of BDM (**Figure 3.9** and **Table 3.1**).

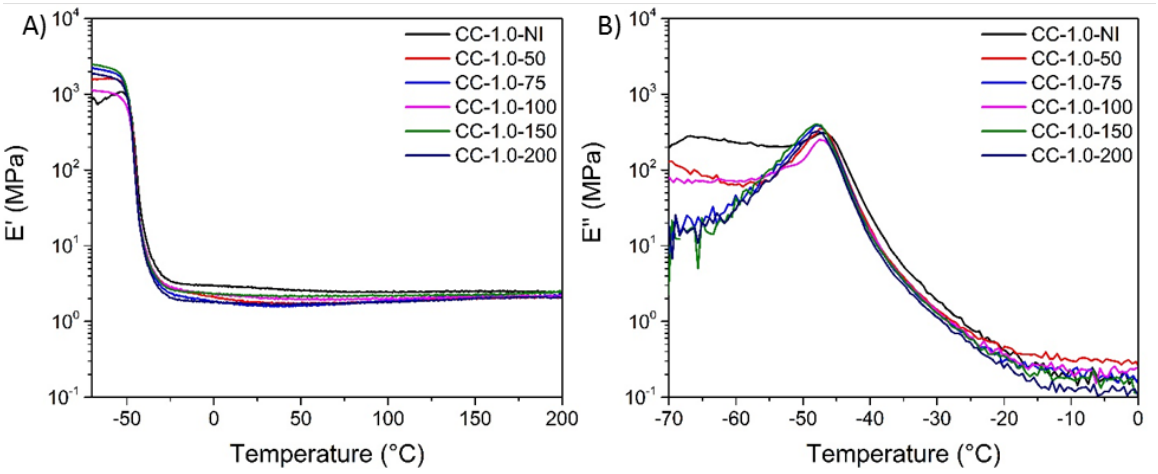

Figure 3.9. DMTA of CC while varying the initiator loading and maintaining a 1 mol% B6CC. **A)** Storage modulus (*E'*) and **B)** loss modulus (*E''*). Samples were measured from –70 to 200 °C at a strain rate of 0.05% and a frequency of 1 Hz.

In addition to the tandem copolymerization/cross-linking strategy, we also explored a sequential approach where linear PMVL homopolymer was synthesized and cross-linked using a free radical generator (**Figure 3.1**). This was accomplished by melt blending linear PMVL with BPO in a twin-screw extruder at 70 °C and cured in a press mold at 150 °C. We fixed the initial molar mass of the PMVL prepolymer (M_n = 162 kg mol^{-1}) and varied the mass percent of BPO in the blend. In some cases, we also added a hydrophobic fumed

silica filler (Aerosil® R 812). The characteristics of these samples and blends are summarized in **Table 3.4**.

Table 3.4. Post-polymerization Cross-linking of PMVL with BPO.

PC-*Z*-FS*Q*[a]	Gel %	FS (%)	*E'* at 25 °C (MPa)	$M_{x,eff}$ (kg mol^{-1})[b]	$T_{g\ DMTA}$ (°C) [c]	$T_{g\ DSC}$ (°C)[d]	T_d (°C)[e]
PC-1.0-FS0	76	0	1.4	5.8	–50	–50	264
PC-2.0-FS0	93	0	1.7	4.8	–49	–50	244
PC-3.0-FS0	95	0	1.8	4.5	–50	–49	246
PC-4.0-FS0	96	0	2.1	3.9	–50	–49	242
PC-5.0-FS0	97	0	2.1	3.9	–49	–48	241
PC-2.0-FS10	96	9	2.4	3.4	–49	–50	256
PC-2.0-FS20	95	16	2.9	2.8	–50	–51	259
PC-2.0-FS30	95	25	5.0	1.6	–48	–51	256

[a]*Z* is the wt% BPO with respect to PMVL and FS*Q* is the wt% fumed silica added with respect to PMVL; all samples produced with 162 kg mol^{-1} PMVL relative to polystyrene standards in RI-SEC with $CHCl_3$ as the mobile phase. [b]Calculated using *E'* from DMTA in equation 1. [c]Determined from the maximum of the loss modulus from DMTA. [d]Taken on the second heating ramp at a rate of 10 °C min^{-1}. [e]Taken under air, defined as the temperature at which 5% mass loss is observed.

To our knowledge, the exact mechanism by which saturated polyesters cross-link in the presence of radicals has not been studied. Hermans and Eyk suggest that the reaction of cyclohexane with BPO produces carbon radicals capable of a variety of reactions, most commonly resulting in dimers and other oligomers.[51] The tertiary carbon within the backbone of PMVL is the most stable position for carbon radicals, and thus, we assume that the longer-lived radicals at the tertiary carbons allow for a more efficient reaction than at the methylene units along the backbone. Indeed, the PC elastomers exhibited higher gel fractions when compared to PCL cross-linked with BPO, which contains no tertiary carbons.[41]

The reaction of PMVL with BPO did not afford a high degree of cross-linking at 0.1 and 0.5 wt% of BPO. PC elastomers prepared with 2 and 3 wt% BPO exhibited very desirable tensile properties (**Figure 3.10**, **Figure 3.11**, and

Table 3.5) and outperformed all CC samples. At BPO loadings of 4 and 5 wt%, the materials began to drastically lose toughness, exhibiting significant decreases in tensile strength and elongation; furthermore, these samples no longer exhibited significant strain hardening. Indeed, this phenomenon has previously been observed with vulcanized rubber and has been attributed to variations in the viscoelastic properties of the material rather than a reduction in its inherent strength.[48] However, Smith and Chu posit that no simple correlation can be attributed to this occurrence as tensile failure depends on a variety of factors.[52] All of the PC samples exhibited a grayish yellow discoloration. We surmise that the yellow discoloration in the absence of FS is due to slight oxidative degradation while the gray discoloration is due to impurities attained in the extruder. Indeed, samples prepared by solvent casting in DCM also had a yellow discoloration, however, no gray discoloration was observed. No significant difference in mechanical or thermal properties were observed between samples prepared by solvent casting and extrusion.

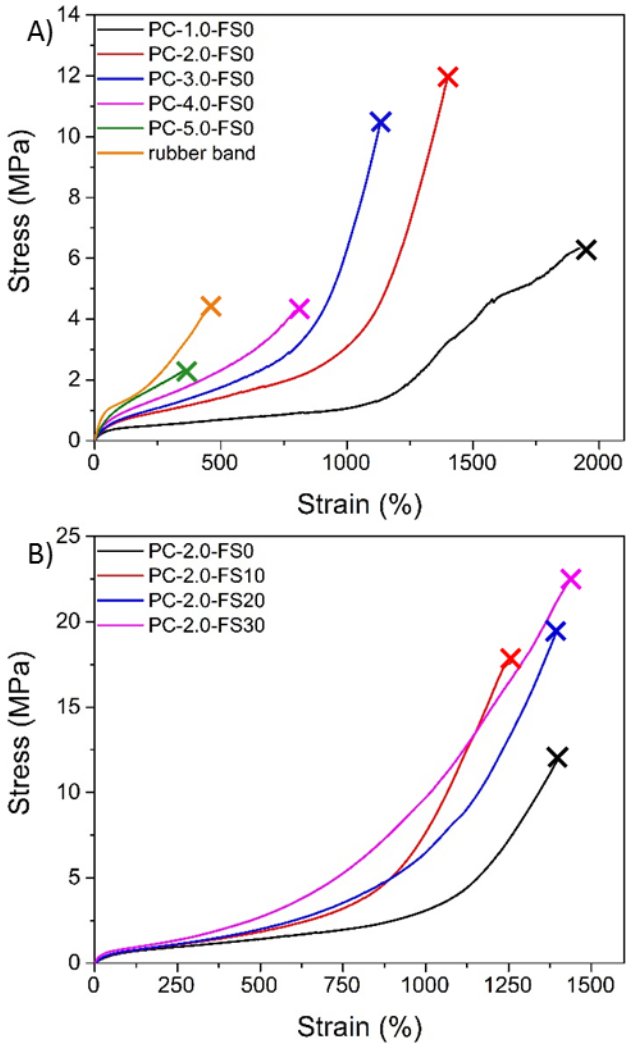

Figure 3.10. A) Representative tensile data for PC elastomers and a commercially available generic rubber band. The 1 wt% BPO sample (black line) begins to tear near the grip above 1500% strain, making the observable tensile strength at break lower than its actual value. **B)** Tensile data for PC-FS composites prepared with 2 wt% BPO relative to the mass of PMVL.

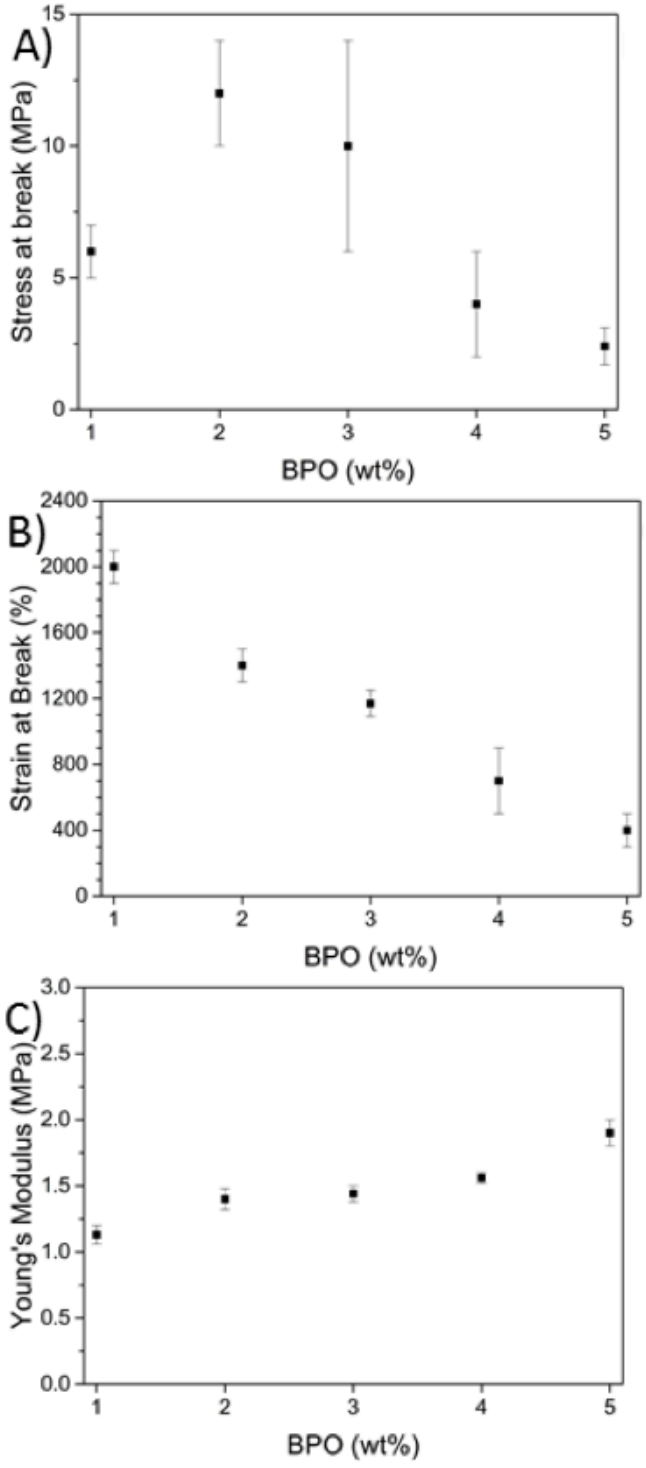

Figure 3.11. Tensile properties of PC while varying wt% of BPO: **A)** Stress at break, **B)** strain at break, and **C)** Young's modulus.

Table 3.5. Tensile properties of PC and PC-FS materials.

PC-*Z*-FS*Q*[a]	Stress at break (MPa)	Strain at break (%)	Young's modulus (MPa)[a]
PC-1.0-FS0	6 ± 1	2000 ± 100	1.13 ± 0.07
PC-2.0-FS0	12 ± 2	1400 ± 100	1.40 ± 0.08
PC-3.0-FS0	10 ± 4	1170 ± 80	1.44 ± 0.06
PC-4.0-FS0	4 ± 2	700 ± 200	1.56 ± 0.04
PC-5.0-FS0	2.4 ± 0.7	400 ± 100	1.9 ± 0.1
PC-2.0-FS10	18 ± 2	1300 ± 80	1.7 ± 0.2
PC-2.0-FS20	19 ± 2	1400 ± 100	1.8 ± 0.3
PC-2.0-FS30	22 ± 5	1400 ± 100	2.2 ± 0.2

[a] *Z* is the wt% BPO with respect to PMVL and FS*Q* is the wt% fumed silica added with respect to PMVL; all samples produced with 162 kg mol^{-1} PMVL relative to polystyrene standards in RI-SEC with $CHCl_3$ as the mobile phase. [b] Calculated from the slope of the stress-strain data from 0-10% strain.

Similarly to the CC elastomers, the radically cross-linked materials exhibited higher plateau moduli and better hysteresis recovery when the loading of BPO was increased (**Figure 3.12**, **Figure 3.13**, **Table 3.3**, and **Table 3.4**). At low BPO loading, we also observe a negatively sloping plateau modulus, similar to CC samples with low B6CC loading, which we attributed dangling chain ends[49] and the relaxation of transient entanglements within the network. The large increase in tensile strength from CC to PC was not entirely expected. We hypothesize that the difference in reactivity ratios between MVL and B6CC may have resulted in more network defects and a less uniform distribution of cross-links than in the PC elastomers. The radicals formed in the production of PC samples should theoretically have an equal probability of reacting with each repeat unit, which would result in a more uniform distribution of cross-links. As previously discussed, an applied force is more evenly dispersed in materials with evenly distributed cross-links,

than in those with more network defects; as a result, the more uniform materials should be significantly stronger.[30]

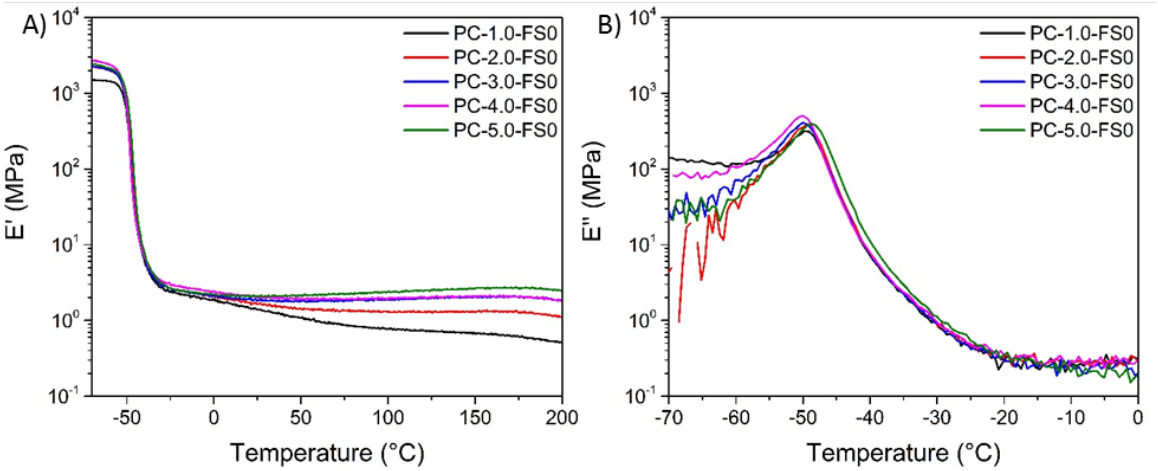

Figure 3.12. DMTA of PC while varying BPO wt%. **A)** *E'* and **B)** *E"*. Samples were measured from –70 to 200 °C at a strain rate of 0.05% and a frequency of 1 Hz.

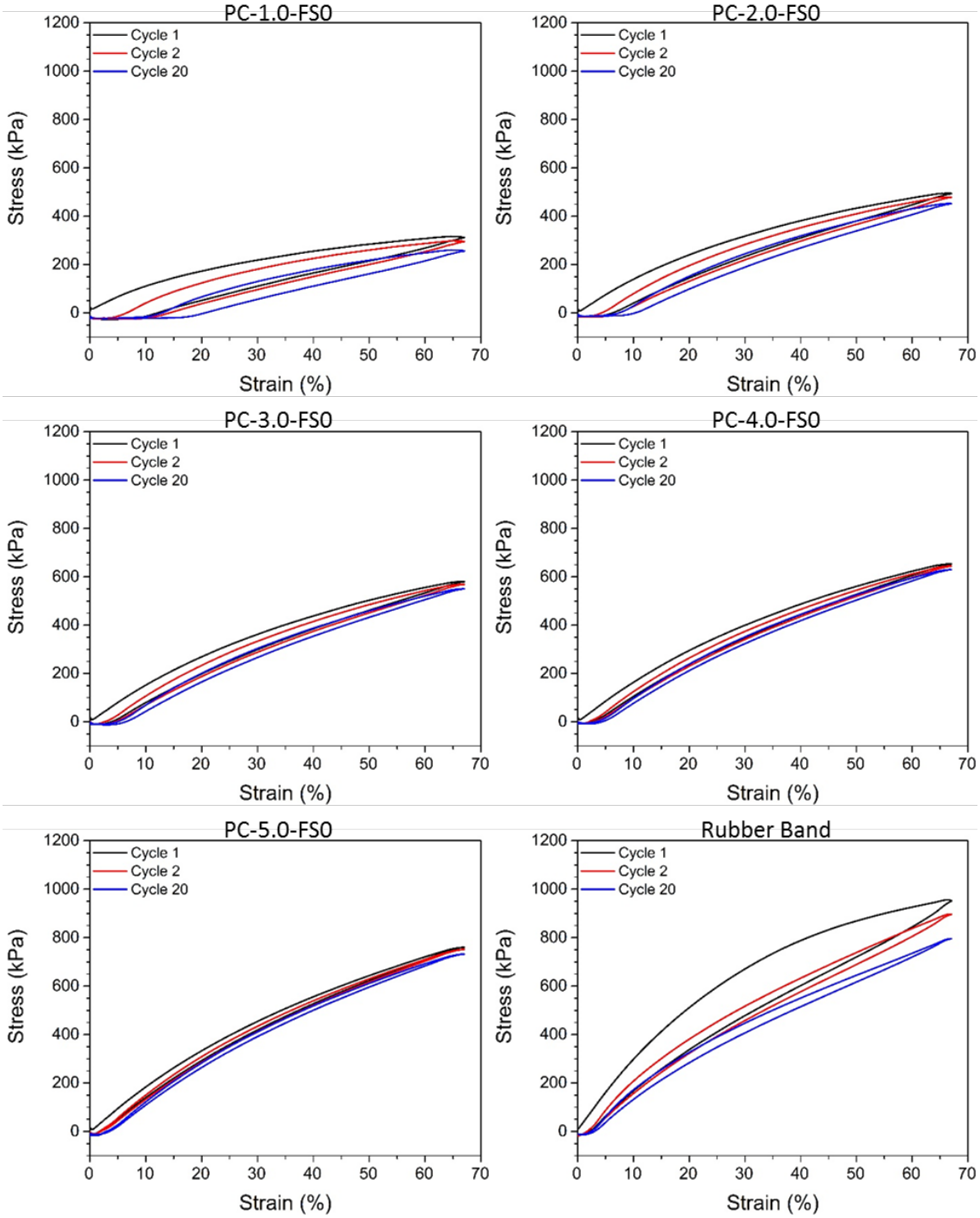

Figure 3.13. Cycles 1, 2, and 20 of the hysteresis of PC while varying the amount of BPO as well as a rubber band. Samples were stretched at a rate of 50 mm min^{-1}.

In an attempt to further improve the properties of the PMVL elastomers and to reduce the total cost of the elastomer, we prepared composites containing fumed silica, Aerosil® R 812.[53] We recently demonstrated that this FS could be homogenously dispersed in cross-linked hydrogenated polyolefins and also impart dramatic improvements in the mechanical properties.[54] Although we also attempted to produce filler reinforced materials using both the tandem cross-linking strategy, we observed that TBD catalyst used for the copolymerization reaction was intolerant of the FS. However, we found that FS reinforced elastomers could easily be prepared using the sequential radical melt blending route. For all samples, the BPO loading was fixed at 2 wt% with respect to PMVL, and blends containing 10 to 30 wt% FS were prepared. The TGA data indicated that in all cases the incorporation of FS into the polymer matrix during twin-screw extrusion was slightly lower than the feed amount (**Table 3.4**). Since the TGA of Aerosil® R 812 exhibited no mass loss up to 550 °C, we believe this minor discrepancy is due to inefficient extrusion rather than FS degradation, loss of water, or volatile small molecules adsorbed to the surface of the filler.

As expected, the mechanical properties of the PC elastomers improved dramatically when blended with FS (**Figure 3.10**, **Figure 3.14**, and

Table 3.5). The tensile strengths of the composites were improved by 50 to 83% relative to the neat elastomer and the elongation at break remained nearly constant at all filler loadings. Furthermore, the Young's modulus increased from 1.4 to 2.2 MPa when 25 wt% FS was incorporated. This significant stiffening effect from the FS was also observed by DMTA; the plateau modulus rose from 1.7 to 5.0 MPa when 25 wt% FS was incorporated (**Figure 3.15** and **Table 3.4**). As we anticipated, increasing the amount of FS

filler also increased the extent of the Mullins effect observed during hysteresis (**Figure 3.16** and **Table 3.3**). Even at 9 wt% incorporation of FS, the appearance of the resulting elastomer was colorless and translucent in contrast to the samples in the absence of FS which were a grayish yellow color. It is likely that the FS behaves as a white dye in the materials.

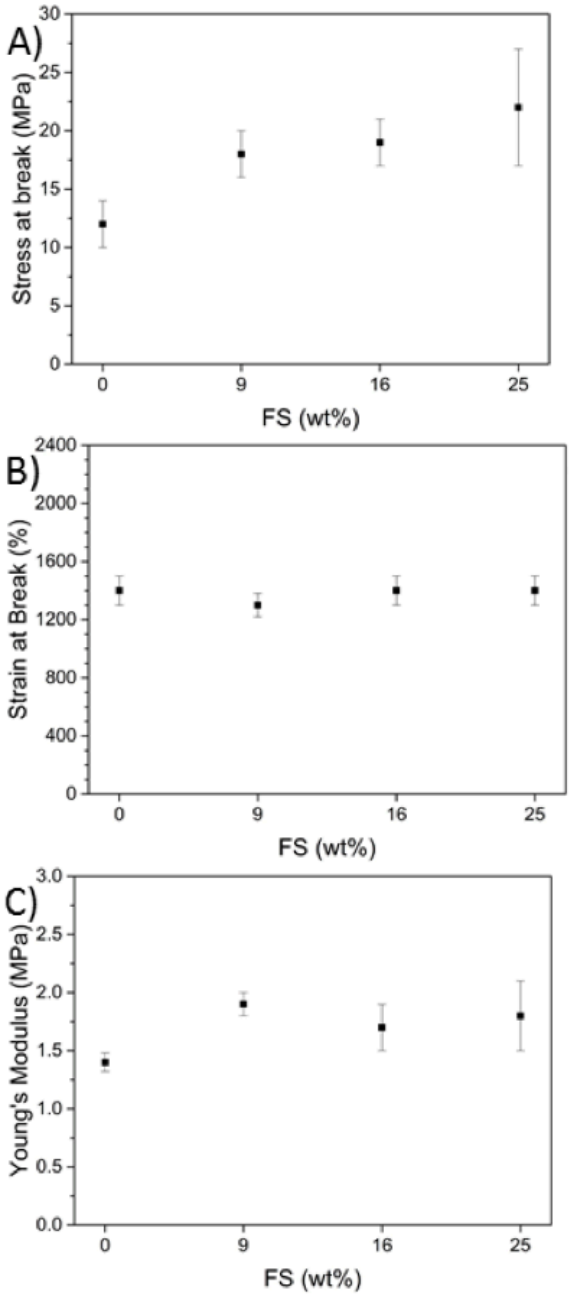

Figure 3.14. Tensile properties of PC-FS composites. **A)** Stress at break, **B)** strain at break, and **C)** Young's modulus.

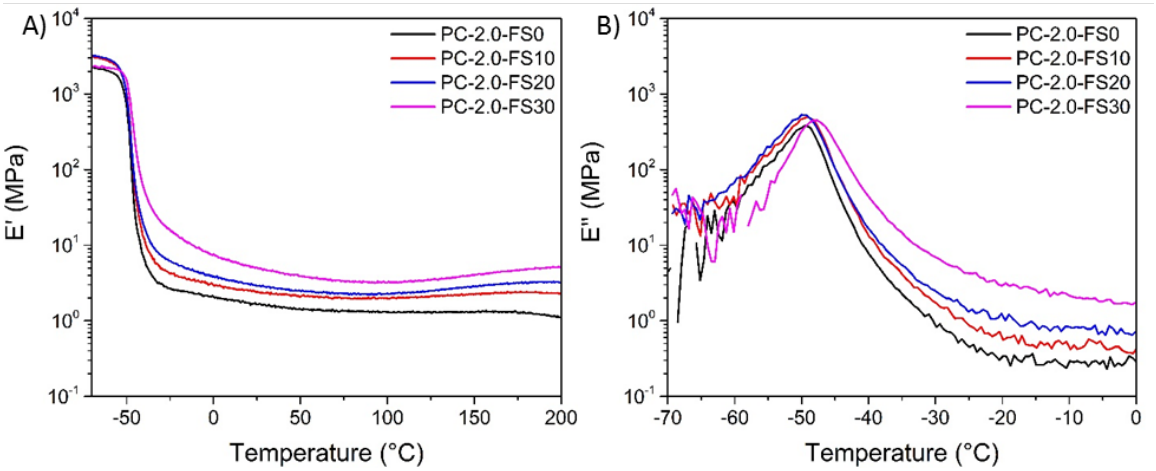

Figure 3.15. DMTA of PC-FS composites. **A)** *E'* and **B)** *E''*. Samples were measured from –70 to 200 °C at a strain rate of 0.05% and a frequency of 1 Hz.

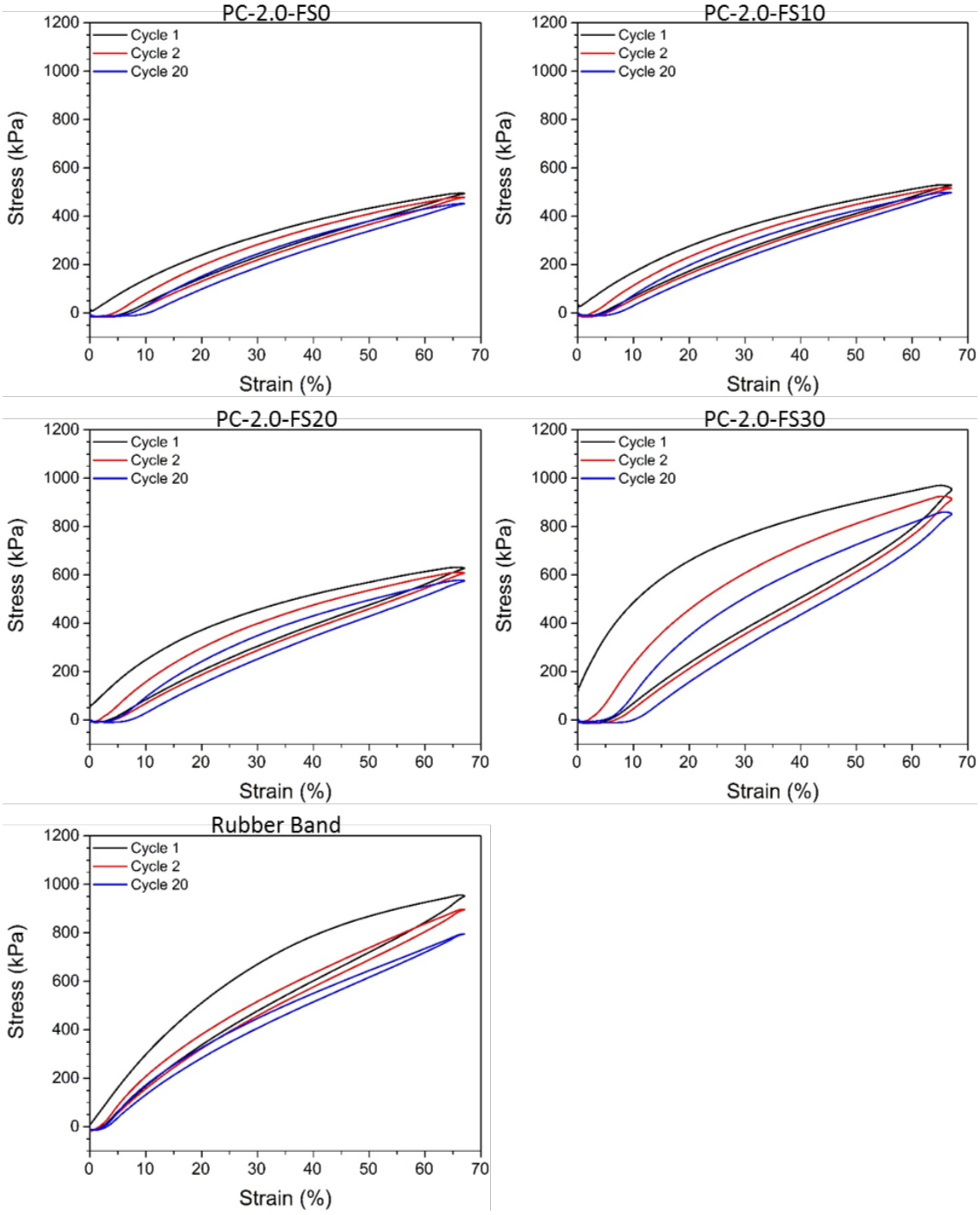

Figure 3.16. Cycles 1, 2, and 30 of the hysteresis of PC-FS composites. All samples contained 2 wt% BPO with respect to PMVL. Hysteresis of a rubber band is also shown. Samples were stretched at a rate of 50 mm min^{-1}.

To demonstrate the recyclability of the PMVL elastomers, we determined the percentage of monomer that was recoverable via chemical depolymerization of CC-0.50-100 and PC-2.0-FS0. While CC materials should be easily depolymerizable, the backbones of the PC materials are chemically altered by the radical cross-linking reaction. We were therefore unsure as to whether the covalent linkages formed during the radical reactions would inhibit the depolymerization. To facilitate MVL recovery via depolymerization, we added stannous octoate and pentaerythritol ethoxylate (a high boiling tetraol) to the elastomers and heated them to 150 °C overnight under vacuum. Both CC and PC elastomers were both capable of depolymerization. We were able to recover 91% of pure MVL from CC-0.50-100 and 93% from PC-2.0-FS0 (**Figure 3.17**).

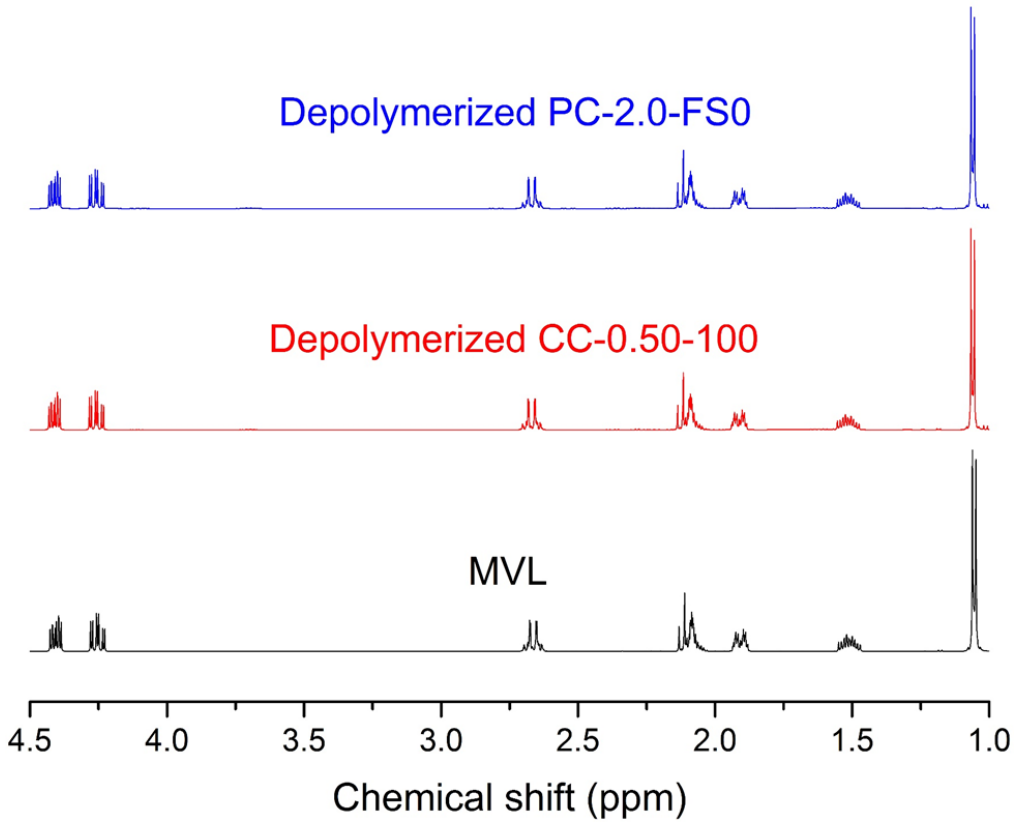

Figure 3.17. ^{1}H NMR in $CDCl_3$ of pure MVL and MVL recovered from the depolymerization of CC-0.50-100 and PC-2.0-FS0.

Finally, we investigated the hydrolytic degradation of the elastomers in aqueous media. Samples were placed in PBS (pH = 7.4), 1 M hydrochloric acid, and 1 M sodium hydroxide (**Figure 3.18**). The elastomers proved to be resilient to degradation in PBS solutions at physiological conditions (37 °C) and in acidic solutions at room temperature, though PC-2.0-FS0 exhibited slight degradation in the basic solutions at room temperature. The poor hydrolytic degradability is likely due to the hydrophobic nature of the materials. Increasing the temperature to 60 °C dramatically improved the degradation of the samples in both acid and base. As hydrochloric acid can behave as a polymerization catalyst for MVL, it is also capable of depolymerizing PMVL at elevated temperature and therefore, capable of degrading the samples. We hypothesize that the increased temperature improved the penetration of polar moieties into the network, allowing accelerated basic degradation of PC-2.0-FS0. Interestingly, CC-0.50-100 appeared to be highly resistant to the basic solution, even at 60 °C; this is somewhat counterintuitive given that esters are easily cleaved in the presence of hydroxide ions. The Young's modulus, plateau modulus, and gel content of PC-2.0-FS0 and CCP-0.50-100 are almost identical, suggesting that either the carbonate moieties lend chemical resistance or that peroxide cross-linking may alter the chemical structure of PMVL in a way that leaves it more susceptible to degradation in basic conditions.

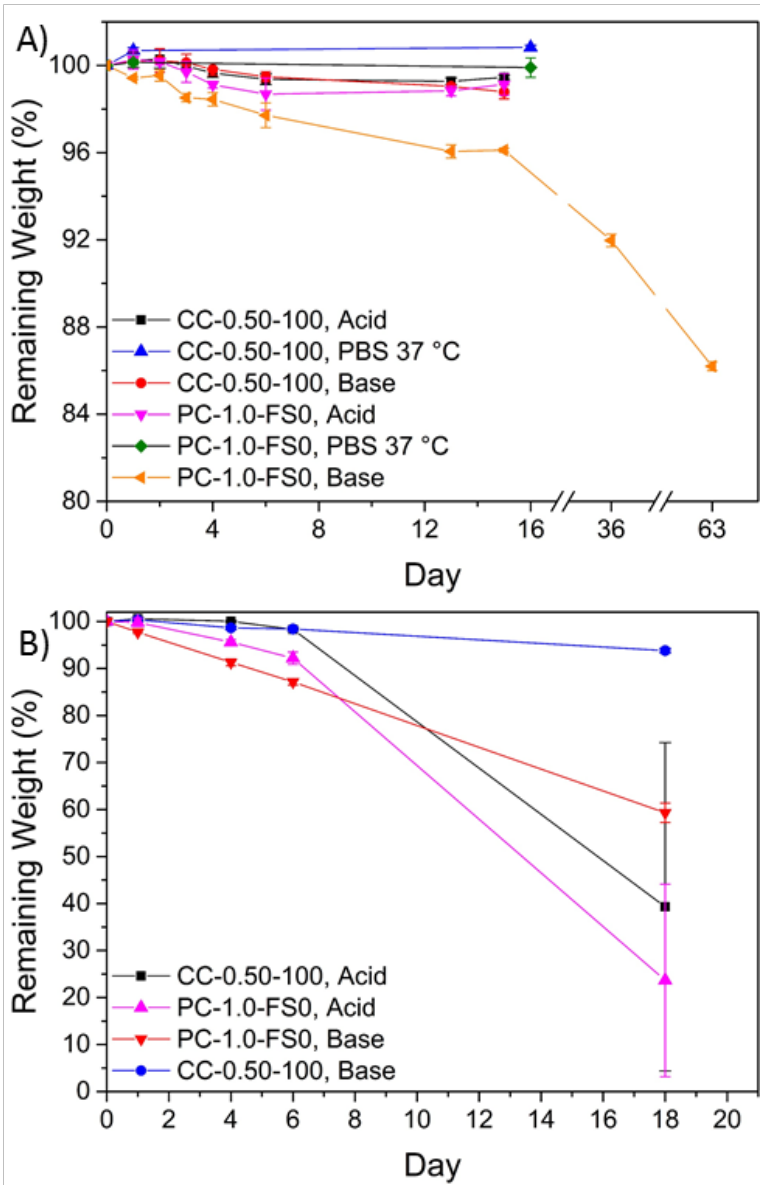

Figure 3.18. Degradation studies of CC-0.50-100 and PC-2.0-FS0 in aqueous PBS (37 °C), 1 M hydrochloric acid (aqueous), and 1 M sodium hydroxide (aqueous). Samples were studied at **A)** room temperature (excluding PBS buffer) and at **B)** 60 °C. Degradation was not performed in PBS buffer at 60 °C as we sought to mimic physiological conditions.

3.5. Conclusions

We have demonstrated that elastomers with a wide range of mechanical properties can be produced from PMVL. Tandem and radical cross-linking methodologies can both be successfully implemented depending on the desired processing conditions and

physical/mechanical properties of the material. The mechanical properties of the reported materials were far superior to similar low T_g, amorphous polyester elastomers reported in the literature, and the toughness could be improved further by incorporating FS. The Young's modulus and tensile strength were improved by 57% and 83%, respectively, without sacrificing the elongation at break by incorporating up to 25 wt% FS in PC. Furthermore, PC-FS materials were produced with similar tensile strength and elongation at break compared to synthetically challenging thermoplastic elastomers based on MVL and lactide.[17] The ability to produce tough composite elastomers facilely with PC will greatly improve its viability as a commodity rubber. Moreover, the recyclability of CC and PC was successfully demonstrated, as they were both able to depolymerize in the presence of catalyst to provide up to 93% recovery of MVL. Finally, both polymers showed the ability to degrade under acidic conditions at 60 °C, while only PC was capable of degradation in basic conditions; this apparent degradation is promising towards the sustainability of these materials.

3.6. References

[1] *The New Plastics Economy—Rethinking the future of plastics*; World Economic Forum; Ellen MacArthur Foundation and McKinsey & Company: London, 2016.

[2] Wu, D. Y.; Meure, S.; Solomon, D. Self-healing polymeric materials: A review of recent developments. *Prog. Polym. Sci.* **2008**, *33*, 479-522.

[3] Montarnal, D.; Capelot, M.; Tournilhac, F.; Leibler, L. Silica-Like Malleable Materials from Permanent Organic Networks. *Science* **2011**, *334*, 965-968.

[4] Altuna, F. I.; Pettarin, V.; Williams, R. J. J. Self-healable polymer networks based on the cross-linking of epoxidised soybean oil by an aqueous citric acid solution. *Green Chem.* **2013**, *15*, 3360-3366.

[5] Tyagi, P.; Deratani, A.; Quemener, D. Self-Healing Dynamic Polymeric Systems. *Isr. J. Chem.* **2013**, *53*, 53-60.

[6] Brutman, J. P.; Delgado, P. A.; Hillmyer, M. A. Polylactide Vitrimers. *ACS Macro Lett.* **2014**, *3*, 607-610.

[7] Fortman, D. J.; Brutman, J. P.; Cramer, C. J.; Hillmyer, M. A.; Dichtel, W. R. Mechanically Activated, Catalyst-Free Polyhydroxyurethane Vitrimers. *J. Am. Chem. Soc.* **2015**, *137*, 14019-14022.

[8] Denissen, W.; Winne, J. M.; Du Prez, F. E. Vitrimers: permanent organic networks with glass-like fluidity. *Chem. Sci.* **2016**, *7*, 30-38.

[9] Albertsson, A.-C.; Varma, I. K. Aliphatic Polyesters: Synthesis, Properties and Applications. *Degradable Aliphatic Polyesters*; Springer Berlin Heidelberg: Berlin, Heidelberg, 2002; pp 1-40.

[10] Lecomte, P.; Jérôme, C. Recent Developments in Ring-Opening Polymerization of Lactones. In *Synthetic Biodegradable Polymers*; Rieger, B., Künkel, A., Coates, W. G., Reichardt, R., Dinjus, E., Zevaco, A. T., Eds.; Springer Berlin Heidelberg: Berlin, Heidelberg, 2012; pp 173-217.

[11] Hillmyer, M. A.; Tolman, W. B. Aliphatic Polyester Block Polymers: Renewable, Degradable, and Sustainable. *Acc. of Chem. Res.* **2014**, *47*, 2390-2396.

[12] Wanamaker, C. L.; O'Leary, L. E.; Lynd, N. A.; Hillmyer, M. A.; Tolman, W. B. Renewable-Resource Thermoplastic Elastomers Based on Polylactide and Polymenthide. *Biomacromolecules* **2007**, *8*, 3634-3640.

[13] Martello, M. T.; Hillmyer, M. A. Polylactide–Poly(6-methyl-ε-caprolactone)–Polylactide Thermoplastic Elastomers. *Macromolecules* **2011**, *44*, 8537-8545.

[14] Shin, J.; Lee, Y.; Tolman, W. B.; Hillmyer, M. A. Thermoplastic Elastomers Derived from Menthide and Tulipalin A. *Biomacromolecules* **2012**, *13*, 3833-3840

[15] Lin, J.-O.; Chen, W.; Shen, Z.; Ling, J. Homo- and Block Copolymerizations of ε-Decalactone with l-Lactide Catalyzed by Lanthanum Compounds. *Macromolecules* **2013**, *46*, 7769-7776.

[16] Olsén, P.; Borke, T.; Odelius, K.; Albertsson, A.-C. ε-Decalactone: A Thermoresilient and Toughening Comonomer to Poly(l-lactide). *Biomacromolecules* **2013**, *14*, 2883-2890.

[17] Xiong, M.; Schneiderman, D. K.; Bates, F. S.; Hillmyer, M. A.; Zhang, K. Scalable production of mechanically tunable block polymers from sugar. *PNAS* **2014**, *111*, 8357-8362.

[18] Martello, M. T.; Schneiderman, D. K.; Hillmyer, M. A. Synthesis and Melt Processing of Sustainable Poly(ε-decalactone)-block-Poly(lactide) Multiblock Thermoplastic Elastomers. *ACS Sustainable Chem. Eng.* **2014**, *2*, 2519-2526.

[19] Huang, Y.; Chang, R.; Han, L.; Shan, G.; Bao, Y.; Pan, P. ABA-Type Thermoplastic Elastomers Composed of Poly(ε-caprolactone-co-δ-valerolactone) Soft Midblock and Polymorphic Poly(lactic acid) Hard End Blocks. *ACS Sustainable Chem. Eng.* **2016**, *4*, 121-128.

[20] Zhang, J.; Li, T.; Mannion, A. M.; Schneiderman, D. K.; Hillmyer, M. A.; Bates, F. S. Tough and Sustainable Graft Block Copolymer Thermoplastics. *ACS Macro Lett.* **2016**, *5*, 407-412.

[21] Schneiderman, D. K.; Hillmyer, M. A. Aliphatic Polyester Block Polymer Design. *Macromolecules* **2016**, *49*, 2419-2428.

[22] Lee, S.; Lee, K.; Kim, Y.-W.; Shin, J. Preparation and Characterization of a Renewable Pressure-Sensitive Adhesive System Derived from ε-Decalactone, l-Lactide, Epoxidized Soybean Oil, and Rosin Ester. *ACS Sustainable Chem. Eng.* **2015**, *3*, 2309-2320.

[23] Grady, B. P.; Cooper, S. L.; Robertson, C. G. Thermoplastic Elastomers. *The Science and Technology of Rubber*, 4th ed.; Academic Press: Boston, 2013; Chapter 13, pp 591-652.

[24] Storey, R. F.; Hickey, T. P. Degradable polyurethane networks based on d,l-lactide, glycolide, ε-caprolactone, and trimethylene carbonate homopolyester and copolyester triols. *Polymer* **1994**, *35*, 830-838.

[25] Wietor, J.-L.; Dimopoulos, A.; Govaert, L. E.; van Benthem, R. A. T. M.; de With, G.; Sijbesma, R. P. Preemptive Healing through Supramolecular Cross-Links. *Macromolecules* **2009**, *42*, 6640-6646.

[26] Gurusamy-Thangavelu, S. A.; Emond, S. J.; Kulshrestha, A.; Hillmyer, M. A.; Macosko, C. W.; Tolman, W. B.; Hoye, T. R. Polyurethanes based on renewable polyols from bioderived lactones. *Polym. Chem.* **2012**, *3*, 2941-2948.

[27] Yang, J.; Lee, S.; Choi, W. J.; Seo, H.; Kim, P.; Kim, G.-J.; Kim, Y.-W.; Shin, J. Thermoset Elastomers Derived from Carvomenthide. *Biomacromolecules* **2015**, *16*, 246-256.

[28] Storey, R. F.; Warren, S. C.; Allison, C. J.; Wiggins, J. S.; Puckett, A. D. Synthesis of bioabsorbable networks from methacrylate-endcapped polyesters. *Polymer* **1993**, *34*, 4365-4372.

[29] Helminen, A. O.; Korhonen, H.; Seppälä, J. V. Structure modification and crosslinking of methacrylated polylactide oligomers. *J. Appl. Polym. Sci.* **2002**, *86*, 3616-3624.

[30] Lewis, C. L.; Meng, Y.; Anthamatten, M. Well-Defined Shape-Memory Networks with High Elastic Energy Capacity. *Macromolecules* **2015**, *48*, 4918-4926.

[31] Spathis, G. Non-Gaussian stress-strain constitutive equation for crosslinked elastomers. *Polymer* **1995**, *36*, 309-313.

[32] Grijpma, D. W.; Kroeze, E.; Nijenhuis, A. J.; Pennings, A. J. Poly(l-lactide) crosslinked with spiro-bis-dimethylene-carbonate. *Polymer* **1993**, *34*, 1496-1503.

[33] Palmgren, R.; Karlsson, S.; Albertsson, A.-C. Synthesis of degradable crosslinked polymers based on 1,5-dioxepan-2-one and cross-linker of bis-ε-caprolactone type. *J. Polym. Sci. Part A: Polym. Chem.* **1997**, *35*, 1635-1649.

[34] Nijenhuis, A. J.; Grijpma, D. W.; Pennings, A. J. Crosslinked poly(l-lactide) and poly(ε-caprolactone). *Polymer* **1996**, *37*, 2783-2791.

[35] Yang, L.-Q.; He, B.; Meng, S.; Zhang, J.-Z.; Li, M.; Guo, J.; Guan, Y.-M.; Li, J.-X.; Gu, Z.-W. Biodegradable cross-linked poly(trimethylene carbonate) networks for implant applications: Synthesis and properties. *Polymer* **2013**, *54*, 2668-2675.

[36] Mecerreyes, D.; Humes, J.; Miller, R. D.; Hedrick, J. L.; Detrembleur, C.; Lecomte, P.; Jérôme, R.; San Roman, J. First example of an unsymmetrical difunctional monomer polymerizable by two living/controlled methods. *Macromol. Rapid Commun.* **2000**, *21*, 779-784.

[37] Campos, L. M.; Killops, K. L.; Sakai, R.; Paulusse, J. M. J.; Damiron, D.; Drockenmuller, E.; Messmore, B. W.; Hawker, C. J. Development of Thermal and Photochemical Strategies for Thiol-Ene Click Polymer Functionalization. *Macromolecules* **2008**, *41*, 7063-7070.

[38] Claudino, M.; van der Meulen, I.; Trey, S.; Jonsson, M.; Heise, A.; Johansson, M. Photoinduced thiol-ene crosslinking of globalide/ε-caprolactone copolymers: Curing performance and resulting thermoset properties. *J. Polym. Sci. Part A: Polym. Chem.* **2012**, *50*, 16-24.

[39] Narkis, M.; Wallerstein, R. Cross-linking of polycaprolactone with peroxides. *Polym. Commun.* **1986**, *27*, 314-317.

[40] Semba, T.; Kitagawa, K.; Ishiaku, U. S.; Hamada, H. The effect of crosslinking on the mechanical properties of polylactic acid/polycaprolactone blends. *J. Appl. Polym. Sci.* **2006**, *101*, 1816-1825.

[41] Han, C.; Ran, X.; Su, X.; Zhang, K.; Liu, N.; Dong, L. Effect of peroxide crosslinking on thermal and mechanical properties of poly(ε-caprolactone). *Polym. Int.* **2007**, *56*, 593-600.

[42] Liu, G.-C.; He, Y.-S.; Zeng, J.-B.; Li, Q.-T.; Wang, Y.-Z. Fully Biobased and Supertough Polylactide-Based Thermoplastic Vulcanizates Fabricated by Peroxide-Induced Dynamic Vulcanization and Interfacial Compatibilization. *Biomacromolecules* **2014**, *15*, 4260-4271.

[43] Målberg, S.; Plikk, P.; Finne-Wistrand, A.; Albertsson, A.-C. Design of Elastomeric Homo- and Copolymer Networks of Functional Aliphatic Polyester for Use in Biomedical Applications. *Chem. Mater.* **2010**, *22*, 3009-3014.

[44] Tran, R. T.; Thevenot, P.; Gyawali, D.; Chiao, J.-C.; Tang, L.; Yang, J. Synthesis and characterization of a biodegradable elastomer featuring a dual crosslinking mechanism. *Soft Matter* **2010**, *6*, 2449-2461.

[45] Schneiderman, D. K.; Vanderlaan, M. E.; Mannion, A. M.; Panthani, T. R.; Batiste, D. C.; Wang, J. Z.; Bates, F. S.; Macosko, C. W.; Hillmyer, M. A. Chemically Recyclable Biobased Polyurethanes. *ACS Macro Lett.* **2016**, 515-518.

[46] Longley, R. I.; Emerson, W. S.; Shafer, T. C. Some Reactions of 2-Alkoxy-3,4-dihydro-2H-pyrans. *J. Am. Chem. Soc.* **1952**, *74*, 2012-2015.

[47] Coady, D. J.; Fukushima, K.; Horn, H. W.; Rice, J. E.; Hedrick, J. L. Catalytic insights into acid/base conjugates: highly selective bifunctional catalysts for the ring-opening polymerization of lactide. *Chem. Commun.* **2011**, *47*, 3105-3107.

[48] Gent, A. N. Strength of Elastomers. In *Science and Technology of Rubber,* 3rd ed.; Mark, J. E., Erman, B., Eirich, F. R., Eds.; Academic Press: Burlington, MA, 2005; pp 455-495.

[49] Yamaguchi, M.; Maeda, R.; Kobayashi, R.; Wada, T.; Ono, S.; Nobukawa, S. Autonomic healing and welding by interdiffusion of dangling chains in a weak gel. *Polym. Int.* **2012**, *61*, 9-16.

[50] Hiemenz, P. C.; Lodge, T. P. *Polymer Chemistry*, 2nd ed.; CRC Press: Boca Raton, FL, 2007; pp 408-409.

[51] Hermans, P. H.; Eyk, J. V. The reaction of benzoyl peroxide with cyclohexane and cyclohexene. Contribution to the mechanism of the catalyzing action of peroxides in the polymerization of vinyl derivatives. *J. Polym. Sci.* **1946**, *1*, 407-418.

[52] Smith, T. L.; Chu, W. H. Ultimate tensile properties of elastomers. VII. Effect of crosslink density on time–temperature dependence. *J. Polym. Sci. A-2: Polym. Phys.* **1972**, *10*, 133-150.

[53] Chen, D.; Hu, M.; Huang, C.; Zhang, R. Preparation and Properties of Natural Rubber Composites and Nanocomposites. *Natural Rubber Materials: Composites and Nanocomposites*; The Royal Society of Chemistry: London, 2014; Vol. 2, Chapter 4, pp 112-135.

[54] Ren, N.; Matta, M. E.; Martinez, H.; Walton, K. L.; Munro, J. C.; Schneiderman, D. K.; Hillmyer, M. A. Filler-Reinforced Elastomers Based on Functional Polyolefin Prepolymers. *Ind. Eng. Chem. Res.* **2016**, *55*, 6106-6112.

Chapter 4. Sustainable Polyester Elastomers from Lactones: Synthesis, Properties, and Enzymatic Hydrolyzability*

* Reprinted (adapted) with permission from De Hoe, G. X.; Zumstein, M. T.; Tiegs, B. J.; Brutman, J. P.; McNeill, K.; Sander, M.; Coates, G. W.; Hillmyer, M A. Sustainable Polyester Elastomers from Lactones: Synthesis, Properties, and Enzymatic Hydrolyzability. *J. Am. Chem. Soc.* **2018**, *140*, 963-973.

4.1. Abstract

Chemically cross-linked elastomers are an important class of polymeric materials with excellent temperature and solvent resistance. However, nearly all elastomers are petroleum-derived and persist in the environment or in landfills long after they are discarded; this work strives to address these issues by demonstrating the synthesis of renewable, enzymatically hydrolyzable, and mechanically competitive polyester elastomers. The elastomers described were synthesized using a novel bis(β-lactone) cross-linker and star-shaped, hydroxyl-terminated poly(γ-methyl-ε-caprolactone). Using model compounds, we determined that the bis(β-lactone) cross-linker undergoes acyl bond cleavage to afford β-hydroxyesters at the junctions. The mechanical properties of the cross-linked materials were tunable and competitive with a commodity rubber band. Furthermore, the elastomers demonstrated high thermal stability and a low glass transition (–50 °C), indicating a wide range of use temperatures. The polyester networks were also subjected to enzymatic hydrolysis experiments to investigate the potential for these materials to biodegrade in natural environments. We found that they readily hydrolyzed at neutral pH and environmentally relevant temperatures (2–40 °C); complete hydrolysis was achieved in all cases at temperature-dependent rates. The results presented in this work exemplify the development of high performance yet sustainable alternatives to conventional elastomers.

4.2. Introduction

Enhanced thermal stability and solvent resistance has facilitated the use of chemically cross-linked polymers (CCPs) in a range of applications including coatings, tires, contact lenses, elastomers, adhesives, and foams. However, there are two major environmental concerns regarding these materials: nearly all CCPs are derived from petroleum, a non-renewable resource, and they typically do not biodegrade on reasonable timescales. Furthermore, the chemical junctions in these polymer networks preclude traditional recycling strategies, which leads to one of the following typical outcomes after use: 1) down-cycling into a lower-value materials, 2) incineration for energy capture, 3) disposal in a landfill, or 4) release into the environment.[1] All compare unfavorably with primary recycling from a value standpoint, and detrimental environmental consequences accompany incineration, landfilling, and release.[2,3] Although the hazards associated with incineration and landfilling are minimized by establishing controls and regulations, it is difficult to mitigate the detrimental effects of plastic released into the environment. Plastic waste poses multiple hazards to ecosystems such as ingestion and entanglement risk for animals, leaching of contaminants, and concentration of organic pollutants.[4] Furthermore, the hydrocarbon-based backbones in plastics are relatively resilient to chemical degradation in natural systems, either by microorganisms and their enzymes (i.e., biodegradation) or by abiotic transformations (e.g., photo-oxidation and non-enzymatic hydrolysis). The extremely slow environmental degradation of these materials—cross-linked or not—coupled with the relatively short use time of many plastics has led to an alarming and continuously increasing amount of plastic waste in the environment.[3,5] It is therefore crucial to continue developing competitive yet biodegradable alternatives to

commercial CCPs, as biodegradable materials will reduce the costs of waste management and the accumulation of waste in the environment.[6]

Aliphatic polyesters with properties ranging from rigid thermosets to flexible elastomers have been studied as sustainable alternatives to non-biodegradable CCPs.[7,8,9,10,11,12,13,14] The inherent susceptibility of ester linkages to hydrolysis can facilitate polyester biodegradation. It is often assumed that accelerated hydrolysis of a cross-linked polyester under alkaline and high temperature conditions (e.g., 1 M NaOH at 60 °C) or simply the mere presence of ester bonds in the network can substantiate the claim that the material is biodegradable. However, not every polyester will readily degrade in the environment; biodegradability is heavily dependent on the conditions (e.g., pH, temperature, presence of oxygen), characteristics of the bulk polymer (e.g., crystallinity, hydrophobicity), the microorganisms present and the competence of their extracellular esterases, as well as the ability of the microorganisms to assimilate and metabolize the hydrolysis products.[6,15] The most important of these considerations is the presence of efficient extracellular microbial esterases, as the hydrolysis of ester bonds is expected to be the rate-limiting step of polyester biodegradation.

In addition to their potential for biodegradability, polyester materials can be made more sustainable if they are obtained from renewable feedstocks. Many bio-sourced precursors can be used to synthesize cross-linked polyesters, such as carboxylic acid, epoxide, and alcohol monomers[10,16] and/or lactone monomers.[17] If using lactones, low dispersity ($Đ$) polyesterols of a desired number-average molar mass (M_n) can be synthesized and cross-linked *in situ*,[9,11,18,19,20] after modification,[8,21,22,23,24,25,26] or post-

polymerization without modification.[9,12,13,27,28] We have previously demonstrated that high performance CCPs can be synthesized from a renewable lactone, β-methyl-δ-valerolactone, but the relatively low ring strain of this monomer led to practical difficulties due to residual monomer at equilibrium.[9,29] To overcome this issue, we more recently reported that high performance thermoplastic elastomers could be synthesized using γ-methyl-ε-caprolactone (MCL),[30] a 7-membered lactone that reaches near quantitative conversion at equilibrium and could potentially be sourced from *para*-cresol or *para*-cymene, both of which can be obtained from biomass.[31,32,33]

In this work, we used potentially bio-based lactones to synthesize polyester elastomers that are mechanically competitive with a commercial CCP and can be readily hydrolyzed by extracellular esterases. We employed ring-opening polymerization (ROP) of MCL to generate prepolymers that are cross-linked without modification by using a novel bis(β-lactone) type cross-linker. The motivation for bis(β-lactone) cross-linkers stems from their high ring strain and potential to be derived from biomass. β-lactones can undergo two mechanisms of ring-opening in the presence of various initiators and catalysts: carboxylate generation via alkyl-oxygen cleavage or alkoxide generation via acyl-oxygen cleavage.[34] The polymerization of monofunctional β-lactones has been well studied,[34,35] but to our knowledge, the use of multifunctional β-lactones in polymers has only been reported once in 1979.[36] This is likely a result of the practical difficulties associated with the traditional ring-closing and [2+2] cycloaddition syntheses of β-lactones. However, recent developments in catalysis have enabled a relatively facile route to β-lactones from epoxides via carbon monoxide insertion.[37] This approach greatly increases access to a

broad array of β-lactone monomers, including those derived from renewable resources. The bis(β-lactone) cross-linker we employ could be obtained by carbonylation of the diepoxide from 1,5-hexadiene, which itself can be formed by deoxygenation of suberic acid from seed oil.[38] Besides dienes, we envision that multifunctional epoxides can be prepared using epichlorohydrin from glycerol[39] and various bio-based alcohols;[40,41,42] subsequent carbonylation of these epoxide precursors would give access to a novel class of bis(lactone) type cross-linkers.

We employed commercially relevant stannous octoate ($SnOct_2$) as the catalyst for prepolymer synthesis as well as cross-linking; despite the widespread use of this catalyst for ROP of lactones, there are few reports of $SnOct_2$-catalyzed ROP for β-lactones due to poor polymerization control.[43,44,45] Though impractical for polymerization of β-lactones, $SnOct_2$ was successful at facilitating the ring opening of β-lactones during cross-linking. Using model compound studies, we demonstrate that the $SnOct_2$-catalyzed ring-opening proceeds via an acyl-oxygen cleavage mechanism. Furthermore, we show that the resultant elastomers have high thermal stability and tunable mechanical properties. The mechanical properties of industrially-relevant cross-linked elastomers (i.e., those based on polyisoprene, polybutadiene, polyisobutylene, and polysiloxanes) strongly depend on the cross-link density and the filler used to toughen them (if any). We therefore selected a common polyisoprene-based elastomer (i.e., a rubber band) as a representative high-performance elastomer and compared its elastic performance with that of our polyester elastomers. Lastly, we investigated the susceptibility of our elastomers to enzymatic

hydrolysis at conditions that are environmentally relevant and found that these new materials show great promise as biodegradable elastomers.

4.3. Experimental

4.3.1. Materials.

All reagents were used as received unless otherwise indicated. Dichloromethane (DCM), ethyl acetate, hexanes, and anhydrous tetrahydrofuran (THF) were purchased from Fisher Scientific, whereas methanol was purchased from Sigma-Aldrich. THF was purified by passing through two neutral alumina-packed columns followed by a third column packed with activated 4Å molecular sieves under nitrogen pressure, and was degassed by three freeze-pump-thaw cycles prior to use. All other solvents were reagent grade or better and used as received. Bis(tetrahydrofuran)-*meso*-tetra(4-chlorophenyl)porphyrinato aluminum tetracarbonyl cobaltate, $[ClTPPAl(THF)_2]^+[Co(CO)_4]^-$, was synthesized as previously reported.[46] Carbon monoxide (Airgas, 99.99% minimum purity) was used as received. Carbonylation reactions were performed in a 100-mL Parr Series 4560 Mini Bench Top Reactor. Because carbon monoxide is a highly toxic gas, all carbonylation reactions were performed in a well-ventilated fume hood equipped with a CO sensor. $SnOct_2$ used for polymerization and the model compound study (see below) was purified by triple distillation under high vacuum and argon (50-100 mTorr and 130-150 °C) and was stored under nitrogen atmosphere. The $SnOct_2$ used for elastomer synthesis was purchased from Alfa Aesar (96%) and was stored in a refrigerator after being placed under vacuum for 1 week to remove residual 2-ethylhexanoic acid. The deuterium-labeled solvents used for NMR spectroscopy, $CDCl_3$ (99.8% with 0.05 vol % tetramethylsilane

(TMS) as reference standard) and D_2O (99.9% with 0.75 wt. % 3-(trimethylsilyl)propionic-2,2,3,3-d_4 acid, sodium salt (TSP) as reference standard), were purchased from Cambridge Isotope Laboratories and Sigma-Aldrich respectively. Rubber bands were manufactured in Thailand for Universal (product number UNV00432) and purchased from the University of Minnesota chemistry stockroom.

4.3.2. Synthesis of bis(β-lactone) Cross-linker (4,4'-(ethane-1,2-diyl)bis(oxetan-2-one)).

In a nitrogen glove box, a 20 mL glass vial equipped with a Teflon-coated magnetic stir bar was charged with 96.4 mg (0.088 mmol, 2.0 mol %) of $[ClTPPAl(THF)_2]^+[Co(CO)_4]^-$ and tetrahydrofuran (4.4 mL). The vial and a 100-mL Parr stainless steel high-pressure reactor were placed in the glove box freezer at –30 °C to cool for 30 minutes. In the absence of CO, isomerization of the epoxide to ketone products can be minimized by keeping the temperature of the reactor below 0 °C.[47] Chilled (also –30 °C for 30 minutes) 1,2,5,6-diepoxyhexane (506 mg, 4.4 mmol) was then added to the vial. After adding a cap with a Teflon-coated septum pierced with an 18 G needle, which prevented the reaction solvent from refluxing into the reactor chamber, the vial was placed quickly into the high-pressure reactor. The reactor was subsequently sealed, taken out of the glove box, placed in a well-ventilated hood, and pressurized with carbon monoxide (900 psi). The reactor was then heated to 60 °C in an oil bath and the reaction mixture stirred for six hours. The reactor was cooled on dry ice for 10 minutes and carefully vented in a fume hood. The crude reaction mixture was purified on a plug of silica (300 mL) using 50% ethyl acetate in hexanes to 100% ethyl acetate. After removing solvent by rotary evaporation, the crystalline product was dissolved in ~10 mL of tetrahydrofuran and

precipitated into hexanes (~150 mL). After cooling in a freezer (−10 °C), the product was collected by filtration and then dried *in vacuo* to afford 4,4'-(ethane-1,2-diyl)bis(oxetan-2-one) (0.513 g, 68%) as a white powder. The melting point was measured by differential scanning calorimetry to be approximately 80 °C (determined by the onset in the melting endotherm). The product was a mixture of racemic and meso isomers as evidenced by 8 peaks in the ^{13}C NMR spectrum. ^{1}H NMR (500 MHz, $CDCl_3$, **Figure 4.1**): δ 4.61–4.54 (m, 2H), 3.59 (ddd, J = 16.4, 5.8, 1.4 Hz, 2H), 3.16 (dt, J = 16.4, 4.4 Hz, 2H), 2.08–1.89 (m, 4H). ^{13}C NMR (125 MHz, $CDCl_3$, **Figure 4.2**): δ 167.61, 167.53, 70.55, 70.05, 43.37, 43.15, 31.05, 30.28. High resolution mass spectrometry (ESI-TOF) m/z: Calculated for $C_8H_{10}O_4Na^+$ 193.0471; Found 193.0477. ATR-FTIR (neat, **Figure 4.3**): 2967, 2916, 2851, 1873, 1799 (strong), 1440, 1408, 1387, 1301, 1283, 1239, 1209, 1196, 1133, 1096, 1083, 1030, 1002, 946, 848, 823, 798, 783, 702, 567, 536, 511 cm^{-1}.

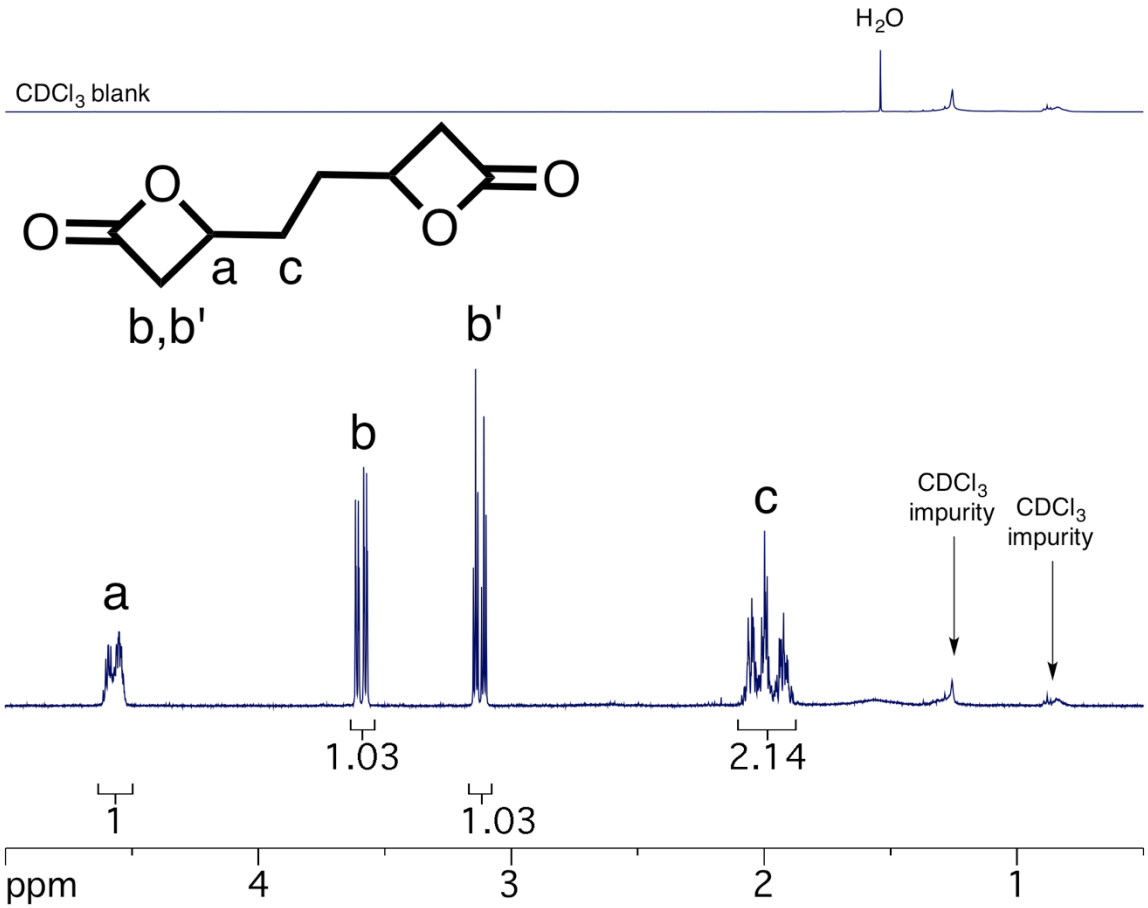

Figure 4.1. ^{1}H NMR spectrum (500 MHz, $CDCl_3$) of the bis(β-lactone) cross-linker; a blank of the NMR solvent is overlaid to show that two impurities in the bis(β-lactone) spectrum are from the NMR solvent.

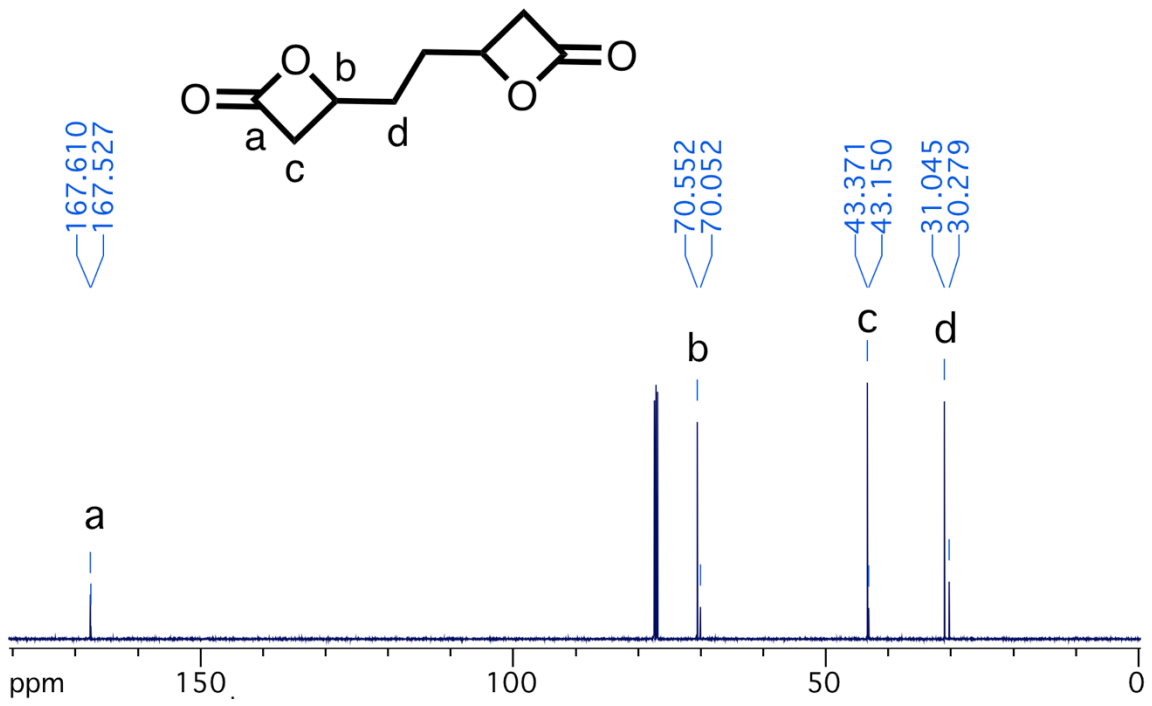

Figure 4.2. ^{13}C NMR spectrum (125 MHz, $CDCl_3$) of the bis(β-lactone) cross-linker; the racemic and meso isomers produce 4 peaks each.

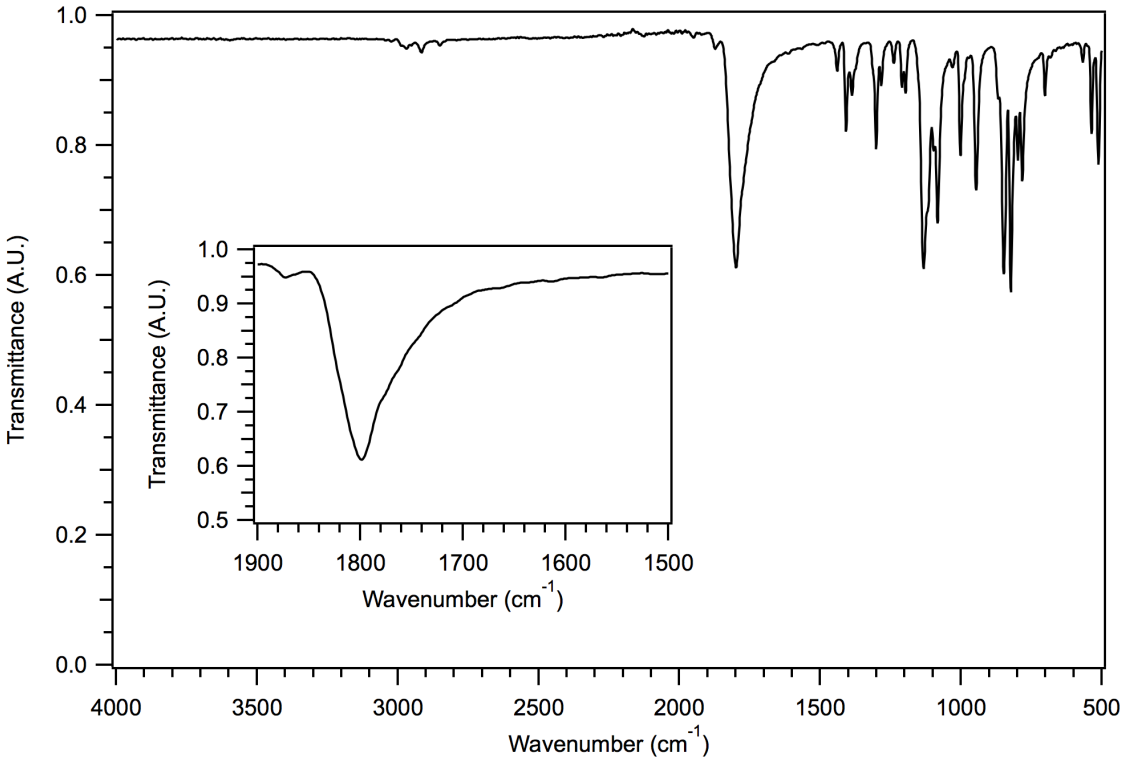

Figure 4.3. IR spectrum (neat) of the bis(β-lactone) cross-linker, with an inset showing the distinctive strained carbonyl stretching frequency at 1799 cm^{-1}.

4.3.3. Synthesis of β-Valerolactone (4-ethyl-oxetan-2-one).

Carbonylation of 1-butene oxide was performed using previously reported procedures.[48] The crude product was purified by distillation over calcium hydride (*ca.* 1.7 torr, 55-57 °C). ^{1}H NMR (500 MHz, $CDCl_3$, **Figure 4.4**): δ 4.47–4.43 (m, 1H), 3.48 (dd, *J* = 16.3, 5.8 Hz, 1H), 3.05 (dd, *J* = 16.3, 4.3 Hz, 1H), 1.92–1.74 (m, 2H), 1.00 (t, *J* = 7.4 Hz).

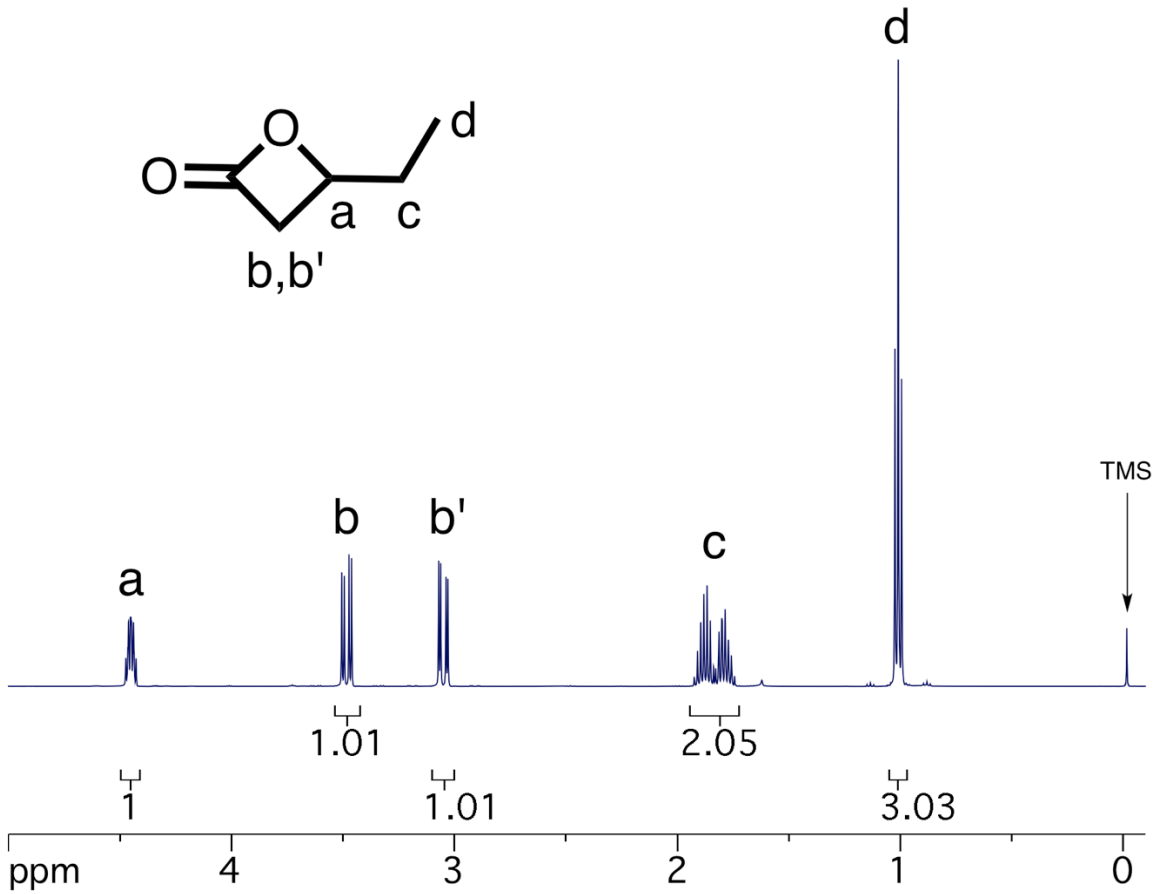

Figure 4.4. ^{1}H NMR spectrum (500 MHz, $CDCl_3$) of the β-valerolactone used for the model compound study.

4.3.4. Large Scale Synthesis of γ-Methyl-ε-caprolactone (MCL) Monomer.

This monomer was synthesized via the Baeyer-Villiger oxidation of γ-methyl cyclohexanone (MC). Small-scale synthesis (approx. 100 g MC) was achieved using previously reported procedures,[30] but this reaction was also performed on a large scale (approx. 1 kg MC). First, a 15 gallon (38 L, HxD = 26.25”x14”) HDPE drum with half of the top sawn off was placed in a 17 gallon tub (HxD = 22”x16”) and tethered to the fume hood lab frame kit via a string. A stainless-steel siphon hand pump was screwed into the threaded opening opposite the sawed-off opening. The drum was then charged with 2.407

kg of *meta*-chloroperoxybenzoic acid (*m*CPBA, ≥77%, 10.7 mol, 1.1 eq.) and DCM (22 L). The solution was stirred with a stainless-steel mechanical stirrer through the top opening until the *m*CPBA dissolved, after which an ice/salt bath was prepared in the gallon tub. The solution was allowed to cool to 5 ºC as a 4 L separatory funnel was charged with a solution of γ-methylcyclohexanone (1.103 kg, 9.8 mol, 1 eq.) in 2 L of DCM. Evaporation of DCM was observed in the reaction vessel and thus another 2 L of DCM was added. Once the solution reached 5 °C, the γ-methylcyclohexanone solution was added dropwise over the course of an hour (exact time: 59 m 30 s). After the addition was complete (final temperature: 11 °C), the temperature was allowed to rise to 21 °C over the course of the next hour by allowing the ice to melt. The reaction mixture was analyzed by ^{1}H NMR spectroscopy over the course of the next 2 h 45 m and a maximum conversion of approximately 90% was attained before filtration began (**Figure 4.5**).

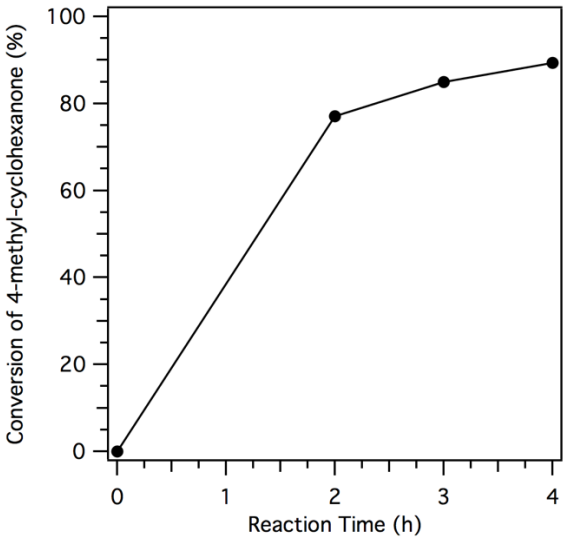

Figure 4.5. Plot indicating the progress of Baeyer-Villiger oxidation over time for the large-scale reaction (1 kg ketone); this is in contrast to the 99% conversion observed after 1 h on a smaller scale (100 g ketone). The conversion was measured via integration of ^{1}H NMR spectra of aliquots, specifically using the –CH_2–C(O)–signals for the ketone starting material and the lactone product.

Once reaction progress plateaued at 90% conversion, the heterogeneous reaction mixture (the *meta*-chlorobenzoic acid has low solubility in DCM) was siphoned using the pump into a tabletop Buchner funnel connected to another 15-gallon HDPE drum fitted with a vacuum adaptor. Once all the filtrate was collected, the drum pump was switched to the receiving drum and used to pump the filtrate into large (4 or 6 L) Erlenmeyer flasks. The filtrate was concentrated via rotary evaporation and filtered in 1-2 L amounts until the majority of *meta*-chlorobenzoic acid and DCM is removed (23 L of DCM was stored for re-use). Each portion of crude γ-methyl-ε-caprolactone was then combined (total of *ca.* 1-1.5 L), washed with 10% aqueous Na_2SO_3 (3 x 500 mL), brine (1 x 500 mL), dried over $MgSO_4$, and filtered through Celite. The crude product was then transferred to a 2 L round bottom flask and stirred over CaH_2 for 48 h. Finally, the crude product was fractionally distilled over CaH_2 (1 Torr, 80-100 °C), stirred over CaH_2 again, and then redistilled once more in the same manner to afford pure γ-methyl-ε-caprolactone in 60 % yield. ^{1}H NMR (500 MHz, $CDCl_3$, **Figure 4.6**): δ 4.28 (ddd, *J* = 12.9, 5.8, 1.9 Hz, 1H), 4.19 (dd, *J* = 12.9, 10.4 Hz, 1H), 2.69–2.59 (m, 2H), 1.96–1.86 (m, 2H), 1.78 (m, 1H), 1.51 (dtd, *J* = 15.4, 10.8, 1.6 Hz, 1H), 1.34 (dtd, *J* = 14.1, 11.4, 2.7 Hz, 1H), 1.00 (d, *J* = 6.7 Hz, 3H).

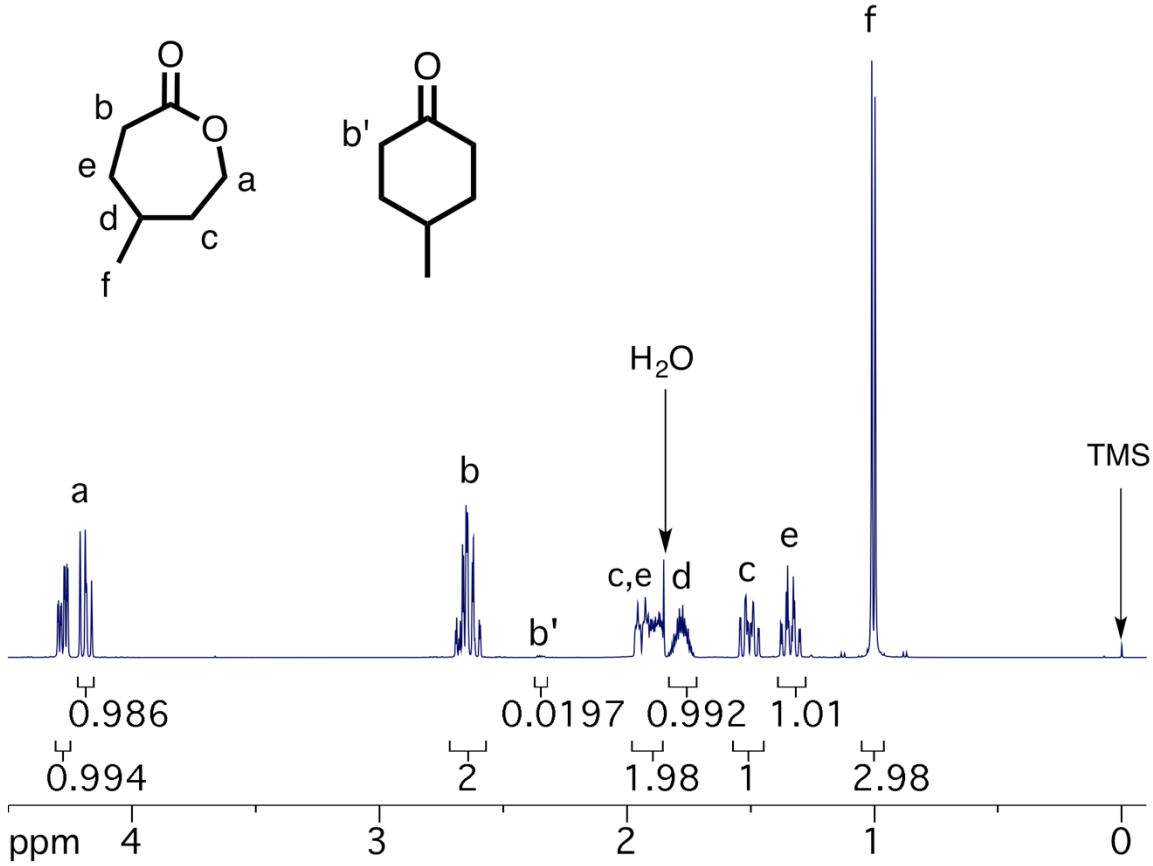

Figure 4.6. ^{1}H NMR spectrum (500 MHz, $CDCl_3$) of γ-methyl-ε-caprolactone after distillation; approximately 1 mol% γ-methyl-cyclohexanone is present.

4.3.5. Synthesis of Star-shaped Hydroxyl-terminated Poly(γ-methyl-ε-caprolactone) (PMCL).

In a typical polymerization, a 50-mL pressure vessel was loaded with MCL (20.0 g, 156 mmol) and pentaerythritol (137 mg, 1.01 mmol) under inert atmosphere. A stock solution of $SnOct_2$ was prepared in toluene and added (90 μL stock solution, 12.7 mg, 31.2 μmol $SnOct_2$) to the pressure vessel. A Teflon-coated magnetic stir bar was added to the pressure vessel, which was subsequently sealed, removed from inert atmosphere, and placed in a pre-heated silicone oil bath. The polymerization was allowed to proceed for 2

h at 160 °C; by the end of the reaction, the contents were still clear but had a slight yellow tinge, and the viscosity had increased drastically such that the stir bar was not stirring effectively. DCM was added to approximately double the volume in the pressure vessel and the crude PMCL was dissolved overnight. PMCL was then precipitated from DCM twice—first into methanol, then using hexanes—and consolidated into a tared jar. The pure polymer was then dried under a stream of nitrogen gas for 24 h before being placed in a vacuum oven, where it was dried under vacuum for 2 days. The temperature in the vacuum oven was then elevated to 60 °C and the polymer was dried under vacuum for 2 more days. Typical conversions of monomer were greater than 98% and typical yields were greater than or equal to 90%. The pure polymers were analyzed via ^{1}H NMR, ^{13}C NMR, and FTIR spectroscopy (analyses for representative polymer shown in **Figure 4.7**, **Figure 4.8**, and **Figure 4.9**), SEC (**Figure 4.10** and **Table 4.1**), TGA, and DSC. ^{1}H NMR (500 MHz, $CDCl_3$, **Figure 4.7**): δ 4.13–4.08 (m, 172H), 3.75–3.64 (m, 8H), 2.36–2.29 (m, 173H), 1.71–1.44 (m, 444H), 0.92 (d, J = 6.6 Hz, 258H). ^{13}C NMR (125 MHz, $CDCl_3$, **Figure 4.8**): δ 173.89, 62.77, 35.38, 32.05, 31.92, 29.73, 19.18. ATR-FTIR (neat, **Figure 4.9**): 2958, 2928, 2873, 1729, 1459, 1421, 1382, 1340, 1253, 1166, 1100, 1052, 965, 774 cm^{-1}.

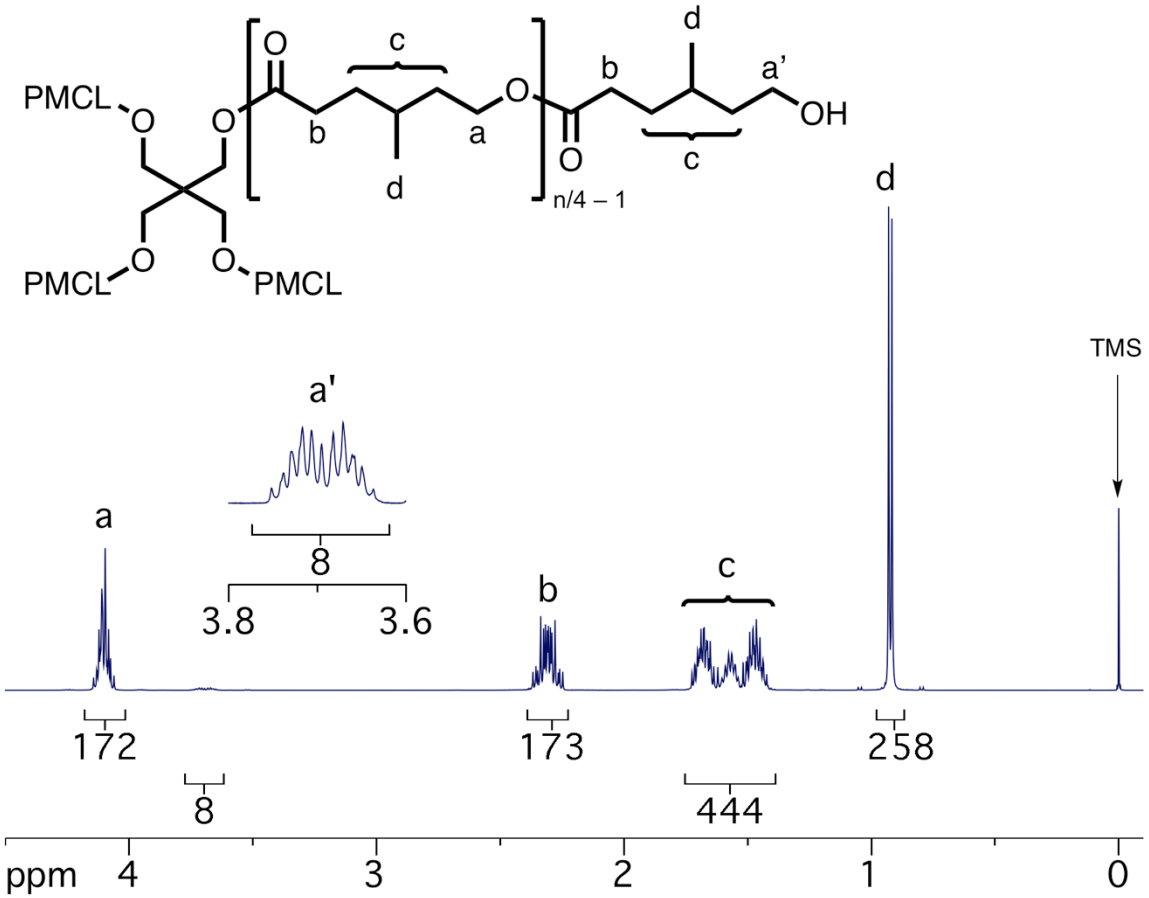

Figure 4.7. ^{1}H NMR spectrum (500 MHz, $CDCl_3$) of star-shaped hydroxyl-terminated PMCL of target M_n = 10 kg/mol (i.e., prepolymer for CE-11) after purification, with an inset showing the signal corresponding to the end group. The CH_2 signals for the pentaerythritol core overlap with the signal denoted "a".

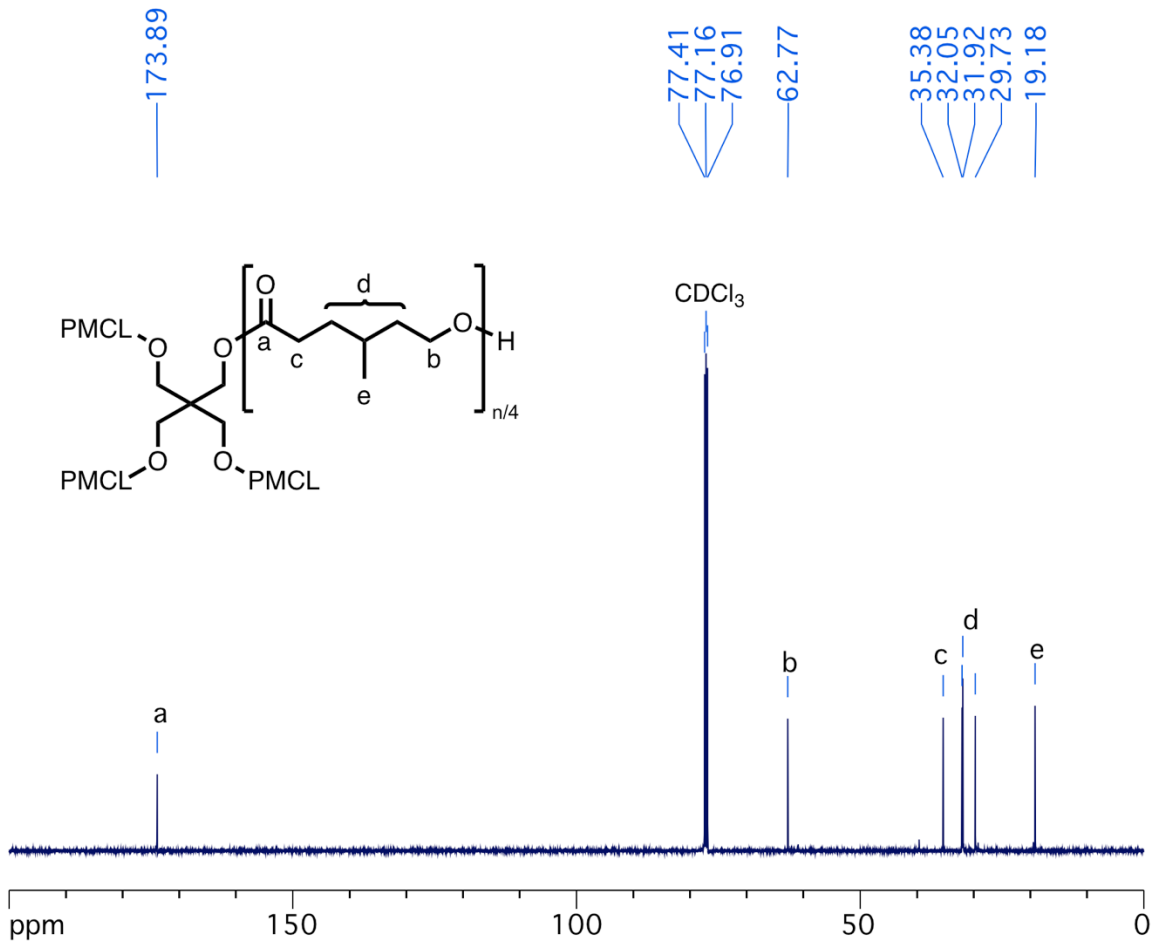

Figure 4.8. ^{13}C NMR spectrum (125 MHz, $CDCl_3$) of star-shaped hydroxyl-terminated PMCL of target M_n = 10 kg/mol (i.e., prepolymer for CE-11) after purification.

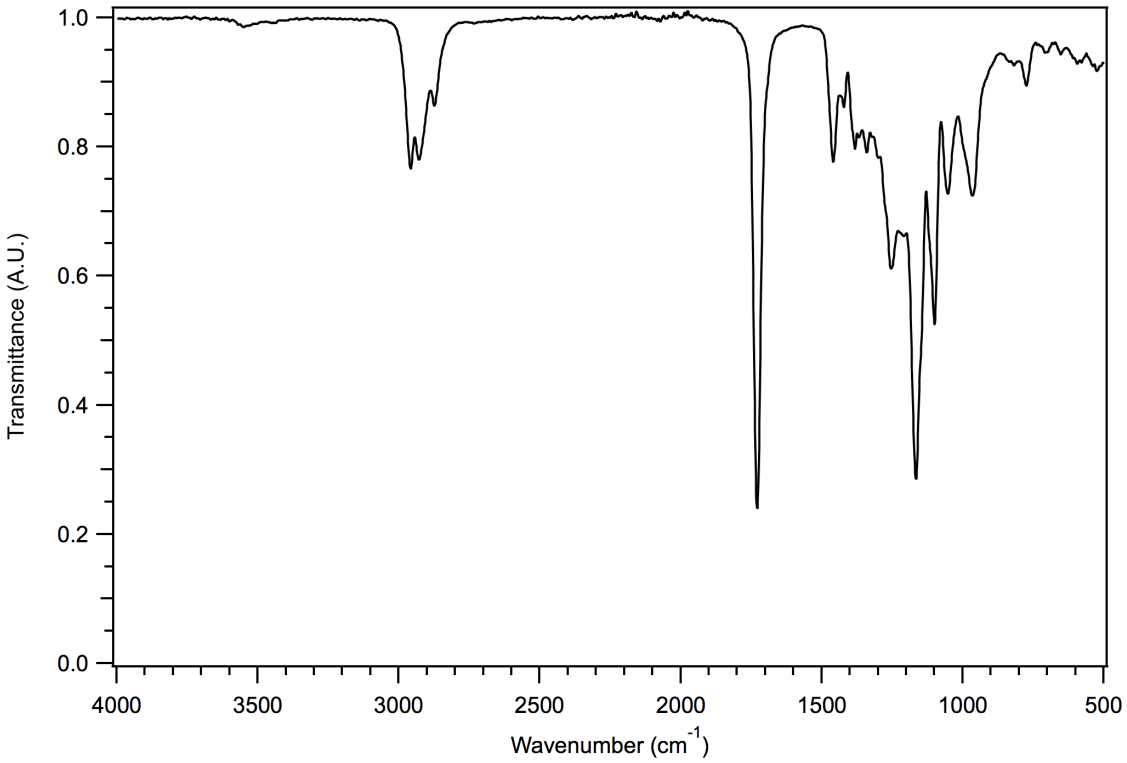

Figure 4.9. IR spectrum (neat) of star-shaped hydroxyl-terminated PMCL of target M_n = 10 kg/mol (i.e., prepolymer for CE-11) after purification.

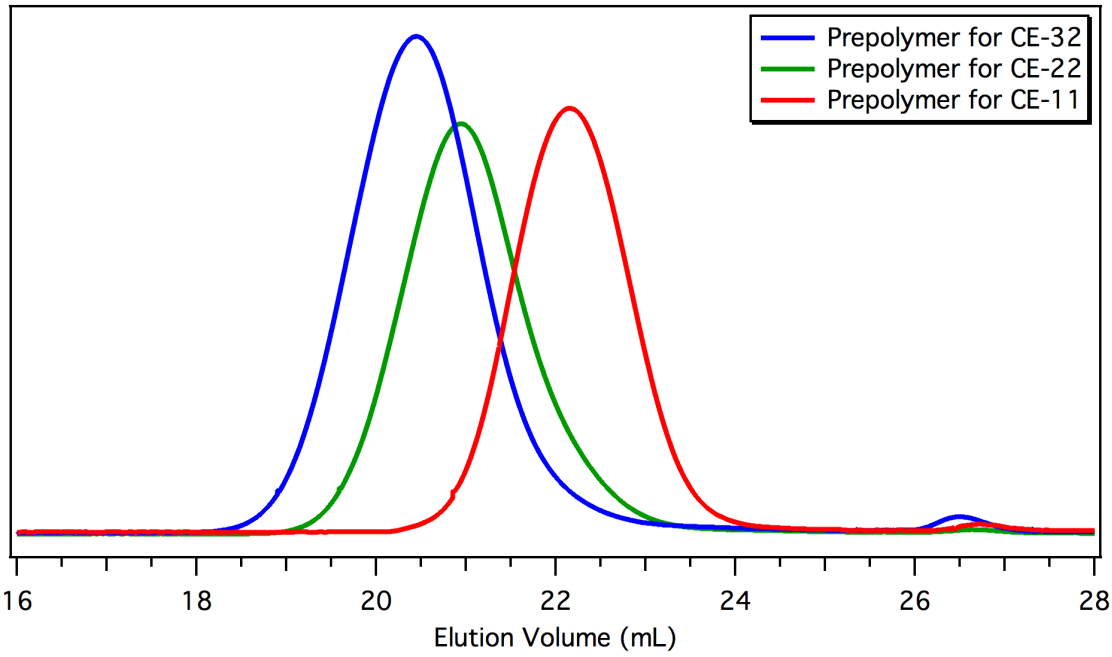

Figure 4.10. SEC traces of star-shaped PMCL of various molar masses used to produce the cross-linked elastomers (denoted CE-X, where X is the prepolymer molar mass calculated used ^{1}H NMR spectroscopy).

Table 4.1. Molar mass characterization of PMCL samples used for elastomers.

Prepolymer for	M_n (kg/mol)[a]	M_n (kg/mol)[b]	$Đ$[b]
CE-32	31.5	52.8	1.30
CE-22	22.4	36.2	1.29
CE-11	11.2	17.6	1.23

[a]Calculated using end-group analysis via ^{1}H NMR spectroscopy in $CDCl_3$, specifically using the integrations corresponding to the protons adjacent to the hydroxyl end group and adjacent to the carbonyl in each repeat unit. [b]Measured using size-exclusion chromatography in $CHCl_3$ by comparison to polystyrene standards.

4.3.6. Synthesis of Star-shaped Carboxylic-acid-terminated PMCL.

The same procedure as above was performed except for the following modification. After polymerization, the pressure vessel was returned to the glovebox to add succinic anhydride (606 mg, 6.06 mmol, 1.5 eq. relative to polymer end groups) to the crude polymer. The pressure vessel was then closed, taken out of the glovebox, and placed back in the oil bath for 1 h. After this time, the crude polymer was purified as described above

and analyzed by ^{1}H NMR spectroscopy. ^{1}H NMR (500 MHz, $CDCl_3$, **Figure 4.11.** ^{1}H NMR spectrum (500 MHz, $CDCl_3$) of star-shaped carboxylic acid-terminated PMCL of target M_n = 10 kg/mol after purification, with an inset showing the signal corresponding to the end group. The CH_2 signals for the pentaerythritol core overlap with the signal denoted "a".): δ 4.14–4.06 (m, 168H), 2.68–2.61 (m, 16H), 2.37–2.25 (m, 165H), 1.72–1.42 (m, 415H), 0.92 (d, J = 6.5 Hz, 249H).

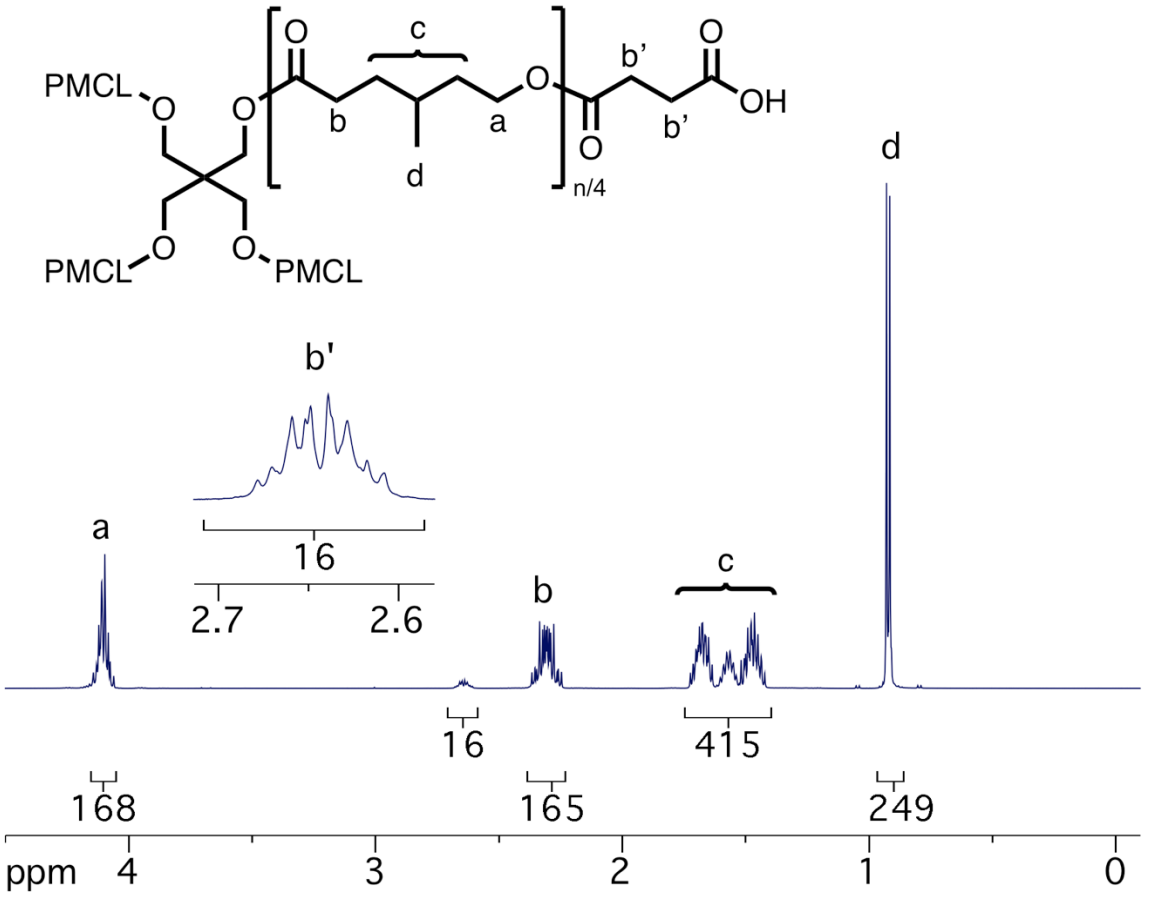

Figure 4.11. ^{1}H NMR spectrum (500 MHz, $CDCl_3$) of star-shaped carboxylic acid-terminated PMCL of target M_n = 10 kg/mol after purification, with an inset showing the signal corresponding to the end group. The CH_2 signals for the pentaerythritol core overlap with the signal denoted "a".

4.3.7. Preparation of Cross-linked Polyester Elastomers (CEs).

To produce the elastomers that were used for all experiments, star-shaped PMCL (4.0 g) of M_n = 11, 22, or 32 kg/mol was dissolved in DCM (4 mL) in a 20-mL vial using a small Teflon-coated magnetic stir bar. To each vial, bis(β-lactone) cross-linker was added such that the PMCL end group to β-lactone ratio was 1.0 to 1.5 (180, 91, and 65 mg respectively). Next, $SnOct_2$ was added (100 mg/mL stock solution in DCM) in amounts corresponding to 2.5 mol% with respect to the PMCL end groups (15, 7, and 5 mg respectively). After stirring for 30 seconds, the homogenous mixture was poured into aluminum weigh pans (7 cm diameter). A small amount of DCM (1-2 mL) was used to finish the transfer, and the solvent cast mixtures were put under a stream of nitrogen gas for 24 h to evaporate solvent. Though we tested several solvents for this procedure—tetrahydrofuran, acetone, and dichloromethane—we found that only dichloromethane effectively solubilized all components without deactivating the $SnOct_2$. After drying, the pans were put in a pre-heated oven (120 °C) under nitrogen atmosphere for 24 h. The resultant films were *ca.* 1 mm thick, clear, colorless, and almost completely free of visible defects. The notation of the films is CE-*X*, where *X* represents the M_n of the PMCL used to make the film. Each film was characterized using swell tests, DSC, TGA, DMTA, tensile testing, and ATR-FTIR. Small scale films were produced using 0.5 g of PMCL using the same procedure but were only characterized via swell tests.

4.3.8. Model Compound Study.

Under inert atmosphere, a 2-mL amber vial with a rubber septum cap was charged with three reagents in the following order: $SnOct_2$ (57 mg, 14 μmol, 0.025 eq.), β-

valerolactone (502 mg, 5.0 mmol, 0.91 eq.), and benzyl alcohol (595 mg, 5.5 mmol, 1.0 eq.). The homogenous mixture (*ca.* 0.5 mL) was sampled for later analysis, tightly sealed, and placed in a pre-heated heating block element on a hot plate at 120 °C. Aliquots were removed at various time points (0.25, 0.5, 1, 2, 4, and 24 h) and immediately cooled to below room temperature. Each aliquot was then analyzed by GC-MS, ATR-FTIR spectroscopy, and ^{1}H NMR spectroscopy.

4.3.9. Characterization.

The NMR spectroscopy data for MCL, PMCL, the bis(β-lactone) cross-linker, and the model study were obtained at the University of Minnesota using a 500 MHz Bruker Avance III HD spectrometer with a SampleXpress auto-sampler. The NMR spectroscopy data for the hydrolysis products was obtained at ETH Zurich using a 400 MHz Bruker Avance III spectrometer. All spectra were analyzed using the *iNMR* software. The Fourier transform infrared (FTIR) spectra were obtained on a Bruker Alpha Platinum spectrometer equipped with a diamond crystal in attenuated total reflection (ATR) mode at a resolution of 4 cm^{-1}, and 32 scans were obtained for each spectrum. High resolution mass spectrometry data for the bis(β-lactone) cross-linker was obtained using a Bruker BioTOF II instrument in electrospray ionization (ESI) mode with poly(ethylene glycol) added as an internal standard and calibrant. Gas chromatography mass spectrometry (GC-MS) data for the model compound study was obtained using an Agilent 6890N Network GC system equipped with a 7683 Series injector and auto-sampler; the electron impact (70 eV) mass spectroscopy detector for this system was an Agilent 5975 MSD equipped with an Agilent HP-5 column (0.25 μm film thickness, 30 m long, 0.32 mm inner diameter). The GC-MS

method used the following sequence: 5 min hold at 35 °C, temperature ramp at 20 °C min^{-1} to 250 °C, and 2.25 min hold at 250 °C. Size exclusion chromatography (SEC) data for hydroxyl-terminated PMCL was obtained at 35 °C using an HP/Agilent 1100 series size-exclusion chromatograph equipped with a HP 1047A refractive index detector. The mobile phase was chloroform (1 mL min^{-1} flow rate); prior to reaching the detector, the sample passed through a PLgel 5 μm guard column before passing through three successive PLgel Mixed C columns. The M_n and $Đ$ for each polymer was determined using a 10-point calibration curve generated using EasiCal polystyrene standards purchased from Agilent.

Thermal characterization data was obtained using a TA Instruments Discovery Series differential scanning calorimeter and thermogravimetric analysis was performed on a TA Instruments Q500 Analyzer. Samples subjected to calorimetry (*ca.* 5 mg) were placed in T-Zero hermetic pans and cooled to –90 °C before the first and second heating ramp to 150 °C; all temperature sweeps were performed at 10 °C min^{-1} and under nitrogen atmosphere. During the first heat, the samples were held at 150 °C for 60 seconds to erase any thermal history. The glass transition temperature was taken as the midpoint of the transition using the *Trios* software. Thermogravimetric analysis was performed on all samples (*ca.* 10 mg) at 10 °C min^{-1} under nitrogen or air to 500 °C.

Extractions of sol fractions (i.e., swell tests) were performed using DCM. A small amount of each cross-linked sample (*ca.* 50-100 mg) was immersed in DCM for 48 h before the solvent was decanted. The swollen sample was then dried in a vacuum oven for 48 h before the final mass was measured. The gel fraction was calculated by taking the ratio of the final mass to the initial mass.

A Shimadzu Autograph AGS-X series instrument was used to conduct uniaxial extension and hysteresis measurements at room temperature with dogbone-shaped specimens [*ca.* 1 mm (T) x 2.5 mm (W) x 27 mm (L) with a gauge length of *ca.* 15 mm]. For both measurements, metal grips were used and the test speed was set to a ramp rate of 50 mm min^{-1}. The data obtained were analyzed using the *Trapezium* software. The extension to break tests were performed with 5 replicates per CE sample and the values reported are averages and standard deviations for each set. The Young's modulus was calculated by taking the slope of the stress-strain curve from 0-10% strain. For hysteresis tests, one dogbone from each CE sample was subjected to cyclical loading (67% strain) and unloading for 20 cycles. The hysteresis energy loss per cycle was calculated by subtracting the area of the unloading curve from that of the loading curve, whereas the tensile set per cycle was determined from the residual strain present when the unloading cycle afforded zero stress.

Dynamic mechanical thermal analysis (DMTA) was performed using a TA Instruments RSA-G2 analyzer with dogbone-shaped specimens (same dimensions as above) in a tensile geometry. Liquid nitrogen was used to cool the sample to –90 °C and the axial force was continuously adjusted to 0.00 N (sensitivity 0.01 N) while the sample was cooling. After equilibration, the axial force was adjusted to 0.20 N of tension (sensitivity 0.01 N) to ensure no buckling of the sample. The proportional force mode was set to force tracking to maintain an axial force that was at least 100% greater than the dynamic oscillatory force. The strain adjust was set to 30% with minimum and maximum strain values of 0.05% and 10% and minimum and maximum forces of 0.01 N and 0.2 N, respectively; these settings prevented the sample from going outside the specified strain

range. The sample was then heated to 200 °C at a rate of 5 °C min^{-1} with an oscillating strain of 0.05% at an angular frequency of 6.28 rad s^{-1} (1 Hz). The T_g was determined using the maximum value in tan δ, which is defined as the ratio of the loss modulus (*E''*) to the storage modulus (*E'*). The effective molar mass between cross-links $M_{x,eff}$ was calculated using eq 1:

$$E'(T) = 3G'(T) = 3RT\nu_e = \frac{3\rho RT}{M_{x,eff}} \quad (1)$$

where *E'* and *G'* denote the storage modulus under tension and shear, respectively, *R* is the universal gas constant, *T* denotes the absolute temperature in the rubbery plateau region, ν_e is the effective cross-link density, and ρ is the density of the CE samples (approx. 1.065 g cm^{-3} as measured by a density gradient column).

Shear rheology was performed on a TA Instruments Rheometric Series ARES Classic using 8 mm diameter parallel plates under a nitrogen atmosphere. Prior to performing frequency sweeps, a strain sweep was performed from 0.1% to 10% and a linear response in the signal was observed. The PMCL sample was then equilibrated at the desired temperature for 10 minutes before performing a frequency sweep from 0.01 to 100 rad/s at an oscillating strain of 1.0%. Each sweep was performed at one of the following temperatures: 10, 0, –10, –20, –30, –40, and –50 °C. Time-temperature superposition was then used to generate a master curve (reference temperature of 273 K) and the entanglement molar mass M_e was determined from the plateau modulus G_N' using eq 2:

$$M_e = \frac{\rho RT}{G_N'} \quad (2)$$

where ρ is the density of the PMCL (assumed to be 1.065 g cm^{-3}), T denotes the absolute temperature, and R is the universal gas constant. The plateau modulus was defined as the shear storage modulus at the minimum of tan δ.

4.3.10. Enzyme Solutions for Polyester Enzymatic Hydrolysis Experiments.

The enzymatic hydrolysis experiments were performed with a cutinase from *Fusarium solani* (FsC, M_w = 20.8 kg/mol and pI = 8.4 as calculated from the sequence entry 1AGY[49] in the RCSB protein data bank (PDB) using the pI/MW compute tool from ExPASy[50]) that was obtained as a solution from ChiralVision (product number Novozym 51032). The cutinase concentration of the obtained solution was determined to be 4.24 ± 0.16 mM (mean ± standard deviation for triplicate measurement) by absorbance measurements at 280 nm using a molar extinction coefficient of 13610 M^{-1} cm^{-1}.[51] The obtained solution was diluted to a final cutinase concentration of 4.1 mg FsC/mL using 10 mM KCl prepared with Milli-Q H_2O (resistivity = 18.2 MΩ cm, Barnstead NANOpure Diamond); aliquots of the dilute solution were stored in 2 mL Eppendorf tubes in a freezer at –20 °C and thawed before use. In between experiments, the thawed enzyme solutions were kept in a 5 °C refrigerator and were not used if more than one week had passed since thawing.

4.3.11. Aqueous Solutions for pH-Stat Titrations and Batch Reactors.

Two solutions were prepared in Milli-Q H_2O with 10 mM of KCl as background electrolyte: one for the pH-stat titrations and one for the batch reactors coupled to total organic carbon (TOC) analysis (see section below). The solution used in titration experiments additionally contained a small amount of phosphate buffer (0.067 mM) to

facilitate adjustment of the initial solution pH at the start of each experiment close to the desired pH value of 7.0; the effect of buffer on the extent of hydrolysis was considered negligible because the amount of phosphate present corresponded to less than 0.1 mol% of the acid produced from complete hydrolysis. The solution used for hydrolysis experiments coupled to solution TOC analysis contained a higher phosphate buffer concentration (340 mM, pH 7.1) to keep the pH close to 7.0 over the course of the hydrolysis; the final pH values for all incubations were between 6.8 and 6.9.

4.3.12. Polyester Elastomer Enzymatic Hydrolysis Experiments

A Titrando 907 (Metrohm) and the *Tiamo 2.5* software were used for automated pH-stat titration experiments with a KOH solution (approx. 30 mM) as the titrant. The exact titrant concentration was determined before and after each experiment by titrating a citric acid solution (10 mM, initial pH of approx. 2.5). This experimental setup was used at temperatures between 20 and 40 °C. Hydrolysis at lower temperatures (≤ 20 °C) was studied in batch systems using repeated solution TOC analysis. A circular die cut (4.3 mm inner diameter) was used to punch out discs of polyester elastomer for either experimental set-up; this cutting procedure resulted in high reproducibility in the surface area between experiments. Based on the dimensions of the die cut and the thicknesses of the polyester films, the surface areas present in a pH-stat titration and a batch reactor experiment were 85 ± 1 mm^2 and 86 ± 1 mm^2 (mean ± standard deviation), respectively. Due to the high reproducibility in the first set of titrations performed in triplicate (i.e., CE-22 at 40 °C) as well as time constraints due to the sample throughput (only two titrations could be run in parallel), all subsequent experiments were performed in duplicate.

For a typical pH-stat titration experiment, 10 mL of enzyme-free solution was pipette-transferred into a water-jacketed 25-mL glass vessel sitting atop a stir plate. A stir bar was added and the temperature was equilibrated. A circular Teflon sheet was taped over the vessel to form a lid, and pre-cut holes in the Teflon were used to position the pH probe, buret line for KOH delivery from the titrator, nitrogen gas line, and temperature probe in the solution. The Teflon cap and the nitrogen gas line served to minimize artifacts from carbon dioxide in-gassing (explained in the section below). Data collection was then started and two discs of elastomer were submerged in the solution. The solution was left to stir for approximately 24 h before enzyme addition to monitor the background titration rate (no FsC present) for data correction (see section below). Freshly thawed cutinase solution (193 μL, see above) was then added using a micropipette ($[FsC]_0$ = 78 μg/mL) and subsequent hydrolysis was monitored by KOH addition. During hydrolysis, the pH remains constant because the carboxylic acid moieties created via ester hydrolysis are neutralized; the amount of titrant used therefore corresponds to the number of esters hydrolyzed, and this number can be compared to the expected ester content based on the sample mass and the structure of the repeat unit.

For a hydrolysis experiment monitored by TOC analysis, 10 mL of enzyme-free solution was pipette-transferred into a batch reactor (i.e., a 20-mL amber glass vial). Two elastomer discs were added and the reactor was placed in either a temperature-controlled incubator with a shaking unit (a Kühner AG LT-W or a Kühner AG ISF1-X for 10 °C and 20 °C experiments, respectively) or in a refrigerator (Electrolux ZFX31401WA) equipped with a stir plate (for 2 °C experiments). The incubations were sampled twice (2 and 7 day time points) before enzyme addition on day 7. Sampled aliquots were 0.5 mL and were

transferred into 2 mL Eppendorf tubes using a micropipette. The aliquots were stored in a freezer and thawed before TOC analysis. The TOC measurements were conducted on 80 μL aliquots that were collected from each batch reactor at various time points; this volume was diluted with Milli-Q water to a final volume of 8 mL, mixed well, and analyzed on a Shimadzu TOC-L analyzer. The TOC content in each sample was determined using a standard calibration curve (0 to 100 mg C/L) that was obtained by analyzing solutions made from a TOC standard (Sigma-Aldrich, product number 76067). The data obtained from TOC analysis (mg C/L) was compared to the expected mass of carbon in the added elastomer to calculate the extent of hydrolysis. The temperature around the batch reactors was monitored every few days using a thermocouple (Digi-Sense Type K), and the exact temperatures of each chamber and the fridge were recorded over a 24 h period using Thermochron iButton devices (DS1921 and DS1922).

After terminating each hydrolysis experiment, a small portion of the solution was transferred into a glass vial and evaporated at 105 °C in an oven. The solid, white, seemingly crystalline residue (i.e., the major hydrolysis product) was then reconstituted in D_2O (0.75 wt% TSP) for subsequent analysis by ^{1}H and ^{13}C NMR spectroscopy. We verified that the elevated temperature did not change the hydrolysis product observed by NMR spectroscopy by instead employing either freeze-drying or evaporation at 60 °C to remove solvent; the obtained spectra were indistinguishable from those obtained after evaporation at 105 °C.

4.3.13. Titration Controls and Data Correction.

Preliminary results at pH 7 demonstrated significant amounts of base titrated over experimentally relevant timespans (several days) without polymer or enzyme present. This observation was attributed to the equilibrium of CO_2 dissolving in solution to form carbonic acid, which was continually titrated because the equilibrium pH lies below 7. To mitigate this effect, a Teflon sheet was formed into a lid and holes were cut out to allow for the pH probe, temperature probe, buret, and nitrogen gas line. The nitrogen gas stream in the headspace was kept at a constant, low pressure throughout the experiment to displace and inhibit further introduction of CO_2. Furthermore, the nitrogen gas was run through two sealed flasks before reaching the vessel; the first was used to bubble the gas through water and saturate it, whereas the second was empty and served to catch any condensation.

With all these controls in place, the rate of titration attributed to CO_2 ingassing was minimized to two orders of magnitude less than the enzymatic hydrolysis rate. To demonstrate this comparison, the first titration was allowed to run for 24 h before adding polymer. The addition of polymer causes a negligible change in the titration rate observed in the absence of polymer and enzyme, whereas the subsequent addition of enzyme increases the titration rate by a factor of 25 (**Figure 4.12**). The contributions of ingassing and non-enzymatic hydrolysis to the observed enzymatic hydrolysis rate were 3% and 1%, respectively. The initial slope was therefore used to correct the hydrolysis data obtained (**Figure 4.13**). The contribution of non-enzymatic hydrolysis was thereafter considered negligible, and the slopes used for the correction of all subsequent data corresponds to the titration rate observed with polymer and solution (no enzyme) over *ca.* 24 h.

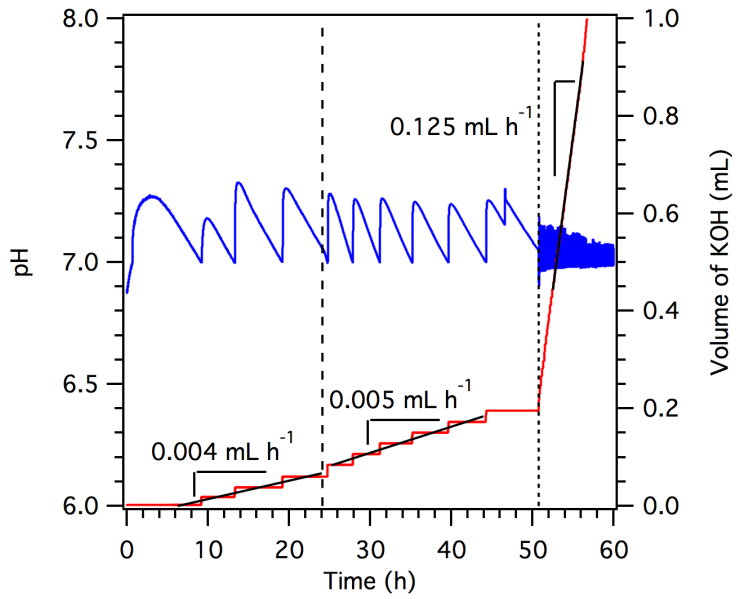

Figure 4.12. The first 60 h during the first titration experiment with CE-22 elastomer at pH 7 and 40 °C; polymer was added to the solution at 24 h (dashed line) and enzyme was added after 51 h (dotted line). The initial titration rate observed in the absence of polymer and enzyme is low, and addition of polymer results in a negligible change in the titration rate, indicating that non-enzymatic hydrolysis is insignificant. The subsequent addition of enzyme at *ca.* 50 h increases the titration rate by two orders of magnitude.

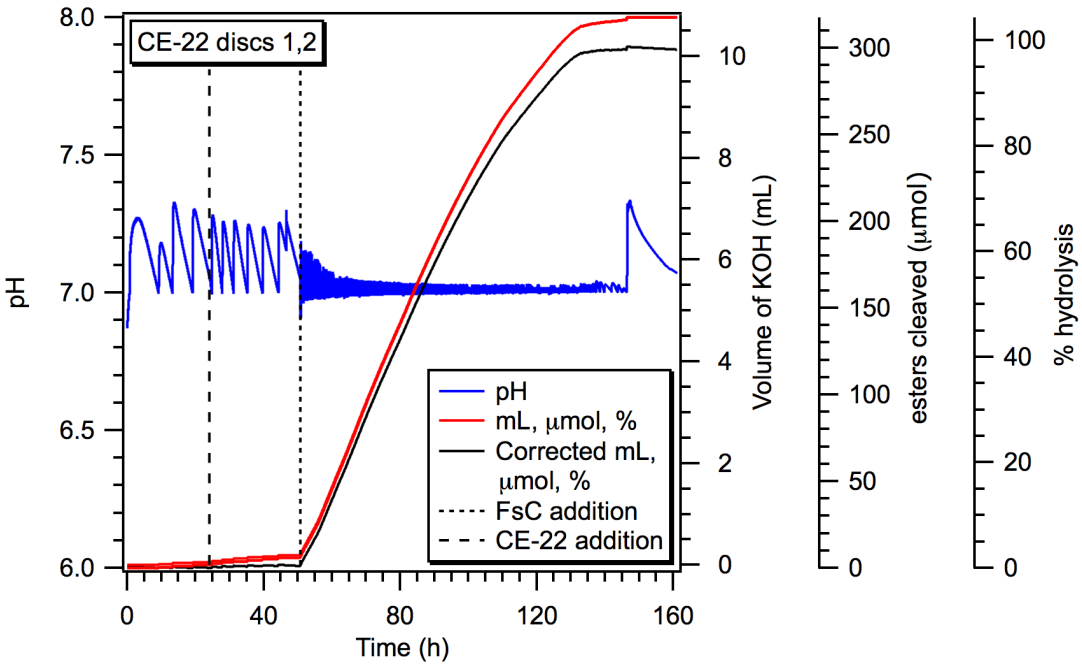

Figure 4.13. The first titration experiment with CE-22 elastomer at pH 7 and 40 °C, demonstrating the data correction for the entire pH-stat titration curve.

4.3.14. Non-enzymatic Hydrolysis Control in Phosphate Buffer.

The non-enzymatic degradation of the elastomers was also investigated by incubating CE samples in phosphate buffered saline (PBS, 1 M, pH = 7.4) at room temperature and 37 °C. Three replicates of each CE sample were used (*ca.* 50 mg each); each replicate was immersed in 20 mL of the aqueous PBS solution in separate scintillation vials and either left at room temperature or heated to 37 °C. The insoluble mass was recorded after removing each sample from the solution and patting it dry with a Kimwipe™, after which the sample was re-immersed in the same solution. Solutions were checked weekly with litmus paper to ensure their pH remained stable; none of the solutions showed pH variance by this method. The data presented in the plots of insoluble mass % (percentage of original mass) over time includes the averages and standard deviations of the triplicate samples at each temperature (**Figure 4.14**). No mass loss was observed over *ca.* 15 days at either temperature, which strongly supports the conclusion that hydrolysis of CE samples is very slow when enzymes are absent.

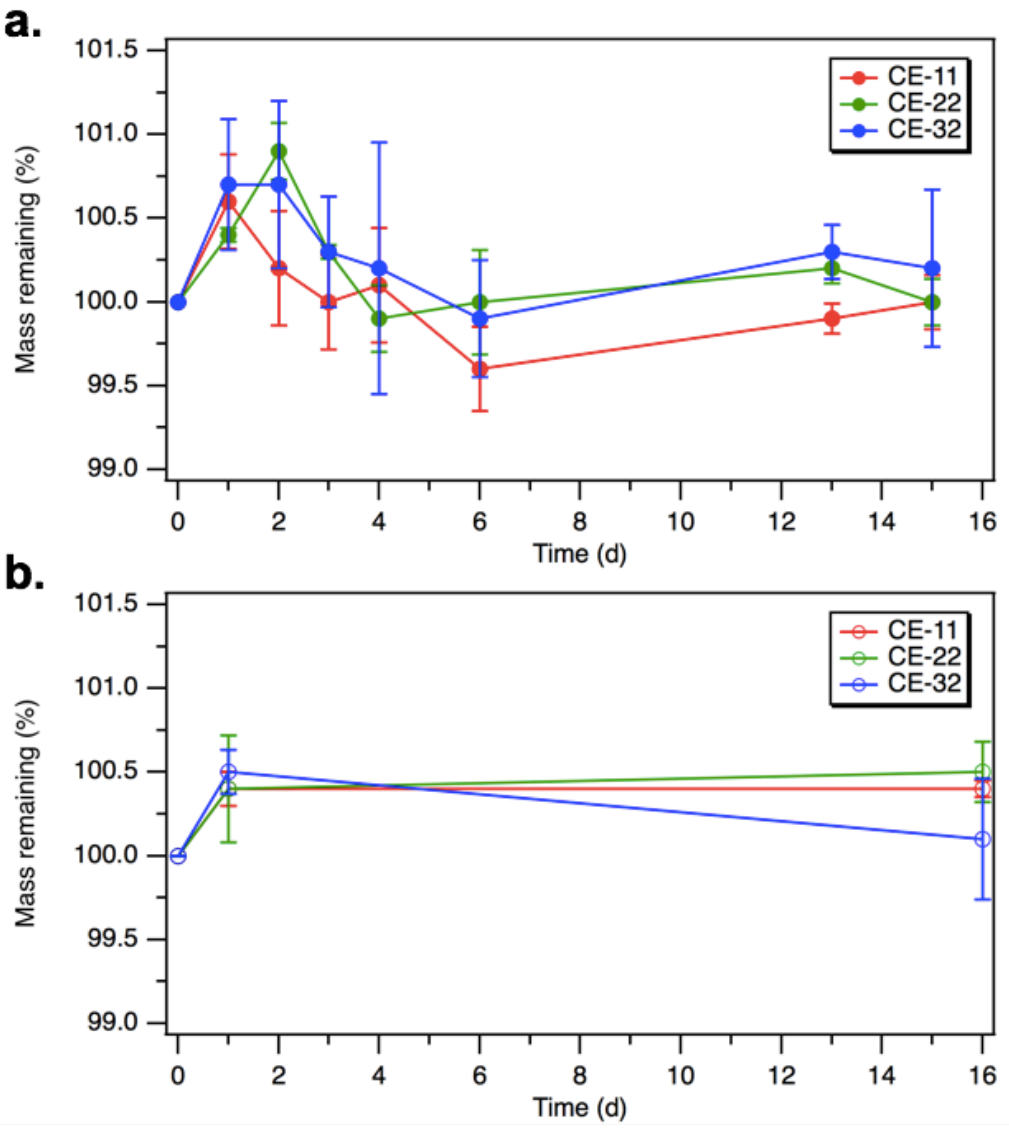

Figure 4.14. Gravimetric analyses of the CE samples in phosphate buffered saline (1 M, pH = 7.4) for *ca.* 15 days at (**a**) room temperature and (**b**) 37 °C. The negligible change in the insoluble mass over this time period supports that non-enzymatic hydrolysis is very slow.

4.4. Results and Discussion

4.4.1. Synthesis of Polyester Elastomers and Investigation of Stannous Octoate Catalyzed β-Lactone Ring-Opening.

Industrial-scale Baeyer-Villiger oxidation is typically performed with organic peracids, which is a robust and effective approach for synthesizing lactones.[52] We employed this approach to convert γ-methyl-cyclohexanone to MCL on both the small and large laboratory scale (up to 1 kg). With MCL in hand, we prepared a series of hydroxyl-terminated, star-shaped poly(γ-methyl-ε-caprolactone) (PMCL) with varying molar mass by $SnOct_2$-catalyzed ring-opening transesterification polymerization with a pentaerythritol initiator (**Figure 4.15**). Solvent casted mixtures of these PMCLs, the bis(β-lactone) cross-linker (0 to 5 eq. β-lactone to OH), and $SnOct_2$ were heated overnight to afford cross-linked polyester networks (**Figure 4.15**).

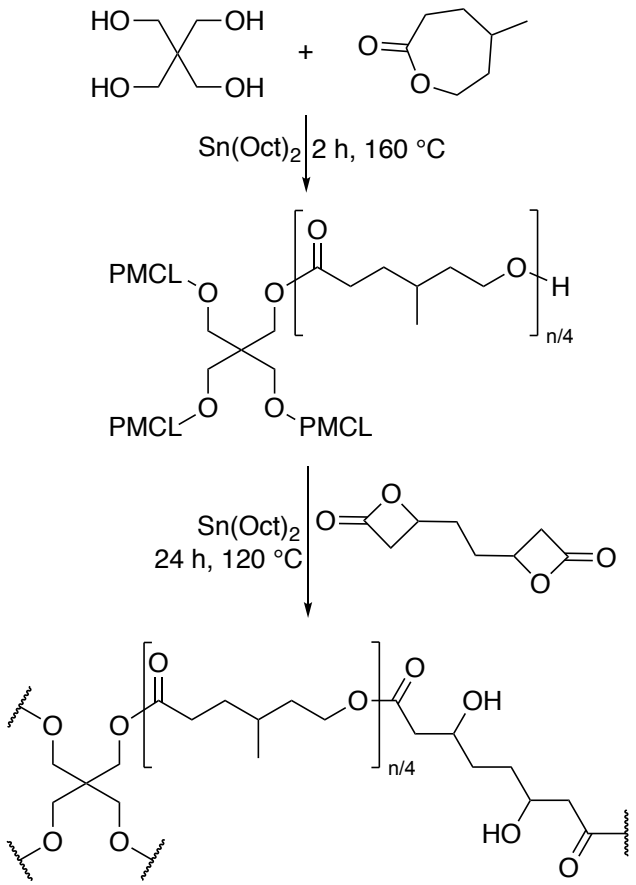

Figure 4.15. Hydroxyl-terminated star-shaped poly(γ-methyl-ε-caprolactone) (PMCL) was synthesized via ring-opening polymerization of γ-methyl-ε-caprolactone using stannous octoate ($SnOct_2$) as a transesterification catalyst. The star polymers were then cross-linked using a bis(β-lactone) monomer and $SnOct_2$ to afford polyester networks.

The degree of cross-linking was evaluated by swelling the films in DCM and extracting the soluble (sol) fraction. The gel fraction increased from 0 to 0.92 as the ratio of β-lactone to hydroxyl groups (i.e., the amount of cross-linker for a given mass of polymer) was increased from 0 to 1. Furthermore, use of excess bis(β-lactone) resulted in gel fractions greater than 0.90 (**Figure 4.16** and **Table 4.2**); this suggested that the cross-linking proceeded by ring-opening of the lactones to generate reactive β-hydroxyesters, similar to a chain-growth mechanism rather than one that relies on addition reactions, which are less tolerant to deviations from ideal stoichiometry. When holding the

stoichiometric ratio constant (2.0 β-lactones per hydroxyl), we found that the gel fraction decreased when the molar mass of PMCL used was more than 30 kg/mol (**Figure 4.16** and **Table 4.2**). Although gel fractions of 0.80 were achieved with 41 kg/mol PMCL on a small scale, later attempts to scale the synthesis were unsuccessful in yielding cross-linked polyester over 24 h. Increasing the reaction time to 72 h did not result in any measurable gel fraction despite further β-lactone ring-opening detected by IR spectroscopy (i.e., decreasing signal for β-lactone carbonyl stretch, **Figure 4.17**); we therefore attributed the low cross-linking efficiency to a significant decrease in the rate of reaction due to the low concentration of hydroxyl end-groups present in a given amount of high M_n prepolymer. No significant cross-linking was observed in the absence of catalyst and/or when the end-groups of the prepolymer were modified to carboxylic acids (**Table 4.2**). The success of cross-linking under these conditions (i.e., 120 °C for 24 h) was thus found to rely on the presence of hydroxyl end-groups, $SnOct_2$, and prepolymer M_n less than or equal to 30 kg/mol. Although we could not analyze the chemical junctions of the insoluble networks, we hypothesized that $SnOct_2$ facilitated ring-opening of the β-lactone by the hydroxyl end-groups to generate reactive β-hydroxyesters.

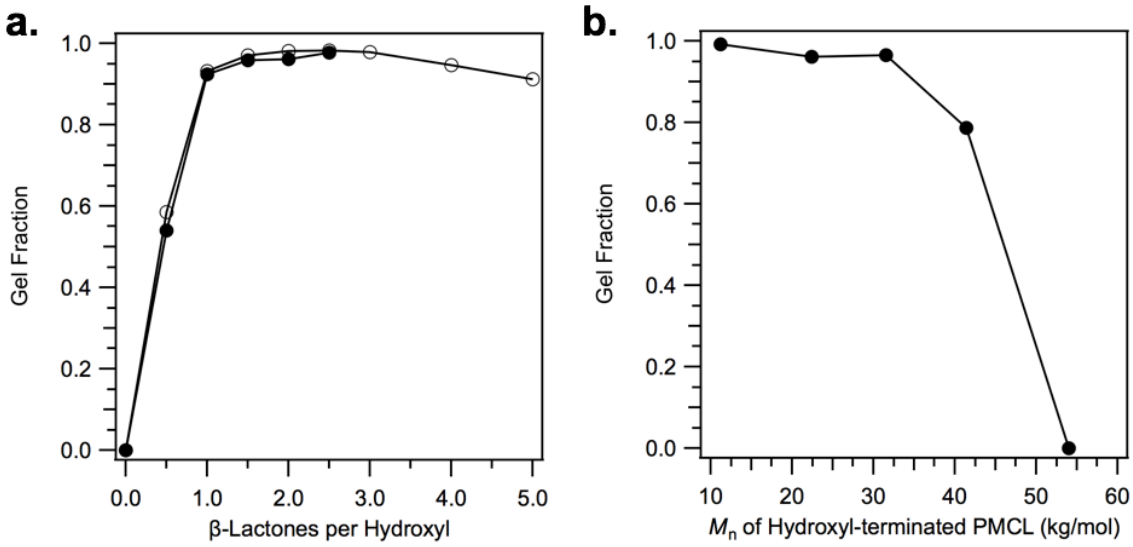

Figure 4.16. Plots of gel fraction as a function of (**a.**) the number of β-lactones per hydroxyl end-group of PMCL and (**b.**) the molar mass of the PMCL at a constant 2.0 β-lactones per hydroxyl. The experiment shown at left was performed two times (open and closed circles), and the results imply that the cross-linking is not governed by simple A_4 + B_2 step growth statistics. The statistical approach developed by Flory and Stockmayer predicts that gelation should be impossible for an A_4 + B_2 system (i.e., star-PMCL and bis(β-lactone) respectively) when the stoichiometric ratio of A and B groups r drops under 0.33, as the critical extent of conversion ρ_c for gelation exceeds 1.0 at this value. In this case, values of $r \leq 0.33$ corresponds to β-lactone to hydroxyl ratios of ≥ 3. No precipitous drop in the gel fraction was observed experimentally at β-lactone to hydroxyl ratios ≥ 3, which suggested that the cross-linking was not governed by simple A_4 + B_2 step-growth statistics.

Table 4.2. Small-scale cross-linking PMCL experiments with bis(β-lactone).

M_n (kg/mol)[a]	$Đ$[b]	EG[c]	Lac:EG[c]	$SnOct_2$ mol %[e]	Gel fraction[f]
12.6	1.26	OH	0.0	2.5	0.000
12.6	1.26	OH	0.5	2.5	0.540
12.6	1.26	OH	1.0	2.5	0.924
12.6	1.26	OH	1.5	2.5	0.959
12.6	1.26	OH	2.0	2.5	0.962
12.6	1.26	OH	2.5	2.5	0.977
12.6	1.26	OH	2.0	0.0	0.000
11.2	1.23	OH	0.0	2.5	0.000
11.2	1.23	OH	0.5	2.5	0.586
11.2	1.23	OH	1.0	2.5	0.933
11.2	1.23	OH	1.5	2.5	0.971
11.2	1.23	OH	2.0	2.5	0.982
11.2	1.23	OH	2.5	2.5	0.982
11.2	1.23	OH	3.0	2.5	0.979
11.2	1.23	OH	4.0	2.5	0.946
11.2	1.23	OH	5.0	2.5	0.912
11.2	1.23	OH	2.0	2.5	0.992
22.4	1.29	OH	2.0	2.5	0.962
31.5	1.30	OH	2.0	2.5	0.966
41.4	1.38	OH	2.0	2.5	0.787
54.0	1.40	OH	2.0	2.5	0.000
11.1	–	COOH	2.0	2.5	0.000
11.1	–	COOH	2.0	0.0	0.000

[a] Calculated using end-group analysis via ^{1}H NMR spectroscopy in $CDCl_3$, specifically using the integrations corresponding to the protons adjacent to the hydroxyl end group and adjacent to the carbonyl in each repeat unit. [b] Measured using size-exclusion chromatography in $CHCl_3$ by comparison to polystyrene standards. [c] EG denotes end group; the COOH terminated PMCL was made by adding succinic anhydride after polymerization (one-pot, sequential addition). [d] The number of β-lactones per end group of the pre-polymer. [e] This mol % is based on the moles of pre-polymer end-groups present (i.e., 4 times the moles of pre-polymer). [f] Measured using dichloromethane as the swelling solvent.

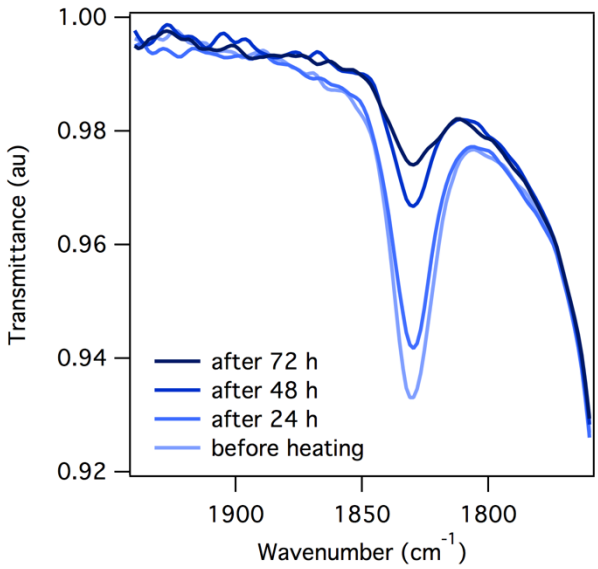

Figure 4.17. An overlay of IR spectra of reaction mixture (4 g scale) containing PMCL (41 kg/mol), bis(β-lactone) (1.5 β-lactones per hydroxyl), and $SnOct_2$ (2.5 mol% with respect to hydroxyl end-groups of PMCL) after several periods of heating the mixture for 24 h at 120 °C. The decreasing intensity of the β-lactone carbonyl stretch at 1830 cm^{-1} indicates that more β-lactones are ring-opening as the reaction time is increased, but after 72 h the product after 72 h was still fully soluble (*i.e.*, not cross-linked).

We tested our hypothesis by performing a model compound study with benzyl alcohol (1.0 equiv) and β-valerolactone (0.9 equiv). These compounds were reacted in the presence of $SnOct_2$ (0.025 equiv) and monitored over 24 h at 120 °C; aliquots were removed periodically and analyzed using GC-MS, ^{1}H NMR spectroscopy, and ATR-FTIR spectroscopy. Although we hypothesized that ring-opening would occur via acyl-oxygen scission, several other products were possible due to dehydration at elevated temperature or ring-opening by alkyl-oxygen scission (**Figure 4.18**).

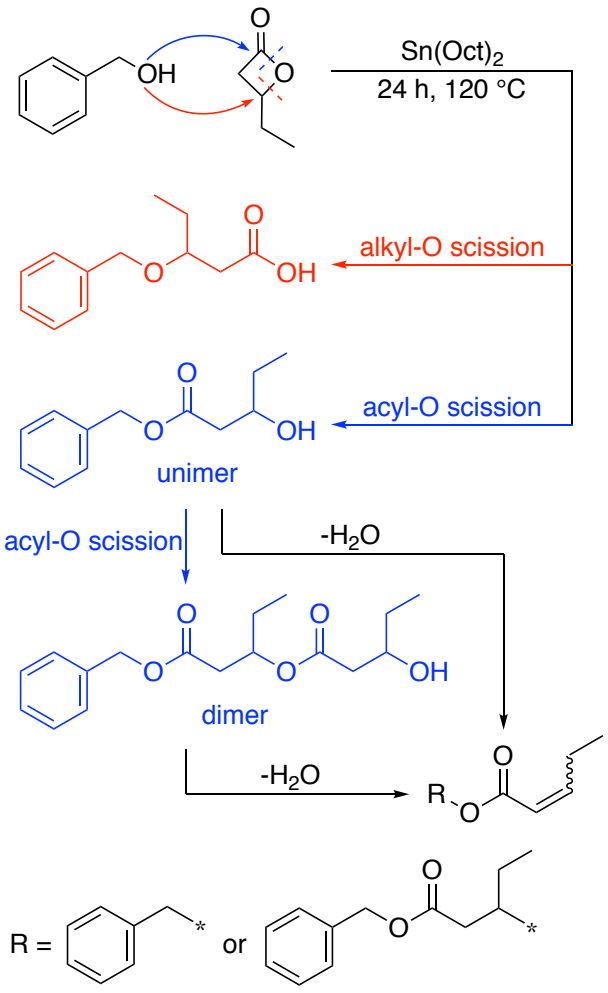

Figure 4.18. Model compound study and expected products. The major products obtained from the reaction of benzyl alcohol and β-valerolactone after 24 hours were unimer and dimer, accompanied by some minor dehydration products.

The disappearance of the carbonyl peak at approximately 1820 cm^{-1} from the strained β-lactone and the appearance of a carbonyl peak at 1730 cm^{-1} from the ring-opened product indicated that all of the β-lactone ring opened to yield aliphatic ester bonds; no evidence of alkyl-oxygen scission or substantial dehydration is apparent in the ATR-FTIR spectra, and the O–H stretching frequency remained relatively unchanged (**Figure 4.19** and **Figure 4.20**). Monitoring the reaction progress by GC-MS supported corroborated the ATR-FTIR spectroscopy finding that the initial reaction mixture contained primarily unreacted benzyl

alcohol and β-valerolactone (**Figure 4.21**, **Figure 4.22**, and **Figure 4.23**). Upon heating for 30 min, the starting materials were partially converted into two major products; after 24 h of heating, the presence of residual benzyl alcohol and two additional minor products were observed (**Figure 4.24** and **Figure 4.25**). The mass spectrum of all products exhibited a peak at 91.1 m/z, which is characteristic of a tropylium cation and indicated that benzyl groups were present in each structure (**Figure 4.26**, **Figure 4.27**, **Figure 4.28**, and **Figure 4.29**).

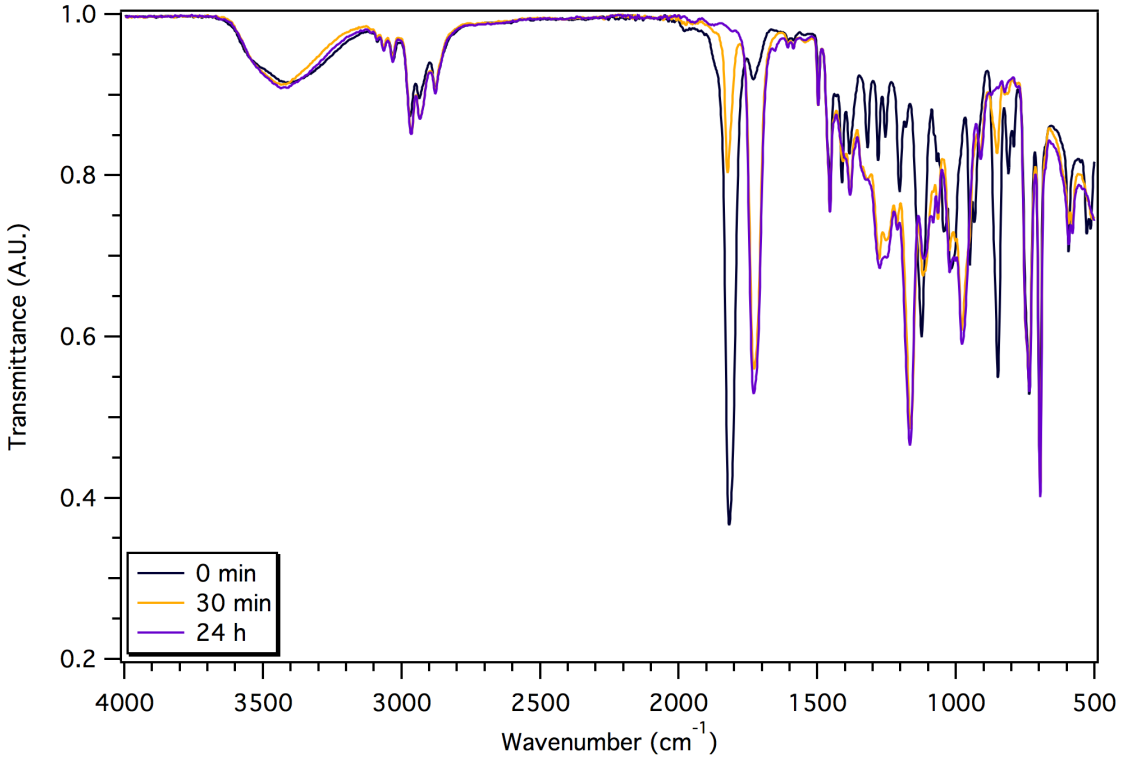

Figure 4.19. Overlay of IR spectra for three time points during the $SnOct_2$-catalyzed reaction of benzyl alcohol and β-valerolactone.

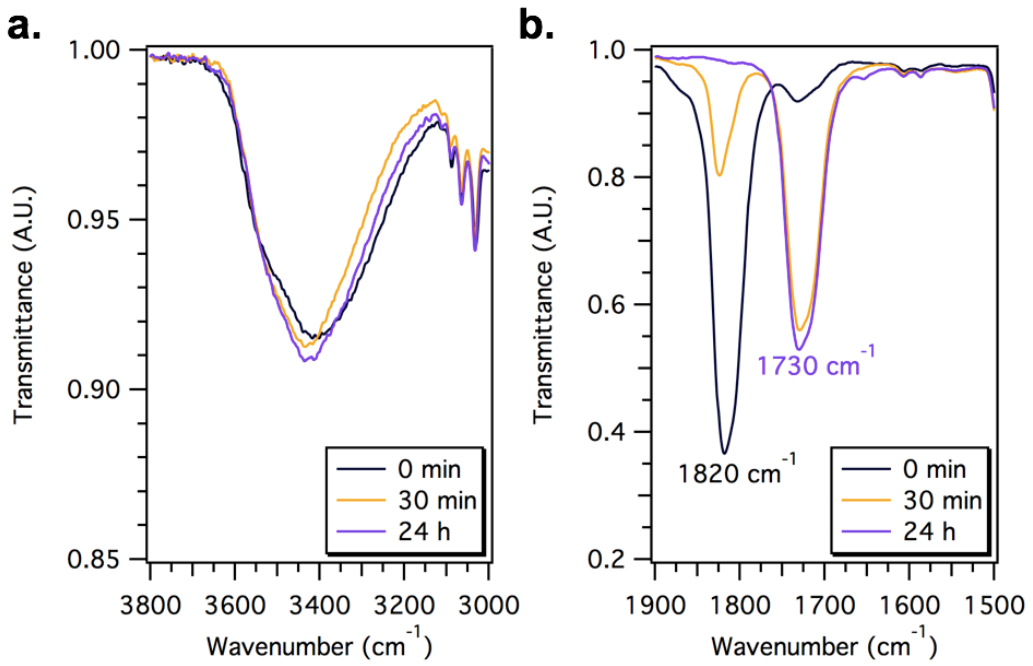

Figure 4.20. Enhanced sections of the IR spectra for three time points during the $SnOct_2$-catalyzed reaction of benzyl alcohol and β-valerolactone; the presence of a hydroxyl remains throughout the reaction (**a.**) and the β-lactone ring opens to form an ester (**b.**)

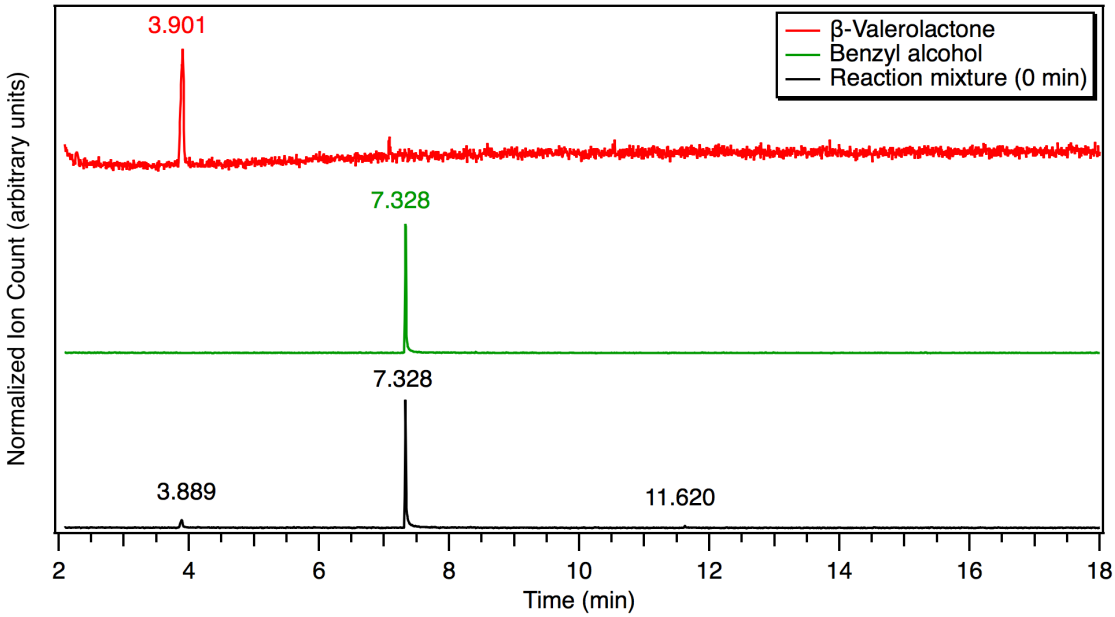

Figure 4.21. Overlay of gas chromatographs for the initial time point of the model study and the two reactants: benzyl alcohol and β-valerolactone. A minute amount of product is present in the reactant mixture prior to heating, as evidenced by the small peak at a retention time of 11.6 minutes.

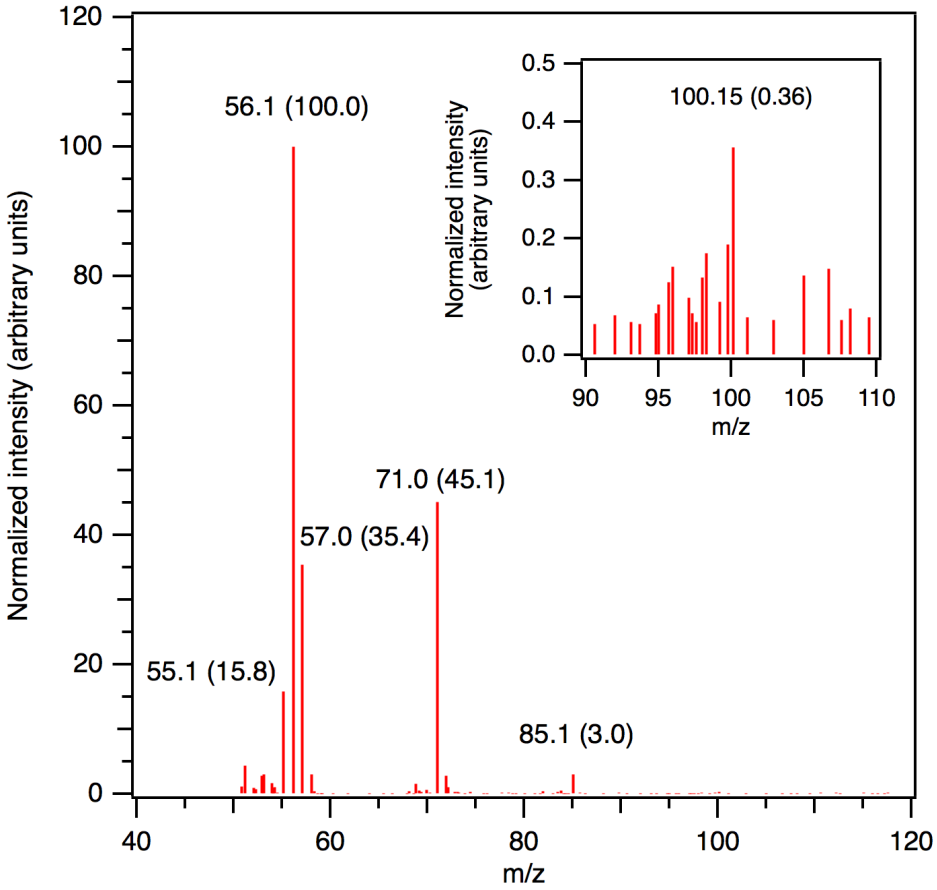

Figure 4.22. The extracted mass spectrum for the peak in the gas chromatograph of the β-valerolactone; the peak labeled in the inset is likely the molecular ion peak.

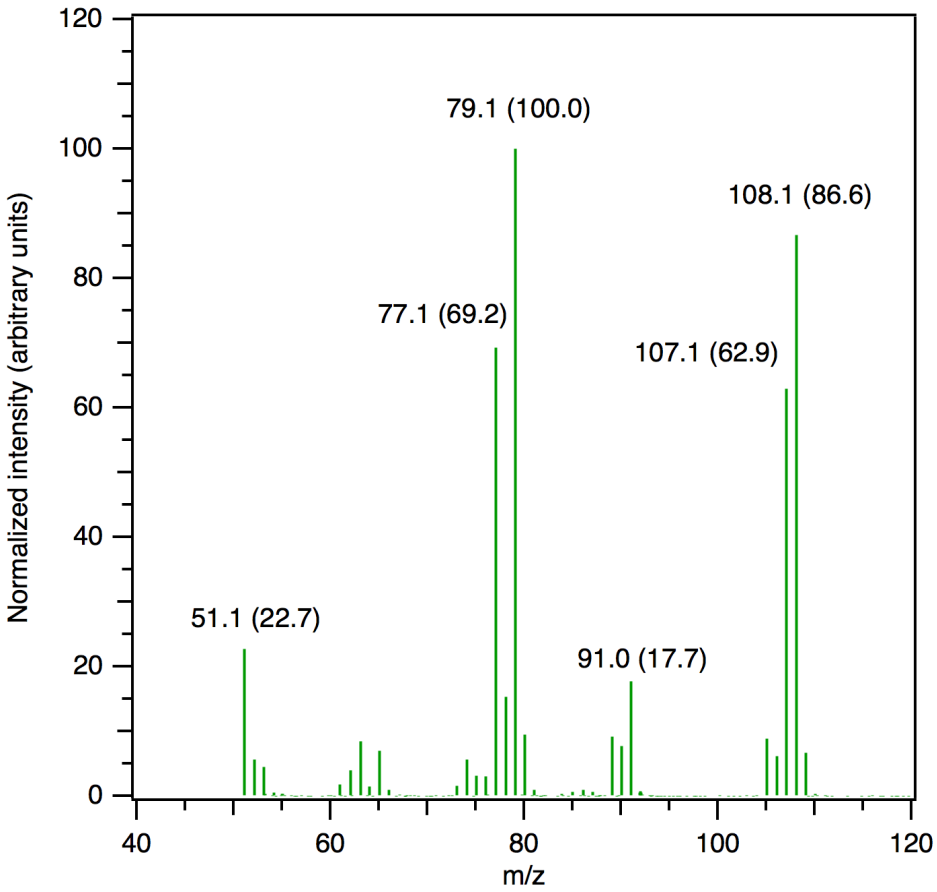

Figure 4.23. The extracted mass spectrum for the peak in the gas chromatograph of benzyl alcohol.

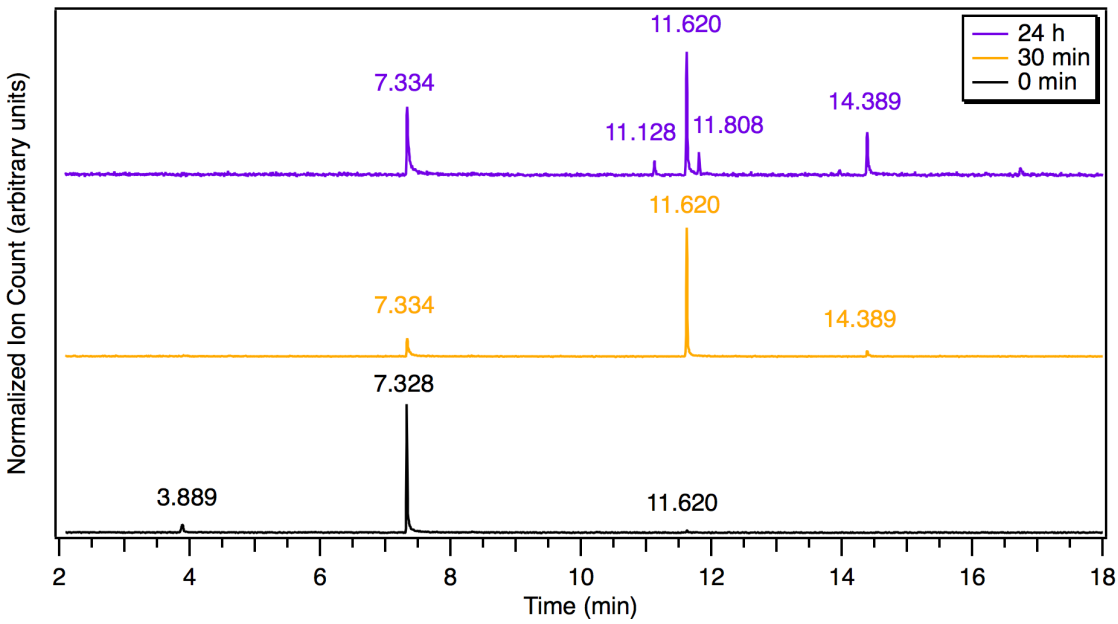

Figure 4.24. Overlay of gas chromatographs for three time points during the $SnOct_2$-catalyzed reaction of benzyl alcohol and β-valerolactone.

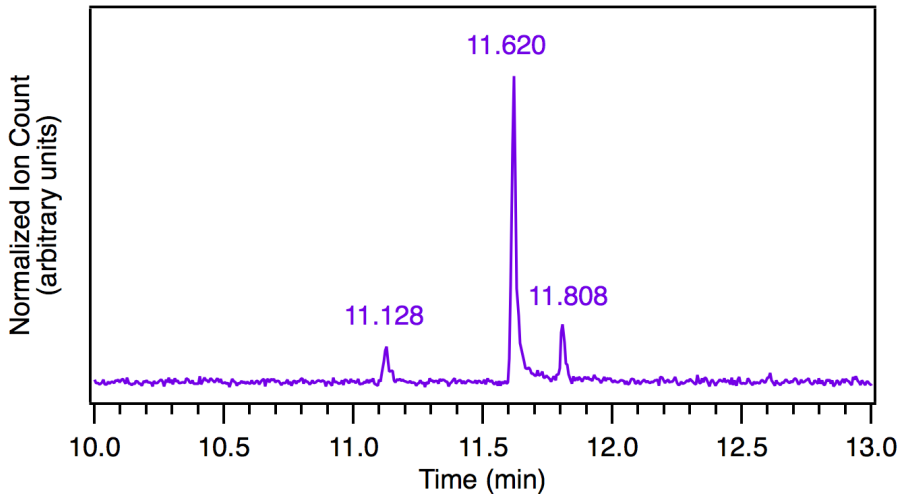

Figure 4.25. Enhanced section of the gas chromatograph for the 24 h time point of the model study, showing two minor peaks flanking the major peak at a retention time of 11.6 minutes.

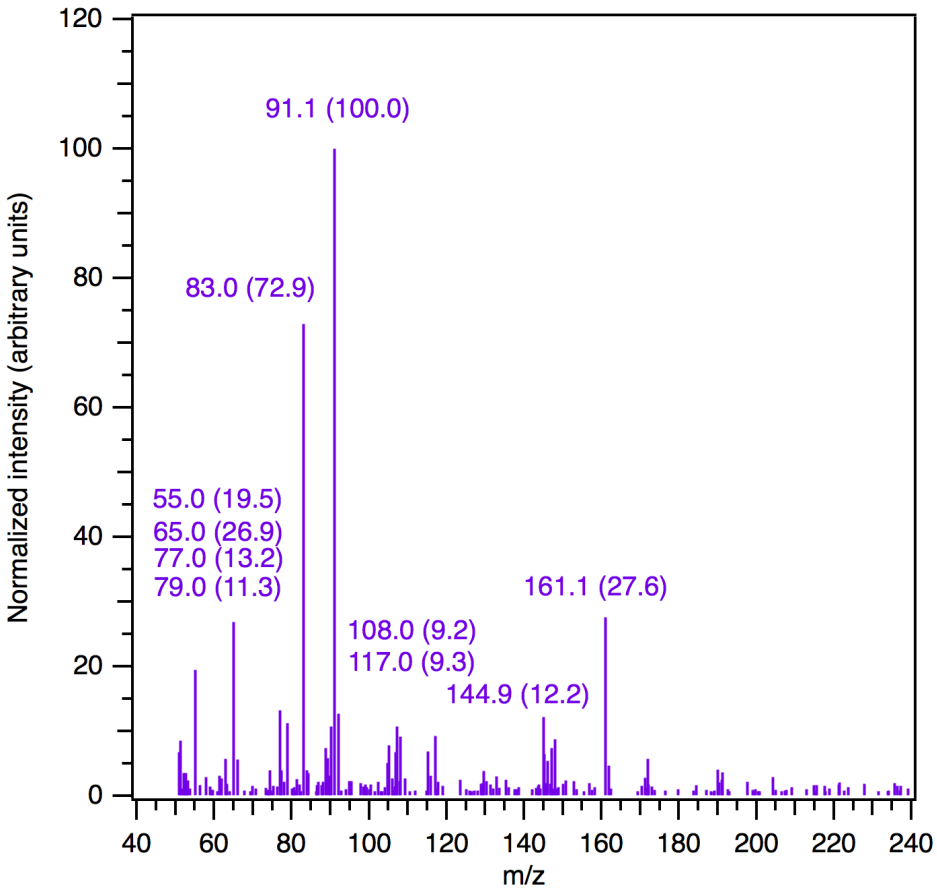

Figure 4.26. The extracted mass spectrum for the peak at a retention time of 11.1 minutes in the gas chromatograph of the 24 h time point. This spectrum likely corresponds to the dehydration product for the unimer formed by the reaction of benzyl alcohol with one β-valerolactone.

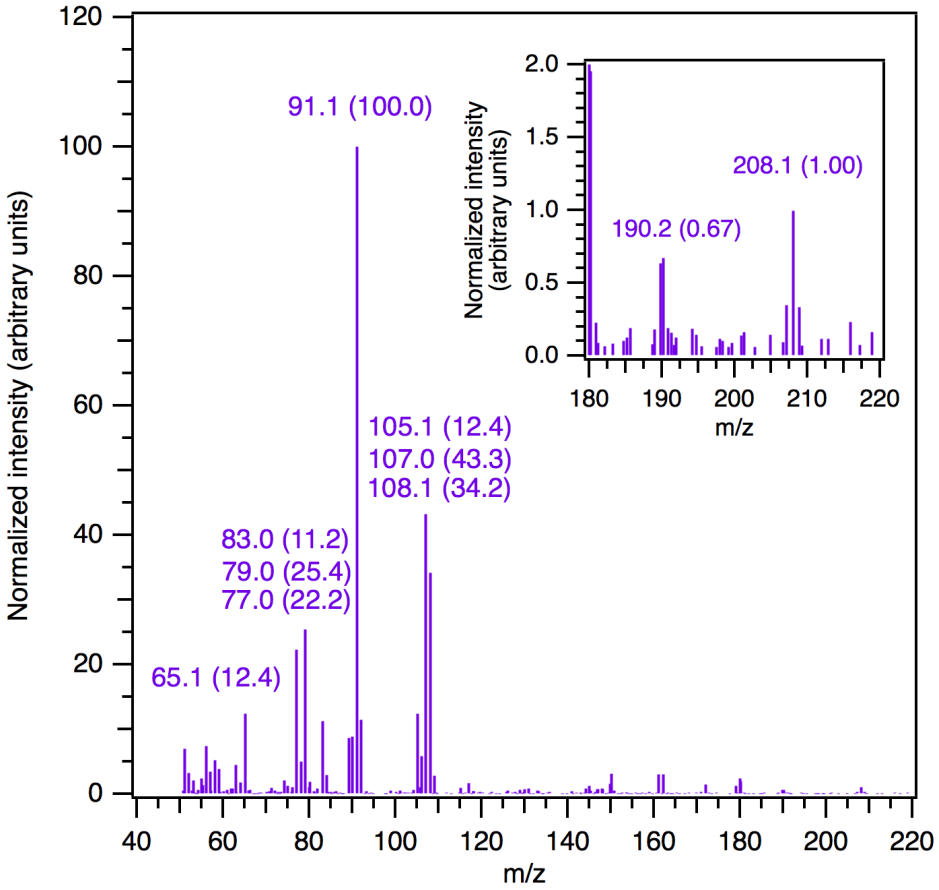

Figure 4.27. The extracted mass spectrum for the peak at a retention time of 11.6 minutes in the gas chromatograph of the 24 h time point; this mass spectrum is likely the unimer formed by the reaction of benzyl alcohol with one β-valerolactone. The inset shows the signals that likely correspond to the molecular ion peak (theoretical m/z of 208.11) and the molecular ion after a loss of H_2O.

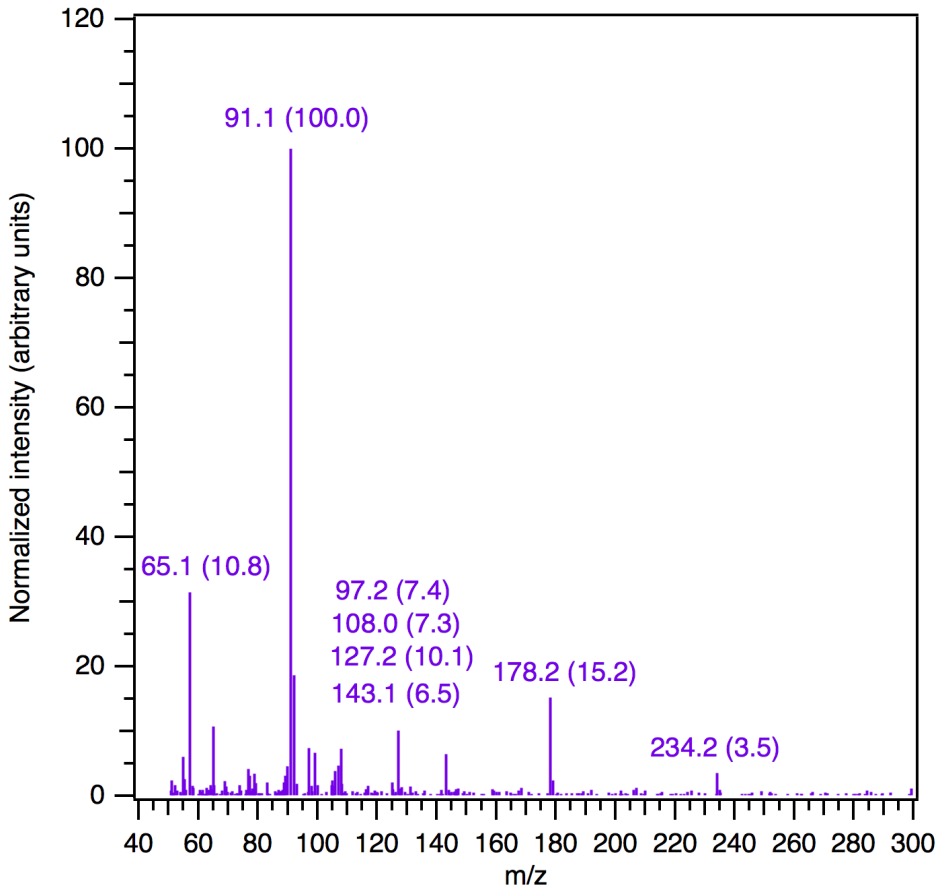

Figure 4.28. The extracted mass spectrum for the peak at a retention time of 11.8 minutes in the gas chromatograph of the 24 h time point. This spectrum likely corresponds to the dehydration product for the dimer; however, no significantly distinct peak for the molecular ion is observed at the expected m/z of 290.15 amu.

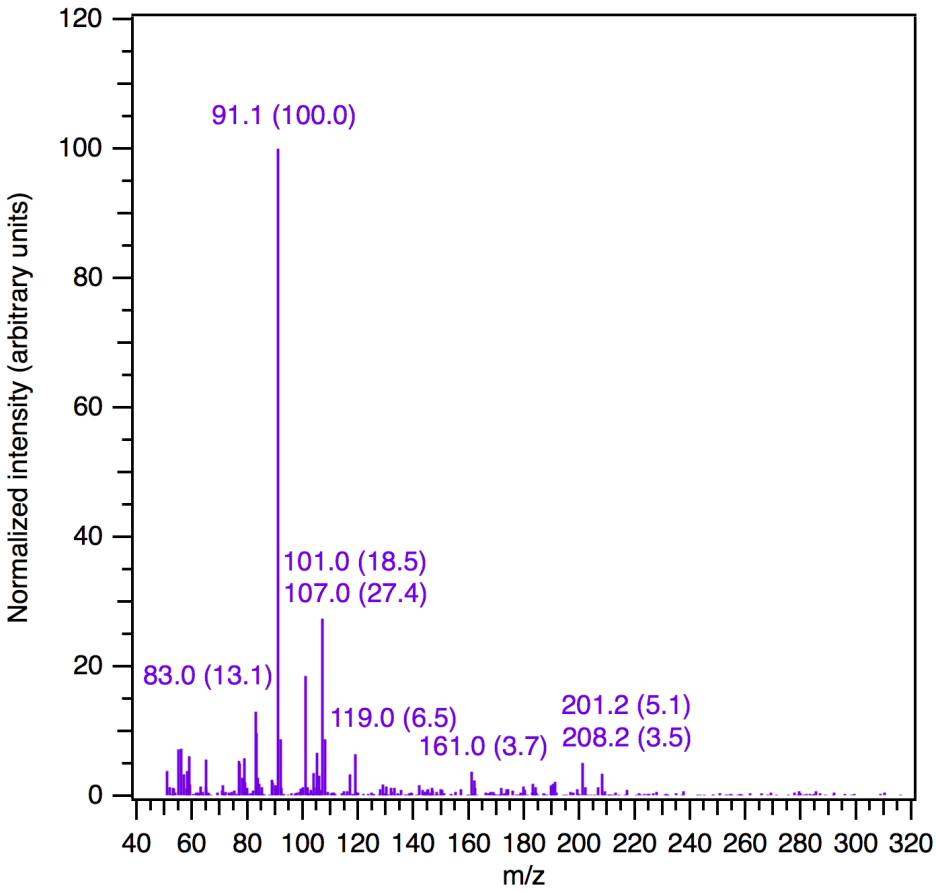

Figure 4.29. The extracted mass spectrum for the peak at a retention time of 14.4 minutes in the gas chromatograph of the 24 h time point. This spectrum likely corresponds to the dimer formed by the reaction of benzyl alcohol with two β-valerolactone molecules; however, no significantly distinct peak for the molecular ion is observed at the expected m/z of 308.16 amu.

The presence of residual benzyl alcohol at 24 h was corroborated by ^{1}H NMR spectroscopy, and the two major products were identified as the unimer and dimer from one or two β-lactone ring-opening events (**Figure 4.30**, **Figure 4.31**, **Figure 4.32**, and **Figure 4.33**). Additionally, there was no detectable signal for benzyl ether protons, which further confirmed that only acyl-oxygen scission was occurring in the presence of $SnOct_2$. The protons in the dimer had similar chemical environments to the unimer, which significantly complicated the ^{1}H NMR spectra for the products at longer reaction times.

Although the methyl and α-CH_2 proton resonances in each acyl-oxygen scission product overlapped significantly, the other protons had distinct enough chemical environments such that the peaks corresponding to the unimer could be integrated separately to those corresponding to the dimer, which allowed for determination of their molar ratio (**Figure 4.34**, 2:1 unimer:dimer). Remarkably, the reaction was left at 120 °C for 24 h but only very small amounts of dehydration products were observed at equilibrium (**Figure 4.35**). The two minor peaks in the gas chromatogram of the 24 h aliquot were therefore attributed to the dehydration products arising from the unimer and dimer. Thus, the results of this model compound study supported our hypothesis that the $SnOct_2$-catalyzed cross-linking with the bis(β-lactone) yielded reactive β-hydroxyesters at the junctions between star-shaped PMCL. Although $SnOct_2$ has been deemed non-toxic and was effective for our purposes, more environmentally benign (organo)catalysts could be used for polymerization and cross-linking.

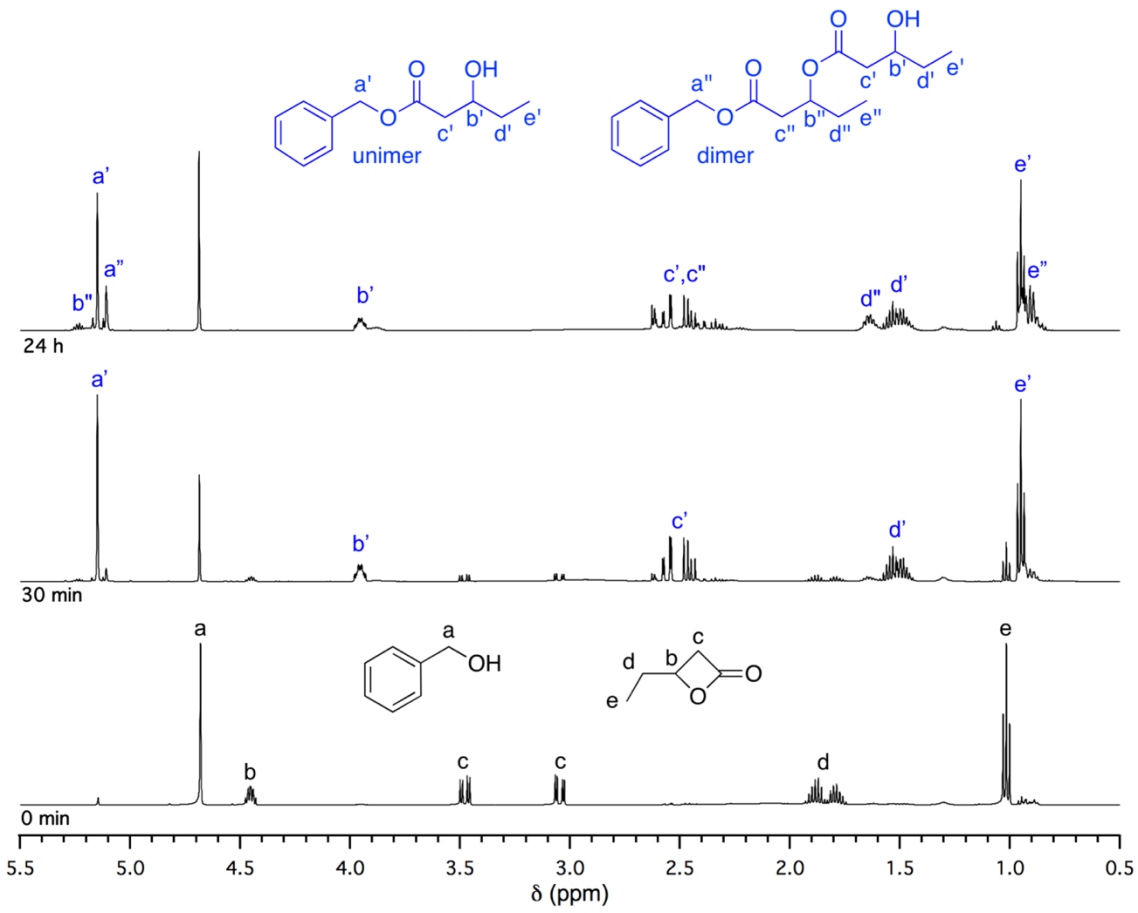

Figure 4.30. Overlay of ^{1}H NMR spectra showing the disappearance of the β-valerolactone peaks and the appearance of the unimer and dimer peaks.

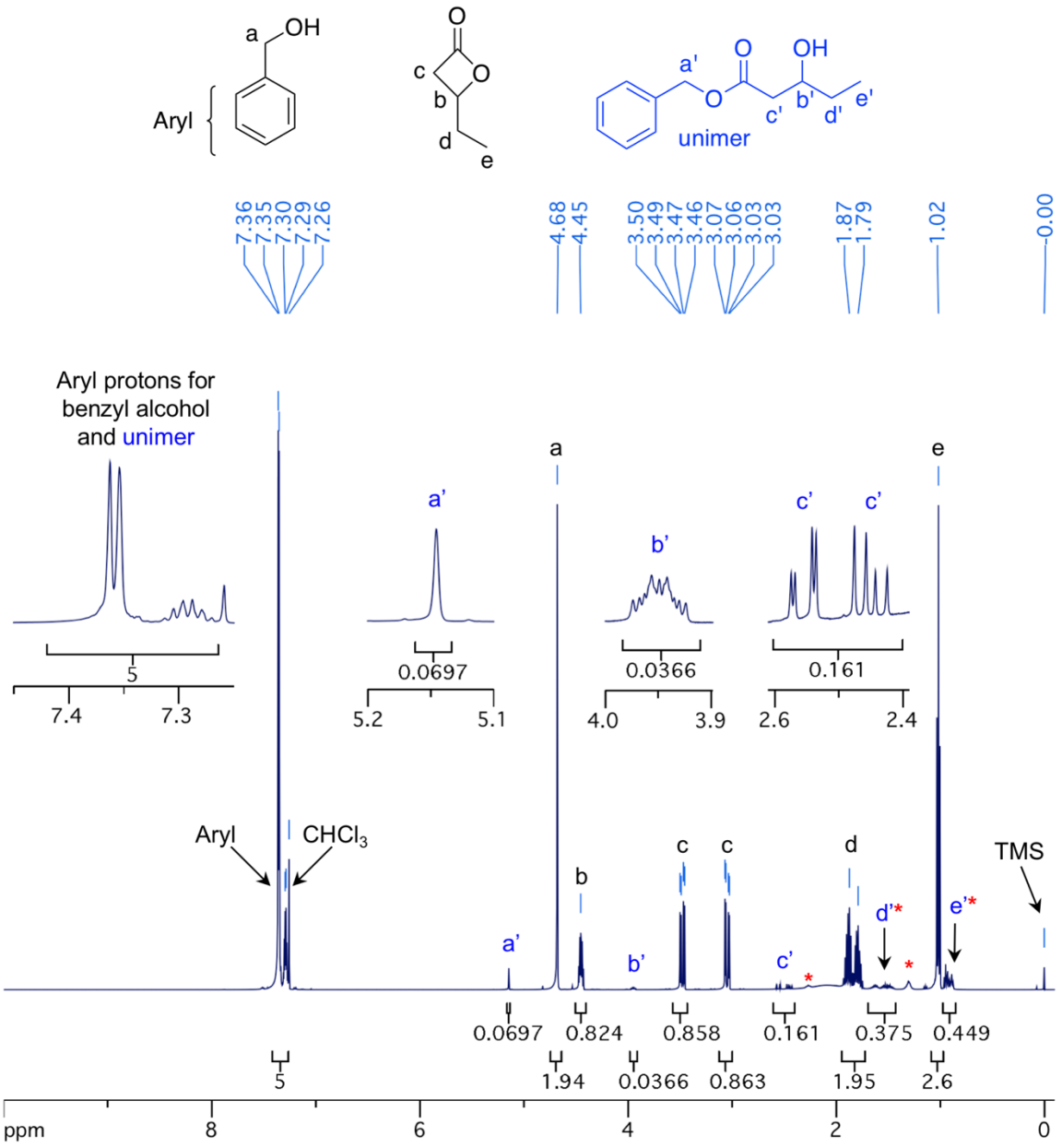

Figure 4.31. The full ^{1}H NMR spectrum (500 MHz, $CDCl_3$) for the first model study time point (0 min). The red asterisks (*) designate peaks that can be wholly or partially attributed to the $SnOct_2$ catalyst (determined by comparison to a spectrum of $SnOct_2$ in $CDCl_3$). Though not labeled on the figure, the broad OH peak from the benzyl alcohol is present between 1.7 and 2.7 ppm. The integrations match well for the peaks that do not overlap with the OH signal or the $SnOct_2$ signals. The insets show peaks relevant to the unimer, which is present in small amounts after mixing the components together. In fact, the J-values for the unimer α-CH_2 signals (c') are 16.4, 9.1, and 3.1 Hz; this last value matches exactly with the first and only coupling constant that can be confidently extracted from the peak for the b' proton.

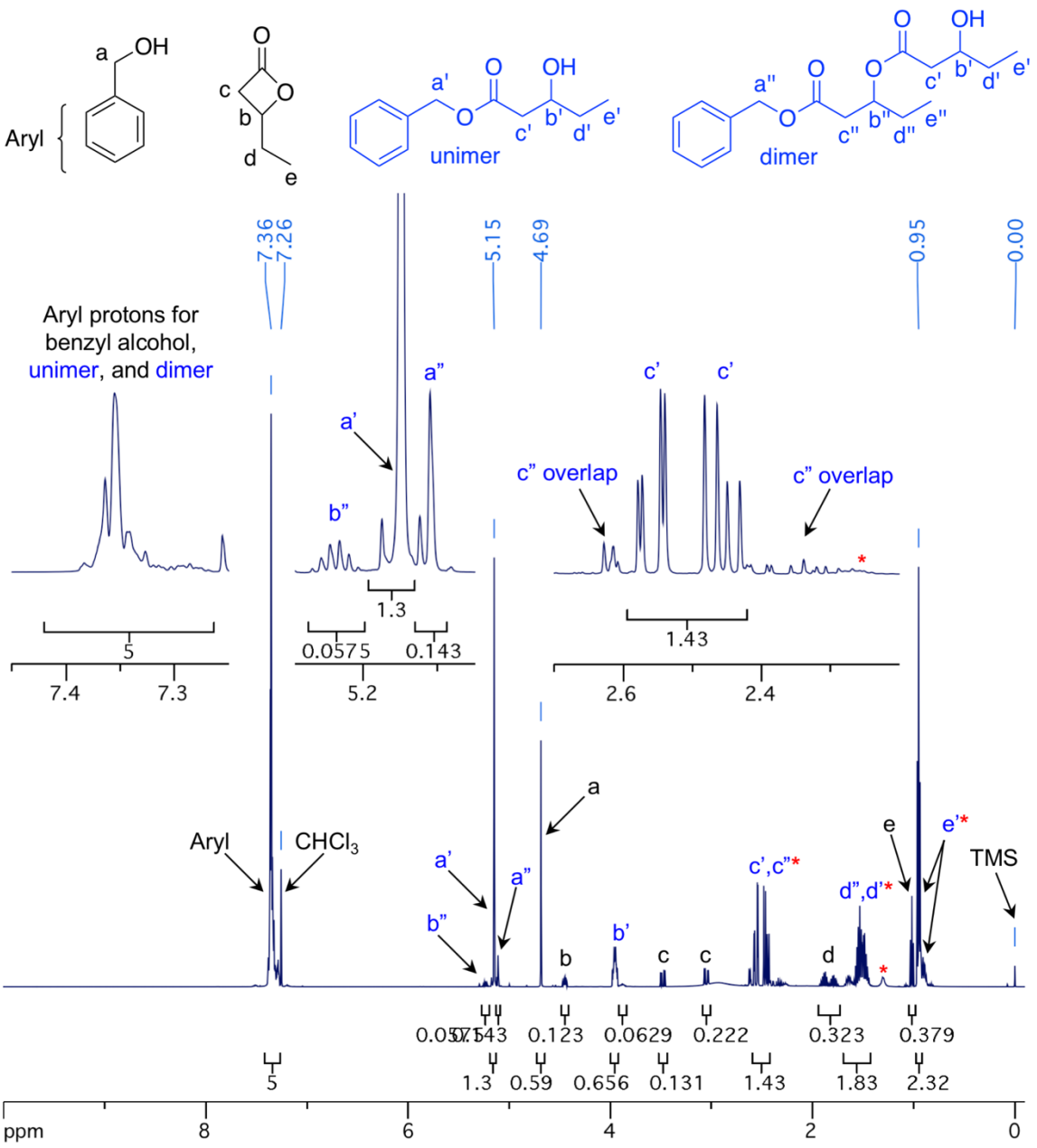

Figure 4.32. The full ^{1}H NMR spectrum (500 MHz, $CDCl_3$) for the second model study time point (30 min). The red asterisks (*) designate peaks that can be wholly or partially attributed to the $SnOct_2$ catalyst (determined by comparison to a spectrum of $SnOct_2$ in $CDCl_3$). Though not labeled on the figure, the broad OH peak is present between 2.4 and 3.4 ppm (not the same at 0 min). The insets show peaks relevant to the unimer and dimer; it is clear that the doublet of doublets around 2.5 ppm are the same α-CH_2 signals observed at 0 min, which are now higher intensity but slightly complicated by the underlying peaks from the small amount of dimer present.

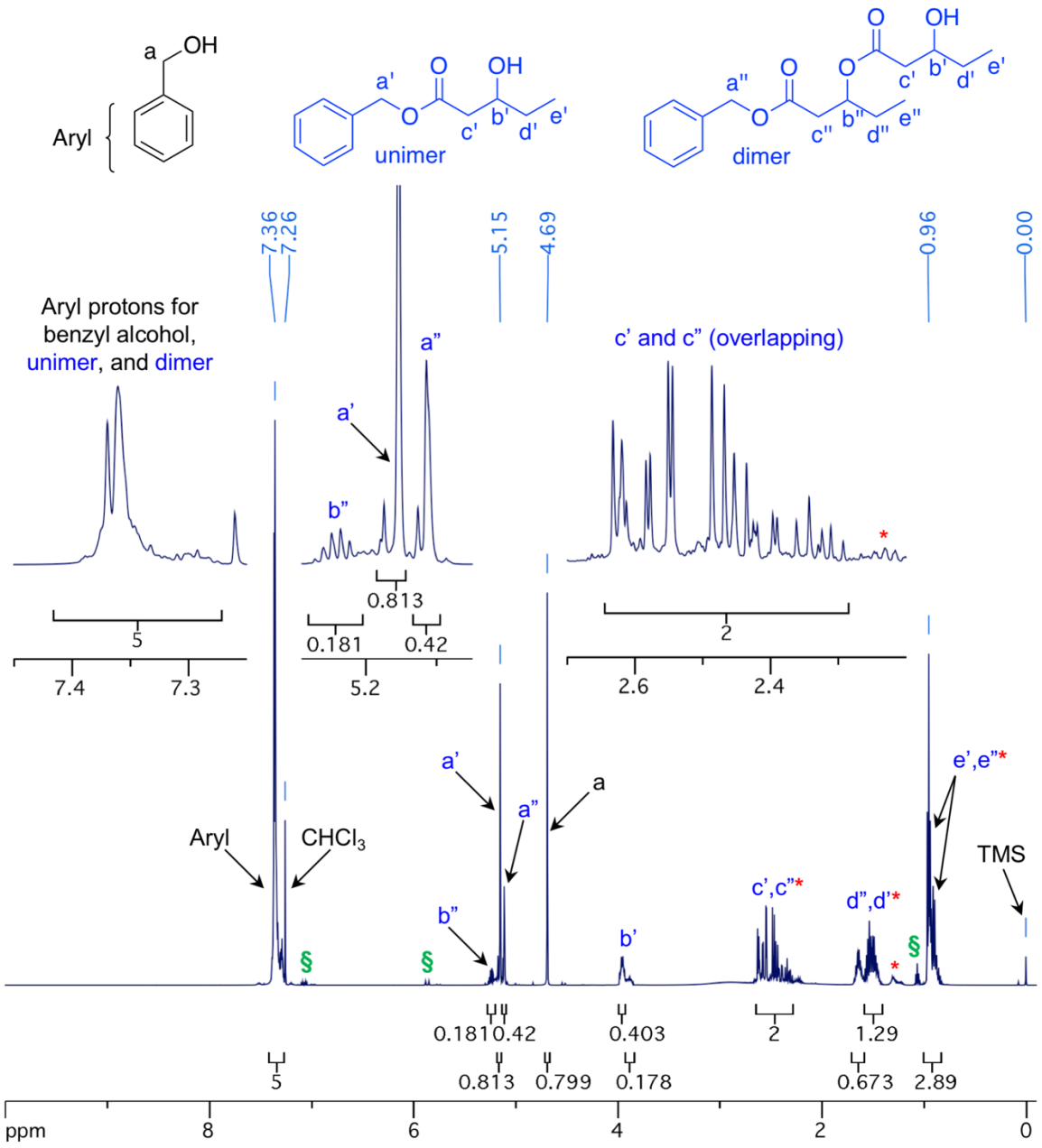

Figure 4.33. The full ^{1}H NMR spectrum (500 MHz, $CDCl_3$) for the last model study time point (24 h), with insets showing peaks relevant to the unimer and dimer. The red asterisks (*) designate peaks that can be wholly or partially attributed to the $SnOct_2$ catalyst (determined by comparison to a spectrum of $SnOct_2$ in $CDCl_3$). Though not labeled on the figure, the broad OH peak is present between 2.4 and 3.4 ppm (similar for 30 min time point). The green section signs (§) denote peaks attributed to the dehydration products.

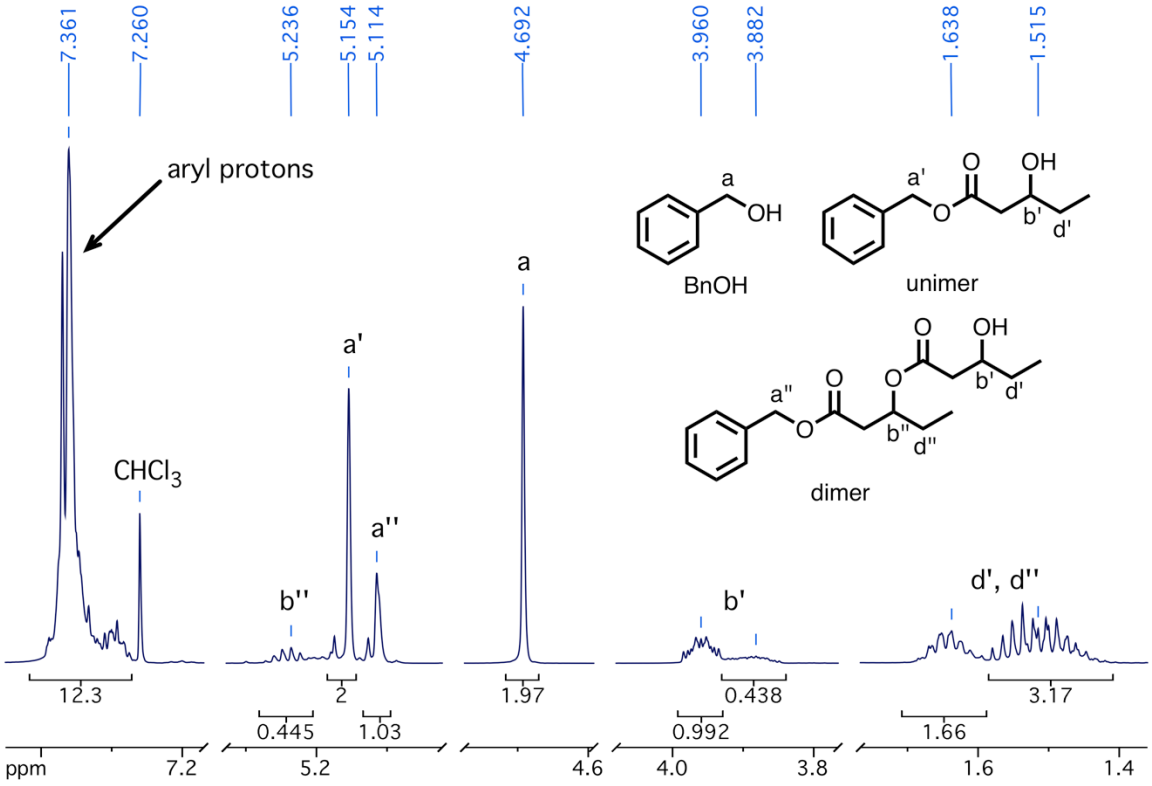

Figure 4.34. ^{1}H NMR spectrum (500 MHz, $CDCl_3$) of the model compound study at 24 h, which shows the signals for the protons of BnOH, unimer, and dimer. The peak at 5.24 ppm (denoted b'') is specific for the dimer. All other peaks exist in pairs, and the ratio of the integration areas indicates that the unimer and dimer are present in a 2 to 1 ratio. The integration area of the aryl protons is equal to what is expected for the ratio of the three species; a total benzyl proton peak area of 5 (a + a' + a") should correspond to an aryl proton peak area of 12.5. Furthermore, the peak area for the BnOH benzyl protons (denoted a) is in good agreement with the residual amount expected after 5.5 mmoles of BnOH reacts with 5 mmoles of β-valerolactone to afford a 2 to 1 ratio of unimer to dimer. After 3.75 mmoles of lactone is converted to unimer—leaving 2.25 mmoles of BnOH—the remaining lactone reacts with unimer to yield 1.25 mmoles of dimer. The resultant molar ratio of BnOH:unimer:dimer is 2.25:2.50:1.25, and the integration area for BnOH is therefore expected to be roughly the same as that of unimer, which agrees well with the ^{1}H NMR spectrum.

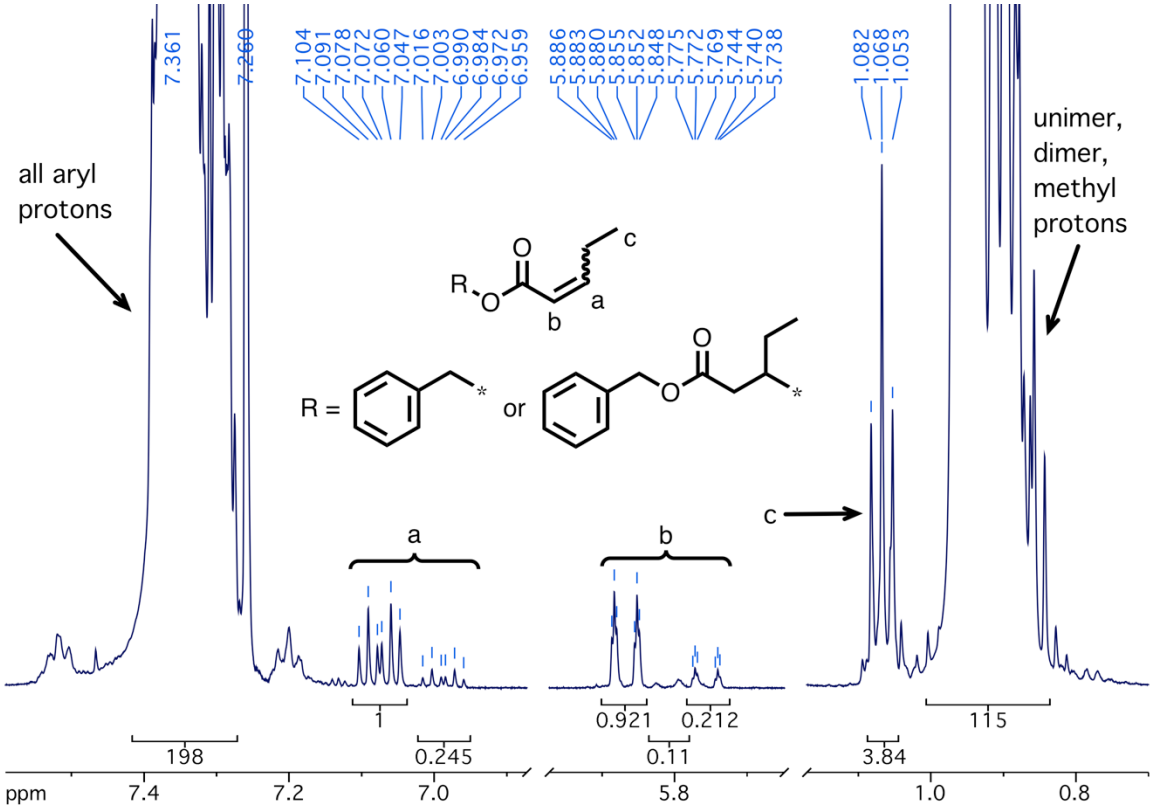

Figure 4.35. ^{1}H NMR spectrum (500 MHz, $CDCl_3$) of the model compound study at 24 h, which shows the methyl and alkene protons for the dehydration products. Using the integration areas for the alkene proton signals most downfield (total area = 1.245) and the aryl proton signals, it was determined that the dehydration products comprise only 3 mol% of the total amount of products present.

4.4.2. Thermal and Mechanical Characterization of Polyester Elastomers.

With some insight as to the identity of the cross-links, film preparation was scaled up to afford enough material for an investigation of the thermal and mechanical properties as well as the enzymatic hydrolyzabilities. The resultant elastomers were clear, colorless, and had high gel fractions (**Figure 4.36** and **Table 4.3**). The disappearance of the β-lactone carbonyl stretching frequency at 1830 cm^{-1} was used as a measure of cross-linking progress (**Figure 4.37**, **Figure 4.38**, and **Figure 4.39**). The samples were subjected to thermal characterization by differential scanning calorimetry and thermogravimetric analysis. The

glass transition temperatures of the elastomers were all approximately –55 °C, a few degrees higher than the prepolymers (**Figure 4.40**). The 5% mass loss temperatures in air for all elastomers were greater than 200 °C, similar to the prepolymers (**Figure 4.41**, **Table 4.3**, and **Table 4.4**).

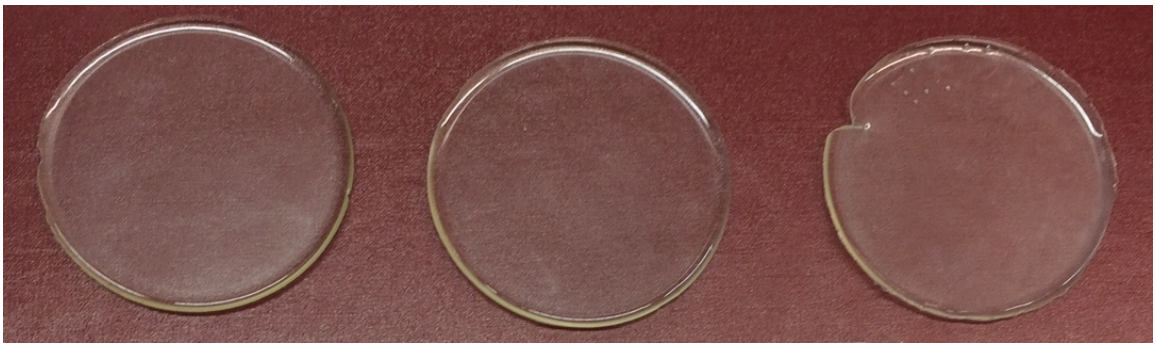

Figure 4.36. Picture of cross-linked elastomers after peeling them out of the aluminum pans. From left to right: CE-11, CE-22, CE-32, where the number after CE represents the pre-polymer molar mass.

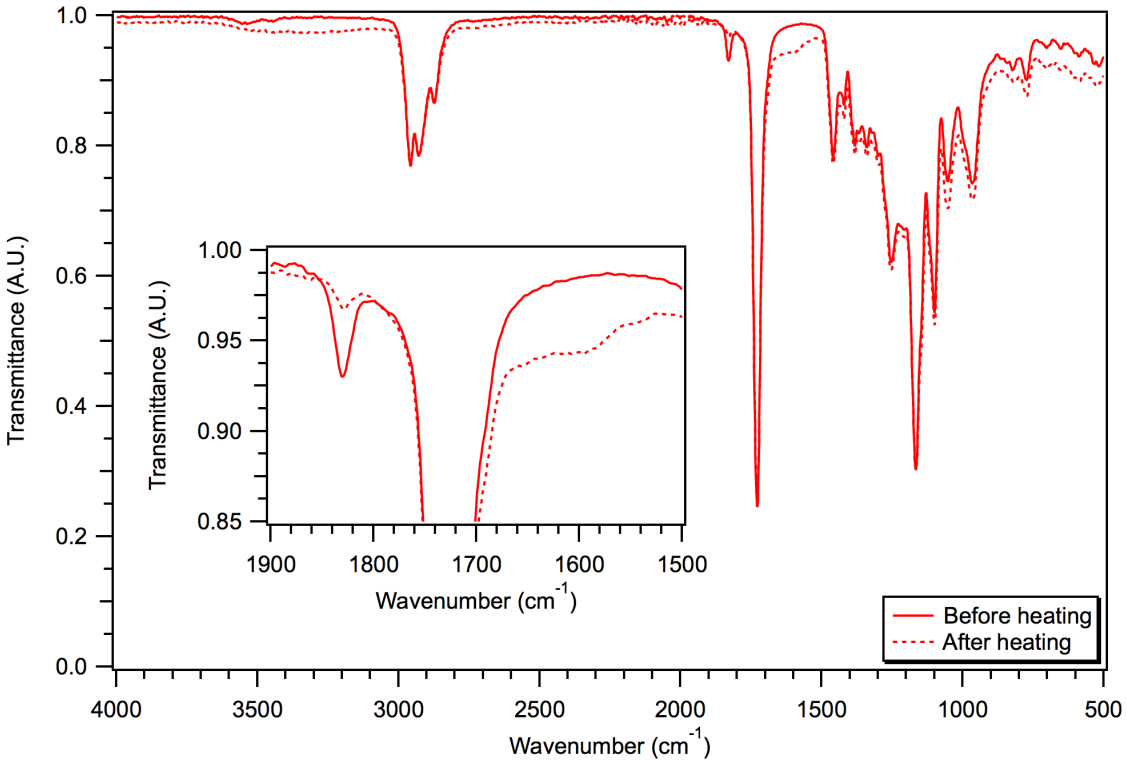

Figure 4.37. IR spectra (neat) of solvent-casted pre-polymer, catalyst, and cross-linker before and after heating; the inset shows the disappearance of the β-lactone stretching frequency after cross-linking. The elastomer produced in this case was CE-11.

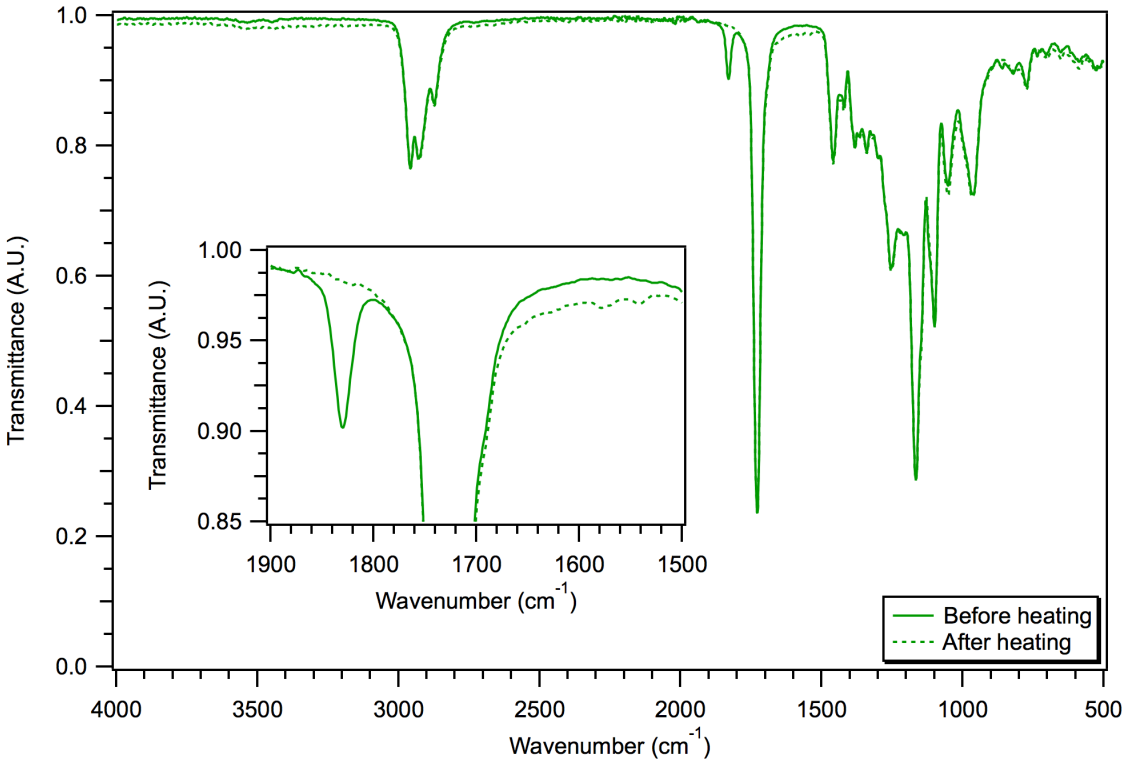

Figure 4.38. IR spectra (neat) of solvent-casted pre-polymer, catalyst, and cross-linker before and after heating; the inset shows the disappearance of the β-lactone stretching frequency after cross-linking. The elastomer produced in this case was CE-22.

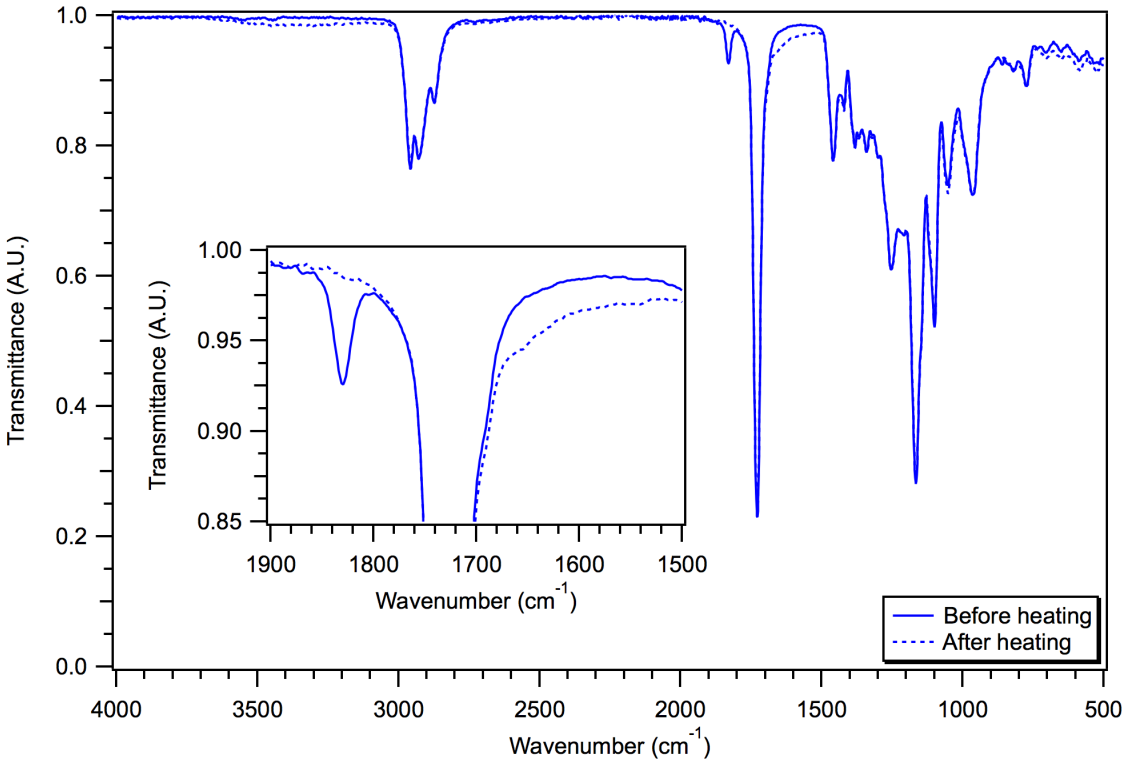

Figure 4.39. IR spectra (neat) of solvent-casted pre-polymer, catalyst, and cross-linker before and after heating; the inset shows the disappearance of the β-lactone stretching frequency after cross-linking. The elastomer produced in this case was CE-32.

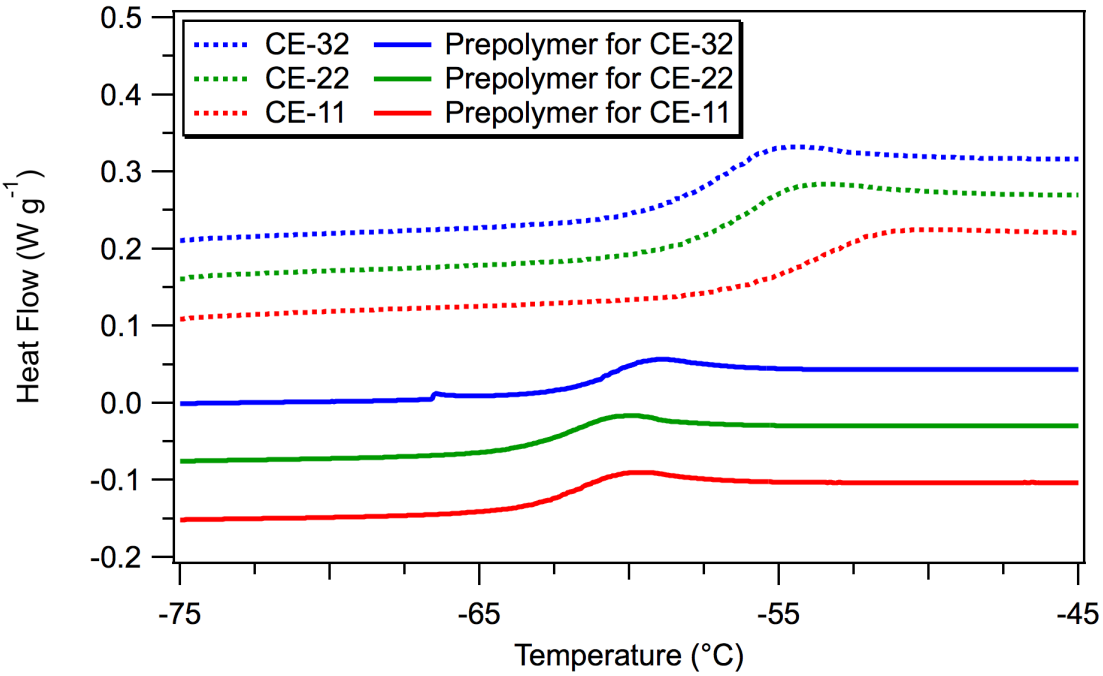

Figure 4.40. An overlay of the second heating ramps obtained via differential scanning calorimetry for the pre-polymers and respective cross-linked elastomers; there is a small increase in the glass transition temperature after cross-linking. Curves are vertically shifted for clarity.

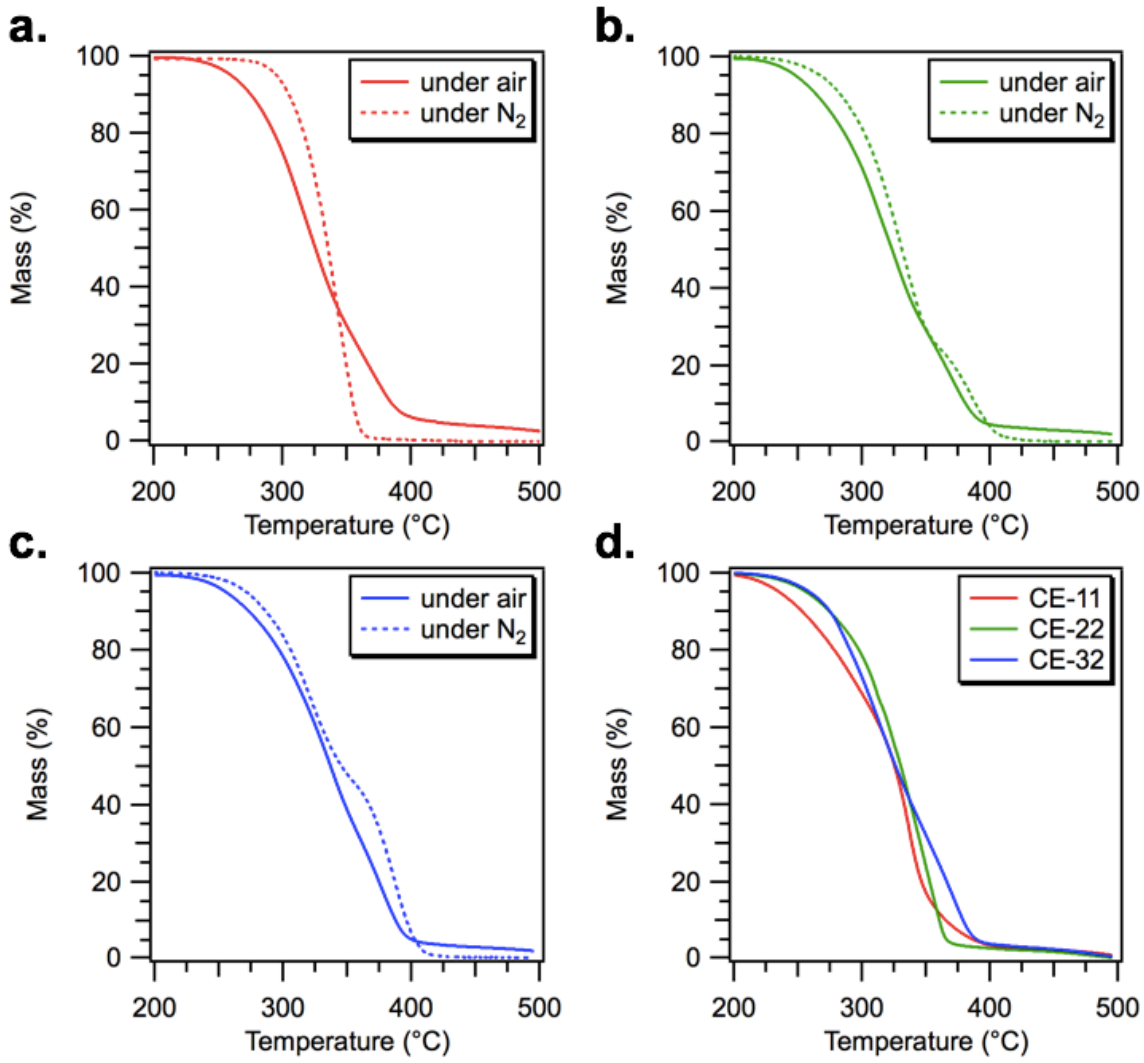

Figure 4.41. TGA traces of the prepolymers for (**a.**) CE-11 (**b.**) CE-22, (**c.**) CE-32 and (**d.**) cross-linked polyester elastomers under air atmosphere.

Table 4.3. Thermal properties and gel fractions for cross-linked elastomers.

Elastomer[a]	T_g (°C)[b]	T_g (°C)[c]	$T_{d,5\%}$ (°C)[d]	Gel fraction [e]
CE-32	–57	–54	259	0.994
CE-22	–57	–53	256	0.997
CE-11	–54	–50	235	0.989

[a]The notation of the films is CE-*X*, where *X* represents the M_n of the PMCL used to make the film. [b]Measured using differential scanning calorimetry; the reported value is taken from the second heat. [c]Measured using dynamic mechanical thermal analysis; the reported value is taken from the maximum in tan δ. [d]Measured using thermogravimetric analysis in an air atmosphere. [e]Measured using swell tests with dichloromethane.

Table 4.4. Thermal properties of PMCL samples used for elastomers.

Prepolymer for	T_g (°C)[a]	$T_{d,1\%}$ (°C)[b]	$T_{d,5\%}$ (°C)[b]	$T_{d,1\%}$ (°C)[c]	$T_{d,5\%}$ (°C)[c]
CE-32	–61	242	271	223	255
CE-22	–63	237	268	220	248
CE-11	–62	269	296	233	260

[a]Measured using differential scanning calorimetry; the reported value is taken from the second heat. [b]Measured using thermogravimetric analysis in a nitrogen atmosphere. [c]Measured using thermogravimetric analysis in air.

Each elastomer was subjected to dynamic mechanical thermal analysis and the storage and loss moduli were monitored as a function of temperature from –90 to 200 °C in a tensile geometry; except during the glass transition, the storage modulus was greater than the loss modulus over the entire temperature range, which provided further evidence that the elastomers were indeed chemically cross-linked (**Figure 4.42**, **Figure 4.43**, and **Figure 4.44**). For all elastomers, the rubbery plateau moduli were relatively constant throughout the temperature sweep, which indicated that the mechanical integrity of the network was maintained.

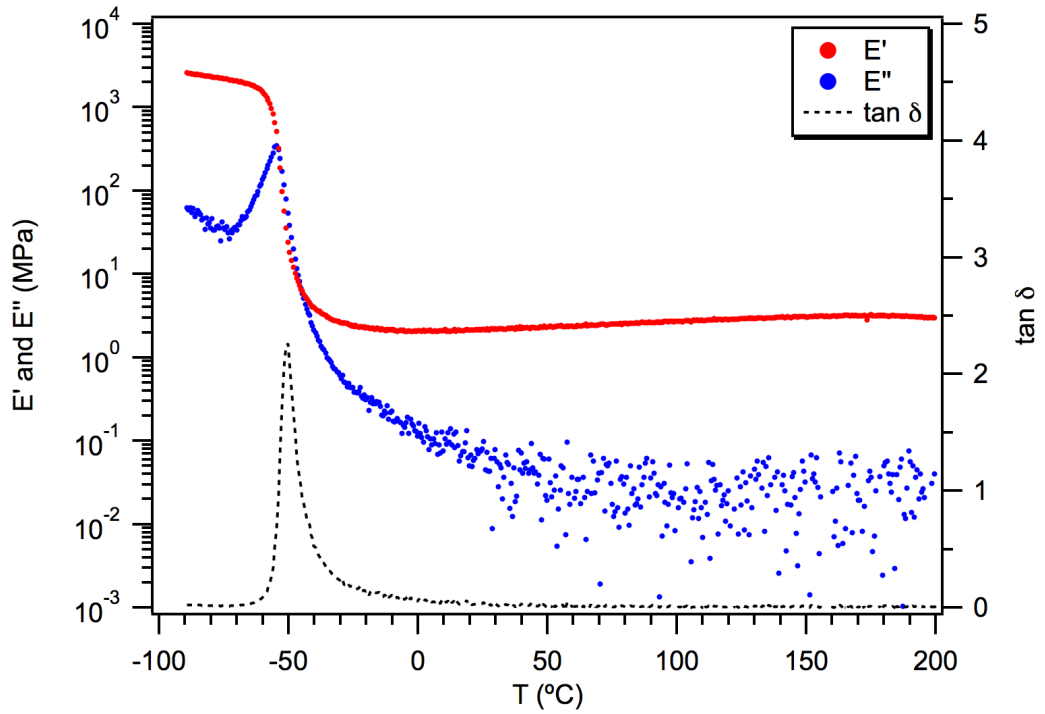

Figure 4.42. Dynamic mechanical thermal analysis of CE-11.

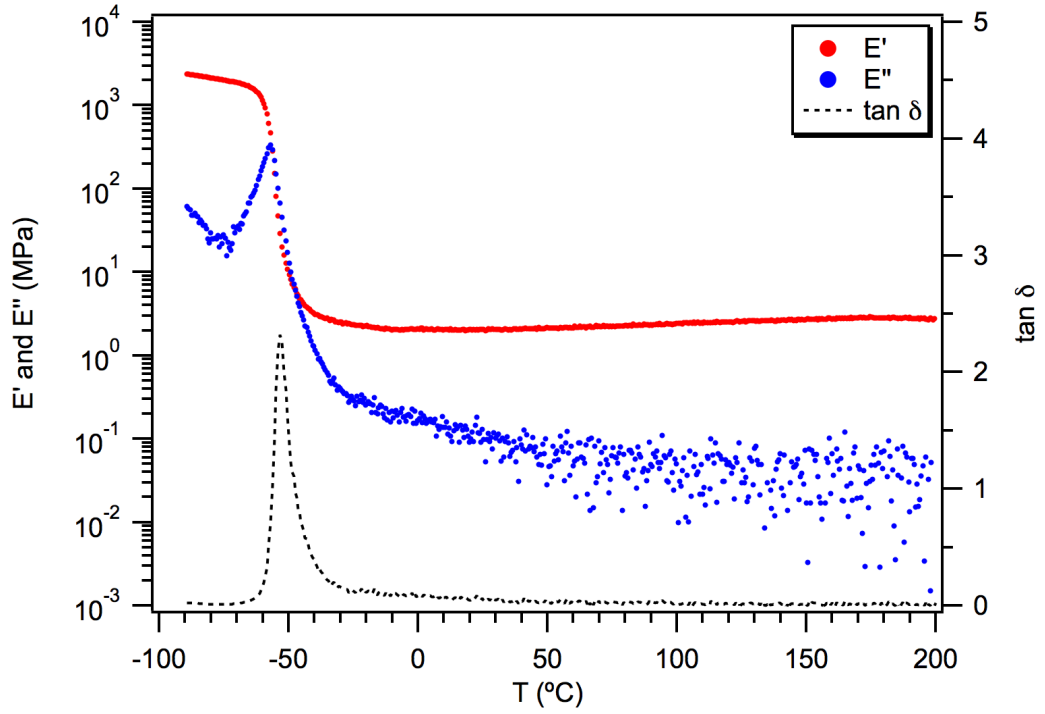

Figure 4.43. Dynamic mechanical thermal analysis of CE-22.

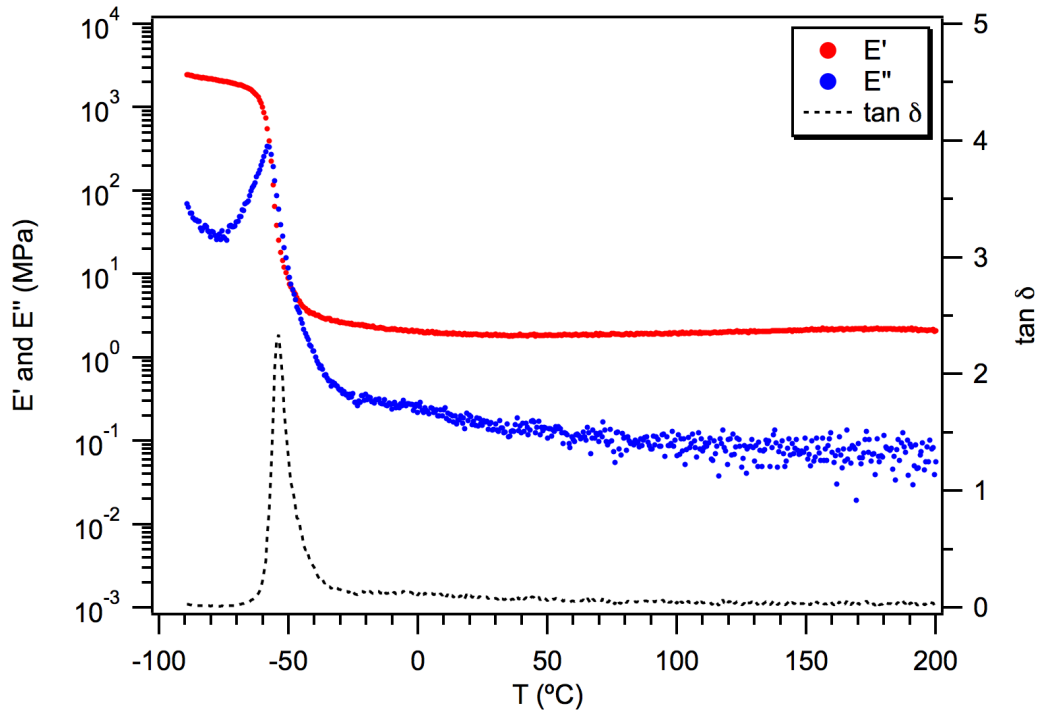

Figure 4.44. Dynamic mechanical thermal analysis of CE-32.

A comparison of all three elastomers revealed that the rubbery plateau moduli (denoted E_N') were within 1 MPa of one another (**Figure 4.45**). This is not what one would expect if E_N' were dictated by the molar mass between chemical cross-links M_x, which increased by roughly a factor of three from CE-11 to CE-32 (**Table 4.5**). Instead, E_N' was related to the *effective* molar mass between cross-links $M_{x,eff}$ (see equation 1 in experimental), which includes contributions from transient cross-links such as entanglements. Shear rheology measurements were performed on the star-shaped PMCL (**Figure 4.46**, **Figure 4.47**, and **Figure 4.48**). Based on the obtained data, we calculated an entanglement molar mass M_e (see equation 2 in experimental) of 4.6 kg/mol. The critical molar mass M_c characterizes the actual molar mass where entanglements are observed in rheological tests, and is typically a factor of 2–3 times the M_e.[53] The theoretical M_x for CE-11 was 5.6 kg/mol, which was too small to expect a substantial amount of entanglements

in the CE-11 network. By comparison, the theoretical M_x values for CE-22 and CE-32 were large enough that entanglements could have been present between cross-links. Indeed, the calculated values for $M_{x,eff}$ of CE-22 and CE-32 were respectively 3.8 and 4.1 kg/mol (**Table 4.5**), which correspond more closely with the M_e of PMCL than with the theoretical M_x. The lack of a strong trend in $M_{x,eff}$ indicated that the mechanical properties at low strains were primarily dictated by the inherent entanglements in the network rather than by the chemical cross-links.

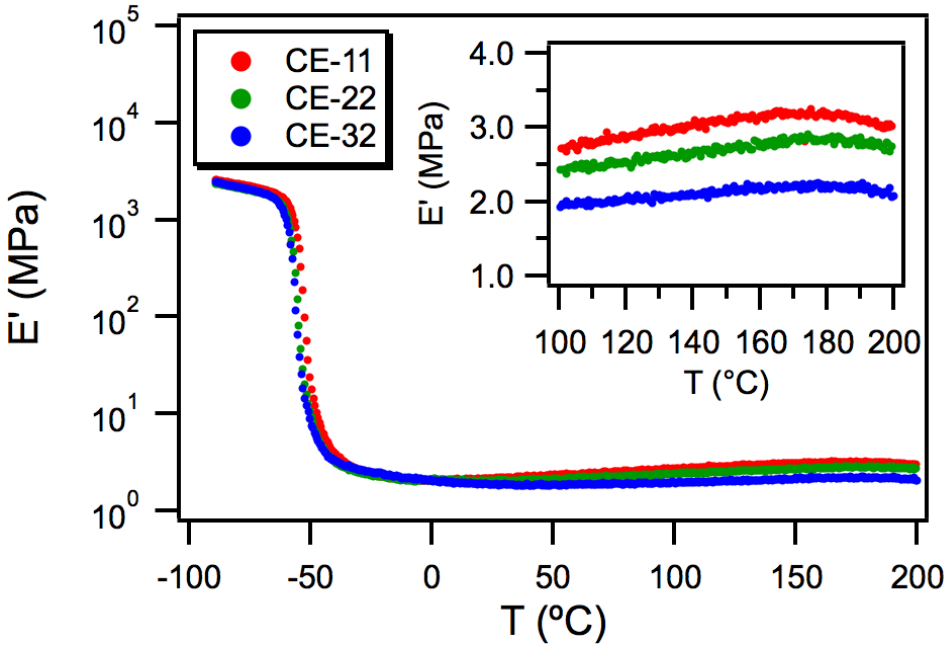

Figure 4.45. An overlay of the storage modulus curves for the three polyester elastomers of varying chemical cross-link density, where CE-*X* denotes the cross-linked elastomer made with a prepolymer of molar mass *X*.

Table 4.5. Theoretical and measured parameters for elastomers.

Elastomer[a]	M_n (kg/mol)[b]	M_{arm} (kg/mol)[b]	M_x (kg/mol)[c]	E_N' (MPa)[d]	$M_{x,eff}$ (kg/mol)[e]
CE-32	31.5	7.9	15.8	1.90	4.1
CE-22	22.4	5.6	11.2	2.05	3.8
CE-11	11.2	2.8	5.6	2.14	3.7

[a]The notation of the films is CE-*X*, where *X* represents the M_n of the PMCL used to make the film. [b]Molar masses determined by end-group analysis via ^{1}H NMR spectroscopy and correspond to pre-polymer. [c]Theoretical molar mass between chemical cross-link junctions if each arm of the pre-polymer was joined to another during cross-linking (i.e., $M_x = 2M_{arm}$). [d]Value at 21.5 °C from dynamic mechanical thermal analysis of cross-linked elastomers. [e]Calculated from equation 1 in the main text using a density of 1.065 g cm^{-1} and a temperature of 21.5 °C

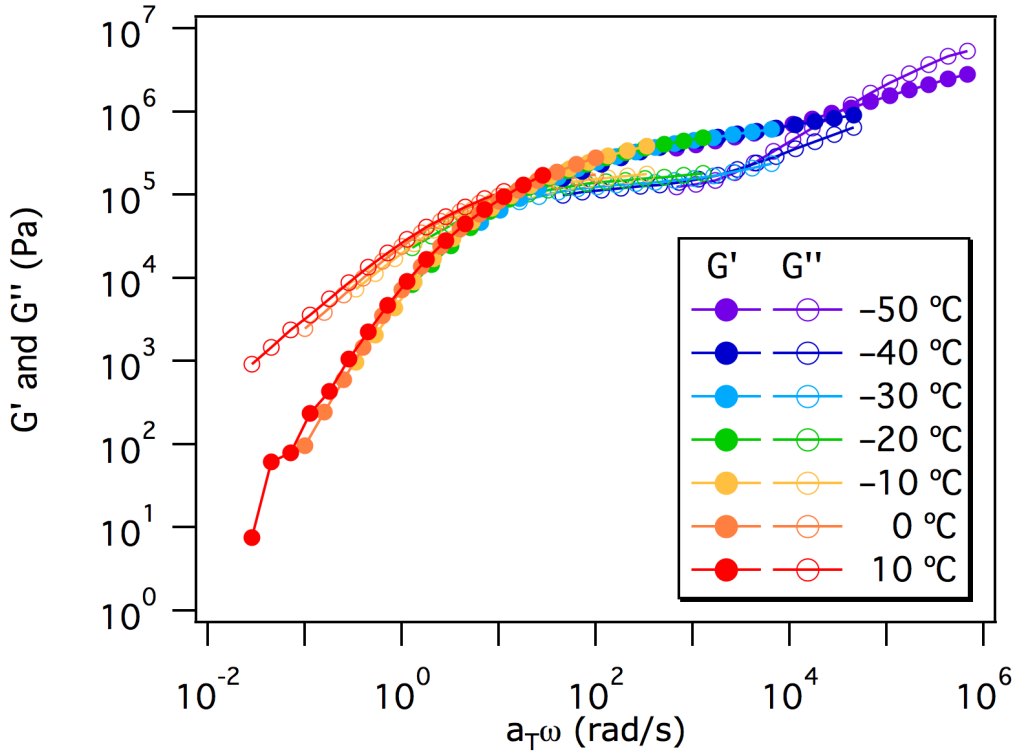

Figure 4.46. Master curve for star-shaped hydroxyl-terminated PMCL of M_n = 31.5 kg/mol (i.e., prepolymer for CE-32) obtained using time-temperature superposition; shift factors were obtained by shifting tan δ.

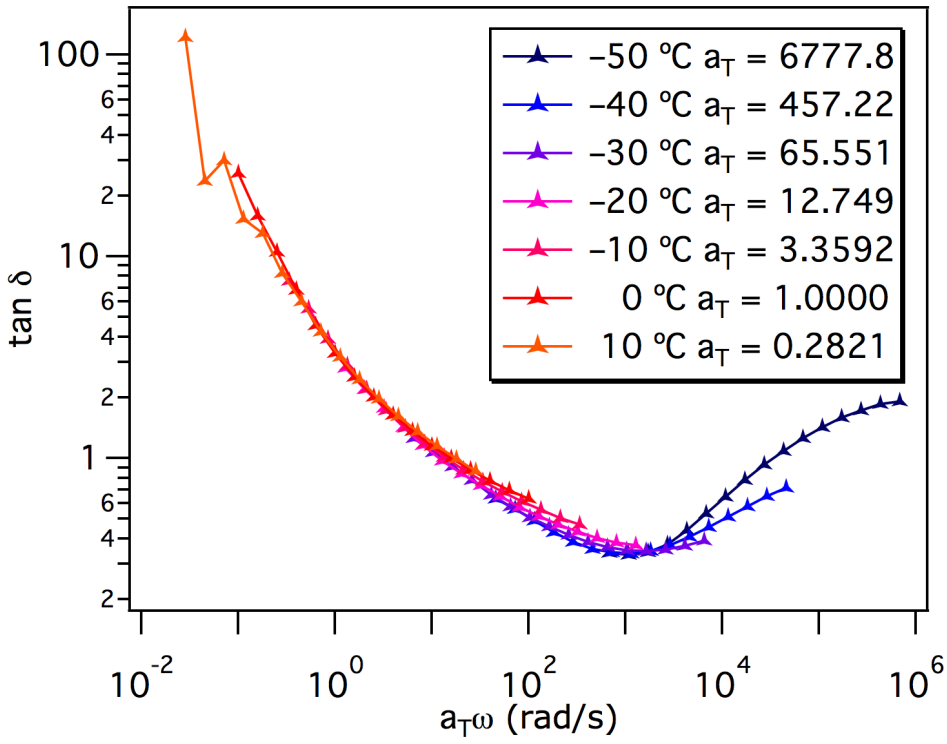

Figure 4.47. Time-temperature superposition of tan δ for star-shaped hydroxyl-terminated PMCL of M_n = 31.5 kg/mol (i.e., prepolymer for CE-32).

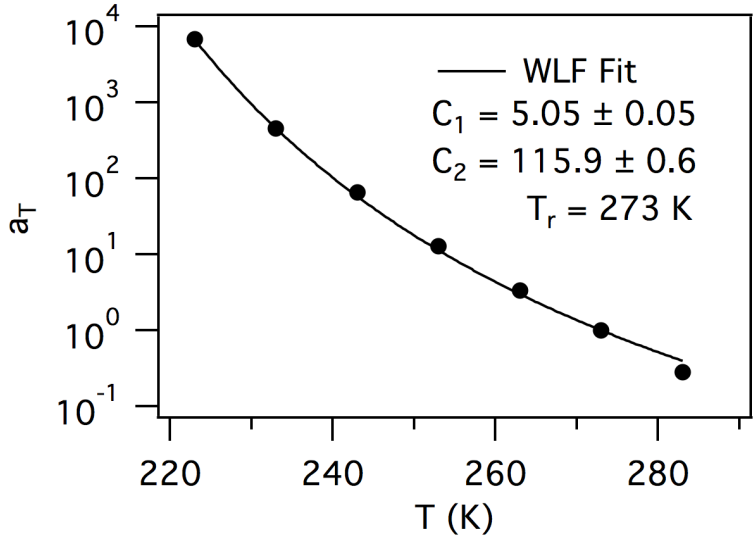

Figure 4.48. William-Landel-Ferry fitting of the shift factors obtained via time-temperature superposition of tan δ for star-shaped hydroxyl-terminated PMCL of M_n = 31.5 kg/mol (i.e., prepolymer for CE-32).

Linear and cyclical tensile tests were performed to investigate the elastic performance of the elastomers; vulcanized natural rubber (i.e., a rubber band) was also tested as a benchmark for tensile performance of a commercially available CCP (**Figure 4.49**). The Young's modulus *E* of each elastomer was determined from the slope of the stress-strain curve in the linear viscoelastic regime (i.e., low strain behavior); all three elastomers had moduli in the range of 1.6 to 2.0 MPa, which was in good agreement with the results obtained via dynamic mechanical thermal analysis (**Table 4.6**). However, distinct trends arose in both the ultimate tensile strength, σ_b, and the ultimate elongation, ε_b, as the samples were stretched to their breaking point. Materials with a larger M_x were able to stretch to higher strain values before failure. Furthermore, the change to positive curvature observed in the stress-strain curve of CE-32 indicated that the M_x was large enough to enable strain hardening, which resulted in a significant improvement in the σ_b. The CE-32 elastomer outperformed the rubber band with respect to ultimate tensile strength and elongation; however, the Young's modulus of the rubber band was approximately 3 MPa, which was higher than all three CE samples. This was expected, as rubber bands are composite materials with hard filler particles—usually clay—that increase the rigidity and lower the water permeability of the vulcanized natural rubber.[54] We have previously reported that fumed silica filler can be incorporated into polyester elastomers with a very similar chemical structure as those presented here,[9] and we believe the same strategy could be applied to increase the σ_b and *E* of MCL-based elastomers.

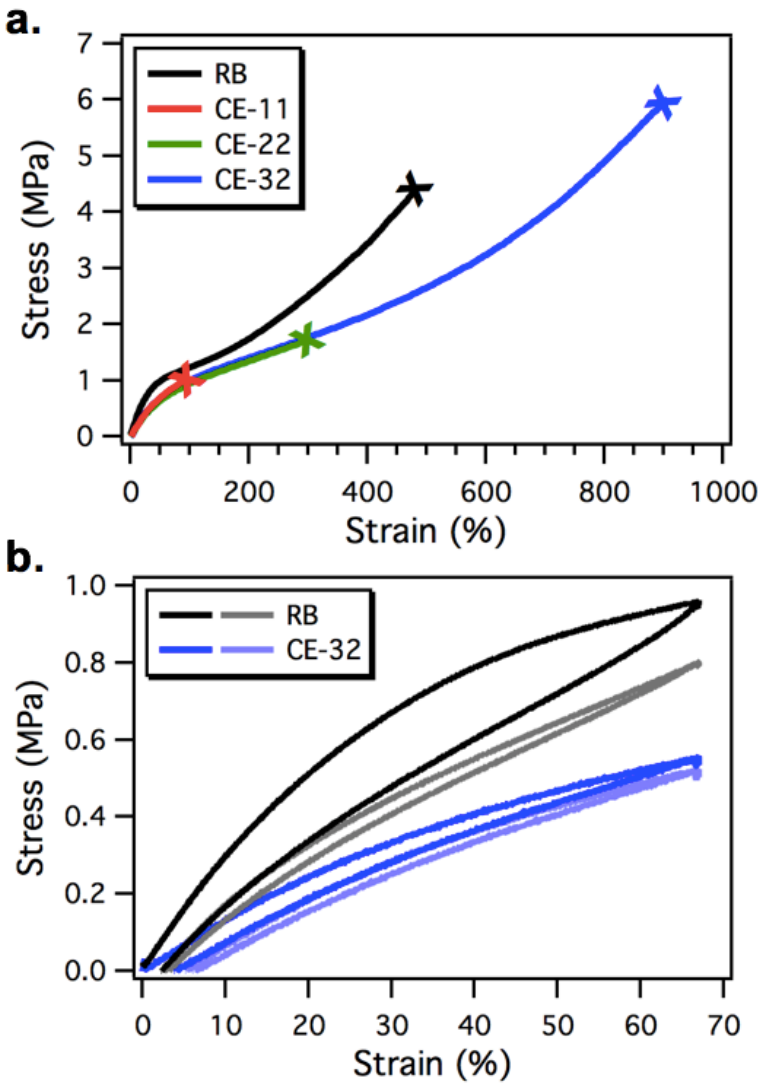

Figure 4.49. (**a.**) An overlay of representative uniaxial extension tensile testing data for a conventional rubber band (RB) and three elastomers of varying cross-link density, where CE-*X* denotes the cross-linked elastomer made with a prepolymer of molar mass *X*. (**b.**) An overlay of the first and twentieth cycles (dark and light shades, respectively) of cyclical uniaxial extension tensile tests for the RB and CE-32 (black and blue, respectively).

Table 4.6. Tensile testing data for elastomers.

Elastomer[a]	Young's Modulus (MPa)[b,c]	Stress at Break (MPa)[c]	Strain at Break (%)[c]
CE-32	1.6 ± 0.4	6 ± 1	900 ± 100
CE-22	1.77 ± 0.07	1.7 ± 0.3	290 ± 80
CE-11	2.0 ± 0.6	1.0 ± 0.1	90 ± 20

[a]The notation of the films is CE-*X*, where *X* represents the M_n of the PMCL used to make the film. [b]Obtained between 0-10 % strain. [c]Values shown are average ± standard deviations for 5 or more replicates.

Cyclical deformation across all CE samples indicated that the hysteresis energy loss and the tensile set per cycle both decreased when going from CE-32 to CE-11 (**Figure 4.50** and **Figure 4.51**). The rubber band was also tested and compared to the highest performing elastomer, CE-32. The hysteresis energy loss of the rubber band was significantly larger during the first cycle but compared well with the CE-32 elastomer for all subsequent cycles. CE-32 also exhibited very low tensile deformation (approximately 6% on 20th cycle) but still higher than that of the rubber band for all cycles.

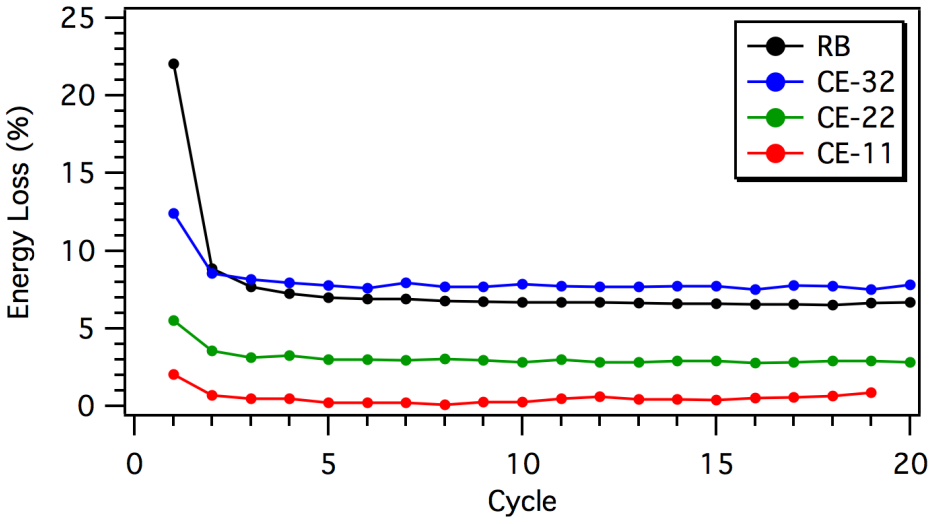

Figure 4.50. An overlay of hysteresis energy loss during 20 cycles of tensile testing for a conventional rubber band (RB) and the cross-linked polyester elastomers. The last data point for CE-11is missing because the material broke during the last cycle.

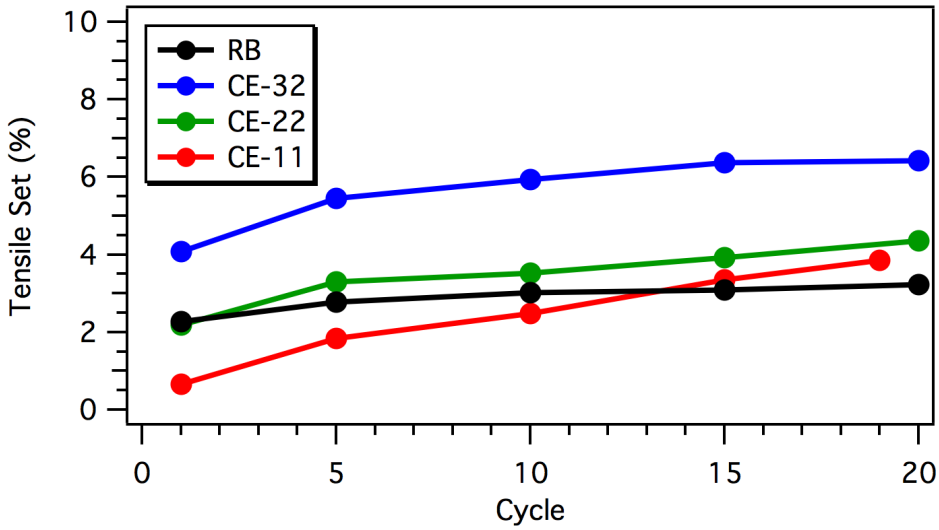

Figure 4.51. An overlay of the tensile set (i.e., % strain at zero stress) during 20 cycles of tensile testing for a conventional rubber band (RB) and the cross-linked polyester elastomers. The last data point for CE-11is missing because the material broke during the last cycle.

4.4.3. Investigation of the Enzymatic Hydrolysis of Polyester Elastomers.

We then set our sights toward the enzymatic hydrolyzabilities of these elastomers. The first and overall rate-limiting step of polyester biodegradation in natural systems is expected to be polyester hydrolysis.[55] While non-enzymatic hydrolysis may be slow, extracellular esterases secreted by naturally-occurring microorganisms colonizing the polyesters can largely facilitate hydrolysis. During this process, the esterases cleave the polyesters into smaller, water-soluble oligomers and monomers that can subsequently be taken up and utilized by microorganisms, resulting in the conversion of polyester carbon to CO_2 and microbial biomass.[15,55] Providing proof of enzymatic hydrolyzability of a polyester in a model system using naturally-occurring esterases strongly supports that these materials will also undergo enzymatic hydrolysis in the environment.

For our enzymatic hydrolysis experiments, we chose a model cutinase from

Fusarium solani, a filamentous fungus. While the natural substrate for *Fusarium solani* cutinase (FsC) is cutin, FsC has also been found to hydrolyze a variety of polyesters including poly(caprolactone),[56] poly(ethylene terephthalate),[57] and poly(butylene adipate).[58] To study complete enzymatic hydrolysis within reasonable experimental timescales, we used elevated FsC concentrations that resulted in polyester surface-limited and enzyme-saturated conditions. We used two complementary techniques to monitor hydrolysis: pH-stat titration to quantify the number of carboxylic acids formed during polyester hydrolysis and batch reaction vessels coupled to solution TOC analysis to quantify soluble hydrolysis products. We performed our experiments at pH 7 and temperatures between 2 and 40 °C to simulate conditions found in natural soils.

The first set of pH-stat titrations (CE-22, 40 °C) were performed in triplicate and demonstrated that hydrolysis experiments were highly reproducible; all subsequent experiments were therefore performed in duplicate. CE-11, CE-22, and CE-32 were each subjected to pH-stat titration experiments at 40 °C wherein the FsC was added at least 24 hours after the elastomers were placed in solution (**Figure 4.52**). The pH was stable without base addition over this 24 h period, which demonstrated that non-enzymatic (i.e., abiotic) hydrolysis of the elastomers was negligible. For all CE samples, the addition of the enzyme immediately resulted in base titration due to the hydrolysis of ester bonds in the elastomer. The titration progressed at a relatively linear rate until the hydrolyzed ester bonds approached 100% (after approximately 3.5 days). We demonstrated in a separate experiment that the rate was proportional to the surface area of elastomer (**Figure 4.53**). Although it has been previously shown that increases in surface area—and therefore accelerated hydrolysis—can be detected during the enzymatic hydrolysis of polymer thin

films,[59,60,61,62,63] the constant slopes of the hydrolysis curves for CE samples indicated that there were no appreciable increases in the surface areas throughout the experiments. Furthermore, the similarity in the hydrolysis rates between all CE samples suggested that the polymer chains in each network were equally accessible to FsC regardless of the M_x, which in these cases ranged from 6 to 16 kg/mol (**Table 4.7**). The hydrolysis curves began to plateau as the available substrate was depleted; these final stages of hydrolysis were concomitant with visual observations of pitting and near complete disappearance of the CE samples. For all CE samples, the plateau occurred at approximately 100% of esters hydrolyzed (with an average and standard deviation of 97 ± 4%), which indicated that the primary hydrolysis product was monomeric. Indeed, the analysis of the hydrolysis products by ^{1}H and ^{13}C NMR spectroscopy was consistent with the 6-hydroxy-4-methylhexanoic acid expected from full hydrolysis of PMCL (**Figure 4.54**, **Figure 4.55**, **Figure 4.56**, **Figure 4.57**, **Figure 4.58**, and **Figure 4.59**).

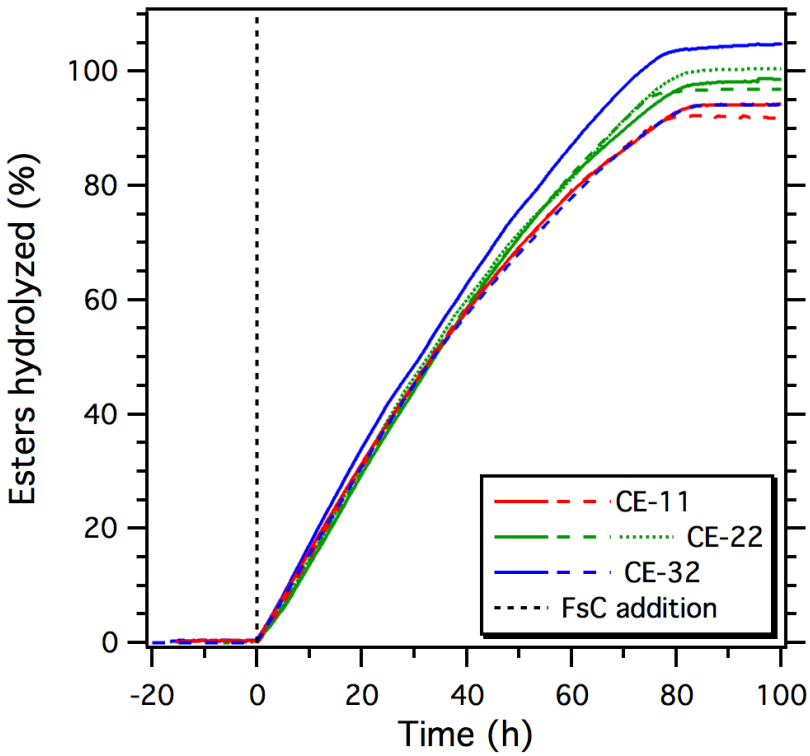

Figure 4.52. Hydrolysis curves for the polyester elastomers (CE-11, CE-22, and CE-32) by *Fusarium solani* cutinase (FsC) at 40 °C and pH 7 as measured by pH-stat titration. The curves are horizontally offset such that FsC addition occurs at t = 0 h. Experiments were run in triplicates (CE-22) or duplicates (CE-11 and CE-32).

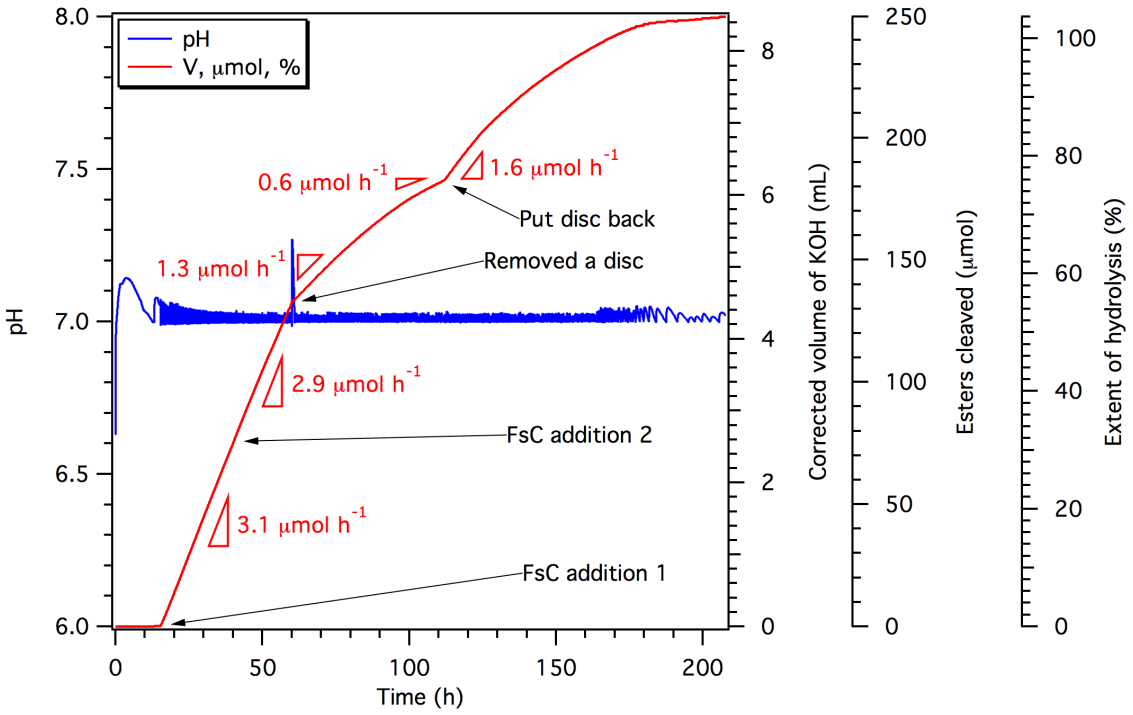

Figure 4.53. Control experiment at 30 °C and pH 7 demonstrating that the pH-stat titrations performed in this work are at enzyme saturation conditions and the hydrolysis rate is proportional to the surface area. The rate does not change upon the addition of more enzyme, but it does change when one of the two discs is removed from or returned to the solution.

Table 4.7. Hydrolysis rates and esters hydrolyzed for each elastomer at pH 7 and 40 °C.

Elastomer	Mass Used (mg)	Total Esters (µmol)	Surface Area (mm^2)	Rate (µmol esters h^{-1})[a]	Average Rate (µmol esters h^{-1})
CE-32	37.84	296.3	86.2	4.86	4.71
CE-32	38.90	304.6	87.3	4.57	
CE-22	38.81	304.2	86.7	4.62	4.56
CE-22	36.03	282.4	85.8	4.36	
CE-22	37.55	294.4	86.6	4.67	
CE-11	36.45	299.8	85.7	4.50	4.55
CE-11	36.52	300.4	85.8	4.61	

[a] Obtained from 0 to 50% hydrolysis as measured by pH-stat titration.

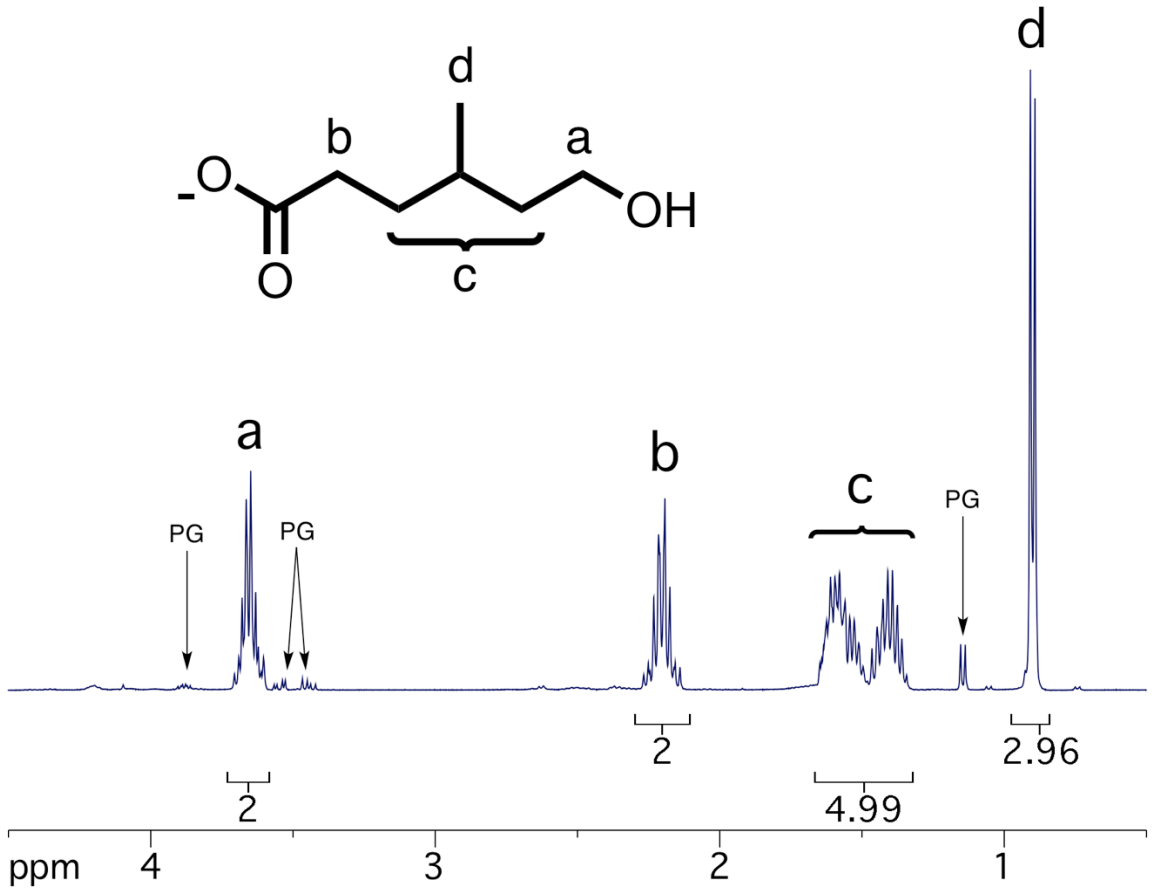

Figure 4.54. ^{1}H NMR spectrum (400 MHz, D_2O) of the dissolved solid in the degradation solution of CE-11; the peaks corresponding to the major hydrolysis product are indicated as well as those from propylene glycol (PG), which is a stabilizer used in enzyme solutions (see **Figure 4.56** and **Figure 4.57**).

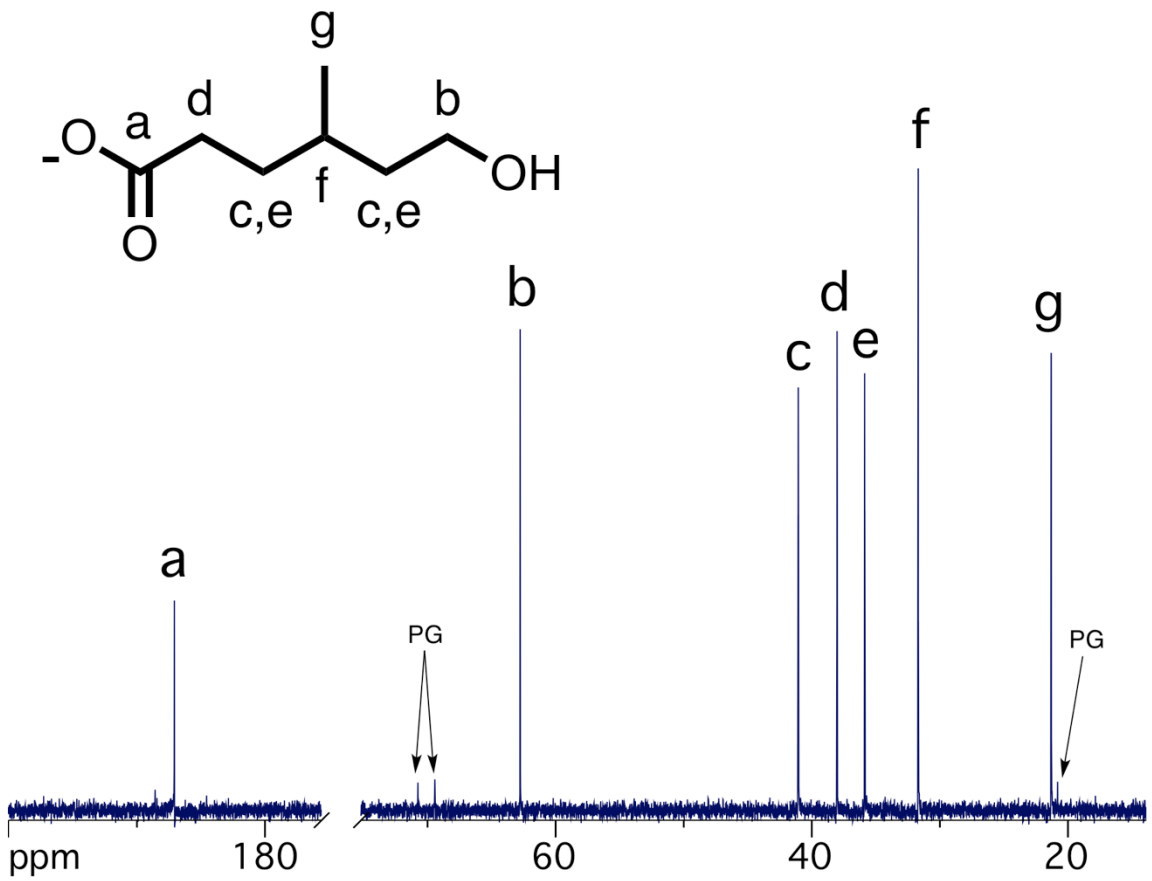

Figure 4.55. ^{13}C NMR spectrum (100 MHz, D_2O) of the dissolved solid in the degradation solution of CE-11; the peaks corresponding to the major hydrolysis product are indicated as well as those from propylene glycol (PG).

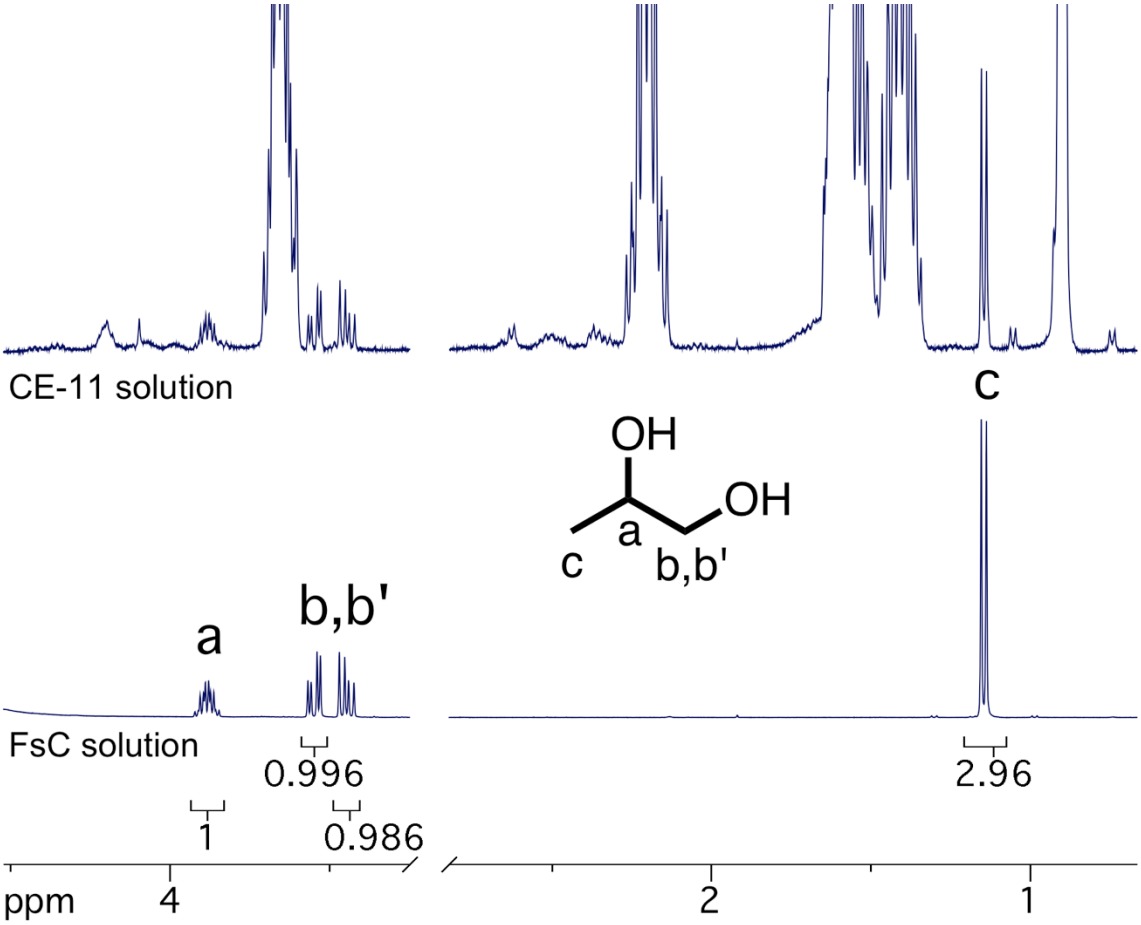

Figure 4.56. ^{1}H NMR spectrum (400 MHz, D_2O) of the dissolved solid in the degradation solution of CE-11 overlaid with the spectrum for the *Fusarium solani* cutinase solution; the peaks for the propylene glycol stabilizer are indicated.

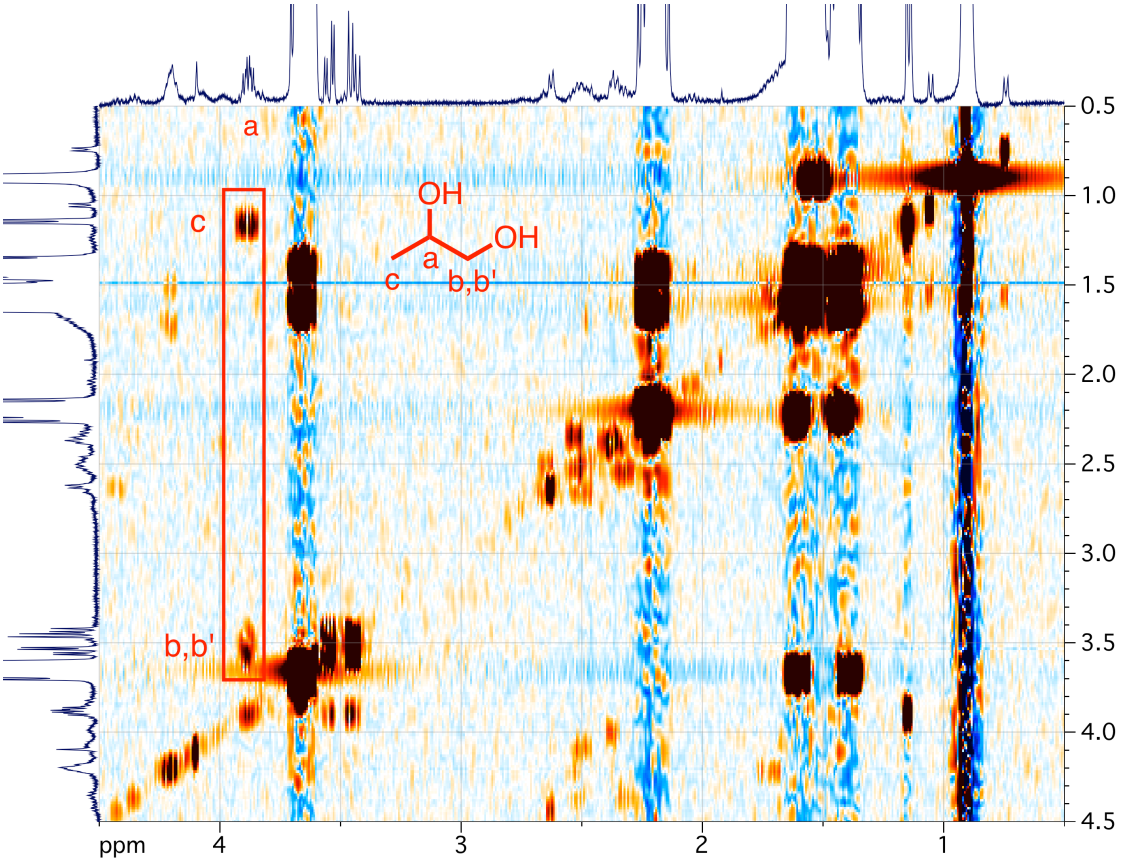

Figure 4.57. ^{1}H NMR COSY spectrum (400 MHz, D_2O) of the dissolved solid in the degradation solution of CE-11; the propylene glycol peaks are indicated. Although there are other small cross-peaks that could belong to minor hydrolysis products, is difficult to determine their structure as some peaks are overlapping with those of the major hydrolysis product.

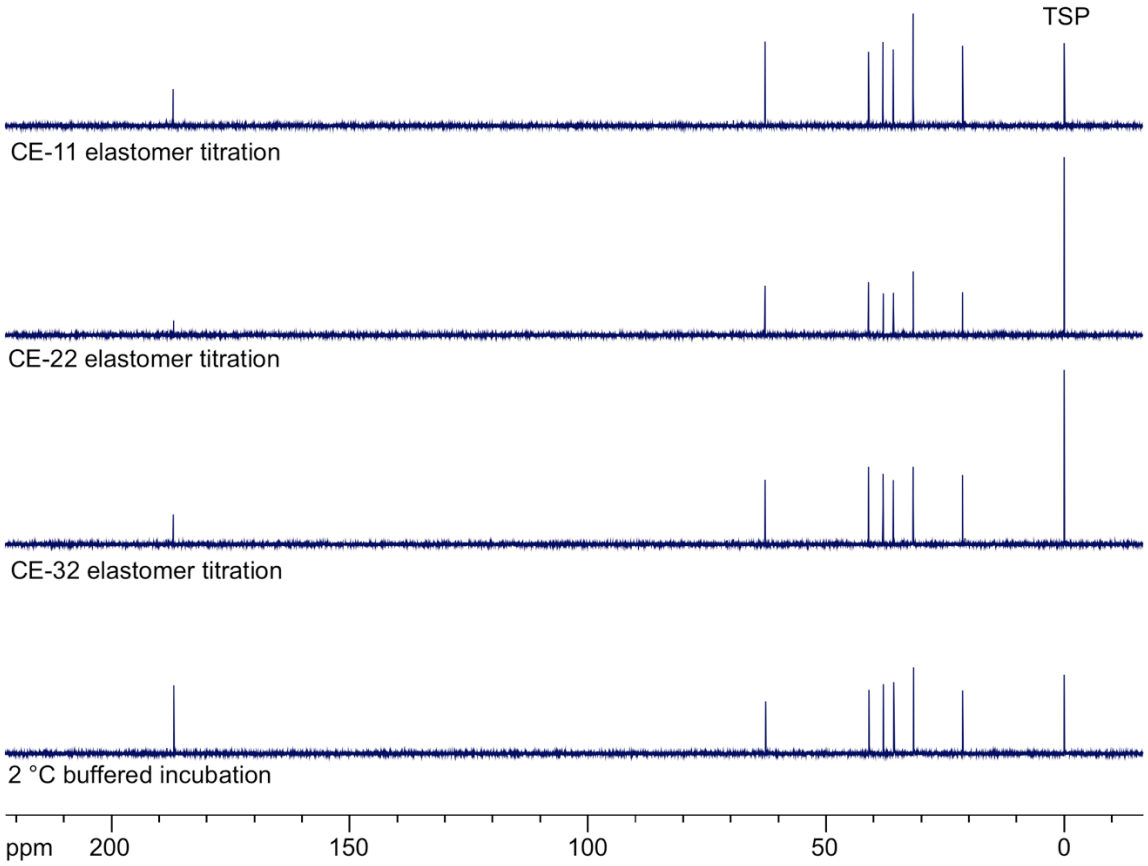

Figure 4.58. ^{13}C NMR spectra (100 MHz, D_2O) overlay showing a consistent major hydrolysis product for all elastomers and both methods: pH-stat titrations and buffered incubations. The spectra are standardized to 3-(trimethylsilyl)propanoate-2,2,3,3-d_4 (TSP).

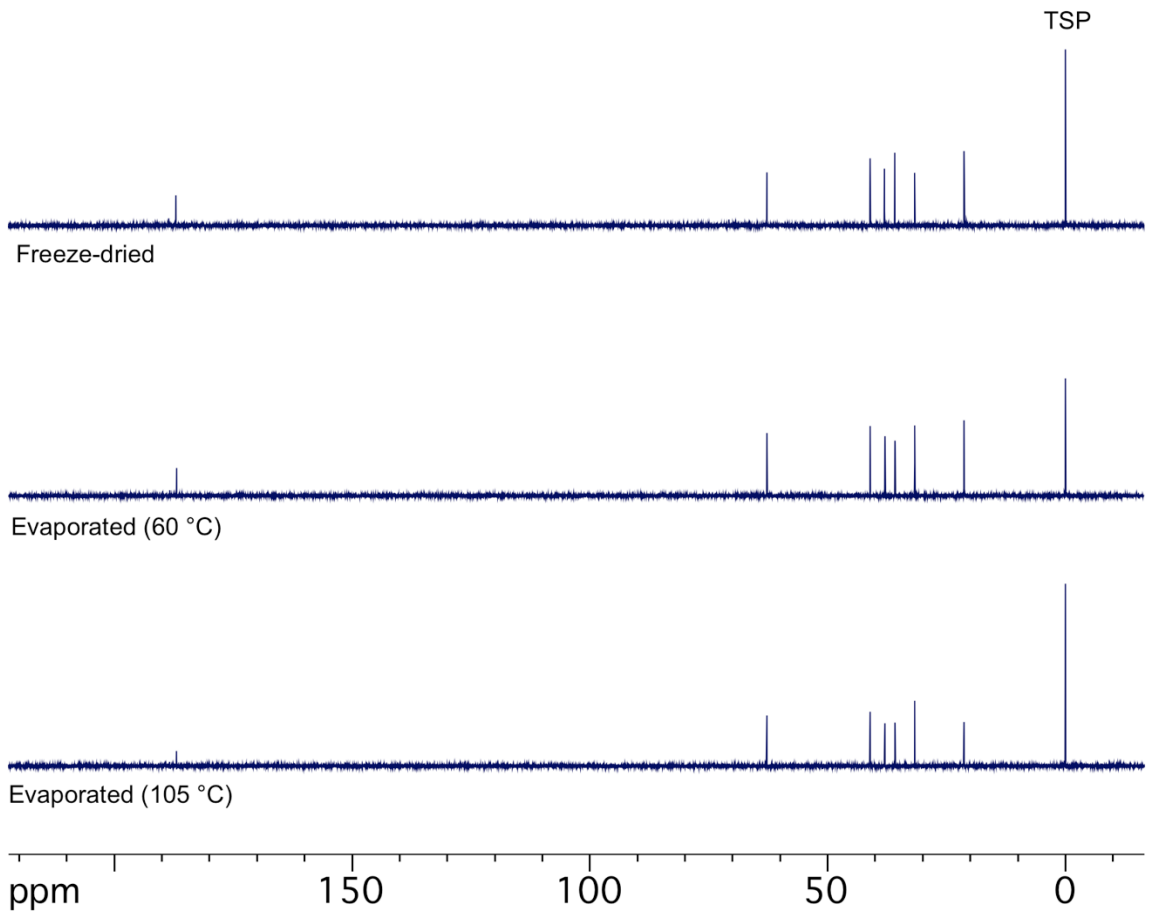

Figure 4.59. ^{13}C NMR spectra (100 MHz, D_2O) overlay comparing various methods of removing the water prior to NMR analysis of the solid residue of CE-22 degradation solution; side products are not formed during evaporation at elevated temperature. The spectra are standardized to 3-(trimethylsilyl)propanoate-2,2,3,3-*d*$_4$ (TSP).

We also investigated enzymatic hydrolysis at more environmentally relevant temperatures, specifically between 30 and 2 °C. Although pH-stat titration was used to monitor hydrolysis at 30 and 20 °C, the slow hydrolysis at temperatures lower than 20 °C made the use of pH-stat titration impractical. Thus, hydrolysis experiments at 2, 10, and 20 °C were conducted in batch vessels coupled to repeated solution TOC analysis. As there was high reproducibility and good agreement in the observed hydrolysis rates of the different CE samples at 40 °C, only CE-22 was used for the variable temperature hydrolysis

experiments (**Figure 4.60**). The pH-stat titration data indicated that complete hydrolysis was achieved in 5.5 and 10 days after enzyme addition at 30 and 20 °C, respectively. For all temperatures, the extent of hydrolysis was 98 ± 2% (average ± standard deviation), which was in very good agreement with the titration results obtained at 40 °C.

In the cases of hydrolysis monitored by TOC analysis, the lack of any appreciable dissolved organic carbon (*ca*. 1% of added elastomer carbon) after one week of incubation without FsC indicated that both non-enzymatic (abiotic) hydrolysis of the elastomers and leaching of water-soluble organic compounds from the elastomers were negligible, the latter of which would not necessarily be observable via pH-stat titration (**Figure 4.61**). Just as in pH-stat titration, the addition of enzyme resulted in the immediate formation of soluble hydrolysis products, which resulted in relatively linear evolution of TOC over time until the substrate was depleted. TOC analyses of the solutions containing polyester and enzyme indicated complete hydrolysis in 16, 28, or 53 days after enzyme addition at 20, 10, and 2 °C respectively. The final TOC concentrations in each batch reactor were in very good agreement with the expected carbon contents if all of the added elastomer was converted into soluble monomers; the TOC content was 100 ± 2% (average ± standard deviation) of the TOC expected for complete hydrolysis). We speculate that the discrepancy between the TOC analysis data and pH-stat titration data at 20 °C (16 days versus 10 days) was due to the presence of a significant amount of phosphate buffer (340 mM) in the batch reactors, which was necessary to keep the pH close to 7. The increased ionic strength of the solution likely resulted in a lower enzyme activity.[64,65] More importantly from an environmental fate perspective, complete hydrolysis was achieved on a reasonable timescale even at the lowest tested temperature of 2 °C. This finding strongly

suggests that the investigated elastomers would undergo complete enzymatic hydrolysis in natural systems such as soils as well as engineered systems such as landfills. Many previous investigations on the enzymatic hydrolysis of polyesters have shown that the presence of crystalline domains typically slows down hydrolysis;[57,59,60,61] the amorphous nature of the polyester elastomers presented here enabled facile and complete hydrolysis over a wide range of temperatures.

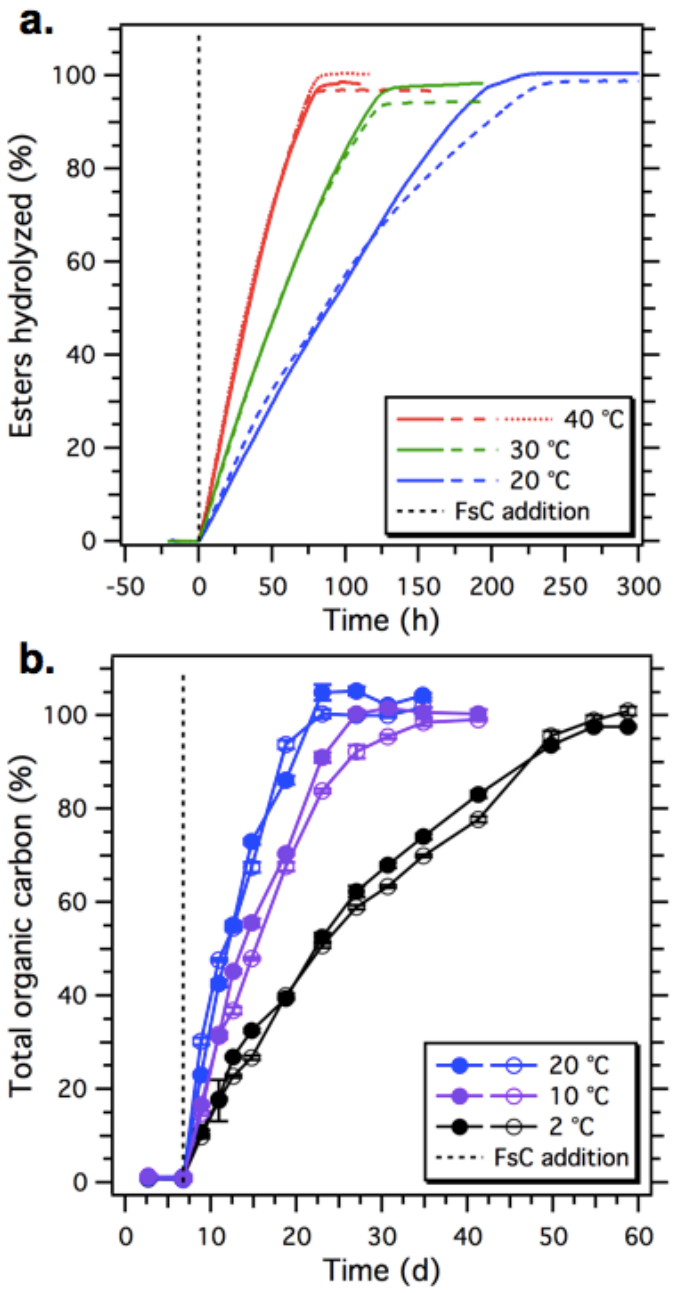

Figure 4.60. (**a.**) Hydrolysis curves for CE-22 with *Fusarium solani* cutinase (FsC) as measured by pH-stat titration at various temperatures and pH 7. The curves are horizontally offset such that FsC addition occurs at t = 0 h. (**b.**) Evolution of total organic carbon (% of added elastomer) during the hydrolysis of CE-22 by FsC at various temperatures and pH 7. The error bars represent standard deviations for three technical replicates per sample.

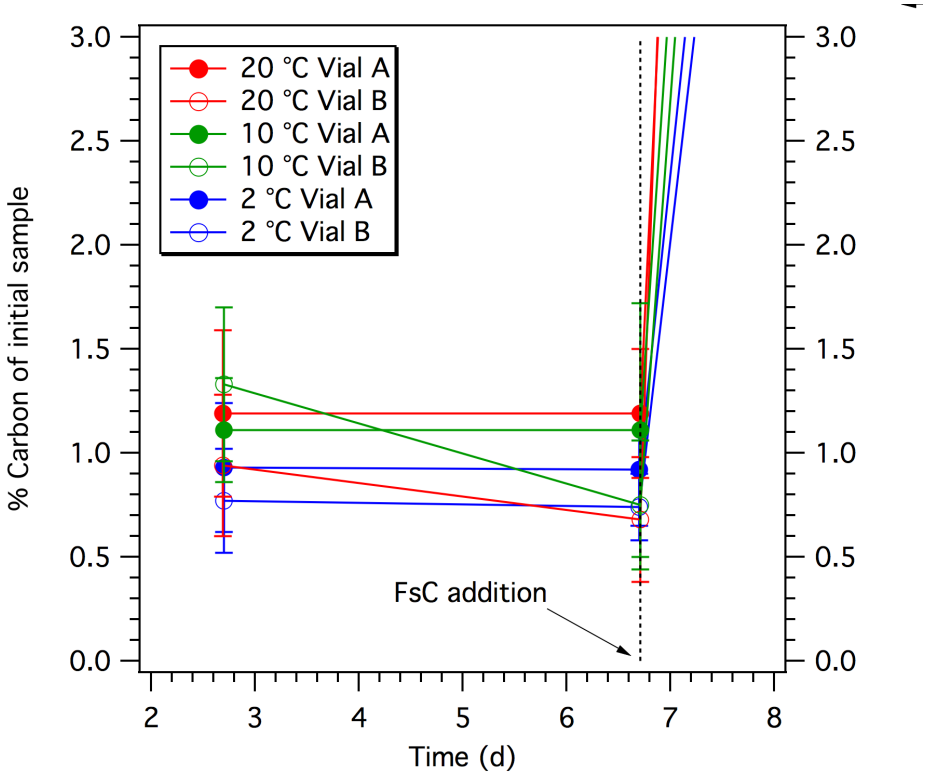

Figure 4.61. An enhanced section of the TOC analyses, demonstrating the carbon content at day 2 and day 5 for each batch reactor. For all samples, the carbon content in the solution did not increase from the first data point to the second, indicating that there is no detectable non-enzymatic hydrolysis over this time period. We ascribe the measured carbon (1%) to leaching of low-molecular weight compounds from the elastomer.

4.5. Conclusion.

We have demonstrated that MCL can be used to produce well-defined, star-shaped polyesters with hydroxyl end groups, which can react with a novel bis(β-lactone) monomer in the presence of $SnOct_2$ to afford cross-linked elastomers. Through soluble model compound studies, we determined that the $SnOct_2$-catalyzed ring-opening of β-valerolactone with benzyl alcohol proceeds via acyl-oxygen cleavage to generate β-hydroxyesters. Over 24 h, these moieties did not undergo substantial dehydration, and we therefore concluded that the junctions between the arms of the star-polymers in the insoluble network were β-hydroxyesters. The mechanical properties of the elastomer were

tuned by changing the molar mass of the star-polymer used to prepare the network. Although all elastomers demonstrated a very wide operating temperature range (–50 to 200 °C), the elastomer prepared with PMCL of M_n = 32 kg/mol demonstrated tensile properties that were competitive with a commercial rubber band. Enzymatic hydrolysis, the rate-limiting step in polyester biodegradation, of the elastomers was investigated at pH 7 and monitored using pH-stat titration or solution TOC analysis. With titration experiments, we showed that all CE samples hydrolyzed with similar rates. To further approach environmental conditions, hydrolysis was investigated at lower temperatures. Remarkably, the samples fully hydrolyzed at all temperatures (i.e., from 2 to 40 °C) and the primary hydrolysis product in each case was confirmed to be 6-hydroxy-4-methylhexanoic acid from the PMCL chains. The implications of these results for renewable CCPs are promising: lignin and various bio-based multifunctional epoxides could potentially be transformed into an easily polymerizable monomer and a versatile class of cross-linkers, respectively. These building blocks could then be used to make useful materials whose mechanical properties can be tuned without compromising their susceptibility to enzymatic hydrolysis. The materials investigated here are promising candidates as renewable and biodegradable alternatives to commercially available elastomers; as such, we expect future efforts to overcome the remaining challenges regarding the sustainability of MCL-based elastomers, namely by developing and optimizing the conversion of biomass to MCL using green chemistry principles.[66,67,68]

4.6. References

[1] Imbernon, L.; Norvez, S. *Eur. Polym. J.* **2016**, *82*, 347-376.

[2] Hopewell, J.; Dvorak, R.; Kosior, E. *Philos. Trans. R. Soc., B* **2009**, *364*, 2115-2126.

[3] World Economic Forum, Ellen MacArthur Foundation and McKinsey and Company, The New Plastics Economy: Rethinking the Future of Plastics; 2016; [report] http://www.ellenmacarthurfoundation.org/publications. Accessed July 5, 2016.

[4] Schneiderman, D. K.; Hillmyer, M. A. *Macromolecules*, **2017**, *50*, 3733-3749.

[5] Geyer, R.; Jambeck, J. R.; Law, K. L. *Sci. Adv.* **2017**, *3*, 1–5.

[6] Tokiwa, Y.; Calabia, B. P.; Ugwu, C. U.; Aiba, S. *Int. J. Mol. Sci.* **2009**, *10*, 3722-3742.

[7] Gallagher, J. J.; Hillmyer, M. A.; Reineke, T. M. *Macromolecules* **2014**, *47*, 498-505.

[8] Yang, J.; Lee, S.; Choi, W. J.; Seo, H.; Kim, P.; Kim, G.-J.; Kim, Y.-W.; Shin, J. *Biomacromolecules* **2015**, *16*, 246-256.

[9] Brutman, J. P.; De Hoe, G. X.; Schneiderman, D. K.; Le, T. N.; Hillmyer, M. A. *Ind. Eng. Chem. Res.* **2016**, *55*, 11097-11106.

[10] Wang, Y.; Ameer, G. A.; Sheppard, B. J.; Langer, R. *Nature Biotechnology* **2002**, *20*, 602-606.

[11] Andronova, A.; Srivastava, A.; Albertsson, A.-C. *Polymer* **2005**, *46*, 6746-6755.

[12] Amsden, B.; Wang, S.; Wyss, U. *Biomacromolecules* **2004**, *5*, 1399-1404.

[13] Younes, H. M.; Bravo-Grimaldo, E.; Amsden, B. G. *Biomaterials* **2004**, *25*, 5261-5269.

[14] Liu, Q.; Lei, J.; Shi, R.; Zhang, L. *Prog. Polym. Sci.* **2012**, *37*, 715-765.

[15] Andrady, A. *J. Macromol. Sci, Polym. Rev.* **1994**, *34*, 25-76.

[16] Altuna, F. I.; Pettarin, V.; Williams, R. J. J. *Green Chem.* **2013**, *15*, 3360-3366.

[17] Tang, X.; Hong, M.; Falivene, L.; Caporaso, L.; Cavallo, L.; Chen, E. Y.-X. *J. Am. Chem. Soc.* **2016**, *138*, 14326-14337.

[18] Palmgren, R.; Karlsson, S.; Albertsson, A.-C. *J. Polym. Sci., Part A: Polym. Chem* **1997**, *35*, 1635-1649.

[19] Nijenhuis, A. J.; Grijpma, D. W.; Pennings, A. J. *Polymer* **1996**, *37*, 2783-2791.

[20] Gripjma, D. W.; Kroeze, E.; Nijenhuis, A. J.; Pennings, A. J. *Polymer* **1993**, *34*, 1496-1503.

[21] Storey, R. F.; Warren, S. C.; Allison, C. J.; Wiggins, J. S.; Puckett, A. D. *Polymer* **2003**, *34*, 4365-4372.

[22] Helminen, A.; Korhonen, H.; Seppälä, J. *J. Polym. Sci., Part A: Polym. Chem.* **2003**, *41*, 3788-3797.

[23] Helminen, A.; Korhonen, H.; Seppälä, J. *J. Appl. Polym. Sci.* **2002**, *86*, 3616-3624.

[24] Helminen, A.; Korhonen, H.; Seppälä, J. *Macromol. Chem. Phys.* **2002**, *18*, 2630-2639.

[25] Lewis, C. L.; Meng, Y.; Anthamatten, M. *Macromolecules* **2015**, *48*, 4918-4926.

[26] Gurusamy-Thangavelu, S. A.; Emond, S. J.; Kulshrestha, A.; Hillmyer, M. A.; Macosko, C. W.; Tolman, W. B.; Hoye, T. R. *Polym. Chem.* **2012**, *3*, 2941-2948.

[27] Brutman, J. P.; Delgado, P. A.; Hillmyer, M. A. *ACS Macro Lett.* **2014**, *3*, 607-610.

[28] Storey, R. F.; Hickey, T. P. *Polymer* **1994**, *35*, 830-838.

[29] Schneiderman, D. K.; Vanderlaan, M. E.; Mannion, A. M.; Panthani, T. R.; Batiste, D. C.; Wang, J. Z.; Bates, F. S.; Macosko, C. W.; Hillmyer, M. A. *ACS Macro Lett.* **2016**, *5*, 515-518.

[30] Watts, A.; Kurokawa, N; Hillmyer, M. A. *Biomacromolecules*, **2016**, *18*, 1845-1854.

[31] Roberge, D. M.; Buhl, D.; Niederer, J. P. M.; Hölderich, W. F. *Appl. Catal., A* **2001**, *215*, 111-124.

[32] Linnekoski, J. A.; Asikainen, M.; Heikkinen, H.; Kaila, R. K.; Räsänen, J.; Laitinen, A.; Harlin, A. *Org. Process Res. Dev.* **2014**, *18*, 1468-1475.

[33] Schutyser, W.; Van Den Bosch, S.; Dijkmans, J.; Turner, S.; Meledina, M.; Van Tendeloo, G.; Debecker, D. P.; Sels, B. F. *ChemSusChem* **2015**, *8*, 1805-1818.

[34] Coulembier, O.; Dubois, P. Polyesters from β-Lactones. In *Handbook of Ring-Opening Polymerization*, Dubois, P., Coulembier, O.; Raquez, J.-M., Eds. Wiley-VCH Verlag GmbH & Co. KGaA: Weinheim, Germany, 2009, pp. 227-254.

[35] Carpentier, J.-F. *Macromol. Rapid Comm.* **2010**, *31*, 1696-1705.

[36] Ueda, M.; Takahashi, M.; Imai, Y. *J. Polym. Sci., Polym. Chem. Ed.* **1979**, *17*, 2477-2482.

[37] Kramer, J.; Rowley, J.; Coates, G. W. *Org. React.* **2015**, *86*, 1-104.

[38] Ayorinde, F.; Osman, G.; Shepard, R.; Powers, F. T. *J. Am. Oil. Chem. Soc.* **1988**, *65*, 1774-1777.

[39] Bell, B. M.; Briggs, J. R.; Campbell, R. M.; Chambers, S. M.; Gaarenstroom, P. D.; Hippler, J. G.; Hook, B. D.; Kearns, K.; Kenney, J. M.; Kruper, W. J.; Schreck, D. J.; Theriault, C. N.; Wolfe, C. P. *Clean: Soil, Air, Water* **2008**, *36*, 657-661.

[40] Lligadas, G.; Ronda, J. C.; Galià, M.; Cádiz, V. *Biomacromolecules* **2010**, *11*, 2825-2835.

[41] De Espinosa, L. M.; Meier, M. A. R. *Eur. Polym. J.* **2011**, *47*, 837-852.

[42] Gandini, A. *Green Chem.* **2011**, *13*, 1061-1083.

[43] Liu, X.-Q., Wang, M.-X.; Li, Z.-C.; Li, F.-M. *Macromol. Chem. Phys.* **1999**, *200*, 468-473.

[44] Coulembier, O.; Degée, P.; Barbaud, C.; Guérin, P.; Dubois, P. *Polym. Bull.* **2004**, *51*, 365-372.

[45] Hong, J. H.; Hyun, J. J.; Yoo, J. H.; Yu, W.-R.; Youk, J. H. *Polym. Degrad. Stab.* **2007**, *92*, 1186-1192.

[46] Rowley, J. M.; Lobkovsky, E. B.; Coates, G. W. *J. Am. Chem. Soc.* **2007**, *129*, 4948-4960.

[47] Church, T. L.; Getzler, Y. D. Y. L.; Coates, G. W. *J. Am. Chem. Soc.* **2006**, *128*, 10125-10133.

[48] Getzler, Y. D. Y. L.; Mahadevan, V.; Lobkovsky, E. B.; Coates, G. W. *J. Am. Chem. Soc.* **2002**, *124*, 1174-1175.

[49] Longhi, S.; Czjzek, M.; Lamzin, V.; Nicolas, A.; Cambillau, C. *J. Mol. Biol.* **1997**, *268*, 779-799.

[50] Gasteiger, E.; Hoogland, C.; Gattiker, A.; Duvaud, S.; Wilkins, M.; Appel, R.; Bairoch, A. Protein Identification and Analysis Tools on the ExPASy Server. In *The Proteomics Protocols Handbook*, Walker, J. M. Ed. Humana Press Inc: Totowa, NJ, 2005, pp. 571-607.

[51] Baker, P. J.; Poultney, C.; Liu, Z.; Gross, R.; Montclare, J. K. *Appl. Microbiol. Biotechnol.* **2012**, *93*, 229-240.

[52] Teles, J. H.; Hermans, I.; Franz, G.; Sheldon, R. H. Oxidation. In *Ullman's Encyclopedia of Industrial Chemistry*, Wiley-VCH Verlag GmbH & Co. KGaA: Weinheim, Germany, 2015, pp. 1-103.

[53] Hiemenz, P. C.; Lodge, T. P. *Polymer Chemistry* 2nd ed.; CRC Press: Boca Raton, FL, 2007.

[54] Nirmal Ghosh, O. S.; Gayathri, S.; Sudhakara, P.; Misra, S. K.; Jayaramudu, J. Natural Rubber Nanoblends: Preparation, Characterization, and Applications. In *Rubber Nano Blends*, Markovic, G.; Visakh, P. M., Eds. Springer International Publishing AG: Cham, Switzerland, 2017, pp. 15-65.

[55] Mueller, R.-J. *Process Biochem.* **2006**, *41*, 2124-2128.

[56] Murphy, C. A.; Cameron, J. A.; Huang, S. J.; Vinopal, R. T. *Appl. Environ. Microbiol.* **1996**, *62*, 456-460.

[57] Ronkvist, Å. M.; Xie, W.; Lu, W.; Gross, R. A. *Macromolecules* **2009**, *42*, 5128-5138.

[58] Perz, V.; Bleymaier, K.; Sinkel, C.; Kueper, U.; Bonnekessel, M.; Ribitsch, D.; Guebitz, G. M. *New Biotechnol.* **2016**, *33*, 295-304.

[59] Zumstein, M. T.; Kohler, H.-P. E.; McNeill, K.; Sander, M. *Environ. Sci. Technol.* **2016**, *50*, 197-206.

[60] Zumstein, M. T.; Kohler, H.-P. E.; McNeill, K.; Sander, M. *Environ. Sci. Technol.* **2017**, *51*, 4358-4367.

[61] Zumstein, M. T.; Rechsteiner, D.; Roduner, N.; Perz, V.; Ribitsch, D.; Guebitz, G. M.; Kohler, H.-P. E.; McNeill, K.; Sander, M. *Environ. Sci. Technol.* **2017**, *51*, 7476-7485.

[62] Turon, X.; Rojas, O. J.; Deinhammer, R. S. *Langmuir* **2008**, *24*, 3880-3887.

[63] Wang, C.; Kittle, J. D.; Qian, C.; Roman, M.; Esker, A. R. *Biomacromolecules* **2013**, *14*, 2622-2628.

[64] Salis, A.; Bilaničová, D.; Ninham, B. W.; Monduzzi, M. *J. Phys. Chem. B* **2007**, *111*, 1149-1156.

[65] Schmidt, J.; Wei, R.; Oeser, T.; Belisário-Ferrari, M. R.; Barth, M.; Then, J.; Zimmermann, W. *FEBS Open Bio* **2016**, *6*, 919-927.

[66] Corma, A.; Nemeth, L. T.; Renz, M.; Valencia, S. *Nature* **2001**, *412*, 423-425.

[67] ten Brink, G.-J.; Arends, W. C. E.; Sheldon, R. *Chem. Rev.* **2004**, *104*, 4105-4123.

[68] Yakabi, K.; Mathieux, T.; Milne, K.; López-Vidal, E. M.; Buchard, A.; Hammond, C. *ChemSusChem* **2017**, *10*, 3652-3659.

Chapter 5. Mechanistic Study of Stress Relaxation in Urethane-Containing Polymer Networks.*

* Reprinted (adapted) with permission from Brutman, J. P.; Fortman, D. J.; De Hoe, G. X.; Dichtel, W. R.; Hillmyer M. A. A Mechanistic Study of Stress Relaxation in Urethane-Containing Polymer Networks. *J. Phys. Chem. B* **2019**, *123*, 1432–1441. Copyright © 2019 American Chemical Society.

5.1. Abstract

Cross-linked polymers are used in many commercial products and are traditionally incapable of recycling via melt reprocessing. Recently, tough and reprocessable cross-linked polymers have been realized by incorporating cross-links that undergo associative exchange reactions, such as transesterification, at elevated temperatures. Here we investigate how cross-linked polymers containing urethane linkages relax stress under similar conditions, which enables their reprocessing. Materials based on hydroxyl-terminated star-shaped poly(ethylene oxide) and poly((±)-lactide) were cross-linked with methylene diphenyldiisocyanate in the presence of stannous octoate catalyst. Polymers with lower plateau moduli exhibit faster rates of relaxation. Reactions of model urethanes suggest that exchange occurs through tin-mediated exchange of the urethanes that does not require free hydroxyl groups. Furthermore, samples were incapable of elevated temperature dissolution in a low polarity solvent (1,2,4-trichlorobenzene) but readily dissolved in a high polarity aprotic solvent (DMSO, 24 to 48 h). These findings indicate that urethane linkages, which are straightforward to incorporate, impart dynamic character to polymer networks of diverse chemical composition, possibly through a urethane reversion mechanism.

5.2. Introduction

Cross-linked polymer networks are prevalent in adhesives, composites, and other durable products. Unlike thermoplastics, traditional cross-linked polymer networks are effectively irreparable, cannot be reshaped, and are non-recyclable through traditional means. Many studies have explored their reprocessing by incorporating dynamic cross-links.[1,2,3,4,5,6] Early examples relied on thermally reversible moieties such as Diels-Alder

cycloadducts, which allowed the materials to depolymerize and be reformed in a new shape.[7,8] Although this approach represented a significant conceptual advance in the reprocessing of cross-linked polymers, the materials often exhibited poor thermal stability and solvent resistance, which limited their potential applications.[9]

A new class of reprocessable polymer networks, termed vitrimers,[10,11,12] feature cross-links that typically undergo exchange through associative rather than dissociative processes. Vitrimers maintain their cross-linked nature at elevated temperature and/or in the presence of solvents, as demonstrated for polyester epoxy resins containing a Zn(II) transesterification catalyst.[10,13,14] The cured resins were capable of reprocessing and injection molding at 280 °C; however, they only swelled in hot solvent (180 °C) rather than dissolving, as is typical for cross-linked polymers. The temperature dependence of the viscosity of vitrimers is gradual and follows an Arrhenius relationship, which differs from the typical Williams-Landel-Ferry response observed for thermoplastics. This strong glass-forming behavior confers a topology freezing transition temperature (T_v) when it occurs above or at the T_g. Below T_v the vitrimer behaves as a traditional thermoset, and above T_v the cross-links undergo dynamic exchange reactions that give rise to thermally activated stress relaxation.

Vitrimers and vitrimer-like materials have been developed based on dynamic chemistries including alkene metathesis,[15,16] hindered urea exchange,[17,18,] disulfide/polysulfide metathesis,[19,20,21,22] thiol-disulfide exchange,[23] vinylogous urethane exchange,[24,25] transcarbamoylation,[26,27] siloxane equilibrium,[28,29] and boronic ester exchange.[30,31,32] We previously reported reprocessable materials based on poly((±)-lactide) (PLA) cross-linked with a diisocyanate in the presence of stannous octoate catalyst.[33] We

initially hypothesized that transesterification caused stress relaxation (**Figure 5.1A**) and that the high concentration of ester functionalities in the PLA backbone was responsible for the rapid stress relaxation and efficient reprocessability of these materials. However, the Arrhenius activation energy (E_a) for stress relaxation (150 kJ mol^{-1}) was much higher than that determined for PLA transesterification (80 kJ mol^{-1}),[34] which indicated that other stress relaxation mechanisms were more likely. We later showed that cross-linked polyhydroxyurethanes relax stress through hydroxyl-urethane exchange (e.g., transcarbamoylation, **Figure 5.1B**),[26,27] suggesting that the urethane linkages might also be responsible for stress relaxation in the PLA networks. Furthermore, stress relaxation of polyurethane networks lacking free hydroxyl groups, which are required for transcarbamoylation, was reported by Tobolsky in the 1950s and was hypothesized to occur via urethane reversion (**Figure 5.1C**).[35,36] Exploiting the dynamic nature of urethane bonds has recently become a promising approach for reshaping polyurethane networks, although mechanistic aspects of these processes are not entirely clear. For example, Zheng, *et al.* hypothesized that urethanes were responsible for stress relaxation in polyurethane elastomers in the presence of dibutyltin dilaurate.[37] Yan, *et al.* further studied the tin-mediated relaxation of polyurethanes and showed preliminary results indicating that this behavior can be correlated to reprocessability of cross-linked polyurethanes.[38,39] Additional work by Zheng, *et al.* demonstrated that networks based on *N*-aryl urethanes relax stress at elevated temperatures even in the absence of an external catalyst,[40] although no explicit evidence for urethane reversion was presented in any of these systems. Yang and Urban postulated that repair of cross-linked polyurethanes occurs through the generation of amines upon mechanical failure, which react further with urethanes to form ureas.[41]

Although modest changes in the Raman and IR spectra were consistent with this hypothesis, more definitive characterization was not obtained. Considering these findings, a robust understanding of the mechanisms of stress relaxation for urethane-containing polymer networks has not yet been established.

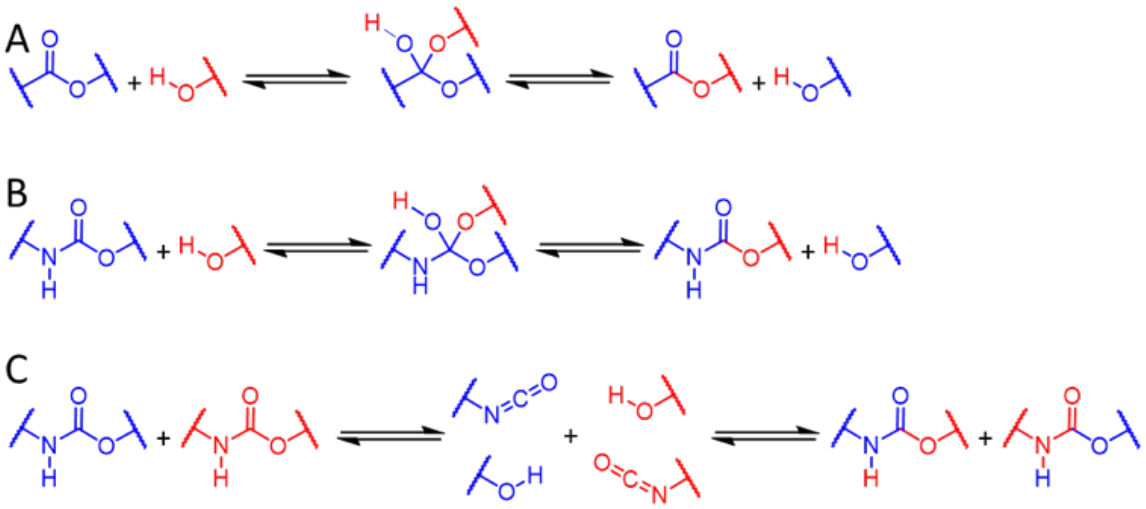

Figure 5.1. Proposed relaxation mechanisms for urethane cross-linked PLA: **A)** transesterification, **B)** transcarbamoylation, and **C)** urethane reversion.

Here we investigate the thermally activated stress relaxation of urethane-containing polymer networks as a function of temperature, catalyst content, and polymer structure. The similarity of E_a values for stress relaxation of PLA- and poly(ethylene oxide) (PEO)-based polymers cross-linked with aryl isocyanates indicates that urethane bonds are the dynamic linkages in both networks and further suggests that transesterification-based relaxation is negligible in PLA-derived urethane networks. Exchange studies of urethane model compounds at elevated temperature provide further insight into the mechanism responsible for stress relaxation. Variable-temperature NMR spectroscopy and polymer swelling experiments are consistent with urethane reversion being the predominant mechanism of stress relaxation in polymer networks cross-linked by *N*-aryl urethanes.

5.3. Experimental

5.3.1. Materials

All reagents were purchased from Sigma-Aldrich (Milwaukee, WI) and were used as received unless otherwise stated. All glassware was heated to 105 °C overnight prior to use unless otherwise specified. (±)-Lactide was kindly provided by Altasorb (Piedmont, SC) and used as received. Stannous octoate [$Sn(Oct)_2$] was purified by vacuum distillation (3x, ~130-150 °C, *ca.* 30-50 mTorr argon). Dichloromethane (DCM) and methanol were purchased from Fisher Scientific (Hampton, NH); DCM was purified via a GC-SPS-4-CM glass contour 800-L solvent purification system obtained from Pure Process Technologies (Nashua, NH). 4-Arm hydroxyl-terminated PLA and urethane cross-linked PLA were synthesized using a literature procedure; the number average molar mass (M_n) of the prepolymer was determined by ^{1}H NMR spectroscopy.[33] Urethane cross-linked PEO was synthesized under the same conditions as the PLA samples using commercially available pentaerythritol ethoxylate (M_n ~ 797 g mol^{-1}). PLA and PEO samples are respectively denoted PLA-*X*-*Y* and PEO-*X*-*Y*, where *X* is the M_n of the prepolymer (kg mol^{-1}) and *Y* is the cross-linker used: either methylene diphenyl diisocyanate (MDI) or poly(methylene diphenyl diisocyanate) (PMDI). In some cases, a sample was swelled in methanol (see characterization methods section) or contains no catalyst, denoted by SM and NC at the end of the sample name, respectively.

5.3.2. Synthesis of Epoxide Cross-linked Poly(4-methylcaprolactone)

The 4-methylcaprolactone monomer was synthesized using a literature procedure.[42] $Sn(Oct)_2$ (4 mg, 0.025 mol%) was dissolved in toluene (*ca.* 0.1 mL) and charged in a

pressure vessel, along with 4-methylcaprolactone (5 g, 39 mmol) and pentaerythritol (0.073 g, 0.54 mmol). The reaction mixture was heated to 160 °C for 3 h, then succinic anhydride (0.3 g, 3 mmol) was added under N_2 and stirred for 1 h. The mixture was cooled, dissolved using DCM, and then precipitated into methanol (*ca.* 10 times volume of product solution). The crude polymer was again dissolved in DCM and reprecipitated in hexanes (*ca.* 10 times volume of product solution). The resulting carboxylic acid-terminated poly(4-methylcaprolactone) (P4MCL) was dried under N_2 for 24 h, then dried under vacuum (20 mTorr) at 60 °C for 72 h; the isolated yield was 76%. ^{1}H NMR (500 MHz, $CDCl_3$; 25 °C): δ (ppm) = 4.20-4.01 (m, 158 H), 2.64 (m, 16 H), 2.42-2.23 (m, 150 H), 1.74-1.39 (m, 390 H), 0.97-0.87 (m, 240 H). M_n = 10.1 kg mol^{-1}. DSC: T_g = –60 °C.

P4MCL (1.52 g, 1.0 eq. COOH groups), triglycidyl isocyanurate (64 mg, 1.0 eq. epoxide groups), and $Sn(Oct)_2$ (6 mg, 2.5 mol% to COOH groups) were dissolved in DCM. The solution was poured into a polypropylene container and allowed to sit for 24 h before heating under N_2 at 120 °C for 3 h. The gel percent of the resultant epoxide cross-linked P4MCL network was 95%.

5.3.3. Representative Synthesis of N-H Model Compounds

To a flame-dried round-bottom flask under nitrogen atmosphere was added alcohol (16.8 mmol) and anhydrous tetrahydrofuran (20 mL). A solution of $Sn(Oct)_2$ (130 mg, 0.34 mmol, 2 mol%) dissolved in anhydrous tetrahydrofuran (1 mL) was added, followed by addition of isocyanate (16.8 mmol) using a syringe. The resulting solution was stirred at room temperature for 24 h, and solvent was removed at reduced pressure to yield a white solid. The crude solid was chromatographed on silica gel in 20% ethyl acetate/hexanes to yield the product.

N-phenyl-O-octyl urethane: White solid, 82% yield. ^{1}H NMR (400 MHz, $CDCl_3$) δ 7.38 (d, *J* = 8.0 Hz, 2H), 7.35-7.23 (m, 2H), 7.05 (tt, *J* = 7.1, 1.2 Hz, 1H), 6.56 (br s, 1H), 4.16 (t, J = 6.7 Hz, 2H), 1.71-1.63 (m, 2H), 1.43-1.23 (m, 10H), 0.89 (t, *J* = 7.8 Hz, 3H). ^{13}C NMR (100 MHz, $CDCl_3$) δ 153.7, 138.0, 128.9, 123.2, 118.5, 65.4, 31.7, 29.19, 29.15, 28.9, 25.8, 22.6, 14.0. IR (neat, ATR) 3304, 2956, 2920, 2853, 1698, 1599, 1544, 1444, 1236, 1055, 747 cm^{-1}.

N-tolyl-*O*-decyl urethane: White solid, 85% yield. ^{1}H NMR (400 MHz, $CDCl_3$) δ 7.28-7.22 (m, 2H), 7.10 (d, J = 8.3 Hz, 2H), 6.49 (br s, 1H), 4.14 (t, J = 6.7 Hz, 2H), 2.30 (s, 3H), 1.72-1.60 (m, 2H), 1.44-1.24 (m, 14H), 0.92-0.84 (m, 3H). ^{13}C NMR (100 MHz, $CDCl_3$) δ 153.8, 135.4, 132.8, 129.4, 118.7, 65.3, 31.9, 29.51, 29.50, 29.27, 29.25, 28.9, 25.8, 22.6, 20.7, 14.1. IR (neat, ATR) 3327, 2919, 2851, 1696, 1596, 1531, 1314, 1235, 1071, 814 cm^{-1}.

N-tolyl-*O*-(triethyleneglycol monomethyl ether) urethane: Colorless oil, 57% yield. ^{1}H NMR (400 MHz, $CDCl_3$) δ 7.25 (d, *J* = 8.6 Hz, 2H), 7.10 (d, *J* = 8.0 Hz, 2H), 6.73 (br s, 1H), 4.35-4.28 (m, 2H), 3.78-3.71 (m, 2H), 3.73-3.62 (m, 6H), 3.59-3.52 (m, 2H), 3.38 (s, 3H), 2.30 (s, 3H). ^{13}C NMR (100 MHz, $CDCl_3$) δ 153.5, 135.3, 132.7, 129.3, 118.7, 71.8, 70.42, 70.41, 70.40, 69.3, 63.9, 58.8, 20.6. IR (neat, ATR) 3306, 2873, 1727/1709, 1599, 1530, 1315, 1222, 1207, 1102, 1069, 816 cm^{-1}.

5.3.4. Representative Synthesis of *N*-CH_3 Model Compounds

To a flame-dried round-bottom flask under nitrogen atmosphere was added urethane (4 mmol) and anhydrous dimethylformamide (15 mL). The mixture was cooled in an ice bath, and sodium hydride (192 mg, 8.0 mmol, 320 mg dispersion in mineral oil) was added, resulting in gas evolution. The resulting mixture was stirred for 10 minutes, then

iodomethane (1.419 g, 10 mmol, 0.62 mL) was added using a syringe. The resulting mixture was stirred at room temperature for 18 h, then diluted with water (150 mL). This solution was extracted with diethyl ether (200 mL), which was washed with water (2 x 150 mL), dried over $MgSO_4$, and filtered. Solvent was removed at reduced pressure to yield a colorless oil. The crude oil was chromatographed on silica gel using 10% ethyl acetate/hexanes to yield the product as a colorless oil.

N-methyl-*N*-phenyl-*O*-octyl urethane: Colorless oil, 65% yield. ^{1}H NMR (400 MHz, $CDCl_3$) δ 7.34 (m, 2H), 7.27-7.15 (m, 3H), 4.09 (t, J = 6.7 Hz, 2H), 3.30 (s, 3H), 1.63-1.53 (m, 2H), 1.33-1.22 (m, 10H), 0.88 (t, J = 6.8 Hz, 3H). ^{13}C NMR (100 MHz, $CDCl_3$) δ 155.7, 143.4, 128.7, 125.8, 125.6, 65.8, 37.5, 31.7, 29.11, 29.08, 28.8, 25.8, 22.6, 14.0. IR (neat, ATR) 2925, 2855, 1703, 1598, 1498, 1346, 1154, 695 cm^{-1}.

N-methyl-*N*-tolyl-*O*-decyl urethane: Colorless oil, 55% yield. ^{1}H NMR (400 MHz, $CDCl_3$) δ 7.18-7.07 (m, 4H), 4.08 (t, J = 6.7 Hz, 2H), 3.27 (s, 3H), 2.34 (s, 3H), 1.64-1.54 (m, 2H), 1.35-1.23 (m, 14H), 0.89 (t, J = 6.9 Hz, 3H). ^{13}C NMR (100 MHz, $CDCl_3$) δ 155.9, 140.8, 135.6, 129.3, 125.6, 65.8, 37.7, 31.9, 29.5, 29.4, 29.3, 29.1, 28.9, 25.8, 22.6, 20.9, 14.0. IR (neat, ATR) 2923, 2854, 1703, 1515, 1343, 1155, 1111, 820, 768 cm^{-1}.

5.3.5. Model Alcohol-Urethane Exchange Reaction analyzed by GC-MS Analysis

To a vial was added $Sn(Oct)_2$ (11.9 mg, 0.03 mmol, 2.5 mol% to urethane), *N*-phenyl-*O*-octyl urethane (293 mg, 1.17 mmol), 1-decanol (1.86 g, 11.7 mmol), and triphenylmethane (27.0 mg, 0.11 mmol) as an internal standard. The resulting mixture was heated and stirred in a preheated oil bath. Aliquots were removed using a syringe at various time points, diluted with DCM, and subjected to GC-MS analysis. Concentrations of the transcarbamoylation product *N*-phenyl-*O*-decyl urethane could not be determined

quantitatively due to partial decomposition of the urethanes on the GC column at temperatures required to sufficiently volatilize them.

5.3.6. Model Alcohol-Urethane Exchange Reaction analyzed by NMR Spectroscopy

To a vial was added $Sn(Oct)_2$ (11.6 mg, 0.03 mmol, 2.5 mol% to urethane), *N*-tolyl-*O*-(triethyleneglycol monomethyl ether) urethane (340 mg, 1.14 mmol), and 1-decanol (1.81 g, 11.4 mmol). The resulting mixture was then heated and stirred in a preheated oil bath. Aliquots of *ca*. 10 mg were removed using a syringe at various time points, dissolved in $CDCl_3$ (containing 10.0 mg/mL tribromobenzene as an external standard) to a concentration of 50.0 mg/mL, and analyzed by ^{1}H NMR spectroscopy (the -C*H*$_2$O- peaks of the starting material and transcarbamoylation product are distinct). Concentrations of the transcarbamoylation product *N*-tolyl-*O*-decyl urethane could not be determined quantitatively due to overlap of the product resonance at *ca.* 4.1 ppm with a side product (the calculated amount of product formed is greater than the amount of starting material lost; running the reaction to high conversion clearly shows an overlapping resonance convoluting the product peak).

5.3.7. Model Urethane-Urethane Crossover Reaction

To a vial was added $Sn(Oct)_2$ (23.9 mg, 0.059 mmol, 2.5 mol% to urethane), *N*-phenyl-*O*-octyl urethane (294 mg, 1.18 mmol), *N*-tolyl-*O*-decyl urethane (344 mg, 1.18 mmol), and triphenylmethane (30.5 mg, 0.12 mmol) as an internal standard. The resulting mixture was heated and stirred in an oil bath preheated to the desired temperature. Aliquots were removed using a syringe at various time points, diluted with DCM, and subjected to GC-MS analysis. Concentrations of the urethane exchange product *N*-phenyl-*O*-decyl

urethane could not be determined quantitatively due to partial decomposition of the urethanes on the GC column at temperatures required to sufficiently volatilize them.

5.3.8. Synthesis of Diethyl Urethane Adduct of MDI

To a round-bottom flask was added MDI (10 g, 40 mmol), ethanol (9.3 mL, 160 mmol) and DCM (10 mL) under stirring. Once the solution was homogenous, it was cooled to 0 °C and $Sn(Oct)_2$ (0.81 g, 2 mmol, 2.5 mol% to –NCO) in DCM (10 mL) was added. After 10 min at 0 °C, the solution was left at room temperature for 20 h before concentrating by rotary evaporation and drying under high vacuum (~20 mTorr) for 48 h. The crude product was then dissolved in dimethylformamide (*ca.* 20 mL) and precipitated into deionized water (*ca.* 200 mL) yielding a yellow solid that was dried under vacuum (20 mTorr) for 48 h (quantitative yield). ^{1}H NMR (500 MHz, DMSO-d_6): δ 9.52 (s, 2H), 7.38 (d, 4H), 7.10 (d, 4H), 4.12 (q, 4H), 3.79 (s, 2H), 1.24 (t, 6H). ^{13}C NMR (125 MHz, DMSO-d_6): δ 154, 138, 136, 129, 119, 60, 40, 15.

5.3.9. Characterization Methods[26,33,43]

NMR spectroscopy was performed on a 500 MHz Bruker Avance III HD with SampleXpress spectrometer (Billerica, MA) or an Agilent DD MR-400 400 MHz spectrometer. Solutions were prepared in 99.8% $CDCl_3$ (Cambridge Isotope Laboratories). All NMR spectra were acquired at 20 °C with at least 16 scans and a 1 s delay unless otherwise specified. Chemical shifts are reported in ppm with respect to residual $CHCl_3$ (7.26 ppm). Variable temperature (VT) NMR was performed on a 500 MHz Bruker III at 100 °C and 140 °C. DMSO-d_6 (Cambridge Isotope Laboratories, 99.9%) was purified by distillation over CaH_2. The solution for VT-NMR was prepared and sealed in a high-

pressure NMR tube under N_2. The same solution was allowed to equilibrate at the desired temperature for 10 min before acquiring the ^{1}H NMR and ^{13}C NMR spectra.

FT-IR was performed on a Bruker Alpha Platinum with a single reflection diamond ATR head or a Thermo Nicolet iS10 equipped with a ZnSe ATR attachment. Spectra were obtained from 400 to 4000 cm^{-1} using a minimum of 16 scans. For each spectrum, the transmission intensity data were normalized with respect to the carbonyl stretch.

Gas chromatography/electron impact mass spectrometry (GC-MS) was performed on an Agilent 6890N Network GC System with a JEOL JMS-GCmate II Mass Spectrometer (magnetic sector). Triphenylmethane was used as an internal standard.

Dynamic mechanical thermal analysis (DMTA) was performed on a TA Instruments RSA-G2 analyzer (New Castle, DE) using dog bone shaped films (*ca.* 0.5 mm (T) × 3 mm (W) × 25 mm (L) and a gauge length of 14 mm). DMTA experiments were conducted in tension film mode, where the axial force was first adjusted to 0.2 N of tension (sensitivity of 0.01 N) to ensure no buckling of the sample. The proportional force mode was set to force tracking to ensure that the axial force was at least 100% greater than the dynamic oscillatory force. The strain adjust was then set to 30% with a minimum strain of 0.05%, a maximum strain of 5%, and a maximum force of 0.2 N to prevent the sample from going out of the specified strain range. A temperature ramp was then performed from –50 °C to 200 °C at a rate of 5 °C min^{-1}, with an oscillating strain of 0.05% and an angular frequency of 6.28 rad s^{-1}. PLA samples required a higher starting temperature (25 to 35 °C) due to transducer overload in the brittle regime. The glass transition temperature (T_g) was determined from the maximum value of the loss modulus. The cross-link density (v_e) and

the molar mass between cross-links (M_x) were calculated using the storage modulus (E') at 100 °C and equation 1.

$$E'(T) = 3G'(T) = 3RT\nu_e = \frac{3\rho RT}{M_x} \quad (1)$$

Where G' is the storage modulus under shear, R is the universal gas constant, T refers to the absolute temperature in the rubbery region (*ca.* 373 K) and ρ is the density of PLA (1.25 g cm^{-3}) or PEO (1.13 g cm^{-3}).

The stress-relaxation analysis (SRA) experiments were performed under strain control at a specified temperature (110-170 °C depending on the sample). The samples were allowed to equilibrate at this temperature for approximately 10 minutes, after which the axial force was then adjusted to 0 N with a sensitivity of 0.05 N. Each sample was then subjected to an instantaneous 5% strain. The stress decay was monitored while maintaining a constant strain (5%) until the stress relaxation modulus had relaxed to 37% (1/e) of its initial value. The characteristic relaxation time (τ^*), or the time required for the modulus to reach 37% (1/e) of its initial value, was measured three times in succession for each sample at each temperature. These points were then plotted versus 1/T and fit to the Arrhenius relationship in equation 2.

$$\tau^*(T) = \tau_0 e^{Ea/RT} \quad (2)$$

Where τ_0 is the characteristic relaxation time at infinite T, E_a is the activation energy of stress relaxation (kJ mol^{-1}), R is the universal gas constant, and T is the temperature in K at which SRA was performed.

The T_v is defined as the point at which a material exhibits a viscosity of 10^{12} Pa s, also known as the liquid to solid transition viscosity (η_v).[44,45,46] Using Maxwell's relation

(equation 3)[47] and the E' measured by DMTA at 100 °C, the τ^* at T_v (τ_v^*) was determined for each sample. The Arrhenius fit for each sample was then extrapolated to the corresponding τ_v^* to determine T_v.

$$\eta_v = \frac{1}{3} E' * \tau_v^* \quad (3)$$

Differential scanning calorimetry (DSC) was conducted on a TA Instruments Discovery DSC (New Castle, DE). The instrument was calibrated using an indium standard. All samples (*ca.* 3–7 mg) were analyzed using T-Zero hermetic pans under a N_2 purge of 50 mL min^{-1}. The samples were initially cooled to –80 °C and then heated to 150 °C at 10 °C min^{-1}. After a 1-minute isotherm, the samples were then cooled to –80 °C at 10 °C min^{-1} and heated again to 150 °C at the same rate. Values for T_g were acquired at the midpoint of each transition in the second heating curve using the Trios® software. Thermogravimetric analysis (TGA) was performed on a TA Instruments Q500 (New Castle, DE) under air at a heating rate of 10 °C/min from room temperature to 550 °C. A typical sample size was between 8-15 mg.

Solvent extraction experiments were performed by placing a small amount of cross-linked polymer (*ca.* 20 to 100 mg) into a 20-mL vial filled with DCM or MeOH. The vial was then closed and stirred for 48 h before removing the solvent by gravity filtration. The recovered sample was dried under reduced pressure for 48 h at 20 mTorr, after which the sample was weighed and the gel percent was determined. A high temperature swell test was also performed with PEO-0.8-MDI (with and without catalyst) submerged in 1,2,4-trichlorobenzene (TCB) or anhydrous dimethylsulfoxide (DMSO) at 140 °C for 7 days or until full dissolution.

Trace Sn analysis was performed by Chemical Solutions Ltd. using inductively coupled plasma mass spectrometry (ICP-MS) after microwave digestion of the samples. Five samples were subjected to trace Sn analysis: PEO-0.8-PMDI (0.44 wt% Sn), PEO-0.8-MDI (0.54 wt% Sn), PEO-0.8-PMDI-SM (0.96 wt% Sn), PEO-0.8-MDI-SM (0.52 wt% Sn), and PEO-0.8-MDI-NC (0.000053 wt% Sn).

5.4. Results and Discussion

In our previous study of urethane cross-linked PLA,[33] the E_a of stress relaxation (150 kJ mol^{-1}) was far higher than that reported for Sn(Oct)$_2$-catalyzed transesterification in a PLA melt (80 kJ mol^{-1}).[34] To further investigate, we substituted the PLA component with PEO; if transesterification reactions are the dominant mechanism of stress relaxation, then PEO-based materials would exhibit distinctly different stress relaxation behavior due to the lack of ester linkages in PEO. Urethane cross-linked PEO materials were prepared using similar conditions to those used for urethane cross-linked PLA (**Figure 5.2**).[33] The commercially available PEO prepolymer was combined with MDI (NCO functionality of 2, 0.75 NCO groups per OH group) and Sn(Oct)$_2$ (2.5 mol% relative to initial OH groups) to afford cross-linked networks. The cross-link density of the PEO-based materials was varied by using PMDI (average NCO functionality of 3.2, 0.75 NCO groups per OH group) as an alternate cross-linker. The NCO:OH ratio was chosen in order to maintain consistency between this study and our previous study.[33] To directly compare these materials with PLA-based polymers, we prepared hydroxyl-terminated, star-shaped PLA prepolymers with M_n of 1.0, 3.8, and 10 kg mol^{-1} and cross-linked them under the same conditions as those used for the PEO prepolymers (**Figure 5.2**). Some PEO-based samples

were swelled in methanol (MeOH) after curing to study the effect of alcohol treatment on stress relaxation. Similarly, a control PEO-based sample was prepared without catalyst.

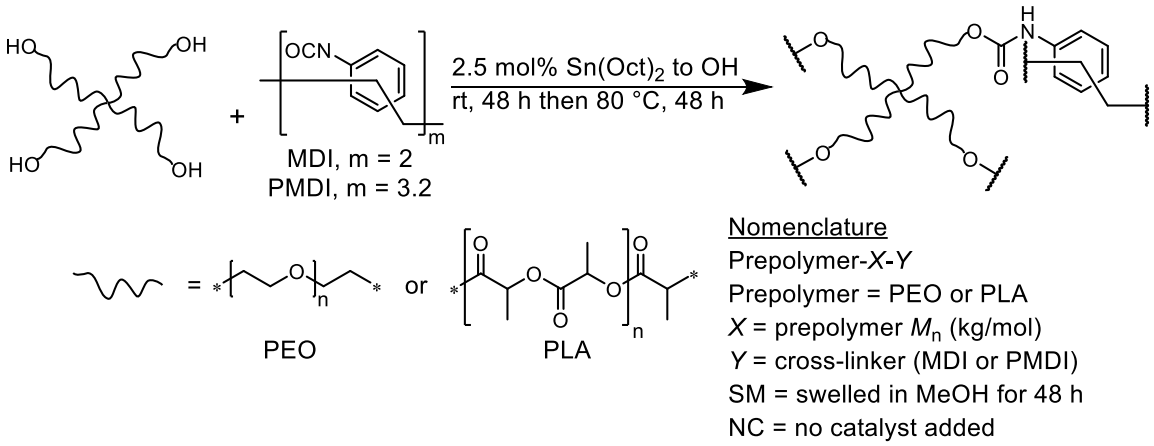

Figure 5.2. Synthesis of urethane cross-linked PEOs and PLAs. The bracketed representation for MDI and PMDI is used to show that PMDI is a mixture of regioisomers and oligomers with an average functionality of 3.2 isocyanate groups, or an average M_n ~ 400 g/mol.

DMTA of the PEO-based materials exhibited a plateau modulus of 3.7 MPa for the MDI-based materials and a modulus of 6.6 MPa for those prepared with PMDI, indicating that the higher isocyanate functionality of PMDI increased the cross-link density as expected (**Figure 5.3** and **Table 5.1**). During the DMTA experiment, an increase in the modulus of the materials with catalyst was observed above 150 °C. After cooling the samples back to room temperature, we subjected them to a second DMTA experiment and found that the plateau moduli had increased slightly (**Figure 5.4**). These increases in the moduli are likely the outcome of further cross-linking at ≥ 150 °C. By comparison with the DMTA data for materials without catalyst and those swollen in MeOH, it is apparent that the presence of catalyst was necessary to observe further cross-linking at high temperature. Varying the M_n of the PLA prepolymer affected the plateau modulus as expected: higher M_n prepolymers yielded less densely cross-linked materials and thus lower plateau moduli.

We attributed the similar plateau moduli of PLA-3.8-MDI and PLA-10-MDI to the presence of trapped entanglements, which became more prevalent as the prepolymer M_n was increased (**Figure 5.3** and **Table 5.1**); the molar mass between entanglements (M_e) for PLA is 4 kg mol^{-1} and the critical molar mass (M_c) at which entanglements are experimentally observed for PLA is 9 kg mol^{-1},[48] which is consistent with the M_x of 8.9 kg mol^{-1} determined for these samples.

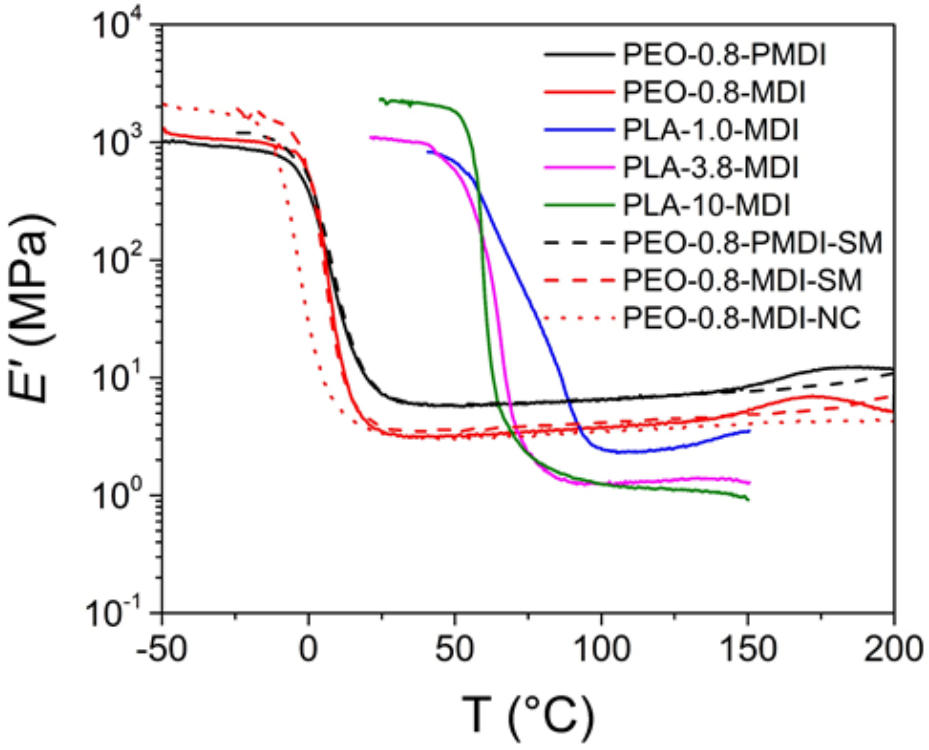

Figure 5.3. DMTA of urethane cross-linked PEO and PLA samples; the dashed lines are for samples after being soaked in methanol (SM) and dried under vacuum, whereas the dotted line is for the control sample with no catalyst (NC). The analysis was run at 1 Hz with an oscillation strain of 0.05%. PLA samples were tested below 150 °C to avoid thermal decomposition and higher initial temperatures to avoid transducer overload in the glassy regime.

Table 5.1. Mechanical and thermal data of urethane cross-linked PEOs and PLAs.

Sample[a]	Gel %[b]	E' (MPa)[c]	$v_e \times 10^4$ (mol mL^{-1})[d]	M_x (kg mol^{-1})[d]	T_g (°C)[e]	T_g (°C)[f]	$T_{d,5\%}$ (°C)[g]	E_a (kJ mol^{-1})[h]	T_v (°C)[i]
PEO-0.8-PMDI	99	6.6	7.1	1.6	3	1	303	142 ± 11	83
PEO-0.8-MDI	100	3.7	4.0	2.8	-1	-3	294	139 ± 5	76
PLA-1-MDI	99	2.4	2.6	4.8	63	55	189	155 ± 5	67
PLA-3.8-MDI	99	1.3	1.4	8.9	54	55	188	153 ± 3	56
PLA-10-MDI	99	1.3	1.4	8.9	53	53	202	165 ± 3	59
PEO-0.8-PMDI-SM	100	6.6	7.1	1.6	0	-1	299	127 ± 31	108
PEO-0.8-MDI-SM	100	4.2	4.5	2.5	0	-4	293	87 ± 27	81
PEO-0.8-MDI-NC	95	3.5	3.8	3	-10	-14	309	102 ± 37	91

[a]Samples are named as prepolymer type-molar mass (kg mol^{-1})-cross-linker used. SM denotes the samples swelled in methanol, and NC denotes the sample made without catalyst. [b]Determined as the ratio of the dry mass after a swell test to the mass before the swell test multiplied by 100. [c]Determined at 100 °C. [d]Determined using equation 1. [e]Defined as the temperature where the maximum of the loss modulus (E'') occurs in DMTA. [f]Measured by DSC after erasing the thermal history at 150 °C for 1 min, cooling to –80 °C, and back to 150 °C at a rate 10 °C min^{-1}. [g]Determined by heating from 20 °C to 550 °C under air at 10 °C min^{-1}. [h]Determined from the Arrhenius fit from SRA (equation 2). Standard error as determined by Origin® software is shown with these values. [i]Determined by extrapolating the Arrhenius fit from SRA to τ_v^* for each individual sample, which is determined using equation 3.

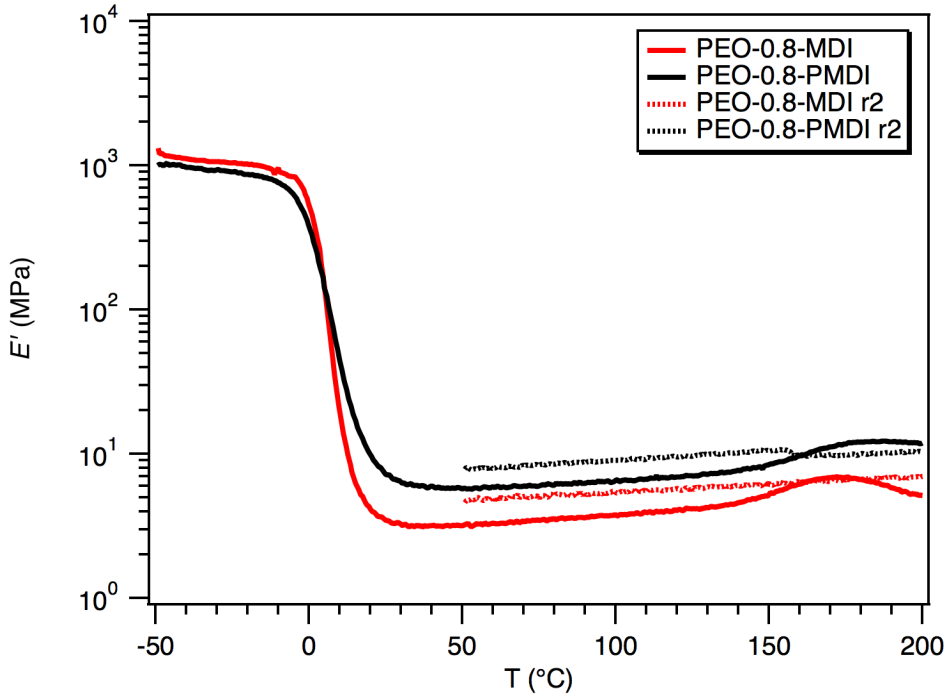

Figure 5.4. Multiple DMTA experiments of PEO-based samples containing 2.5 mol % $Sn(Oct)_2$. An increase in storage modulus is observed above 150 ºC during the first heating (solid lines); this increased modulus is present during the second heating (dashed lines), suggesting that irreversible cross-linking occurs in the presence of catalyst during the first heating.

SRA of the PEO-based materials revealed stress relaxation similar to PLA-based materials (**Figure 5.5A**), suggesting that urethanes—not esters—are the dominant functional groups contributing to stress relaxation. These findings are further consistent with the remarkably slow stress relaxation observed for an aliphatic polyester network containing $Sn(Oct)_2$ but no urethanes (epoxide cross-linked poly(4-methylcaprolactone), **Figure 5.6**). Furthermore, the lack of significant transesterification observed in poly(4-methylcaprolactone) and PLA-based materials is in agreement with a recently reported model compound study using $Sn(Oct)_2$; transesterification between benzyl alcohol and a β-lactone was rapid at 120 °C, but no linear transesterification with the resultant products was observed after 24 hours.[42]

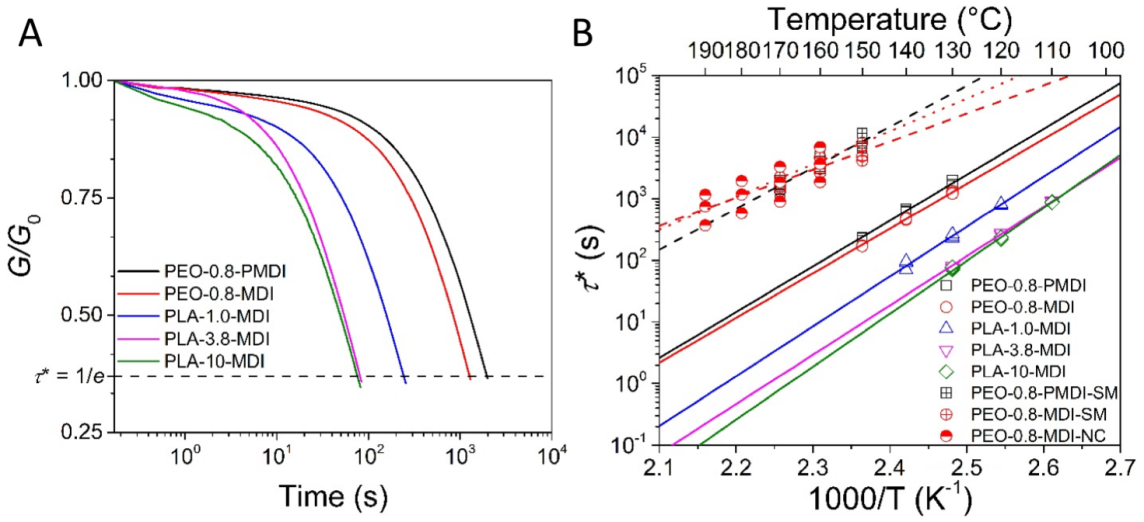

Figure 5.5. A) SRA for PEO- and PLA-based materials at 130 °C and 5% strain; the experiments were stopped once the sample reached 1/*e* (37%) of the initial stress relaxation modulus (G_0). **B)** Arrhenius analyses of the characteristic relaxation times for each sample; three experiments at each temperature are plotted. Dashed lines are for samples that were swelled in MeOH and the dotted line is for the sample prepared with no catalyst.

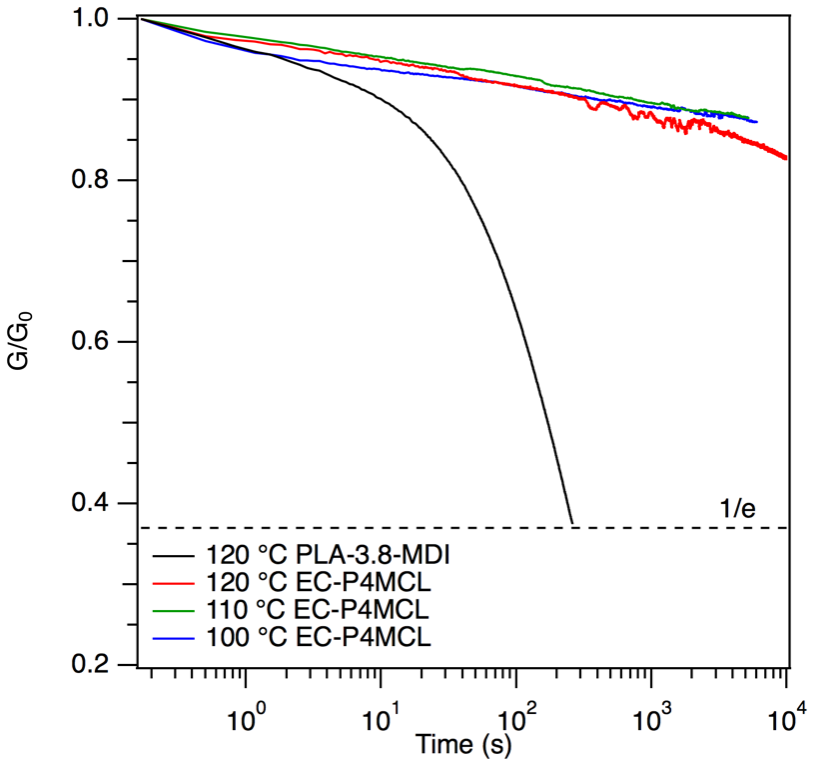

Figure 5.6. Stress relaxation analyses of epoxide cross-linked poly(4-methylcaprolactone) (EC-P4MCL) containing $Sn(Oct)_2$ at three separate temperatures, as compared to the stress-relaxation of urethane cross-linked PLA at 120 °C.

The characteristic relaxation times (τ^*) for PEO and PLA-based materials at various temperatures were fitted to an Arrhenius model (equation 2), from which an E_a of stress relaxation was extracted (**Figure 5.5B** and **Table 5.1**). The E_a did not vary significantly between the PEO- and PLA-based materials containing $Sn(Oct)_2$ (the range was 139–165 kJ mol^{-1}, consistent with our previous work), providing further evidence that the urethane functionality dominates the stress relaxation behavior in all cases. FT-IR spectra of all materials before and after SRA are indistinguishable from one another, indicating that the functional groups in the networks are stable at the elevated temperatures employed in this study (**Figure 5.7**, **Figure 5.8**, and **Figure 5.9**). Explicitly, we see no formation of common by-products seen in polyurethanes, such as allophanates, ureas, biurets, and isocyanurates.

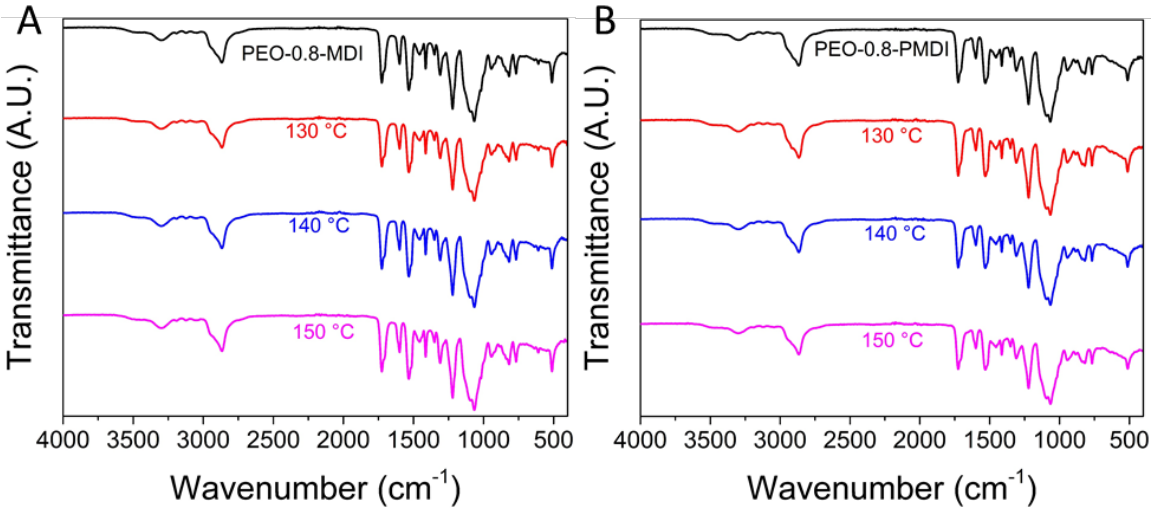

Figure 5.7. FT-IR spectra before and after stress relaxation analysis (SRA) at various temperatures on **A)** PEO-0.8-MDI and **B)** PEO-0.8-PMDI.

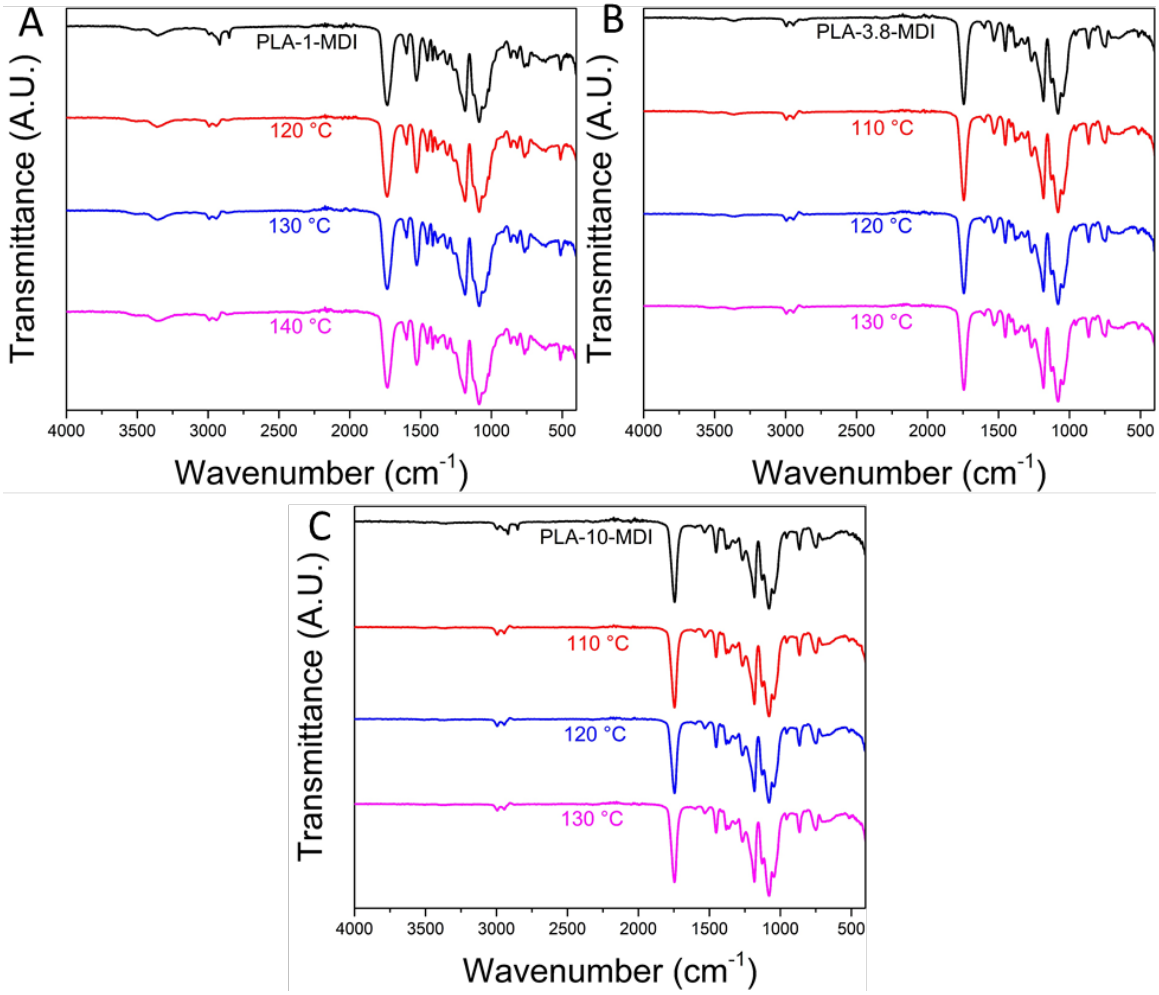

Figure 5.8. FT-IR spectra before and after stress relaxation analysis (SRA) at various temperatures on **A)** PLA-1.0-MDI **B)** PLA-3.8-MDI, and **C)** PLA-10-MDI.

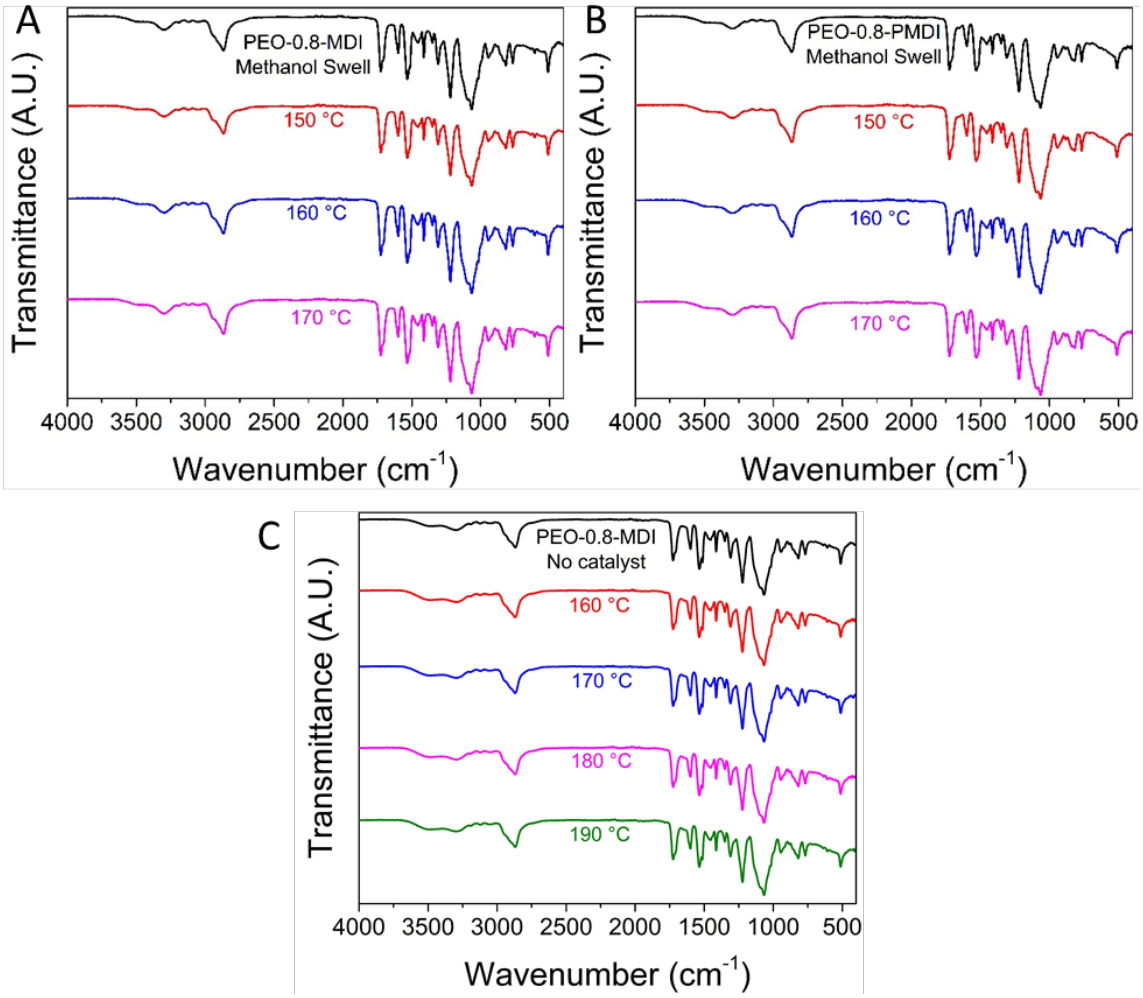

Figure 5.9. FT-IR spectra before and after stress relaxation analysis (SRA) at various temperatures on **A)** PEO-0.8-MDI-SM, **B)** PEO-0.8-PMDI-SM, and **C)** PEO-0.8-MDI-NC.

While the E_a values were similar across all polymers studied, the rates of relaxation differed significantly depending on the structure of the networks. Relaxation rates increased dramatically with decreasing plateau modulus (**Figure 5.10A**), which is consistent with previous studies performed on polyester vitrimers.[49] Based on stoichiometry, PEO-0.8-PMDI and PEO-0.8-MDI have nearly identical residual hydroxyl group concentrations ($[OH]_{res}$); however, the slower stress relaxation behavior of PEO-0.8-PMDI suggested that the modulus influenced the relaxation rate more strongly than the

$[OH]_{res}$ (**Figure 5.10**). Likewise, PLA-3.8-MDI and PLA-10-MDI had similar plateau moduli and vastly different $[OH]_{res}$ values, yet their rates of stress relaxation were essentially identical (**Figure 5.10**). Although it is difficult to completely decouple the influence of E' and $[OH]_{res}$ on the stress relaxation rate, it is apparent that across all samples—both in this work and our previous study—the modulus has a stronger influence on the relaxation rate than the residual hydroxyl concentration.[33] Furthermore, samples with a lower plateau modulus had a lower urethane concentration. We speculate that relaxation is more rapid at lower cross-link density due to the increased ability for reactive groups to diffuse within the network; in addition, each urethane reversion has a proportionally greater effect on the reduction of overall cross-link density for networks with lower cross-link density as compared to those with higher cross-link density.

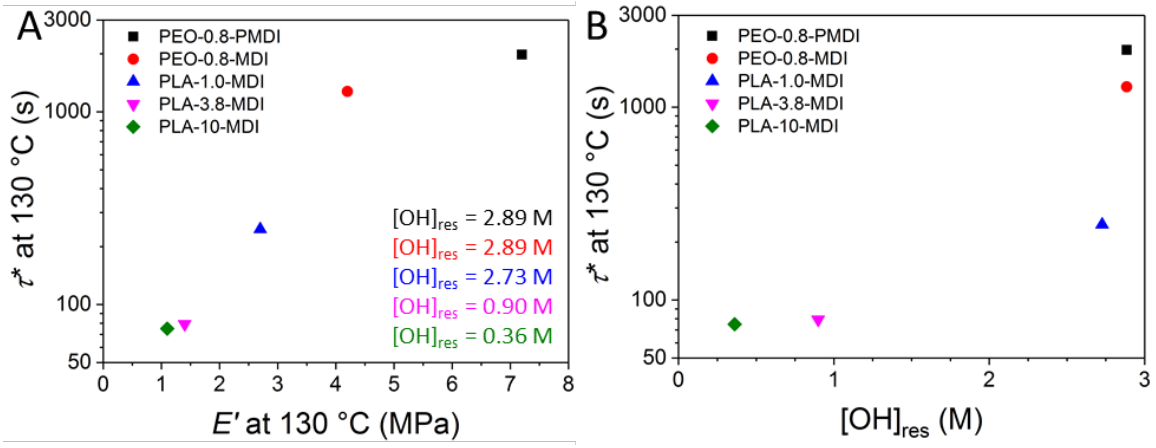

Figure 5.10. Plots of characteristic relaxation time (τ^*) at 130 °C as a function of **A)** storage modulus (E') at 130 °C and **B)** $[OH]_{res}$, which was estimated from the cross-linking reaction stoichiometry. The values of $[OH]_{res}$ are also shown in **A)** using the color that corresponds to each material.

In our previous studies with PLA-based materials, we found that urethane-based stress relaxation occurred more rapidly in the presence of $Sn(Oct)_2$;[33] however, we did not determine an E_a for stress relaxation in the absence of $Sn(Oct)_2$. Therefore, we investigated

the stress relaxation of PEO-based materials prepared without catalyst as well as catalyst-containing materials that had been swelled in MeOH. The rate of relaxation was approximately 30 times slower in the absence of $Sn(Oct)_2$ (**Figure 5.5B**, dotted line), indicating that the presence of tin greatly facilitates stress relaxation. We observed similar slow relaxation behavior in the samples swelled in MeOH (PEO-0.8-MDI-SM and PEO-0.8-PMDI-SM, **Figure 5.5B**, dashed lines). Although we initially hypothesized that MeOH treatment would completely remove the catalyst, the Sn contents of samples pre- and post-swelling were evaluated by ICP-MS and determined to be between 0.4 and 1 wt%, which indicated that Sn was not effectively removed by swelling the samples in MeOH. The Sn content of a sample prepared without catalyst was negligible (< 1 ppm). Therefore, the ICP-MS and SRA results suggest that swelling in excess MeOH possibly deactivates the $Sn(Oct)_2$ catalyst towards urethane exchange rather than removing it. However, the origin of slowed stress relaxation after the MeOH treatment remains an open question. For the MeOH-treated and catalyst-free samples, the τ^* values increased significantly after each successive run at a given temperature, resulting in large errors for the calculated activation energies. There were no evident changes in the FT-IR spectra before and after SRA for these samples as well as no significant mass loss observed before 290 °C (**Figure 5.9** and **Figure 5.11**). However, SRA resulted in discoloration of the samples, and we suspect that the inconsistent stress relaxation behavior between successive runs was at least partially due to decomposition of the reactive functionalities or formation of additional non-dynamic cross-links. The multiple processes contributing to stress relaxation in the absence of active tin species convolute the comparison of the measured activation energies between MeOH-treated and catalyst-free samples and those with $Sn(Oct)_2$ present.

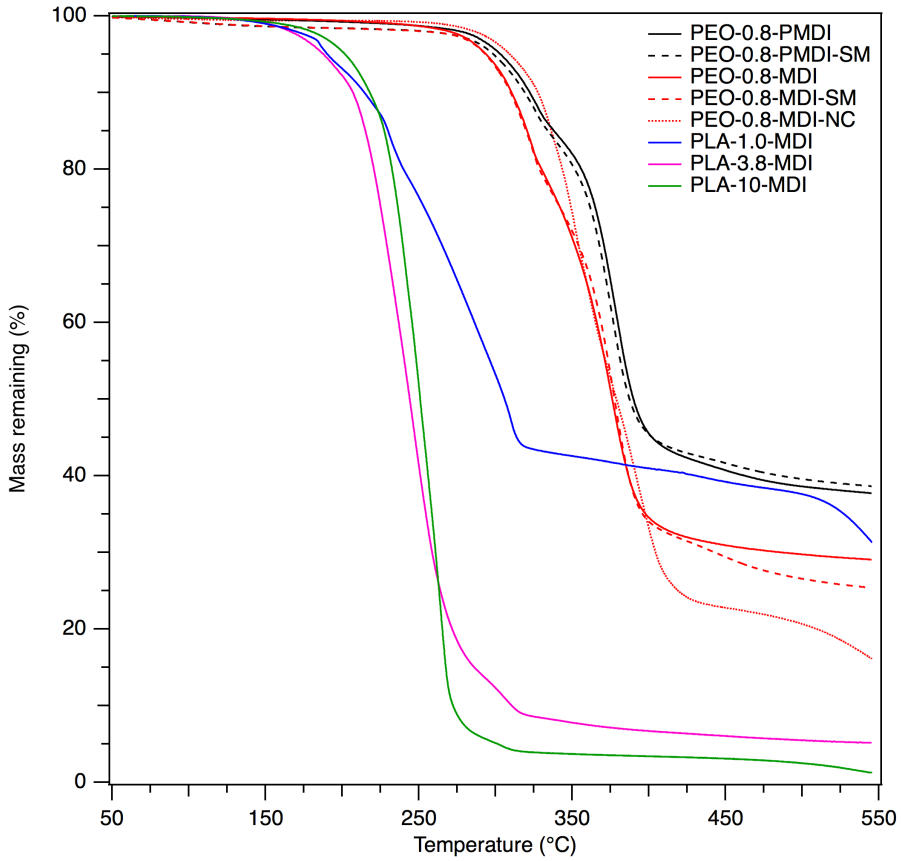

Figure 5.11. TGA traces of the polymer networks used in this study.

To further understand the exchange reactions of urethanes and the effects of hydroxyl groups on these processes, we studied the behavior of urethane-containing model compounds at elevated temperature. In the presence of excess 1-decanol and $Sn(Oct)_2$ (2.5 mol% with respect to urethane) at 150 °C, *N*-phenyl-*O*-octyl urethane reacts to yield the *O*-decyl urethane at a much slower rate compared to the timescale of the stress relaxation (**Figure 5.12A**). We therefore analyzed the reaction between two discrete urethanes in the absence of exogenous alcohol (**Figure 5.12B**). Under these conditions, the formation of crossover products is observed more quickly and at timescales more similar to stress relaxation, suggesting that urethane reversion—not alcohol-induced associative

exchange—is the dominant exchange mechanism (**Figure 5.12B**). Furthermore, when two discrete urethanes are heated in the presence of exogenous alcohol, only exchange with the free alcohol was observed (at a similar rate to urethane-hydroxyl exchange) (**Figure 5.13A**). These results indicate that excess free alcohols trap the isocyanate intermediates that would otherwise enable urethane-urethane exchange. However, the free alcohols also slow the rate of exchange by coordinating to the Sn atoms, thereby attenuating their ability to catalyze urethane exchange. Decreasing the concentration of free alcohol in this model exchange reactions leads to a recovery of the reactivity, consistent with this interpretation (**Figure 5.14**). These findings are consistent with the slower stress relaxation observed for the MeOH-treated samples—although Sn atoms are still present, the rates of relaxation are similar to the catalyst-free material.

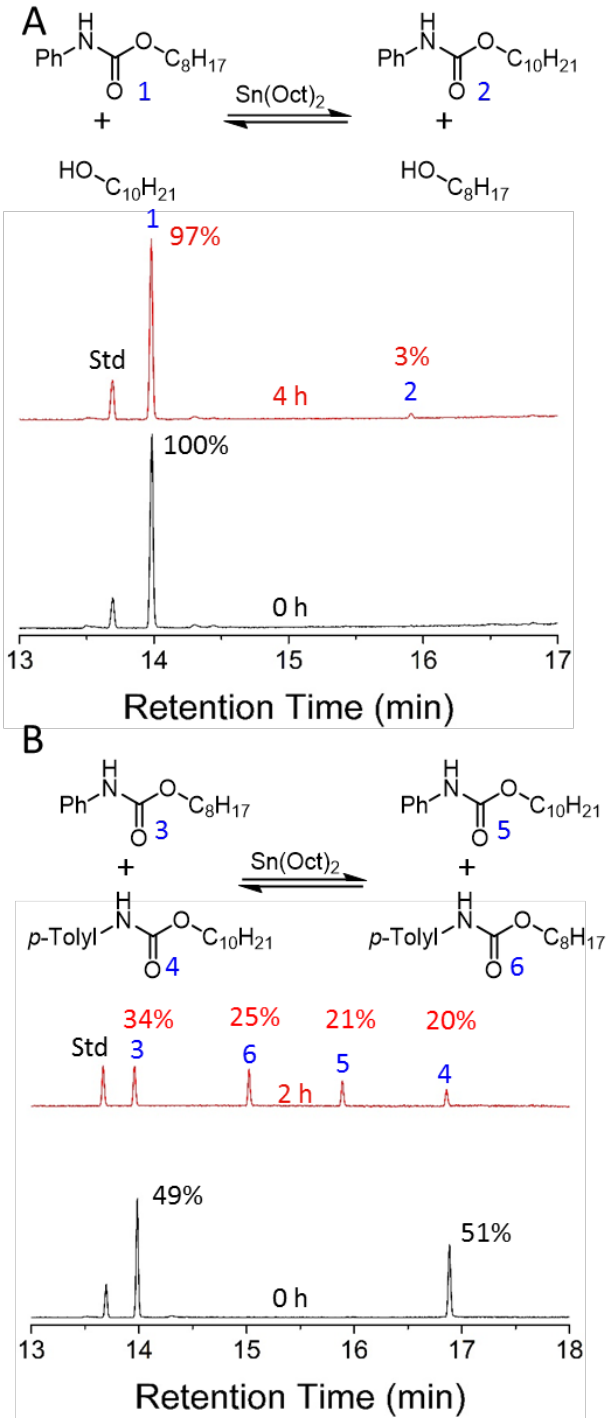

Figure 5.12. GC-MS of model compound studies. **A)** Urethane-hydroxyl exchange conducted at 150 °C for 4 h (10 OH groups per urethane) and **B)** Urethane-urethane exchange performed at 150 °C for 2 h (equimolar in both urethanes). Peak intensities are normalized to triphenylmethane (retention time = 13.7 min). Relative area percentages of each compound are shown and while qualitatively significant, compound degradation on the GC column prevented quantitative determination.

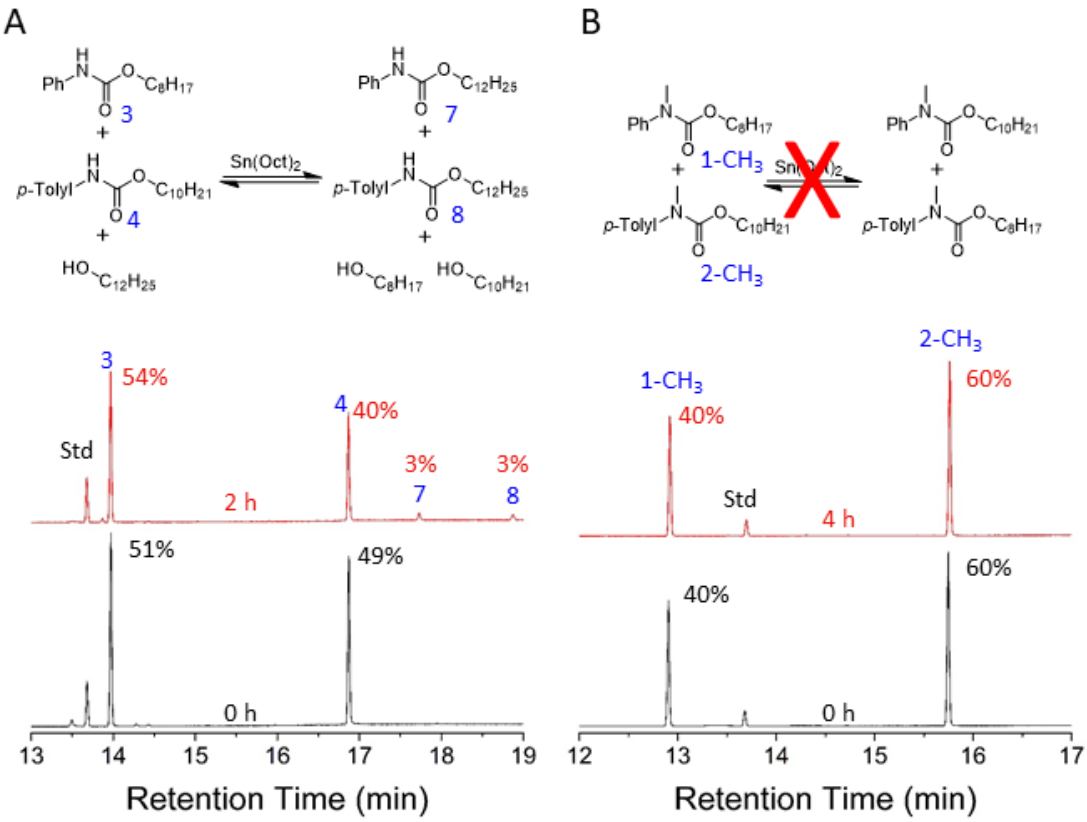

Figure 5.13. Model compound studies. **A)** Urethane-urethane-hydroxyl exchange performed for 2 h at 150 °C (equimolar –OH to both urethanes) and **B)** urethane-urethane exchange with *N*-methylated urethanes conducted at 150 °C for 4 h (equimolar in both urethanes). Peak intensities are normalized to triphenylmethane (retention time = 13.7 min). Relative percentages of each compound are shown and while qualitatively significant, compound degradation on the GC column (>270 °C) prevented a quantitative determination of the product distributions; the degradation temperature of *N*-aryl-*O*-alkyl urethanes are typically around 200 °C.[50,51]

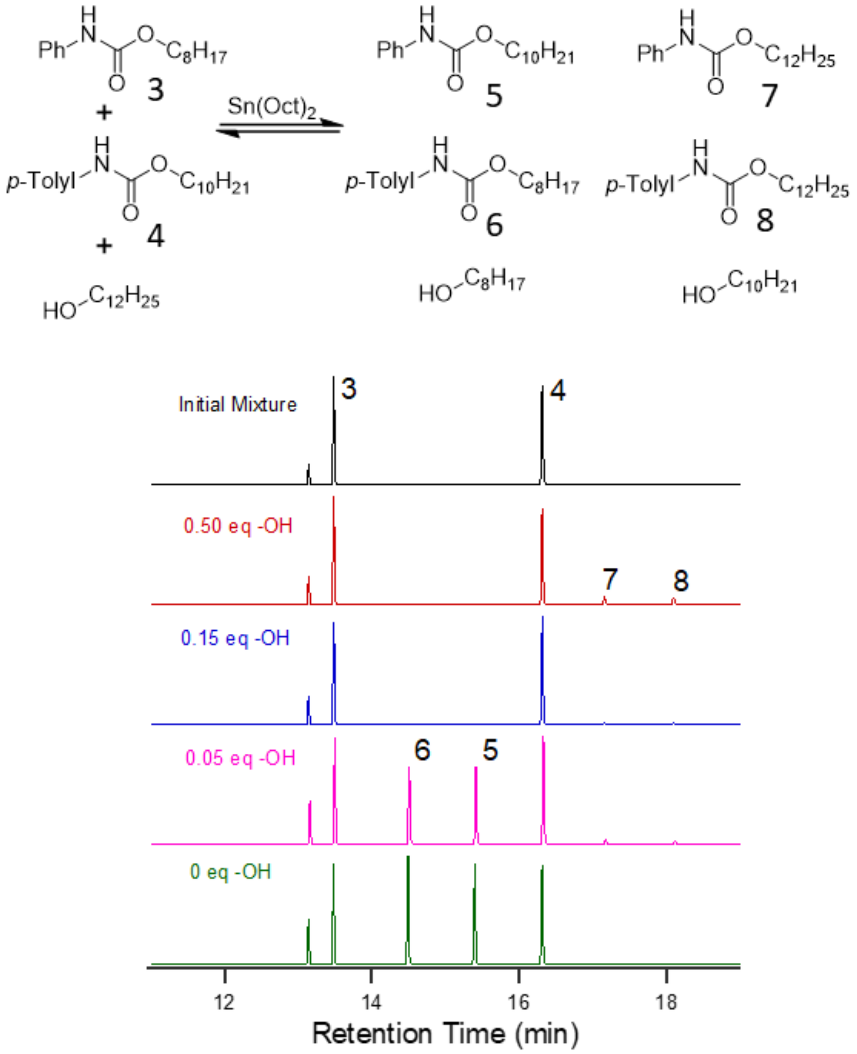

Figure 5.14. Urethane-urethane exchange in the presence of different amounts of additional free alcohol, performed with 2.5 mol% $Sn(Oct)_2$ to total urethane at 150 ºC for 2 h. Large concentrations of dodecanol (0.50 and 0.15 equivalents) inhibit urethane-urethane exchange, and only small amounts of products 7 and 8 are observed. With low concentrations of free dodecanol (0.05 eq), significant urethane-urethane exchange is observed to generate products 5 and 6.

A urethane-urethane crossover experiment was also conducted on analogous *N*-methylated urethanes to explore the possibility of a distinct metathesis mechanism (**Figure 5.13B**), as *N,N*-disubstituted urethanes are incapable of reversion.[26,52] Neither exchange products nor byproducts were observed, again supporting a dissociative, urethane exchange

mechanism in the non-methylated urethanes. Unfortunately, the GC-MS results for all model studies were not amenable to quantitative reaction rate determination due to partial decomposition on the GC column (see **Figure 5.13** for more information). Attempts to use ^{1}H NMR spectroscopy as an alternative method to quantitatively determine the rate of reaction of a free alcohol with a model urethane were complicated by side reactions (**Figure 5.15**).

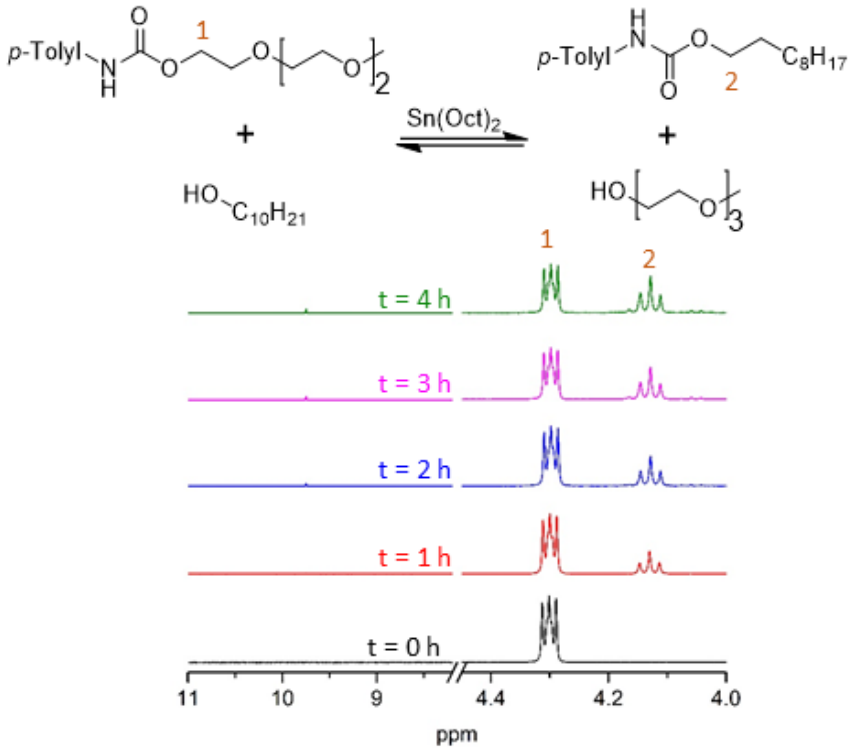

Figure 5.15. ^{1}H NMR spectra of the neat reaction between *N*-tolyl-*O*-(triethyleneglycol monomethyl ether) urethane and decanol at 180 °C. The reaction was allowed to proceed for the specified amount of time and then an aliquot was removed for analysis. The reaction progress was monitored by the protons of the *O*-methylene unit, whose peaks are shown above. Each spectrum was normalized to an external standard, 1,3,5-tribromobenzene. The signals from an undesired byproduct overlapped with peak 2 and compromised the determination of an E_a for this reaction by skewing the amount of product towards higher values. This byproduct is not consistent with typical side reactions that occur with urethanes, as the ^{1}H NMR spectrum does not indicate the formation of ureas and allophanates/biurets, whose *N*-aryl N-H peaks usually appear at ~8.5 and ~10.9 ppm in $CDCl_3$, respectively.[53,54,55]

Although it appeared that a urethane reversion pathway was operative in these systems, this mechanism was inconsistent with the insolubility of these networks in TCB at 140 °C.[33] Other reprocessable cross-linked polymers based on reversible reactions, such as Diels-Alder cycloadditions, are capable of full dissolution at elevated temperatures.[9] Therefore, we posited that the low polarity of TCB was not appropriate for dissolving the polymers, but that a polar aprotic solvent such as DMSO could favor dissolution. Indeed, all three variations of PEO-0.8-MDI as well as PLA-1.0-MDI were insoluble in TCB but dissolved fully in anhydrous DMSO at elevated temperature (**Figure 5.16** and **Figure 5.17**). Model urethane-urethane exchange studies performed with addition of DMSO and TCB show very similar reactivity, suggesting that the samples dissolve in DMSO due to the increased swellability or solubility of the samples in DMSO, rather than a significant difference in the reactivity of the urethane functional groups (**Figure 5.18**). The samples swelled in TCB were dried under vacuum and analyzed using FT-IR spectroscopy. While there were some minor detectable differences, no significant change in the carbonyl resonances were observed despite substantial discoloration (**Figure 5.19**). In contrast to our expectations based on rates of stress relaxation, the samples treated with MeOH dissolved in DMSO significantly faster (24 h) than samples with (36 h) and without catalyst (48 h to be mostly dissolved, 96 h for complete dissolution). We hypothesize that the additional alcohols in the MeOH-treated samples result in a net loss of cross-links during the swelling experiment.

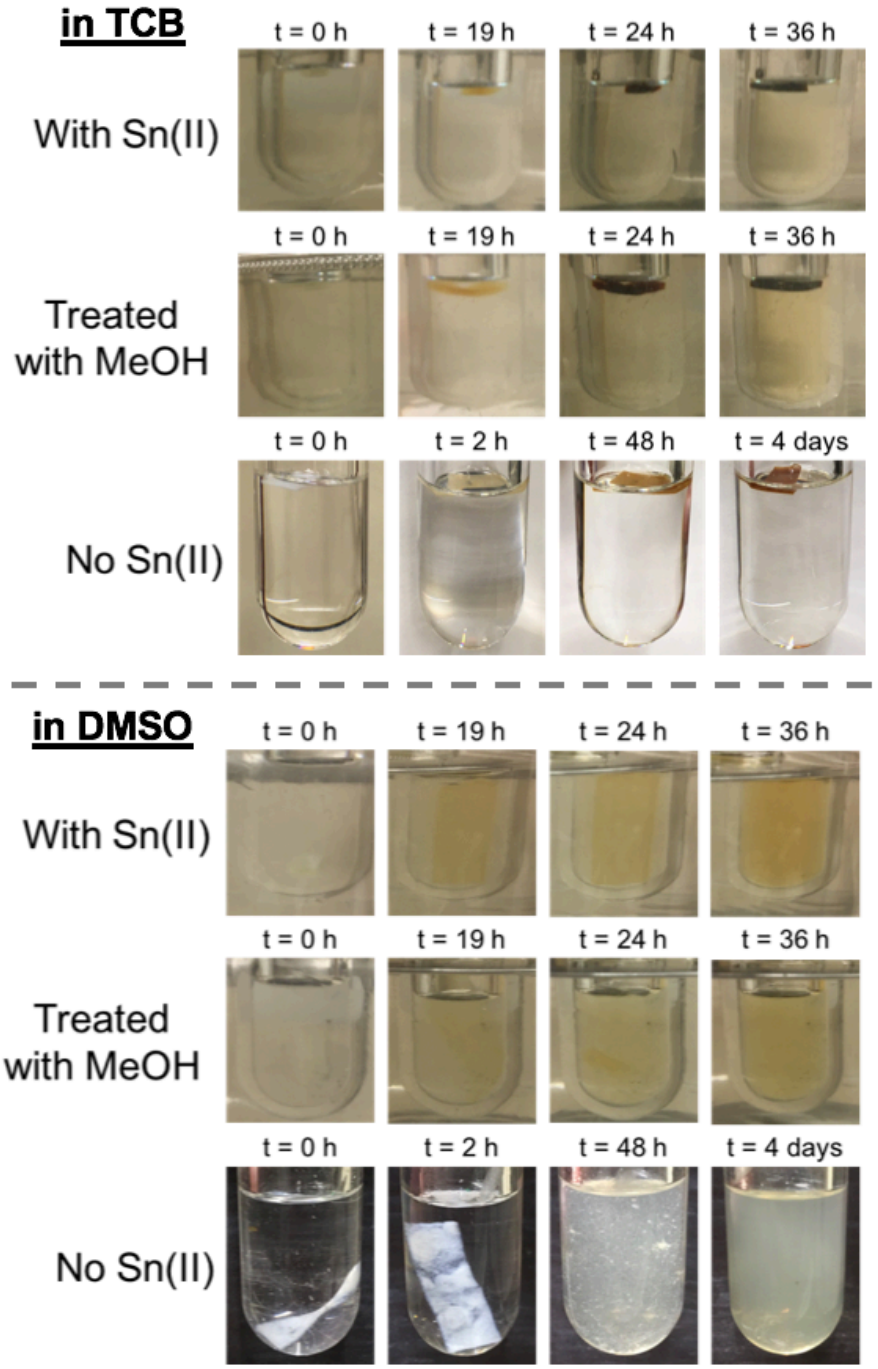

Figure 5.16. High temperature (140 °C) dissolution studies with PEO-0.8-MDI, PEO-0.8-MDI-SM, or PEO-0.8-MDI-NC in anhydrous DMSO and TCB. Samples are denser than DMSO, though less dense than TCB, explaining the difference in location in the pressure vessels. Eventually, the samples discolor, making them easier to visualize in the solvent. Both samples with Sn(II) are completely dissolved within 36 h for DMSO; the sample without Sn(II) catalyst takes 4 days to fully dissolve. Meanwhile, the three materials swell in TCB but do not eventually dissolve, even after 7 days.

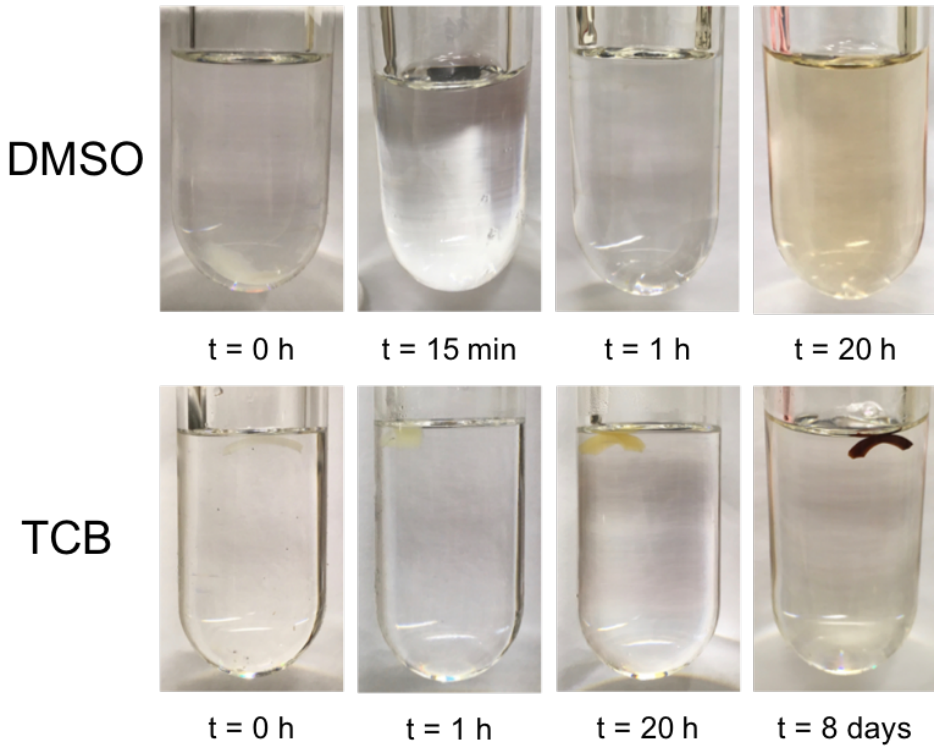

Figure 5.17. High temperature (140 °C) dissolution studies with PLA-1.0-MDI in anhydrous DMSO (top) and TCB (bottom). Samples are denser than DMSO, though less dense than TCB, explaining the difference in location in the pressure vessels. In DMSO, the sample turned clear and was still intact at 15 minutes, had fully dissolved after 1 hour, and the solution had discolored after 20 h. Meanwhile, the sample swelled and discolored in TCB but did not dissolve.

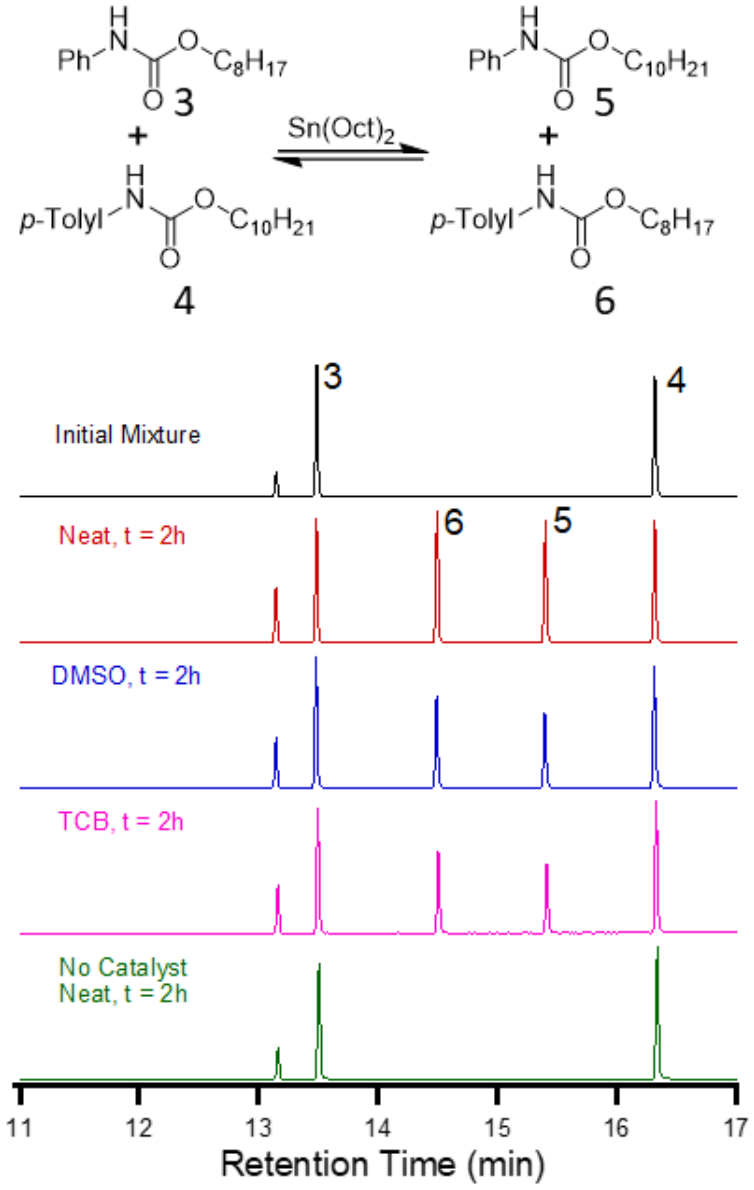

Figure 5.18. Urethane-urethane exchange in the presence of different solvents, performed with 2.5 mol% $Sn(Oct)_2$ to total urethane at 150 ºC for 2 hours. Similar results are obtained performing the reaction at a concentration of 1 M total urethane in both DMSO and TCB, suggesting that solvent does not significantly affect the urethane-urethane exchange. Omission of catalyst also prevents exchange.

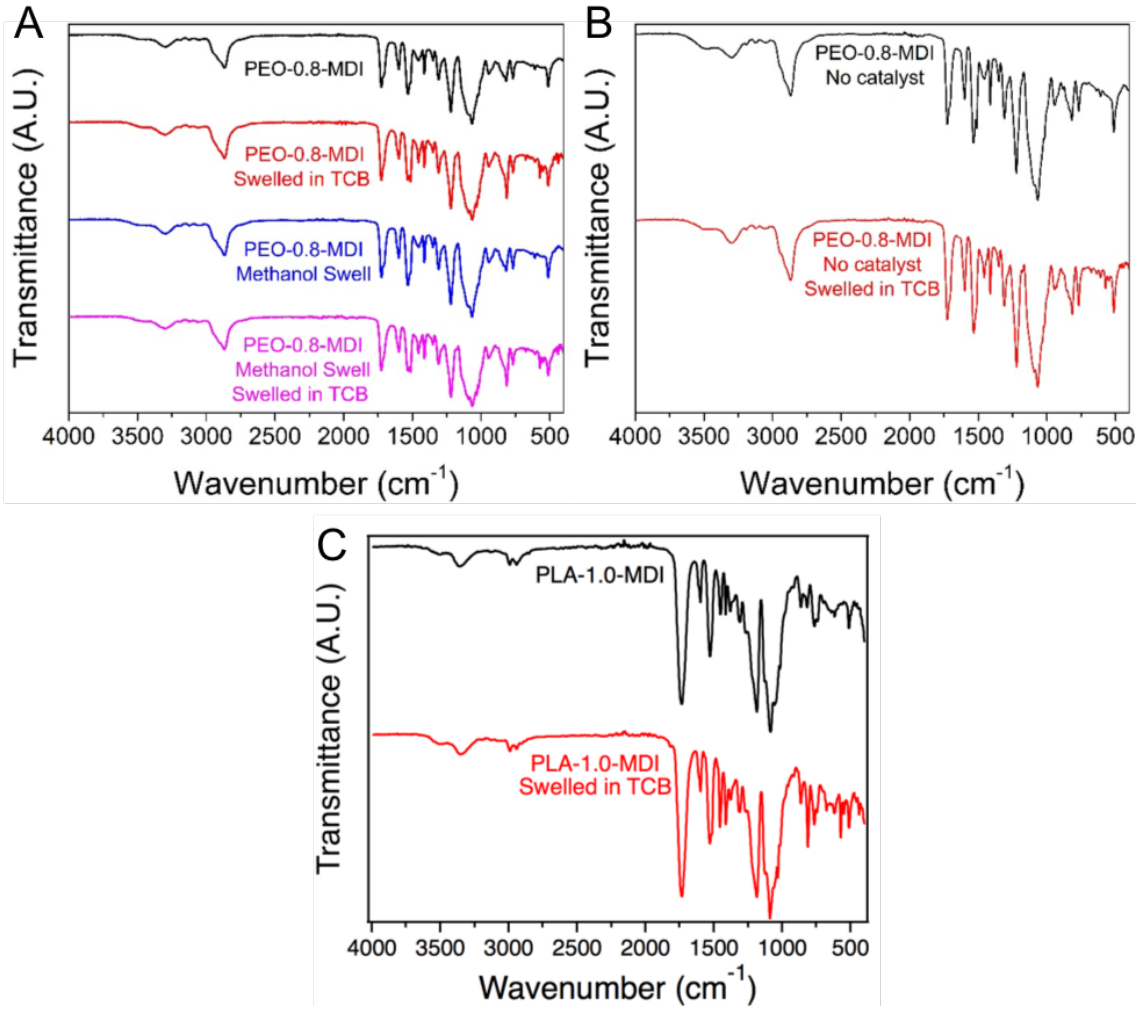

Figure 5.19. FT-IR spectra of urethane cross-linked samples before and after swelling in TCB for 7 or 8 days at 140 °C: **A)** PEO-based samples prepared with catalyst, **B)** PEO-based samples prepared without catalyst, and **C)** PLA-based sample prepared with catalyst. Swelled samples were dried for 48 h under vacuum (*ca.* 30 mTorr) before the spectra were obtained.

As DMSO was capable of completely dissolving the PEO-based samples, we sought to directly detect the formation of the isocyanate intermediates. We acquired a ^{13}C NMR spectrum of the diethyl urethane adduct of MDI in DMSO-d_6 at 25, 100, and 140 °C (**Figure 5.20**). No peaks were observed in the ^{13}C NMR spectrum that corresponded to the isocyanate, suggesting that the equilibrium was significantly shifted toward the urethane at

these temperatures. A ^{1}H NMR spectrum showed only an upfield shift of the N–H peak due to loss of hydrogen bonding (**Figure 5.21**), further indicating that the isocyanate concentration at these temperatures is below the detection limit of NMR spectroscopy. The fact that urethane is strongly favored at equilibrium is consistent with the Arrhenius-type dependence of stress relaxation, as the cross-links never dissociate to the degree required to cause a rapid drop in viscosity.

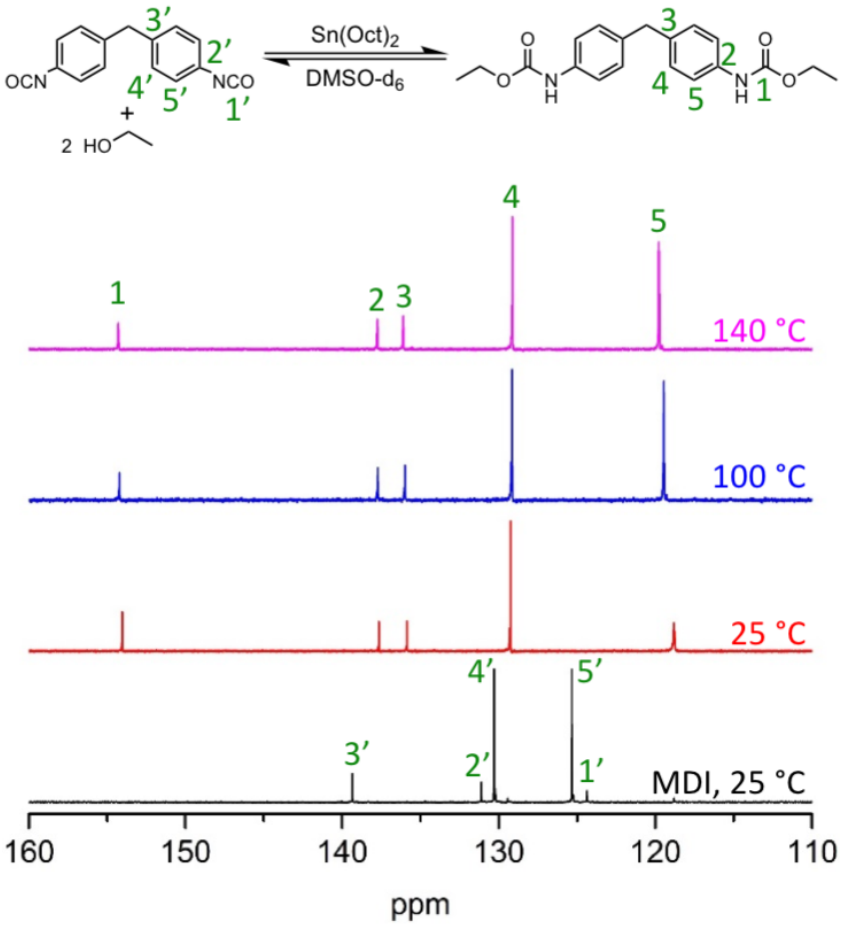

Figure 5.20. ^{13}C VT-NMR spectra (125 MHz, DMSO-d_6) of MDI and the diethyl urethane adduct of MDI; concentrations of approximately 100 mg mL^{-1} were used to achieve better signal to noise. The diethyl urethane solution was under N_2 atmosphere and contained $Sn(Oct)_2$ (2.5 mol% to urethanes); the solution was allowed to equilibrate at the desired temperature for 10 min before 128 scans were collected.

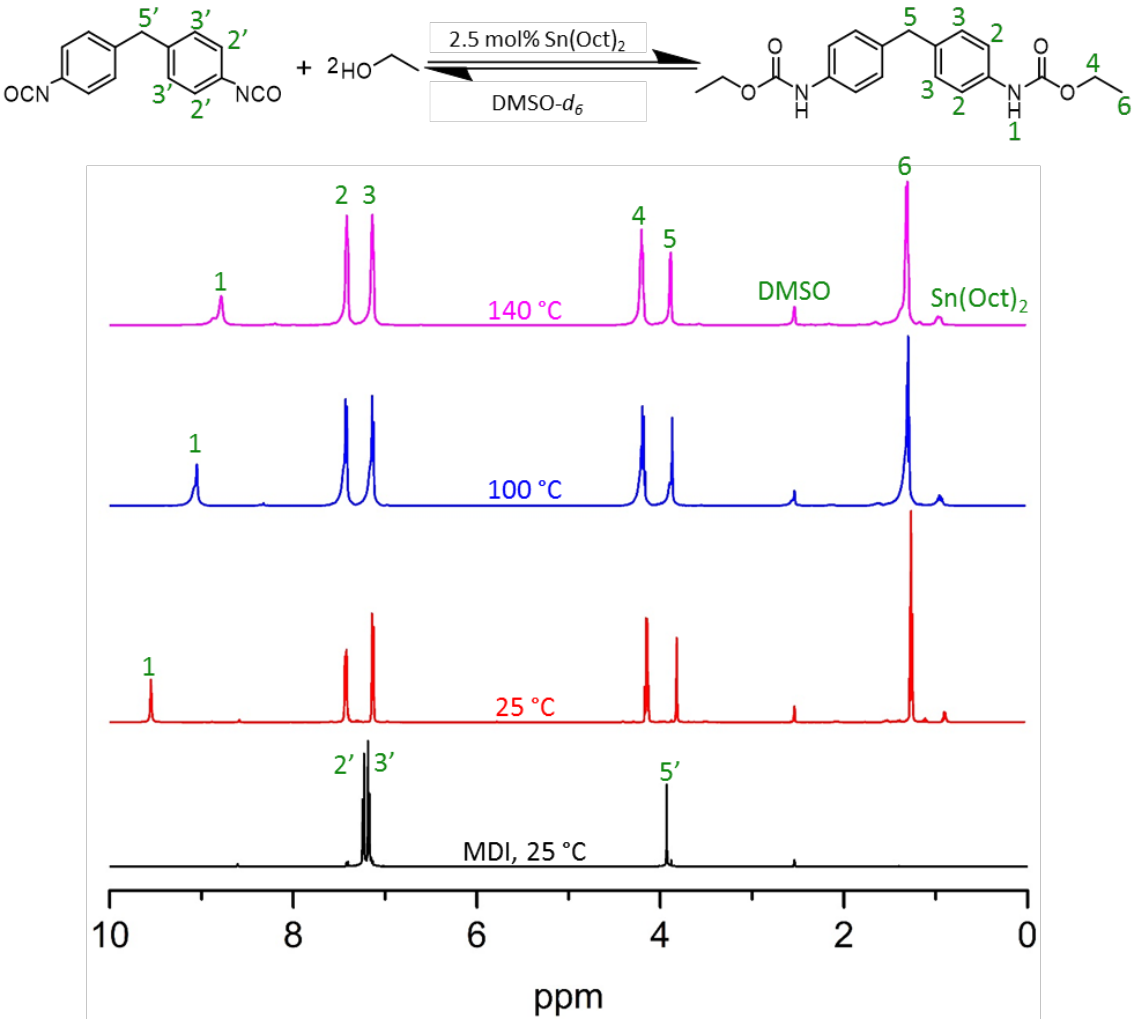

Figure 5.21. ^{1}H VT-NMR spectra (500 MHz, DMSO-d_6) of MDI and the diethyl urethane of MDI in. The same solutions from ^{13}C VT-NMR were utilized for this experiment (100 mg mL^{-1}). The diethyl urethane solution was under N_2 atmosphere and contained 2.5 mol% $Sn(Oct)_2$ to urethanes; the solution was allowed to equilibrate at the desired temperature for 10 min before 16 scans were collected.

We sought other evidence for a reversion mechanism by indirectly detecting isocyanate-derived species upon removal of alcohol. A mixture of the diethyl urethane adduct of MDI and $Sn(Oct)_2$ (2.5 mol% to urethane) was heated in a distillation apparatus to drive the formation of MDI by removal of ethanol. We found that no ethanol was recovered after 24 h at 140 °C or 150 °C; at 160 °C, however, some ethanol was recovered

(18% of the theoretical amount) and we observed an insoluble brown solid in the distillation pot. The FT-IR spectrum of the solid indicated the presence of isocyanurate moieties (1509, 1411, and 1171 cm^{-1}, **Figure 5.22**),[56] which is consistent with the formation of isocyanates followed by trimerization to isocyanurates during alcohol removal. This experiment confirmed that the isocyanate species was transient at temperatures relevant to stress relaxation (140-150 °C) and is consistent with a reversion-based mechanism.

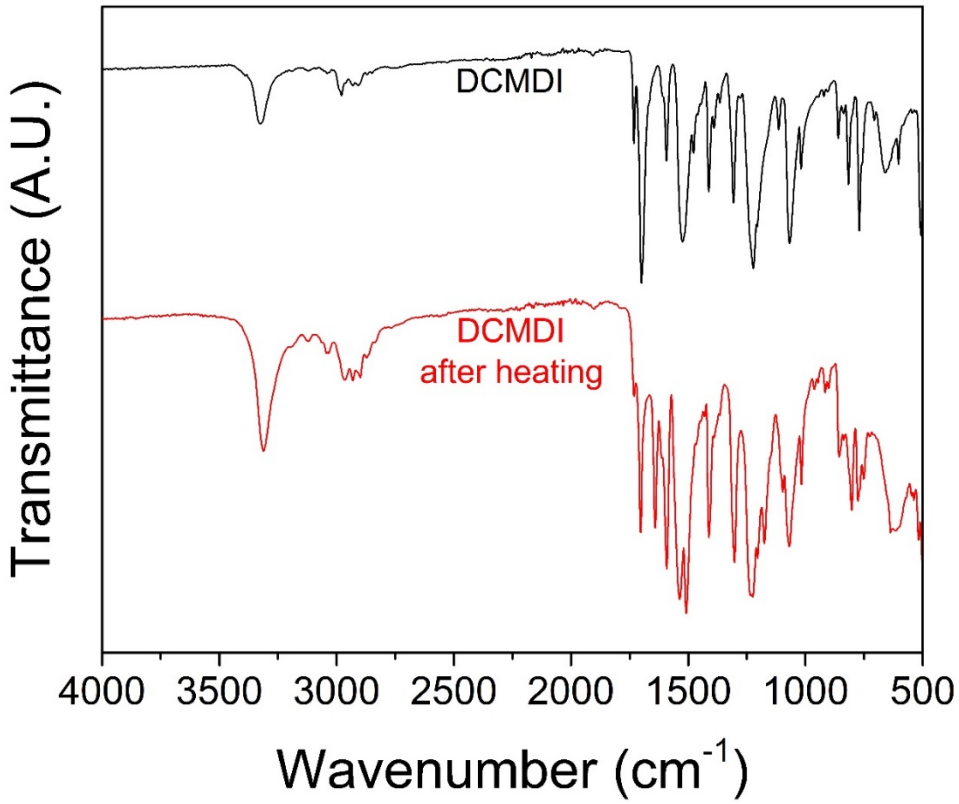

Figure 5.22. FT-IR spectra of the diethyl carbamate of methylene diphenyl diisocyanate (DCMDI) before and after heating at 140 °C for 24 h, then 150 °C for 24 h, and finally 160 °C for 24 h.

On the basis of SRA, model reactions, and literature precedent,[51,57] we propose two potential mechanisms of stress relaxation in these materials (**Figure 5.23**). In the presence of exogenous alcohol, the mechanism in **Figure 5.23A** would predominate. Low

conversion observed in the hydroxyl-urethane exchange model reactions (10 OH groups per urethane) and low relaxation rates in the MeOH-treated samples may arise from the coordination of the Sn(II) metal center by alcohols, inhibiting its ability to catalyze urethane reversion. However, rates would increase as the [OH] decreases, which is consistent with the fast urethane-urethane exchange observed in the absence of exogenous alcohol. Furthermore, because the $[OH]_{res}$ in the cross-linked materials is low, inhibition of the Sn(II) centers by excess alcohol is less likely to occur. Meanwhile, in the absence of exogenous alcohol, urethanes can more freely bind to the catalytic Sn(II) center, allowing for full reversion and subsequently, fast exchange (**Figure 5.23B**). This mechanism is consistent with previous observations of polyurethane stress relaxation both in the presence[37,38] and absence[35,36,40] of tin catalysts.

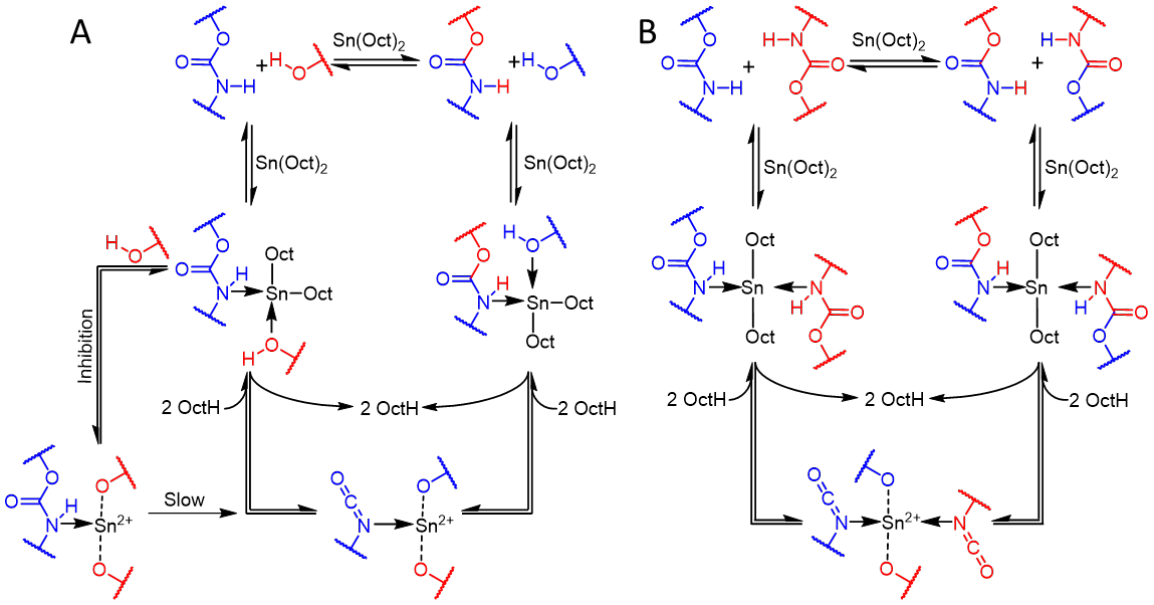

Figure 5.23. Proposed stress relaxation mechanisms of **A)** hydroxyl-urethane exchange (urethane reversion and reaction with a new hydroxyl) and **B)** urethane-urethane exchange (urethane reversion and recombination).

5.5. Conclusions

We demonstrate that PEO- and PLA-based networks with urethane cross-links are capable of stress relaxation at elevated temperature, likely by urethane reversion. The modulus of the materials is apparently the principal factor controlling the relaxation time, as samples with lower moduli relax more quickly. Although an increase in the concentration of residual hydroxyl moieties slightly lowers the E_a of stress relaxation, the $[OH]_{res}$ in these materials does not affect the overall rate of relaxation as significantly as the storage modulus, suggesting that reversion is the primary mechanism for urethane exchange. Urethane reversion is further supported by model compound studies, in which rapid urethane exchange is observed in the absence of free hydroxyl groups and only when the urethane contains an N-H as opposed to N-Me. Furthermore, the alcohol-based inhibition of $Sn(Oct)_2$ catalyst is apparent in samples treated with MeOH as well as model compound reactions performed in large excess of exogenous alcohol. While we were unable to observe the presence of isocyanates using NMR spectroscopy at elevated temperatures, generation of isocyanurate moieties after distillation of ethanol from the diethyl urethane adduct of MDI provides further evidence for the formation of isocyanate intermediates. These studies yield insight into the vitrimer-like behavior of polyurethane networks at elevated temperatures and suggest that further investigations of the reprocessability of commercially ubiquitous cross-linked polyurethanes will be a beneficial approach to their recycling.

5.6. References

[1] Wu, D. Y.; Meure, S.; Solomon, D. Self-healing Polymeric Materials: A Review of Recent Developments. *Prog. Polym. Sci.* **2008,** *33*, 479-522.

[2] Tyagi, P.; Deratani, A.; Quemener, D. Self-Healing Dynamic Polymeric Systems. *Isr. J. Chem.* **2013,** *53*, 53-60.

[3] Kloxin, C. J.; Bowman, C. N. Covalent Adaptable Networks: Smart, Reconfigurable and Responsive Network Systems. *Chem. Soc. Rev.* **2013,** *42*, 7161-7173.

[4] Wool, R. P. Self-healing Materials: A Review. *Soft Matter* **2008,** *4*, 400-418.

[5] Wojtecki, R. J.; Meador, M. A.; Rowan, S. J. Using the Dynamic Bond to Access Macroscopically Responsive Structurally Dynamic Polymers. *Nat. Mater.* **2011**, *10*, 14–27.

[6] Roy, N.; Bruchmann, B.; Lehn, J.-M. DYNAMERS: Dynamic Polymers as Self-healing Materials. *Chem. Soc. Rev.* **2015,** *44*, 3786-3807

[7] Chen, X.; Dam, M. A.; Ono, K.; Mal, A.; Shen, H.; Nutt, S. R.; Sheran, K.; Wudl, F. A Thermally Re-mendable Cross-Linked Polymeric Material. *Science* **2002,** *295*, 1698-1702.

[8] Chen, X.; Wudl, F.; Mal, A. K.; Shen, H.; Nutt, S. R. New Thermally Remendable Highly Cross-Linked Polymeric Materials. *Macromolecules* **2003,** *36*, 1802-1807.

[9] Zhang, Y.; Broekhuis, A. A.; Picchioni, F. Thermally Self-Healing Polymeric Materials: The Next Step to Recycling Thermoset Polymers? *Macromolecules* **2009,** *42*, 1906-1912

[10] Montarnal, D.; Capelot, M.; Tournilhac, F.; Leibler, L. Silica-Like Malleable Materials from Permanent Organic Networks. *Science* **2011,** *334*, 965-968.

[11] Imbernon, L.; Norvez, S. From Landfilling to Vitrimer Chemistry in Rubber Life Cycle. *Eur. Polym. J.* **2016,** *82*, 347-376.

[12] Denissen, W.; Winne, J. M.; Du Prez, F. E. Vitrimers: Permanent Organic Networks With Glass-like Fluidity. *Chem. Sci.* **2016,** *7*, 30-38.

[13] Capelot, M.; Montarnal, D.; Tournilhac, F.; Leibler, L. Metal-Catalyzed Transesterification for Healing and Assembling of Thermosets. *J. Am. Chem. Soc.* **2012,** *134*, 7664-7667.

[14] Capelot, M.; Unterlass, M. M.; Tournilhac, F.; Leibler, L. Catalytic Control of the Vitrimer Glass Transition. *ACS Macro Lett.* **2012,** *1*, 789-792.

[15] Lu, Y.-X.; Tournilhac, F.; Leibler, L.; Guan, Z. Making Insoluble Polymer Networks Malleable via Olefin Metathesis. *J. Am. Chem. Soc.* **2012,** *134*, 8424-8427.

[16] Lu, Y.-X.; Guan, Z. Olefin Metathesis for Effective Polymer Healing via Dynamic Exchange of Strong Carbon–Carbon Double Bonds. *J. Am. Chem. Soc.* **2012,** *134*, 14226-14231.

[17] Ying, H.; Zhang, Y.; Cheng, J. Dynamic Urea Bond for the Design of Reversible and Self-Healing Polymers. *Nat. Commun.* **2014**, *5*, 3218-3227.

[18] Zhang, Y.; Ying, H.; Hart, K. R.; Wu, Y.; Hsu, A. J.; Coppola, A. M.; Kim, T. A.; Yang, K.; Sottos, N. R.; White, S. R.; Cheng, J. Malleable and Recyclable Poly(urea-urethane) Thermosets Bearing Hindered Urea Bonds. *Adv. Mater.* **2016**, *28*, 7646–7651.

[19] Martin, R.; Rekondo, A.; Ruiz de Luzuriaga, A.; Cabanero, G.; Grande, H. J.; Odriozola, I. The Processability of a Poly(urea-urethane) Elastomer Reversibly Crosslinked With Aromatic Disulfide Bridges. *J. Mater. Chem. A* **2014,** *2*, 5710-5715.

[20] Rekondo, A.; Martin, R.; Ruiz de Luzuriaga, A.; Cabanero, G.; Grande, H. J.; Odriozola, I. Catalyst-free Room-temperature Self-healing Elastomers Based on Aromatic Disulfide Metathesis. *Mater. Horiz.* **2014,** *1*, 237-240.

[21] Xiang, H. P.; Qian, H. J.; Lu, Z. Y.; Rong, M. Z.; Zhang, M. Q. Crack Healing and Reclaiming of Vulcanized Rubber by Triggering the Rearrangement of Inherent Sulfur Crosslinked Networks. *Green Chem.* **2015**, *17*, 4315-4325.

[22] Xiang, H. P.; Rong, M. Z.; Zhang, M. Q. Self-healing, Reshaping, and Recycling of Vulcanized Chloroprene Rubber: A Case Study of Multitask Cyclic Utilization of Cross-linked Polymer. *ACS Sustainable Chem. Eng.* **2016,** *4*, 2715-2724.

[23] Pepels, M.; Filot, I.; Klumperman, B.; Goossens, H. Self-healing Systems Based on Disulfide-thiol Exchange Reactions. *Polym. Chem.* **2013,** *4*, 4955-4965.

[24] Denissen, W.; Rivero, G.; Nicolaÿ, R.; Leibler, L.; Winne, J. M.; Du Prez, F. E. Vinylogous Urethane Vitrimers. *Adv. Funct. Mater.* **2015,** *25*, 2451–2457.

[25] Denissen, W.; Droesbeke, M.; Renaud, N.; Leibler, L.; Winne, J. M.; Du Prez, F. Chemical Control of the Viscoelastic Properties of Vinylogous Urethane Vitrimers. *Nat. Commun.* **2017**, *8*, 14857.

[26] Fortman, D. J.; Brutman, J. P.; Cramer, C. J.; Hillmyer, M. A.; Dichtel, W. R. Mechanically Activated, Catalyst-Free Polyhydroxyurethane Vitrimers. *J. Am. Chem. Soc.* **2015,** *137*, 14019-14022.

[27] Fortman, D. J.; Brutman, J. P.; Hillmyer, M. A.; Dichtel, W. R. Structural Effects on the Reprocessability and Stress relaxation of Cross-linked Polyhydroxyurethanes. *J. Appl. Polym. Sci.* **2017**, *134*, 44984.

[28] Zheng, P.; McCarthy, T. J. A Surprise from 1954: Siloxane Equilibration Is a Simple, Robust, and Obvious Polymer Self-Healing Mechanism. *J. Am. Chem. Soc.* **2012,** *134*, 2024-2027.

[29] Schmolke, W.; Perner, N.; Seiffert, S. Dynamically Cross-Linked Polydimethylsiloxane Networks with Ambient-Temperature Self-Healing. *Macromolecules* **2015,** *48*, 8781-8788.

[30] Cash, J. J.; Kubo, T.; Bapat, A. P.; Sumerlin, B. S. Room-Temperature Self-Healing Polymers Based on Dynamic-Covalent Boronic Esters. *Macromolecules* **2015,** *48*, 2098-2106.

[31] Cromwell, O. R.; Chung, J.; Guan, Z. Malleable and Self-Healing Covalent Polymer Networks through Tunable Dynamic Boronic Ester Bonds. *J. Am. Chem. Soc.* **2015,** *137*, 6492-6495.

[32] Roettger, M.; Domenech, T.; van der Weegen, R.; Breuillac, A.; Renaud, N.; Leibler, L. High-performance Vitrimers from Commodity Thermoplastics through Dioxaborolane Metathesis. *Science* **2017**, *356*, 62-65.

[33] Brutman, J. P.; Delgado, P. A.; Hillmyer, M. A. Polylactide Vitrimers. *ACS Macro Lett.* **2014,** *3*, 607-610.

[34] Yu, Y.; Storti, G.; Morbidelli, M. Kinetics of Ring-Opening Polymerization of l,l-Lactide. *Ind. Eng. Chem. Res.* **2011,** *50*, 7927-7940.

[35] Colodny, P. C.; Tobolsky, A. V. Chemorheological Study of Polyurethan Elastomers. *J. Am. Chem. Soc.* **1957,** *79*, 4320-4323.

[36] Offenbach, J. A.; Tobolsky, A. V. Chemical Relaxation of Stress in Polyurethane Elastomers. *J. Colloid Sci.* **1956,** *11*, 39-47.

[37] Zheng, N.; Fang, Z.; Zou, W.; Zhao, Q.; Xie, T. Thermoset Shape-Memory Polyurethane with Intrinsic Plasticity Enabled by Transcarbamoylation. *Angew. Chem. Int. Ed.* **2016,** *55*, 11421–11425.

[38] Yan, P.; Zhao, W.; Fu, X.; Liu, Z.; Kong, W.; Zhou, C.; Lei, J. Multifunctional Polyurethane-Vitrimers Completely Based on Transcarbamoylation of Carbamates: Thermally-Induced Shape Memory Effect and Self-Welding. *RSC Adv.* **2017**, *7*, 26858-26866.

[39] Yan, P; Zhao, W.; Wang, Y.; Jiang, Y.; Zhou, C.; Lei, J. Carbon Nanotubes-Polyurethane Vitrimer Nanocomposites with the Ability of Surface Welding Controlled by Heat and Near-Infrared Light. *Macromol. Chem. Phys*. **2017**, *218*, 1700265.

[40] Zheng, N.; Hou, J.; Xu, Y.; Fang, Z.; Zou, W.; Zhao, Q.; Xie, T. Catalyst-Free Thermoset Polyurethane with Permanent Shape Reconfigurability and Highly Tunable Triple-Shape Memory Performance. *ACS Macro Lett.* **2017**, *6*, 326-330.

[41] Yang, Y.; Urban, M. W. Self-Healing of Glucose-Modified Polyurethane Networks Facilitated by Damage-Induced Primary Amines. *Polym. Chem.* **2016,** *8*, 303-309.

[42] De Hoe, G. X.; Zumstein, M. T.; Tiegs, B. J.; Brutman, J. P.; McNeill, K.; Sander, M.; Coates, G. W.; Hillmyer, M. A. Sustainable Polyester Elastomers from Lactones: Synthesis, Properties, and Enzymatic Hydrolyzability. *J. Am. Chem. Soc.* **2018**, *140*, 963-973.

[43] Brutman, J. P.; De Hoe, G. X.; Schneiderman, D. K.; Le, T. N.; Hillmyer, M. A. Renewable, Degradable, and Chemically Recyclable Cross-Linked Elastomers. *Ind. Eng. Chem. Res.* **2016,** *55*, 11097-11106.

[44] Angell, C. A. Formation of Glasses from Liquids and Biopolymers. *Science* **1995,** *267*, 1924-1935.

[45] Ediger, M. D.; Angell, C. A.; Nagel, S. R. Supercooled Liquids and Glasses. *J. Phys. Chem.* **1996,** *100*, 13200-13212.

[46] Dyre, J. C. *Colloquium*: The Glass Transition and Elastic Models of Glass-forming Liquids. *Rev. Mod. Phys.* **2006,** *78*, 953-972.

[47] Hiemenz, P. C.; Lodge, T. P. *Polymer Chemistry*. 2nd ed.; CRC Press INC: Boca Raton, FL, 2007.

[48] Auras, R. A.; Lim, L. T.; Selke, S. E. M.; Tsuji, H. *Poly(lactic acid): Synthesis, Structures, Properties, Processing, and Applications*. John Wiley & Sons, Inc.: Hoboken, NJ, 2010.

[49] Yu, K.; Taynton, P.; Zhang, W.; Dunn, M. L.; Qi, H. J. Influence of Stoichiometry on the Glass Transition and Bond Exchange Reactions in Epoxy Thermoset Polymers. *RSC Adv.* **2014**, *4*, 48682-48690.

[50] Yang, W. P.; Macosko, C. W.; Wellinghoff, S. T. Thermal degradation of urethanes based on 4,4′-diphenylmethane diisocyanate and 1,4-butanediol (MDI/BDO). *Polymer* **1986,** *27*, 1235-1240.

[51] Delebecq, E.; Pascault, J.-P.; Boutevin, B.; Ganachaud, F. On the Versatility of Urethane/Urea Bonds: Reversibility, Blocked Isocyanate, and Non-isocyanate Polyurethane. *Chem. Rev.* **2012,** *113*, 80-118.

[52] Gaylord, N. G.; Sroog, C. E. The Reactions of Carbamates with Alcohols. *J. Org. Chem.* **1953,** *18*, 1632-1637.

[53] Ghosh, R.; Nethaji, M.; Samuelson, A. G. Reversible double insertion of aryl isocyanates into the Ti–O bond of titanium(IV) isopropoxide. *J. Organomet. Chem.* **2005,** *690*, 1282-1293.

[54] Kumar, A.; Samuelson, A. G. Room temperature metathesis of aryl isocyanates and aromatic aldehydes catalyzed by group(IV) metal alkoxides: An experimental and computational study. *J. Organomet. Chem.* **2010,** *695*, 338-345.

[55] Becerra-Figueroa, L.; Ojeda-Porras, A.; Gamba-Sánchez, D. Transamidation of Carboxamides Catalyzed by Fe(III) and Water. *J. Org. Chem.* **2014,** *79*, 4544-4552.

[56] Pawar, G. M.; Buchmeiser, M. R. Polymer-Supported, Carbon Dioxide-Protected N-Heterocyclic Carbenes: Synthesis and Application in Organo- and Organometallic Catalysis. *Adv. Synth. Catal.* **2010,** *352*, 917-928.

[57] Bloodworth, A. J.; Davies, A. G. 975. Organometallic Reactions. Part I. The Addition of Tin Alkoxides to Isocyanates. *J. Chem. Soc. Res.* **1965**, 5238-5244.

Bibliography

A

Ahner, J.; Micheel, M.; Geitner, R.; Schmitt, M.; Popp, J.; Dietzek, B.; Hager, M. D. Self-healing Functional Polymers: Optical Property Recovery of Conjugated Polymer Films by Uncatalyzed Imine Metathesis. *Macromolecules* **2017**, *50*, 3789–3795.

Albertsson, A.-C.; Varma, I. K. Aliphatic Polyesters: Synthesis, Properties and Applications. *Degradable Aliphatic Polyesters*; Springer Berlin Heidelberg: Berlin, Heidelberg, 2002; pp 1-40.

Altuna, F. I.; Pettarin, V.; Williams, R. J. J. Self-healable polymer networks based on the cross-linking of epoxidised soybean oil by an aqueous citric acid solution. *Green Chem.* **2013**, *15*, 3360-3366.

Álvarez-Chávez, C. R.; Edwards, S.; Moure-Eraso, R.; Geiser, K. Sustainability of bio-based plastics: general comparative analysis and recommendations for improvement. *J Clean Prod* **2012**, 23, 47–56.

Amato, D. N.; Strange, G. A.; Swanson, J. P.; Chavez, A. D.; Roy, S. E.; Varney, K. L.; Machado, C. A.; Amato, D. V.; Costanzo, P. J. Synthesis and evaluation of thermally-responsive coatings based upon Diels-Alder chemistry and renewable materials. *Polym. Chem.* **2013**, *5*, 69–76.

American Chemistry Council, Economic Impact of Plastics-to-Oil Facilities in the U.S. October, 2014.

American Chemistry Council, U.S. Resin Production and Sales, March 2017. https://plastics.americanchemistry.com/Sales-Data-by-Resin.pdf

Ammala, A.; Bateman, S.; Dean, K.; Petinakis, E.; Sangwan, P.; Wong, S.; Yuan, Q.; Yu, L.; Patrick, C.; Leong, K. H. An overview of degradable and biodegradable polyolefins. *Prog. Polym. Sci.* **2011**, *36*, 1015–1049.

Amsden, B.; Wang, S.; Wyss, U. *Biomacromolecules* **2004**, *5*, 1399-1404.

Andrady, A. J. Assessment of Environmental Biodegradation of Synthetic Polymers. *Macromol. Sci., Polym. Rev.* **1994**, *34*, 25−76.

Andrady, A. L.; Neal, M. A. Applications and societal benefits of plastics. *Phil. Trans. R. Soc., B* **2009**, *364*, 1977–1984.

Andronova, A.; Srivastava, A.; Albertsson, A.-C. *Polymer* **2005**, *46*, 6746-6755.

Angell, C. A. Formation of Glasses from Liquids and Biopolymers. *Science* **1995,** *267*, 1924-1935.

Araujo, R.; Silva, C.; O'Neill, A.; Micaelo, N.; Guebitz, G.; Soares, C. M.; Casal, M.; Cavaco-Paulo, A. Tailoring cutinase activity towards polyethylene terephthalate and polyamide 6,6 fibers. *J. Biotechnol.* **2007**, *128*, 849–857.

ASTM D 2765–16 Standard Test Methods for Determination of Gel Content and Swell Ratio of Cross-linked Ethylene Plastics, ASTM International, West Conshohocken, PA, 2016.

Auras, R. A.; Lim, L. T.; Selke, S. E. M.; Tsuji, H. *Poly(lactic acid): Synthesis, Structures, Properties, Processing, and Applications*. John Wiley & Sons, Inc.: Hoboken, NJ, 2010.

Ayorinde, F.; Osman, G.; Shepard, R.; Powers, F. T. *J. Am. Oil. Chem. Soc.* **1988**, *65*, 1774-1777.

B

Baekeland, L. H. Method of making insoluble products of phenol and formaldehyde. U.S. Patent 942699A, December 7. 1909.

Bai, J.; Li, Z.; Shi, Z.; Yin, J. An eco-friendly scheme for the cross-linked polybutadiene elastomer via thiol-ene and Diels-Alder click chemistry. *Macromolecules* **2015**, *48*, 3539–3546.

Bai, N.; Saito, K.; Simon, G. P. Synthesis of a diamine cross-linker containing Diels-Alder adducts to produce a self-healing thermosetting epoxy polymer form a widely used epoxy monomer. *Polym. Chem.* **2013**, *4*, 724–730.

Baker, P. J.; Poultney, C.; Liu, Z.; Gross, R.; Montclare, J. K. Identification and comparison of cutinases for synthetic polyester degradation. *Appl. Microbiol. Biotechnol.* **2011**, *93*, 229–240.

Barnes, D. K. A.; Galgani, F.; Thompson, R. C.; Barlaz, M. Accumulation and fragmentation of plastic debris in global environments. *Philos. Trans. R. Soc., B* **2009**, *364*, 1985−1998.

Bassampour, Z. S.; Budy, S. M.; Son, D. Y. Degradable epoxy resins based on bisphenol A diglycidyl ether and silyl ether amine curing agents. *J. Appl. Polym. Sci.* **2017,** *134*, 44620.

Becerra-Figueroa, L.; Ojeda-Porras, A.; Gamba-Sánchez, D. Transamidation of Carboxamides Catalyzed by Fe(III) and Water. *J. Org. Chem.* **2014,** *79*, 4544-4552.

Bell, B. M.; Briggs, J. R.; Campbell, R. M.; Chambers, S. M.; Gaarenstroom, P. D.; Hippler, J. G.; Hook, B. D.; Kearns, K.; Kenney, J. M.; Kruper, W. J.; Schreck, D. J.; Theriault, C. N.; Wolfe, C. P. *Clean: Soil, Air, Water* **2008**, *36*, 657-661.

Bloodworth, A. J.; Davies, A. G. 975. Organometallic Reactions. Part I. The Addition of Tin Alkoxides to Isocyanates. *J. Chem. Soc. Res.* **1965**, 5238-5244.

Blossey, E. C.; Neckers, D. C. Concerning the use of polymer based photosensitizers. *Tetrahedron Lett.* **1974**, *15*, 323–326.

Boutelle, R. C.; Northrop, B. H. Substituent Effects on the Reversibility of Furan-Maleimide Cycloadditions. *J. Org. Chem.* **2011**, *76*, 7994–8002.

Brooks, A. L.; Wang, S.; Jambeck, J. R. The Chinese import ban and its impact on global plastic waste trade. *Sci. Adv.* **2018**, *4*, eaat0131.

Brutman, J. P.; De Hoe, G. X.; Schneiderman, D. K.; Le, T. N.; Hillmyer, M. A. Renewable, Degradable, and Chemically Recyclable Cross-Linked Elastomers. *Ind. Eng. Chem. Res.* **2016,** *55*, 11097-11106.

Brutman, J. P.; Delgado, P. A.; Hillmyer, M. A. Polylactide Vitrimers. *ACS Macro Lett.* **2014**, *3*, 607-610.

Brutman, J. P.; Fortman, D. J.; De Hoe, G. X.; Dichtel, W. R.; Hillmyer, M. A. A Mechanistic Study of Stress Relaxation in Urethane-Containing Polymer Networks. *J. Phys. Chem. B* **2019**, *123*, 1432–1441.

Brydson, J. A. *Plastics Materials*, 6th ed.; Butterworth Heinemann: Oxford, 1995.

Buekens, A. Introduction to Feedstock Recycling of Plastics. In *Feedstock Recycling and Pyrolysis of Waste Plastics*, John Wiley & Sons, Ltd: 2006; pp 1–41.

Butler, E.; Devlin, G.; McDonnell, K. Waste Polyolefins to Liquid Fuels via Pyrolysis: Review of Commercial State-of-the-Art and Recent Laboratory Research. *Waste and Biomass Valoriz.* **2011,** *2*, 227–255.

C

Campos, L. M.; Killops, K. L.; Sakai, R.; Paulusse, J. M. J.; Damiron, D.; Drockenmuller, E.; Messmore, B. W.; Hawker, C. J. Development of Thermal and Photochemical Strategies for Thiol-Ene Click Polymer Functionalization. *Macromolecules* **2008**, *41*, 7063-7070.

Canary, S. A.; Stevens, M. P. Thermally reversible crosslinking of polystyrene via the furan-maleimide Diels-Alder reaction. *J. Polym. Sci. A Polym. Chem.* **1992**, *30*, 1755–1760.

Capelot, M.; Montarnal, D.; Tournilhac, F.; Leibler, L. Metal-Catalyzed Transesterification for Healing and Assembling of Thermosets. *J. Am. Chem. Soc.* **2012,** *134*, 7664-7667.

Capelot, M.; Unterlass, M. M.; Tournilhac, F.; Leibler, L. Catalytic Control of the Vitrimer Glass Transition. *ACS Macro Lett.* **2012,** *1*, 789-792.

Carlsson, D. J.; Wiles, D. M. The Photooxidative Degradation of Polypropylene. Part I. Photooxidation and Photoinitiation Processes. *J. Macromol. Sci., Polym. Rev.* **1976**, *14*, 65–106.

Carpentier, J.-F. *Macromol. Rapid Comm.* **2010**, *31*, 1696-1705.

Cash, J. J.; Kubo, T.; Bapat, A. P.; Sumerlin, B. S. Room-Temperature Self-Healing Polymers Based on Dynamic-Covalent Boronic Esters. *Macromolecules* **2015,** *48*, 2098-2106.

Chao, A.; Negulescu, I.; Zhang, D. Dynamic Covalent Polymer Networks Based on Degenerative Imine Bond Exchange: Tuning the Malleability and Self-Healing Properties by Solvent. *Macromolecules* **2016**, *49*, 6277–6284.

Chen, D.; Hu, M.; Huang, C.; Zhang, R. Preparation and Properties of Natural Rubber Composites and Nanocomposites. *Natural Rubber Materials: Composites and Nanocomposites*; The Royal Society of Chemistry: London, 2014; Vol. 2, Chapter 4, pp 112-135.

Chen, X.; Dam, M. A.; Ono, K.; Mal, A.; Shen, H.; Nutt, S. R.; Sheran, K.; Wudl, F. A Thermally Re-mendable Cross-Linked Polymeric Material. *Science* **2002,** *295*, 1698-1702.

Chen, X.; Wudl, F.; Mal, A. K.; Shen, H.; Nutt, S. R. New Thermally Remendable Highly Cross-Linked Polymeric Materials. *Macromolecules* **2003,** *36*, 1802-1807.

Chinmayanandam, B. R.; Melville, H. W. Photosensitization of polymerization reactions. *Trans. Faraday Soc.* **1954**, *50*, 73–10.

Chujo, Y.; Sada, K.; Saegusa, T. Reversible gelation of polyoxazoline by means of Diels-Alder reaction. *Macromolecules* **1990**, *23*, 2636–2641.

Church, T. L.; Getzler, Y. D. Y. L.; Coates, G. W. *J. Am. Chem. Soc.* **2006**, *128*, 10125-10133.

Ciaccia, M.; Cacciapaglia, R.; Mencarelli, P.; Mandolini, L.; Di Stefano, S. Fast transimination in organic solvents in the absence of proton and metal catalysts. A key to imine metathesis catalyzed by primary amines under mild conditions. *Chem. Sci.* **2013**, *4*, 2253–2261.

Ciaccia, M.; Di Stefano, S. Mechanisms of imine exchange reactions in organic solvents. *Org. Biomol. Chem.* **2015**, *13*, 646–654.

Ciaccia, M.; Pilati, S.; Cacciapaglia, R.; Mandolini, L.; Di Stefano, S. Effective catalysis of imine metathesis by means of fast transiminations between aromatic-aromatic or aromatic-aliphatic amines. *Org. Biomol. Chem.* **2014**, *12*, 3282–3287.

Claudino, M.; van der Meulen, I.; Trey, S.; Jonsson, M.; Heise, A.; Johansson, M. Photoinduced thiol-ene crosslinking of globalide/ε-caprolactone copolymers: Curing performance and resulting thermoset properties. *J. Polym. Sci. Part A: Polym. Chem.* **2012**, *50*, 16-24.

Coady, D. J.; Fukushima, K.; Horn, H. W.; Rice, J. E.; Hedrick, J. L. Catalytic insights into acid/base conjugates: highly selective bifunctional catalysts for the ring-opening polymerization of lactide. *Chem. Commun.* **2011**, *47*, 3105-3107.

Colodny, P. C.; Tobolsky, A. V. Chemorheological Study of Polyurethan Elastomers. *J. Am. Chem. Soc.* **1957,** *79*, 4320-4323.

Connor, E. F.; Nyce, G. W.; Myers, M.; Möck, A.; Hedrick, J. L. First Example of N-Heterocyclic Carbenes as Catalysts for Living Polymerization: Organocatalytic Ring-Opening Polymerization of Cyclic Esters. *J. Am. Chem. Soc.* **2002**, *124*, 914–915.

Corma, A.; Nemeth, L. T.; Renz, M.; Valencia, S. *Nature* **2001**, *412*, 423-425.

Coulembier, O.; Degée, P.; Barbaud, C.; Guérin, P.; Dubois, P. *Polym. Bull.* **2004**, *51*, 365-372.

Coulembier, O.; Dubois, P. Polyesters from β-Lactones. In *Handbook of Ring-Opening Polymerization*, Dubois, P., Coulembier, O.; Raquez, J.-M., Eds. Wiley-VCH Verlag GmbH & Co. KGaA: Weinheim, Germany, 2009, pp. 227-254.

Craven, J. M. Cross-linked thermally reversible polymers produced from condensation polymers with pendant furan groups cross-linked with maleimides. US Patent 3,435,003, March 25, 1969.

Cromwell, O. R.; Chung, J.; Guan, Z. Malleable and Self-Healing Covalent Polymer Networks through Tunable Dynamic Boronic Ester Bonds. *J. Am. Chem. Soc.* **2015,** *137*, 6492-6495.

D

De Espinosa, L. M.; Meier, M. A. R. *Eur. Polym. J.* **2011**, *47*, 837-852.

De Hoe, G. X.; Zumstein, M. T.; Tiegs, B. J.; Brutman, J. P.; McNeill, K.; Sander, M.; Coates, G. W.; Hillmyer, M. A. Sustainable Polyester Elastomers from Lactones: Synthesis, Properties, and Enzymatic Hydrolyzability. *J. Am. Chem. Soc.* **2018**, *140*, 963-973.

Delebecq, E.; Pascault, J.-P.; Boutevin, B.; Ganachaud, F. On the Versatility of Urethane/Urea Bonds: Reversibility, Blocked Isocyanate, and Non-isocyanate Polyurethane. *Chem. Rev.* **2012,** *113*, 80-118.

Deng, G.; Tang, C.; Li, F.; Jiang, H.; Chen, Y. Covalent Cross-Linked Polymer Gels with Reversible Sol−Gel Transition and Self-Healing Properties. *Macromolecules* **2010**, *43*, 1191–1194.

Denissen, W.; Droesbeke, M.; Renaud, N.; Leibler, L.; Winne, J. M.; Du Prez, F. Chemical Control of the Viscoelastic Properties of Vinylogous Urethane Vitrimers. *Nat. Commun.* **2017**, *8*, 14857.

Denissen, W.; Rivero, G.; Nicolaÿ, R.; Leibler, L.; Winne, J. M.; Du Prez, F. E. Vinylogous Urethane Vitrimers. *Adv. Funct. Mater.* **2015,** *25*, 2451–2457.

Denissen, W.; Winne, J. M.; Du Prez, F. E. Vitrimers: permanent organic networks with glass-like fluidity. *Chem. Sci.* **2016**, *7*, 30-38.

Dotan, A. Biobased Thermosets. In *Handbook of Thermoset Plastics*, 3rd Ed.; Dodiuk, H. and Goodman, S. H., Eds.; Elsevier Inc.: Oxford, UK, 2013; pp 572–622.

Dyre, J. C. *Colloquium*: The Glass Transition and Elastic Models of Glass-forming Liquids. *Rev. Mod. Phys.* **2006,** *78*, 953-972.

E

Ediger, M. D.; Angell, C. A.; Nagel, S. R. Supercooled Liquids and Glasses. *J. Phys. Chem.* **1996,** *100*, 13200-13212.

Electronic Code of Federal Regulations, Title 21 – Food and Drugs, Chapter 1 – Food and Drug Administration, Department of Health and Services, Subchapter B – Food for Human Consumption (continued), Part 175 – Indirect Food Additives: Adhesives and Components of Coatings, §175.105 – Adhesives. https://www.ecfr.gov/cgi-bin/text-idx?SID=01e3cc9e948472d4a75ecaeed3cd532b&mc=true&node=se21.3.175_1105&rgn=div8 (accessed September 10, 2019).

Electronic Code of Federal Regulations, Title 21 – Food and Drugs, Chapter 1 – Food and Drug Administration, Department of Health and Services, Subchapter B – Food for Human Consumption (continued), Part 175 – Indirect Food Additives: Adhesives and Components of Coatings, §175.300 – Resinous and Polymeric Coatings. https://www.ecfr.gov/cgi-bin/text-idx?SID=01e3cc9e948472d4a75ecaeed3cd532b&mc=true&node=se21.3.175_1300&rgn=div8 (accessed September 10, 2019).

Enthaler, S.; Trautner, A. Iron-Catalyzed Ring-Closing Depolymerization of Poly(tetrahydrofuran). *ChemSusChem* **2013,** *6*, 1334–1336.

Eubeler, J. P.; Bernhard, M.; Knepper, T. P. Environmental biodegradation of synthetic polymers II. Biodegradation of different polymer groups. *Trends Anal. Chem.* **2010**, *29*, 84–100.

F

Fortman, D. J.; Brutman, J. P.; Cramer, C. J.; Hillmyer, M. A.; Dichtel, W. R. Mechanically Activated, Catalyst-Free Polyhydroxyurethane Vitrimers. *J. Am. Chem. Soc.* **2015**, *137*, 14019-14022.

Fortman, D. J.; Brutman, J. P.; De Hoe, G. X.; Snyder, R. L.; Dichtel, W. R.; Hillmyer, M. A. Approaches to Sustainable and Continually Recyclable Cross-Linked Polymers. *ACS Sus. Chem. Eng.* **2018**, *6*, 11145–11159.

Fortman, D. J.; Brutman, J. P.; Hillmyer, M. A.; Dichtel, W. R. Structural Effects on the Reprocessability and Stress relaxation of Cross-linked Polyhydroxyurethanes. *J. Appl. Polym. Sci.* **2017**, *134*, 44984.

Freinkel, S. *Plastic: A Toxic Love Story*; Houghton Mifflin Harcourt Publishing Company: New York, 2011.

Fukushima, K.; Coulembier, O.; Lecuyer, J. M.; Almegren, H. A.; Alabdulrahman, A. M.; Alsewailem, F. D.; McNeil, M. A.; Dubois, P.; Waymouth, R. M.; Horn, H. W.; Rice, J. E.; Hedrick, J. L. Organocatalytic Depolymerization of Poly(ethylene terephthalate). *J. Polym. Sci. Part A – Polym. Chem.* **2011**, *49*, 1273–1281.

Fukushima, K.; Lecuyer, J. M.; Wei, D. S.; Horn, H. W.; Jones, G. O.; Al-Megren, H. A.; Alabdulrahman, A. M.; Alsewailem, F. D.; McNeil, M. A.; Rice, J. E.; Hedrick, J. L. Advanced chemical recycling of poly(ethylene terephthalate) through organocatalytic aminolysis. *Polym. Chem.* **2013,** *4*, 1610–1616.

G

Gallagher, J. J.; Hillmyer, M. A.; Reineke, T. M. *Macromolecules* **2014**, *47*, 498-505.

Galloway, T. S.; Cole, M.; Lewis, C. Interactions of microplastic debris throughout the marine ecosystem. *Nat. Ecol. Evol.* **2017**, *1*, 0116.

Gandini, A. *Green Chem.* **2011**, *13*, 1061-1083.

Gandini, A. The furan/maleimide Diels-Alder reaction: A versatile click-unlick tool in macromolecular synthesis. *Prog. Polym. Sci.* **2013**, *38*, 1–29.

Gandini, A.; Lacerda, T. M.; Carvalho, A. J. F.; Trovatti, E. Progress of Polymers from Renewable Resources: Furans, Vegetable Oils, and Polysaccharides. *Chem. Rev.* **2016**, *116*, 1637−1669.

Gao, J. Coal, Oil Shale, Natural Bitumen, Heavy Oil, and Peat. In *Coal, Oil Shale, Natural Bitumen, Heavy Oil, and Peat*; Gao, J., Ed.; Eolss Publishers Co. Ltd.: Oxford, UK, 2009; Vol. 1, pp 1–39.

Gasteiger, E.; Hoogland, C.; Gattiker, A.; Duvaud, S.; Wilkins, M.; Appel, R.; Bairoch, A. Protein Identification and Analysis Tools on the ExPASy Server. In *The Proteomics Protocols Handbook*, Walker, J. M. Ed. Humana Press Inc: Totowa, NJ, 2005, pp. 571-607.

Gaylord, N. G.; Sroog, C. E. The Reactions of Carbamates with Alcohols. *J. Org. Chem.* **1953,** *18*, 1632-1637.

Gent, A. N. Strength of Elastomers. In *Science and Technology of Rubber,* 3rd ed.; Mark, J. E., Erman, B., Eirich, F. R., Eds.; Academic Press: Burlington, MA, 2005; pp 455-495.

Getzler, Y. D. Y. L.; Mahadevan, V.; Lobkovsky, E. B.; Coates, G. W. *J. Am. Chem. Soc.* **2002**, *124*, 1174-1175.

Gewert, B.; Plassmann, M.; Sandblom, O.; MacLeod, M. Identification of Chain Scission Products Released to Water by Plastic Exposed to Ultraviolet Light. *Environ. Sci. Technol. Lett.* **2018**, *5*, 272–276.

Geyer, R.; Jambeck, J. R.; Law, K. L. Production, use, and fate of all plastics ever made. *Sci. Adv.* **2017**, *3*, e1700782.

Geyer, R.; Kuczenski, B; Zink, T.; Henderson, A. Common Misconceptions about Recycling. *J. Ind. Ecol.* **2015**, *20*, 1010–1017.

Ghosh, R.; Nethaji, M.; Samuelson, A. G. Reversible double insertion of aryl isocyanates into the Ti–O bond of titanium(IV) isopropoxide. *J. Organomet. Chem.* **2005,** *690*, 1282-1293.

Grady, B. P.; Cooper, S. L.; Robertson, C. G. Thermoplastic Elastomers. *The Science and Technology of Rubber*, 4th ed.; Academic Press: Boston, 2013; Chapter 13, pp 591-652.

Gregory, M. R. Environmental implications of plastic debris in marine settings—entanglement, ingestion, smothering, hangers-on, hitch-hiking and alien invasions. *Phil. Trans. R. Soc., B* **2009**, *364*, 2013–2025.

Grijpma, D. W.; Kroeze, E.; Nijenhuis, A. J.; Pennings, A. J. Poly(l-lactide) crosslinked with spiro-bis-dimethylene-carbonate. *Polymer* **1993**, *34*, 1496-1503.

Gross, R. A. Biodegradable Polymers for the Environment. *Science* **2002**, *297* (5582), 803–807.

Grün, F.; Watanabe, H.; Zamanian, Z.; Maeda, L.; Arima, K.; Cubacha, R.; Gardiner, D. M.; Kanno, J.; Iguchi, T.; Blumberg, B. Endocrine-disrupting organotin compounds are potent inducers of adipogenesis in vertebrates. *Mol Endocrinol.* **2006**, 20, 2141–2155.

Guillory, J. P.; Cook, C. F. Mechanism of stabilization of polypropylene by ultraviolet absorbers. *J. Polym. Sci., Part A-1: Polym. Chem.* **1971**, *9*, 1529–1536.

Gurusamy-Thangavelu, S. A.; Emond, S. J.; Kulshrestha, A.; Hillmyer, M. A.; Macosko, C. W.; Tolman, W. B.; Hoye, T. R. Polyurethanes based on renewable polyols from bioderived lactones. *Polym. Chem.* **2012**, *3*, 2941-2948.

H

Han, C.; Ran, X.; Su, X.; Zhang, K.; Liu, N.; Dong, L. Effect of peroxide crosslinking on thermal and mechanical properties of poly(ε-caprolactone). *Polym. Int.* **2007**, *56*, 593-600.

Han, X.; Liu, W.; Huang, J.-W.; Ma, J.; Zheng, Y.; Ko, T.-P.; Xu, L.; Cheng, Y.-S.; Chen, C.-C.; Guo, R.-T. Structural insight into catalytic mechanism of PET hydrolase. *Nat. Commun.* **2017**, *8*, 1–6.

Helminen, A. O.; Korhonen, H.; Seppälä, J. V. Structure modification and crosslinking of methacrylated polylactide oligomers. *J. Appl. Polym. Sci.* **2002**, *86*, 3616-3624.

Helminen, A.; Korhonen, H.; Seppälä, J. *J. Polym. Sci., Part A: Polym. Chem.* **2003**, *41*, 3788-3797.

Helminen, A.; Korhonen, H.; Seppälä, J. *Macromol. Chem. Phys.* **2002**, *18*, 2630-2639.

Hermans, P. H.; Eyk, J. V. The reaction of benzoyl peroxide with cyclohexane and cyclohexene. Contribution to the mechanism of the catalyzing action of peroxides in the polymerization of vinyl derivatives. *J. Polym. Sci.* **1946**, *1*, 407-418.

Herrera, R.; Franco, L.; Rodríguez-Galán, A.; Puiggalí, J. Characterization and degradation behavior of poly(butylene adipate- co-terephthalate)s. *J. Polym. Sci. A Polym. Chem.* **2002**, *40*, 4141–4157.

Herrero Acero, E.; Ribitsch, D.; Steinkellner, G.; Gruber, K.; Greimel, K.; Eiteljoerg, I.; Trotscha, E.; Wei, R.; Zimmermann, W.; Zinn, M.; et al. Enzymatic Surface Hydrolysis of PET: Effect of Structural Diversity on Kinetic Properties of Cutinases from Thermobifida. *Macromolecules* **2011**, *44*, 4632–4640.

Hiemenz, P. C.; Lodge, T. P. *Polymer Chemistry*. 2nd ed.; CRC Press INC: Boca Raton, FL, 2007.

Hillmyer, M. A. The promise of plastics from plants. *Science* **2017**, *358*, 868–870.

Hillmyer, M. A.; Tolman, W. B. Aliphatic Polyester Block Polymers: Renewable, Degradable, and Sustainable. *Acc. of Chem. Res.* **2014**, *47*, 2390-2396.

Hong, J. H.; Hyun, J. J.; Yoo, J. H.; Yu, W.-R.; Youk, J. H. *Polym. Degrad. Stab.* **2007**, *92*, 1186-1192.

Hong, M., Chen, E. Y. X. Chemically Recyclable Polymers: A Circular Economy Approach to Sustainability. *Green Chem.* **2017**, 19, 3692–3706.

Hong, M.; Chen, E. Y. X. Completely recyclable biopolymers with linear and cyclic topologies via ring-opening polymerization of γ-butyrolactone. *Nat. Chem.* **2016,** *8*, 42–49.

Hopewell, J.; Dvorak, R.; Kosior, E. Plastics Recycling: Challenges and Opportunities. *Philos. Trans. R. Soc., B* **2009**, *364*, 2115−2126.

Horie, K.; Barón, M.; Fox, R. B.; He, J.; Kahovec, J.; Kitayama, T.; Kubisa, P.; Maréchal, E.; Mormann, W.; Stepto, R. F. T.; Tabak, D.; Vohlídal, T.; Wilks, E. S.; Work, W. J. Definitions of terms relating to reactions of polymers and to functional polymeric materials (IUPAC Recommendations 2003). *Pure Appl. Chem.* **2004**, *76*, 889–906.

Huang, Y.; Chang, R.; Han, L.; Shan, G.; Bao, Y.; Pan, P. ABA-Type Thermoplastic Elastomers Composed of Poly(ε-caprolactone-co-δ-valerolactone) Soft Midblock and Polymorphic Poly(lactic acid) Hard End Blocks. *ACS Sustainable Chem. Eng.* **2016**, *4*, 121-128.

I

Iji, M.; Inoue, K.; Yamashiro, M. Recyclable shape-memory and mechanical strength of poly(lactic acid) compounds cross-linked by thermo-reversible Diels-Alder reaction. *Polym. J.* **2008**, *40*, 657–662.

Ikeda, T.; Oikawa, D.; Shimasaki, T.; Teramoto, N.; Shibata, M. Organogelation behavior, thermal and mechanical properties of polymer network formed by the Diels-Alder reaction of furan- and maleimide-terminated four-arm star-shaped ε-caprolactone oligomers. *Polymer* **2013**, *54*, 3206–3216.

Imbernon, L.; Norvez, S. From Landfilling to Vitrimer Chemistry in Rubber Life Cycle. *Eur. Polym. J.* **2016,** *82*, 347-376.

ISO 10147:2011, Pipes and fittings made of crosslinked polyethylene (PE-X)—estimation of the degree of cross-linking by determination of the gel content, International Organization for Standardization: Geneva, Switzerland, 2011.

Ito, H.; Willson, C. G. Chemical amplification in the design of dry developing resist materials. *Polym. Eng. Sci.* **1983,** *23*, 1012–1018.

J

Jambeck, J. R.; Geyer, R.; Wilcox, C.; Siegler, T. R.; Perryman, M.; Andrady, A.; Narayan, R.; Law, K. L. Plastic waste inputs from land into the ocean. *Science*, **2015**, *347*, 768–771.

K

Kaitz, J. A.; Lee, O. P.; Moore, J. S. Depolymerizable polymers: preparation, applications, and future outlook. *MRS Comm.* **2015,** *5*, 191–204.

Kamber, N. E.; Jeong, W.; Waymouth, R. M. Organocatalytic Ring-Opening Polymerization. *Chem. Rev.* **2007**, *49*, 2419–2428.

Kaminsky, W.; Franck, J. Monomer recovery by pyrolysis of poly(methyl methacrylate) (PMMA). *J. Anal. Appl. Pyrolysis* **1991**, *19*, 311−318.

Kathan, M.; Kovaříček, P.; Jurissek, C.; Senf, A.; Dallmann, A.; Thünemann, A. F.; Hecht, S. Control of Imine Exchange Kinetics with Photoswitches to Modulate Self-Healing in Polysiloxane Networks by Light Illumination. *Angew. Chem., Int. Ed.* **2016**, *55*, 13882–13886.

Kauffman, G. B.; Seymour, R. B. Elastomers: I. Natural Rubber. *J. Chem. Educ.* **1990**, *67*, 422–425.

Kaufmann, C. B. *Grand Duke, Wizard, and Bohemian*; Meta4Press LLC: 2012.

Kienle, R. H.; Hovey, A. G. The Polyhydric Alcohol-Polybasic Acid Reaction. I. Glycerol-Phthalic Anhydride. *J. Am. Chem. Soc.* **1929**, *51*, 509–519.

Kijchavengkul, T.; Auras, R.; Rubino, M. Measuring gel content of aromatic polyesters using FTIR spectrophotometry and DSC. *Polym. Test.* **2008**, *27*, 55–60.

Kijchavengkul, T.; Auras, R.; Rubino, M.; Alvarado, E.; Montero, J. R. C.; Rosales, J. M. Atmospheric and soil degradation of aliphatic-aromatic polyester films. *Polym. Degrad. Stab.* **2010**, *95*, 99–107.

Kijchavengkul, T.; Auras, R.; Rubino, M.; Ngouajio, M.; Fernandez, R. T. Assessment of aliphatic–aromatic copolyester biodegradable mulch films. Part I: Field study. *Chemosphere* **2008**, *71*, 942–953.

Kijchavengkul, T.; Auras, R.; Rubino, M.; Ngouajio, M.; Fernandez, R. T. Assessment of aliphatic–aromatic copolyester biodegradable mulch films. Part II: Laboratory simulated conditions. *Chemosphere* **2008**, *71*, 1607–1616.

Kijchavengkul, T.; Auras, R.; Rubino, M.; Selke, S.; Ngouajio, M.; Fernandez, R. T. Biodegradation and hydrolysis rate of aliphatic aromatic polyester. *Polym. Degrad. Stab.* **2010**, *95*, 2641–2647.

Kijchavengkul, T.; Auras, R.; Rubino, M.; Selke, S.; Ngouajio, M.; Fernandez, R. T. Formulation selection of aliphatic aromatic biodegradable polyester film exposed to UV/solar radiation. *Polym. Degrad. Stab.* **2011**, *96*, 1919–1926.

Kloxin, C. J.; Bowman, C. N. Covalent Adaptable Networks: Smart, Reconfigurable and Responsive Network Systems. *Chem. Soc. Rev.* **2013,** *42*, 7161-7173.

Kramer, J.; Rowley, J.; Coates, G. W. *Org. React.* **2015**, *86*, 1-104.

Kumar, A.; Samuelson, A. G. Room temperature metathesis of aryl isocyanates and aromatic aldehydes catalyzed by group(IV) metal alkoxides: An experimental and computational study. *J. Organomet. Chem.* **2010,** *695*, 338-345.

Künkel, A.; Becker, J.; Börger, L.; Hamprecht, J.; Koltzenburg, S.; Loos, R.; Schick, M. B.; Schlegel, K.; Sinkel, C.; Skupin, G.; et al. Polymers, Biodegradable. In *Ullmann's Encyclopedia of Industrial Chemistry*; Wiley-VCH Verlag GmbH & Co. KGaA: Weinheim, 2016.

Kuwabara, K.; Gan, Z.; Nakamura, T.; Abe, H.; Doi, Y. Crystalline/Amorphous Phase Structure and Molecular Mobility of Biodegradable Poly(butylene adipate-co-butylene terephthalate) and Related Polyesters. *Biomacromolecules* **2002**, *3*, 390–396.

L

Laszakovits, J. R.; Berg, S. M.; Anderson, B. G.; O'Brien, J. E.; Wammer, K. H.; Sharpless, C. M. p-Nitroanisole/Pyridine and p-Nitroacetophenone/Pyridine Actinometers Revisited: Quantum Yield in Comparison to Ferrioxalate. *Environ. Sci. Technol. Lett.* **2017**, *4*, 11–14.

Lecomte, J.; Jérôme, C. Recent Developments in Ring-Opening Polymerization of Lactones. *Adv. Polym. Sci.* **2012**, *245*, 173–218.

Lecomte, P.; Jérôme, C. Recent Developments in Ring-Opening Polymerization of Lactones. In *Synthetic Biodegradable Polymers*; Rieger, B., Künkel, A., Coates, W. G., Reichardt, R., Dinjus, E., Zevaco, A. T., Eds.; Springer Berlin Heidelberg: Berlin, Heidelberg, 2012; pp 173-217.

Lee, S.; Lee, K.; Kim, Y.-W.; Shin, J. Preparation and Characterization of a Renewable Pressure-Sensitive Adhesive System Derived from ε-Decalactone, l-Lactide, Epoxidized Soybean Oil, and Rosin Ester. *ACS Sustainable Chem. Eng.* **2015**, *3*, 2309-2320.

Lee, S.Y., Kim, H.U., Chae, T.U., Cho, J.S., Kim, J.W., Shin, J.H., Kim, D.I., Ko, Y.-S., Jang, W.D., Jang, Y.-S. A comprehensive metabolic map for production of bio-based chemicals. *Nat. Catal.* **2019**, *2*, 18–33.

Lee, Y. N. Malaysia, following in China's footsteps, bans imports of plastic waste. *CNBC News*, January 25, 2019.

Lei, Z. Q.; Xie, P.; Rong, M. Z.; Zhang, M. Q. Catalyst-free dynamic exchange of aromatic Schiff base bonds and its application to self-healing and remolding of crosslinked polymers. *J. Mater. Chem. A* **2015**, *3*, 19662–19668.

Lewis, C. L.; Meng, Y.; Anthamatten, M. Well-Defined Shape-Memory Networks with High Elastic Energy Capacity. *Macromolecules* **2015**, *48*, 4918-4926.

Li, H.; Bai, J.; Shi, Z.; Yin, J. Environmental friendly polymers based on schiff-base reaction with self-healing, remolding and degradable ability. *Polymer* **2016**, *85*, 106–113.

Lin, J.-O.; Chen, W.; Shen, Z.; Ling, J. Homo- and Block Copolymerizations of ε-Decalactone with l-Lactide Catalyzed by Lanthanum Compounds. *Macromolecules* **2013**, *46*, 7769-7776.

Linnekoski, J. A.; Asikainen, M.; Heikkinen, H.; Kaila, R. K.; Räsänen, J.; Laitinen, A.; Harlin, A. *Org. Process Res. Dev.* **2014**, *18*, 1468-1475.

Liu, E. K.; He, W. Q.; Yan, C. R. 'White revolution' to 'white pollution'— agricultural plastic film mulch in China. *Environ. Res. Lett.* **2014**, *9*, 1–4.

Liu, G.-C.; He, Y.-S.; Zeng, J.-B.; Li, Q.-T.; Wang, Y.-Z. Fully Biobased and Supertough Polylactide-Based Thermoplastic Vulcanizates Fabricated by Peroxide-Induced Dynamic Vulcanization and Interfacial Compatibilization. *Biomacromolecules* **2014**, *15*, 4260-4271.

Liu, Q.; Lei, J.; Shi, R.; Zhang, L. *Prog. Polym. Sci.* **2012**, *37*, 715-765.

Liu, X.-Q., Wang, M.-X.; Li, Z.-C.; Li, F.-M. *Macromol. Chem. Phys.* **1999**, *200*, 468-473.

Lligadas, G.; Ronda, J. C.; Galià, M.; Cádiz, V. *Biomacromolecules* **2010**, *11*, 2825-2835.

Lohmeijer, B. G. G.; Pratt, R. C.; Leibfarth, F.; Logan, J. W.; Long, D. A.; Dove, A. P.; Nederberg, F.; Choi, J.; Wade, C.; Waymouth, R. M.; Hedrick, J. L. Guanidine and Amidine Organocatalysts for Ring-Opening Polymerization of Cyclic Esters. *Macromolecules* **2006**, *39*, 8574–8583.

Longhi, S.; Czjzek, M.; Lamzin, V.; Nicolas, A.; Cambillau, C. Atomic resolution (1.0 A) crystal structure of Fusarium solani cutinase: stereochemical analysis. *J. Mol. Biol.* **1997**, *268*, 779–799.

Longley, R. I.; Emerson, W. S.; Shafer, T. C. Some Reactions of 2-Alkoxy-3,4-dihydro-2H-pyrans. *J. Am. Chem. Soc.* **1952**, *74*, 2012-2015.

Lu, Y.-X.; Guan, Z. Olefin Metathesis for Effective Polymer Healing via Dynamic Exchange of Strong Carbon–Carbon Double Bonds. *J. Am. Chem. Soc.* **2012,** *134*, 14226-14231.

Lu, Y.-X.; Tournilhac, F.; Leibler, L.; Guan, Z. Making Insoluble Polymer Networks Malleable via Olefin Metathesis. *J. Am. Chem. Soc.* **2012,** *134*, 8424-8427.

Lucas, N.; Bienaime, C.; Belloy, C.; Queneudec, M.; Silvestre, F.; Nava-Saucedo, J.-E. Polymer biodegradation: Mechanisms and estimation techniques *Chemosphere* **2008**, *73*, 429–442.

M

MacDonald, J. P.; Shaver, M. P. An aromatic/aliphatic polyester prepared via ring-opening polymerisation and its remarkably selective and cyclable depolymerisation to monomer. *Polym. Chem.* **2016,** *7*, 553–559.

Målberg, S.; Plikk, P.; Finne-Wistrand, A.; Albertsson, A.-C. Design of Elastomeric Homo- and Copolymer Networks of Functional Aliphatic Polyester for Use in Biomedical Applications. *Chem. Mater.* **2010**, *22*, 3009-3014.

Mandelkern, L. *Crystallization of Polymers*, Second Edition. Cambridge University Press: New York, 2004; Vol. 1.

Martello, M. T.; Hillmyer, M. A. Polylactide–Poly(6-methyl-ε-caprolactone)–Polylactide Thermoplastic Elastomers. *Macromolecules* **2011**, *44*, 8537-8545.

Martello, M. T.; Schneiderman, D. K.; Hillmyer, M. A. Synthesis and Melt Processing of Sustainable Poly(ε-decalactone)-block-Poly(lactide) Multiblock Thermoplastic Elastomers. *ACS Sustainable Chem. Eng.* **2014**, *2*, 2519-2526.

Marten, E.; Müller, R.-J.; Deckwer, W.-D. Studies on the enzymatic hydrolysis of polyesters. II. Aliphatic–aromatic copolyesters. *Polym. Degrad. Stab.* **2005**, *88*, 371–381.

Marten, E.; Müller, R.-J.; Deckwer, W.-D. Studies on the enzymatic hydrolysis of polyesters I. Low molecular mass model esters and aliphatic polyesters. *Polym. Degrad. Stab.* **2003**, *80*, 485–501.

Martin, R.; Rekondo, A.; Ruiz de Luzuriaga, A.; Cabanero, G.; Grande, H. J.; Odriozola, I. The Processability of a Poly(urea-urethane) Elastomer Reversibly Crosslinked With Aromatic Disulfide Bridges. *J. Mater. Chem. A* **2014,** *2*, 5710-5715.

McCarthy, S. Biodegradable Polymers. In *Plastics and the Environment*; Andrady, A., Ed.; John Wiley & Sons, Inc.: Hoboken, NJ, 2003; pp 359–377.

McNaughton, S.; Nowakowski, K. How China's plastic waste ban forced a global recycling reckoning. *National Geographic*, June 2019.

Mecerreyes, D.; Humes, J.; Miller, R. D.; Hedrick, J. L.; Detrembleur, C.; Lecomte, P.; Jérôme, R.; San Roman, J. First example of an unsymmetrical difunctional monomer polymerizable by two living/controlled methods. *Macromol. Rapid Commun.* **2000**, *21*, 779-784.

Montarnal, D.; Capelot, M.; Tournilhac, F.; Leibler, L. Silica-Like Malleable Materials from Permanent Organic Networks. *Science* **2011**, *334*, 965-968.

Morris, J. Recycling versus incineration: an energy conservation analysis. *J. Hazard. Mater.* **1996**, *47*, 277–293.

Mueller, R.-J. Biological degradation of synthetic polyesters—Enzymes as potential catalysts for polyester recycling. *Process Biochem.* **2006**, *41*, 2124–2128

Muller, P. Glossary of terms used in physical organic chemistry (IUPAC Recommendations 1994). *Pure Appl. Chem.* **1994**, *66*, 1077–1184.

Murphy, C. A.; Cameron, J. A.; Huang, S. J.; Vinopal, R. T. *Appl. Environ. Microbiol.* **1996**, *62*, 456-460.

N

Narkis, M.; Wallerstein, R. Cross-linking of polycaprolactone with peroxides. *Polym. Commun.* **1986**, *27*, 314-317.

Neffgen, S.; Keul, H.; Höcker, H. Ring-opening polymerization of cyclic urethanes and ring-closing depolymerization of the respective polyurethanes. *Macromol. Rapid Commun.* **1996**, *17*, 373–382.

Nijenhuis, A. J.; Grijpma, D. W.; Pennings, A. J. Crosslinked poly(l-lactide) and poly(ε-caprolactone). *Polymer* **1996**, *37*, 2783-2791.

Nimmo, C. M.; Owen, S. C.; Shoichet, M. S. Diels-Alder click cross-linked hyaluronic acid hydrogels for tissue engineering. *Biomacromolecules* **2011**, *12*, 824–830.

Nirmal Ghosh, O. S.; Gayathri, S.; Sudhakara, P.; Misra, S. K.; Jayaramudu, J. Natural Rubber Nanoblends: Preparation, Characterization, and Applications. In *Rubber Nano*

Blends, Markovic, G.; Visakh, P. M., Eds. Springer International Publishing AG: Cham, Switzerland, 2017, pp. 15-65.

O

Odian, G. *Principles of Polymerization*; 4th ed.; John Wiley & Sons: Hoboken, NJ, 2004.

Offenbach, J. A.; Tobolsky, A. V. Chemical Relaxation of Stress in Polyurethane Elastomers. *J. Colloid Sci.* **1956,** *11*, 39-47.

Olsén, P.; Borke, T.; Odelius, K.; Albertsson, A.-C. ε-Decalactone: A Thermoresilient and Toughening Comonomer to Poly(l-lactide). *Biomacromolecules* **2013**, *14*, 2883-2890.

Olsén, P.; Undin, J.; Odelius, K.; Keul, H.; Albertsson, A-C. Switching from Controlled Ring-Opening Polymerization (cROP) to Controlled Ring-Closing Depolymerization (cRCDP) by Adjusting the Reaction Parameters that Determine the Ceiling Temperature. *Biomacromolecules* **2016**, *17*, 3995–4002.

Our Common Future, Report of the World Commission on Environment and Development, World Commission on Environment and Development, 1987. Published as Annex to General Assembly document A/42/427, Development and International Co-operation: Environment August 2, 1987.

P

Palmgren, R.; Karlsson, S.; Albertsson, A.-C. Synthesis of degradable crosslinked polymers based on 1,5-dioxepan-2-one and cross-linker of bis-ε-caprolactone type. *J. Polym. Sci. Part A: Polym. Chem.* **1997**, *35*, 1635-1649.

Parker, L. China's ban on trash imports shifts waste crisis to Southeast Asia. Laura Parker. *National Geographic*, November 16, 2018.

Paszun, D.; Spychaj, T. Chemical Recycling of Poly(ethylene terephthalate). *Ind. Eng. Chem. Res.* **1997,** *36*, 1373–1383.

Pawar, G. M.; Buchmeiser, M. R. Polymer-Supported, Carbon Dioxide-Protected N-Heterocyclic Carbenes: Synthesis and Application in Organo- and Organometallic Catalysis. *Adv. Synth. Catal.* **2010,** *352*, 917-928.

Pepels, M.; Filot, I.; Klumperman, B.; Goossens, H. Self-healing Systems Based on Disulfide-thiol Exchange Reactions. *Polym. Chem.* **2013,** *4*, 4955-4965.

Perz, V.; Bleymaier, K.; Sinkel, C.; Kueper, U.; Bonnekessel, M.; Ribitsch, D.; Guebitz, G. M. Substrate specificities of cutinases on aliphatic-aromatic polyesters and on their model substrates. *New Biotechnol.* **2016**, *33*, 295–304.

Piver, W. T. Organotin Compounds: Industrial Applications and Biological Investigation. *Environ. Health Perspect.* **1973**, 4, 61.

Pratt, R. C.; Lohmeijer, B. G. G.; Long, D. A.; Waymouth, R. M.; Hedrick, J. L. Triazabicyclodecene : A Simple Bifunctional Organocatalyst for Acyl Transfer and Ring-Opening Polymerization of Cyclic Esters Triazabicyclodecene : A Simple Bifunctional Organocatalyst for Acyl Transfer and Ring-Opening Polymerization of Cyclic Esters. *J. Am. Chem. Soc.* **2006**, *128*, 4556–4557.

Prioreschi, P. *A History of Medicine: Primitive and ancient medicine*, 2nd ed.; Horatius Press: Omaha, NE, 1996.

R

Rahimi, A.; García, J. Chemical recycling of waste plastics for new materials production. *Nat. Rev. Chem.* **2017**, *1*, 0046.

Raqueza, J.-M.; Deléglise, M; Lacrampe, M.-F.; Krawczak, P. Thermosetting (bio)materials derived from renewable resources: A critical review. *Prog. Polym. Sci.* **2010**, *35*, 487–509.

Rekondo, A.; Martin, R.; Ruiz de Luzuriaga, A.; Cabanero, G.; Grande, H. J.; Odriozola, I. Catalyst-free Room-temperature Self-healing Elastomers Based on Aromatic Disulfide Metathesis. *Mater. Horiz.* **2014,** *1*, 237-240.

Ren, N.; Matta, M. E.; Martinez, H.; Walton, K. L.; Munro, J. C.; Schneiderman, D. K.; Hillmyer, M. A. Filler-Reinforced Elastomers Based on Functional Polyolefin Prepolymers. *Ind. Eng. Chem. Res.* **2016**, *55*, 6106-6112.

Rillig, M. C. Microplastic in Terrestrial Ecosystems and the Soil? *Environ. Sci. Technol.* **2012**, *46*, 6453–6454.

Rivaton, A.; Gardette, J.-L. Photo-oxidation of aromatic polymers. *Angew. Makromol. Chem.* **1998**, *261-262*, 173–188.

Roberge, D. M.; Buhl, D.; Niederer, J. P. M.; Hölderich, W. F. *Appl. Catal., A* **2001**, *215*, 111-124.

Rochman, C. M.; Browne, M. A.; Halpern, B. S.; Hentschel, B, T.; Hoh, E.; Karapanagioti, H. K.; Rios-Mendoza, L. M.; Takada, H.; Teh, S.; Thompson, R. C. Classify plastic waste as hazardous. *Nature* **2013**, *494*, 169−171.

Roettger, M.; Domenech, T.; van der Weegen, R.; Breuillac, A.; Renaud, N.; Leibler, L. High-performance Vitrimers from Commodity Thermoplastics through Dioxaborolane Metathesis. *Science* **2017**, *356*, 62-65.

Romera-Castillo, C.; Pinto, M.; Langer, T. M.; Álvarez-Salgado, X. A.; Herndl, G. J. Dissolved organic carbon leaching from plastics stimulates microbial activity in the ocean. *Nat. Comm.* **2018**, *9*, 1430.

Ronkvist, Å. M.; Xie, W.; Lu, W.; Gross, R. A. Cutinase-Catalyzed Hydrolysis of Poly(ethylene terephthalate). *Macromolecules* **2009**, *42*, 5128–5138.

Rowley, J. M.; Lobkovsky, E. B.; Coates, G. W. Catalytic Double Carbonylation to Succinic Anhydrides: Catalyst Discovery, Reaction Scope, and Mechanism. *J. Am. Chem. Soc.* **2007**, *129*, 4948–4960.

Roy, N.; Bruchmann, B.; Lehn, J.-M. DYNAMERS: Dynamic Polymers as Self-healing Materials. *Chem. Soc. Rev.* **2015,** *44*, 3786-3807

S

Salis, A.; Bilaničová, D.; Ninham, B. W.; Monduzzi, M. *J. Phys. Chem. B* **2007**, *111*, 1149-1156.

Sander, M. Biodegradation of Polymeric Mulch Films in Agricultural Soils: Concepts, Knowledge Gaps, and Future Research Directions. *Environ. Sci. Technol.* **2019**, *53*, 2304–2315.

Sanford, M. J.; Peña Carrodeguas, L.; Van Zee, N. J.; Kleij, A. W.; Coates, G. W. Alternating Copolymerization of Propylene Oxide and Cyclohexene Oxide with Tricyclic Anhydrides: Access to Partially Renewable Aliphatic Polyesters with High Glass Transition Temperatures. *Macromolecules* **2016**, *49*, 6394–6400.

Sanford, M. J.; Van Zee, N. J.; Coates, G. Reversible-deactivation anionic alternating ring-opening copolymerization of epoxides and cyclic anhydrides: access to orthogonally functionalizable multiblock aliphatic polyesters. *Chemical Science* **2018**, *9*, 134–142.

Sangroniz, A.; Sangroniz, L.; Aranburu, N.; Fernández, M.; Santamaria, A.; Iriarte, M.; Etxeberria, A. Blends of biodegradable poly(butylene adipate-co-terephthalate) with poly(hydroxi amino ether) for packaging applications: Miscibility, rheology and transport properties. *Eur. Polym. J.* **2018**, *105*, 348–358.

Santa Barbara County Resource Recovery & Waste Management Division, What happens to trash? http://lessismore.org/materials/177-what-happens-to-trash/ (accessed on 3 September 2019).

Sato, M. Thermochemistry of the formation of fossil fuels. In *Fluid-Mineral Interactions: A Tribute to H.P. Eugster*; Spencer, R. J., Chou, I. M., Eds.; Geological Society of America, 1990; Special Publication 2, pp 271−283.

Schmidt, J.; Wei, R.; Oeser, T.; Belisário-Ferrari, M. R.; Barth, M.; Then, J.; Zimmermann, W. *FEBS Open Bio* **2016**, *6*, 919-927.

Schmolke, W.; Perner, N.; Seiffert, S. Dynamically Cross-Linked Polydimethylsiloxane Networks with Ambient-Temperature Self-Healing. *Macromolecules* **2015,** *48*, 8781-8788.

Schneiderman, D. K.; Hillmyer, M. A. 50th Anniversary Perspective: There Is a Great Future in Sustainable Polymers. *Macromolecules* **2017**, *50*, 3733–3749.

Schneiderman, D. K.; Hillmyer, M. A. Aliphatic Polyester Block Polymer Design. *Macromolecules* **2016**, *49*, 2419-2428.

Schneiderman, D. K.; Vanderlaan, M. E.; Mannion, A. M.; Panthani, T. R.; Batiste, D. C.; Wang, J. Z.; Bates, F. S.; Macosko, C. W.; Hillmyer, M. A. Chemically Recyclable Biobased Polyurethanes. *ACS Macro Lett.* **2016**, 515-518.

Schutyser, W.; Van Den Bosch, S.; Dijkmans, J.; Turner, S.; Meledina, M.; Van Tendeloo, G.; Debecker, D. P.; Sels, B. F. *ChemSusChem* **2015**, *8*, 1805-1818.

Searle, N. D. Environmental Effects on Polymeric Materials. In *Plastics and the Environment*; Andrady, A., Ed.; John Wiley & Sons, Inc.: Hoboken, NJ, 2003; pp 311–358.

Semba, T.; Kitagawa, K.; Ishiaku, U. S.; Hamada, H. The effect of crosslinking on the mechanical properties of polylactic acid/polycaprolactone blends. *J. Appl. Polym. Sci.* **2006**, *101*, 1816-1825.

Shah, A. A.; Hasan, F.; Hameed, A.; Ahmed, S. Biological degradation of plastics: A comprehensive review. *Biotechnol. Adv.* **2008**, *26*, 246–265.

Sharuddin, S. D. A.; Abnisa, F.; Daud, W. M. A. W.; Aroua, M. K. A Review on Pyrolysis of Plastic Wastes. *Energy Convers. Manag*. **2016**, *115*, 308–326.

Shi, Q.; Yu, K.; Dunn, M. L.; Wang, T.; Qi, H. J. Solvent Assisted Pressure-Free Surface Welding and Reprocessing of Malleable Epoxy Polymers. *Macromolecules* **2016**, *49*, 5527–5537.

Shin, J.; Lee, Y.; Tolman, W. B.; Hillmyer, M. A. Thermoplastic Elastomers Derived from Menthide and Tulipalin A. *Biomacromolecules* **2012**, *13*, 3833-3840

Sintim, H. Y.; Flury, M. Is Biodegradable Plastic Mulch the Solution to Agriculture's Plastic Problem? *Environ Sci Technol* **2017**, *51*, 1068–1069.

Smith, T. L.; Chu, W. H. Ultimate tensile properties of elastomers. VII. Effect of crosslink density on time–temperature dependence. *J. Polym. Sci. A-2: Polym. Phys.* **1972**, *10*, 133-150.

Souza, P. M. S.; Morales, A. R.; Sanchez, E. M. S.; Mei, L. H. I. Study of PBAT Photostabilization with Ultraviolet Absorber in Combination with Hindered Amine Light

Stabilizer and Vitamin E, Aiming Mulching Film Application. *J. Polym. Environ.* **2018**, *15*, 125.

Spathis, G. Non-Gaussian stress-strain constitutive equation for crosslinked elastomers. *Polymer* **1995**, *36*, 309-313.

Speight, J. G. *The Chemistry and Technology of Petroleum*; Marcel Dekker: New York, 1980.

Stjerndahl, A.; Wistrand, A. F.; Albertsson, A.-C. Industrial Utilization of Tin-Initiated Resorbable Polymers: Synthesis on a Large Scale with a Low Amount of Initiator Residue. *Biomacromolecules* **2007**, *8*, 937–940.

Storey, R. F.; Hickey, T. P. Degradable polyurethane networks based on d,l-lactide, glycolide, ε-caprolactone, and trimethylene carbonate homopolyester and copolyester triols. *Polymer* **1994**, *35*, 830-838.

Storey, R. F.; Warren, S. C.; Allison, C. J.; Wiggins, J. S.; Puckett, A. D. Synthesis of bioabsorbable networks from methacrylate-endcapped polyesters. *Polymer* **1993**, *34*, 4365-4372.

Sun, Z.; Fridrich, B.; de Santi, A.; Elangovan, S.; Barta, K. Bright Side of Lignin Depolymerization: Toward New Platform Chemicals. *Chem. Rev.* **2018**, *118*, 614−678.

Susperregui, N.; Delcroix, D.; Martin-Vaca, B.; Bourissou, D.; Maron, L. Ring-Opening Polymerization of ε-Caprolactone Catalyzed by Sulfonic Acids: Computational Evidence for Bifunctional Activation. *J. Org. Chem.* **2010**, 75, 6581–6587.

T

Tabankia, M. H.; Gardette, J.-L. Photo-oxidation of Block Copoly(Ether-Ester) Thermoplastic Elastomers: Part 2—Origins of the Photo-Yellowing. *Polym. Degrad. Stab.* **1987**, *19*, 113-123.

Tang, X.; Hong, M.; Falivene, L.; Caporaso, L.; Cavallo, L.; Chen, E. Y.-X. *J. Am. Chem. Soc.* **2016**, *138*, 14326-14337.

Tanzi, M. C.; Verderio, P.; Lampugnani, M. G.; Resnati, M.; Dejana, E.; Sturani, E. Cytotoxicity of some catalysts commonly used in the synthesis of copolymers for biomedical use. *J. Mater. Sci. – Mater. Med.* **1994**, 5, 393–396.

Taylor, M. Dumping plastic waste in Asia found destroying crops and health. *Reuters*, April 22, 2019.

Taynton, P.; Ni, H.; Zhu, C.; Yu, K.; Loob, S.; Jin, Y.; Qi, H. J.; Zhang, W. Repairable Woven Carbon Fiber Composites with Full Recyclability Enabled by Malleable Polyimine Networks. *Adv. Mater.* **2016**, *28*, 2904–2909.

Taynton, P.; Yu, K.; Shoemaker, R. K.; Jin, Y.; Qi, H. J.; Zhang, W. Heat- or Water-Driven Malleability in a Highly Recyclable Covalent Network Polymer. *Adv. Mater.* **2014**, *26*, 3938–3942.

Taynton, P.; Zhu, C.; Loob, S.; Shoemaker, R.; Pritchard, J.; Jin, Y.; Zhang, W. Re-healable polyimine thermosets: polymer composition and moisture sensitivity. *Polym. Chem.* **2016**, *7*, 7052–7056.

Teles, J. H.; Hermans, I.; Franz, G.; Sheldon, R. H. Oxidation. In *Ullman's Encyclopedia of Industrial Chemistry*, Wiley-VCH Verlag GmbH & Co. KGaA: Weinheim, Germany, 2015, pp. 1-103.

ten Brink, G.-J.; Arends, W. C. E.; Sheldon, R. *Chem. Rev.* **2004**, *104*, 4105-4123.

Teramoto, N.; Arai, Y.; Shibata, M. Thermo-reversible Diels-Alder polymerization of difurfurylidene trehalose and bismaleimides. *Carbohydr. Polym.* **2006**, *64*, 78–84.

Teuten, E. L.; Saquing, J. M.; Knappe, D. R. U.; Barlaz, M. A.; Jonsson, S.; Björn, A.; Rowland, S. J.; Thompson, R. C.; Galloway, T. S.; Yamashita, R.; Ochi, D.; Watanuki, Y.; Moore, C.; Viet, P. H.; Tana, T. S.; Prudente, M.; Boonyatumanond, R.; Zakaria, M. P.; Akkhavong, K.; Ogata, Y.; Hirai, H.; Iwasa, S.; Mizukawa, K.; Hagino, Y.; Imamura, A.; Saha, M.; Takada, H. Transport and release of chemicals from plastics to the environment and to wildlife. *Philos. Trans. R. Soc., B* **2009**, *364*, 2027−2045.

The New Plastics Economy—Rethinking the future of plastics; World Economic Forum; Ellen MacArthur Foundation and McKinsey & Company: London, 2016.

Themelis, N. J., Mussche, C. 2014 Energy and Economic Value of Municipal Solid Waste (MSW) and Non-Recycled Plastics (NRP) Currently Landfilled in the Fifty States. Columbia University Earth Engineering Center; http://www.seas.columbia.edu/earth/wtert/sofos/2014_Energy_value_of_MSW.pdf (accessed on 9 September 2019).

Thompson, R. C.; Moore, C. J.; vom Saal, F. S.; Swan, S. H. Plastics, the environment and human health: current consensus and future trends. *Phil. Trans. R. Soc., B* **2009**, *364*, 2153–2166.

Tokiwa, Y.; Calabia, B. P.; Ugwu, C. U.; Aiba, S. Biodegradability of Plastics. *Int. J. Mol. Sci.* **2009**, *10*, 3722–3742.

Tokiwa, Y.; Suzuki, T. Hydrolysis of copolyesters containing aromatic and aliphatic ester blocks by lipase. *J. Appl. Polym. Sci.* **1981**, *26*, 441–448.

Tokiwa, Y.; Suzuki, T. Hydrolysis of polyesters by lipases. *Nature* **1977**, *270*, 76–78.

Tokiwa, Y.; Suzuki, T. Hydrolysis of Polyesters by Rhizopus delemar Lipase. *Agric. Biol. Chem.* **1978**, *42*, 1071–1072.

Tran, R. T.; Thevenot, P.; Gyawali, D.; Chiao, J.-C.; Tang, L.; Yang, J. Synthesis and characterization of a biodegradable elastomer featuring a dual crosslinking mechanism. *Soft Matter* **2010**, *6*, 2449-2461.

Turon, X.; Rojas, O. J.; Deinhammer, R. S. *Langmuir* **2008**, *24*, 3880-3887.

Tyagi, P.; Deratani, A.; Quemener, D. Self-Healing Dynamic Polymeric Systems. *Isr. J. Chem.* **2013**, *53*, 53-60.

U

Ueda, M.; Takahashi, M.; Imai, Y. *J. Polym. Sci., Polym. Chem. Ed.* **1979**, *17*, 2477-2482.

United Nations Environmental Programme (UNEP) Valuing Plastic: The business Case for Measuring Managing and Disclosing Plastic Use in the Consumer Goods Industry, 2014.

V

Van Zee, N. J.; Coates, G. W. Alternating Copolymerization of Propylene Oxide with Biorenewable Terpene-Based Cyclic Anhydrides: A Sustainable Route to Aliphatic Polyesters with High Glass Transition Temperatures. *Angew. Chem., Int. Ed.* **2015**, *54*, 2665–2668.

Vert, M.; Doi, Y.; Hellwich, K.-H.; Hess, M.; Hodge, P.; Kubisa, P.; Rinaudo, M.; Schué, F. Terminology for biorelated polymers and applications (IUPAC Recommendations 2012). *Pure Appl. Chem.* **2012**, *84*, 377–410.

W

Wanamaker, C. L.; O'Leary, L. E.; Lynd, N. A.; Hillmyer, M. A.; Tolman, W. B. Renewable-Resource Thermoplastic Elastomers Based on Polylactide and Polymenthide. *Biomacromolecules* **2007**, *8*, 3634-3640.

Wang, C.; Kittle, J. D.; Qian, C.; Roman, M.; Esker, A. R. *Biomacromolecules* **2013**, *14*, 2622-2628.

Wang, Y.; Ameer, G. A.; Sheppard, B. J.; Langer, R. *Nature Biotechnology* **2002**, *20*, 602-606.

Watts, A.; Kurokawa, N; Hillmyer, M. A. *Biomacromolecules*, **2016**, *18*, 1845-1854.

Whiteley, J. M.; Taynton, P.; Zhang, W.; Lee, S. H. Ultra-thin Solid-State Li-Ion Electrolyte Membrane Facilitated by a Self-Healing Polymer Matrix. *Adv. Mater.* **2015**, *27*, 6922–6927.

Wietor, J.-L.; Dimopoulos, A.; Govaert, L. E.; van Benthem, R. A. T. M.; de With, G.; Sijbesma, R. P. Preemptive Healing through Supramolecular Cross-Links. *Macromolecules* **2009**, *42*, 6640-6646.

Wojtecki, R. J.; Meador, M. A.; Rowan, S. J. Using the Dynamic Bond to Access Macroscopically Responsive Structurally Dynamic Polymers. *Nat. Mater.* **2011**, *10*, 14–27.

Wool, R. P. Self-healing Materials: A Review. *Soft Matter* **2008,** *4*, 400-418.

World Economic Forum, Ellen MacArthur Foundation and McKinsey and Company, The New Plastics Economy Rethinking the Future of Plastics; 2016; [report] http://www.ellenmacarthurfoundation.org/publications.

Wu, D. Y.; Meure, S.; Solomon, D. Self-healing polymeric materials: A review of recent developments. *Prog. Polym. Sci.* **2008**, *33*, 479-522.

X

Xiang, H. P.; Qian, H. J.; Lu, Z. Y.; Rong, M. Z.; Zhang, M. Q. Crack Healing and Reclaiming of Vulcanized Rubber by Triggering the Rearrangement of Inherent Sulfur Crosslinked Networks. *Green Chem.* **2015**, *17*, 4315-4325.

Xiang, H. P.; Rong, M. Z.; Zhang, M. Q. Self-healing, Reshaping, and Recycling of Vulcanized Chloroprene Rubber: A Case Study of Multitask Cyclic Utilization of Cross-linked Polymer. *ACS Sustainable Chem. Eng.* **2016,** *4*, 2715-2724.

Xiong, M.; Schneiderman, D. K.; Bates, F. S.; Hillmyer, M. A.; Zhang, K. Scalable production of mechanically tunable block polymers from sugar. *Proc. Natl. Acad. Sci. U. S. A.* **2014**, *111*, 8357−8362.

Y

Yakabi, K.; Mathieux, T.; Milne, K.; López-Vidal, E. M.; Buchard, A.; Hammond, C. *ChemSusChem* **2017**, *10*, 3652-3659.

Yamaguchi, M.; Maeda, R.; Kobayashi, R.; Wada, T.; Ono, S.; Nobukawa, S. Autonomic healing and welding by interdiffusion of dangling chains in a weak gel. *Polym. Int.* **2012**, *61*, 9-16.

Yan, P; Zhao, W.; Wang, Y.; Jiang, Y.; Zhou, C.; Lei, J. Carbon Nanotubes-Polyurethane Vitrimer Nanocomposites with the Ability of Surface Welding Controlled by Heat and Near-Infrared Light. *Macromol. Chem. Phys*. **2017**, *218*, 1700265.

Yan, P.; Zhao, W.; Fu, X.; Liu, Z.; Kong, W.; Zhou, C.; Lei, J. Multifunctional Polyurethane-Vitrimers Completely Based on Transcarbamoylation of Carbamates:

Thermally-Induced Shape Memory Effect and Self-Welding. *RSC Adv.* **2017**, *7*, 26858-26866.

Yang, J.; Lee, S.; Choi, W. J.; Seo, H.; Kim, P.; Kim, G.-J.; Kim, Y.-W.; Shin, J. Thermoset Elastomers Derived from Carvomenthide. *Biomacromolecules* **2015**, *16*, 246-256.

Yang, L.-Q.; He, B.; Meng, S.; Zhang, J.-Z.; Li, M.; Guo, J.; Guan, Y.-M.; Li, J.-X.; Gu, Z.-W. Biodegradable cross-linked poly(trimethylene carbonate) networks for implant applications: Synthesis and properties. *Polymer* **2013**, *54*, 2668-2675.

Yang, W. P.; Macosko, C. W.; Wellinghoff, S. T. Thermal degradation of urethanes based on 4,4′-diphenylmethane diisocyanate and 1,4-butanediol (MDI/BDO). *Polymer* **1986,** *27*, 1235-1240.

Yang, W.; Dong, Q.; Liu, S.; Xie, H.; Liu, L.; Li, J. Recycling and Disposal Methods for Polyurethane Foam Wastes. *Procedia Environ. Sci.* **2012,** *16*, 167–175.

Yang, Y.; Urban, M. W. Self-Healing of Glucose-Modified Polyurethane Networks Facilitated by Damage-Induced Primary Amines. *Polym. Chem.* **2016,** *8*, 303-309.

Ying, H.; Zhang, Y.; Cheng, J. Dynamic Urea Bond for the Design of Reversible and Self-Healing Polymers. *Nat. Commun.* **2014**, *5*, 3218-3227.

Yokouchi, M.; Sakakibara, Y.; Chatani, Y.; Tadokoro, H.; Tanaka, T.; Yoda, K. Structures of Two Crystalline Forms of Poly(butylene terephthalate) and Reversible Transition between Them by Mechanical Deformation. *Macromolecules* **1976**, *9*, 266–273.

Yoshida, S.; Hiraga, K.; Takehana, T.; Taniguchi, I.; Yamaji, H.; Maeda, Y.; Toyohara, K.; Miyamoto, K.; Kimura, Y.; Oda, K. A bacterium that degrades and assimilates poly(ethylene terephthalate). *Science* **2016**, *351*, 1196–1199

Younes, H. M.; Bravo-Grimaldo, E.; Amsden, B. G. *Biomaterials* **2004**, *25*, 5261-5269.

Yu, K.; Taynton, P.; Zhang, W.; Dunn, M. L.; Qi, H. J. Influence of Stoichiometry on the Glass Transition and Bond Exchange Reactions in Epoxy Thermoset Polymers. *RSC Adv.* **2014**, *4*, 48682-48690.

Yu, Y.; Storti, G.; Morbidelli, M. Kinetics of Ring-Opening Polymerization of l,l-Lactide. *Ind. Eng. Chem. Res.* **2011,** *50*, 7927-7940.

Z

Zhang, D.; Dumont, J-M. Reprocessable 5-hydroxymethylfurfural derivative-based thermoset elastomers synthesized through the thiol-Michael and Diels-Alder reactions. *J. Mater. Sci*. **2018**, *53*, 11116–11129.

Zhang, J.; Li, T.; Mannion, A. M.; Schneiderman, D. K.; Hillmyer, M. A.; Bates, F. S. Tough and Sustainable Graft Block Copolymer Thermoplastics. *ACS Macro Lett.* **2016**, *5*, 407-412.

Zhang, X.; Fevre, M; Jones, G. O.; Waymouth, R. M. Catalysis as an Enabling Science for Sustainable Polymers. *Chem. Rev.* **2018**, *118*, 839–885.

Zhang, Y.; Broekhuis, A. A.; Picchioni, F. Thermally Self-Healing Polymeric Materials: The Next Step to Recycling Thermoset Polymers? *Macromolecules* **2009,** *42*, 1906-1912

Zhang, Y.; Tao, L.; Li, S.; Wei, Y. Synthesis of Multiresponsive and Dynamic Chitosan-Based Hydrogels for Controlled Release of Bioactive Molecules. *Biomacromolecules* **2011**, *12*, 2894–2901.

Zhang, Y.; Yang, B.; Zhang, X.; Xu, L.; Tao, L.; Li, S.; Wei, Y. A magnetic self-healing hydrogel. *Chem. Commun.* **2012**, *48*, 9305–9307.

Zhang, Y.; Ying, H.; Hart, K. R.; Wu, Y.; Hsu, A. J.; Coppola, A. M.; Kim, T. A.; Yang, K.; Sottos, N. R.; White, S. R.; Cheng, J. Malleable and Recyclable Poly(urea-urethane) Thermosets Bearing Hindered Urea Bonds. *Adv. Mater.* **2016**, *28*, 7646–7651.

Zhang, Z. P.; Rong, M. Z.; Zhang, M. Q. Polymer engineering based on reversible covalent chemistry: A promising innovative pathway towards new materials and new functionalities. *Prog. Polym. Sci.* **2018**, *80*, 39–93.

Zheng, N.; Fang, Z.; Zou, W.; Zhao, Q.; Xie, T. Thermoset Shape-Memory Polyurethane with Intrinsic Plasticity Enabled by Transcarbamoylation. *Angew. Chem. Int. Ed.* **2016,** *55*, 11421–11425.

Zheng, N.; Hou, J.; Xu, Y.; Fang, Z.; Zou, W.; Zhao, Q.; Xie, T. Catalyst-Free Thermoset Polyurethane with Permanent Shape Reconfigurability and Highly Tunable Triple-Shape Memory Performance. *ACS Macro Lett.* **2017**, *6*, 326-330.

Zheng, P.; McCarthy, T. J. A Surprise from 1954: Siloxane Equilibration Is a Simple, Robust, and Obvious Polymer Self-Healing Mechanism. *J. Am. Chem. Soc.* **2012,** *134*, 2024-2027.

Zia, K. M.; Bhatti, H. N.; Ahmad Bhatti, I. Methods for polyurethane and polyurethane composites, recycling and recovery: A review. *React. Funct. Polym.* **2007,** *67*, 675–692.

Zou, W. K.; Dong, J. T.; Luo, Y. W.; Zhao, Q.; Xie, T. Dynamic Covalent Polymer Networks: from Old Chemistry to Modern Day Innovations. *Adv. Mater*. **2017**, *29*, 1606100.

Zumstein, M. T.; Kohler, H.-P. E.; McNeill, K.; Sander, M. Enzymatic Hydrolysis of Polyester Thin Films: Real-Time Analysis of Film Mass Changes and Dissipation Dynamics. *Environ. Sci. Technol.* **2016**, *50*, 197–206.

Zumstein, M. T.; Kohler, H.-P. E.; McNeill, K.; Sander, M. High-Throughput Analysis of Enzymatic Hydrolysis of Biodegradable Polyesters by Monitoring Cohydrolysis of a Polyester-Embedded Fluorogenic Probe. *Environ. Sci. Technol.* **2017**, *51*, 4358–4367.

Zumstein, M. T.; Rechsteiner, D.; Roduner, N.; Perz, V.; Ribitsch, D.; Guebitz, G. M.; Kohler, H.-P. E.; McNeill, K.; Sander, M. Enzymatic Hydrolysis of Polyester Thin Films at the Nanoscale: Effects of Polyester Structure and Enzyme Active-Site Accessibility. *Environ. Sci. Technol.* **2017**, *51*, 7476–7485.

Zumstein, M. T.; Schintlmeister, A.; Nelson, T. F.; Baumgartner, R.; Woebken, D.; Wagner, M.; Kohler, H.-P. E.; McNeill, K.; Sander, M. Biodegradation of synthetic polymers in soils: Tracking carbon into CO_2 and microbial biomass. *Sci. Adv.* **2018**, *4*, eaas9024.

Appendix A. Rigid, Reprocessable Polyester Networks with Imine Cross-links

A.1. Introduction

There are many examples of thermosets which leverage dynamic covalent chemistry to circumvent the problem that plagues thermoset recycling: network architectures preclude dissolution and flow at elevated temperatures. Many dynamic bonds have been explored (described briefly in **Chapter 1**), but few reports focus on improving the sustainable characteristics of the networks. We identified the alternating copolymerization of epoxides and cyclic anhydrides as an excellent platform for the synthesis of polyesters with chemical handles which could be used for cross-linking post-polymerization.[1,2,3] In particular, vanillin glycidyl ether (VGE) was chosen as a bio-based monomer which would ultimately be used to create polyesters with pendant aldehydes; these prepolymers could then be reacted with multifunctional amines to yield imine cross-linked networks (**Figure A.1.)**. The networks would be reprocessable due to imine exchange but also potentially biodegradable by virtue of the ester bonds present.

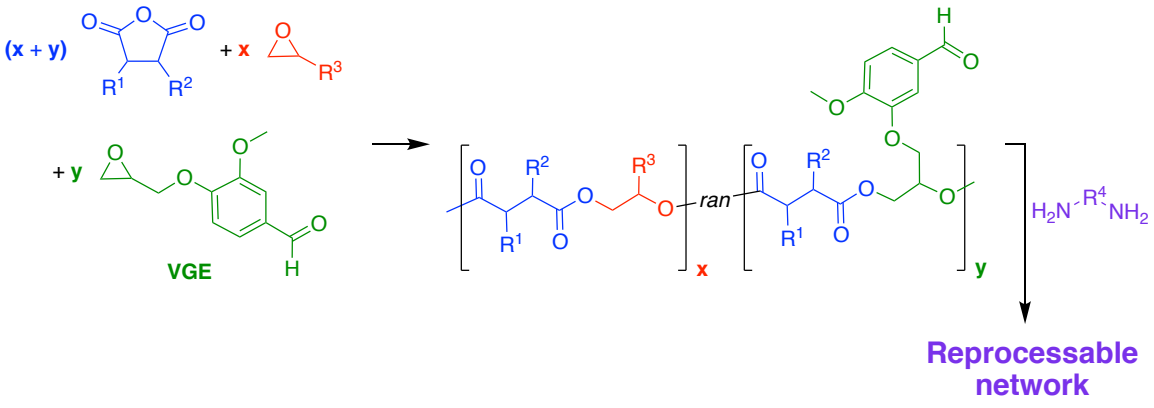

Figure A.1. Scheme depicting the production and cross-linking of polyesters with pendant aldehydes, which are incorporated using vanillin glycidyl ether (VGE).

Imine exchange can be catalyzed by small amounts of residual primary amine (from the equilibrium of imine formation)[4,5,6,7] and therefore does require addition of an exogenous metal catalyst. Omission of added catalysts is convenient synthetically but also avoids potential issues which can hinder long-term reprocessability of dynamic materials with embedded catalysts (i.e., leaching or deactivation). Previous reprocessable imine-linked materials include small molecule networks,[8,9,10,11,12,13] PEG and chitosan-based hydrogels,[14,15,16] polythiophene-derived materials,[17] or polyacrylate[18] or PMDS imine-linked networks.[19] To the best of our knowledge, no high-T_g polyester imine crosslinked networks have been reported to date. The broad monomer scope available to our selected polymerization platform allows for tunability of the bio-based content and various physical properties such as the glass transition temperature. Among the list of available monomers, tricyclic anhydrides and epoxides containing aromatic or cyclic functionalities have been shown to yield high glass transition polymers and are accessible from bio-based and/or petroleum-derived precursors. Herein, we present initial work on reprocessable imine-crosslinked polyester networks derived from high-T_g prepolymers made from tricyclic anhydrides, vanillin glycidyl ether, and epoxide comonomers.

A.2. Summary of Initial Work

We chose to first investigate the CPMA/PO/VGE system because CPMA and PO are easily purchased and polymerized (**Figure A.2.**). After initial successes with material synthesis—indeed, reacting prepolymer and diamine afforded insoluble yet reprocessable materials—we sought to systematically vary the VGE content in the polymer and determine whether or not we could tune the dynamic behavior. Initial results were promising: lower %VGE resulted in slower stress-relaxation without changing the

activation energy. However, we found that reproducing this trend was unsuccessful. Ultimately, it seems systems with *ca.* 15, 25, 40 mol% VGE seem to relax stress at similar rate with similar activation energies. In reproducing the *ca.* 15, 25, 40 mol% VGE samples, we also found that the gel fraction of samples with < 40 %VGE is close to zero, indicating that you need significant VGE incorporation to get an insoluble network.

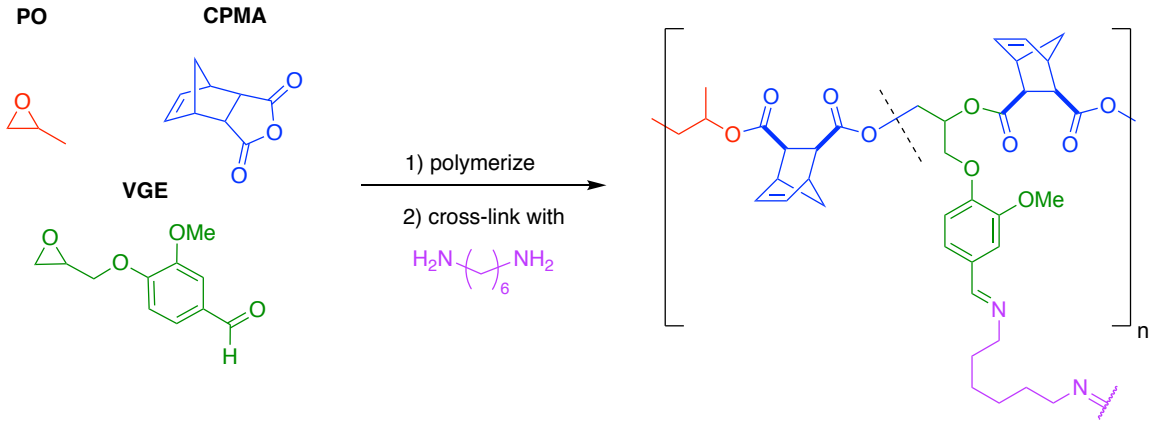

Figure A.2. Scheme depicting the production and cross-linking of polyesters derived from propylene oxide (PO), the tricyclic anhydride derived from cyclopentadiene and maleic anhydride (CPMA), and vanillin glycidyl ether (VGE).

The results obtained using CPMA/PO/VGE-based networks were also consistent with experiments involving other epoxide/anhydride systems (**Figure A.3.**); these systems have > 40% VGE and can reproducibly afford a gel fraction closer to 1. Although TMA and PCA-containing polymers afford insoluble materials with characteristic imine signals in the IR spectra, these materials are sometimes non-reprocessable! Consequently, tensile bars cannot be made and stress-relaxation is not measurable. For the TMA and PCA-based materials that are reprocessable, we observed that the relaxation times and activation energies were similar to those of CPMA/PO-based materials. So, it seems that across the board (i.e., %VGE content, different anhydrides/epoxides), *if the material is reprocessable*, we reproducibly observe characteristic relaxation times on the order of 10-100 seconds and

activation energies of *ca.* 70-80 kJ/mol. Furthermore, the reprocessable materials only have a high gel fraction (i.e., approaching 1) if the VGA content is ≥ 40 mol%.

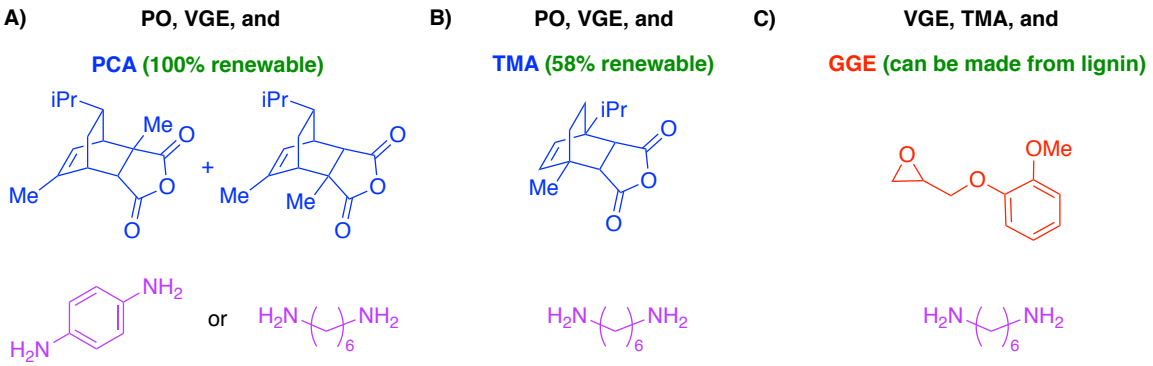

Figure A.3. Scheme depicting the various monomer systems used to make prepolymers including: A) PO, VGE, and the tricyclic anhydride derived from α-phellandrene and citraconic anhydride (PCA), B) PO, VGE, and the tricyclic anhydride derived α-terpinene and maleic anhydride (TMA), and C) VGE, TMA, and guaiacol glycidyl ether (GGE).

To compare our activation energies for the polymeric systems with a model system, we performed small-molecule exchange studies and monitored the results by ^{1}H NMR spectroscopy. We found that the imine exchange was so rapid that the kinetics had to be investigated at ≤ 0 °C. The small-molecule activation energy for imine exchange was 37 ± 2 kJ/mol—approximately half of what we measured for the polymers; one possibility for the higher activation energy of the polymers is that the imine exchange is so fast that segmental motion is limiting flow at high T.

A.3. References

[1] Van Zee, N. J.; Coates, G. W. Alternating Copolymerization of Propylene Oxide with Biorenewable Terpene-Based Cyclic Anhydrides: A Sustainable Route to Aliphatic Polyesters with High Glass Transition Temperatures. *Angew. Chem., Int. Ed.* **2015**, *54*, 2665–2668.

[2] Sanford, M. J.; Peña Carrodeguas, L.; Van Zee, N. J.; Kleij, A. W.; Coates, G. W. Alternating Copolymerization of Propylene Oxide and Cyclohexene Oxide with Tricyclic Anhydrides: Access to Partially Renewable Aliphatic Polyesters with High Glass Transition Temperatures. *Macromolecules* **2016**, *49*, 6394–6400.

[3] Sanford, M. J.; Van Zee, N. J.; Coates, G. Reversible-deactivation anionic alternating ring-opening copolymerization of epoxides and cyclic anhydrides: access to orthogonally functionalizable multiblock aliphatic polyesters. *Chemical Science* **2018**, *9*, 134–142.

[4] Chao, A.; Negulescu, I.; Zhang, D. Dynamic Covalent Polymer Networks Based on Degenerative Imine Bond Exchange: Tuning the Malleability and Self-Healing Properties by Solvent. *Macromolecules* **2016**, *49*, 6277–6284.

[5] Ciaccia, M.; Cacciapaglia, R.; Mencarelli, P.; Mandolini, L.; Di Stefano, S. Fast transimination in organic solvents in the absence of proton and metal catalysts. A key to imine metathesis catalyzed by primary amines under mild conditions. *Chem. Sci.* **2013**, *4*, 2253–2261.

[6] Ciaccia, M.; Di Stefano, S. Mechanisms of imine exchange reactions in organic solvents. *Org. Biomol. Chem.* **2015**, *13*, 646–654.

[7] Ciaccia, M.; Pilati, S.; Cacciapaglia, R.; Mandolini, L.; Di Stefano, S. Effective catalysis of imine metathesis by means of fast transiminations between aromatic-aromatic or aromatic-aliphatic amines. *Org. Biomol. Chem.* **2014**, *12*, 3282–3287.

[8] Taynton, P.; Ni, H.; Zhu, C.; Yu, K.; Loob, S.; Jin, Y.; Qi, H. J.; Zhang, W. Repairable Woven Carbon Fiber Composites with Full Recyclability Enabled by Malleable Polyimine Networks. *Adv. Mater.* **2016**, *28*, 2904–2909.

[9] Taynton, P.; Yu, K.; Shoemaker, R. K.; Jin, Y.; Qi, H. J.; Zhang, W. Heat- or Water-Driven Malleability in a Highly Recyclable Covalent Network Polymer. *Adv. Mater.* **2014**, *26*, 3938–3942.

[10] Whiteley, J. M.; Taynton, P.; Zhang, W.; Lee, S. H. Ultra-thin Solid-State Li-Ion Electrolyte Membrane Facilitated by a Self-Healing Polymer Matrix. *Adv. Mater.* **2015**, *27*, 6922–6927.

[11] Li, H.; Bai, J.; Shi, Z.; Yin, J. Environmental friendly polymers based on schiff-base reaction with self-healing, remolding and degradable ability. *Polymer* **2016**, *85*, 106–113.

[12] Taynton, P.; Zhu, C.; Loob, S.; Shoemaker, R.; Pritchard, J.; Jin, Y.; Zhang, W. Re-healable polyimine thermosets: polymer composition and moisture sensitivity. *Polym. Chem.* **2016**, *7*, 7052–7056.

[13] Chao, A.; Negulescu, I.; Zhang, D. Dynamic Covalent Polymer Networks Based on Degenerative Imine Bond Exchange: Tuning the Malleability and Self-Healing Properties by Solvent. *Macromolecules* **2016**, *49*, 6277–6284.

[14] Zhang, Y.; Tao, L.; Li, S.; Wei, Y. Synthesis of Multiresponsive and Dynamic Chitosan-Based Hydrogels for Controlled Release of Bioactive Molecules. *Biomacromolecules* **2011**, *12*, 2894–2901.

[15] Zhang, Y.; Yang, B.; Zhang, X.; Xu, L.; Tao, L.; Li, S.; Wei, Y. A magnetic self-healing hydrogel. *Chem. Commun.* **2012**, *48*, 9305–9307.

[16] Deng, G.; Tang, C.; Li, F.; Jiang, H.; Chen, Y. Covalent Cross-Linked Polymer Gels with Reversible Sol−Gel Transition and Self-Healing Properties. *Macromolecules* **2010**, *43*, 1191–1194.

[17] Ahner, J.; Micheel, M.; Geitner, R.; Schmitt, M.; Popp, J.; Dietzek, B.; Hager, M. D. Self-healing Functional Polymers: Optical Property Recovery of Conjugated Polymer Films by Uncatalyzed Imine Metathesis. *Macromolecules* **2017**, *50*, 3789–3795.

[18] Lei, Z. Q.; Xie, P.; Rong, M. Z.; Zhang, M. Q. Catalyst-free dynamic exchange of aromatic Schiff base bonds and its application to self-healing and remolding of crosslinked polymers. *J. Mater. Chem. A* **2015**, *3*, 19662–19668.

[19] Kathan, M.; Kovaříček, P.; Jurissek, C.; Senf, A.; Dallmann, A.; Thünemann, A. F.; Hecht, S. Control of Imine Exchange Kinetics with Photoswitches to Modulate Self-Healing in Polysiloxane Networks by Light Illumination. *Angew. Chem., Int. Ed.* **2016**, *55*, 13882–13886.

Appendix B. Mineralization of Poly(4-methylcaprolactone) Elastomers

B.1. Introduction

The enzymatic hydrolysis experiments described in **Chapter 4** showed great promise toward the ultimate biodegradation of elastomers derived from poly(4-methylcaprolactone). These results were obtained *in vitro* with purified enzymes, and thus can only be considered a successful demonstration of *potential* for biodegradation. Therefore, the next steps to provide a solid case for the biodegradability of poly(4-methylcaprolactone) would be to monitor the degradation of the materials in systems where microorganisms are present, such as natural soils or composts.

Typically, biodegradation experiments which assess mineralization (defined in **Chapter 1**) are performed using respirometric techniques: CO_2 evolution or O_2 consumption by microorganisms.[1] The former provides a direct measurement of the carbon which leaves the system by virtue of microbial activity, whereas the latter provides an indirect measure of mineralization. Neither of these techniques provides a direct measurement of the proportion of carbon which remains as the analyte (i.e., residual material) versus the carbon which has been assimilated into the microorganism (i.e., biomass); it is therefore not possible to provide closed mass balances on the carbon introduced to the system.[2,3] Furthermore, significant error is introduced if the analyte mineralizes slowly because there are other sources of organic matter in the soils which are also being mineralized concurrently.[4]

The methods which are being used to circumvent these challenges involve isotopically-labeled substrates, typically using ^{14}C or ^{13}C-enriched (macro)molecules.[1,2,3] Of these two, the use of ^{13}C-enriched analytes is preferred because they are not radioactive.[3] The amount of $^{13}CO_2$ formed is therefore strictly from polymer mineralization and is independent from that of soil organic matter. The $^{13}CO_2$ can be measured using gas chromatography coupled to mass spectrometry or cavity ring down spectroscopy.[3] Furthermore, the remaining ^{13}C in the system can be investigated by soil combustion (for residual analyte) and extraction or microscopy techniques (for assimilated biomass).[3] The use of ^{13}C-labeled substrates therefore provides a promising approach to systematic investigations of ultimate biodegradation across different soil types and microorganisms; furthermore, these labels can be placed at specific positions in the analyte to determine which carbon atoms are more readily mineralized.

We sought to build upon our previous work by investigating the ultimate biodegradation of poly(4-methylcaprolactone)-based materials using the ^{13}C-labeling approach. Our previous studies were performed in the absence of microorganisms, which allowed us to isolate and characterize the enzymatic hydrolysis products by NMR spectroscopy; we found that all of the poly(4-methylcaprolactone)-based elastomers were degraded into the monomeric subunit: 6-hydroxy-4-methylhexanoic acid. Given these findings, we designed synthetic routes to two ^{13}C-labeled variants of 6-hydroxy-4-methylhexanoic acid in order to probe the mineralization of the carbon atoms at multiple positions. The substrates will then be placed in incubation vessels containing natural soils, and the evolution of $^{13}CO_2$ will be measured by cavity ring down spectroscopy (**Figure B.1**). We opted to focus on the monomeric substrate rather than ^{13}C-labeled polymer for

two reasons: 1) the desired overall ^{13}C-enrichment of the analyte could be easily tuned by mixing pure ^{12}C-variant with varying amounts of ^{13}C-variant, and 2) extra (co)polymerization steps were avoided.

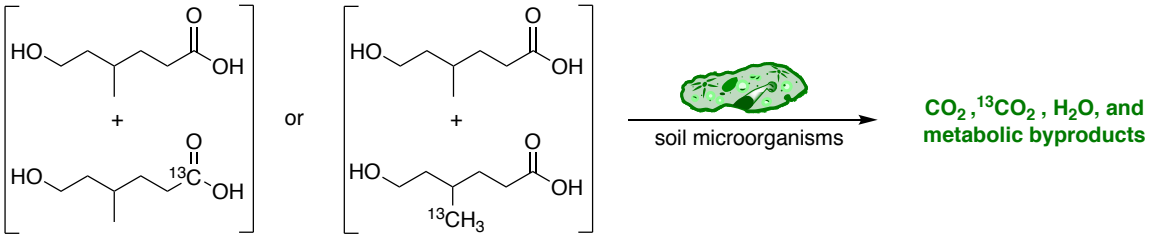

Figure B.1. The mineralization of two ^{13}C-labeled variants of 6-hydroxy-4-methylhexanoic acid; the ^{12}C-variant is mixed with the ^{13}C-variant to achieve the desired overall ^{13}C-enrichment for the analyte.

B.2. Synthesis of Isotopically-labeled 6-hydroxy-4-methylhexanoic acid

The mineralization of carbon in the substrate is expected to proceed more rapidly for carbon atoms that are readily amenable to metabolic pathways within the microorganism, such as those adjacent to the ester bond. Therefore, the first target ^{13}C-labeled compound was **1a**, and the proposed synthetic routes employed a Grignard reaction with $^{13}CO_2$ to install the isotopic label (**Figure B.2**). As Grignard reagents will readily deprotonate hydroxyl groups, a tetrahydropyranyl ether was used and would be removed after the installation of the carboxylic acid. The starting material, 3-methyl-1,5-pentanediol (**MPD**), is commercially available.

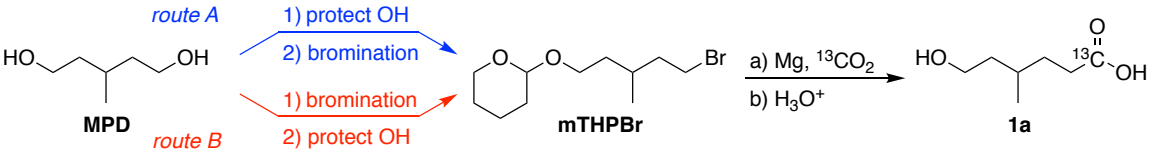

Figure B.2. Proposed scheme for the synthesis of ^{13}C-labeled 6-hydroxy-4-methylhexanoic acid

For the bromination and protection steps, we presumed that the separation of mono- and di-brominated products would be slightly more difficult than mono- and di-protected products and therefore elected to pursue route A. The protection was performed using 3,4-dihydropyran and catalytic tosic acid in dry ether at room temperature; this reaction provided mono-protected product (**mTHP**) in 47% yield after purification via column chromatography. Bromination was achieved using an Appel reaction and the mono-protected alkyl bromide (**mTHPBr**) was obtained in 75% yield. The Grignard reaction was to be performed with ^{13}C-enriched CO_2, but this reagent is expensive and thus trial runs were performed using bone dry CO_2 gas; conversion of the alkyl bromide to the Grignard reagent was repeatedly successful but its reaction with the CO_2 to achieve the carboxylate failed in our hands. A trial was also done with a *tert*-butyl-dimethyl-silyl-protected alkyl bromide (**mTBDMSBr**); again, Grignard reagent formation was observed but carboxylation was unsuccessful (**Figure B.3**). Therefore, a new synthetic route was proposed which employed nucleophilic substitution of the bromide with a cyano group; conversion to the carboxylic acid could then be done under basic or acidic conditions (**Figure B.4**).

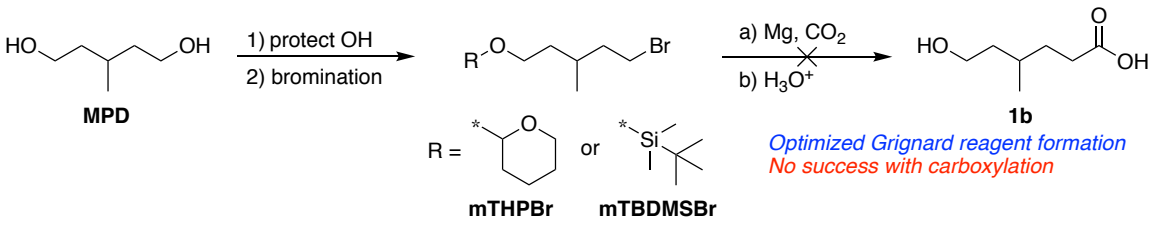

Figure B.3. Scheme depicting the two alkyl bromides which were unsuccessfully converted into 6-hydroxy-4-methylhexanoic acid (**1b**).

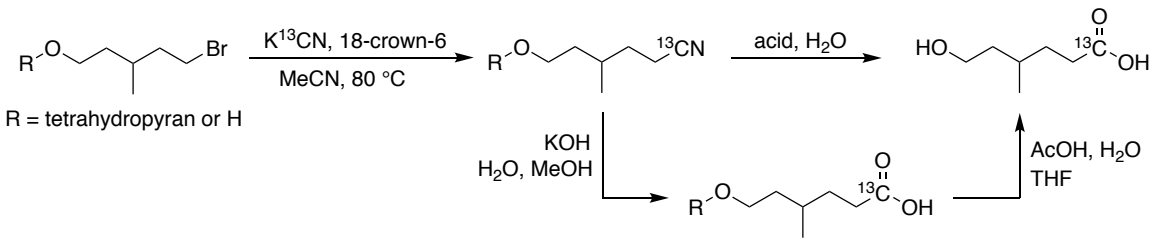

Figure B.4. Proposed scheme for the synthesis of ^{13}C-labeled 6-hydroxy-4-methylhexanoic acid using isotopically enriched potassium cyanide.

Again, due to the high cost of isotopically enriched substances, each reaction was first optimized using normal (i.e., ^{12}C) reagents and compounds. The cyanation was attempted with **mTHPBr** as well as the mono-brominated alcohol produced directly from **MPD**. The reaction of KCN with **mTHPBr** proceeded much more cleanly than with the bromo-alcohol; therefore, the synthesis was continued with the THP-protected cyano compound (**mTHPCN** or **mTHP^{13}CN**), which could be produced in 38% yield. The one-step acid-catalyzed hydrolysis of **mTHPCN** was attempted several times but was ultimately unsuccessful; the deprotection of the alcohol occurred much more readily than the hydrolysis of the cyano group, which required harsher conditions but resulted in a dark brown viscous liquid presumed to be a mix of polymeric and degraded compounds. We therefore switched to a more careful route involving the base-catalyzed hydrolysis of the cyano group, which preserves the protecting group, followed by deprotection of the crude product under acidic conditions. This sequence was successful, and the final compounds **1a** and **1b** were purified using column chromatography. A summary of the reaction conditions and isolated yields of all compounds is shown below in **Figure B.5**.

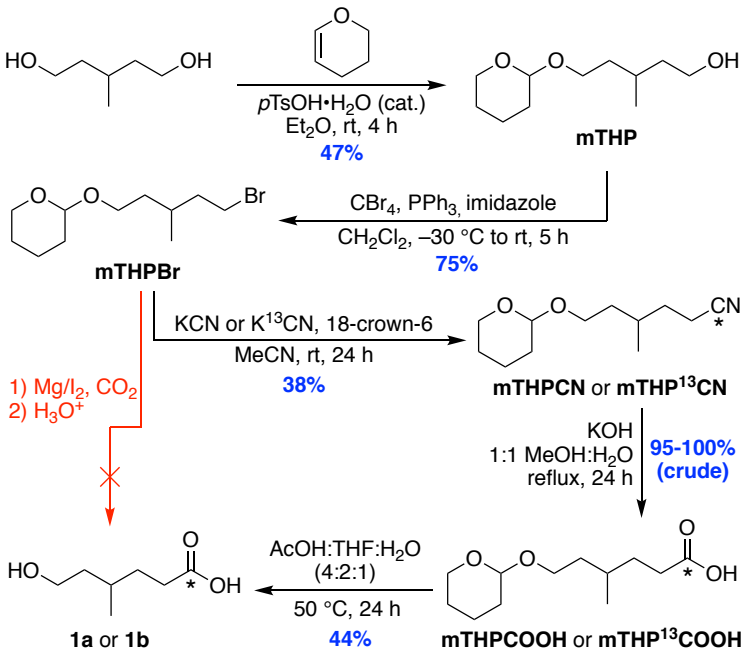

Figure B.5. A summary of the reactions and associated yields for the synthesis of **1a** and **1b**.

Compounds **1a** and **1b** were characterized using IR spectroscopy, gas chromatography, mass spectrometry, and NMR spectroscopy. The IR spectra of both compounds are shown in **Figure B.6**; prominent peaks including those arising from the hydroxyl and carboxyl moieties are listed in the figure caption. The gas chromatography results indicated some minor peaks for both compounds (**Figure B.7**). One of the minor impurities was indentified as trace lactone arising from esterification of the hydroxy-acid; the elution time and extracted mass spectrum for each minor peak agreed well with a separate analysis of pure 4-methyl caprolactone. The other, broad minor peaks were not definitively attributable to a particular impurity. Analysis of **1a** and **1b** by electrospray ionization time-of-flight mass spectrometry yielded experimental *m*/*z* values close to the theoretical values: Calculated for $C_6{}^{13}CH_{14}NaO_3^+$ 170.0869 and for $C_7H_{14}NaO_3^+$ 169.0835, respectively found 170.0864 (–2.94 ppm) and 169.0830 (–2.96 ppm). The ^1H and ^{13}C NMR

spectroscopy results are consistent with the expected resonances from **1a** and **1b** (**Figure B.8**, **Figure B.9**, **Figure B.10**, **Figure B.11**, **Figure B.12**, and **Figure B.13**). Due to the high isotopic enrichment at the carbonyl position of **1a**, trace amounts of lactone and putative dimer are also visible (see insets in **Figure B.11**); the signals at ca. 176 and ca. 174 ppm agree well with carbonyl (ester) signals observed in separate analyses of 4-methylcaprolactone and poly(4-methylcaprolactone), respectively. A purity analysis using quantitative ^{1}H-NMR spectroscopy in $CDCl_3$ with an internal standard (dimethyl sulfone) indicated that both compounds were ≥ 95% pure by mass (**Figure B.14** and **Figure B.15**).

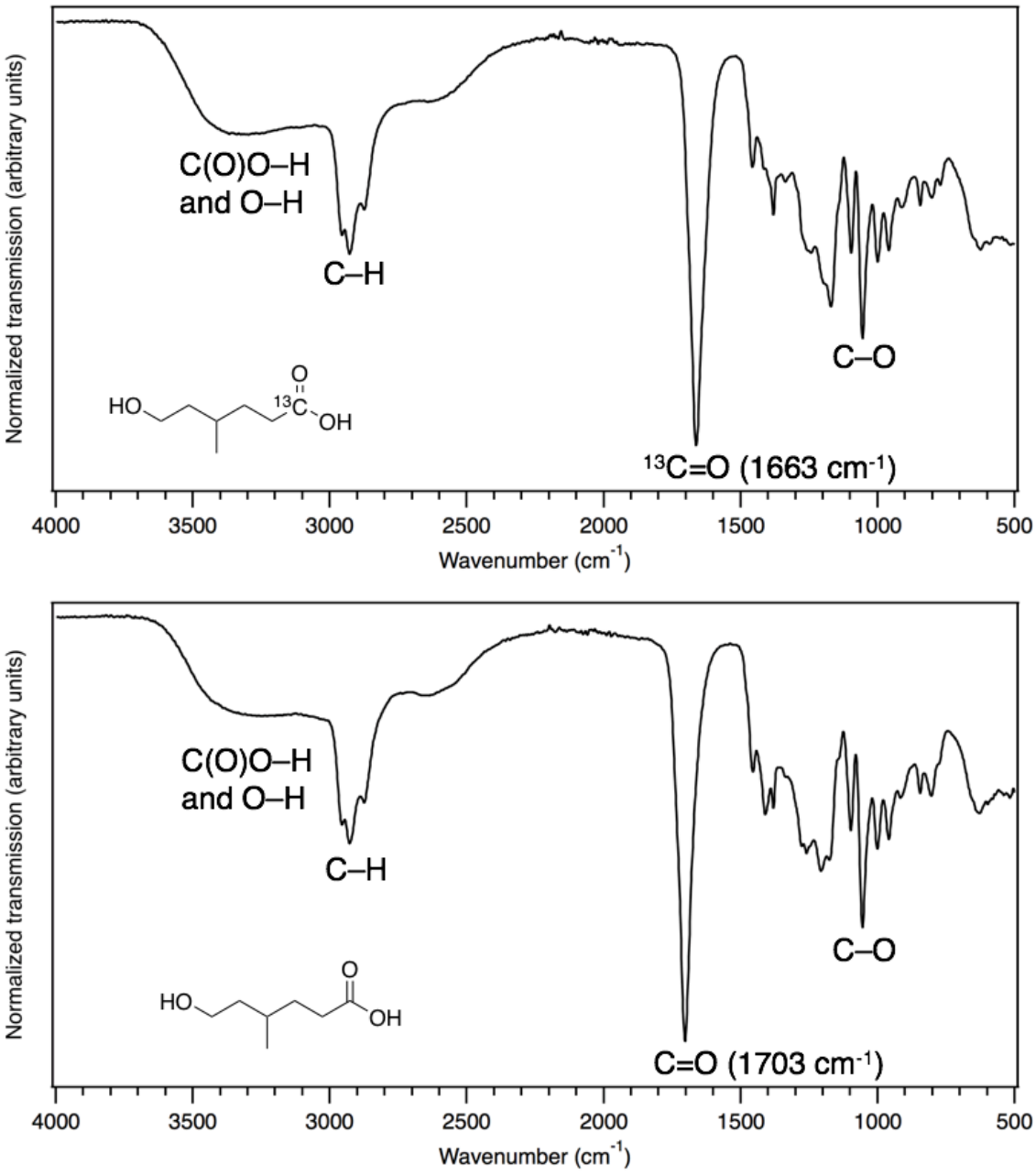

Figure B.6. IR spectroscopy of **1a** (top) and **1b** (bottom). Selected signals for **1a**: 3296, 2928, 2874, 1663, and 1055 cm^{-1}. Selected signals for **1b**: 3296, 2928, 2874, 1703, and 1055 cm^{-1}.

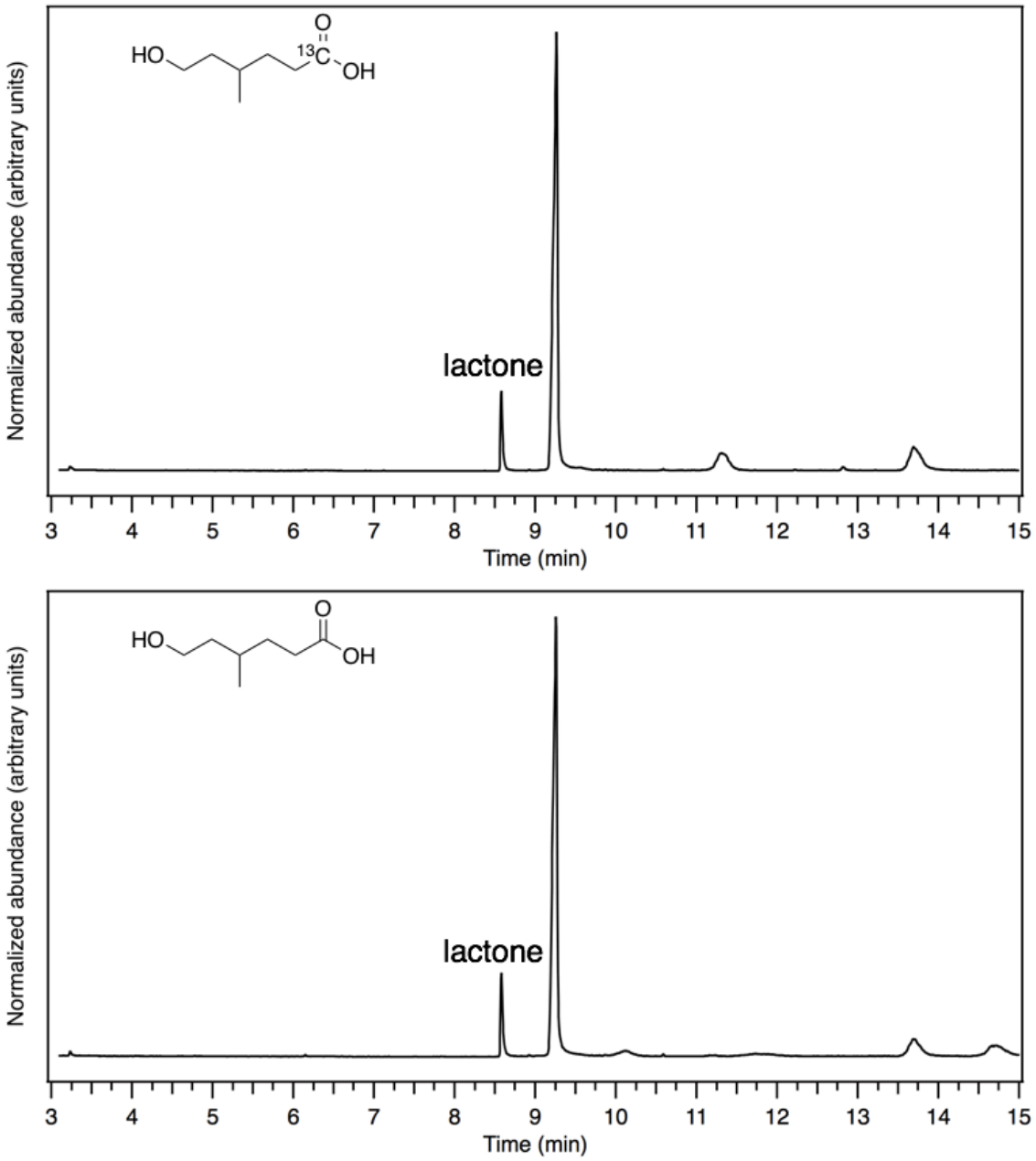

Figure B.7. Gas chromatography results for purified **1a** (top) and **1b** (bottom).

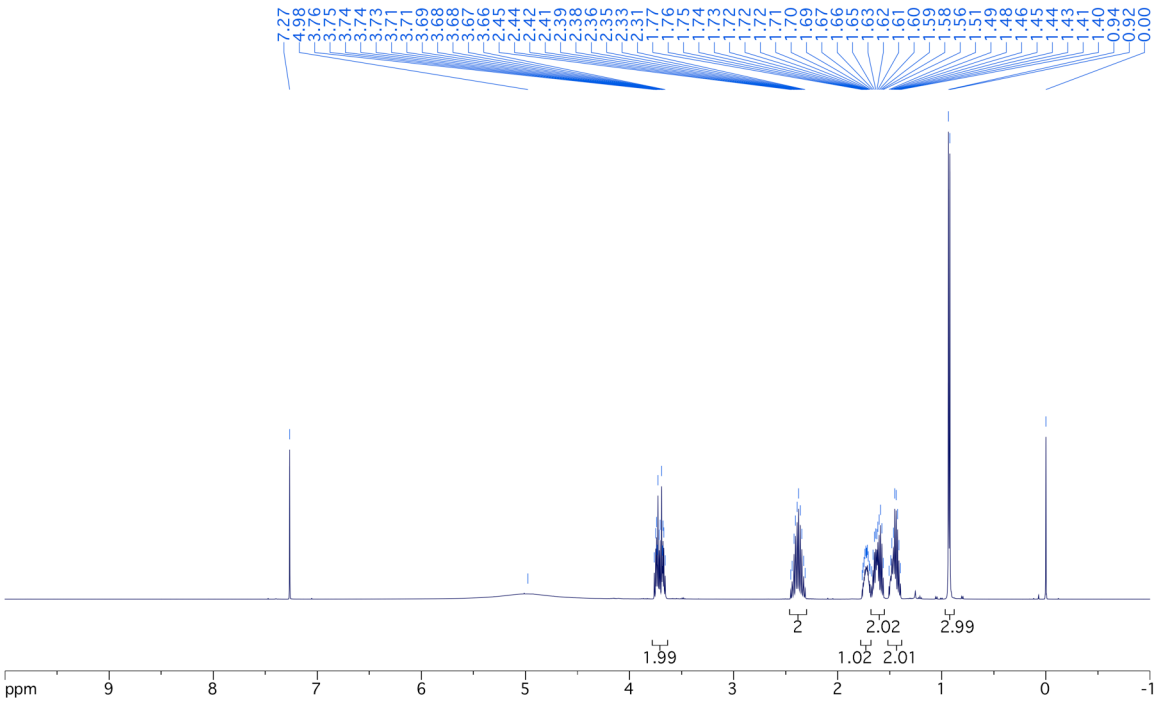

Figure B.8. ^{1}H NMR spectrum (500 MHz) of **1a** in $CDCl_3$: δ 3.76-3.66 (m, 2H), 2.45-2.31 (m, 2H), 1.77-1.69 (m, 1H), 1.67-1.56 (m, J = 6.1 Hz, 2H), 1.51-1.40 (m, 2H), 0.93 (d, J = 6.5 Hz, 3H).

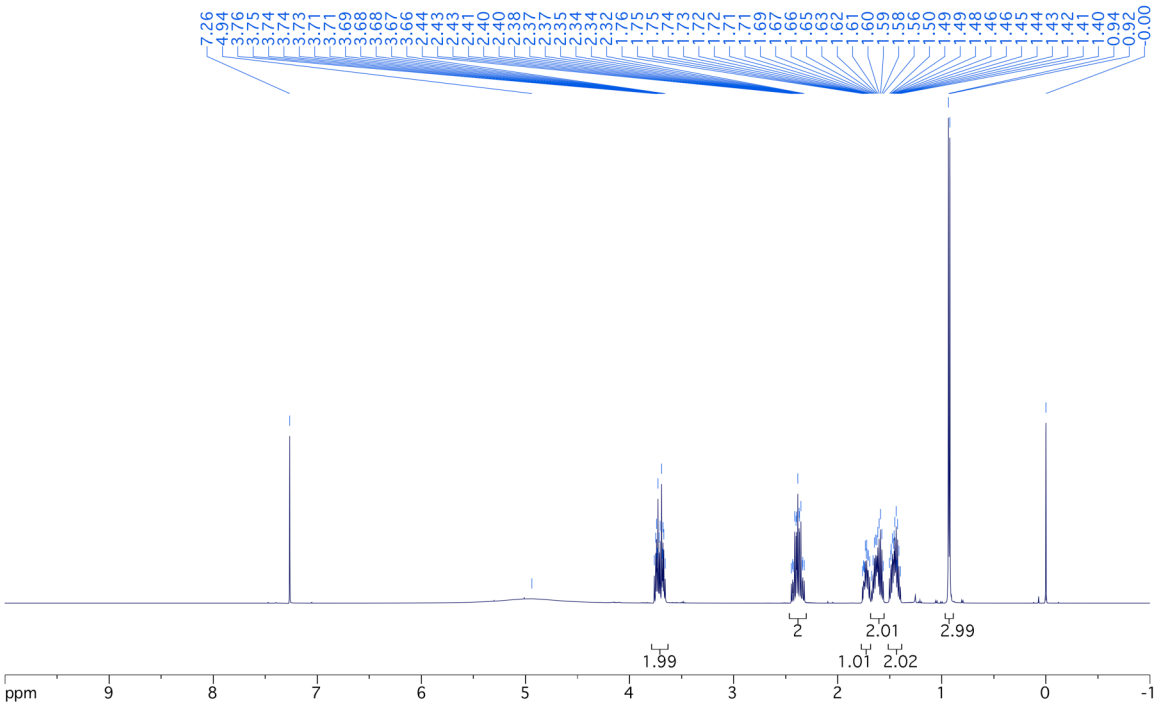

Figure B.9. ^{1}H NMR spectrum (500 MHz) of **1b** in $CDCl_3$: δ 3.76-3.66 (m, 2H), 2.32-2.44 (m, 2H), 1.76-1.69 (m, 1H), 1.67-1.56 (m, J = 6.1 Hz, 2H), 1.50-1.40 (m, 2H), 0.93 (d, J = 6.5 Hz, 3H).

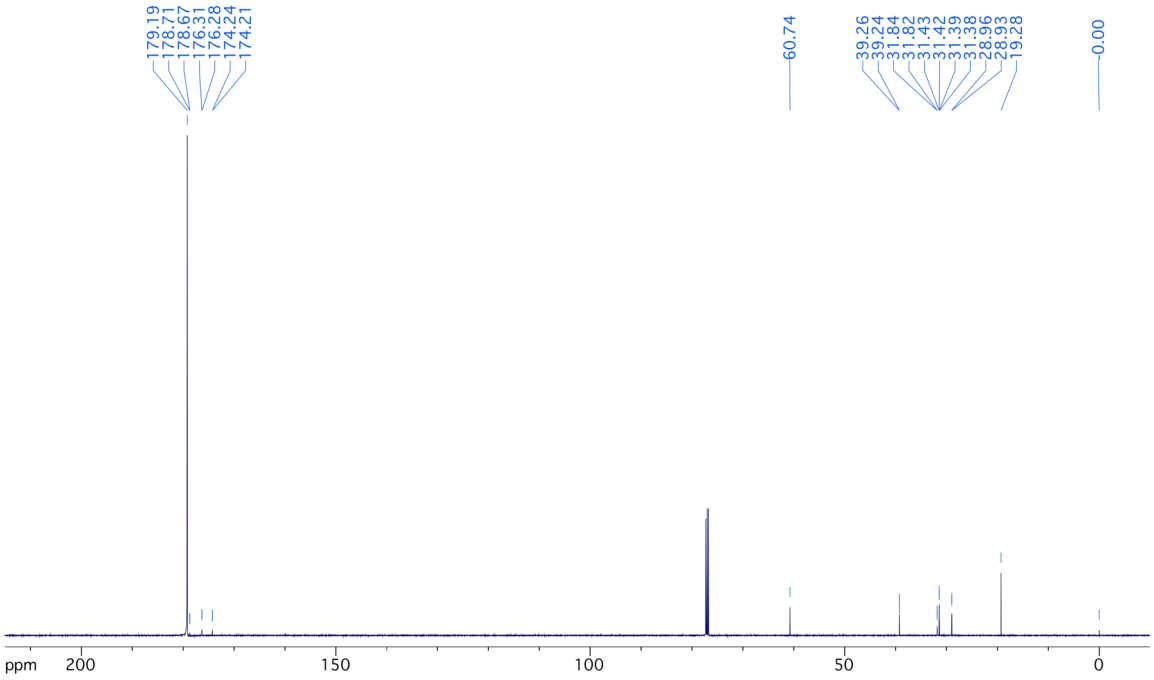

Figure B.10. ^{13}C NMR spectrum (125 MHz) of **1a** in $CDCl_3$: δ 179.2, 60.7, 39.24, 39.26, 31.84, 31.82, 31.43, 31.42, 31.39, 31.38, 28.96, 28.93, 19.28.

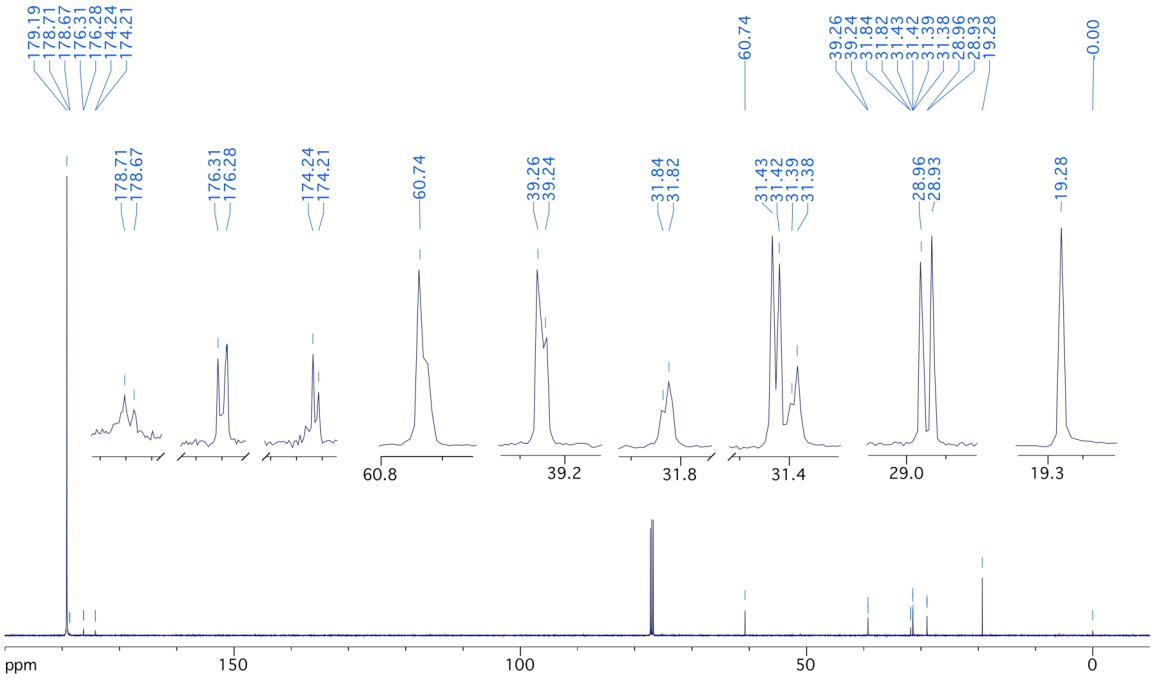

Figure B.11. ^{13}C NMR spectrum (125 MHz) of **1a** in $CDCl_3$ with insets: δ 179.2, 60.7, 39.24, 39.26, 31.84, 31.82, 31.43, 31.42, 31.39, 31.38, 28.96, 28.93, 19.28.

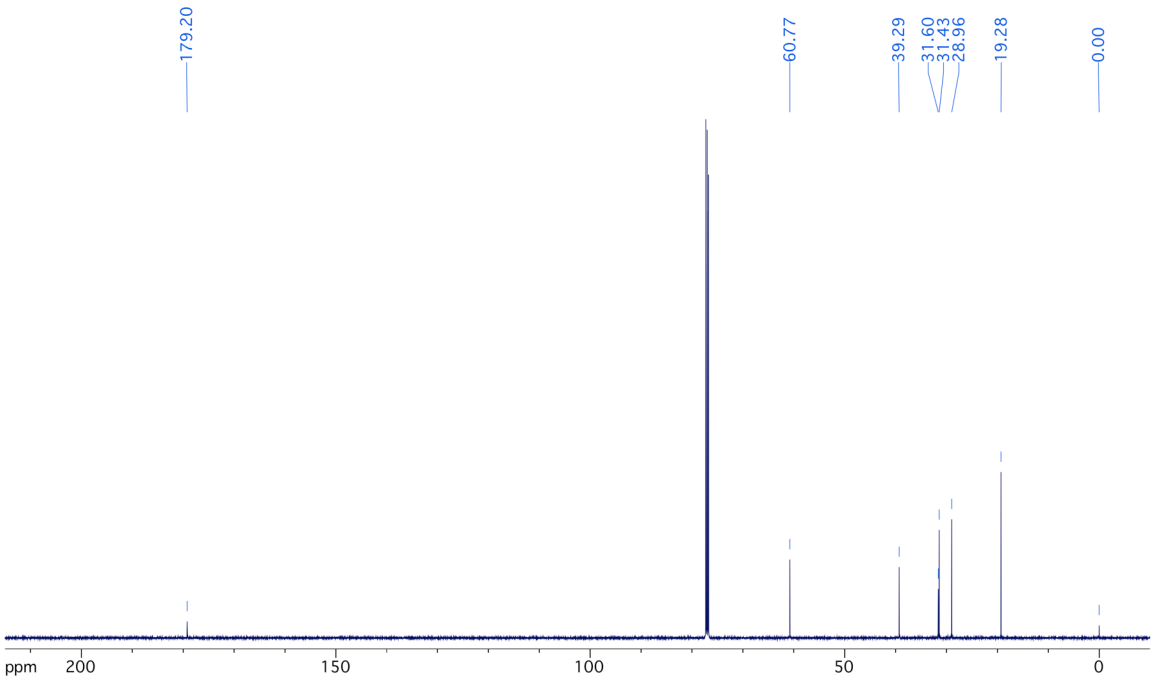

Figure B.12. ^{13}C NMR spectrum (125 MHz) of **1b** in $CDCl_3$: δ 179.2, 60.8, 39.3, 31.60, 31.43, 28.96, 19.28.

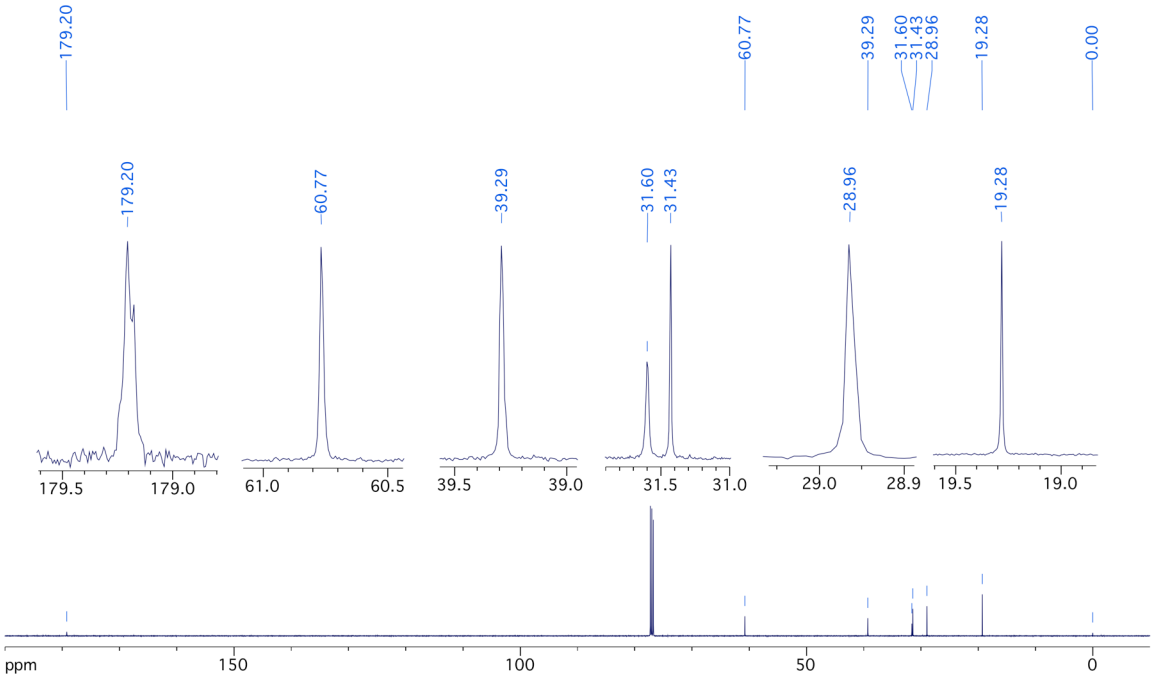

Figure B.13. ^{13}C NMR spectrum (125 MHz) of **1b** in $CDCl_3$ with insets: δ 179.2, 60.8, 39.3, 31.60, 31.43, 28.96, 19.28.

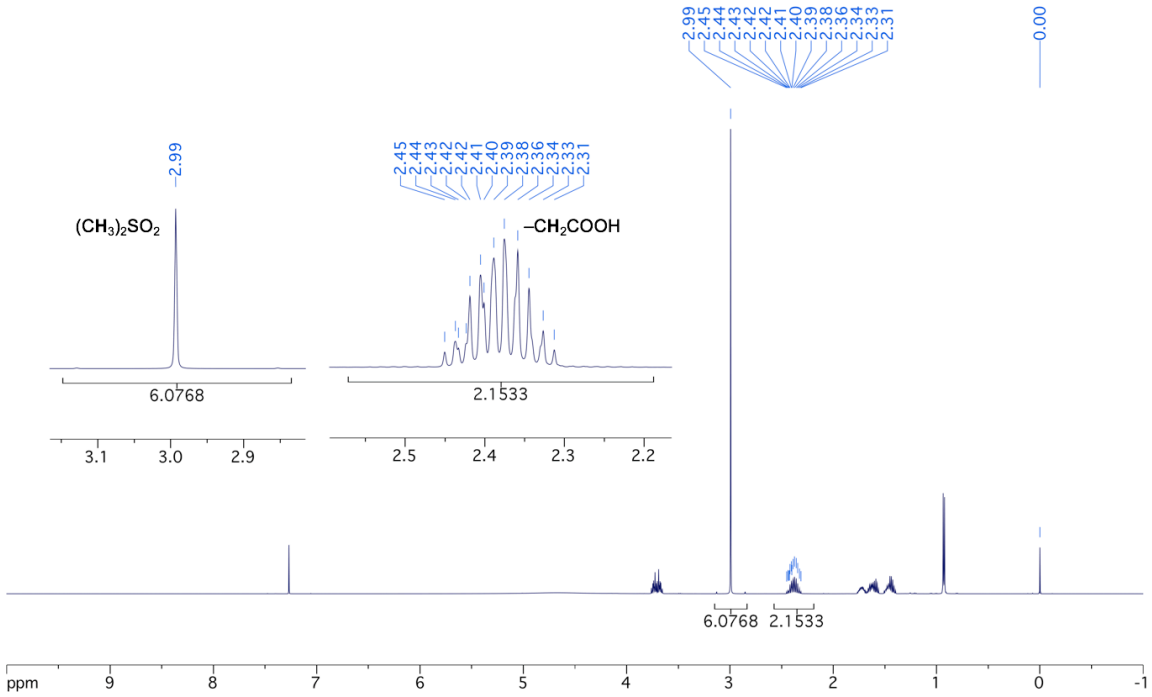

Figure B.14. ^{1}H NMR spectrum (500 MHz) of **1a** and dimethyl sulfone in $CDCl_3$; both integrations include ^{13}C satellites and purity calculations indicate that **1a** is ≥ 94.8% pure.

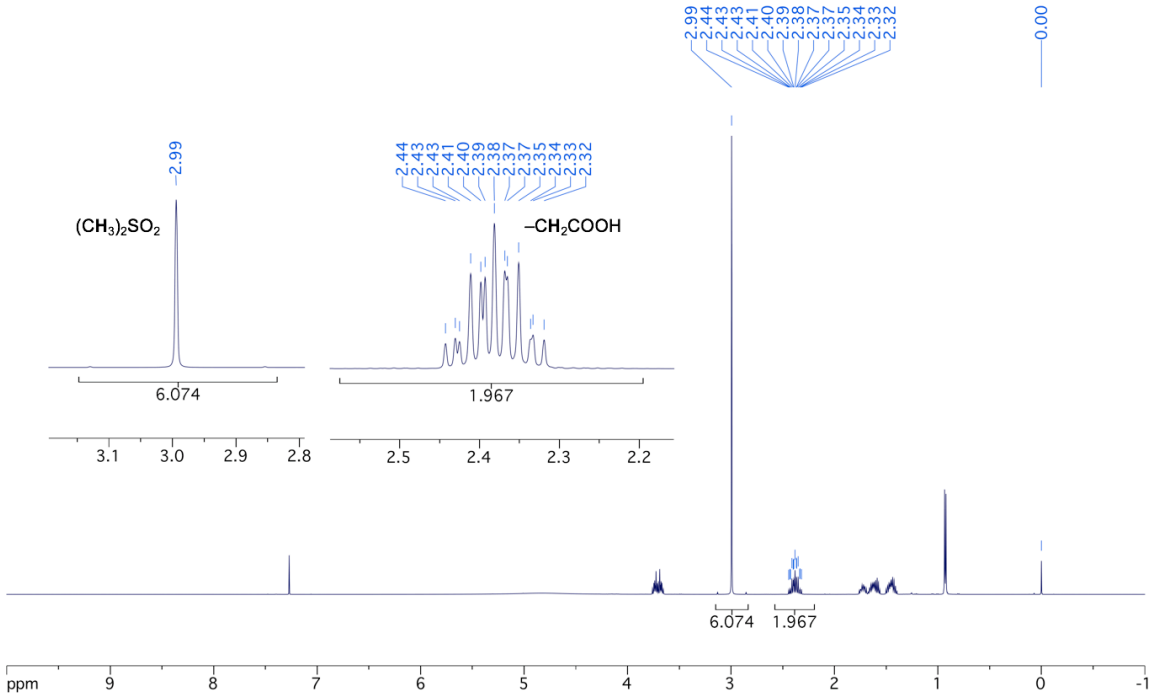

Figure B.15. ^{1}H NMR spectrum (500 MHz) of **1b** and dimethyl sulfone in $CDCl_3$; both integrations include ^{13}C satellites and purity calculations indicate that **1b** is ≥ 95.6% pure.

B.3. Future Work

To perform the mineralization experiments using cavity ring down spectroscopy, an overall ^{13}C-enrichment of 3-5% is optimal. On its own, **1a** has an overall ^{13}C-enrichment of ~15% because one position is 99% enriched and the other six positions correspond to natural abundance (1.1%); therefore, compound **1a** must be "diluted" with **1b** in order to lower the overall ^{13}C-enrichment. These compounds are very viscous oils and difficult to mix in their pure form, but their solubility in water will allow for stock solutions to be made, mixed in the appropriate properties, and ultimately distributed throughout soils collected from the environment. The evolution of $^{13}CO_2$ will then be monitored and used to calculate the extent of mineralization over time. An analogous set of experiments using commercially available ^{13}C-labeled lactic acid (mixed with pure ^{12}C lactic acid) will likely be performed as a benchmark for the mineralization of 6-hydroxy-4-methylhexanoic acid.

Once the mineralization data for these compounds is obtained, the next ^{13}C-labeled 6-hydroxy-4-methylhexanoic acid variant must be synthesized; a proposed route is shown below in **Figure B.16**. The mineralization of this variant is of great interest because the methyl position should be least accessible to the microorganisms; significant mineralization would therefore provide a solid foundation for the case that poly(4-methylcaprolactone)-based plastics are fully biodegradable. The next demonstration of ultimate biodegradability would require the preparation of ^{13}C-enriched poly(4-methylcaprolactone), presumably through (co)condensation or ring-opening (co)polymerization of ^{13}C/^{12}C 6-hydroxy-4-methylhexanoic acid or 4-methylcaprolactone, respectively.

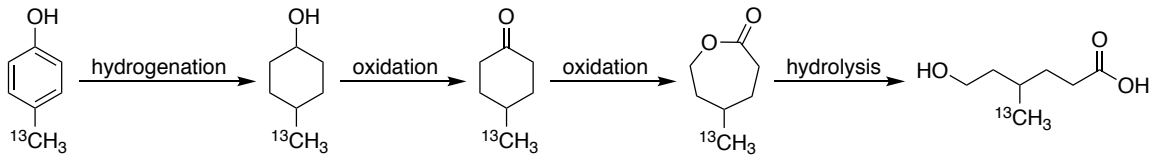

Figure B.16. Proposed scheme for the synthesis of ^{13}C-labeled 6-hydroxy-4-methylhexanoic acid from isotopically enriched 4-methylcresol.

B.4. References

[1] Lucas, N.; Bienaime, C.; Belloy, C.; Queneudec, M.; Silvestre, F.; Nava-Saucedo, J.-E. Polymer biodegradation: Mechanisms and estimation techniques *Chemosphere* **2008**, *73*, 429–442.

[2] Zumstein, M. T.; Schintlmeister, A.; Nelson, T. F.; Baumgartner, R.; Woebken, D.; Wagner, M.; Kohler, H.-P. E.; McNeill, K.; Sander, M. Biodegradation of synthetic polymers in soils: Tracking carbon into CO_2 and microbial biomass. *Sci. Adv.* **2018**, *4*, eaas9024.

[3] Sander, M. Biodegradation of Polymeric Mulch Films in Agricultural Soils: Concepts, Knowledge Gaps, and Future Research Directions. *Environ. Sci. Technol.* **2019**, *53*, 2304−2315

[4] Shah, A. A.; Hasan, F.; Hameed, A.; Ahmed, S. Biological degradation of plastics: A comprehensive review. *Biotechnol. Adv.* **2008**, *26*, 246–265.

Appendix C. Poly(4-methylcaprolactone) Elastomers from Bis(anhydride) Cross-linkers

C.1. Introduction

The poly(4-methylcaprolactone)-based elastomers described in **Chapter 4** demonstrated outstanding mechanical properties and have therefore inspired work aimed at improving upon the sustainable characteristics of the materials. In particular, the use of stannous octoate ($SnOct_2$) for prepolymer synthesis and for cross-linking is non-ideal. Though $SnOct_2$ is FDA-approved for use in food packaging materials,[1,2] the general use of $SnOct_2$ (and other organotin catalysts) should be avoided in sustainable material design because of cytotoxicity concerns.[3,4,5,6,7] The elemental analysis in **Chapter 5** demonstrates that removal of $SnOct_2$ from cross-linked materials is quite difficult; in fact, the persistence of organotin compounds in purified polyesters has also been reported by others.[8] Therefore, it is desirable to develop synthetic strategies which exclude $SnOct_2$ entirely (if possible). Many organocatalysts and Brønsted acid catalysts have been shown to effectively facilitate the ring-opening polymerization of cyclic esters;[9,10,11,12,13,14] furthermore, anhydrides can react readily with hydroxyl moieties at elevated temperature without exogenous catalyst.[15] Herein, we present initial work that demonstrates the feasibility for bis(anhydrides) to cross-link poly(4-methylcaprolactone) made using $SnOct_2$ or diphenylphosphoric acid (DPP), a Brønsted acid catalyst.

C.2. Poly(4-methylcaprolactone) Elastomers Made Using Bis(anhydrides)

The early work for this project was done using poly(4-methylcaprolactone) (PMCL) tetraols similar to those employed in **Chapter 4**, hence the use of $SnOct_2$ mentioned above;

the tetraol prepolymers used for large scale films had molar masses of 10.7, 21, 31.2, and 41.4 kg/mol (by ^{1}H NMR end group analysis) with dispersities of 1.19, 1.22, 1.26, and 1.38, respectively (by chloroform SEC with respect to polystyrene standards). The later work for this project was done using poly(4-methylcaprolactone) triols made using DPP. Both sets of polymers were purified by repeated precipitation (once in methanol, once in hexanes). Although it was presumed that the precipitation in methanol removes the catalysts, the methanol-swelled materials in **Chapter 5** (and the references provided in **Appendix A**) indicate that there is likely residual tin catalyst embedded in the polymer. However, the maximum gel fractions for cross-linked materials obtained using either $SnOct_2$-derived or DPP-derived prepolymers were similar (ca. 0.95), which can be interpreted one of two ways: 1) there is also residual DPP in the prepolymers after repeated precipitation, and it is catalyzing cross-linking to the same extent as the residual $SnOct_2$, or 2) there is no residual DPP and thus the residual tin in the $SnOct_2$-derived prepolymers is not significantly catalyzing the cross-linking process.

Initially, the bis(anhydride) being explored was made using the same carbonylation approach presented for the bis(β-lactone) synthesis in **Chapter 4**, except with two equivalents of carbon monoxide per epoxide rather than one (i.e., double carbonylation, **Figure C.1)**.[16] An important practical note about the bis(anhydride) **1** is that its solubility is much different than that of the corresponding bis(β-lactone); the latter is soluble in dichloromethane (DCM), tetrahydrofuran (THF), and acetone whereas the former is only soluble in THF and acetone. All of these solvents solubilize the prepolymer, though it is most soluble is DCM and least soluble in acetone.

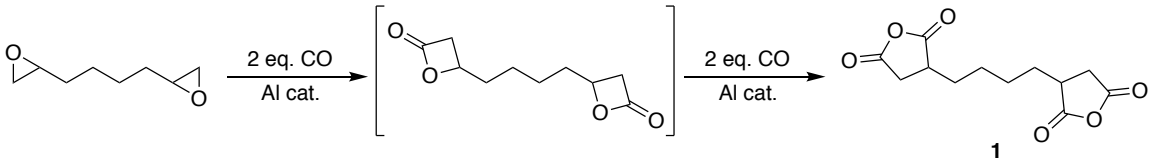

Figure C.1. Scheme for the production of bis(anhydride) cross-linker **1** via double carbonylation of the corresponding epoxide.

Small-scale films of PMCL tetraol and **1** were solvent cast in THF and heated to 120 °C for 24 h, which yielded optically clear elastomers. As with the bis(β-lactone) elastomers in **Chapter 4**, the elastomers derived using **1** also had glass transitions similar to the prepolymer (–60 °C by differential scanning calorimetry). To investigate the parameter space that would be available for scale-up, two series of films were made: 1) constant prepolymer M_n (11 kg/mol) and variable amounts of cross-linker, and 2) constant amount of cross-linker (targeted at stoichiometric equivalence between anhydride and hydroxyl groups) and variable prepolymer M_n. The gel fractions of these films were evaluated in DCM and subsequently compared to those presented in **Chapter 4**.

Varying the amount of cross-linker for a given mass of PMCL produced a trend wherein a maximum in gel fraction was observed at stoichiometric equivalence, which is much different than that which is obtained for cross-linking with the bis(β-lactone) (**Figure C.2**). The underlying reason for this difference is that the reaction of an anhydride and a hydroxyl group produces a carboxylic acid that is likely unreactive toward further reaction with another anhydride; by contrast, the reaction of a β-lactone with a hydroxyl group produces a β-hydroxyl which can react with another β-lactone. Therefore, the most successful conditions for the bis(anhydride) system are those of stoichiometric equivalence, just as with any step-growth polymerization. Furthermore, statistical gelation

theory can be used to predict the stoichiometry at which the reaction will fail entirely; these conditions are obtained when the critical extent of conversion (ρ_{crit}) is greater than or equal to unity.[17] Varying the prepolymer molar mass for the bis(anhydride) system produced a gel fraction trend very similar to that observed for the bis(β-lactone) system: optimal cross-linking was observed with molar masses ≤ 30 kg/mol. It is unclear why the datum corresponding to a prepolymer molar mass of ca. 54 kg/mol is so different across both systems.

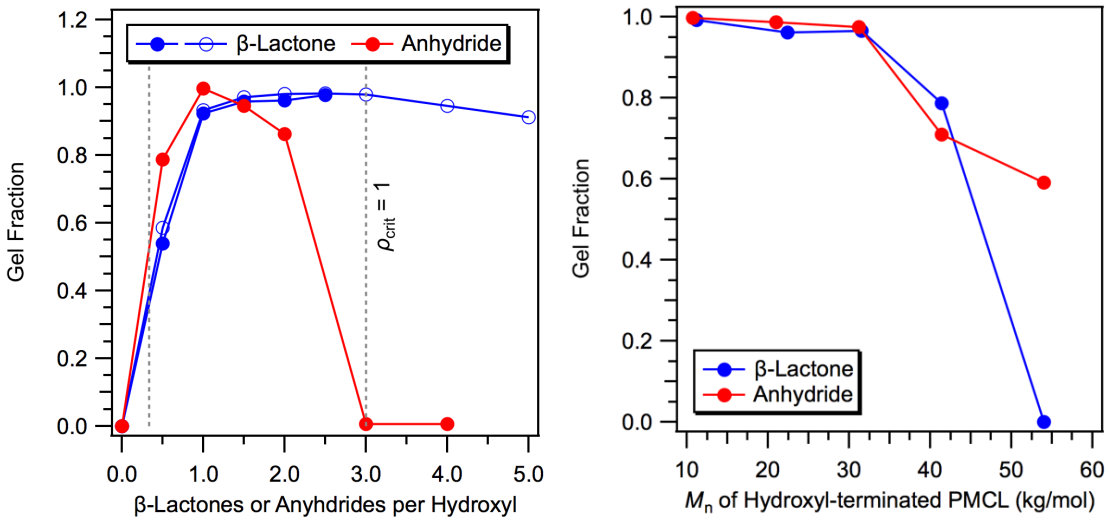

Figure C.2. Gel fractions evaluated in DCM for films made from **1** and PMCL tetraols: (left) varying the amount of **1** (i.e., stoichiometry) using 11 kg/mol PMCL, (right) varying the prepolymer molar mass while maintaining stoichiometric equivalence. The bis(anhydride) results are shown in red and compared to the bis(β-lactone) results from **Chapter 4**, which are shown in blue.

Film preparation was then scaled up using prepolymers of molar mass ≤ 41 kg/mol with amounts of **1** corresponding to stoichiometric equivalence. Just as with the bis(β-lactone), bis(anhydride) cross-linking could be easily visualized by infrared (IR) spectroscopy (**Figure C.3**); even though there was only a small amount of **1** present (≤ 5 wt%), the disappearance of signals arising from the anhydride was diagnostic of ring-

opening (i.e., cross-linking). However, there was one practical issue which had not previously been encountered with the bis(β-lactone) system: the films were much more difficult to remove from the aluminum weigh pans in which they were made. Switching to Teflon dishes helped somewhat, but unpredictable dewetting and the presence of small trapped bubbles were unfortunately observed. The films were still optically clear in all cases and all but the one produced from 41 kg/mol prepolymer had high gel fractions (> 0.95).

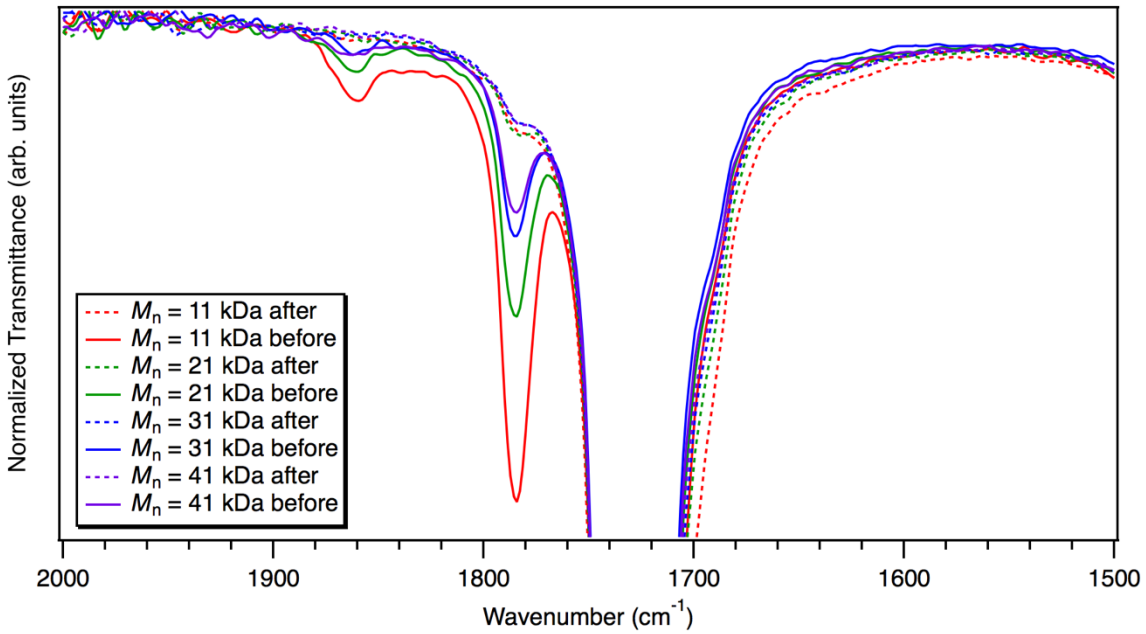

Figure C.3. IR spectroscopy of the bis(anhydride) films prepared on large scale; the indicated molar mass is for the PMCL prepolymer, solid lines represent the mixture before heating, and dotted lines represent the cross-linked materials (i.e., after heating). The large signal at ca. 1735 cm^{-1} is from the aliphatic esters present in PMCL whereas the signals at 1785 cm^{-1} and 1860 cm^{-1} correspond to the bis(anhydride).

In spite of the practical issues mentioned above, enough usable material was made for the purposes of mechanical testing. First, dynamic mechanical thermal analyses (DMTA) were performed in tension mode to probe the rigidity as a function of temperature. Materials made using **1** demonstrated stable plateau moduli between the glass transition

and the upper testing temperature (**Figure C.4**). Across the samples, the change in plateau modulus was not significant enough to be caused primarily by the difference in chemical cross-link density, similar to the results observed for the bis(β-lactone) system (see discussion in **Section 4.4.2**).

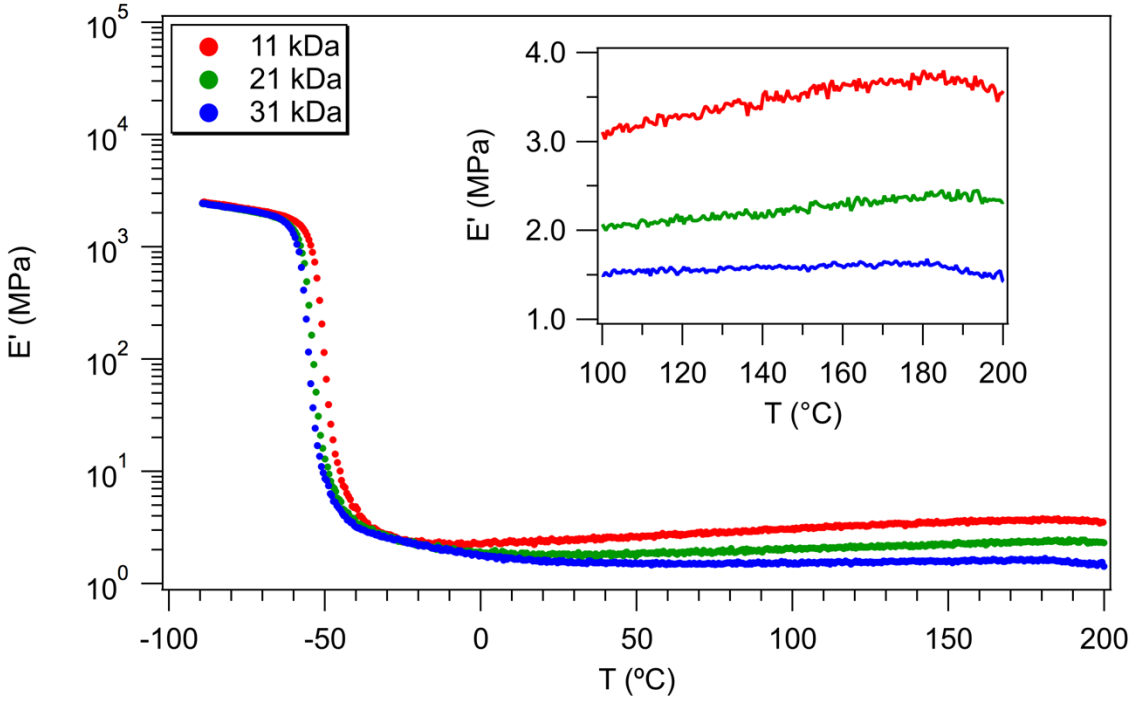

Figure C.4. DMTA (0.05% – 5% strain, 1 Hz, 5 °C/min) of the bis(anhydride) films prepared on large scale; the indicated molar mass is for the PMCL prepolymer.

The tensile properties until material failure were then evaluated and compared with the bis(β-lactone) system (**Figure C.5**). Unsurprisingly, the bis(anhydride) films exhibited classic elastomeric behavior. Across both systems, materials made with ~10 kg/mol PMCL and ~30 kg/mol had essentially identical Young's moduli, strain at break, and stress at break values. However, the bis(anhydride) material made with ~22 kg/mol far outperformed its bis(β-lactone) analogue with respect to stress and strain at break; the reason for this discrepancy is unclear. Regardless, these findings collectively demonstrate

that high-performance materials can be obtained using catalyst-free cross-linking conditions by employing a bis(anhydride) instead of a bis(β-lactone) compound.

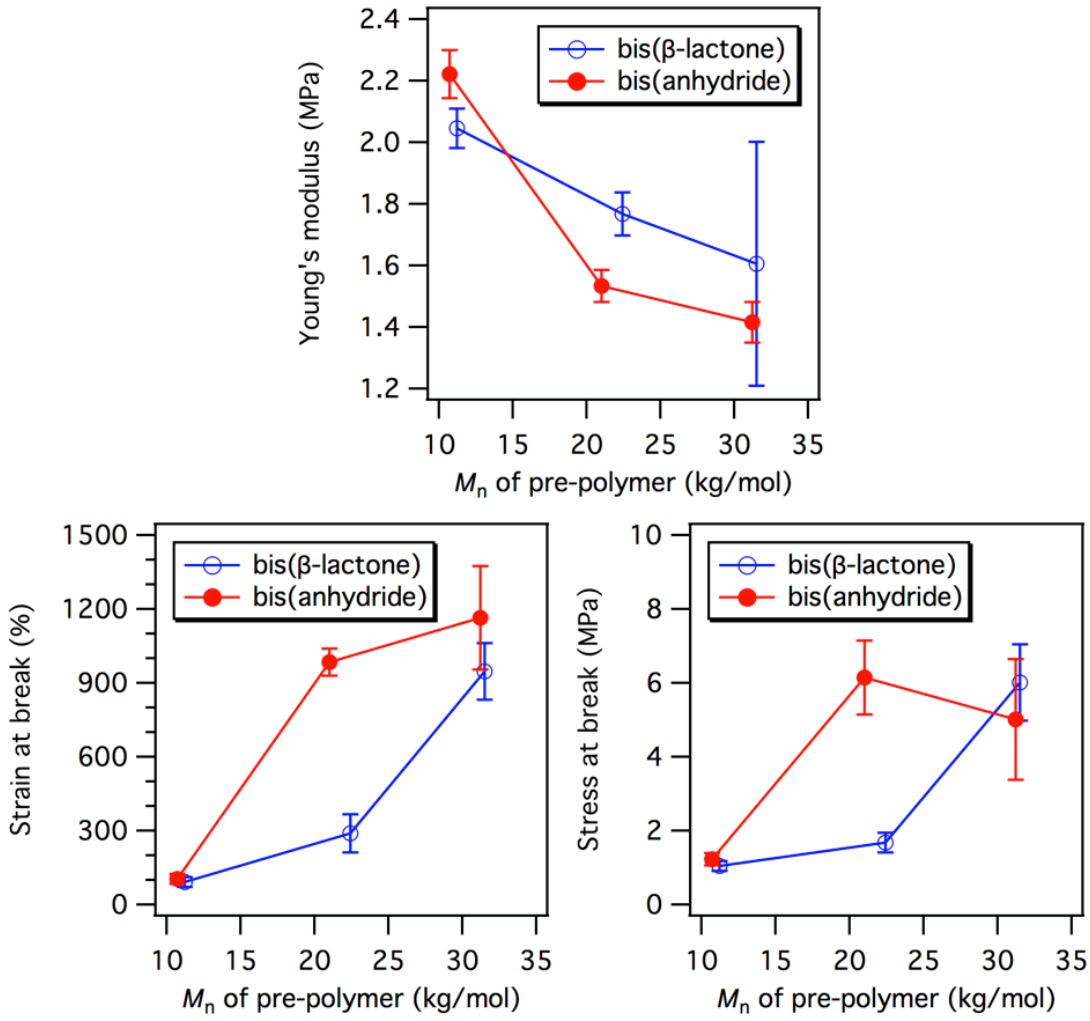

Figure C.5. Results obtained from tensile testing (50 mm/min) of the bis(anhydride) films prepared on large scale. The bis(anhydride) results are shown in red and compared to the bis(β-lactone) results from **Chapter 4**, which are shown in blue.

In the second phase of this project, both components were changed: PMCL triols were made using DPP-catalyzed ring-opening polymerization, and a slew of commercially available bis(anhydrides) were screened as potential candidates for elastomer synthesis. Four bis(anhydrides) were purchased and their solubilities in relevant organic solvents (i.e.,

those that can dissolve PMCL) were tested (**Figure C.6**). Unfortunately, the solubility of compounds **2**, **3**, and **4** was very poor in THF, which was the solvent previously used to homogenize PMCL and cross-linker.

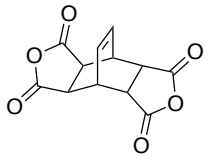

2

insoluble in DCM and THF
soluble in acetone

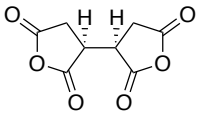

3

insoluble in DCM, THF,
and acetone

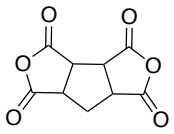

4

insoluble in DCM
sparingly soluble in THF
soluble in acetone

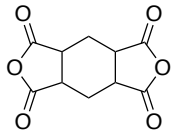

5

insoluble in DCM
soluble in THF and acetone

Figure C.6. Four commercially available bis(anhydrides) and a qualitative assessment of their solubility in the three organic solvents which dissolve PMCL.

The first cross-linker investigated was **5** and analogous sets of films were made in dry THF and dry acetone to test if similar gel fractions would be obtained with either solvent. Blankets of inert gas were used throughout film preparation (i.e., homogenization, evaporation, and heating) to avoid significant introduction of atmospheric moisture. As before, the amount of cross-linker was varied to probe the association between stoichiometry and successful gel formation (**Figure C.7**) From these results, it appeared that the choice of solvent for casting did not significantly affect the observed trend in gel fraction, which agreed nicely with the predictions made using statistical gelation theory. Gel fractions were evaluated in THF because DCM was found to artificially skew the results toward higher gel fraction, presumably because excess cross-linker (and perhaps chemically-modified polymer) was not soluble in DCM (**Figure C.7**).

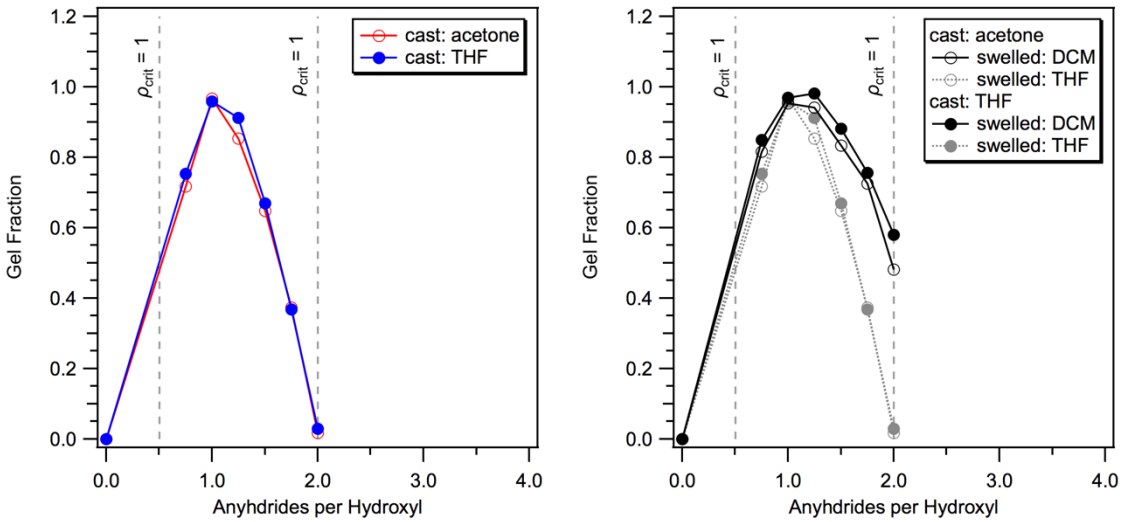

Figure C.7. left) Gel fractions evaluated in THF for films made from **5** and PMCL triols using acetone or THF for solvent casting. (right) A comparison of the gel fractions evaluated in THF (gray) versus the gel fractions evaluated in DCM (black) for films made from **5** and PMCL triols using acetone or THF for solvent casting. Note that the data in grey in the right figure is the same as the data shown in the left figure.

Based on the results with **5**, it seemed that acetone would be suitable for the preparation of cross-linked PMCL using **4** and **2**. Therefore, a series of films was made wherein the molar mass of prepolymer and the stoichiometry was varied for all three cross-linkers (excluding the variable stoichiometry series already performed for **5**). Though all solutions of bis(anhydride) and PMCL were initially homogenous and clear, evaporation under inert gas caused **2**—and to a lesser extent, **4**—to precipitate and settle at the bottom of the vials. Unsurprisingly, all cross-linking with **2** failed. Cross-linking with **4** was non-negligible but unsatisfactory as compared to results obtained with **5** (**Figure C.8**). Similar to prior results, the choice of solvent for film casting with **5** did not significantly affect the observed gel fractions. The low solubility of **2** and **4** in the prepolymer (compared to **5**) evidently makes the use of these bis(anhydrides) impossible going forward. Future work

will therefore focus on the scale-up of PMCL films made using **5** as well as subsequent thermal and mechanical characterization.

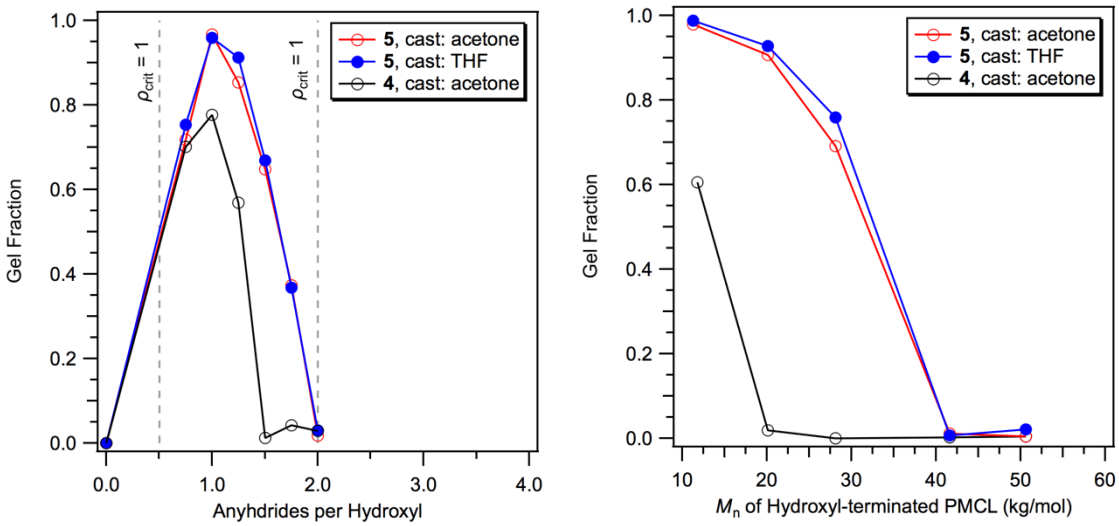

Figure C.8. (left) Gel fractions evaluated in THF for films made from **5** or **4** and PMCL triols using acetone or THF for solvent casting. Note that the data for **5** is the same as in the previous figure. (right) Gel fractions evaluated in THF for films made from **5** or **4** and PMCL triols with variable molar mass using acetone or THF for solvent casting.

C.3. References

[1] Electronic Code of Federal Regulations, Title 21 – Food and Drugs, Chapter 1 – Food and Drug Administration, Department of Health and Services, Subchapter B – Food for Human Consumption (continued), Part 175 – Indirect Food Additives: Adhesives and Components of Coatings, §175.105 – Adhesives. https://www.ecfr.gov/cgi-bin/text-idx?SID=01e3cc9e948472d4a75ecaeed3cd532b&mc=true&node=se21.3.175_1105&rgn=div8 (accessed September 10, 2019).

[2] Electronic Code of Federal Regulations, Title 21 – Food and Drugs, Chapter 1 – Food and Drug Administration, Department of Health and Services, Subchapter B – Food for Human Consumption (continued), Part 175 – Indirect Food Additives: Adhesives and Components of Coatings, §175.300 – Resinous and Polymeric Coatings. https://www.ecfr.gov/cgi-bin/text-idx?SID=01e3cc9e948472d4a75ecaeed3cd532b&mc=true&node=se21.3.175_1300&rgn=div8 (accessed September 10, 2019).

[3] Lecomte, J.; Jérôme, C. Recent Developments in Ring-Opening Polymerization of Lactones. *Adv. Polym. Sci.* **2012**, *245*, 173–218.

[4] Piver, W. T. Organotin Compounds: Industrial Applications and Biological Investigation. *Environ. Health Perspect.* **1973**, 4, 61.

[5] Álvarez-Chávez, C. R.; Edwards, S.; Moure-Eraso, R.; Geiser, K. Sustainability of bio-based plastics: general comparative analysis and recommendations for improvement. *J Clean Prod* **2012**, 23, 47–56.

[6] Grün, F.; Watanabe, H.; Zamanian, Z.; Maeda, L.; Arima, K.; Cubacha, R.; Gardiner, D. M.; Kanno, J.; Iguchi, T.; Blumberg, B. Endocrine-disrupting organotin compounds are potent inducers of adipogenesis in vertebrates. *Mol Endocrinol.* **2006**, 20, 2141–2155.

[7] Tanzi, M. C.; Verderio, P.; Lampugnani, M. G.; Resnati, M.; Dejana, E.; Sturani, E. Cytotoxicity of some catalysts commonly used in the synthesis of copolymers for biomedical use. *J. Mater. Sci. – Mater. Med.* **1994**, 5, 393–396.

[8] Stjerndahl, A.; Wistrand, A. F.; Albertsson, A.-C. Industrial Utilization of Tin-Initiated Resorbable Polymers: Synthesis on a Large Scale with a Low Amount of Initiator Residue. *Biomacromolecules* **2007**, *8*, 937–940.

[9] Lohmeijer, B. G. G.; Pratt, R. C.; Leibfarth, F.; Logan, J. W.; Long, D. A.; Dove, A. P.; Nederberg, F.; Choi, J.; Wade, C.; Waymouth, R. M.; Hedrick, J. L. Guanidine and

Amidine Organocatalysts for Ring-Opening Polymerization of Cyclic Esters. *Macromolecules* **2006**, *39*, 8574–8583.

[10] Pratt, R. C.; Lohmeijer, B. G. G.; Long, D. A.; Waymouth, R. M.; Hedrick, J. L. Triazabicyclodecene : A Simple Bifunctional Organocatalyst for Acyl Transfer and Ring-Opening Polymerization of Cyclic Esters Triazabicyclodecene : A Simple Bifunctional Organocatalyst for Acyl Transfer and Ring-Opening Polymerization of Cyclic Esters. *J. Am. Chem. Soc.* **2006**, *128*, 4556–4557.

[11] Connor, E. F.; Nyce, G. W.; Myers, M.; Möck, A.; Hedrick, J. L. First Example of N-Heterocyclic Carbenes as Catalysts for Living Polymerization: Organocatalytic Ring-Opening Polymerization of Cyclic Esters. *J. Am. Chem. Soc.* **2002**, *124*, 914–915.

[12] Schneiderman, D. K.; Hillmyer, M. A. Aliphatic Polyester Block Polymer Design. *Macromolecules*, **2016**, 49, 2419–2428.

[13] Kamber, N. E.; Jeong, W.; Waymouth, R. M. Organocatalytic Ring-Opening Polymerization. *Chem. Rev.* **2007**, *49*, 2419–2428.

[14] Susperregui, N.; Delcroix, D.; Martin-Vaca, B.; Bourissou, D.; Maron, L. Ring-Opening Polymerization of ε-Caprolactone Catalyzed by Sulfonic Acids: Computational Evidence for Bifunctional Activation. *J. Org. Chem.* **2010**, 75, 6581–6587.

[15] Kienle, R. H.; Hovey, A. G. The Polyhydric Alcohol-Polybasic Acid Reaction. I. Glycerol-Phthalic Anhydride. *J. Am. Chem. Soc.* **1929**, *51*, 509–519.

[16] Rowley, J. M.; Lobkovsky, E. B.; Coates, G. W. Catalytic Double Carbonylation to Succinic Anhydrides: Catalyst Discovery, Reaction Scope, and Mechanism. *J. Am. Chem. Soc.* **2007**, *129*, 4948–4960.

[17] Odian, G. *Principles of Polymerization*; 4th ed.; John Wiley & Sons: Hoboken, NJ, 2004.